Small Molecule Activation by Multimetallic Uranium Complexes

Thèse N° 9539

Présentée le 14 juin 2019

à la Faculté des sciences de base
Groupe SCI SB MM
Programme doctoral en chimie et génie chimique

pour l'obtention du grade de Docteur ès Sciences

par

Marta FALCONE

Acceptée sur proposition du jury

Prof. K. Sivula, président du jury
Prof. M. Mazzanti, directrice de thèse
Prof. G. Cloke, rapporteur
Prof. P. Arnold, rapporteuse
Prof. X. Hu, rapporteur

2019

ÉCOLE POLYTECHNIQUE
FÉDÉRALE DE LAUSANNE

ABSTRACT

The development of new processes for the selective and sustainable transformation of abundant small molecules constitutes one of the major research areas in inorganic and organometallic chemistry. These molecules as CO_2, CO, N_2 and H_2 are abundant reservoirs of chemical energy, readily available sources of carbon, nitrogen and hydrogen. In a patent from 1909, Haber reported that uranium and uranium nitride were very efficient catalysts for ammonia synthesis. In order to perform multi-electron transfer, multimetallic complexes need to be designed. Reactivity of uranium bridging nitrides remained unexplored since we investigated the nitride based reactivity of a dinuclear uranium(IV) bridging nitride complex towards small molecules such as CO_2, yielding the first example of a uranium complex containing a bridging dicarbamate ligand, or CO, resulting in the complete cleavage in mild conditions of one of the strongest bonds in nature, or H_2, yielding one of the few examples in *f*-elements of metal hydride, which is readily transferred to substrates such as CO_2. Beyond the ligand based reactivity, we were interested in reducing the two metal centers to access a diuranium(III) bridging nitride, to pursue nitrogen activation. This complex was shown to have high flexibility, provided by the siloxide ligands, high reducing power and a bridging atom, the nitride, that holds together the uranium centers, with the possibility to bend upon nitrogen activation. This approach led us to the isolation of a hydrazido complex, resulting from the four-electron reduction of dinitrogen by the two metal centers. Moreover, complete cleavage of the N–N single bond was achieved by addition of CO to give two cyanate ligands or by addition of H_2 to give ammonia. The nitride atom linker is nonetheless, too reactive to act as a spectator and it is involved in reactivity. Hence, we target the isolation of the analogue dinuclear U(III) complex with an oxide ligand as linker. This complex showed the same reactivity towards nitrogen but DFT revealed a more ionic character of the U–O bond nature with respect to the U–N bond, leading to different reactivity of the hydrazido fragment upon addition of CO and upon addition of H_2, showing a smaller extent of activation in the oxo complex with respect to the nitride. The diuranium(III) bridging oxide complex showed interesting reactivity with H_2, forming a bis-hydride complex capable of reducing CO_2 beyond the formate level, to methanol.

Keywords: uranium, nitride, bridging nitride, bridging oxide, ammonia formation, hydrogen activation, carbon monoxide, carbon dioxide, hydrides, small molecules, siloxide ligands.

RIASSUNTO

Lo sviluppo di nuovi processi per l'utilizzo e la trasformazione selettiva di piccole molecole costituisce una delle aree di ricerca più vaste in chimica inorganica. Queste molecole, come CO_2, CO, N_2 e H_2 sono abbondanti fonti di carbonio, azoto e idrogeno. Nel 1909, Haber riportò un patent in cui uranio e nitruri di uranio venivano descritti come catalizzatori altamente efficienti per la produzione di ammoniaca. Importante è quindi il design di complessi multimetallici al fine di ottenere trasferimento di più di un elettrone da un complesso di uranio. Prima del lavoro qui presentato, la reattività di nitruri a ponte di uranio era essenzialmente inesplorata. Abbiamo intrapreso così lo studio di reattività del complesso dinucleare di uranio(IV) con nitruro a ponte verso CO_2, che ha portato al primo esempio contenente un dicarbammato tra i due atomi di uranio; verso CO, che ha portato alla completa rottura del triplo legame; e verso H_2, che ha portato a isolare uno dei rari esempi di idruri metallici tra gli elementi *f*, che facilmente viene trasferito a substrati quali diossido di carbonio. Oltre alla reattività basata sul legante nitruro, abbiamo riportato la sintesi del complesso dinucleare di uranium(III) con nitruro a ponte, per studiarne la reattività con l'azoto. Le caratteristiche di questo complesso comprendono una grande flessibilità, data dai leganti silossanici e un alto potere riducente, permettendo di isolare un complesso contenente un legante idrazinico, risultante dalla riduzione a quattro elettroni dell'azoto da parte dei due centri metallici. Inoltre, la completa rottura del legame N–N è resa possibile attraverso l'aggiunta di reagenti quali CO per dare cianato o H_2 per dare ammoniaca. Il nitruro a ponte è tuttavia reattivo nel confronti di tali reagenti. Con lo scopo di trovare un atomo a ponte che fungesse da spettatore, l'analogo composto con un legante ossido a ponte è stato sintetizzato. Questo complesso mostra la stessa reattività con l'azoto, ma i calcoli DFT hanno rivelato una netta differenza della natura del legame U–O rispetto a quella del legame U–N. Questo si riflette in un minor grado di attivazione dell'azoto che risulta in una diversa reattività nei confronti di CO e H_2. Il complesso di diuranio(III) con un ossido a ponte ha mostrato anche una reattività interessante con l'idrogeno, formando un bis-idruro, il quale, facilmente riduce CO_2 a metanolo.

Parole chiave: uranio, nitruri, nitruri a ponte, ossido a ponte, ammoniaca, attivazione di idrogeno, monossido di carbonio, diossido di carbonio, idruri, piccole molecole, leganti silossanici.

ACKNOWLEDGEMENTS

I would like to first thank all the members of my committee for accepting to review the present thesis.

I would like to express my deepest gratitude to Prof. Marinella Mazzanti for giving me the opportunity to undertake my PhD work with her. She passed on to me the passion for coordination chemistry and taught me what it really means to rigorously work in a laboratory. Through the feed-back, guidance, scientific discussions and freedom I was provided with, I have been able to achieve a lot through these years.

I am grateful to my Master's thesis supervisor, prof. Lorenzo Di Bari for the support he gave me after my thesis and throughout my PhD years.

A lot of people have been essential for the positive outcome of my PhD and deserve my gratitude. First of all, Rosario Scopelliti, together with Farzaneh Fadaei Tirani for the solution of the crystallographic structures and for the knowledge they shared regarding crystallography. Secondly, I thank Euro Solari, for all the performed elemental analysis and for the help with any technical issues in the laboratory. I thank Ivica Zivkovic who carried out and interpreted the magnetic measurement on the uranium complexes. I thank prof. Laurent Maron who carried out computational mechanistic studies. I thank prof. Clémence Corminboeuf and Alberto Fabrizio for the computational analysis on the nitride and oxide complexes, which added value to the work. I also want to thank prof. Kay Severin for the collaboration in part of the work. Finally, I would like to thank Aurélien Bornet for the technical help with NMR spectroscopy.

Then I would like to thank all the members of the GCC group for their help, support and for making these years special. Thank to Anne Sophie for her support and help. Thank to Lucile Chatelain as she introduced me to uranium chemistry and laboratory techniques. Thank to Juliè Andrez for the scientific contribution. Thank to Rory P. Kelly for the help in the lab and profitable discussions but most of all for being part of

some of the best memories I will bring along of this PhD. Thank to all the actual members of the group, which I consider more than colleagues, for the support, the scientific discussions and for the fun we had together. In particular, thanks to Luciano for his amazing personality, thanks to Radmila and her ability in conveying self-confidence, thanks to Davide for his never ending jokes, thanks to Chad for his availability, thanks to Nadir for his spontaneous selflessness, thanks to Aurélien for his relaxed approach to PhD life. A special thanks to Masoud, for introducing me to life out of EPFL, for the support and the great scientific and non-scientific exchange of ideas and beliefs.

This PhD thesis wouldn't exist without the support and the trust of my husband, friend and life partner Daniele. He sustained me through all the good and bad times related to research and personal life, giving me strength even from afar.

I thank my big family for the support and the distraction they have been during these years: mamma and babbo, the rock on which I stand when I feel weak, Filippo and Federico, the wisest brothers I could have, Sandy and Anto, sisters in law and friends; Alex and Dani, brothers in law and friends; Noemi, Rebecca and Rachele, sisters, friends and inspiring people. All my precious nephews: Daniele, Samuele, Miriam, Benjamin, Ryan, Levi and Sophie.

I thank God who goes before me and behind me, whose hand guided me, whose strength supported me, who saw me before I was born, who knew every moment before a single day had gone by.

ABBREVIATIONS

18c6	1,4,7,10,13,16-hexaoxacyclooctadecane
Ad	adamantyl
COT	cyclooctatetraene
cryptand	1,10-diaza-4,7,13,16,21,24-hexaoxabicyclo[8.8.8]hexacosane
Cp	cyclopentadienyl
Cp*	pentamethylcyclopentadienyl
DFT	density functional theory
DMAP	4-dimethylaminopyridine
DMBS	dimethytertbutylsilyl
DME	dimetoxyethane
dmit	1,3-dithiole-2-thione-4,5-dithiolate
Et	ethyl
equiv	equivalents
ESI-MS	electro-spray ionization mass spectrometry
HMDS	bis(trimethylsilyl)amine
Hz	Herz
^{i}Pr	isopropyl
Ln	lanthanide
Me	methyl
Mes	mesityl (2,4,6-$Me_3C_6H_2$)
NMR	nuclear magnetic resonance
OTf	triflate: $CF_3SO_3^-$
Ph	phenyl
ppm	parts per million
r.t.	room temperature
SQUID	superconducting quantum interference device
tacn	triazacyclononane
tren	tris(2-aminoethyl)amine
^{t}Bu	tert-butyl
THF	tetrahydrofuran
TMS	trimethylsilyl

TABLE OF CONTENTS

CHAPTER 1
INTRODUCTION

1.1. The Uranium element

"Nothing in life is to be feared, it is only to be understood..." – M. Curie

When a black powder was found after heating a yellow compound obtained from pitchblende, an oxide of a new element was being discovered (Klaproth, 1789). This new element was named Uranus and isolated as the first sample of uranium metal in 1841, by heating uranium tetrachloride with potassium.

Uranium is an *f*-element, more precisely an actinide (Figure 1) and it is long-lived and significantly abundant in the earth, along with thorium, while actinium and protactinium are present in small amounts, as decay products of ^{235}U (7.13 x 10^8 years, natural 0.7204% abundance) and ^{238}U (4.50 x 109 years, natural 99.2739% abundance), the most abundant uranium isotopes.[1]

57 La	58 Ce	59 Pr	60 Nd	61 Pm	62 Sm	63 Eu	64 Gd	65 Tb	66 Dy	67 Ho	68 Er	69 Tm	70 Yb	71 Lu
89 Ac	90 Th	91 Pa	92 U	93 Np	94 Pu	95 Am	96 Cm	97 Bk	98 Cf	99 Es	100 Fm	101 Mb	102 No	103 Lr

Figure 1. *f*-elements block of the periodic table, showing lanthanides and actinides.

Actinides present some unique characteristics, such as large ionic radii, high coordination numbers and unusual coordination geometries.[2] A particular aspect is the radial extension of the 5f and 6d orbitals of the early actinides elements (from thorium to neptunium), allowing some overlap with the ligand orbitals (Figure 2).[3]

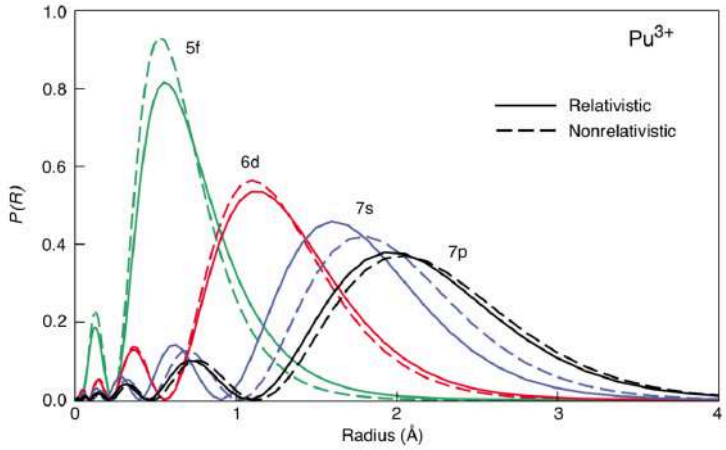

Figure 2. Radial Extent of the electronic orbitals for the Pu^{3+} ion.

1.1.1. Overview on the oxidation states

The actinides in the first half of the series present lower energies for the 5f → 6d promotion than for the 4f → 5d promotion in the lanthanides series, resulting in a higher range of oxidation states. The uranium element exhibits a wide range of oxidation states, from +2 to +6. The coordination chemistry of U(VI), in particular of compounds containing the uranyl(VI) ion, UO_2^{2+},[4] has been significantly studied, due to its implication in the nuclear waste recycling process. A significant example of non uranyl-contaning U(VI) compound is the hexafluoride complex of U(VI), UF_6, currently used in nuclear plants for the separation of uranium isotopes. Pentavalent uranyl-containing compounds are not so common because of the tendency to disproportionate to U(IV) and U(VI), however, while stable UO_2^+ complexes have been reported in organic media,[5] only recently the first example of water stable UO_2^+ complex was discovered.[6] The +4 oxidation state is very stable in non-aqueous media and in inert atmosphere of argon and stable starting materials consist of halides complexes as UCl_4 and $UI_4(Et_2O)_2$, while many compounds with many different ligands are formed by oxidation of U(III) compounds. These will be described in details in the following section.

Only few examples are reported with the uranium in the oxidation state +2 (Figure 3).[7]

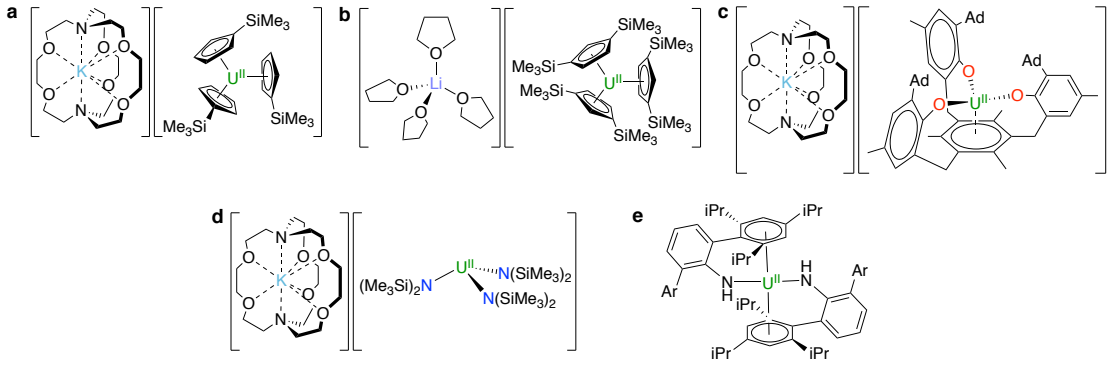

Figure 3. Isolated compounds of uranium(II) with Cp ligands (**a**;**b**), with a chelating trisaryloxide ligand (**c**), with bis(trimethylsilyl)amide ligands (**d**) and with terphenylamide ligands (**e**).

1.2. Trivalent uranium compounds

Trivalent uranium exhibits a strong reducing potential (between –1.5V to –2.9V vs $[(C_5H_5)_2Fe]^{+/0}$),[8] which depends on the ligand environment as well [8b] (the reducing ability increases with electron donating ligands) and a large Van der Waals radius (1.86 Å),[9] resulting in high coordination numbers. Low coordination numbers can be accessed with sterically hindered ligands, such as bis(trimethylsilyl)amide.[10] At last, even if the metal-ligand bonding is still prevalently electrostatic and the geometries determined by steric repulsion, trivalent uranium complexes show π and δ back-bonding ligation.[11] Stable uranium(III) complexes can be prepared by ligand exchange (Scheme 1) or by reduction of a tetravalent compound (Scheme 2).

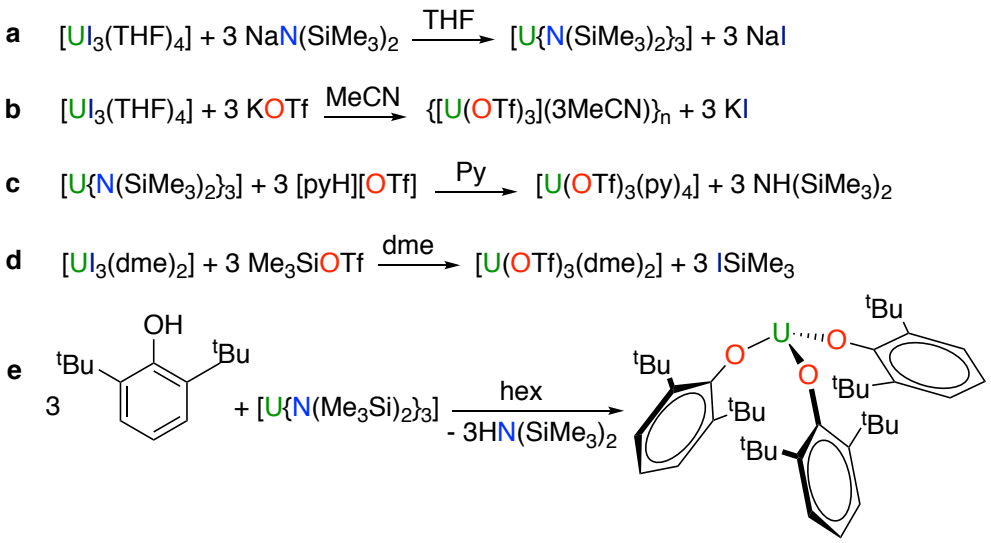

Scheme 1. Trivalent uranium complexes prepared by ligand exchange.

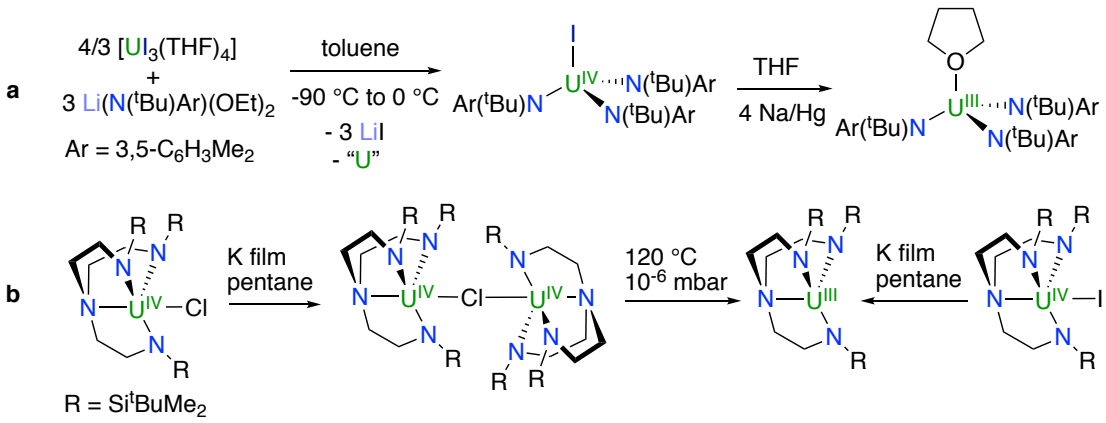

Scheme 2. Trivalent uranium complexes prepared by tetravalent compound reduction.

1.2.1. Ligands in U(III) chemistry

Cyclopentadienyl (Cp) supporting ligands have been widely studied in uranium chemistry as they provide the required bulkiness to form stable species of uranium in low oxidation states (+2 and +3). Uranium chemistry was for a long time dominated by complexes formed with cyclopentadienyl-derived and other carbocyclic ligands (Figure 4), as they provide complexes with only a few available coordination sites for reactivity. Many examples of U(III) complexes stabilized by Cp ligands will be presented in the next section.

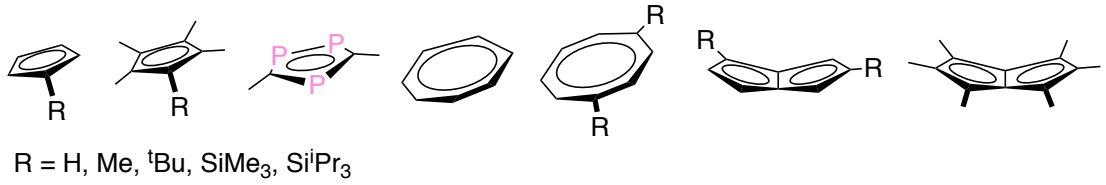

Figure 4. Classic organouranium spectator ligands.

Heteroatom-based ligands were shown to stabilize U(III) compounds, especially organoboron anionic ligands,[12] or oxygen-donor and nitrogen-donor monodentate ligands, including alkoxides, aryloxides,[13] amides [14] and silylamides [15] (Figure 5). The hard character of such ligands brings to an easy bonding of low-valent uranium, enhancing the reducing character towards reactivity. As the cone angle of cyclopentadienyl is estimated to be 130°, any alkoxide analogue would require the use of a bulky group, greater in size than ^{t}Bu (cone angle of ^{t}Bu < 90°). In contrast to hindered amides, an alkoxide has only one substituent on the heteroatom, two bond length from the metal, and hence it must be extremely large in order to have steric control.

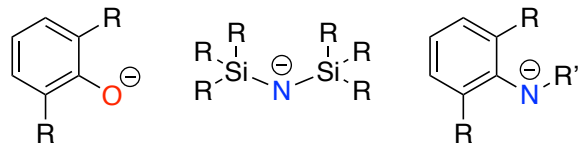

Figure 5. Common aryloxide, silylamide and amide ligands in uranium chemistry.

Many other ligands containing amido or phenolate donor fragments have been synthetized with various coordination modes as well as ligands that combine hard and soft atoms (such as sulfur and phosphorous) to be used as ancillary ligands for uranium in +3 oxidation state (Figure 6).[16]

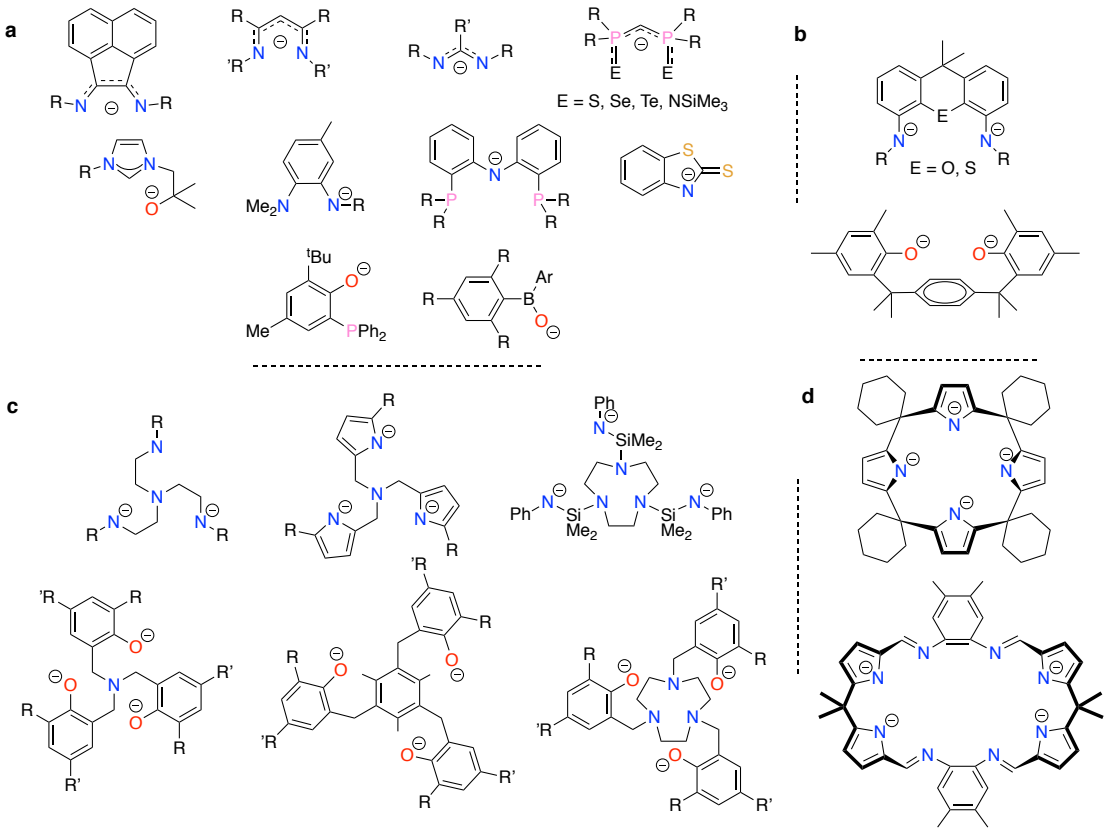

Figure 6. Multidentate anionic supporting ligands used in U(III) chemistry: monoanionic (**a**), dianionic (**b**), trianionic (**c**) and tetraanionic (**d**) ligands.

1.3. Small molecule activation

In the current energetic context, the search for renewable alternatives to fossil fuels is attracting increasing attention towards the low energy conversion of cheap and largely available C_1 sources such as CO_2 and CO, or N sources such as N_2, into higher value organic molecules. CO_2 is a cheap, very largely available and renewable C1 source and as such, the possibility of using it in fine chemical synthesis, or its

conversion into liquid fuels is highly attractive.[17] CO is readily available as part of syngas (CO + H_2, usually obtained from coal or biomass) and is used as feedstock in the industrial Fischer-Tropsch process for the production of alkanes, alkenes and alcohols. This heterogeneous catalytic process is energy consuming, as the reduction of CO by H_2 is performed under high temperatures and pressures (200 - 350 °C, 20 - 44 bar). Furthermore, in spite of the importance in agriculture of ammonia derived fertilizers, the only industrial process that uses N_2 as feedstock is the Haber-Bosch. This process allows the production of large amounts of ammonia from dinitrogen and dihydrogen, but imposes the use of harsh conditions (about 450 °C and 300 bar) and consumes about 2% of the world's annual energy supply.

However, this is a very challenging problem due to the low reactivity of such molecules. Metal complexes have been widely used to promote activation of small molecules under mild conditions. Uranium compounds offer an attractive alternative to metals of s, p and d blocks because of their unique properties and large availability from spent nuclear fuel, and the efforts in this area have been summarized in several recent reviews.[18]

1.3.1. Binding at mononuclear uranium complexes

A few rare examples of mononuclear uranium complexes binding CO,[19] N_2 [20] or CO_2 [21] in a terminal fashion were reported (Figure 7).

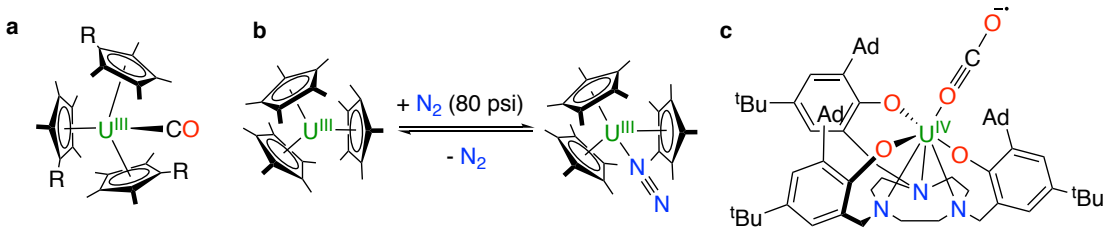

Figure 7. Carbonyl complex of U(III) (**a**); dinitrogen coordination at a U(III) center (**b**); end-on bound CO_2 at a U(IV) center (**c**).

In the carbonyl and dinitrogen U(III) complexes, the CO and N_2 bonds are unchanged with respect to the free molecules, suggesting a very low degree of activation. The ability of U(III) complexes to bind CO contrasts with the lack of reported carbonyl complexes of Ln(III) and is interpreted in terms of a more covalent U–C interaction.

In contrast, an important degree of activation is reported for the bound CO_2 in the [U{(^{Ad}ArO)$_3$tacn}(η^1-OCO)] complex, which shows a unique end-on bound CO_2 unit. The structural and spectroscopic data suggested the presence of a U(IV) complex of the charge-separated $CO_2^{-\cdot}$ radical anion, U(IV)($OCO^{-\cdot}$).[21] The unusual reactivity leading to [U{(^{Ad}ArO)$_3$tacn}(η^1-OCO)] was explained in terms of the sterically protected environment provided by the bulky (^{Ad}ArO)$_3$tacn system that stabilises an end-on bound $CO_2^{-\cdot}$ radical anion. This was confirmed by the reactivity of the less bulky ligand system (^{tBu}ArO)$_3$tacn, leading to a very stable bridging oxo species and evolution of CO.[22]

1.3.2. Reactivity of uranium complexes with CO and heteroallenes

Beside the unique examples of small molecules binding at mononuclear uranium complexes, reduction of CO, CO_2 or N_2 at U(III) centers involves, in the vast majority of reported studies, mono-electron transfer by mononuclear and monometallic complexes of uranium(III). In most cases two mononuclear complexes bind the substrate and effect the reduction to afford a dinuclear complex, in which two uranium(IV) centers are bridged by the reduced substrate. Usually, each uranium center is involved in one-electron transfer process.

In scheme 3 some key examples of this type of reactivity with CS_2, CO_2 and CO are summarized.

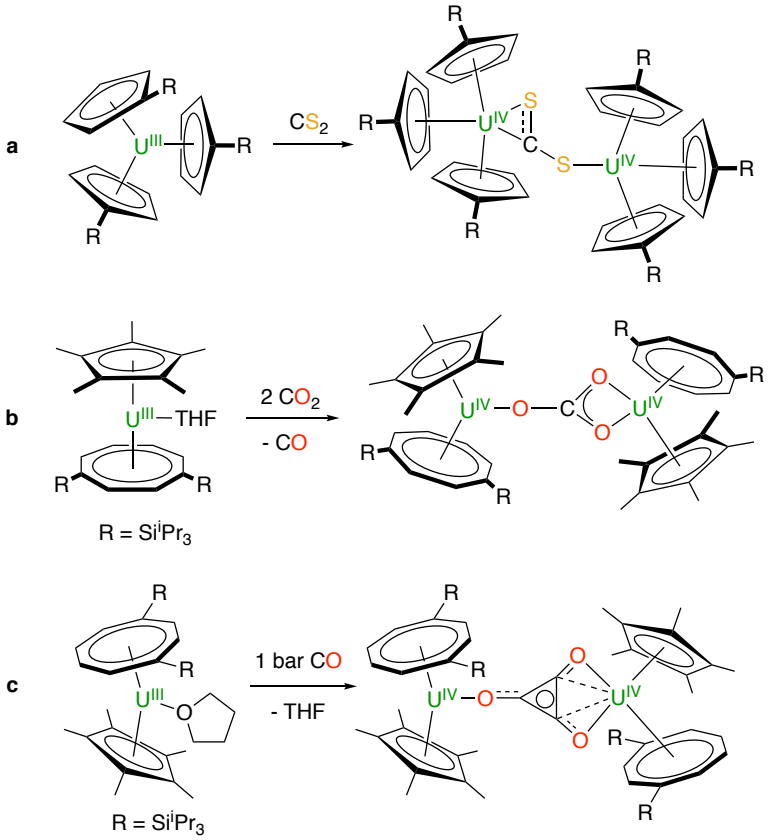

Scheme 3. Reduction of CS_2 to afford a dinuclear U(IV) complex (**a**); disproportionation of CO_2 to give a bridged carbonate dinuclear U(IV) complex (**b**); carbon monoxide reduction to give the deltate bridged dinuclear U(IV) complex (**c**).

One trivalent uranium metallocene complex reduces CS_2 by a one-electron transfer to form a dinuclear U(IV) complex.[23] Reduction of CO_2 has resulted in the cleavage of one CO double bond, reductive disproportionation and reductive dimerization depending on the electronic and steric properties of the supporting ligands.[24] Furthermore, U(IV) salts of squarate were obtained, yielding the first carbocycle synthesis only from CO_2 as carbon source. Carbon monoxide reduction by U(III) mixed sandwhich or amide complexes afforded a range of linear and cyclic homologation products $(C_nO_n)^{2-}$, the ethynediolate,[25] deltate dianions [26] and squarate. [27]

1.3.3. Reactivity of uranium complexes with chalcogenides

Activation of chalcogens and functionalization of chalcogenides is attracting increasing interest in uranium chemistry [28] due to its importance in catalysis and in spent nuclear fuel processing. However, uranium compounds capable of activating elemental chalcogens remain relatively scarce and most of them, even if chalgogens are formally two-electron oxidizing agents, resulted in one electron transfer from the

uranium center. Notably, U(III) mononuclear complexes are known to promote the reduction of elemental sulfur providing a pathway to sulfide bridged diuranium(IV) complexes (Scheme 4).[29] In contrast, the reaction of a dinuclear U(III) complex with excess sulfur leads to a persulfide bridged diuranium(IV) complex.[30] The formation of the persulfide versus sulfide could be explained by a cooperative binding of sulfur by the two metal centers associated to simultaneous one electron transfer.

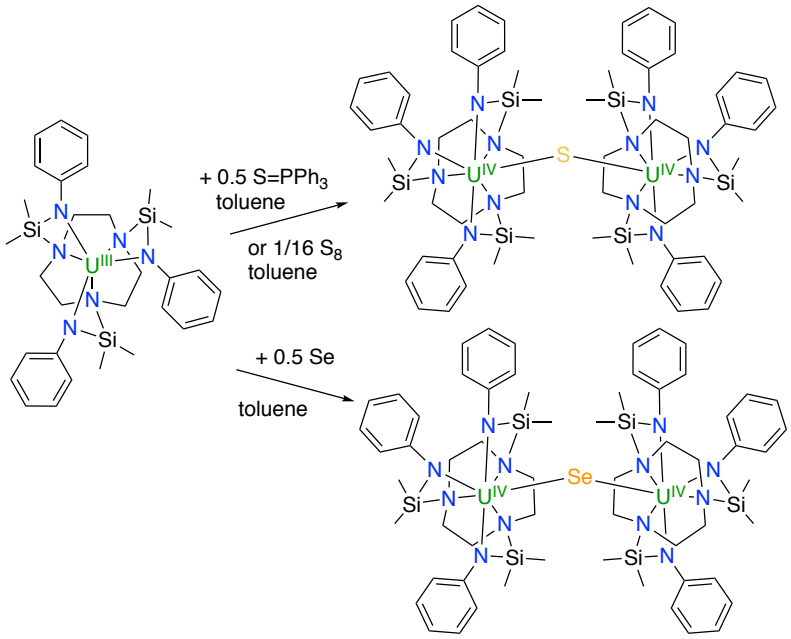

Scheme 4. Synthesis of sulfide-bridged and selenide-bridged complexes of U(IV) with the tacn-based ligand system.

The first terminal U(IV) sulfide was reported by Hayton and coworkers by using a ylide protecting group that disfavors the formation of bridging sulfide complexes during sulfur transfer from S_8 to a U(III) amido complex.[31] Single electron chalcogen reduction was also reported for dimeric bis(imido) U(V) complexes leading to the formation of E^{2-} or $[E_4]^{2-}$ (E = S, Se) bridged diuranium(VI) complexes.[32]

1.3.4. Nitrogen activation

Dinitrogen activation at any metal center is very challenging because of its strong chemical bonds and high barrier to activation. The nitrogen-nitrogen triple bond is one of the strongest found in nature (945 kJ mol^{-1}) and it is apolar with tightly bound σ and π electrons. These characteristics make N_2 a very poor ligand with respect to the isoelectronic CO, as it is both a weaker σ-donor and a poorer π-acceptor, resulting in a much less developed chemistry. Nitrogen chemistry is well

developed for d-block metals, and stoichiometric or catalytic conversion of dinitrogen into ammonia are reported [33] (Figure 8). Most catalysts involve N_2 terminally bound mononuclear complexes as intermediates but the importance of multimetallic cooperativity in dinitrogen activation is evident in the iron compounds reported by Holland and Leslie, that allow full cleavage of dinitrogen.

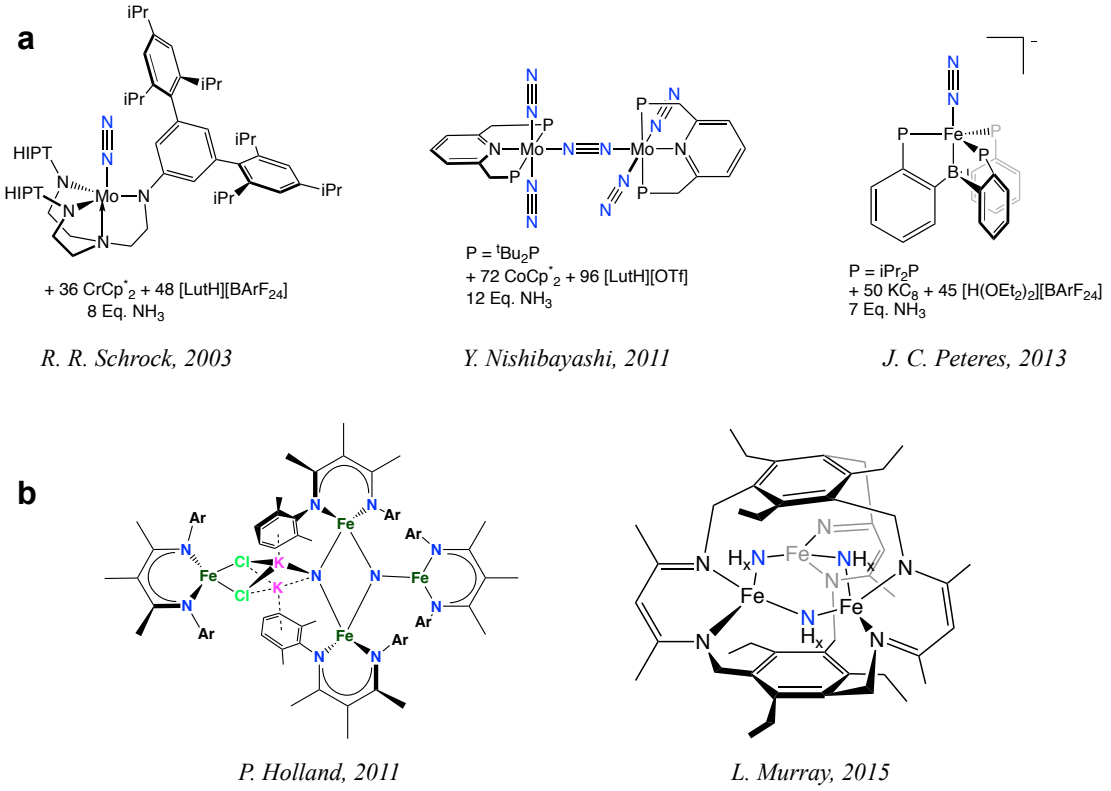

Figure 8. Activation of N_2 by d-block metals complexes leading to the catalytic formation of ammonia (**a**) or to the stoichiometric formation of ammonia (**b**).

In 1909, Haber noted and reported the high efficiency of uranium and uranium nitride materials as catalysts for ammonia production,[34] before the iron-based process was adopted. Uranium could be a valid alternative in molecular processes, as it is largely available from spent nuclear fuel, it can access several oxidation states and it might form complexes with unusual coordination numbers and geometries, possibly resulting in complementary reactivity compared to transition metals. However, only few examples have been reported in uranium chemistry. The reaction of U(III) complexes supported by various ligands leads to side-on bridged dinitrogen complexes (Scheme 5), in which the extent of dinitrogen reduction varies from 0 to –2.[16l, 35]

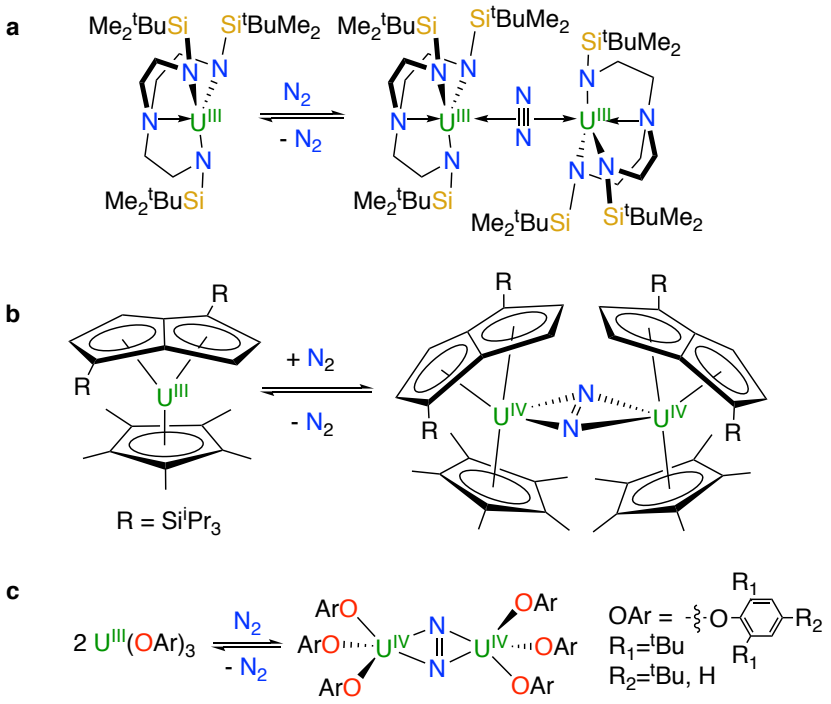

Scheme 5. Reversible coordination/reduction of dinitrogen by U(III) complexes: side-on coordination (**a**); two electron reduction to afford the side-on N_2^{2-} bridged diuranium(IV) complexes with Cp ligands (**b**) and aryloxide ligands (**c**).

Most of the products show a side-on activation mode, especially in group 4 metals as zirconium and hafnium, for which the side-on activated dinitrogen can be further functionalized with hydrogen to give ammonia.[36] For the few reported examples of uranium N_2 complexes, N_2 is reversibly bound and reduced by two electrons, in equilibrium with the U(III) monomer, it is easily lost under vacuum and any attempt to cleave or further functionalize the uranium bound dinitrogen resulted in N_2 displacement. The only stable uranium dinitrogen(2–) complex, supported by bulky trimesitylsiloxide ligands, was reported by P. Arnold (Scheme 6).[37]

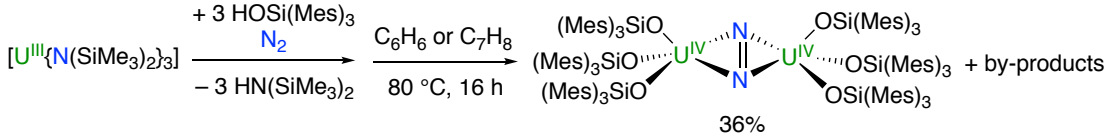

Scheme 6. Non reversible two-electron reduction of N_2 to give the robust complex $[\{U(OSi(Mes)_3)_3\}_2(\mu\text{–}\eta^2\text{:}\eta^2\text{-}N_2)]$.

These results anticipated that cooperative binding of substrates by homo- and heteromultimetallic U(III) complexes would be more effective in the reduction of small molecules but examples of such systems remain extremely rare for uranium.

Particularly relevant is the fact that the first example of two electron reduction of N_2 at a uranium center was reported for an heterodimetallic U/Mo system (Scheme 7).[14]

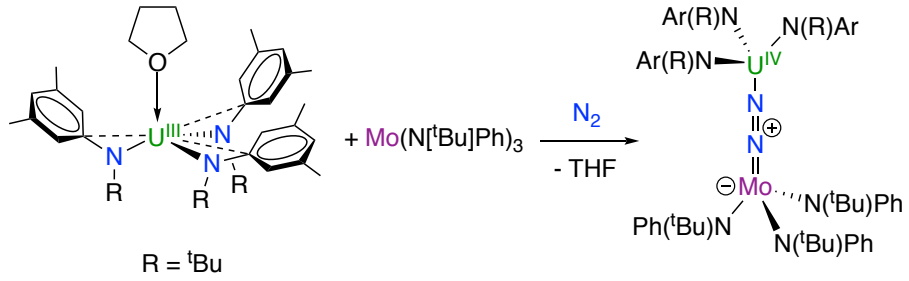

Scheme 7. Non reversible two-electron reduction of dinitrogen by an heterodimetallic U/Mo system.

The only example of dinitrogen cleavage reported for an uranium complex was isolated from the reduction of the U(III) complex [(Et_8-calix[4]tetrapyrrole)U-(dme)][K(dme)] under nitrogen (Scheme 8).[38]

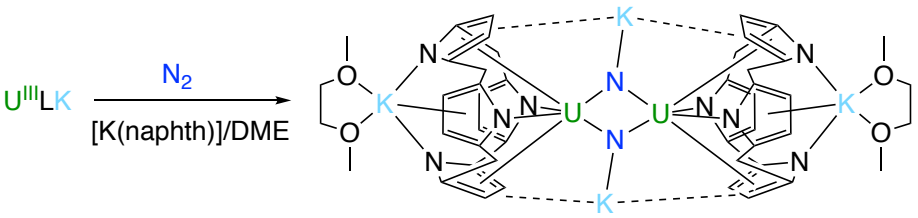

Scheme 8. Reaction of [(Et_8-calix[4]tetrapyrrole)U(dme)][K(dme)] and [K(naphthalenide)] under N_2.

So far, complete cleavage of the strong N_2 and of the isoelectronic CO triple bonds by uranium systems has not been reported, but carefully tailored multimetallic complexes should be able to effect such transformations.

1.3.5. Tris(tert)butoxysiloxide as ligand

The previously presented ligand systems are mainly based on hindered polydentate aryl oxides or classic Cp derivatives. Siloxide ligands, like tris(tert)butoxysiloxide, that possess three equivalent bulky groups, are considered to occupy a regular cone of space around the metal just as in Cp derivatives.[39] The use of a silyl rather than alkyl substituent on the oxygen renders the ligand less donating: a R_3Si group possesses empty low-lying 3d/σ* orbitals that can interact with pπ-orbitals of oxygen, attenuating the O(pπ)→M(dπ) donation and hence, supporting reduced metal centers. The tris(tert)butoxysiloxide represents a valid ancillary ligand, characterized by the ability to bind the metal center in a mono- or bidentate fashion (Figure 9), increasing the stability and the flexibility of such ligand framework.

Moreover, due to their lower basicity they are less prone to insert small molecules in the M–L bond as found for monodentate phenoxide [35b] or amides.[40]

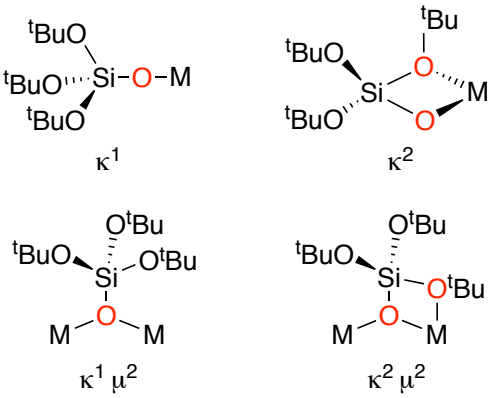

Figure 8. Different binding modes of the tris(tert)butoxysiloxide ligand.

This ligand has been used extensively in d-block chemistry [41] but only recently extended to lanthanides [42] and to uranium chemistry.[43] It was found that it could be used to build homopolymetallic and heteropolymetallic complexes of uranium in low oxidation state. The reaction of $[UI_4(OEt_2)_2]$ with the potassium salt of the tris(tert)butoxysiloxide ligand leads to the homoleptic complex $[U(OSi(O^tBu)_3)_4]$ (Scheme 9). The siloxide ligands act as polydentate supporting ligands in the absence of coordinating solvents or other substrates.

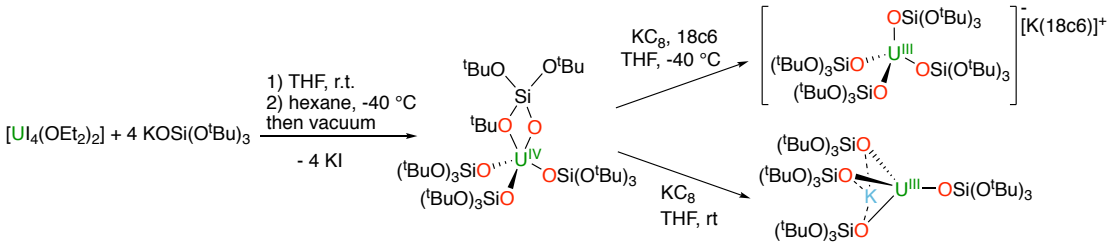

Scheme 9. Formation of $[U(OSi(O^tBu)_3)_4]$ by salt metathesis and further reduction with KC_8 with and without crown ether to obtain the *ate* and the heterodimetallic complexes.

The reduction of $[U(OSi(O^tBu)_3)_4]$ with KC_8 leads to the formation of the neutral heterodimetallic U(III) complex $[KU(OSi(O^tBu)_3)_4]$ and addition of crown ether affords the ion-pair analogue $[K(18c6)][U(OSi(O^tBu)_3)_4]$ (Scheme 9). The homoleptic dinuclear complex of U(III) $[U(OSi(O^tBu)_3)_3]_2$, can be synthesised from the metathesis reaction of the tris-silylamide complex $[U(N(SiMe_3)_2)_3]$ with the silanol ligand (Scheme 10).[44]

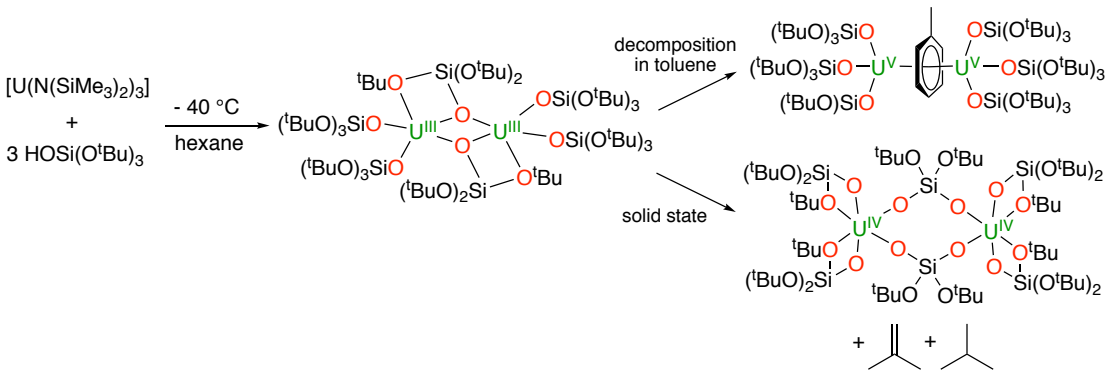

Scheme 10. Synthesis of the dinuclear U(III) complex and its decomposition products in toluene solution and in solid state.

This dinuclear complex decomposes slowly at room temperature, affording the dinuclear U(IV) complex $[U(OSi(O^tBu)_3)_2(\mu\text{-}O_2Si(O^tBu)_2)]_2$,[43b] and in toluene solution to afford the inverted arene sandwich $[K\{U(OSi(O^tBu)_3)_3\}_2(\mu\text{-}\eta^6\text{:}\eta^6\text{-}C_7H_8)]$, which was identified as the product of four-electron reduction of toluene (U(V)–(arene)$^{4-}$–U(V)).

The uranium(III) siloxide complexes provide a versatile platform to investigate cooperative effects in small molecule activation by U(III) complexes.

1.3.6. Activation of heteroallenes by U(III) siloxide complexes

The U(III) siloxide complexes previously described can react with CS_2 to give different products (Scheme 11). The dinuclear complex $[U(OSi(O^tBu)_3)_3]_2$, effects the two-electron reduction of CS_2 in ambient conditions to afford $[\{U(OSi(OtBu)_3)_3\}_2(\mu\text{-}CS_2)]$ [43a] where the CS_2^{2-} ligand bridges two U(IV) centers in a rare $\mu\text{-}\kappa^2(C,S1)\text{:}\kappa^2(S1,S2)$ fashion (Scheme 11a).[45] This is one of the rare examples of diuranium(IV) complexes bridged by a CS_2^{2-} ligand, together with the complex $[(RC_5H_4)_3U]_2[\mu\text{-}\eta^1\text{:}\eta^2\text{-}CS_2]$, reported by Andersen and coworkers,[23] resulting from CS_2 reduction by the U(III) complex $[(RC_5H_4)_3U]$. In contrast, Meyer *et al*. reported the formation of a mixture of trithiocarbonate and tetrathiooxalate complexes when the uranium(III) complex of a multidentate phenolate ligand, $[(^{Ad}ArO)_3N)U(DME)]$ was reacted with CS_2.[46] DFT studies on these systems identified a CS_2^{2-} bridged U(IV)/U(IV) dimer as the most probable intermediate in the formation of the trithiocarbonate and tetrathiooxalate complexes, but this intermediate was not experimentally characterized.[43a]

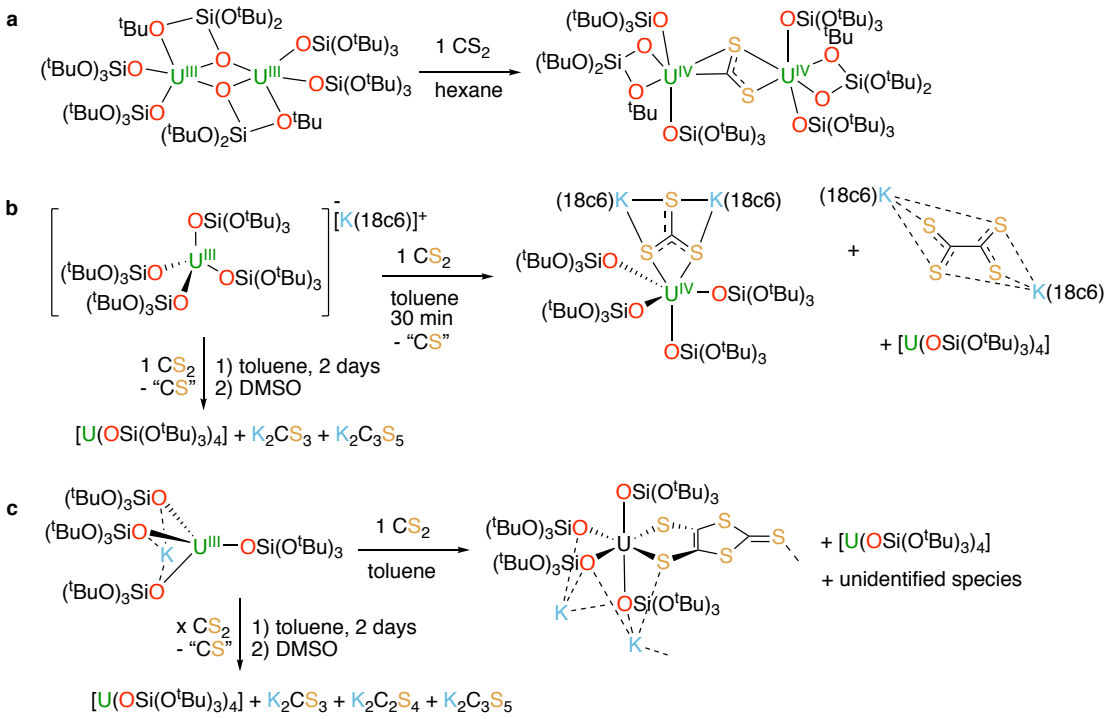

Scheme 11. Reduction of CS_2 by the dinuclear U(III) complex to give the bridging CS_2^{2-} diuranium(IV) complex (**a**); reduction of CS_2 by the *ate* complex (**b**) and by the heterodimetallic complex (**c**).

However, when the number of siloxide ligands bound to the uranium(III) centers is increased from three to four, the reaction with CS_2 proceeds differently leading to the formation of the reductive coupling and disproportionation products that are rapidly released from the coordination sphere of the metal center due to the bulkiness. The *ate* complex $[K(18c6)][U(OSi(O^tBu)_3)_4]$, and the heterobimetallic U/K complex $[KU(OSi(O^tBu)_3)_4]$, both effect the parallel reductive dimerization and reductive disproportionation of CS_2 (Scheme 11b and c). However, the bound potassium cation in the heterobimetallic U/K complex, with its Lewis acidic character, favors the reductive dimerization of CS_2 while, the *ate* complex $[K(18c6)][U(OSi(O^tBu)_3)_4]$ leads to reductive disproportionation. The unstable intermediates $[U(OSi(O^tBu)_3)_4(\mu\text{-}CS_3)K_2(18c6)_2]$ and $[U(OSi(O^tBu)_3)_4K_2(C_3S_5)]_n$ contain bound trithiocarbonate and bound dmit dianion ($dmit^{2-}$ = $C_3S_5^{2-}$ = 1,3-dithiole-2-thione-4,5-dithiolate, formed from the reaction of $C_2S_4^{2-}$ with CS). The terminal thiocarbonate was found to rapidly release the K_2CS_3 substrate rendering the system attractive for the development of catalytic cycles.[47] The differences in reactivity were interpreted in terms of different multimetallic U/K cooperativity. In contrast, the lower stability of the putative CS_2^{2-} intermediates is probably the result of combined factors, electronic and steric, introduced by the additional electron-rich, bulky siloxide present in the

[K(18c6)][U(OSi(O^{t}Bu)$_3$)$_4$] and [KU(OSi(O^{t}Bu)$_3$)$_4$] complexes compared to the dinuclear one.

In ambient conditions, the U(III) siloxide complexes react with CO_2 as well and the reactions are summarized in Scheme 12. The dinuclear complex effects the reductive disproportionation of CO_2 to afford the carbonate-bridged diuranium(IV) complex [{U(OSi(O^{t}Bu)$_3$)$_3$}$_2$(μ-η^1:η^2-CO$_3$)], and CO (Scheme 12a). The disproportionation of CO_2 to CO and uranium carbonate derivatives had been previously reported for mixed sandwich U(III),[24] and tris(aryloxide) systems.[48]

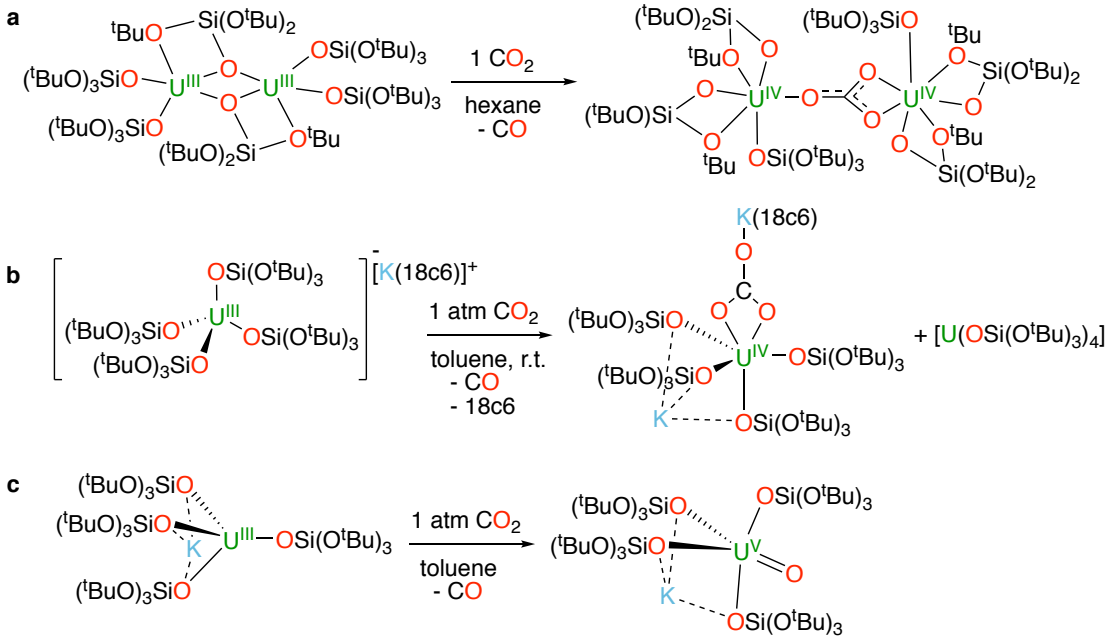

Scheme 12. Carbon dioxide reduction reactions by the dinuclear U(III) complex to give the bridging carbonate dinuclear U(IV) complex (**a**); carbon dioxide reduction by the *ate* and the heterobimetallic complexes to give the U(IV) carbonate complex (**b**), and the U(V) terminal oxo complex (**c**).

However, the disproportionation mechanism proposed on the basis of DFT computational studies, differs significantly for the previously reported systems. In the case of mononuclear tris(aryloxide) U(III) and mixed sandwich systems, a diuranium(IV) oxo bridged intermediate was postulated to form upon extrusion of CO from a the bimetallic species [U^{IV}]–(CO$_2^{2-}$)–[U^{IV}]. The oxo dimer further inserts a second CO_2 molecule to afford the final carbonate.[49] In contrast, for the dinuclear siloxide complex, the [U^{IV}]–(CO$_2^{2-}$)–[U^{IV}] intermediate brings to the carbonate product through a different mechanism, which shows a concerted attack of CO_2 and release of CO.[43a] This alternative concerted mechanism of CO_2 reduction is probably

favored by the dinuclear nature of the complex. This reactivity is in contrast with the one reported for mononuclear uranium(III) complexes supported by aryloxide or amide ligands with carbon dioxide, for which carbonate products were not isolated and multiple products of reduction and insertion were found.[35b, 40] This could be attributed to the different ligand properties, both electronic and steric, confirming the interest of siloxide as an alternative ancillary ligand in U(III) chemistry. The ion-pair complex readily reacts in ambient condition with CO_2 to afford CO, the terminal U(IV) carbonate complex $[K(18c6)][KU(\mu\text{-}\eta^1\text{:}\eta^2CO_3)(OSi(O^tBu)_3)_4]$, and the U(IV) tetrasiloxide complex (Scheme 12b).[50] Thus, both the dinuclear tris(siloxide) complex and the mononuclear tetrasiloxide complex promote selectively the reductive disproportionation of CO_2. The pathway leading to reductive dimerization of CO_2 to oxalate was not observed. Oxalate formation from CO_2 is rare and only three examples have been reported for uranium(III) that were obtained as the kinetic products of the reaction controlled by steric effects.[49b, 51] In contrast, the heterobimetallic complex shows a dramatically different and unprecedented reactivity with CO_2 (Scheme 12c). This complex effects the two electron reduction of CO_2 under ambient conditions leading to the terminal U(V) oxo complex $[UO(OSi(O^tBu)_3)_4K]$ and CO.[50] This reaction is the first example of the two-electron reductive cleavage of CO_2 mediated by a single U(III) complex. One example of two-electron reduction of CO_2 had been previously reported but involved the concerted oxidation of two U(III) complexes.[22] Notably, addition of carbon dioxide to the U(III) complex $[((^{tBu}ArO)_3tacn)U]$ resulted in the formation of a oxo-bridged diuranium(IV) species with extrusion of carbon monoxide. The one electron reduction of CO_2 by a very bulky aminophenolate U(III) complex afforded the $[((^{Ad}ArO)_3tacn)U^{IV}(CO_2)]$ complex presenting a unique linear coordinated CO_2 radical anion.[21] All the other reported examples of CO_2 reduction by U(III) complexes involve one-electron transfer by two metal complexes and resulted either in the reductive disproportionation to yield CO and uranium carbonate or reductive dimerization to afford uranium oxalate.[49b, 51-52] The reactivity of the heterobimetallic complex is remarkable both because two-electron transfer is an unusual redox event in uranium chemistry [8a, 29b, 53] and terminal U(V) oxo complexes are not common. Notably, the use of bulky ligands and the careful choice of the oxo-transfer agent, can prevent the formation of more stable dinuclear oxo-bridged compounds that are usually formed in such reactivity, and yield the formation of a terminal uranium(V)

oxo.[54] U(V) mono-oxo complexes have also been obtained from the reductive cleavage of nitrite by a U(IV) complex,[55] and from the metathesis of a U(V)-imido complex with CO_2.[56] The dramatic difference in the reactivity of the *ate* and the heterobimetallic complexes with carbon dioxide was explained in terms of the presence of a bound potassium cation close to the uranium center in the first. The combination of the reducing power of a U(III) ion and of the electropositivity of the potassium cation is likely to result in a coordination mode of carbon dioxide similar to the one obtained at a Co^{I}–M (M= Li, Na) site.[57] The influence of the potassium cation and the cooperative effect between the metals were supported by DFT studies.[50]

1.3.7. Activation of chalcogenides by U(III) siloxide complexes

The use of bulky ligands has been often employed to favor the formation of bridging sulfide complexes. However, the reaction of $[KU(OSi(O^tBu)_3)_4]$, with 0.125 equiv S_8 leads to a complex mixture of compounds from which the disulfide and the trisulfide diuranium(IV) dimers were isolated.

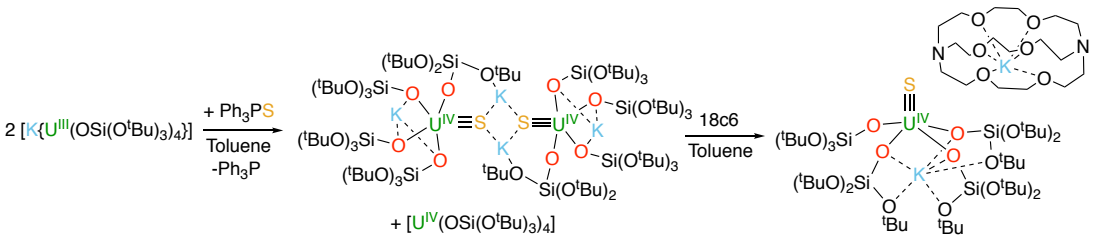

Scheme 13. Syntheses of the U(IV) potassium-capped sulfide complex and of the U(IV) non-capped sulfide complex.

In contrast, the rare potassium-capped $[\{SU(OSi(OtBu)_3)_4K_2\}_2]$, or non-capped $[SU(OSi(OtBu)_3)_4K][Kcryptand]$, U(IV) sulfide complexes, could be selectively formed by reaction with Ph_3PS (Scheme 13) [58] and the bound potassium was shown to be crucial in the S-transfer reaction.

A few studies of the reactivity of bridging and terminal chalcogenides have been reported with different ancillary ligands. Terminal [59] and bridging [60] chalcogenides were reported to further activate elemental chalcogens to afford terminal and polychalcogenido-bridged uranium complexes respectively.

The activation of CS_2, CO_2, and COS by chalcogenide-bridged complexes has also been reported for the $[\{((^{Ad}ArO)_3N)U\}_2(\mu\text{-}E)]$ (E = S, Se) and leads to

trithiocarbonate bridged [{((^{Ad}ArO)$_3$N)U}$_2$(μ−κ^2:κ^2-CS$_3$)] [46a] and mixed-chalcogeno carbonate bridged complexes U−CO$_2$E−U (E = S, Se), U−CS$_2$E−U (E = O, Se), and U−COSSe−U.[61]

The capped and terminal sulfides [{SU(OSi(OtBu)$_3$)$_4$K$_2$}$_2$] and [SU(OSi(OtBu)$_3$)$_4$K][Kcryptand] could react with S$_8$, CS$_2$ and CO$_2$ (Scheme 14). Excess sulfur leads to polychalcogenide-bridged complexes as a result of loss of one siloxide ligand formation, but the reaction with CS$_2$ leads to the formation of terminal thiocarbonate complexes that release the bound K$_2$CS$_3$ over time. The intermediate thiocarbonate complex [U(OSi(O^{t}Bu)$_3$)$_4$(μ^3-k^2:k^2: k^2-CS$_3$)K$_2$(18c6)$_2$], was isolated and crystallographically characterized from the direct reaction of the ion-pair complex [K(18c6)][U(OSi(O^{t}Bu)$_3$)$_4$], with CS$_2$. [47] The reaction of the terminal sulfide with CO$_2$ leads to free COS probably from the decomposition of a U(IV)–CO$_2$S intermediate.[58] Surprisingly, U(V) terminal sulfides could not be obtained from the activation of S$_8$ by U(III) complexes probably due to the high nucleophilic nature of such compounds that results in fast reaction with unreacted U(III).

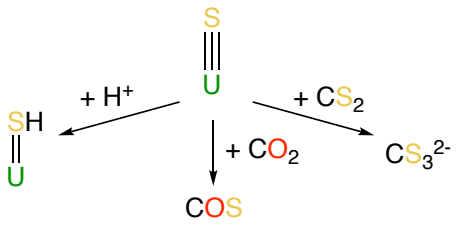

Scheme 14. Reactivity of the U(IV) sulfide complex.

1.3.8. U(III) siloxide complexes reactivity with azides

In view of the high reactivity of the U(III) siloxide complexes with heteroallenes the reactivity with the isoelectronic azide (N_3^-) ligands was investigated, as a possible route to uranium nitride complexes. Metal azides are indeed known as versatile precursors for the synthesis of nitride complexes.

Uranium nitrides are of great fundamental interest for investigating multiple M–Ligand bonding [53a, 62] and nitride transfer reactivity. The synthesis and study of molecular nitride complexes has also attracted attention because of the importance of UN materials as potential alternative nuclear fuel.[63] Moreover, the interest in the high activity of UN materials reported by Haber in the catalytic conversion of N$_2$ and H$_2$ to NH$_3$ drives the attention to the synthesis of molecular uranium nitride as possible materials for nitrogen activation.

The earliest examples of uranium nitrides were obtained by the laboratories of Evans and Mazzanti from reactions of U(III) complexes with alkali-metal azide salts and multimetallic (3-8 uranium atoms) clusters containing both bridging nitrides and bridging azide ligands were obtained.[64] A series of stable nitride bridged diuranium complexes, (U(IV)/U(IV), U(V)/U(IV), U(V)/U(V)) containing a linear U=N=U motif were subsequently reported by Cummins and coworkers. The parent diuranium(IV) complex was prepared from the reaction of a U(III) tris-amide species with unprotected azide and then stepwise oxidized.[65] Only a handful of additional examples of dinuclear and terminal nitrides have been reported to this date from the reaction of U(III) with azides suggesting that the choice of reaction conditions and supporting ligands is critical in the isolation of stable uranium nitrides.[43b, 53a, 62b, 66] The nature of the supporting ligand was also proven very important to attain nitride-containing uranium complexes in low oxidation state and to promote reactivity. The reaction of the dinuclear U(III) tris-siloxide complex with the organic azide AdN_3 yield to a mixture of products, $[U(OSi(O^tBu)_3)_4]$ and a dinuclear bis-imido complex of uranium(VI) $[U_2(NAd)_4(OSi(O^tBu)_3)_4]$ in a ratio 2:1, as a result of U(V) disproportionation. Instead, the increased steric bulk and the difference in charge of the *ate* complex influence the reactivity, resulting in a U(V) imido complex, $[K(18c6)][U(NAd)(OSi(O^tBu)_3)_4]$, (Scheme 15) that does not undergo disproportionation.

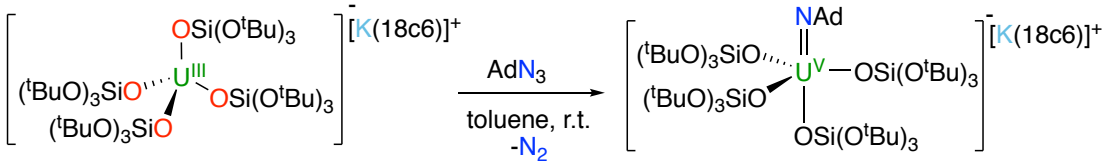

Scheme 15. Reaction of the *ate* complex with the organic azide AdN_3.

1.3.8.1. Synthesis of nitrides

The reaction of the bulky tetra-siloxide *ate* complex with cesium azide (Scheme 16) lead to the formation of multiple products from which the U(IV) azido complex $[K(18c6)U(N_3)(OSi(O^tBu)_3)_4]$ and the bis-nitrido diuranium(V) complex $[KU(\mu\text{-}N)_2(OSi(O^tBu)_3)]_2$ could be isolated and crystallographically characterized.[43b] If a synthetic route to the terminal azide complex could be identified, then it could provide access to a terminal nitride complex.

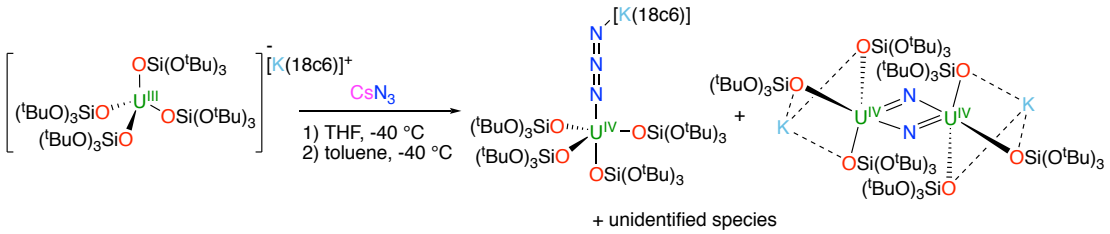

Scheme 16. Reaction of the *ate* complex with cesium azide to give the azido U(IV) complex and the bridging bis-nitrido diuranium(IV) complex.

The bis-nitride is the first isolated U_2N_2 complex, obtained from the reaction of U(III) with azides. The formation of this unprecedented U(V)/U(V) complex may involve a highly reactive intermediate (U(V) terminal nitrido) that affords the bis-nitrido complex via loss of one siloxide ligand. The crowded environment and the high complex charge result in a low stability intermediate that is difficult to trap. This is consistent with what reported for the highly reactive nitride intermediate $[UN\{N(SiMe_3)_2\}(C_5Me_5)_2]$, which is involved in intramolecular C–H bond activation. [67]

The reaction of the dinuclear tris-siloxide complex with CsN_3 (Scheme 17) proceeds in contrast in a more controlled manner and affords the nitride bridged diuranium(IV) complex $[Cs(\mu\text{-}N)\{U(OSi(O^tBu)_3)_3\}_2]$.[43b]

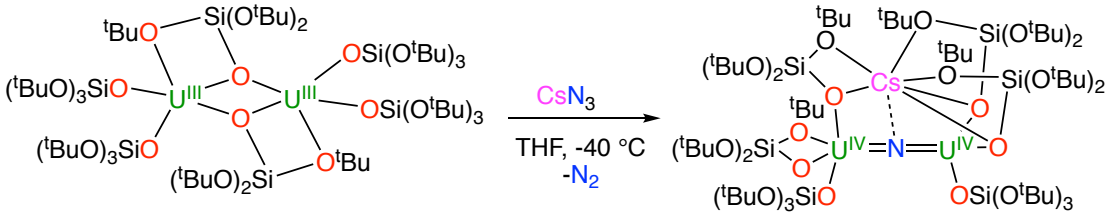

Scheme 17. Synthesis of the bridging nitride diuranium(IV) complex.

The reaction is likely to proceed via the formation of an azide-bridged complex that eliminates dinitrogen to afford the final nitride. The solid-state structure of the product consists of a heterotrinuclear (U, U, Cs) complex. The two U(IV) cations are linked through a bridging nitrido ligand (N^{3-}) in a nearly linear fashion (U–N–U angle : 170.2(3)°). The short U–$N_{nitride}$ bond distances (U1–N1 2.058(5) Å, U2–N1 2.079(5) Å) are in agreement with a multiple bond nature. These values are similar to those found in other nitride-bridged diuranium(IV) complexes presenting a linear U=N=U fragment.[65, 66g] An important structural feature of this complex compared to the other linear nitride-bridged U(IV)/U(IV) complexes is that its cation binds inner-sphere to

the nitride ligand of the U=N=U core. Notably, the six siloxide ligands are multidentate and bridge uranium with the Cs cation through six tert-butoxy oxygen atoms. This cesium cation lies at the apical position of the nitride ligand with a Cs–N distance of 3.393(4) Å.

The reaction of the dinuclear uranium(III) complex with 2 equivalents of KN_3 leads to the formation of the bridged nitride, bridged azide diuranium(IV) complex $[K_2\{[U(OSi(O^tBu)_3)_3]_2\}(\mu\text{-}N)(\mu\text{-}N_3)]$ (Scheme 18a) as the only product is observed. Its decomposition leads to the bis-nitride diuranium(V) complex $[K_2\{[U(OSi(O^tBu)_3)_3]_2(\mu\text{-}N)_2\}]$, (Scheme 18b), which is the second example of a uranium bis-nitride complex, an attractive system for the study of its ability in N–C bond formation reactivity.

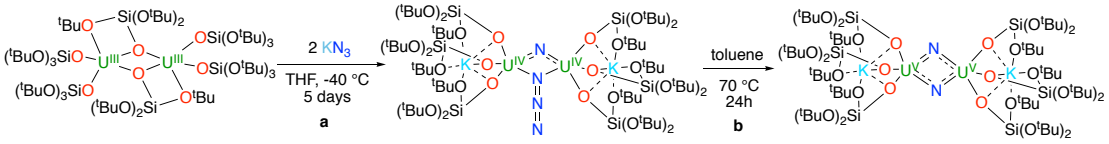

Scheme 18. Reactivity of complex $[U(OSi(O^tBu)_3)_3]_2$, with 2 equivalents of KN_3 (**a**) and formation of the bis-nitride complex $[K_2\{[U(OSi(O^tBu)_3)_3]_2(\mu\text{-}N)_2\}]$ (**b**).

Surprisingly, until 2016, all the nitride complexes contained uranium in high oxidation state (U(IV), U(V), U(VI)) in spite of the fact that one global objective behind the synthesis of these species was to model the properties of uranium mononitride, UN. In our group, we investigated the reduction of diuranium(IV) bridging nitride complex with Cs^0. Stepwise reduction with 1 equivalent or a large excess of Cs^0 in THF at low temperature afforded the U(III)/U(IV) complex $[Cs_2\{[U(OSi(O^tBu)_3)_3]_2(\mu\text{-}N)\}]$, and the U(III)/U(III) complex $[Cs_3\{[U(OSi(O^tBu)_3)_3]_2(\mu\text{-}N)\}]$, respectively (Scheme 19).[66f]

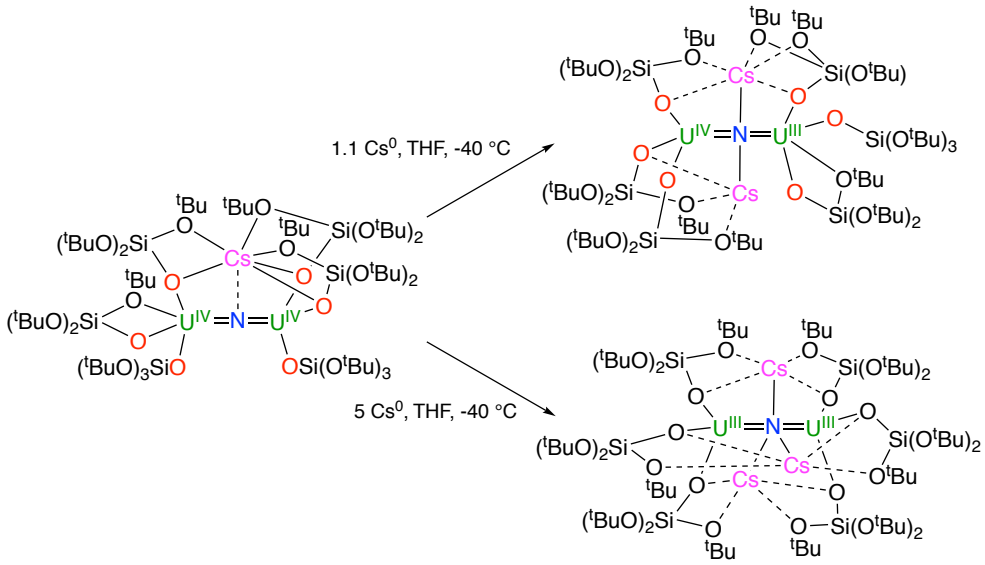

Scheme 19. Syntheses of the U(III)U(IV) bridging nitride, and of the U(III)U(III) bridging nitride.

1.3.9. Ligand based reactivity: N-C bond formation

Beyond as nuclear fuels, uranium nitrides have been recognized as suitable candidates for stoichiometric and catalytic N-atom transfer reactions and small molecules transformations.[68] In recent years, more and more molecular nitride complexes of uranium have been synthetized. [66a] Few terminal uranium nitrides were synthetized using highly sterically encumbered ligands such as $Tren^{TIPS}$ ($Tren^{TIPS}$ = $N(CH_2CH_2NSi^iPr_3)_3$).[53a] In particular, U(V) and U(VI) terminal nitride synthesis and reactivity towards reduction and reductive carbonylation or C–H activation have been reported (Scheme 20). [66e, 67]

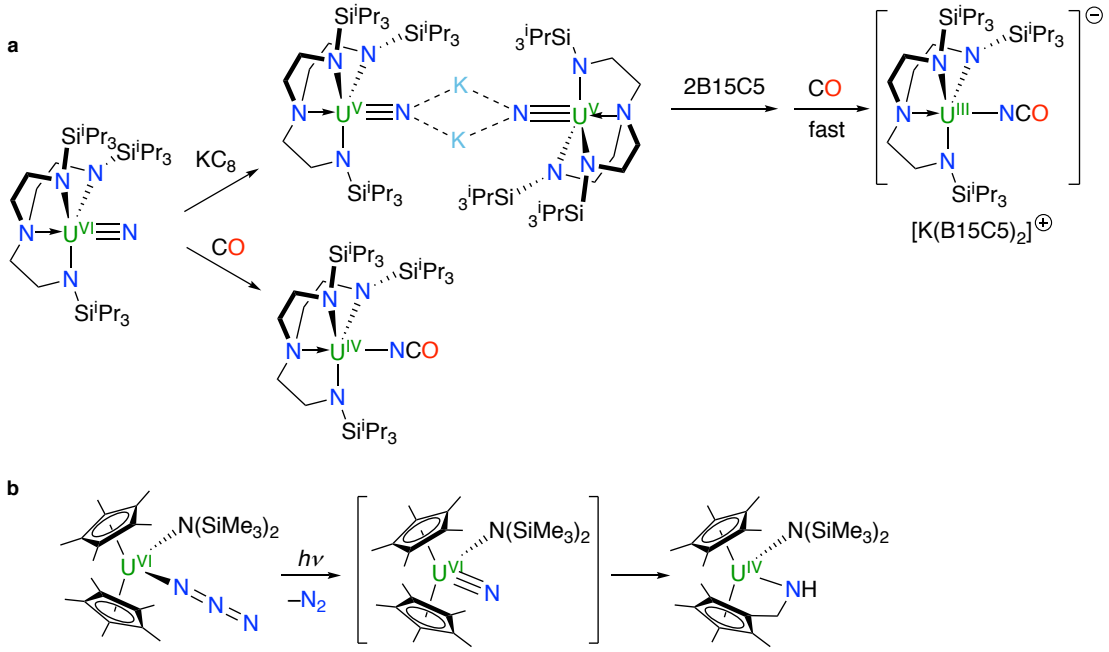

Scheme 20. Reduction of the U(VI) terminal nitride to U(V) terminal nitride and reactivity with carbon monoxide (**a**); insertion of the terminal nitride into the C–H bond of the ligand (**b**).

However, most of nitride complexes contain a bridging nitride but the reactivity of such compounds has only been reported once for a nitride-bridged diuranium(V) complex (Scheme 21). [65]

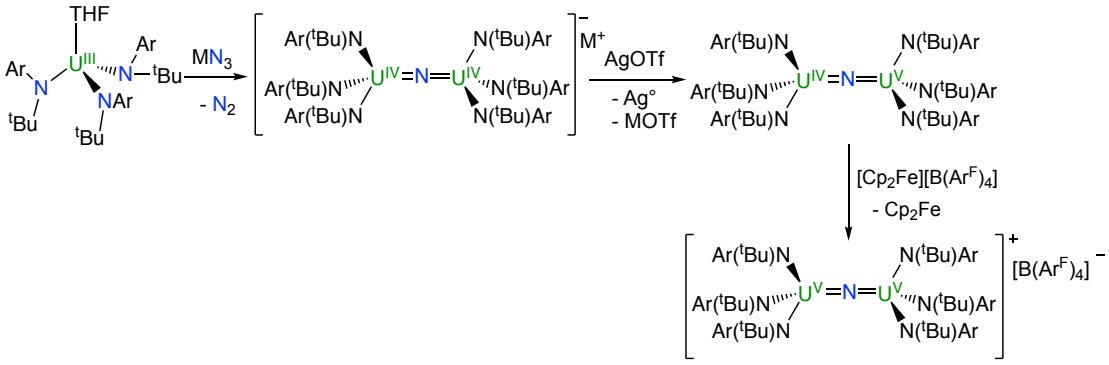

Scheme 21. Oxidation of diuranium nitride complexes from U(IV/IV) to U(V/IV) and U(V/V) (M = Na, N(n-Bu)$_4$).

Very recently, syntheses of a bridging diuranium(IV) nitride and a bridging diuranium(IV/V) nitride with Tren type ligand were reported;[69] they were obtained by reduction of a tetranuclear azide complex, [{U(Tren^{DMBS})(μ-N$_3$)}$_4$], (Scheme 22), but C–H bond activation reactivity was not reported unlike the terminal uranium(IV/VI)-nitrides supported by the same ligand.

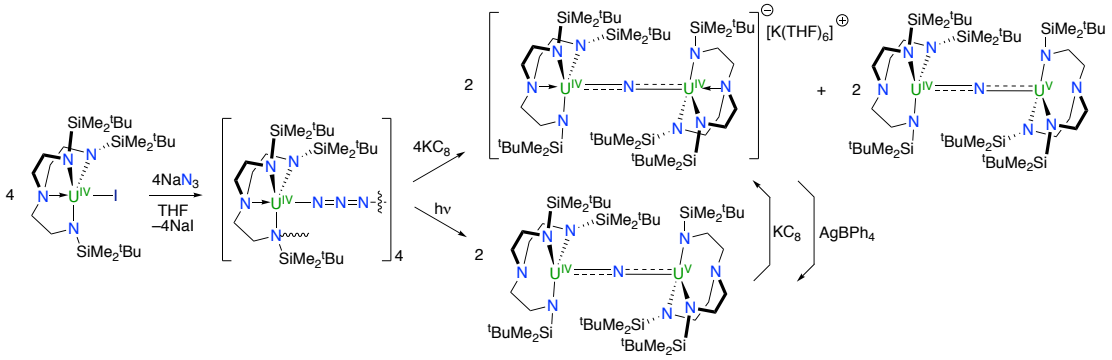

Scheme 22. Syntheses of the tetramer azido complex and its reaction with KC_8 and with hν to give the diuranium(IV/IV) and the diuranium(IV/V) bridging nitride complexes, respectively.

1.3.9.1. Group 4 nitride reactivity

Nitrogen-carbon bond formation reactions are particularly attractive for the production of value-added chemicals such as amino acids, pharmaceuticals or agrochemicals.[70] Synthetic methods using cheap and largely available feedstock such as carbon dioxide are particularly desirable.[17] However, N–C bonds formation reactions from a nitride as nitrogen source and CO_2 as carbon source are rare and so far, described only for transition metals.[71] Chirik et al. were able to activate nitrogen to synthetize a hafnium-N_2 complex, that in presence of DMAP was activated towards reaction with CO to give the corresponding base stabilized nitride complex (Scheme 23).

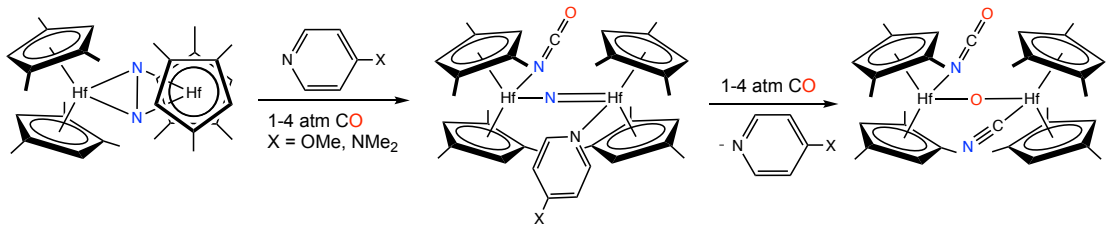

Scheme 23. Synthesis and reactivity with CO of a pyridine-stabilized dihafnocene complex prepared from N_2 cleavage.

This compound can undergo a second carbonylation. The reaction leads to the transfer of the nitrogen atom to form a cyanide ligand after deoxygenation promoted by the hafnium centers. Both the hydrazide and the bridged-nitride complexes were reacted with CO_2. The dihafnium-N_2 complex leaded to the formation of two new C–N bonds, from nitrogen and carbon dioxide (Scheme 24); the subsequent removal of the functionalized nitrogen core gave the dicarboxylated silyl-substituted hydrazine.

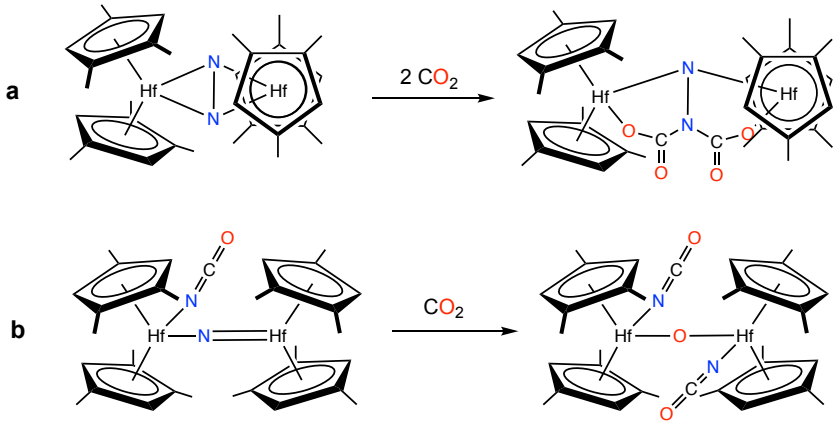

Scheme 24. Reaction of the dihafnium-N_2 complex with CO_2 (**a**); reaction of the dihafnium-nitride complex with CO_2 (**b**).

Nitride-bridged metal complexes of transition metal are usually unreactive to N transfer reactions. Chirik showed that the nitride transfer could be activated by the presence of a cyanate ligand affording, in the reaction with CO_2, oxygen abstraction and isocyanate.

1.4. Purpose and objectives of the project

The PhD work presented in this thesis is in the research area of fundamental molecular uranium chemistry. The redox chemistry of this *f*-element is important in nuclear technology, especially in the nuclear fuel reprocessing and disposal, and also in controlling the mobility of actinides in the environment. Beyond its relevance in the nuclear industry, the chemistry of *f*-elements could provide alternatives for novel supplies of energy. In particular, the great interest in low-valent *f*-elements chemistry arises from their capability in promoting small molecule (CO_2, CO, N_2) activation and atom/group transfer.

Small molecule activation is an attractive field in contemporary catalysis as these molecules could provide renewable chemical feedstock for the production of fertilizers, fuels or fine chemicals.[72] These molecules are generally kinetically inert and thermodynamically stable preventing their facile utilization. One of the best ways to overcome their large activation barriers involves the use of metal ions with a highly negative reduction potential.[72b, 73] To overcome the intrinsic low reactivity of small molecules such as CO_2, CO or N_2, fundamental research focuses on developing bi-functional electron-rich catalysts that can easily bind the small molecule and provide electrons. This implies the use of low valent metallic elements [33b, 74] or the use of bi- or multi-metallic systems [75] for multi-electron transfer.[76]

Hence, the main objective of this work was to design and investigate the reactivity of uranium multimetallic complexes towards small molecules. More specifically, it can be divided into two main targets: the study of the ligand based reactivity of complexes bearing linker atoms such as a bridging nitride or a bridging oxide, between the two uranium metal centers, and the study of the metal based reactivity of low valent diuranium(III) complexes towards dinitrogen.

The reactivity of a bridging nitride diuranium(IV) [43b] complex, $[Cs\{[U(OSi(O^tBu)_3)_3]_2(\mu\text{-}N)\}]$, was studied at the outset of this PhD work, showing unprecedented nitride ligand based reactivity with small molecules. This complex bears a nitride as a linker atom between the metal centers and it is supported by siloxide ligands. The study of its reactivity and the possibility to reduce the metal centers to access the diuranium(III) bridging nitride complex showed that siloxide

ligands constitute a valid alternative [43b] to the ubiquitous Cp ligands, in particular for their different binding modes and flexibility.

Accordingly, the first part of the work will show the reactivity of the bridging nitride diuranium(IV) complex with small molecules, such as CO_2, CS_2, CO and H_2, as a first step towards uranium catalysis for N–C, N–H bond forming reactions. The reactivity of uranium bridging nitrides had essentially been unexplored and the work we presented allowed us to understand the nature of the ligand bonding to uranium and to explore the possibility of both activating the molecule and releasing the product. Attention was focused on the formation of diuranium hydride complexes upon addition of H_2, both with nitride and oxide linker atoms. The importance of such study follows the implication of metal hydrides in both the catalytic hydrogenation of CO_2 and in the ammonia formation from N_2 and H_2. The main goal related to this subject was to isolate uranium hydride complexes, as very few examples are reported in literature and study the reactivity in particular with CO_2, with the purpose of reducing it beyond the formate level, possibly to methanol.

Secondly, knowing the reducing ability of low-valent uranium complexes, the second part of the work consists in the study of the reactivity with dinitrogen of multi-metallic systems of low-valent diuranium(III) with nitride and oxide atoms as linker between the metal centers. The main goal related to this research was to find a system capable of completely cleaving the dinitrogen molecule through redox processes at the metal centers and further addition of H_2 or CO, possibly leading to ammonia formation and to new N–C bonds formation. The flexibility given by the ligand framework in the bridging nitride diuranium(III) complex and its high reducing ability, allowed us to report unprecedented results in dinitrogen reduction and functionalization in uranium chemistry. Moreover, an important target consisted in comparing two multimetallic uranium(III) complexs bearing different bridging ligands, nitride and oxide, in the reactivity with dinitrogen. The goal is to find a spectator ligand, capable of assisting the complex upon N_2 binding and reduction, and not react with reagents used for further functionalization and/or cleavage of dinitrogen. This study let us comprehend the nature of the uranium-ligand bond and how it is possible to tune reactivity by changing the bridging ligand between the uranium atoms in such systems.

Bibliography

[1] S. Cotton, *Lanthanides and Actinides*, MacMillan Education, London, **1991**.

[2] A. F. Cotton, G. Wilkinson, *Advanced inorganic chemistry*, fifth edition ed., Wiley-Interscience, **1988**.

[3] D. L. Clark, S. S. Hecker, G. D. Jarvinen, M. P. Neu, *the Chemistry of the Actinides and Transactinide Elements, Vol. 2*, 3rd ed., Dordrecht, **2006**.

[4] a) M. Ephritikhine, *Dalton T* **2006**, 2501-2516; b) T. E. Albrecht-Schmitt, *Angew Chem Int Edit* **2005**, *44*, 4836-4838; c) M. B. Jones, A. J. Gaunt, J. C. Gordon, N. Kaltsoyannis, M. P. Neu, B. L. Scott, *Chem Sci* **2013**, *4*, 1189-1203; d) J. L. Sessler, P. J. Melfi, G. D. Pantos, *Coordin Chem Rev* **2006**, *250*, 816-843; e) S. Fortier, T. W. Hayton, *Coordin Chem Rev* **2010**, *254*, 197-214; f) M. Nyman, P. C. Burns, *Chem Soc Rev* **2012**, *41*, 7354-7367.

[5] a) P. L. Arnold, J. B. Love, D. Patel, *Coordin Chem Rev* **2009**, *253*, 1973-1978; b) P. L. Arnold, G. M. Jones, S. O. Odoh, G. Schreckenbach, N. Magnani, J. B. Love, *Nat Chem* **2012**, *4*, 221-227; c) G. Nocton, P. Horeglad, V. Vetere, J. Pecaut, L. Dubois, P. Maldivi, N. M. Edelstein, M. Mazzanti, *J Am Chem Soc* **2010**, *132*, 495-508; d) V. Mougel, P. Horeglad, G. Nocton, J. Pecaut, M. Mazzanti, *Chem-Eur J* **2010**, *16*, 14365-14377; e) V. Mougel, L. Chatelain, J. Pecaut, R. Caciuffo, E. Colineau, J. C. Griveau, M. Mazzanti, *Nat Chem* **2012**, *4*, 1011-1017.

[6] R. Faizova, R. Scopelliti, A. S. Chauvin, M. Mazzanti, *J Am Chem Soc* **2018**, *140*, 13554-13557.

[7] a) D. N. Huh, J. W. Ziller, W. J. Evans, *Inorg Chem* **2018**, *57*, 11809-11814; b) H. S. La Pierre, A. Scheurer, F. W. Heinemann, W. Hieringer, K. Meyer, *Angew Chem Int Edit* **2014**, *53*, 7158-7162; c) M. R. MacDonald, M. E. Fieser, J. E. Bates, J. W. Ziller, F. Furche, W. J. Evans, *J Am Chem Soc* **2013**, *135*, 13310-13313; d) B. S. Billow, B. N. Livesay, C. C. Mokhtarzadeh, J. McCracken, M. P. Shores, J. M. Boncella, A. L. Odom, *J Am Chem Soc* **2018**, *140*, 17369-17373; e) A. J. Ryan, M. A. Angadol, J. W. Ziller, W. J. Evans, *Chem Commun* **2019**, *55*, 2325-2327.

[8] a) W. J. Evans, S. A. Kozimor, *Coordin Chem Rev* **2006**, *250*, 911-935; b) D. C. Sonnenberger, J. G. Gaudiello, *Inorg Chem* **1988**, *27*, 2747-2748; c) D. E. Morris, R. E. Da Re, K. C. Jantunen, I. Castro-Rodriguez, J. L. Kiplinger, *Organometallics* **2004**, *23*, 5142-5153; d) E. J. Schelter, P. Yang, B. L. Scott, J. D. Thompson, R. L. Martin, P. J. Hay, D. E. Morris, J. L. Kiplinger, *Inorg Chem* **2007**, *46*, 7477-7488; e) L. R. Avens, D. M. Barnhart, C. J. Burns, S. D. Mckee, W. H. Smith, *Inorg Chem* **1994**, *33*, 4245-4254.

[9] I. Korobkov, S. Gambarotta, in *Progress in Inorganic Chemistry, Vol 54, Vol. 54* (Ed.: K. D. Karlin), **2005**, pp. 321-348.

[10] J. L. Stewart, R. A. Andersen, *Polyhedron* **1998**, *17*, 953-958.

[11] a) P. L. Diaconescu, P. L. Arnold, T. A. Baker, D. J. Mindiola, C. C. Cummins, *J. Am. Chem. Soc.* **2000**, *122*, 6108-6109; b) I. Korobkov, S. Gorelsky, S. Gambarotta, *J. Am. Chem. Soc.* **2009**, *131*, 10406-10420.

[12] a) D. Rabinovich, C. M. Haswell, B. L. Scott, R. L. Miller, J. B. Nielsen, K. D. Abney, *Inorg. Chem.* **1996**, *35*, 1425; b) Y. Sun, R. McDonald, J. Takats, V. Day, W., T. A. Eperspacher, *Inorg. Chem.* **1994**, *33*, 4433-4434; c) A. Carvalho, A. Domingos, P. Gaspar, N. Marques, A. Pires de Matos, I. Santos,

Polyhedron **1992**, *11*, 1481-1488; d) S. R. Daly, G. S. Girolami, *Inorg. Chem.* **2010**, *49*, 5157-5166.
[13] W. G. Vandersluys, C. J. Burns, J. C. Huffman, A. P. Sattelberger, *J. Am. Chem. Soc.* **1988**, *110*, 5924-5925.
[14] A. L. Odom, P. L. Arnold, C. C. Cummins, *Journal of American Chemical Society* **1998**, *120*, 5836-5837.
[15] R. A. Andersen, *Inorg. Chem.* **1979**, *18*, 1507-1509.
[16] a) Gambarotta Sandro, I. Korobkov, G. Yap, *Organometallics* **2001**, *20*, 2552-2559; b) A. J. Lewis, U. J. Williams, J. M. Kikkawa, P. J. Carroll, E. J. Schelter, *Inorg. Chem.* **2012**, *51*, 37-39; c) E. J. Schelter, R. L. Wu, B. L. Scott, J. D. Thompson, T. Cantat, K. D. John, E. R. Batista, D. E. Morris, J. L. Kiplinger, *Inorg. Chem.* **2010**, *49*, 924-933; d) C. Villiers, P. Thuery, M. Ephritikhine, *Eur. J. Inorg. Chem.* **2004**, 4624-4632; e) A. J. Gaunt, B. L. Scott, M. P. Neu, *Chem. Commun.* **2005**, 3215-3217; f) D. P. Mills, F. Moro, J. McMaster, J. van Slageren, W. Lewis, A. J. Blake, S. T. Liddle, *Nat. Chem.* **2011**, *3*, 454-460; g) B. Vidjayacoumar, S. Ilango, M. J. Ray, T. Chu, K. B. Kolpin, N. R. Andreychuk, C. A. Cruz, D. J. H. Emslie, H. A. Jenkins, J. F. Britten, *J. Chem. Soc.-Dalton Trans.* **2012**, *41*, 8175-8189; h) T. Cantat, C. R. Graves, B. L. Scott, J. L. Kiplinger, *Angew. Chem. Int. Ed. Engl.* **2009**, *48*, 3681-3684; i) A. R. Fox, J. S. Silvia, E. M. Townsend, C. C. Cummins, *Comptes Rendus Chimie* **2010**, *13*, 781-789; j) Z. R. Turner, R. Bellabarba, R. P. Tooze, P. L. Arnold, *J. Am. Chem. Soc.* **2010**, *132*, 4050; k) M. Roger, T. Arliguie, P. Thuery, M. Ephritikhine, *Inorg. Chem.* **2008**, *47*, 3863-3868; l) P. Roussel, P. Scott, *J. Am. Chem. Soc.* **1998**, *120*, 1070-1071; m) B. Monteiro, D. Roitershtein, H. Ferreira, J. R. Ascenso, A. M. Martins, A. Domingos, N. Marques, *Inorg. Chem.* **2003**, *42*, 4223-4231; n) O. P. Lam, S. C. Bart, H. Kameo, F. W. Heinemann, K. Meyer, *Chem. Commun.* **2010**, *46*, 3137-3139; o) S. C. Bart, F. W. Heinemann, C. Anthon, C. Hauser, K. Meyer, *Inorg. Chem.* **2009**, *48*, 9419-9426; p) I. Castro-Rodriguez, K. Olsen, P. Gantzel, K. Meyer, *Chemical Communication* **2002**, 2764-2765; q) P. L. Arnold, N. A. Potter, N. Magnani, C. Apostolidis, J. C. Griveau, E. Colineau, A. Morgenstern, R. Caciuffo, J. B. Love, *Inorg. Chem.* **2010**, *49*, 5341-5343; r) C. J. Inman, A. S. P. Frey, A. F. R. Kilpatrick, F. G. N. Cloke, S. M. Roe, *Organometallics* **2017**, *36*, 4539-4545; s) F. Sinclair, J. A. Hlina, J. A. L. Wells, M. P. Shaver, P. L. Arnold, *Dalton T* **2017**, *46*, 10786-10790; t) P. L. Arnold, L. Puig-Urrea, J. A. L. Wells, D. Yuan, F. L. Cruickshank, R. D. Young, *Dalton T* **2019**.
[17] M. Aresta, A. Dibenedetto, *J. Chem. Soc.-Dalton Trans.* **2007**, 2975-2992.
[18] a) P. L. Arnold, Z. R. Turner, *Nat. Rev. Chem.* **2017**, *1*; b) O. T. Summerscales, F. G. N. Cloke, *Struct Bond* **2008**, *127*, 87-117.
[19] a) J. G. Brennan, R. A. Andersen, J. L. Robbins, *J. Am. Chem. Soc.* **1986**, *108*, 335-336; b) J. Parry, E. Carmona, C. Simon, M. Hursthouse, *J. Am. Chem. Soc.* **1995**, *117*, 2649-2650.
[20] W. J. Evans, S. A. Kozimor, J. W. Ziller, *J. Am. Chem. Soc.* **2003**, *125*, 14264-14265.
[21] I. Castro-Rodriguez, H. Nakai, L. N. Zakharov, A. L. Rheingold, K. Meyer, *Science* **2004**, *305*, 1757-1759.
[22] I. Castro-Rodriguez, K. Meyer, *J. Am. Chem. Soc.* **2005**, *127*, 11242-11243.
[23] J. G. Brennan, R. A. Andersen, A. Zalkin, *Inorg. Chem.* **1986**, *25*, 1756-1760.

[24] O. T. Summerscales, A. S. P. Frey, F. Geoffrey, N. Cloke, P. B. Hitchcock, *Chem. Commun.* **2009**, 198-200.
[25] a) P. L. Arnold, Z. R. Turner, R. M. Bellabarba, R. P. Tooze, *Chem. Sci.* **2011**, *2*, 77-79; b) B. M. Gardner, J. C. Stewart, A. L. Davis, J. McMaster, W. Lewis, A. J. Blake, S. T. Liddle, *Proc Natl Acad Sci USA* **2012**, *109*, 9265-9270.
[26] O. T. Summerscales, F. G. N. Cloke, P. B. Hitchcock, J. C. Green, N. Hazari, *Science* **2006**, *311*, 829-831.
[27] O. T. Summerscales, F. G. N. Cloke, P. B. Hitchcock, J. C. Green, N. Hazari, *J. Am. Chem. Soc.* **2006**, *128*, 9602-9603.
[28] M. Ephritikhine, *Coord. Chem. Rev.* **2016**, *319*, 35-62.
[29] a) O. P. Lam, F. W. Heinemann, K. Meyer, *Chem. Sci.* **2011**, *2*, 1538-1547; b) C. Camp, M. A. Antunes, G. Garcia, I. Ciofini, I. C. Santos, J. Pecaut, M. Almeida, J. Marcalo, M. Mazzanti, *Chem. Sci.* **2014**, *5*, 841-846; c) J. L. Brown, G. Wu, T. W. Hayton, *Organometallics* **2013**, *32*, 1193-1198; d) D. E. Smiles, G. Wu, T. W. Hayton, *New J. Chem.* **2015**, *39*, 7563-7566; e) J. G. Brennan, R. A. Andersen, A. Zalkin, *Inorg. Chem.* **1986**, *25*, 1761-1765.
[30] P. L. Arnold, C. J. Stevens, N. L. Bell, R. M. Lord, J. M. Goldberg, G. S. Nichol, J. B. Love, *Chem. Sci.* **2017**, *8*, 3609-3617.
[31] J. L. Brown, S. Fortier, R. A. Lewis, G. Wu, T. W. Hayton, *J. Am. Chem. Soc.* **2012**, *134*, 15468-15475.
[32] L. P. Spencer, P. Yang, B. L. Scott, E. R. Batista, J. M. Boncella, *Inorg. Chem.* **2009**, *48*, 11615-11623.
[33] a) B. A. MacKay, M. D. Fryzuk, *Chem Rev* **2004**, *104*, 385-401; b) D. V. Yandulov, R. R. Schrock, *Science* **2003**, *301*, 76-78; c) K. Arashiba, Y. Miyake, Y. Nishibayashi, *Nat. Chem.* **2011**, *3*, 120-125; d) J. S. Anderson, J. Rittle, J. C. Peters, *Nature* **2013**, *501*, 84; e) M. M. Rodriguez, E. Bill, W. W. Brennessel, P. L. Holland, *Science* **2011**, *334*, 780-783; f) Y. Lee, F. T. Sloane, G. Blondin, K. A. Abboud, R. Garcia-Serres, L. J. Murray, *Angew. Chem. Int. Ed. Engl.* **2015**, *54*, 1499-1503.
[34] F. Haber*, Vol. DE 229126*, Haber, F Ammonia German patent DE 229126, **1909**.
[35] a) G. Cloke, F. N., P. B. Hitchcock, *J. Am. Chem. Soc.* **2002**, *124*, 9352-9353; b) S. M. Mansell, N. Kaltsoyannis, P. L. Arnold, *J. Am. Chem. Soc.* **2011**, *133*, 9036-9051.
[36] J. A. Pool, E. Lobkovsky, P. J. Chirik, *Nature* **2004**, *427*, 527-530.
[37] S. M. Mansell, J. H. Farnaby, A. I. Germeroth, P. L. Arnold, *Organometallics* **2013**, *32*, 4214-4222.
[38] I. Korobkov, S. Gambarotta, G. P. A. Yap, *Angew. Chem. Int. Ed. Engl.* **2002**, *41*, 3433-3436.
[39] P. T. Wolczanski, *Polyhedron* **1995**, *14*, 3335-3362.
[40] C. Camp, L. Chatelain, C. E. Kefalidis, J. Pecaut, L. Maron, M. Mazzanti, *Chem. Commun.* **2015**, *51*, 15454-15457.
[41] a) C. Krempner, *Eur. J. Inorg. Chem.* **2011**, 1689-1698; b) S. Lysenko, J. Volbeda, P. G. Jones, M. Tamm, *Angew. Chem. Int. Ed. Engl.* **2012**, *51*, 6757-6761; c) J. Jarupatrakorn, J. D. Tilley, *J. Am. Chem. Soc.* **2002**, *124*, 8380-8388; d) K. L. Fujdala, A. G. Oliver, F. J. Hollander, T. D. Tilley, *Inorg. Chem.* **2003**, *42*, 1140-1150; e) F. Blanc, C. Coperet, J. Thivolle-Cazat, J. M. Basset, A. Lesage, L. Emsley, A. Sinha, R. R. Schrock, *Angew. Chem. Int. Ed. Engl.* **2006**, *45*, 1216-1220.

[42] a) J. Andrez, J. Pecaut, P.-A. Bayle, M. Mazzanti, *Angew. Chem. Int. Ed. Engl.* **2014**, *53*, 10448-10452; b) G. Lapadula, M. P. Conley, C. Coperet, R. A. Andersen, *Organometallics* **2015**, *34*, 2271-2277; c) T. J. Boyle, L. A. M. Ottley, *Chem. Rev.* **2008**, *108*, 1896-1917; d) M. Nishiura, Z. M. Hou, Y. Wakatsuki, *Organometallics* **2004**, *23*, 1359-1368; e) A. Fischbach, G. Eickerling, W. Scherer, E. Herdtweck, R. Anwander, *Zeitschrift Fur Naturforschung Section B-a Journal of Chemical Sciences* **2004**, *59*, 1353-1364.

[43] a) V. Mougel, C. Camp, J. Pecaut, C. Coperet, L. Maron, C. E. Kefalidis, M. Mazzanti, *Angew. Chem. Int. Ed. Engl.* **2012**, *51*, 12280-12284; b) C. Camp, J. Pecaut, M. Mazzanti, *J. Am. Chem. Soc.* **2013**, *135*, 12101-12111.

[44] C. Camp, V. Mougel, J. Pecaut, L. Maron, M. Mazzanti, *Chem. Eur. J.* **2013**, *19*, 17528-17540.

[45] C. Bianchini, C. Mealli, A. Meli, A. Orlandini, L. Sacconi, *Angewandte Chemie-International Edition in English* **1979**, *18*, 673-674.

[46] a) O. P. Lam, L. Castro, B. Kosog, F. W. Heinemann, L. Maron, K. Meyer, *Inorg. Chem.* **2012**, *51*, 781-783; b) O. P. Lam, F. W. Heinemann, K. Meyer, *Angew. Chem. Int. Ed. Engl.* **2011**, *50*, 5965-5968.

[47] C. Camp, O. Cooper, J. Andrez, J. Pecaut, M. Mazzanti, *J. Chem. Soc.-Dalton Trans.* **2015**, *44*, 2650-2656.

[48] a) O. P. Lam, F. W. Heinemann, K. Meyer, *Comptes Rendus Chimie* **2010**, *13*, 803-811; b) A. C. Schmidt, A. V. Nizovtsev, A. Scheurer, F. W. Heinemann, K. Meyer, *Chem. Commun.* **2012**, *48*, 8634-8636.

[49] a) L. Castro, O. P. Lam, S. C. Bart, K. Meyer, L. Maron, *Organometallics* **2010**, *29*, 5504-5510; b) N. Tsoureas, L. Castro, A. F. R. Kilpatrick, F. G. N. Cloke, L. Maron, *Chem. Sci.* **2014**, *5*, 3777-3788.

[50] O. Cooper, C. Camp, J. Pecaut, C. E. Kefalidis, L. Maron, S. Gambarelli, M. Mazzanti, *J. Am. Chem. Soc.* **2014**, *136*, 6716-6723.

[51] A.-C. Schmidt, F. W. Heinemann, C. E. Kefalidis, L. Maron, P. W. Roesky, K. Meyer, *Chem. Eur. J.* **2014**, *20*, 13501-13506.

[52] H. S. La Pierre, K. Meyer, in *Prog. Inorg. Chem., Vol. 58* (Ed.: K. D. Karlin), **2014**, pp. 303-415.

[53] a) D. M. King, F. Tuna, E. J. L. McInnes, J. McMaster, W. Lewis, A. J. Blake, S. T. Liddle, *Science* **2012**, *337*, 717-720; b) J. G. Brennan, R. A. Andersen, *J. Am. Chem. Soc.* **1985**, *107*, 514-516; c) D. S. J. Arney, C. J. Burns, *J. Am. Chem. Soc.* **1993**, *115*, 9840-9841; d) J. R. Bargar, K. H. Williams, K. M. Campbell, P. E. Long, J. E. Stubbs, E. I. Suvorova, J. S. Lezama-Pacheco, D. S. Alessi, M. Stylo, S. M. Webb, J. A. Davis, D. E. Giammar, L. Y. Blue, R. Bernier-Latmani, *Proc Natl Acad Sci USA* **2013**, *110*, 4506-4511; e) I. Castro-Rodriguez, K. Meyer, *Chem. Commun.* **2006**, 1353-1368; f) C. R. Graves, J. L. Kiplinger, *Chem. Commun.* **2009**, 3831-3853.

[54] S. Fortier, J. L. Brown, N. Kaltsoyannis, G. Wu, T. W. Hayton, *Inorg. Chem.* **2012**, *51*, 1625-1633.

[55] D. M. King, F. Tuna, J. McMaster, W. Lewis, A. J. Blake, E. J. L. McInnes, S. T. Liddle, *Angew. Chem. Int. Ed. Engl.* **2013**, *52*, 4921-4924.

[56] S. C. Bart, C. Anthon, F. W. Heinemann, E. Bill, N. M. Edelstein, K. Meyer, *J. Am. Chem. Soc.* **2008**, *130*, 12536-12546.

[57] S. Gambarotta, F. Arena, C. Floriani, P. F. Zanazzi, *J. Am. Chem. Soc.* **1982**, *104*, 5082-5092.

[58] J. Andrez, J. Pecaut, R. Scopelliti, C. E. Kefalidis, L. Maron, M. W. Rosenzweig, K. Meyer, M. Mazzanti, *Chem. Sci.* **2016**, *7*, 5846-5856.
[59] D. E. Smiles, G. Wu, T. W. Hayton, *Inorg. Chem.* **2014**, *53*, 12683-12685.
[60] S. M. Franke, F. W. Heinemann, K. Meyer, *Chem. Sci.* **2014**, *5*, 942-950.
[61] O. P. Lam, S. M. Franke, F. W. Heinemann, K. Meyer, *J. Am. Chem. Soc.* **2012**, *134*, 16877-16881.
[62] a) T. W. Hayton, *Chem. Commun.* **2013**, *49*, 2956-2973; b) D. M. King, J. McMaster, F. Tuna, E. J. L. McInnes, W. Lewis, A. J. Blake, S. T. Liddle, *J. Am. Chem. Soc.* **2014**, *136*, 5619-5622.
[63] G. W. C. Silva, C. B. Yeamans, A. P. Sattelberger, T. Hartmann, G. S. Cerefice, K. R. Czerwinski, *Inorg. Chem.* **2009**, *48*, 10635-10642.
[64] W. J. Evans, S. A. Kozimor, J. W. Ziller, *Science* **2005**, *309*, 1835-1838.
[65] A. R. Fox, P. L. Arnold, C. C. Cummins, *J. Am. Chem. Soc.* **2010**, *132*, 3250-3251.
[66] a) D. M. King, S. T. Liddle, *Coord. Chem. Rev.* **2014**, *266*, 2-15; b) S. Fortier, G. Wu, T. W. Hayton, *J. Am. Chem. Soc.* **2010**, *132*, 6888-6889; c) L. Maria, I. C. Santos, V. R. Sousa, J. Marcalo, *Inorg. Chem.* **2015**, *54*, 9115-9126; d) D. M. King, F. Tuna, E. J. L. McInnes, J. McMaster, W. Lewis, A. J. Blake, S. T. Liddle, *Nat. Chem.* **2013**, *15*, 482-488; e) P. A. Cleaves, D. M. King, C. E. Kefalidis, L. Maron, F. Tuna, E. J. L. McInnes, J. McMaster, W. Lewis, A. J. Blake, S. T. Liddle, *Angew. Chem. Int. Ed. Engl.* **2014**, *53*, 10412-10415; f) L. Chatelain, R. Scopelliti, M. Mazzanti, *J. Am. Chem. Soc.* **2016**, *138*, 1784-1787; g) N. Tsoureas, A. F. R. Kilpatrick, C. J. Inman, F. G. N. Cloke, *Chem. Sci.* **2016**, *7*, 4624-4632.
[67] R. K. Thomson, T. Cantat, B. L. Scott, D. E. Morris, E. R. Batista, J. L. Kiplinger, *Nat. Chem.* **2010**, *2*, 723-729.
[68] A. R. Fox, S. C. Bart, K. Meyer, C. C. Cummins, *Nature* **2008**, *455*, 341-349.
[69] J. Du, D. M. King, L. Chatelain, E. Lu, F. Tuna, E. J. L. McInnes, A. J. Wooles, L. Maron, S. T. Liddle, *Chem Sci* **2019**, *10*, 3738-3745.
[70] S. D. Roughley, A. M. Jordan, *J. Med. Chem.* **2011**, *54*, 3451-3479.
[71] a) J. M. Smith, *Prog. Inorg. Chem.* **2014**, *58*, 417-470; b) J. K. Brask, V. Dura-Vila, P. L. Diaconescu, C. C. Cummins, *Chem. Commun.* **2002**, 902-903; c) S. P. Semproni, P. J. Chirik, *J. Am. Chem. Soc.* **2013**, *135*, 11373-11383.
[72] a) W. B. Tolman, Wiley VCH, Weinheim, Germany, **2006**; b) T. Sakakura, J.-C. Choi, H. Yasuda, *Chem. Rev.* **2007**, *107*, 2365-2387; c) M. Cokoja, C. Bruckmeier, B. Rieger, W. A. Herrmann, F. E. Kuhn, *Angew. Chem. Int. Ed. Engl.* **2011**, *50*, 8510-8537.
[73] a) A. M. Appel, J. E. Bercaw, A. B. Bocarsly, H. Dobbek, D. L. DuBois, M. Dupuis, J. G. Ferry, E. Fujita, R. Hille, P. J. A. Kenis, C. A. Kerfeld, R. H. Morris, C. H. F. Peden, A. R. Portis, S. W. Ragsdale, T. B. Rauchfuss, J. N. H. Reek, L. C. Seefeldt, R. K. Thauer, G. L. Waldrop, *Chem. Rev.* **2013**, *in press*; b) C. Costentin, S. Drouet, M. Robert, J. M. Saveant, *Science* **2012**, *338*, 90-94.
[74] a) K. C. MacLeod, P. L. Holland, *Nat. Chem.* **2013**, *5*, 559-565; b) W. J. Evans, G. Zucchi, J. W. Ziller, *J. Am. Chem. Soc.* **2003**, *125*, 10-11; c) C. C. Lu, C. T. Saouma, M. W. Day, J. C. Peters, *J. Am. Chem. Soc.* **2007**, *129*, 4-5; d) N. W. Davies, A. S. P. Frey, M. G. Gardiner, J. Wang, *Chem. Commun.* **2006**, 4853-4855.

[75] a) Y. Ohki, M. D. Fryzuk, *Angew. Chem.-Int. Edit.* **2007**, *46*, 3180-3183; b) S. Gambarotta, J. Scott, *Angew. Chem. Int. Ed. Engl.* **2004**, *43*, 5298-5308; c) S. Hui, Y. Yi, A. J. James, P. S. Sharp, *Science* **1997**, *275*, 1460-1462; d) J. P. Krogman, B. M. Foxman, C. M. Thomas, *J. Am. Chem. Soc.* **2011**, *133*, 14582-14585.

[76] a) F. Akagi, T. Matsuo, H. Kawaguchi, *Angew. Chem.-Int. Edit.* **2007**, *46*, 8778-8781; b) J. Ballmann, F. Pick, L. Castro, M. D. Fryzuk, L. Maron, *Inorganic Chemistry* **2013**, *52*, 1685-1687; c) J. Li, M. Hermann, G. Frenking, C. Jones, *Angew. Chem.-Int. Edit.* **2012**, *51*, 8611-8614.

CHAPTER 2

Nucleophilic Reactivity of a Nitride-Bridged Diuranium(IV) Complex: CO_2 and CS_2 Functionalization

Introduction[1]

Uranium nitrides are attractive candidates for both stoichiometric and catalytic nitrogen-transfer reactions and small-molecule transformations.[1] Understanding the reactivity of uranium nitrides is also of great interest because of their importance in many fields of science and engineering (e.g., as nuclear fuels).[2] In recent years, an increasing number of molecular nitride compounds of uranium have been prepared and characterized,[2b, 3] but their reactivity has remained virtually unexplored. The activation of a C−H bond by a transient terminal uranium nitride, which resulted in the formation of new N−H and N−C bonds, was first reported by Kiplinger and co-workers.[3j] More recently, the two-electron reduction of terminal U(V) and U(VI) nitrides to cyanates by carbon monoxide has also been described.[3m] Although most previously reported uranium nitride complexes contain a bridging nitride, the reactivity of the U=N=U fragment has thus far only been studied for a diuranium(V) complex in which the nitride reacted as a masked metallonitrene to afford a cyanoimide diuranium(IV/IV) complex.[3g] N−C bond-formation reactions are very important in the construction of value-added chemical compounds and synthetic methods that use inexpensive and largely available feedstock, such as carbon dioxide, are particularly desirable. A few examples of N−C bond formation from the reaction of carbon dioxide with activated nitride-bridged complexes [4] or terminal nitride complexes [5] have been reported for transition metals but thus before this work, the reactivity of molecular nitride compounds of *f*-block elements with CO_2 had not been investigated.

[1] Portions of this chapter have been published: M. Falcone, L. Chatelain, M. Mazzanti, *Angewandte Chemie Int. Ed.*, **2016**, *55*, 4074.
Author contributions: M.F. carried out the synthetic experiments except for compound **2**. M.M., M.F. and L.C. analyzed the data and wrote the manuscript. M.M. originated the central idea, coordinated the work and analyzed the experimental data.

In this chapter, reactivity studies of a previously described nitride-bridged diuranium(IV) complex, [Cs{[U(OSi(O^{t}Bu)$_3$)$_3$]$_2$(μ-N)}], **1** [3h] are reported. The high nucleophilicity of the nitride bridging ligand is found to promote N–C bond formation reactions with electrophiles such as CO_2 and CS_2, through ligand based reactivity. The metal centers are not involved in redox processes.

Results and discussion

We firstly investigated the temperature-induced decomposition of complex **1** to give fragmentation of one siloxide ligand. The nitride-bridged diuranium(IV) complex [Cs{[U(OSi(O^{t}Bu)$_3$)$_3$]$_2$(μ-N)}], **1** is stable in solution at –40 °C for several months but undergoes decomposition at higher temperatures. Notably, the overnight thermolysis of **1** at 80 °C in toluene solution resulted in the complete transformation of **1** to afford a new imido-bridged siloxide/silanediolate diuranium(IV) complex, [Cs{U$_2$(OSi(O^{t}Bu)$_3$)$_5$(μ-O$_2$Si(O^{t}Bu)$_2$)(μ-N^{t}Bu)}] **2**, in 65 % yield (Scheme 1). The solid-state crystal structure of **2** was determined by single-crystal X-ray diffraction (Figure 1).

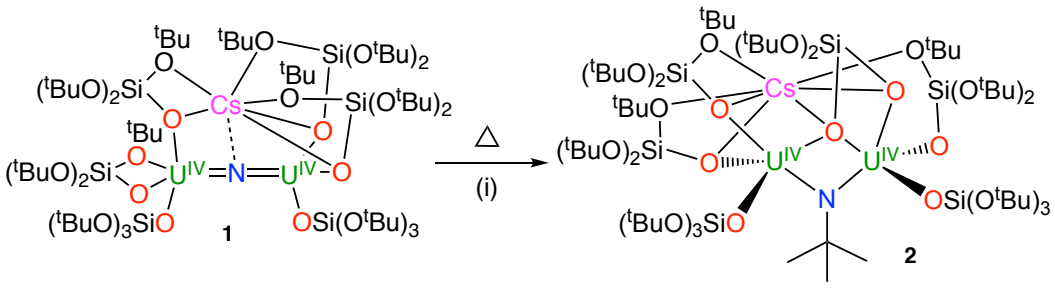

Scheme 1. *tert*-Butyl transfer from a ligand of [Cs{[U(OSi(O^{t}Bu)$_3$)$_3$]$_2$(μ-N)}], **1** to the bridging nitride to form [Cs{U$_2$(OSi(O^{t}Bu)$_3$)$_5$(μ-O$_2$Si(O^{t}Bu)$_2$)(μ-N^{t}Bu)}], **2**. (i) 6 days at room temperature or 12 h at 80 °C.

The structure of **2** shows the presence of a tris(siloxide) U(IV) moiety, [U(OSi(O^{t}Bu)$_3$)$_3$], and of a bis(siloxide)/mono(silanediolate) U(IV) moiety, [U(O$_2$Si(O^{t}Bu)$_2$)(OSi(O^{t}Bu)$_3$)$_2$]. The two uranium ions are bridged by a tert-butylimido group and by one of the oxygen atoms of the silanediolate ligand, affording a non-symmetric structure.

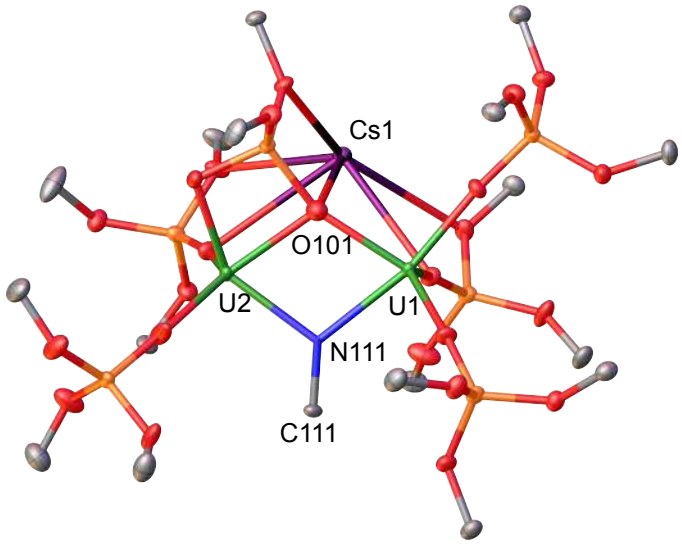

Figure 1. Solid-state molecular structure of [Cs{U_2(OSi(O^{t}Bu)$_3$)$_5$(μ-O_2Si(O^{t}Bu)$_2$)(μ-N^{t}Bu)}] **2**. Thermal ellipsoids set at 50% probability. Hydrogen atoms and methyl groups were omitted for clarity. Selected bond lengths [Å]: U1–N111 2.300(3), U2–N111 2.398(3), N111–C111 1.461(6), U2–O101 2.223(4), U1–O101 2.323(4), Cs1–O101 3.340(4).

This result shows that the thermolysis of complex **1** leads to C–O cleavage in one of the siloxide ligands with concomitant transfer of the *tert*-butyl group to the nitride, giving a dianionic silanediolate ligand that bridges the two uranium centers. C–O cleavage in a *tert*-butoxysiloxide ligand with concomitant elimination of isobutene has previously been observed in the thermolysis of the diuranium(III) complex [U(OSi(O^{t}Bu)$_3$)$_2$(μ-OSi(O^{t}Bu)$_3$)]$_2$.[6] The strong nucleophilic character of the bridging nitride in **1** results in the formation of a new N–C bond with the *tert*-butyl group from the siloxide ligand, yielding the *tert*-butylimido bridging group. The *tert*-butylimide bridges the two uranium centers in a non-symmetric fashion with U–N_{imido} bond lengths of 2.300(3) and 2.398(3) Å, which are slightly longer than those found in the few reported examples of dinuclear imido-bridged U(IV) complexes (2.156(8) - 2.378(3) Å).[7] The high nucleophilic reactivity of the bridging nitride, as evidenced by the slow decomposition of complex **1** at room temperature, inspired us to investigate the reactivity of this complex with the electrophiles CS_2 and CO_2. The addition of two equivalents of CS_2 to **1** resulted in an immediate color change of the solution to green. Storing the solution at –40 °C resulted in the isolation of [Cs{[U(OSi(O^{t}Bu)$_3$)$_3$]$_2$(μ-NCS)(μ-CS_3)}], **3** in 58 % yield (Scheme 2).

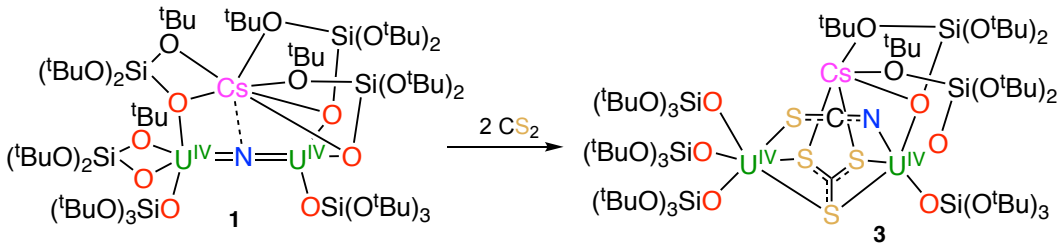

Scheme 2. Reaction of [Cs{[U(OSi(O^{t}Bu)$_3$)$_3$]$_2$(μ-N)}], **1** with CS_2 to form [Cs{[U(OSi(O^{t}Bu)$_3$)$_3$]$_2$(μ-NCS)(μ-CS_3)}], **3**.

The solid-state structure of **3** is disordered with occupancy of 0.85 for the Cs atom in one position (**3a**, Figure 2a) and occupancy of 0.15 in the other position (**3b**, Figure 2b). The structure of **3** consists of a diuranium(IV) complex in which two [U(OSi(O^{t}Bu)$_3$)$_3$] fragments are bridged by a thiocyanate unit and a trithiocarbonate unit that binds the two uranium cations and the cesium cation in a μ_3-k^2:k^2:k^2 fashion.

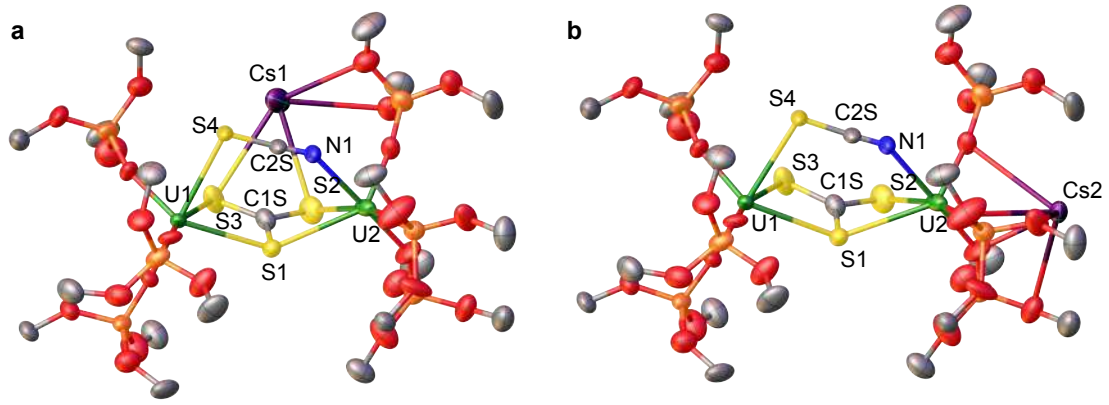

Figure 2. Solid-state molecular structure of the complex [Cs{[U(OSi(O^{t}Bu)$_3$)$_3$]$_2$(μ-NCS)(μ-CS_3)}], **3**. Thermal ellipsoids set at 50% probability. Hydrogen atoms and methyl groups were omitted for clarity. Representation of the two disordered positions occupied by the Cs cation: structure **3a** (Cs occupancy of 0.85) with the cesium cation binding two sulphur atoms of the CS_3 fragment and two oxygen atoms of one siloxide ligans (**a**); structure **3b** (Cs occupancy of 0.15) with cesium cation coordinated by five oxygen atoms of the siloxide ligands (**b**). Selected bond lengths [Å] for **3a**: U1–S1 2.9792(18), U1–S4 3.029(4), U1–S3 2.885(3), U2–S1 3.0411(18), U2–S2 2.881(4), U2–N1 2.501(15), S4–C2S 1.639(15), N1–C2S 1.07(2), S1–C1S 1.740(12), S2–C1S 1.682- (9), S3–C1S 1.712(10), Cs1–S3 3.525(3), Cs1–S4 4.170(6), Cs1–S2 3.408(3), U2–Cs1 4.7200(9).

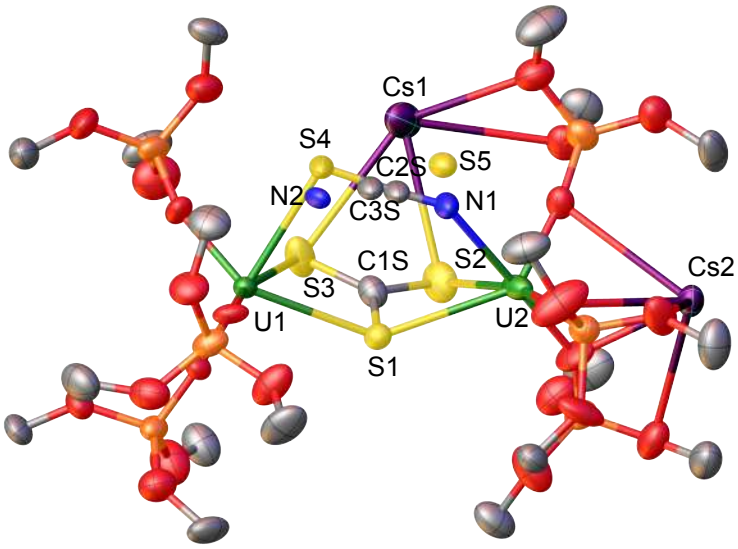

Figure 3. Solid-state molecular structure of the complex $[Cs\{[U(OSi(O^tBu)_3)_3]_2(\mu\text{-}NCS)(\mu\text{-}CS_3)\}]$, **3**. Thermal ellipsoids set at 50% probability. Hydrogen atoms and methyl groups were omitted for clarity. Representation of the two disordered positions of the NCS^- ligand and of the Cs cation. In one position N is bound to U2 and S is bound to U1 (0.61 occupancy) while in the other one N is bound to U1 and S is bound to U2 (0.39 occupancy).

The C–S bond lengths (1.740(12), 1.682(9), 1.712(10) Å) are consistent with electronic delocalization of the negative charge over the CS_3^{2-} unit, and are similar to those found in the two other reported uranium trithiocarbonate complexes.[8] The bridging thiocyanate is disordered over two positions: one with N bound to U2 and S bound to U1, and one with N bound to U1 and S bound to U2 (Figure 3). The U–N bonds (U1–N1 2.501(15) Å, U2–N1 2.62(2) Å) are longer than those reported for terminal N-bound U(IV) thiocyanate complexes (2.385(4) Å).[9] The ^{13}C NMR spectrum of **3** in toluene-d_8 shows a resonance at 124.0 ppm for the bridging NCS^- ligand and one at 195.8 ppm for the bridging CS_3^{2-} ligand. The ^{13}C NMR spectrum of **3** in DMSO-d_6 shows a resonance at 129.3 ppm that was assigned to the NCS^- anion (Appendix 1, Figure S12). The presence of two $\nu(^{13}CN)$ stretches at 2006 and 2085 cm^{-1} in the IR spectrum of a sample of **3** that was prepared with $^{13}CS_2$ is consistent with the presence of a bridging thiocyanate ligand.[10]

The addition of an equimolar amount of CS_2 to **1** led to a mixture of unreacted complex **3** and an additional species, which was transformed into **3** after addition of a second equivalent of CS_2. The ^{13}C NMR spectrum in DMSO-d_6 of the residue obtained after removal of the volatiles allowed us to confirm the presence of the free NCS^- group (Appendix 1, Figure S7). This finding suggests that the formation of the trithiocarbonate- and thiocyanate-bridged complex **3** is most likely the result of the

reaction of a sulfide- and thiocyanate-bridged intermediate, "[Cs{[U(OSi(O^{t}Bu)$_3$)$_3$]$_2$(μ-NCS)(μ-S)}]", with a second molecule of CS_2 (Scheme 3).

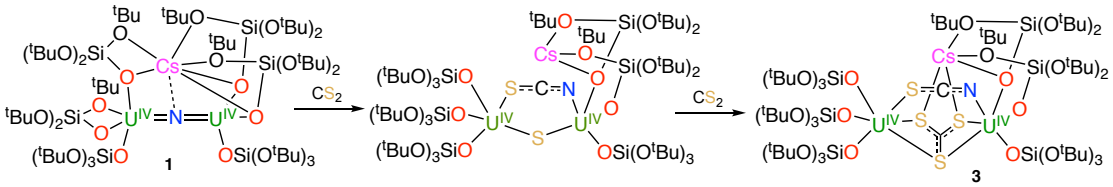

Scheme 3. Proposition of bridging sulphide complex formation as intermediate, that reacts with a second molecule of CS_2 to give **3**.

The formation of a trithiocarbonate-bridged diuranium(IV) complex by the nucleophilic addition of a sulfide-bridged diuranium(IV) complex to CS_2 has previously been described by Meyer et al.[8a] Moreover, the formation of sulfide and thiocyanate species from the nucleophilic addition of CS_2 to a nitride via a dithiocarbamate intermediate has been described for a terminal V(V) nitride.[5b]

Rather different reactivity was observed with CO_2. The addition of three equivalents of CO_2 to **1** in toluene at low temperature (–70 °C) resulted in an immediate color change to yield a blue solution. Storing the solution at –40 °C gave [Cs[U(OSi(O^{t}Bu)$_3$)$_3$]$_2${(μ-NC$_2$O$_4$)}], **4** in 72 % yield (Scheme 4).

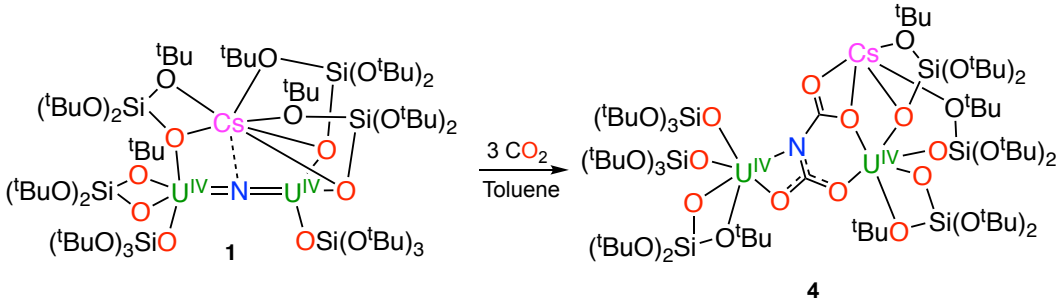

Scheme 4. Reaction of **1** with CO_2 to form [Cs[U(OSi(O^{t}Bu)$_3$)$_3$]$_2${(μ-NC$_2$O$_4$)}], **4**.

Complex **4** is stable in toluene solution at room temperature for up to two weeks. The solid-state structure of **4** (Figure 4) shows the presence of a dicarbamate ligand bridging two [U(OSi(O^{t}Bu)$_3$)$_3$] fragments in an asymmetric fashion. One uranium cation is bound by the nitrogen atom and by a carboxylate oxygen atom, while the second uranium cation is bound by two oxygen atoms, from two different carbamate units. The $U_2NC_2O_4$ core comprises two fused rings, with one six-membered ring (UOCNCO) and one four-membered ring (UNCO). The two rings share the N–C

bond and are arranged in a planar fashion. A carbamate oxygen atom that is not bound to the uranium ion is located above this plane, and it is bound to the Cs cation. The U−N bond length (2.467(3) Å) is longer than those usually found in U(IV) amide complexes (ca. 2.3 Å) [11] but similar to the U(IV)−N bond reported for a sterically demanding amide (2.415 Å) [12] and in the range of U−N bond lengths reported for amido-bridged diuranium(IV) complexes (2.4 - 2.57 Å).[13] The similar values of the O121−C121 and C121−O122 bond lengths (1.292(5) and 1.282(4) Å) are consistent with delocalization of the negative charge. The C122−O124 bond (1.229(6) Å) is shorter than the C122−O123 bond (1.317(4) AÅ), which suggests a localized C=O bond.

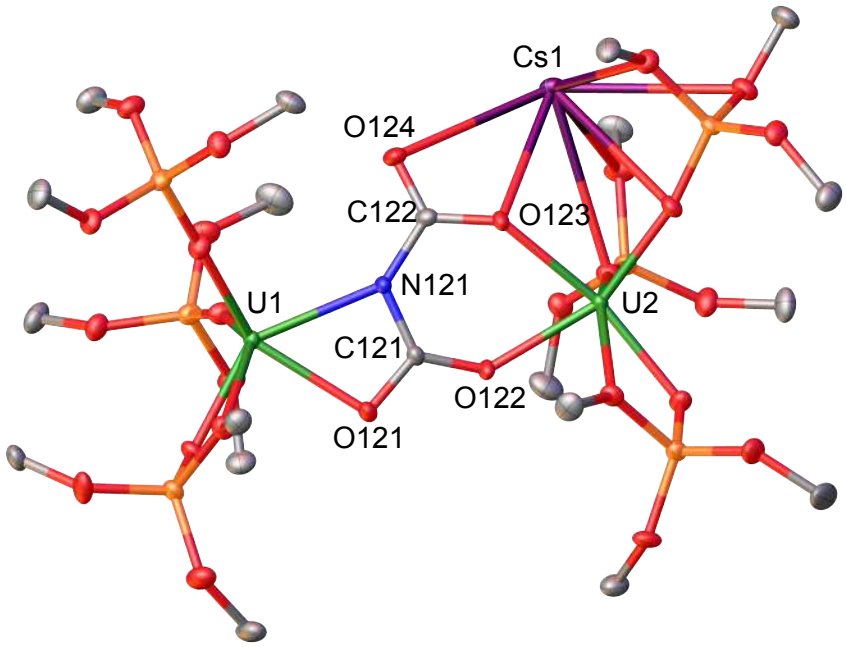

Figure 4. Solid-state molecular structure of the complex $[Cs[U(OSi(O^tBu)_3)_3]_2\{(\mu\text{-}NC_2O_4)\}]$, **4**. Thermal ellipsoids set at 50 % probability. Hydrogen atoms, methyl groups, and solvent molecules were omitted for clarity. Selected bond lengths [Å]: U1–O121 2.360(3), U1–N121 2.467(3), O121–C121 1.292(5), C121–N121 1.347(5), C121–O122 1.282(4), N121–C122 1.396(6), C122–O124 1.229(6), C122–O123 1.317(4), U2–O123 2.252(3), U2–O122 2.283(3), O124–Cs1 3.206(3), O123–Cs1 3.045(3). Torsion angles [°]: O121–C121–N121–C122 178.11, O124–C122–N121–C121 158.03.

The ^{13}C NMR spectrum in D_2O of crystals of complex **4** shows the presence of a peak at 162 ppm (DMSO as reference), assigned to the bicarbonate species, as the salt of the imidodicarboxylic acid hydrolyzes in water to bicarbonate and ammonium hydroxide, as follows:[14]

$$(KCO_2)_2NH + 3H_2O \rightarrow 2KHCO_3 + NH_4OH$$

The ^{13}C NMR spectrum of the crude reaction mixture obtained from the reaction of **1** with three equivalents of $^{13}CO_2$ in toluene-d_8 only shows one peak at –134.1 ppm, which was assigned to the bridging dicarbamate ligand. This result suggests that complex **4** is the only product formed in this reaction. In contrast, ^{1}H and ^{13}C NMR studies showed that when smaller amounts of carbon dioxide (1 - 2 equiv.) are added, a mixture of **4**, unreacted **1**, and an additional species is formed (Scheme 5). This new species cannot be transformed into **4** by the subsequent addition of excess CO_2. X-ray diffraction analysis of crystals obtained from this reaction mixture showed the presence of two co-crystallized complexes, $[Cs\{[U(OSi(O^tBu)_3)_3]_2(\mu\text{-}NCO)(\mu\text{-}O)\}]$, **5** and $[Cs_2\{[U(OSi(O^tBu)_3)_3]_2(\mu\text{-}O)_2\}]$, **6** (Figure 5), in a ratio of 1:0.5.

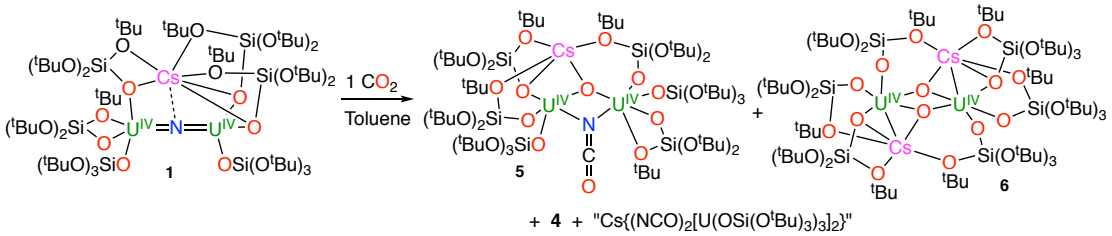

Scheme 5. Reaction of $[Cs\{[U(OSi(O^tBu)_3)_3]_2(\mu\text{-}N)\}]$, **1** with 1 equiv. of CO_2; isolation of co-crystallized $[Cs\{[U(OSi(O^tBu)_3)_3]_2(\mu\text{-}NCO)(\mu\text{-}O)\}]$, **5** and $[Cs_2\{[U(OSi(O^tBu)_3)_3]_2(\mu\text{-}O)_2\}]$, **6**.

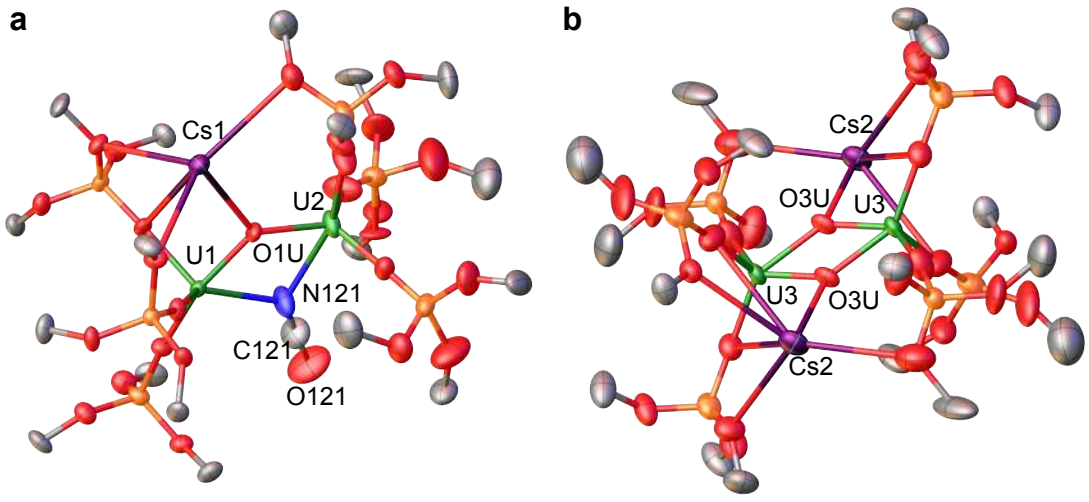

Figure 5. Solid-state molecular structure of the cocrystallized complexes $[Cs\{[U(OSi(O^tBu)_3)_3]_2(\mu\text{-}NCO)(\mu\text{-}O)\}]$, **5** (**a**) and $[Cs_2\{[U(OSi(O^tBu)_3)_3]_2(\mu\text{-}O)_2\}]$, **6** (**b**) in **5.(0.5)6** with probability set at 50%. Hydrogen atoms, methyl groups and solvent molecules were omitted for clarity. Selected bond lengths [Å] of **5**: U1–N121 2.535(9), U2–N121 2.582(9), U1–O1U 2.118(5), U2–O1U 2.127(5), N121–C121 1.178(2), C121–O121 1.180(2). Selected bond lengths [Å] of **6**: U3–O3U 1.897(1), O3U–Cs2 2.876(9).

The ^{13}C NMR spectrum of these crystals in DMSO-d_6 shows the presence of free isocyanate (Appendix 1, Figure S24), indicating that NCO^- is released when the crystals are dissolved in DMSO. The structure of **5** shows the presence of two

tris(siloxide) U(IV) moieties that are bridged by an oxo ligand and an N-bound isocyanate. The U–N bonds (2.535(9) and 2.582(9) Å) are longer than those found in terminally bound isocyanates (around 2.3 Å)[9] but similar to those reported for an isocyanatodioxouranate(VI) (2.58(1) Å), in which the cyanate group adopted a similar bridging mode.[15]

The isolation of compound **5** indicates that at substoichiometric ratios of CO_2, the reaction of **1** with CO_2 proceeds with deoxygenation and N–C bond formation to yield the cyanate/oxo complex, which is probably formed via a bridging carbamate intermediate. Analogous reactivity has been reported for a terminal niobium carbamate, which undergoes intramolecular metathesis to afford a terminal oxo complex and free isocyanate, but only after heating at 80 °C.[5c] The presence of the co-crystallized bis(oxo) complex **6** also suggests that scrambling of the isocyanate and oxo ligands occurs in solution, which is in agreement with the observation of only one peak for this complex in the ^{1}H NMR spectrum of crystals of **5·6$_{0.5}$** (Appendix 1, Figure S23). In the presence of excess CO_2, the addition of a second equivalent of CO_2 to the monocarbamate intermediate is faster than the isocyanate formation. Complexes of the $N(CO_2)_2^{3-}$ ligand are rare, probably because of the difficulty of preparing the parent triprotic species.[14] Only a few examples of the reactivity of the U–N bond with CO_2 have been described before this work. Insertion of CO_2 into U(III)–N_{amide} or U(IV)–N_{amide} bonds resulted in the formation of O-bound carbamate complexes of U(III) or U(IV) [11b, 16] or U(IV) isocyanate complexes,[17] and the reaction of CO_2 with U(V) imido complexes led to isocyanate extrusion and formation of a terminal U(V) oxo complex by multiple metathesis.[16d, 18] Very recently in our group,[19] reactivity of the diuranium(V) bis-nitride complex $[K_2\{[U(OSi(O^tBu)_3)_3]_2(\mu\text{-}N)_2\}]$, with CS_2 has been reported. It shows similar reactivity, but in contrast to the U(IV) mono-nitride presented here, the presence of uranium(V) stabilizes the bridging sulphide formed together with the NCS^- ligand. The resulting nitride-sulfide-thiocyanate bridged diuranium(V) complex (Figure 6a), was isolated in high yield. Similar reactivity was observed upon addition of 1 equiv. of CO_2 to the diuranium(V) bis-nitride, which forms an NCO^- ligand and a bridging oxo (Figure 6b), showing analogous ligand based reactivity with respect to the diuranium(IV) mono-nitride.

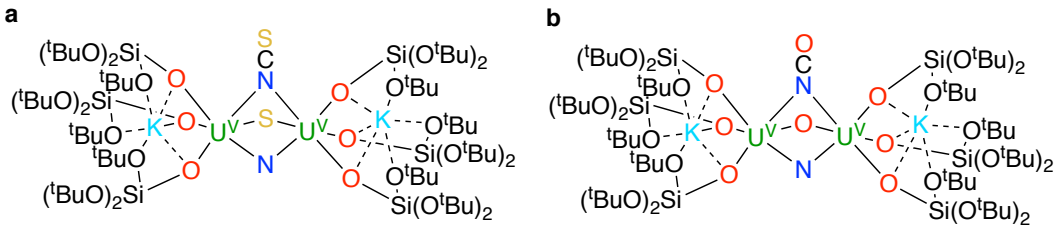

Figure 6. Reaction product of the diuranium(V) bis-nitride complex with 1 equiv. of CS_2 (**a**); reaction product of the diuranium(V) bis-nitride complex with 1 equiv. of CO_2 (**b**).

Conclusions

In this chapter, the first example of insertion of CO_2 into a U–$N_{nitride}$ bond was shown. The high reactivity of **1** with electrophiles is in stark contrast to the often inert character of nitride-bridged transition-metal complexes,[20] which require activation of the nitride group for further functionalization. This result highlights the potential of uranium nitrides in promoting N–C bond-formation reactions, opening up new pathways for the selective synthesis of organic molecules from metal nitrides and the abundant and inexpensive feedstock CO_2, and demonstrate that nitride functionalization with heteroallenes is readily feasible with uranium. This novel reactivity of uranium nitrides inspired us to pursue reactivity with other small molecules.

Experimental

General Considerations. Unless otherwise noted, all manipulations were carried out at ambient temperature under an inert argon atmosphere using Schlenk techniques and an MBraun glovebox equipped with a purifier unit. The water and oxygen levels were always kept at less than 0.1 ppm. Glassware was dried overnight at 130 °C before use.

^{1}H NMR experiments were carried out using NMR tubes adapted with J. Young valves. ^{1}H NMR spectra were recorded on Bruker 400 MHz. NMR chemical shifts are reported in ppm with solvent as internal reference.

Elemental analyses were performed with a Thermo Scientific Flash 2000 Organic Elemental Analyzer.

Starting materials. Unless otherwise noted, reagents were purchased from commercial suppliers and used without further purification. The solvents were purchased from Aldrich or Eurisotop (deuterated solvents) in their anhydrous form, conditioned under argon and vacuum distilled from K/benzophenone (toluene and

THF). [Cs{[U(OSi(OtBu)$_3$)$_3$]$_2$(μ-N)}], **1** was prepared according to the published procedure.[3h]

Caution: Depleted uranium (primary isotope ^{238}U) is a weak α-emitter (4.197 MeV) with a half-life of 4.47×10^9 years. Manipulations and reactions should be carried out in monitored fume hoods or in an inert atmosphere glovebox in a radiation laboratory equipped with α- and β-counting equipment.

Thermal rearrangement of [Cs{[U(OSi(O^{t}Bu)$_3$)$_3$]$_2$(μ-N)}]: synthesis of [Cs{ U$_2$(OSi(O^{t}Bu)$_3$)$_5$(μ-O$_2$Si(O^{t}Bu)$_2$)(μ-N^{t}Bu)}], 2.

A red brown solution of [Cs{[U(OSi(O^{t}Bu)$_3$)$_3$]$_2$(μ-N)}], **1** (27.6 mg, 0.013mmol) in 0.5 mL of toluene was heated at 80 °C overnight, yielding a light green solution. This solution was concentrated and stored at –40°C to afford light green crystals of [Cs{ U$_2$(OSi(O^{t}Bu)$_3$)$_5$(μ-O$_2$Si(O^{t}Bu)$_2$)(μ-N^{t}Bu)}], **2** (18 mg, 65% yield). ^{1}H NMR (400 MHz, toluene-d$_8$, 298K) of crystals: δ = 64.39 (s, 9H), 16.16 (br s, 9H), 9.37 (s, 27H), 5.01 (s, 9H), 3.54 (br s, 9H), –7.47 (s, 27H), –9.72 (s, 62H), –39.66 (s, 9H). Anal. Calcd for [Cs{ U$_2$(OSi(O^{t}Bu)$_3$)$_5$(μ-O$_2$Si(O^{t}Bu)$_2$)(μ-N^{t}Bu)}] ($C_{72}H_{162}CsNO_{24}Si_6U_2$): C, 39.25; H, 7.41; N, 0.64. Found: C, 39.44; H, 7.54; N, 0.76.

Synthesis of [Cs{[U(OSi(O^{t}Bu)$_3$)$_3$]$_2$(μ-NCS)(μ-CS$_3$)}], 3.

The addition of CS_2 (1.2 μL, 0.02 mmol, 2 eq) to a red-brown solution of [Cs{[U(OSi(O^{t}Bu)$_3$)$_3$]$_2$(μ-N)}], **1** (21.9 mg, 0.01 mmol, 1 eq) in toluene (2 mL) led to an immediate colour change affording a brown green solution. The solution was concentrated to 0.5 mL and left standing at –40°C. After 24 hours green crystals suitable for XRD studies formed. The crystals were collected and dried *in vacuo* to give **3** as a pure crystalline solid (14.0 mg, 0.0058 mmol, 58 %,). Complex **3** is stable in solution at –40 °C. It decomposes at room temperature within 24 h. IR, ν^{13}**CN** (cm^{-1}): 2006, 2085. The presence of two ν^{13}**CN** is consistent with the presence of a bridging thiocyanate ligand. ^{1}H NMR (400 MHz, toluene-d$_8$, 298 K): δ = 0.36 (broad s, 162H, C**H**$_3$ terminal siloxide). ^{13}C NMR (400 MHz, toluene-d$_8$, 298 K): δ = 124.0 (bridging N**C**S$^-$), 195.8 (bridging **C**S$_3^{2-}$). ^{13}C NMR (400 MHz, DMSO-d$_6$, 298 K): δ = 129.3 (N**C**S$^-$); 236.0 (bridging **C**S$_3^{2-}$). ^{13}C NMR (400 MHz, DMSO-d$_6$, 298 K, after decomposition): δ = 129.2 (N**C**S$^-$); 260.3 (**C**S$_3^{2-}$). The presence of free thiocarbonate in the spectrum of the decomposed reaction mixture measured in DMSO-d$_6$, suggests

that decomposition involves ligand disproportionation affording the monomeric $[U(IV)(OSi(O^tBu)_3)_4]$ [21] complex (observed by proton NMR) and free thiocyanate and thiocarbonate. ^{13}C NMR (400 MHz, D_2O, 298 K): δ = 134.9 (N**C**S$^-$). Anal. Calcd for $[Cs\{[U(OSi(O^tBu)_3)_3]_2(\mu\text{-}NCS)(\mu\text{-}CS_3)\}].(C_7H_8)_{0.8}$ ($C_{74}H_{162}CsNO_{24}S_4Si_6U_2.(C_7H_8)_{0.8}$): C, 39.35; H, 6.99; N, 0.58. Found: C, 39.37; H, 6.99; N, 0.88

Reaction of $[Cs\{[U(OSi(O^tBu)_3)_3]_2(\mu\text{-}N)\}]$ with 1 equivalent of CS_2.

The addition of 9.9 μL of a 0.8M solution of CS_2 (0.008 mmol, 1 eq) to a red brown solution of $[Cs\{[U(OSi(O^tBu)_3)_3]_2(\mu\text{-}N)\}]$, **1** (15.6 mg, 0.008 mmol, 1 eq) in toluene (0.6 mL) led to an immediate colour change affording a green solution. The proton NMR spectrum of this reaction mixture shows the presence of a major species which was assigned to a putative thiocyanate and sulphide bridged U(IV) complex $[Cs\{[U(OSi(O^tBu)_3)_3]_2(\mu\text{-}NCS)(\mu\text{-}S)\}]$, **a**. The proton NMR shows also the presence of complex **3** suggesting that it forms also at sub-stoichiometric amounts of CS_2. When amounts of CS_2 lower than 1 eq are added to **1,** the proton NMR spectrum of the resulting reaction mixture shows the presence of unreacted complex **1**, of complex **3** and of the SCN/S species **a**. This prevents the isolation of the SCN/S intermediate in a pure form. The ^{13}C NMR in DMSO-d_6 of the 1:1 (1:CS_2) reaction mixture shows the presence of free SCN$^-$ in agreement with the formulation of the intermediate as a thiocyanate and sulphide bridged complex. The addition of a second equivalent of CS_2 to the 1:1 reaction mixture of **1** and CS_2 leads to the formation of **3** as the only species in solution. ^1H NMR of intermediate **a** (400 MHz, toluene-d_8, 298 K): δ = –0.52 (s, 162H, C**H**$_3$ terminal siloxide). ^{13}C NMR of intermediate **a** (400 MHz, toluene-d_8, 298 K): δ = 136.7 (bridging N**C**S$^-$)^{13}C NMR of intermediate **a** (400 MHz, DMSO-d_6, 298 K): δ = 129.3 (N**C**S$^-$).

Synthesis of $[Cs\{[U(OSi(O^tBu)_3)_3]_2(\mu\text{-}NC_2O_4)\}]$, 4.

$^{13}CO_2$ (0.042 mmol, 28 mbar, 3 eq) was added to an NMR tube containing a red brown solution of $[Cs\{[U(OSi(O^tBu)_3)_3]_2(\mu\text{-}N)\}]$, **1** (30 mg, 0.014 mmol, 1 eq) in toluene-d_8 (0.5 mL). Immediately the mixture turned light blue. Blue single crystals, suitable for XRD studies, formed after 24 h at –40 °C. The crystals were collected and dried *in vacuo* to give 23.5 mg of **4** (72%). IR, $\nu^{13}C{=}O$ (cm^{-1}): 1579, 1648, 1645. ^1H NMR (400 MHz, toluene-d_8, 298 K) of crystals of **4**: δ = very broad signal ranging

from –4 to 3 ppm, 162H, C**H**$_3$ terminal siloxide). ^{13}C NMR (400 MHz, toluene-d$_8$, 298 K) of crystals of **4**: δ = –134.2 (bridging (N**C**$_2$O$_4$)$^{3-}$). Anal. Calcd for [Cs{[U(OSi(O^{t}Bu)$_3$)$_3$]$_2$(μ-NC$_2$O$_4$)}].(C$_7$H$_8$) (C$_{74}$H$_{162}$CsNO$_{28}$Si$_6$U$_2$.(C$_7$H$_8$)): C, 40.81; H, 7.19; N, 0.59. Found: C, 40.92; H, 7.44; N, 0.59.

Reaction of [Cs{[U(OSi(O^{t}Bu)$_3$)$_3$]$_2$(μ-N)}] with 1 equivalent of CO$_2$; isolation of co-crystallized [Cs{[U(OSi(O^{t}Bu)$_3$)$_3$]$_2$(μ-NCO){(μ-O)}], 5 and [Cs{[U(OSi(O^{t}Bu)$_3$)$_3$]$_2$(μ-O)$_2$}], 6.

^{13}CO$_2$ (0.012 mmol, 8.2 mbar, 1 eq) was added to an NMR tube containing a red brown solution of [Cs{[U(OSi(O^{t}Bu)$_3$)$_3$]$_2$(μ-N)}], **1** (26.7 mg, 0.012 mmol, 1 eq) in toluene-d$_8$ (0.5 mL). Immediately the mixture turned light blue. The proton NMR shows a mixture of species including complex **4**. A similar result is obtained when 1.5 or 2.2 eq of CO$_2$ are added. Blue single crystals of **4** formed after 24 h at –40 °C and were collected. From the supernatant, light purple single crystals of **5.6**, suitable for XRD, formed after 24 h. The proton NMR of the crystals in toluene shows the presence of only one peak probably due to the presence of ligand scrambling in solution. The stoichiometry of the reaction requires also the presence of an additional species containing two bridging thiocyanate ligands. ^{1}H NMR (400 MHz, toluene-d$_8$, 298 K) of crystals: δ = –2.48.

Bibliography

[1] a) F. Haber, *Vol. DE 229126*, Haber, F Ammonia German patent DE 229126, **1909**; b) A. R. Fox, S. C. Bart, K. Meyer, C. C. Cummins, *Nature* **2008**, *455*, 341-349; c) M. S. Eisen, *Top. Organomet. Chem.* **2010**, *31*, 157-184.

[2] a) G. W. C. Silva, C. B. Yeamans, A. P. Sattelberger, T. Hartmann, G. S. Cerefice, K. R. Czerwinski, *Inorg. Chem.* **2009**, *48*, 10635-10642; b) D. M. King, S. T. Liddle, *Coord. Chem. Rev.* **2014**, *266*, 2-15.

[3] a) T. W. Hayton, *Chem. Commun.* **2013**, *49*, 2956-2973; b) W. J. Evans, S. A. Kozimor, J. W. Ziller, *Science* **2005**, *309*, 1835-1838; c) I. Korobkov, S. Gambarotta, G. P. A. Yap, *Angew. Chem. Int. Ed. Engl.* **2002**, *41*, 3433-3436; d) T. K. Todorova, L. Gagliardi, J. R. Walensky, K. A. Miller, W. J. Evans, *J. Am. Chem. Soc.* **2010**, *132*, 12397-12403; e) G. Nocton, J. Pecaut, M. Mazzanti, *Angew. Chem. Int. Ed. Engl.* **2008**, *47*, 3040-3042; f) S. Fortier, G. Wu, T. W. Hayton, *J. Am. Chem. Soc.* **2010**, *132*, 6888-6889; g) A. R. Fox, P. L. Arnold, C. C. Cummins, *J. Am. Chem. Soc.* **2010**, *132*, 3250-3251; h) C. Camp, J. Pecaut, M. Mazzanti, *J. Am. Chem. Soc.* **2013**, *135*, 12101-12111; i) L. Maria, I. C. Santos, V. R. Sousa, J. Marcalo, *Inorg. Chem.* **2015**, *54*, 9115-9126; j) R. K. Thomson, T. Cantat, B. L. Scott, D. E. Morris, E. R. Batista, J. L. Kiplinger, *Nat. Chem.* **2010**, *2*, 723-729; k) D. M. King, F. Tuna, E. J. L. McInnes, J. McMaster, W. Lewis, A. J. Blake, S. T. Liddle, *Science* **2012**, *337*, 717-720; l) D. M. King, J. McMaster, F. Tuna, E. J. L. McInnes, W. Lewis, A. J. Blake, S. T. Liddle, *J. Am. Chem. Soc.* **2014**, *136*, 5619-5622; m) P. A. Cleaves, D. M. King, C. E. Kefalidis, L. Maron, F. Tuna, E. J. L. McInnes, J. McMaster, W. Lewis, A. J. Blake, S. T. Liddle, *Angew. Chem. Int. Ed. Engl.* **2014**, *53*, 10412-10415.

[4] a) S. P. Semproni, P. J. Chirik, *J. Am. Chem. Soc.* **2013**, *135*, 11373-11383; b) S. P. Semproni, P. J. Chirik, *Angew. Chem. Int. Ed. Engl.* **2013**, *52*, 12965-12969.

[5] a) J. M. Smith, *Prog. Inorg. Chem.* **2014**, *58*, 417-470; b) J. K. Brask, V. Dura-Vila, P. L. Diaconescu, C. C. Cummins, *Chem. Commun.* **2002**, 902-903; c) J. S. Silvia, C. C. Cummins, *J. Am. Chem. Soc.* **2010**, *132*, 2169-2170.

[6] C. Camp, C. E. Kefalidis, J. Pecaut, L. Maron, M. Mazzanti, *Angew. Chem. Int. Ed. Engl.* **2013**, *52*, 12646-12650.

[7] a) J. G. Brennan, R. A. Andersen, A. Zalkin, *J. Am. Chem. Soc.* **1988**, *110*, 4554-4558; b) J. L. Stewart, R. A. Andersen, *New J. Chem.* **1995**, *19*, 587-595; c) R. C. Schnabel, B. L. Scott, W. H. Smith, C. J. Burns, *J. Organomet. Chem.* **1999**, *591*, 14-23.

[8] a) O. P. Lam, L. Castro, B. Kosog, F. W. Heinemann, L. Maron, K. Meyer, *Inorg. Chem.* **2012**, *51*, 781-783; b) C. Camp, O. Cooper, J. Andrez, J. Pecaut, M. Mazzanti, *J. Chem. Soc.-Dalton Trans.* **2015**, *44*, 2650-2656.

[9] C. Camp, N. Settineri, J. Lefevre, A. R. Jupp, J. M. Goicoechea, L. Maron, J. Arnold, *Chem. Sci.* **2015**, *6*, 6379–6384.

[10] M. A. S. Goher, *Coll. Czech. Chem. Commun.* **1977**, *42*, 1478.

[11] a) S. M. Franke, M. W. Rosenzweig, F. W. Heinemann, K. Meyer, *Chem. Sci.* **2015**, *6*, 275-282; b) L. P. Spencer, P. Yang, S. G. Minasian, R. E. Jilek, E. R. Batista, K. S. Boland, J. M. Boncella, S. D. Conradson, D. L. Clark, T. W. Hayton, S. A. Kozimor, R. L. Martin, M. M. MacInnes, A. C. Olson, B. L. Scott, D. K. Shuh, M. P. Wilkerson, *J. Am. Chem. Soc.* **2013**, *135*, 2279-2290;

c) J. A. H. Frey, G. N. Cloke, S. M. Roe, *Organometallics* **2015**, *34*, 2102–2105.
[12] C. A. P. Goodwin, F. Tuna, E. J. L. McInnes, S. T. Liddle, J. McMaster, I. J. Vitorica-Yrezabal, D. P. Mills, *Chem. Eur. J.* **2014**, *20*, 14579-14583.
[13] a) J. G. Reynolds, A. Zalkin, D. H. Templeton, N. M. Edelstein, *Inorg. Chem.* **1977**, *16*, 599-603; b) J. G. Reynolds, A. Zalkin, D. H. Templeton, N. M. Edelstein, L. K. Templeton, *Inorg. Chem.* **1976**, *15*, 2498-2502.
[14] R. B. MacMullin, *Vol. 43178*, US, **1935**.
[15] M. J. Crawford, P. Mayer, H. Noth, M. Suter, *Inorg. Chem.* **2004**, *43*, 6860-6862.
[16] a) P. J. Fagan, J. M. Manriquez, S. H. Vollmer, C. S. Day, V. W. Day, T. J. Marks, *J. Am. Chem. Soc.* **1981**, *103*, 2206-2220; b) E. M. Matson, P. E. Fanwick, S. C. Bart, *Organometallics* **2011**, *30*, 5753-5762; c) A. L. Arduini, J. D. Jamerson, J. Takats, *Inorg. Chem.* **1981**, *20*, 2474-2479; d) S. C. Bart, C. Anthon, F. W. Heinemann, E. Bill, N. M. Edelstein, K. Meyer, *J. Am. Chem. Soc.* **2008**, *130*, 12536-12546.
[17] C. Camp, L. Chatelain, C. E. Kefalidis, J. Pecaut, L. Maron, M. Mazzanti, *Chem. Commun.* **2015**, *51*, 15454-15457.
[18] A.-C. Schmidt, F. W. Heinemann, L. Maron, K. Meyer, *Inorg. Chem.* **2014**, *53*, 13142-13153.
[19] L. Barluzzi, L. Chatelain, F. Fadaei-Tirani, I. Zivkovic, M. Mazzanti, *Chem Sci* **2019**, *10*, 3543-3555.
[20] B. A. MacKay, M. D. Fryzuk, *Chem Rev* **2004**, *104*, 385-401.
[21] O. Cooper, C. Camp, J. Pecaut, C. E. Kefalidis, L. Maron, S. Gambarelli, M. Mazzanti, *J. Am. Chem. Soc.* **2014**, *136*, 6716-6723.

CHAPTER 3

Facile CO cleavage by a Multimetallic CsU_2 Nitride Complex

Introduction[1]

Carbon monoxide is an inexpensive and readily available C_1 feedstock used in industry for the production of a wide variety of chemicals, such as methanol, acetic acid, phosgene, and hydrocarbons.[1] A key step in Fischer-Tropsch hydrocarbon production from CO and H_2 is the cleavage of the CO triple bond, which is the strongest chemical bond (dissociation energy at 298 K: 1076 kJ mol^{-1}). This process requires the use of heterogeneous transition-metal catalysts at elevated temperatures. [2] The cleavage of the CO bond under mild conditions is an important fundamental challenge in the search for new routes for the production of functionalized organic molecules from CO. The direct addition of CO to a metal nitride is a rare event observed only for highly nucleophilic nitride complexes of d-block transition metals, such as V, Fe, and Hf.[3] Notably, a few terminal monometallic nitrido complexes and only one example of nitride-bridged dimetallic complex [3f] effect nitrogen-atom transfer to CO to afford cyanate, which in some cases is spontaneously extruded.[3d] Reductive carbonylation of monometallic U(V) and U(IV) nitrides by CO to afford the isocyanate ligand has also been recently reported.[3e] Several examples of CO cleavage by metal complexes have been reported,[4] and these reactions often yield metal-carbide complexes and oxo clusters. The binding [5] and the reduction [6] of CO by uranium(III) complexes has been demonstrated. Several examples of CO reductive homologation effected by uranium(III) systems with the formation of deltate,[7] squarate,[7b, 8] or ethynediolate dianions [7b, 9] have also been identified. We showed in the previous chapter the high nucleophilic character of the nitride-bridged diuranium complex $[Cs\{[U(OSi(O^tBu)_3)_3]_2(\mu\text{-}N)\}]$, **1**,[10] which reacted under ambient conditions with CO_2 and CS_2. The reaction led to the formation of C–N bonds

[1] Portions of this chapter have been published: M. Falcone, C. E. Kefalidis, R. Scopelliti, M. Mazzanti, *Angewandte Chemie Int. Ed.*, **2016**, *55*, 12290
Author contributions: M.F. carried out the synthetic experiments and analysed the experimental data; C.E.K. performed the DFT calculations; R.S. performed the X-ray single crystal structure analyses. M.M. and M.F. wrote the manuscript.

yielding cyanate, thiocyaniate and unprecedented dicarbamate species. In the present chapter we describe how the high nucleophilicity of **1**, and the multimetallic cooperativity of the CsU_2 core, lead to complete cleavage of the CO triple bond to yield cyanide. The cyanide ligand can be readily transferred to electrophiles, such as MeOTf and Me_3SiI, resulting in the stoichiometric synthesis of organic nitriles.

Results and discussion

The addition of stoichiometric or excess amounts of CO or ^{13}CO (1 equiv.) to the diuranium(IV) complex $[Cs\{[U(OSi(O^tBu)_3)_3]_2(\mu\text{-}N)\}]$, **1** in toluene at room temperature led to an immediate colour change of the solution from brown to light blue (Scheme 1). The proton NMR showed the disappearance of the peak assigned to complex **1** and the appearance of a single new signal at –1.34 ppm, assigned to complex $[Cs\{[U(OSi(O^tBu)_3)_3]_2(\mu\text{-}CN)(\mu\text{-}O)\}]$, **2**.

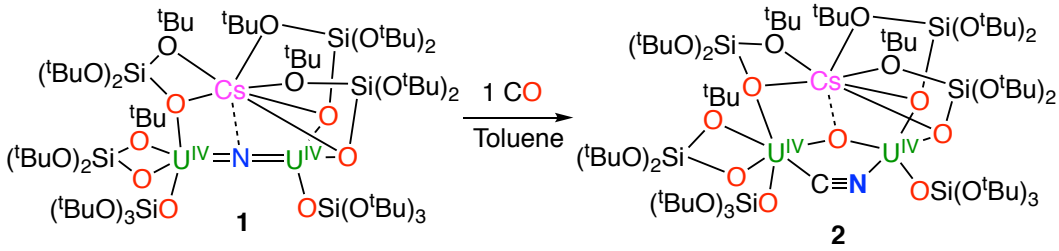

Scheme 1. CO cleavage reaction effected by complex 1 under ambient conditions to afford the complex $[Cs\{[U(OSi(O^tBu)_3)_3]_2(\mu\text{-}CN)(\mu\text{-}O)\}]$, **2**.

Blue crystals of the complex $[Cs\{[U(OSi(O^tBu)_3)_3]_2(\mu\text{-}CN)(\mu\text{-}O)\}]$, **2** were isolated in 60% yield at –40 °C. Proton NMR studies showed that complex **2** was stable in toluene at room temperature for several hours. The ^{13}C NMR spectrum of **2** showed the presence of a signal at 866 ppm, which was assigned to the ^{13}CN ligand. Traces of decomposition, evident from a new NMR peak assigned to the $[U(OSi(O^tBu)_3)_4]$ complex, appeared only after three days, probably as a result of ligand scrambling. The solid-state structure of **2** (Figure 1) shows the presence of a diuranium(IV) complex in which two $[U(OSi(O^tBu)_3)_3]$ framents are bridged by one oxo ligand and one cyanide group. This structure indicates that the highly nucleophilic character of the bridging nitride promotes the ready cleavage and deoxygenation of carbon monoxide to afford a N≡C triple bond and a bridging oxo group. The resulting cyanide ligand adopts a bridging mode with U–C (2.610(7) Å) and U–N (2.576(6) Å) bond distances comparable to those reported for cyanide-bridged diuranium(IV)

complexes (2.549(8) - 2.583(2) Å).[11] The N–C bond distance (1.155(9) Å) compares well to that found in cyanide-bridged diuranium(IV) complexes (1.177(4) Å). [11b]

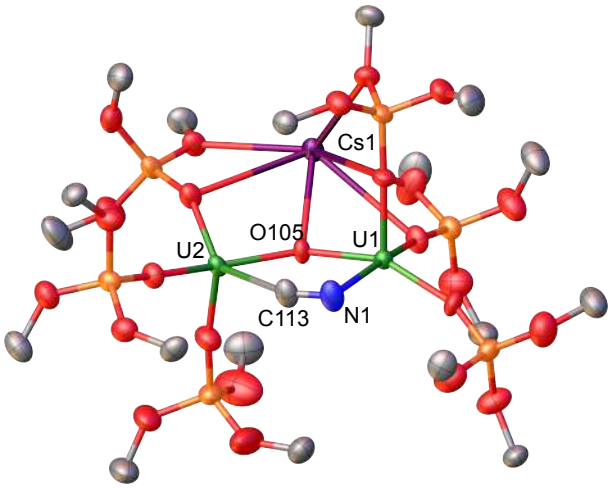

Figure 1. Solid-state molecular structure of [Cs{[U(OSi(O^{t}Bu)$_3$)$_3$]$_2$(μ-CN)(μ-O)}], **2**. Thermal ellipsoids set at 50% probability. Hydrogen atoms and methyl groups were omitted for clarity. Selected bond lengths [Å]: U1–O105 2.124(4), U1–N1 2.576(6), N1–C113 1.155(9), U2–O105 2.144(4), U2–C113 2.610(7).

The structure of complex **2** was determined by X-ray crystallography. In complexes containing very heavy metals, it is quite hard to differentiate between O and N atoms by X-ray crystallography, but a comparative analysis, based on the displacement parameters and on the R factors, with the alternative structure resolution as a putative nitride-carbonyl complex [Cs{[U(OSi(O^{t}Bu)$_3$)$_3$]$_2$(μ-CO)(μ-N)}], strongly supports the presence of the oxo-cyanide complex **2**. In addition, the irreversible binding of neutral CO to a uranium(IV) nitride is rather improbable. The only reported uranium complex containing a bridging CO ligand was identified in a dinuclear U(III)U(IV) complex. However in this case the complex featured a reduced CO^- ligand rather than a neutral CO ligand.[6] No evidence of crystallographic disorder between the C and N atoms was observed.

The outcome of the reaction of **1** with CO is very different from that recently reported for the reaction of mononuclear uranium nitride complexes with CO, which led to the reductive carbonylation of U(V) and U(VI), thus affording U(III)–OCN and U(IV)–OCN complexes, respectively.[3e] This remarkable difference in reactivity shows the importance of multimetallic cooperativity in CO scission. To confirm the presence of a cyanide ligand in complex **2** and to investigate the possibility of transferring the cyanide ligand to organic substrates, we treated complex **2** with Me_3SiI and with MeOTf (Scheme 2).

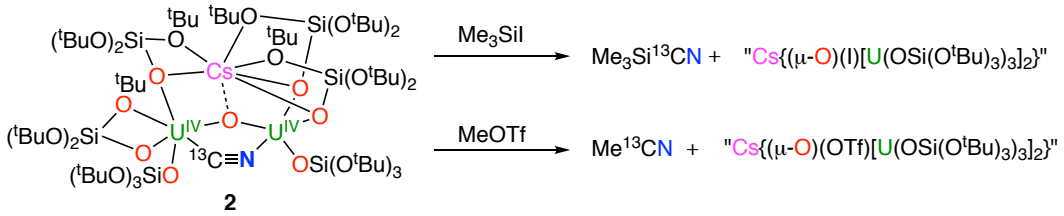

Scheme 2. Reactions of **2** with the electrophiles MeOTf and Me_3SiI to afford MeCN and Me_3SiCN. OTf = trifluoromethanesulfonate.

The reaction of $[Cs\{[U(OSi(O^tBu)_3)_3]_2(\mu\text{-}^{13}CN)(\mu\text{-}O)\}]$ with Me_3SiI (1 equiv.) at room temperature in benzene led to an immediate colour change and afforded a white suspension. The ^{13}C NMR spectrum of the reaction mixture showed the disappearance of the peak assigned to the uranium bound ^{13}CN group and the appearance of a new signal at 126.3 ppm, which was assigned to the cyanide group of $Me_2Si^{13}CN$ (Figure 2). After the addition of Me_3SiI, proton NMR studies showed the immediate disappearance of the peak assigned to complex **2** and the appearance of only one new major signal at –1 ppm. This signal was assigned to an intermediate oxo iodide species "$[Cs\{[U(OSi(O^tBu)_3)_3]_2(\mu\text{-}I)(\mu\text{-}O)\}]$". This species decomposes rapidly and after 48 h only a peak assigned to $[U(OSi(O^tBu)_3)_4]$ was observed. The formation of a stable μ-oxo iodide complex and $Me_3Si^{13}CN$ was observed in the reaction of the dihafnium oxo cyanide complex $[\{(\eta^5\text{-}C_5Me_4H)_2Hf(NCO)\}(\mu\text{-}O)\{(\eta^5\text{-}C_5Me_4H)_2Hf(CN)\}]$ with Me_3SiI.[12] The formation of $[U(OSi(O^tBu)_3)_4]$ from the intermediate iodide is the result of ligand scrambling. Ligand scrambling leading to the formation of bis(oxo) complexes and unidentified products was previously observed for the diuranium(IV) oxo- and cyanate-bridged complex (see chapter 2).[10b]

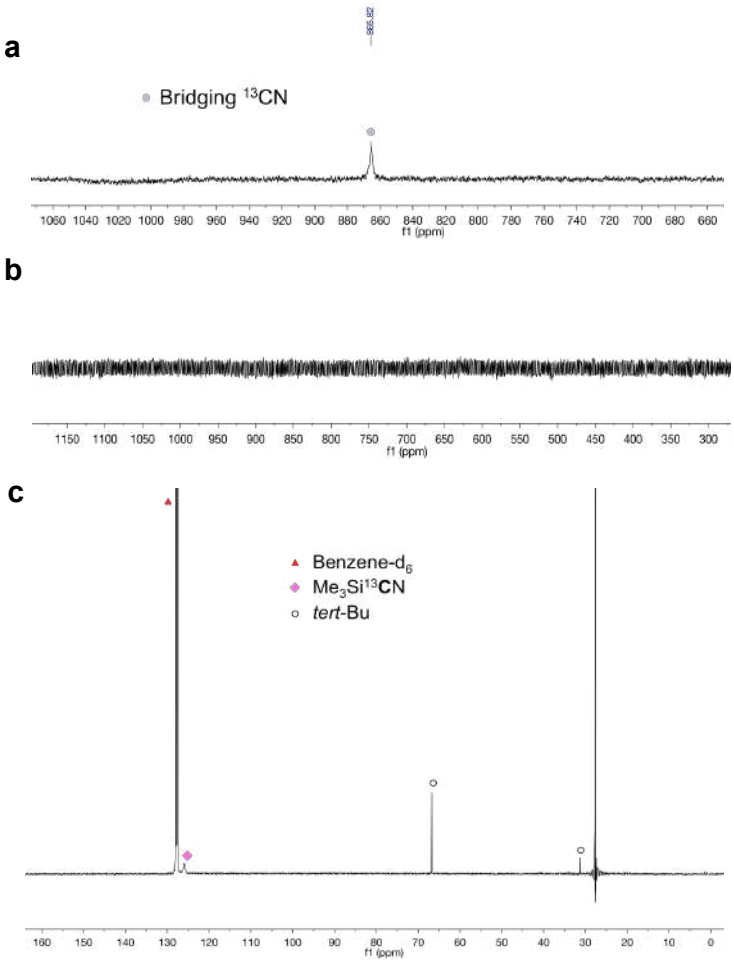

Figure 2. ^{13}C NMR (400 MHz, benzene-d_8, 298 K) of crystals of complex **2** (**a**); ^{13}C NMR (400 MHz, benzene-d_8, 298 K) 48 h after the addition of Me_3SiI to complex **2** showing the disappearance of the signal assigned to the bridging ^{13}CN (**b**); ^{13}C NMR (400 MHz, benzene-d_8, 298 K) 48 h after the addition of Me_3SiI to complex **2** (**c**).

The reaction of **2** with MeOTf proceeded more slowly, and after 24 h at room temperature a large amount of starting material was still present. The ^{1}H NMR spectrum in toluene-d_8 after 24 h showed the presence of the signal assigned to $[U(OSi(O^tBu)_3)_4]$ and a broad signal at 0.63 ppm assigned to $CH_3{}^{13}CN$. The formation of $CH_3{}^{13}CN$ was confirmed by the presence of a signal at 113 ppm in the ^{13}C NMR spectrum. The cyanide-alkylation reaction was complete after overnight heating at 55 °C. NMR studies did not show evidence of products arising from the alkylation of the bridging oxo ligand. Overall, the successive addition of CO and MeOTf or Me_3SiI to complex **1** resulted in the conversion of CO into organic nitrile compounds.

For comparison, we also investigated the reactivity of the nitride complex **1** with MeOTf. The reaction of **1** with MeOTf (1 equiv.) at room temperature resulted in a slow (24 hours) colour change of the solution from brown to green and a mixture of complexes **3** and **4** (Scheme 3). Storage of the solution at −40 °C resulted in the

isolation of light blue crystals of the bis(imido) complex [{U^V(OSi(OtBu)$_3$)$_3$}$_2$(μ-NMe)$_2$], **4**.

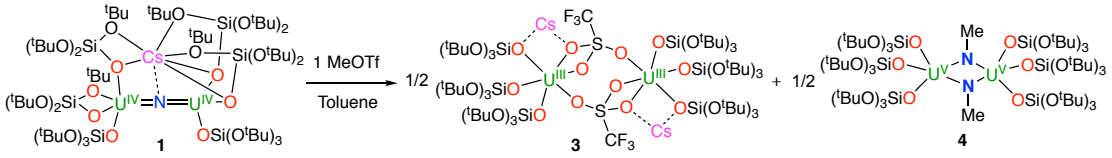

Scheme 3. Methylation reaction of complex **1** with MeOTf to form complexes **3** and **4**.

Attempts to isolate the two products in a pure form from this reaction were not successful. The reaction is faster when **1** is treated with 2 equivalents of MeOTf, but the same mixture of complexes **3** and **4** is obtained, as indicated by the proton NMR spectrum. However, in this case storage of the reaction mixture at −40 °C for 24 h resulted in the isolation of green-blue crystals of the complex [Cs_2{U(OSi(O^{t}Bu)$_3$)$_3$}$_2$(μ-OTf)$_2$]·2(C_7H_8), **3** in 60% yield. The crystallization of complex **3** is probably favored by the presence of an excess of MeOTf in the solution. Subsequent cooling of the mother liquor afforded a few crystals of complex **4**. Owing to its low stability, the isolation of complex **4** in sufficient amounts for further characterization was not possible. The low stability of the U(V) imido complex **4** is consistent with the observed instability of the previously reported "[U^V(OSi(OtBu)$_3$)$_3$}(NR)]" (R= adamantly) intermediate, which could not be isolated because it rapidly disproportionate to afford [U(IV)(OSi(O^{t}Bu)$_3$)$_4$] and [U(VI)$_2$(NR)$_4$(OSi(O^{t}Bu)$_3$)$_4$].[10a]

The solid-state structure of **3** (Figure 3) consists of a diuranium(III) complex where two [U(OSi(O^{t}Bu)$_3$)$_3$] fragments are bridged by two triflate anions, each one binding the two uranium centres and a cesium cation in a μ_3:κ^2(O,O):η^1-O fashion. The mean U–$O_{siloxide}$ bond length is similar (2.165(3) Å) to the U–$O_{siloxide}$ distance found in the U(IV) complex **1** (U–O_{avg} 2.19(3) Å) and in the diuranium(III) tris(siloxide) complex [U(OSi(O^{t}Bu)$_3$)$_2$(μ-OSi(O^{t}Bu)$_3$)]$_2$ (2.193(4) Å).[13] The U−U distance is longer (5.636 Å) than that found in the [U(OSi(O^{t}Bu)$_3$)$_2$(μ-OSi(O^{t}Bu)$_3$)]$_2$ complex (3.9862(2) Å).

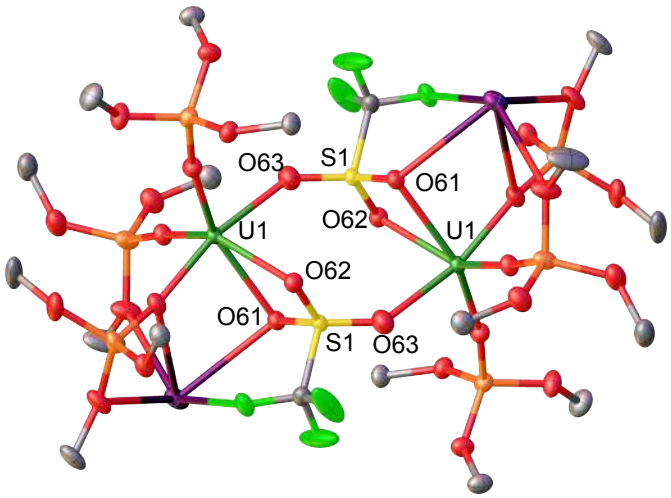

Figure 3. Solid-state molecular structure of $[Cs_2\{U(OSi(O^tBu)_3)_3\}_2(\mu\text{-}OTf)_2]$, **3**. Thermal ellipsoids set at 50% probability. Hydrogen atoms and methyl groups were omitted for clarity. Selected bond lengths [Å]: U1–O61 2.537(3), U1–O62 2.479(3), U1–O63 2.323(3), S1–O61 1.504(3), S1–O62 1.492(3), S1–O63 1.462(3), U1–U1A 5.6356(1).

The solid-state structure of **4** was determined by X-ray crystallography (Figure 4). The unit cell consists of two independent diuranium(V) complexes, **4a** and **4b** where two $[U(OSi(O^tBu)_3)_3]$ fragments are bridged by two methylimido ligands. The mean $U–O_{siloxide}$ bond length (2.110(5) Å) is slightly shorter than that found in the U(V) terminal imido complex $[K(18c6)][U(NSiMe_3)(OSi(O^tBu)_3)_4]$ ($U1–O_{avg}$ 2.16(2) Å).[10a] The average U–U distance in **4** is 3.8612(6) Å. The U–N distances in the two complexes are slightly different (2.319(6) Å in **4a** and 2.309(6) Å in **4b**). These values can be compared to those found in the rare examples of previously reported imido-bridged diuranium(V) complexes (2.387(5) - 2.078(5) Å).[14]

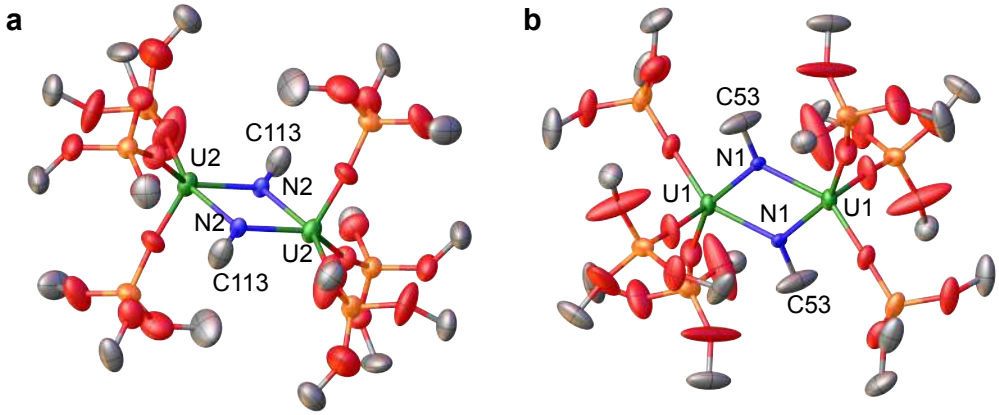

Figure 4. Solid-state molecular structure of $[\{U^V(OSi(OtBu)_3)_3\}_2(\mu\text{-}NMe)_2]$, **4, 4a (a)** and **4b (b)**. Thermal ellipsoids set at 50% probability. Hydrogen atoms and methyl groups were omitted for clarity. Selected bond lengths [Å]: U(1)–N(1)#1 2.314(6), U(1)–N(1) 2.324(6), U(1)–U(1)#1 3.8735(5), U(2)–N(2) 2.309(6), U(2)–N(2)#2 2.309(6), U(2)–U(2)#2 3.8489(6), N(1)–C(53) 1.429(13), N(1)–U(1)#1 2.314(6), N(2)–C(113) 1.441(14), N(2)–U(2)#2 2.309(6).

The formation of imide complexes from the alkylation of nucleophilic bridging nitrides has been reported [15] but did not lead to valence disproportionation. In contrast, the alkylation of **1** promotes the disproportionation of the metal center, leading to the transformation of two U(IV) cations into a U(V) and a U(III) complex. This is exceptional reactivity since U(IV) complexes are generally much more stable than their U(III) and U(V) analogues, which are usually more prone to disproportionation reactions.[16] For instance, the diuranium(IV) imido-bridged complex, $[(MeC_5H)_4U_2(\mu\text{-}NPh)_2]$, was obtained from the comproportionation reaction of the imido complex $(MeC_5H)_3U^{V}NPh$ with the tris-(cyclopentadienyl) complex $[(MeC_5H_5)_3U(III)]$.[17] The reactivity of complex **1** could be explained by the presence of asymmetric bonding in the U(IV)–N–U(IV) core that may be formulated as a mixed valent U(V)–N–U(III) complex, but this formulation is not supported by comparison of the optimized geometry with the experimental metrical parameters in complex **1** (Figure 5).[10a]

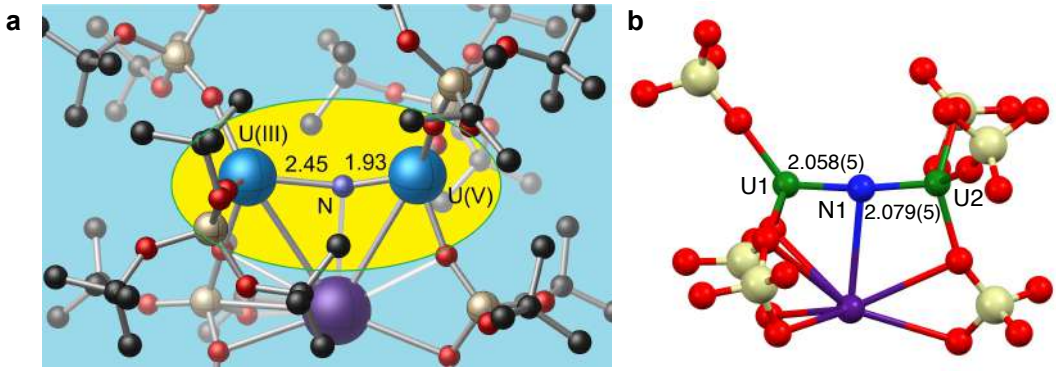

Figure 5. 3D representation of the optimized geometry together with the U(III)-N and U(V)-N bonding distances [Å] for the putative mixed valence complex **1** (**a**); metrical parameters for the solid-state structure of **1** (**b**).[10a]

The unique reactivity of complex **1** towards CO and MeOTf substrates, was further explored by examining plausible reaction pathways with calculations at the DFT level of theory.[18]

Full systems without any simplifications or geometrical constraints were considered in the calculations.[19] In the computed profile for the reaction of **1** with MeOTf (Figure 6) the first step involves the coordination of the MeOTf to complex **1**.

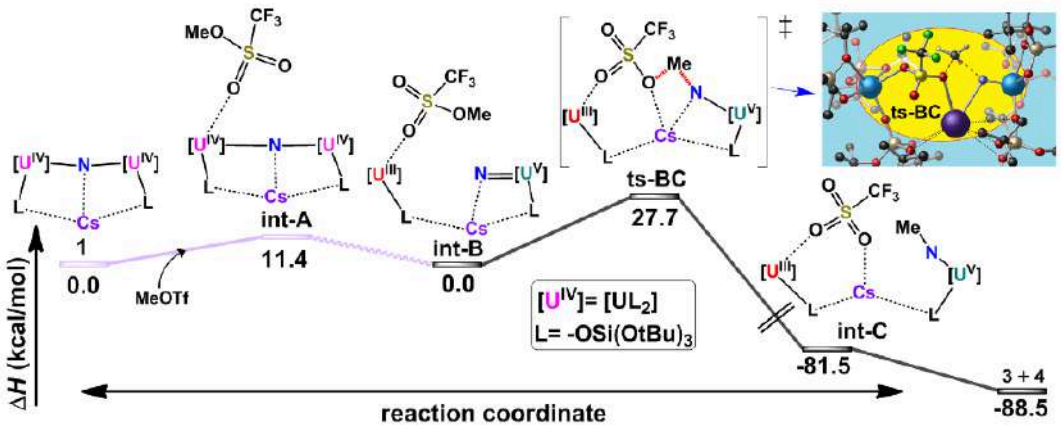

Figure 6. DFT computed enthalpy profile for the reaction of **1** with MeOTf to afford **3** and **4** at room temperature (the values are give in kcal mol^{-1}) and 3D representation of **ts-BC**.

In the non-symmetric coordination environment of the U–N–U core resulting from MeOTf binding, the mixed-valent intermediate **int-B** is enthalpically more stable compared to the charge-delocalized **int-A**, by 11.4 kcal/mol (22 kcal/mol more stable with respect to the separated reactants). Interestingly, no direct methyl-transfer TS from MeOTf to the nitride (in an outer-sphere-type mechanism) could be located, as every attempt lead to either **int-A** or **int-B**. The Cs^+ plays a crucial role in holding the fragments together in the dinuclear mixed valence complex, but also in stabilizing the anionic, monomeric formally U(V) nitride molecular part. From **int-B**, the system can reach the transition state **ts-BC** where the methyl group is transferred from the triflate moiety to terminal nitride. This reaction can be better described as a methyl transfer from oxygen to nitrogen at the Cs atom rather than at the uranium center, as illustrated nicely in Figure 6. Eventually, the uranium atoms act solely as Lewis acid centers to activate the nitride and methyl triflate ligands.

ts-BC leads to the formation of complex **int-C**, which is a mixed-valence bimetallic complex involving two fragments: a U(III) sulfonate (Cs) and a U(V) imido. The formation of the latter, is highly favourable (−81.5 kcal/mol). Complex **int-C** then undergoes a dimerization process to yield the two homoleptic U(III) and U(V) complexes, **3** and **4** respectively. This last step is computed to be favourable by 7.0 kcal/mol, in line with experimental observations.

The computational mechanistic investigation of the reaction between complex **1** and CO was also carried out (Figure 7).

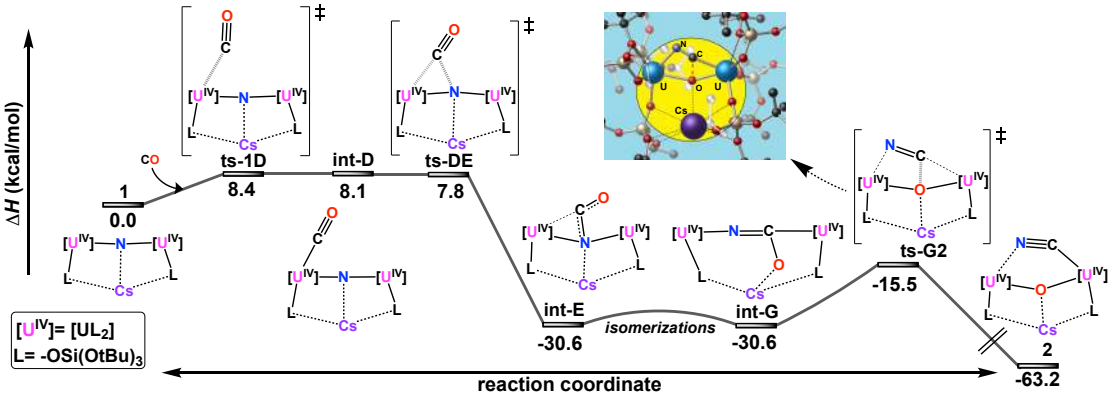

Figure 7. DFT computed enthalpy profile for the reaction of CO with complex **1** to afford complex **2** at room temperature (the values are given in kcal mol^{-1}). The insert shows a 3D representation of the active core of **ts-G2**.

The closest, unique analogue of such exceptional reactivity is the high temperature (110 °C) cleavage of CO by a diazenido di-hafnium complex to yield a μ-oxo/μ-cyanido species that proceeds through the formation of a stable oxamidide intermediate.[12] Computational and experimental studies suggest that this stable oxamidide species forms via an unstable nitride intermediate.[20] However, the uranium nitride reactivity appears to be significantly different. First the CO molecule binds one uranium center with an activation barrier of 8.6 kcal/mol, yielding an unstable CO adduct (endothermic formation of 8.1 kcal/mol). Subsequently, the CO molecule undergoes a barrier-less migratory insertion onto the U–nitride bond. This process is favored by the coordination of the Cs^+ cation to the nitride ligand in a *trans* position with respect to the bound CO. Such binding mode results in the pyramidalization of the nitride ligand that enhances its nucleophilic character. The insertion yields **int-E**, that is a η^2(C,N):κ^2(O,N) bimetallic complex.

The **int-E** then undergoes a isomerization process assisted by the Cs cation to yield the isoenergetic but reactive isomer **int-G** (see SI for the full isomerization part). The geometry of complex **int-G** is quite interesting as the cyanate ligand exhibits a η^1-N coordination with one uranium centre and η^2(C,O) with the other uranium (η^1,η^2 is a classical coordination for bimetallic uranium complexes of triatomic molecules such as CO_2 [13]), but also develops an interaction with the Cs cation that exemplifies the cooperative effect of the Cs cation. From **int-G**, an easy elimination of a CN^- anion (i.e., full C–O bond scission from carbon monoxide) takes place with an activation barrier of 15.1 kcal/mol. Interestingly, at **ts-G2**, it appears that the elimination occurs *trans* to the Cs cation, which acts as a Lewis acid activator for the C–O bond

disruption. Once more, the heteropolymetallic cooperativity is important in explaining the observed facile reactivity.

The cesium cation is found to play an important role in the calculated mechanism; however, it is not necessary to achieve CO cleavage. Indeed, when the butyl ammonium diuranium(IV) bridging nitride is prepared, and in situ reacted with ^{13}CO, the ^{13}C NMR spectrum in D_2O of the crude mixture reveals the presence of cyanide (Scheme 4), confirming that the combination of nucleophilicity of the nitride and oxophilicity of the uranium atoms is enough to cleave the CO triple bond, even in absence of the cesium cation in the core. However, the reaction does not allow the isolation of the cyanide oxide product due to ligand scrambling and formation of multiple species.

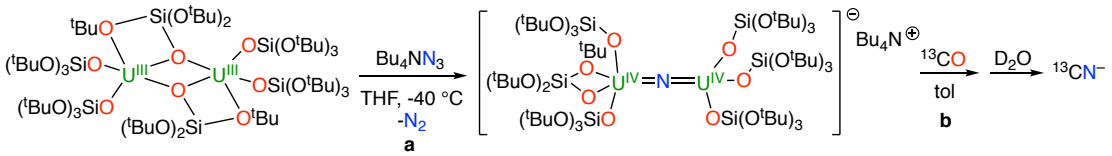

Scheme 4. Reaction of the diuranium(III) siloxide complex with butyl ammonium azide to give the bridging nitride with butyl ammonium as counter cation (**a**); in situ addition of carbon monoxide and subsequent release of the cyanide in D_2O (**b**).

Attempt to coordinate the cesium cation with cryptand did not succeed in removing the cation from the pocket formed by the siloxide ligands and the nitride. When cryptand was added to a solution of complex **1**, no shift of the peak assigned to the siloxide was observed and the reaction with CO proceeded giving the same product, complex **2**.

Conclusions

The high nucleophilic reactivity of the nitride ligand in the heterodimetallic **1** leads to the first example of complete cleavage of CO by a nitride complex under ambient conditions. The CO cleavage affords a complex containing two U(IV) cations bridged by an oxo and a cyanide group. This complex can transfer the cyanide group to electrophiles leading to N–C bond formation and release of organic molecules such as CH_3CN or CH_3SiCN. An exceptional outcome is also observed for the reaction of the U(IV) with the electrophilic MeOTf leading to the unprecedented valence disproportionation of U(IV) to U(III) and U(V) with concomitant formation of a U(V) imido complex. In this case, not only ligand based reactivity of the bridging nitride

was observed but also metal redox activity was involved. The DFT studies support the presence of a multimetallic cooperative effect of the two uranium centres and of the Cs^+ cation in the complete cleavage of CO and in the methyl transfer to the uranium-bound nitride. These results encouraged us to pursue the use of the easily available CO substrate to build C–N or C–H bonds (see next chapters) and may open new pathways for the synthesis of valuable chemicals from CO as a source of carbon.

Experimental

General Considerations. All manipulations were carried out under a dry and oxygen free argon atmosphere using Schlenk techniques and an MBraun glovebox equipped with a purifier unit. The water and oxygen levels were always kept at less than 0.1 ppm. Glassware was dried overnight at 130°C before use. Compounds were characterized by elemental analysis, ^{1}H and ^{13}C NMR, IR, single-crystal X-ray diffraction. Reaction pathways were examined by performing calculations at the DFT level of theory. Further Details are provided in the Supplementary Information.

^{1}H NMR experiments were carried out using NMR tubes adapted with J. Young valves. ^{1}H NMR spectra were recorded on Bruker 400 MHz. NMR chemical shifts are reported in ppm with solvent as internal reference.

Elemental analyses were performed with a Thermo Scientific Flash 2000 Organic Elemental Analyzer.

Starting materials. Unless otherwise noted, reagents were purchased from commercial suppliers and used without further purification. The solvents were purchased from Aldrich or Eurisotop (deuterated solvents) in their anhydrous form, conditioned under argon and vacuum distilled from K/benzophenone (toluene and THF). $[Cs\{[U(OSi(OtBu)_3)_3]_2(\mu\text{-}N)\}]$, **1** was prepared according to the published procedure.[10a]

Caution: Depleted uranium (primary isotope ^{238}U) is a weak α-emitter (4.197 MeV) with a half-life of 4.47×10^9 years. Manipulations and reactions should be carried out in monitored fume hoods or in an inert atmosphere glovebox in a radiation laboratory equipped with α- and β-counting equipment.

Synthesis of complex [Cs{[U(OSi(O^{t}Bu)$_3$)$_3$]$_2$(μ-CN)(μ-O)}], 2.

CO (0.03 mmol, 17.9 mbar, 1 eq) was added at room temperature to an NMR tube containing a red brown solution of [Cs{[U(OSi(OtBu)$_3$)$_3$]$_2$(μ-N)}] (58.7 mg, 0.03 mmol, 1 eq), complex **1** in toluene-d$_8$ (0.5 mL). The solution turned light blue. Blue single crystals, suitable for XRD studies, formed after letting stand the solution for 24 h at -40 °C. The crystals were collected and dried *in vacuo* to give 35 mg of complex [Cs{[U(OSi(O^{t}Bu)$_3$)$_3$]$_2$(μ-CN)(μ-O)}], **2** (60% yield). The same reaction was performed also with labelled ^{13}CO. IR, n^{13}**CN** (cm^{-1}): 2037 (bridging ^{13}CN). ^{1}H NMR (400 MHz, toluene-d$_8$, 298 K): δ = −1.34 (s, 162H, CH$_3$ terminal siloxide). ^{1}H NMR (400 MHz, toluene-d$_8$, 298 K) of crystals: δ = −1.34 (s, 162H, CH$_3$ terminal siloxide). ^{13}C NMR of crystals (400 MHz, benzene-d$_6$, 298 K): δ = 865.82 (bridging ^{13}CN). Anal. Calcd for [Cs{[U(OSi(O^{t}Bu)$_3$)$_3$]$_2$(μ-CN)(μ-O)}] ($C_{73}H_{162}Cs_1N_1O_{25}Si_6U_2$): C, 39.29; H, 7.32; N, 0.63. Found: C, 39.18, H, 7.76, N, 0.63.

Reaction of complex [Cs{[U(OSi(O^{t}Bu)$_3$)$_3$]$_2$(μ-^{13}CN)(μ-O)}], 2, with MeOTf

Complex [Cs{[U(OSi(O^{t}Bu)$_3$)$_3$]$_2$(μ-^{13}CN)(μ-O)}] (15.7 mg, 0.007 mmol, 1 eq) was dissolved in 0.5 mL of benzene-d$_8$ and MeOTf was added (7 mL of a solution 1M in C_6D_6, 1 eq). The reaction proceeds slowly affording the complex [U(OSi(OtBu)$_3$)$_4$] and Me^{13}CN both detected by ^{1}H and ^{13}C NMR. Within 3 days heating at 50 °C, the decomposition is completed and the species [U(OSi(OtBu)$_3$)$_4$(Me^{13}CN)] was detected by ^{1}H and ^{13}C NMR. After addition of an excess of pyridine (5 mL, 10 eq) free Me^{13}CN was detected by ^{1}H (doublet at 0.59 ppm) and ^{13}C NMR. ^{1}H NMR after 1h (400 MHz, benzene-d$_8$, 298 K): δ = 0.66 (CH$_3$^{13}CN). ^{13}C NMR after 1h (400 MHz, benzene-d$_8$, 298 K): δ = 113.15 (CH$_3$^{13}CN). ^{1}H NMR after heating (400 MHz, benzene-d$_8$, 298 K): δ = 1.11 (^{t}Bu of complex [U[(OSi(OtBu)$_3$)$_4$(Me^{13}CN)]). ^{13}C NMR after heating (400 MHz, benzene-d$_8$, 298 K): δ = 114.4 (coordinated CH$_3$^{13}CN). ^{1}H NMR (400 MHz, benzene-d$_8$, 298 K) after addition of pyridine: δ = 0.59 (doublet, free Me^{13}CN). ^{13}C NMR (400 MHz, benzene-d$_8$, 298 K) after addition of pyridine: δ = 115.75 (free Me^{13}CN).

Reaction of complex [Cs{[U(OSi(O^{t}Bu)$_3$)$_3$]$_2$(μ-^{13}CN)(μ-O)}], 2, with Me$_3$SiI

The addition of 8 mL of a 0.64M solution of Me$_3$SiI (0.005 mmol, 1 eq) to a light blue solution of complex [Cs{[U(OSi(O^{t}Bu)$_3$)$_3$]$_2$(μ-^{13}CN)(μ-O)}] (11.4 mg, 0.005 mmol, 1

eq) led to an immediate colour change resulting in a white suspension that after centrifugation and removal of CsI afforded a colourless solution. The presence of $Me_3Si^{13}CN$ was detected by ^{13}C NMR. The solution turns light green within 48 hours at room temperature, yielding quantitatively $[U(OSi(OtBu)_3)_4]$ (titrated by NMR with naphthalene as reference). ^1H NMR immediately after Me_3SiI addition (400 MHz, benzene-d_6, 298 K): $\delta = -1.05$ (s, 162H, CH_3 terminal siloxide). ^{13}C NMR (400 MHz, benzene-d_6, 298 K): δ = 126.7 (Me_3Si^{13}**C**N). ^1H NMR after 48 hours (400 MHz, benzene-d_6, 298 K): δ = 1.09 (CH_3 terminal siloxide of complex $U[OSi(O^tBu)_3]_4$).

Reaction of complex [Cs{[U(OSi(OtBu)$_3$)$_3$]$_2$(μ-N)}], 1, with 1 eq of MeOTf

To a red brown solution of complex [Cs{[U(OSi(OtBu)$_3$)$_3$]$_2$(μ-N)}] (9.6 mg, 0.0044 mmol, 1 eq) in toluene-d_8 (0.5 mL), 5.5 mL of a 0.8M solution of MeOTf in toluene-d_8 (0.0044 mmol, 1 eq) were added at room temperature. The reaction is not immediate. After 24 hours at -40 °C the solution turns light blue green.

The proton NMR (Appendix 2, Figure S17) shows the presence of on broad signal assigned to complex [{U(OSi(OtBu)$_3$)$_3$}$_2$(μ-NMe)$_2$], **4**, and one narrow signal assigned to complex [Cs$_2${U(OSi(OtBu)$_3$)$_3$}$_2$(μ-OTf)$_2$], **3.** Correct integration of the signals was prevented by the poor resolved shape of the signal of complex **4**. It was possible to isolate light blue crystals of the complex **4**, after 24h at -40 °C. Attempts to isolate this complex in larger amount lead to the isolation of mixtures of complexes **3** and **4**.

Reaction of complex [Cs{[U(OSi(OtBu)$_3$)$_3$]$_2$(μ-N)}], 1, with 2 eq of MeOTf

To a red brown solution of complex [Cs{[U(OSi(OtBu)$_3$)$_3$]$_2$(μ-N)}] (46.9 mg, 0.02 mmol, 1 eq) in toluene-d_8 (1.5 mL), 4.8 mL of MeOTf were added (0.04 mmol, 2 eq) at room temperature. After 1 hour stirring at room temperature the solution turns light blue green. Green blue single crystals, suitable for XRD studies, formed after letting the solution stand 24 h at -40 °C. The crystals were collected and dried *in vacuo* to afford the complex [Cs$_2${U(OSi(OtBu)$_3$)$_3$}$_2$(μ-OTf)$_2$]·2(C_7H_8), **3·2(C_7H_8)** in 60% yield (18.0 mg). The supernatant after standing 24 h at -40°C afforded a few crystals of the [{U(OSi(OtBu)$_3$)$_3$}$_2$(μ-NMe)$_2$], complex **4**. The isolation in larger amounts of the complex **4** was prevented by its low stability and by co-crystallization of complex **3** and decomposition products. ^1H NMR (400 MHz, toluene-d_8, 298 K): δ = –2 - 1

(broad, CH_3 siloxide of **4**), –2.45 (CH_3 siloxide of complex **3**). ^{1}H NMR of crystals (400 MHz, toluene-d_8, 298 K): δ = –2.45 (CH_3 siloxide of complex **3**. Anal. Calcd for $[Cs_2\{U(OSi(OtBu)_3)_3\}_2(\mu\text{-}OTf)_2]\cdot 2(C_7H_8)$ $(C_{74}H_{162}Cs_2O_{30}F_6S_2Si_6U_2)(C_7H_8)_2$: C, 37.40; H, 6.90; N, 0.00. Found: C, 37.68, H, 6.40, N, 0.00.

Reaction of complex $[Cs\{[U(OSi(OtBu)_3)_3]_2(\mu\text{-}N)\}]$, 1, with 18c6 crown ether and 2.2.2-cryptand

The addition of excess (2 eq) 18c6 crown ether or 2.2.2-cryptand to a solution of **1** in toluene did not lead to any change on the proton NMR spectrum indicating that the Cs cation remains bound to the complex in toluene. When the addition of 18c6 crown ether or 2.2.2-cryptand is carried out in THF a significant shift (from –0.8 ppm without cryptand to –0.38 ppm with cryptand) of the signal assigned to the complex **1** is observed indicating the formation of a ion pair. Removal of the THF and dissolution of the residue in toluene lead to the restauration of the original neutral complex **1**. Preliminary studies of the reactivity of the complex **1** with CO and MeOTf in THF in the presence of 18c6 crown ether or 2.2.2-cryptand lead to a different reaction product compared to the reactivity in toluene, but these products remain unidentified.

Bibliography

[1] G. W. Parshall, S. D. Ittel, *Homogeneous Catalysis. The Applications and Chemistry of Catalysis by Soluble Transition Metal Complexes*, 2nd ed ed., Wiley Interscience, **1992**.

[2] H. Schulz, *Appl. Catal. A* **1999**, *186*, 3-12.

[3] a) B. Askevold, J. T. Nieto, S. Tussupbayev, M. Diefenbach, E. Herdtweck, M. C. Holthausen, S. Schneider, *Nat. Chem.* **2011**, *3*, 532-537; b) J. J. Scepaniak, R. P. Bontchev, D. L. Johnson, J. M. Smith, *Angew. Chem. Int. Ed. Engl.* **2011**, *50*, 6630-6633; c) B. L. Tran, M. Pink, X. F. Gao, H. Park, D. J. Mindiola, *J. Am. Chem. Soc.* **2010**, *132*, 1458; d) J. S. Silvia, C. C. Cummins, *J. Am. Chem. Soc.* **2009**, *131*, 446-447; e) P. A. Cleaves, D. M. King, C. E. Kefalidis, L. Maron, F. Tuna, E. J. L. McInnes, J. McMaster, W. Lewis, A. J. Blake, S. T. Liddle, *Angew. Chem. Int. Ed. Engl.* **2014**, *53*, 10412-10415; f) S. P. Semproni, C. Milsmann, P. J. Chirik, *Angew. Chem. Int. Ed. Engl.* **2012**, *51*, 5213-5216.

[4] a) F. Calderazzo, U. Englert, A. Guarini, F. Marchetti, G. Pampaloni, A. Segre, *Angew. Chem. Int. Ed. Engl.* **1994**, *33*, 1188-1189; b) N. M. West, A. J.

M. Miller, J. A. Labinger, J. E. Bercaw, *Coord. Chem. Rev.* **2011**, *255*, 881-898; c) D. R. Neithamer, R. E. Lapointe, R. A. Wheeler, D. S. Richeson, G. D. Vanduyne, P. T. Wolczanski, *J. Am. Chem. Soc.* **1989**, *111*, 9056-9072; d) R. L. Miller, P. T. Wolczanski, A. L. Rheingold, *J. Am. Chem. Soc.* **1993**, *115*, 10422-10423; e) T. Shima, Z. Hou, *J. Am. Chem. Soc.* **2006**, *128*, 8124-8125; f) J. Ballmann, F. Pick, L. Castro, M. D. Fryzuk, L. Maron, *Organometallics* **2012**, *31*, 8516-8524; g) A. S. Batsanov, J. A. Cabeza, M. G. Crestani, M. R. Fructos, P. Garcia-Alvarez, M. Gille, Z. Lin, T. B. Marder, *Angew. Chem. Int. Ed. Engl.* **2016**, *55*, 4707-4710; h) P. A. Belmonte, F. G. N. Cloke, R. R. Schrock, *J. Am. Chem. Soc.* **1983**, *105*, 2643-2650; i) J. A. Buss, T. Agapie, *Nature* **2016**, *529*, 72-75; j) D. J. Knobloch, E. Lobkovsky, P. J. Chirik, *J. Am. Chem. Soc.* **2010**, *132*, 10553-10564; k) T. Matsuo, H. Kawaguchi, *J. Am. Chem. Soc.* **2005**, *127*, 17198-17199; l) H. Braunschweig, M. A. Celik, R. D. Dewhurst, S. Kachel, B. Wennemann, *Angew. Chem. Int. Ed. Engl.* **2016**, *55*, 5076-5080.

[5] a) J. G. Brennan, R. A. Andersen, J. L. Robbins, *J. Am. Chem. Soc.* **1986**, *108*, 335-336; b) J. Parry, E. Carmona, S. Coles, M. Hursthouse, *J. Am. Chem. Soc.* **1995**, *117*, 2649-2650; c) W. J. Evans, S. A. Kozimor, G. W. Nyce, J. W. Ziller, *J. Am. Chem. Soc.* **2003**, *125*, 13831-13835.

[6] I. Castro-Rodriguez, K. Meyer, *J. Am. Chem. Soc.* **2005**, *127*, 11242-11243.

[7] a) O. T. Summerscales, F. G. N. Cloke, P. B. Hitchcock, J. C. Green, N. Hazari, *Science* **2006**, *311*, 829-831; b) A. S. Frey, F. G. N. Cloke, P. B. Hitchcock, I. J. Day, J. C. Green, G. Aitken, *J. Am. Chem. Soc.* **2008**, *130*, 13816-13817.

[8] O. T. Summerscales, F. G. N. Cloke, P. B. Hitchcock, J. C. Green, N. Hazari, *J. Am. Chem. Soc.* **2006**, *128*, 9602-9603.

[9] a) P. L. Arnold, Z. R. Turner, R. M. Bellabarba, R. P. Tooze, *Chem. Sci.* **2011**, *2*, 77-79; b) S. M. Mansell, N. Kaltsoyannis, P. L. Arnold, *J. Am. Chem. Soc.* **2011**, *133*, 9036-9051; c) B. M. Gardner, J. C. Stewart, A. L. Davis, J. McMaster, W. Lewis, A. J. Blake, S. T. Liddle, *Proc Natl Acad Sci USA* **2012**, *109*, 9265-9270.

[10] a) C. Camp, J. Pecaut, M. Mazzanti, *J Am Chem Soc* **2013**, *135*, 12101-12111; b)M. Falcone, L. Chatelain, M. Mazzanti, *Angew Chem Int Edit* **2016**, *55*, 4074-4078.

[11] a)J.-C. Berthet, P. Thuery, M. Ephritikhine, *J. Chem. Soc.-Dalton Trans.* **2015**, *44*, 7727-7742; b) A. Herve, Y. Bouzidi, J.-C. Berthet, L. Belkhiri, P. Thuery, A. Boucekkine, M. Ephritikhine, *Inorg. Chem.* **2014**, *53*, 6995-7013.

[12] S. P. Semproni, G. W. Margulieux, P. J. Chirik, *Organometallics* **2012**, *31*, 6278-6287.

[13] V. Mougel, C. Camp, J. Pecaut, C. Coperet, L. Maron, C. E. Kefalidis, M. Mazzanti, *Angew. Chem. Int. Ed. Engl.* **2012**, *51*, 12280-12284.

[14] a) L. P. Spencer, E. J. Schelter, P. Yang, R. L. Gdula, B. L. Scott, J. D. Thompson, J. L. Kiplinger, E. R. Batista, J. M. Boncella, *Angew. Chem. Int. Ed. Engl.* **2009**, *48*, 3795-3798; b) C. R. Graves, J. L. Kiplinger, *Chem. Commun.* **2009**, 3831-3853.

[15] a) F. Akagi, T. Matsuo, H. Kawaguchi, *Angew. Chem. Int. Ed. Engl.* **2007**, *46*, 8778-8781; b) T. M. Powers, A. R. Fout, S.-L. Zheng, T. A. Betley, *J. Am. Chem. Soc.* **2011**, *133*, 3336-3338.

[16] *The Chemistry of the Actinide and Transactinide Elements*, 3rd ed., Springer, Dordrecht, **2006**.

[17] J. G. Brennan, R. A. Andersen, A. Zalkin, *J. Am. Chem. Soc.* **1988**, *110*, 4554-4558.

[18] a) C. E. Kefalidis, L. Castro, L. Perrin, I. Del Rosal, L. Maron, *Chem. Soc. Rev.* **2016**, *45*, 2516-2543; b) C. E. Kefalidis, L. Castro, A. Yahia, L. Perrin, L. Maron, *Computational Methods in Lanthanide and Actinide Chemistry*, John Wiley & Sons Ltd, Chichester, UK, **2015**.

[19] O. Cooper, C. Camp, J. Pecaut, C. E. Kefalidis, L. Maron, S. Gambarelli, M. Mazzanti, *J. Am. Chem. Soc.* **2014**, *136*, 6716-6723.

[20] a) D. J. Knobloch, S. P. Semproni, E. Lobkovsky, P. J. Chirik, *J. Am. Chem. Soc.* **2012**, *134*, 3377-3386; b) X. Zhang, B. Butschke, H. Schwarz, *Chem. Eur. J.* **2010**, *16*, 12564-12569.

CHAPTER 4

Reversible Dihydrogen Activation and Hydride Transfer by a Uranium Nitride Complex

Introduction[1]

Heterolytic H_2 cleavage is an important step in many reactions promoted by enzymes or synthetic catalysts.[1] Hydrogen activation is crucial in the industrial Haber-Bosch process that is used in the production of ammonia from N_2 and H_2 and is also important in nitrogen fixation by nitrogenase enzymes, which is enabled by hydride-containing intermediates.[2] Such hydride intermediates are also believed to play a role in the reduction of other substrates such as CO_2 or nitriles effected by these enzymes.[3] Moreover, hydrogenolysis by metal nitrides intermediates is believed to be a key step in the Haber-Bosch process.[4] However, only three examples of heterolytic splitting of H_2 by a nitride complex have been reported so far.[5] Molecular nitride complexes of uranium can effect N–C formation reactions under mild conditions as shown for the bridging nitride with CO_2 and CO (Chapters 2 and 3).[6] However, in spite of the increasing number of characterized uranium nitride complexes,[7] the study of the reactivity of these systems is still in its infancy and in particular the reaction with dihydrogen has never been explored. In view of the ability of uranium nitrides to effect N–C bond formation reactions we became interested in studying the reaction of the bridging diuranium(IV) nitride with H_2, to explore the possibility of obtaining a highly reactive uranium hydride-imide complex.

Despite the fact that the seminal work of Andersen and Marks on organometallic uranium hydrides goes back to the early 80s,[8] uranium hydrides remain rare and most of the reported examples contain carbocyclic ligands.[8c, 9] In this chapter the facile and reversible heterolytic cleavage of dihydrogen under ambient conditions is presented. The bifunctional Lewis acid-base character of the U–N bond in the

[1] Portions of this chapter have been published: M. Falcone, L. N. Poon, F. F. Tirani, M. Mazzanti, *Angewandte Chemie Int. Ed.*, **2018**, *57*, 3697
Author contributions: M.F. and M.M. originated the idea; M.F. carried out the synthetic experiments and analysed the experimental data; L.N.P. carried out some synthetic experiments, including the isolation of compound **3**. F.F.T. performed the X-ray single crystal structure analyses. M.M. and M.F. wrote the manuscript.

multimetallic U(IV) complex [Cs{U(OSi(O^{t}Bu)$_3$)$_3$}$_2$(μ-N)] **1**,[10] leads to the reversible formation of a imide-hydride complex that can transfer the hydride to acetonitrile and CO_2.

Results and discussion

When a toluene solution of the previously reported [10] complex **1** is exposed to 1 atmosphere of hydrogen the solution turns from brown to yellow within 15 minutes and the proton NMR spectrum shows the disappearance of the siloxides signal of **1** and the appearance of a new signal at 0.32 ppm, assigned to the siloxide ligands of complex [Cs{U(OSi(O^{t}Bu)$_3$)$_3$}$_2$(μ-H)(μ-NH)], **2** (Scheme 1). The resonance at 571.3 ppm in the ^{1}H NMR spectrum of **2** is assigned to the U(IV)-bound hydride and its value is consistent with those reported for other U(IV) hydride complexes.[9g, 11] This resonance is absent in the ^{1}H NMR spectrum of the deuterated analogue [Cs{U(OSi(O^{t}Bu)$_3$)$_3$}$_2$(μ-D)(μ-ND)], **D_2-2** (Appendix 3, Figure S2). Removal of the headspace after reaction of **1** with H_2 results in slow H_2 loss and formation of the nitride complex **1**. Crystals of complex **2** also loose H_2 once removed from the solution resulting in the isolation of complexes **1** and **2** co-crystallized in 30:70% ratio. However, loss of H_2 could be avoided by maintaining at –40 °C the crystals of **2,** obtained at –40 °C under 1 atm H_2, during crystal mounting and by performing X-ray data collection at –133 °C**.** The facile and reversible activation of H_2 by complex **1** is remarkable. Notably, in the only example reported so far of cooperative H_2 activation by a bifunctional metal nitride, the H_2 cleavage is not reversible.[5a]

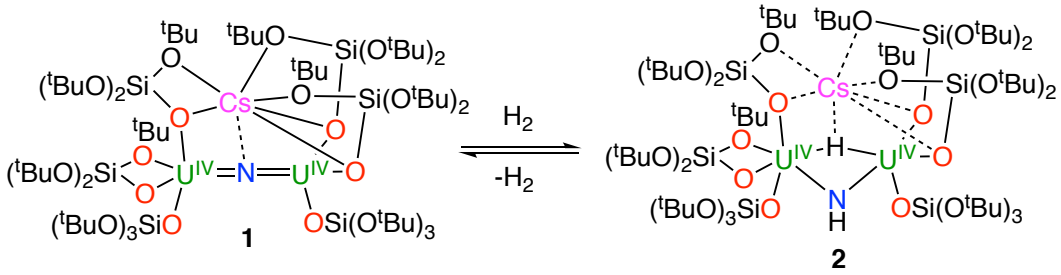

Scheme 1. Reversible cleavage of H_2 by **1** to afford the di-uranium(IV) hydride-imide product **2**.

The molecular structure of **2** (Figure 1) could be determined by X-ray analysis of crystals of **2** and it shows a dinuclear U(IV) complex bridged by an imido and a hydrido ligand. Electron density that could be assigned to the imide and to the hydride

was located and both groups were refined without imposing any constraints. A Cs cation is bound by the siloxide ligands resulting in a dissymmetric structure analogous to that found in the nitride complex **1**.

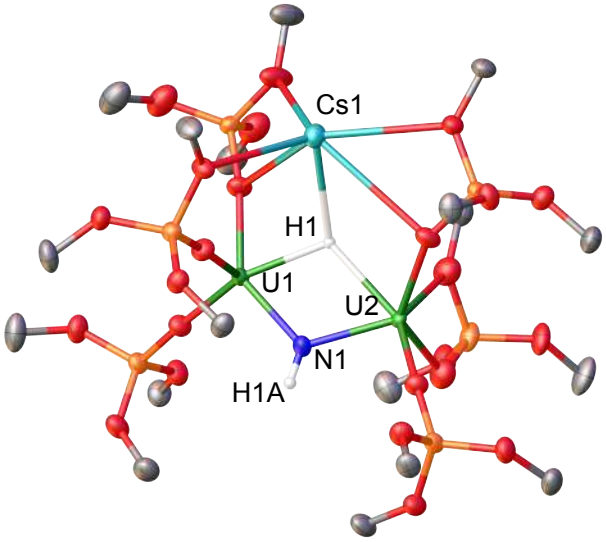

Figure 1. Solid-state molecular structure of $[Cs\{U(OSi(O^tBu)_3)_3\}_2(\mu\text{-}H)(\mu\text{-}NH)]$, **2**. Thermal ellipsoids set at 50% probability. Hydrogen atoms and methyl groups were omitted for clarity. Selected bond distances [Å]: U1–N1 2.187(3), U2–N1 2.204(4), U1–H1 2.18(6), U2–H1 2.30(6), N1–H1A 0.88, H1–Cs1 2.73(6).

Notably, two siloxide ligands bridge the U1 and Cs centers binding the Cs in a bidentate fashion while only one siloxide ligand binding the Cs cation in a bidentate fashion bridges U2 and Cs. The Cs cation was found in the apical position of the nitride at a Cs–N distance of 3.393(4) Å in **1**, while in **2** it lies at the apical position of the hydride ligand with a Cs-H distance of 2.73(6) Å and is located at a non-bonding distance of 4.821(3) Å from N1. Moreover, the U–N–U angle changes dramatically from linear in complex **1** (U–N–U angle: 170.2(3)°) to bent in the diamond core geometry of complex **2** (U–N–U angle: 117.5(3)°) and the U–N bond distances are significantly elongated in **2** (2.187(3), 2.256(4) Å) compared to those found in **1** (2.058(5) - 2.079(5) Å). These data are in agreement with the presence of a protonated NH group and the U–NH distances are in the range of those found in diuranium(IV) imido bridged complexes (2.156(8) - 2.315(8) Å).[12] One terminal parent imido U(IV) complex is known,[13] but a bridging parent imido-U(IV) linkage was not characterized previously. In contrast, the bridging parent imido U(V)U(V) $[K_2\{[U(OSi(O^tBu)_3)_3]_2(\mu\text{-}NH)(\mu\text{-}\eta^2\text{:}\eta^2\text{-}N_2)\}]$ and U(IV)U(V) $[K_2\{[U(OSi(O^tBu)_3)_3]_2(\mu\text{-}NH)_2(\mu\text{-}Cl)\}]$ complexes were previously isolated in our group by protonation of the nitride-hydrazide complex $[K_3\{[U(OSi(O^tBu)_3)_3]_2(\mu\text{-}$

N)(μ-η^2:η^2-N_2)}].[14] The hydride bridges the two uranium cations (U–U 3.786 Å) in a non-symmetric fashion (U–H 2.18(6) and 2.36(6) Å) with the shorter distance being comparable to those determined by neutron diffraction studies for the $[(C_5Me_5)_2UH_2]_2$ complex (2.134(9) Å)[14] where the hydride bridges the two uranium centers in a symmetric fashion. Complex **2** is a rare example of imide-hydride bridged complex.[5a, 15] Such species are very relevant as probable intermediate in N_2 hydrogenation to yield NH_3.[15c, 16]

If the crystals of **2** were not maintained at –40 °C before mounting them to measure the diffraction pattern, the molecular structure showed the presence of the starting material, complex **1**, overlapped to the hydrido- imido- complex **2** (crystal of the mixture called **1.2**). The U–$N_{nitride}$ distances found for **1** (U1–N1B =1.924(17) Å and U–N1B =1.950(17) Å) in the crystal **1.2** (Figure 2a) are significantly shorter than those found in the previously reported structure of complex **1** crystallized as a unique species from toluene (2.058(5) Å and 2.079(5) Å).[10] This difference may be explained by the difference in binding of the Cs cation to the nitride group. Notably in the previously reported structure the N–Cs distance is 3.393(5) Å, but in **1.2** the N(1B)–Cs(1) distance is 3.801(19) Å. This difference results in an increased electron density on the nitride group that explains the shorter U=N distances found for the nitride group in **1.2**. So the different crystallization conditions affect the Cs binding to the nitride. The overlay of the structures of complexes **1** and **2** (Figure 2b) shows an almost perfect overlap of the U and Cs atoms, but slight displacements of the siloxide ligand atoms. The main structural difference is the bending of the U–N–U angle upon protonation of the nitride to afford the imido group. These changes result in significantly different cell parameters in **2** compared to those reported for **1**.

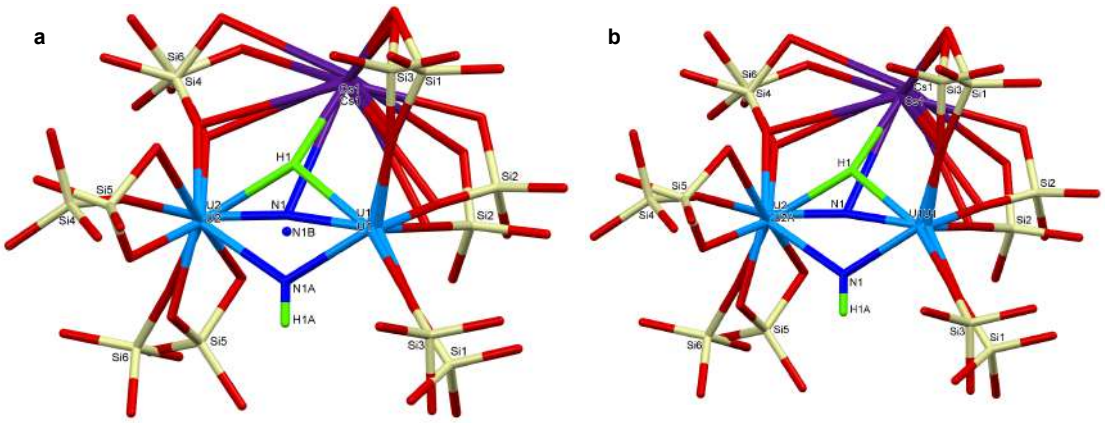

Figure 2. Overlay of the previously reported structure of **1** and of the structure of **1.2** showing perfect overlap of the U and Cs atoms but slight displacement of the siloxide ligand atoms and of the nitride atom (**a**); overlay of the structure of complexes **1** and **2** showing an almost perfect overlap of the U and Cs atoms, but slight displacements of the siloxide ligand atoms.

Complex **2** displays a rich reactivity that unambiguously confirms the presence of the hydride-imide core in **2** and demonstrates the ability of **2** to effect hydride transfer reactions to substrates such as MeCN and CO_2.

Beyond the reducing characters of the hydride, it can react as a base when reacted with acidic substrate such as phenylacetylene. When one equivalent of PhC≡CH is added to a solution of complex **2**, the alkyne proton is easily removed by the hydride to form H_2 and the phenyl acetylide ion, which bridges the two uranium centers in complex [Cs{[U(OSi(O^{t}Bu)$_3$)$_3$](μ-NH)(μ-PhC≡C}], **3** (Scheme 2).

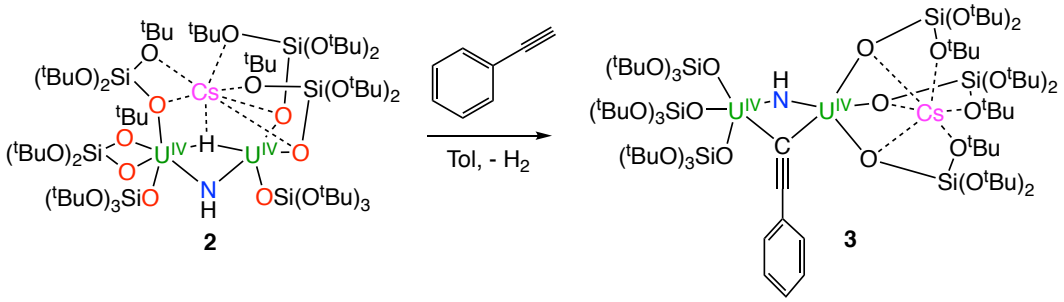

Scheme 2. Reactivity of complex **2** with PhC≡CH to give complex [Cs{[U(OSi(O^{t}Bu)$_3$)$_3$](μ-NH)(μ-PhC≡C}], **3**.

The X-ray structure of **3** (Figure 3) shows a non-symmetric molecule with the cesium cation placed in the pocket created by the three siloxide ligands coordinating U2. The proton H1 is visible by X-ray, leaving no ambiguity on the nature of the NH ligand. The U1–N1 distance (2.259(4) Å) is comparable to the U–NH distance in **2**, while the U2–N1 distance (2.177(4) Å) is considerably shorter, probably to compensate the electron density withdrawing effect of the cesium cation bound to the ligands

coordinated to U1. The C121–C122 distance of 1.217(7) Å is consistent with a typical carbon-carbon triple bond.

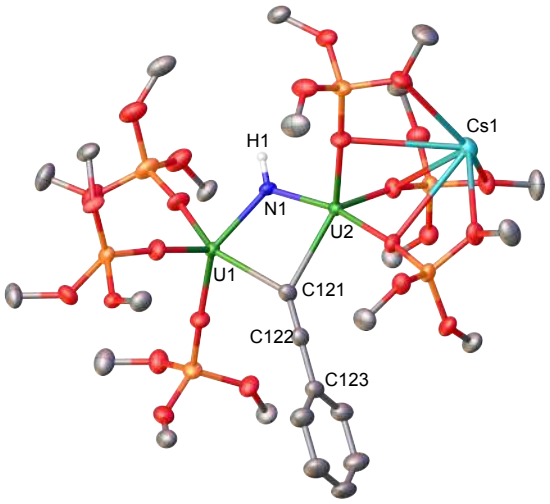

Figure 3. Solid-state molecular structure of [Cs{[U(OSi(O^{t}Bu)$_3$)$_3$](μ-NH)(μ-PhC≡C}], **3**. Thermal ellipsoids set at 50% probability. Hydrogen atoms and methyl groups were omitted for clarity. Selected bond distances [Å]: U1–N1 2.259(4), U1–C121 2.660(5), U2–N1 2.177(4), U2–C121 2.595(5), N1–H1 0.8800, C121–C122 1.217(7), C122–C123 1.439(7), average U1–Osiloxides 2.140(12), average U2–Osiloxides 2.185(13).

The reducing character of the bridging hydride was demonstrated by performing reactions with acetonitrile and carbon dioxide. The addition of MeCN to a toluene solution of **2** (Scheme 3a), led to the formation of the bridging imido-ketimide complex [Cs{U(OSi(O^{t}Bu)$_3$)$_3$}$_2$(μ-NH)(μ-CH$_3$CHN)], **4** that was isolated in high yield (85%) as a yellow crystalline solid.

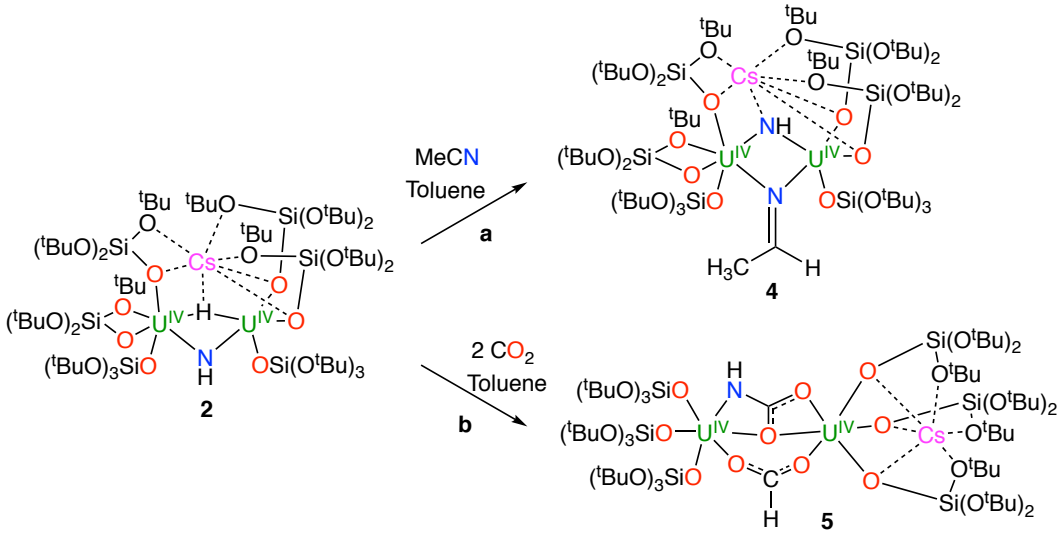

Scheme 3. In situ reactions of 2 with acetonitrile to give **4** (**a**) and 2 equiv. of carbon dioxide to give **5** (**b**).

Thus, the hydride addition to the acetonitrile results in the two-electron reduction of the triple nitrogen-carbon triple bond. The solid-state structure of **4** (Figure 4a) shows the presence of two uranium ions bridged by an imido and a ketimido (or azavinylidene) group. A cesium cation binds in a dissymmetric fashion the imido nitrogen and the siloxide ligands. The carbon atom C121 has a trigonal planar geometry and the C121–N1 distance of 1.273(7) Å is consistent with a carbon-nitrogen double bond. The pseudo tetrahedral geometry of the N2 atom and the U–N2 distances (U1–N2 2.247(4) and U2-N2 2.209(5) Å) are in agreement with the presence of an imido group NH, indicating that the NH group is not involved in the reactivity with MeCN. The IR spectrum shows a peak at 1629 cm^{-1} assigned to the N–C double bond stretching (Appendix 3, Figure S16). The insertion of nitriles into the U–C bond has been used by Kiplinger and co-workers [17] as a convenient method for the synthesis of mono- and multimetallic ketimide complexes. Formation of a ketimide ligand from the insertion of the nitrile triple bond into a uranium hydride complex was also reported previously but the insertion products were not crystallographically characterized.[9g] The ability of **2** to perform hydride transfer reactivity and the consequent reducing behavior of the hydride towards substrates were confirmed in the reaction of **2** with carbon dioxide. Addition of two equivalents of CO_2 (Scheme 3b) to **2** led to the formation of complex $[Cs\{U(OSi(O^tBu)_3)_3\}_2(\mu\text{-}HCOO)(\mu\text{-}NHCOO)]$, **5** in 44% yield. The addition of less that 2 equivalent of CO_2 shows only the presence of unreacted **2** and **5**. The solid state structure of **5** (Figure 4b) shows the presence of two U(IV) cations bridged by a formate and a dianionic carbamate group. A cesium cation is also bound in the pocket formed by three siloxides bound to U1.

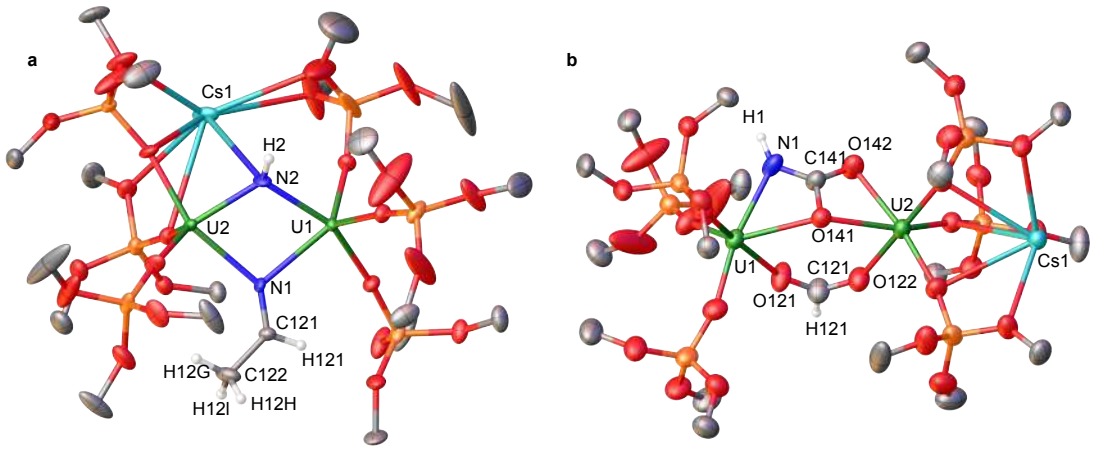

Figure 4. Solid-state molecular structure of $[Cs\{U(OSi(O^tBu)_3)_3\}_2(\mu\text{-}NH)(\mu\text{-}CH_3CHN)]$, **4** (**a**) and of $[Cs\{U(OSi(O^tBu)_3)_3\}_2(\mu\text{-}HCOO)(\mu\text{-}NHCOO)]$, **5** (**b**). Thermal ellipsoids set at 50% probability. Hydrogen atoms and methyl groups were omitted for clarity. Selected bond distances for **4** [Å]: U1-N2 2.247(4), U1-N1 2.480(4), U1-U2 3.7912(5), U2-N2 2.209(5), U2-N1 2.429(4), N2-Cs1 3.429(5), N1-C121 1.273(7), N2-H2 0.8800, C121-C122 1.500(8). Selected bond distances for **5** [Å]: U1–O121 2.409(3), U1–O141 2.574(2), U1–N1 2.423(4), O121–C121 1.225(5), C121–H121 0.950, C121–O122 1.257(5), N1–H1 0.880, N1–C141 1.303(5), C141–O141 1.349(4), C141–O142 1.285(5), U2–O142 2.339(3), U2–O141 2.453(2), U2–O122 2.356(3).

Complex **5** is only the second example of a crystallographically characterized formate complex obtained from the insertion of CO_2 into a U–H bond and the first one containing a bridging formate.[9a] The U–O distances for the bridging formate in **5** (2.409(3) and 2.356(3) Å) are slightly shorter than those found in the reported terminal formate (2.451(3) Å). The proton of the formate was located by X-ray diffraction and was identified in the ^{1}H NMR spectrum. The concomitant cycloaddition of CO_2 to the parent imido linkage affords a bridging κ^3-carbamate group. This reactivity is a rare example of cycloaddition of CO_2 to a metal imido complex [18] and differs from that reported for U(IV)-bound terminal bulky aryl imido groups (N=Ph) that results in N=C bond methathesis and extrusion of the cyanate via a proposed carbamate intermediate.[19] The low sterical pressure of the NH group and its bridging mode result in a high stability of the κ^3-O,O,N-carbamate group. A few examples of U(IV) carbamate have been reported but they all present monoanionic κ^2-O,O-carbamate groups. [19-20]

Conclusions

In summary, the polymetallic U(IV) nitride is able to effect the reversible heterolytic activation of dihydrogen in mild conditions (room temperature and 1 atmosphere of H_2), showing once more the high ligand based activity of this bridging nitride towards small molecules. Notably, the hydride is readily transferred to acetonitrile and CO_2

resulting in the substrate reduction. These results anticipate that metal hydride intermediates may play an important role in the uranium-catalyzed transformation of N_2 and H_2 into ammonia. Moreover, the importance of this study lies in the reduction of carbon dioxide, as it opens new routes for the development of hydrogenation catalysts, with the possibility of reducing CO_2 beyond the formate level and perform direct hydrogenation to methanol (see Chapter 8).

Experimental

Materials. Unless otherwise noted, reagents were purchased from commercial suppliers and used without further purification. Tris(*tert*-butoxy)silanol was purified by sublimation. The solvents were purchased from Aldrich or Cortecnet (deuterated solvents) in their anhydrous form, conditioned under argon and vacuum distilled from K/benzophenone (toluene, toluene-d_6 and n-hexane). DMSO-d_6 was freeze-degassed and stored over activated 3 Å molecular sieves. The complex [Cs(μ-N){U(OSi(O^{t}Bu)$_3$)$_3$}$_2$], **1**,[10] was prepared according to published procedure. Hydrogen gas (99.9999% purity) and carbon dioxide (99.9999% purity) were purchased from Carbagas. $^{13}CO_2$ (93.13% ^{13}C) and D_2 (99.8% D) were purchased from Cortecnet and stored over activated 3 Å molecular sieves. All manipulations were carried out under a dry and oxygen free argon atmosphere using Schlenk techniques and an MBraun glovebox equipped with a purifier unit. The water and oxygen levels were always kept at less than 0.1 ppm. Glassware was dried overnight at 140°C before use. Depleted uranium metal was purchased from Ibilabs, Florida, USA. **Caution:** Depleted uranium (primary isotope ^{238}U) is a weak α-emitter (4.197 MeV) with a half-life of 4.47×10^9 years. Manipulations and reactions should be carried out in monitored fume hoods or in an inert atmosphere glovebox in a radiation laboratory equipped with α- and β-counting equipment. **^{1}H NMR experiments** were carried out using NMR tubes adapted with J. Young valves. ^{1}H NMR spectra were recorded on Bruker 400 MHz. NMR chemical shifts are reported in ppm with solvent as internal reference. **Elemental analyses** CHN elemental microanalysis were obtained using a Thermo Scientific Flash 2000 Organic Elemental Analyzer at the Institut of Chemistry and Chemical Engineering at EPFL. **IR analyses** were performed with a FT-IR Spectrometer Spectrum one Perkin-Elmer.

Reaction of 1 with 1 atm H_2 to afford [Cs{U(OSi(O^{t}Bu)$_3$)$_3$}$_2$(μ-NH)(μ-H)], 2

A brown solution of complex [Cs{U(OSi(O^{t}Bu)$_3$)$_3$}$_2$(μ-N)], **1** (27.8 mg, 0.0126 mmol) in d_8-toluene (0.5 mL) was prepared in an argon filled glove box and placed in an NMR tube equipped with a Young Valve. The tube was transferred to a Schlenk line and degassed by freeze-pump-thawing. Hydrogen gas (1 atmosphere) was added at room temperature. Within 15 minutes a yellow solution was obtained identified as the 97% conversion of **1** into **2** as determined by NMR spectroscopy. The conversion decreases if lower pressure of H_2 is used. While still under a headspace of H_2 the solution was cooled at –40 °C for 24 h to afford yellow crystals of complex [Cs{U(OSi(O^{t}Bu)$_3$)$_3$}$_2$(μ-NH)(μ-H)], **2**. The crystals of **2** were transferred quickly from the cooled solution to oil previously cooled at –40° C to prevent H_2 loss during X-ray data collection and mounted on the diffractometer at low temperature. When the crystals were handled at room temperature during mounting, H_2 loss from the crystals was observed even if the data were collected at low temperature. The structure analysis for the resulting crystals of **1.2** shows the presence of complexes **1** and **2** in 30:70 % ratio (See Figure Appendix 3 S18). ^{1}H NMR (400 MHz, tol-d_8, 298 K): δ (ppm) = 0.32 (s, 162 H, CH_3), 571.3 (s, 1H, hydride); the resonance attributable to NH could not be identified. The hydride resonance was assigned by recording the ^{1}H NMR spectrum of the solution obtained after the reaction of **1** with 0.8 atm of D_2 in d_8-toluene (carried out using a similar procedure to that used in the synthesis of **2**) to afford the deuterated analogue [Cs{U(OSi(O^{t}Bu)$_3$)$_3$}$_2$(μ-ND)(μ-D)], **D_2-2** (85% conversion). The resonance assigned to the hydride is absent from the spectrum of **D_2-2**. Removal of the H_2 headspace from the tube containing a toluene solution of **2** results in the slow formation of **1**, indicating that the reaction is reversible as shown by the evolution of the ^{1}H NMR spectrum over time. Leaving the isolated solid under vacuum for 5 minutes or 1 hour results in a nitride/hydride ratio of 0.2 and 5 respectively. Further analysis and recording of the isolated yield were not possible due to the reversibility of the reaction in the absence of the H_2 headspace that results inevitably in a mixture of complex **1** and **2**. The vibrations of the U–H and U–NH groups could not be identified in the IR spectrum of the isolated mixture of **1** and **2** (Figure Appendix 3 S15). This is surprising but already reported for a imide-hydride bridged iron complex.[5a]

Synthesis of [Cs{[U(OSi(O^{t}Bu)$_3$)$_3$](μ-NH)(μ-PhC≡C}], 3

A solution of complex **2** (25 mg, 0.011 mmol, 1 eq) in toluene (0.5 mL) was prepared by addition of 1 atm of H_2 to a toluene solution of **1** in a NMR tube. The headspace was removed under vacuum and 9.2 mL (0.014 mmol, 1.2 eq) of a 1.5 M solution of phenylacetylene in toluene-d_8 were added to the tube. The solution turned green and darker within 3 days. X-ray suitable amber crystals of complex [Cs{U(OSi(O^{t}Bu)$_3$)$_3$}$_2$(μ-NH)(μ-C≡CPh)], **3** were obtained by letting the solution stand at –40 °C for 24 h (11 mg, 40% yield). ^{1}H NMR (400

MHz, tol-d_8, 298 K) of crystals of **3**: δ (ppm) = 3.42 (t, 1H, H_{para}), –0.16 (s, 162 H, CH_3), –1.02 (t, 2H, H_{meta}), –10.26 (bs, 2H, H_{orto}). Anal. Calcd for [Cs{U(OSi(O^{t}Bu)$_3$)$_3$}$_2$(μ-NH)(μ-C≡CPh)], **3**: $C_{80}H_{168}CsNO_{24}Si_6U_2$: C 41.67; H 7.34; N 0.61; Found: C 41.33; H 7.46; N 0.65.

Synthesis of [Cs{U(OSi(O^{t}Bu)$_3$)$_3$}$_2$(μ-NH)(μ-CH$_3$CHN)], 4

A yellow solution of complex **2** (25 mg, 0.011 mmol, 1 eq) in toluene (0.5 mL) was prepared in situ as described above by addition of 1 atm of H_2 to a toluene solution of **1** in an NMR tube and letting react at room temperature for 15 minutes. The tube was transferred to the glove box, and, while still under H_2 headspace, 6.5 mL (0.011 mmol, 1 eq) of a standard solution (1.74 mM) of acetonitrile in toluene was added to the mixture. The immediate reaction (the ^{1}H NMR spectrum shows complete conversion after few minutes) proceeds without any change in color. The solution was left standing at –40 °C for 24 h and XRD suitable crystals of complex [Cs{U(OSi(O^{t}Bu)$_3$)$_3$}$_2$(μ-NH)(μ-CH$_3$CHN)], **4** were recovered (21.5 mg, 84% yield). ^{1}H NMR (400 MHz, tol-d_8, 298 K) of crystals of **4**: δ (ppm) = –1.22 (s, 162 H, CH_3 terminal siloxides), 3.5 (s, 3H, C**H**$_3$CHN); the resonances attributable to NH and CH could not be identified. ^{13}C NMR (400 MHz, tol-d_8, 298 K) of crystals of **4**: δ (ppm) = 128.7 (s, CH$_3$**C**HN), 69.4 (**C**Me$_3$), 26.0 (**C**H$_3$CHN), 22.5 (CH_3 terminal siloxides). Anal. Calcd for [Cs{U(OSi(O^{t}Bu)$_3$)$_3$}$_2$(μ-NH)(μ-CH$_3$CHN)]: $C_{74}H_{167}CsN_2O_{24}Si_6U_2$: C 39.56; H 7.49; N 1.25; Found: C 39.16; H 7.83; N 1.23.

IR, ν**N=C** (cm^{-1}): 1629

Synthesis of [Cs{[U(OSi(O^{t}Bu)$_3$)$_3$]$_2$(μ-HCOO)(μ-HNCOO)}], 5

A yellow solution of complex **2** (28.2 mg, 0.013 mmol, 1 eq) in toluene (0.5 mL) was in situ prepared by addition of 1 atm of H_2 to a toluene solution of **1** in an NMR tube and by letting react for 15 minutes at room temperature. The tube was transferred to a Schlenk line and placed in liquid nitrogen, the head-space was removed under vacuum and two equivalents of CO_2 or $^{13}CO_2$ and 1 atm of H_2 were subsequently added to the frozen solution of the hydride complex **2**. In view of the reversibility of the hydride formation in the absence of H_2, the addition of 1 atm of H_2 before raising the temperature of the solution ensures that only complex **2** is present to react with CO_2. The reaction mixture was then left to return at room temperature and the solution turned immediately from brown to light green. The proton NMR of the reaction mixture shows the presence of the signals assigned to complex [Cs{[U(OSi(O^{t}Bu)$_3$)$_3$]$_2$(μ-HNCOO)(μ-HCOO)}] **5**, (or the ^{13}C labeled analogue **^{13}C-5**), of the signal assigned to unreacted complex **2** and of signals assigned to [U(OSi(O^{t}Bu)$_3$)$_4$]. Light blue crystals of complexes **5** and **^{13}C-5** (12.8 mg, 44%) were obtained by cooling the resulting solution at –40 °C for 24 h. Conversion of **2** into **5** is higher but due to the presence of minor products the complex **5** could only be isolated analytically pure in 44% yield. ^{1}H NMR (400 MHz, tol-d_8, 298 K) of crystals of **5**: δ (ppm) = 27.7 (bs, 1H, HCOO), 1.14 (bs, 81H, CH_3

terminal siloxide), 0.48 (bs, 81H, CH_3 terminal siloxide), the resonance attributable to NHCOO could not be located as in the case of complex **2**. ^{13}C NMR (400 MHz, tol-d_8, 298 K) of crystals of **^{13}C-5**: δ (ppm) = 147.04 (H**C**OO or NH**C**OO), –96.44 (H**C**OO or NH**C**OO), 69.8 (**C**Me_3), 29.12 (**C**H_3 terminal siloxides). The resonance assigned to the formate proton is not present in the spectrum of the solution obtained from the reaction of **D_2-2** with CO_2.

Anal. Calcd for $[Cs\{U(OSi(O^tBu)_3)_3\}_2(\mu\text{-}NHCOO)(\mu\text{-}HCOO)]$: $C_{74}H_{164}CsNO_{28}Si_6U_2$(0.6 C_7H_8): C 39.99; H 7.24; N 0.60; Found: C 39.90; H 7.05; N 0.64. Only one IR vibration assigned to the COO^- group was found that is assigned to both carbamate and formate ligands. IR, ν^{13}**COO**$^-$ (cm^{-1}): 1550; ν**COO**$^-$ (cm^{-1}): 1593. When only one equivalent of CO_2 is reacted with **2**, only the signals assigned to complex **5** and to unreacted **2** are observed in the ^1H NMR spectrum indicating that both the hydride and the imido group react promptly with CO_2. The addition of 3 equiv. of CO_2 results in the complete conversion of **2**, but also in the decomposition of **5** as indicated by the ^1H NMR spectrum probably as the result of further addition of CO_2 to the carbamate group.

Bibliography

[1] a) M. R. DuBois, D. L. DuBois, *Chem. Soc. Rev.* **2009**, *38*, 62-72; b) S. G. Zhang, A. M. Appel, R. M. Bullock, *J. Am. Chem. Soc.* **2017**, *139*, 7376-7387.

[2] a) G. J. Kubas, *Chem. Rev.* **2007**, *107*, 4152-4205; b) B. M. Hoffman, D. Lukoyanov, Z. Y. Yang, D. R. Dean, L. C. Seefeldt, *Chem. Rev.* **2014**, *114*, 4041-4062.

[3] a) Y. Yu, A. R. Sadique, J. M. Smith, T. R. Dugan, R. E. Cowley, W. W. Brennessel, C. J. Flaschenriem, E. Bill, T. R. Cundari, P. L. Holland, *J. Am. Chem. Soc.* **2008**, *130*, 6624-6638; b) G. M. Henderson, (Eds.: M. Peruzzini, R. Poli), Elsevier, New York, **2001**, pp. 463-505.

[4] a) R. Schlogl, *Angew. Chem. Int. Ed. Engl.* **2003**, *42*, 2004-2008; b) H. P. Jia, E. A. Quadrelli, *Chem. Soc. Rev.* **2014**, *43*, 547-564.

[5] a) S. D. Brown, M. P. Mehn, J. C. Peters, *J. Am. Chem. Soc.* **2005**, *127*, 13146-13147; b) B. Askevold, J. T. Nieto, S. Tussupbayev, M. Diefenbach, E. Herdtweck, M. C. Holthausen, S. Schneider, *Nat. Chem.* **2011**, *3*, 532-537; c) J. Schoffel, A. Y. Rogachev, S. D. George, P. Burger, *Angew. Chem. Int. Ed. Engl.* **2009**, *48*, 4734-4738; d) F. S. Schendzielorz, M. Finger, C. Volkmann, C. Wurtele, S. Schneider, *Angew. Chem. Int. Ed. Engl.* **2016**, *55*, 11417-11420.

[6] a) M. Falcone, L. Chatelain, M. Mazzanti, *Angew. Chem. Int. Ed. Engl.* **2016**, *55*, 4074-4078; b) M. Falcone, C. E. Kefalidis, R. Scopelliti, L. Maron, M. Mazzanti, *Angew Chem Int Edit* **2016**, *55*, 12290-12294; c) P. A. Cleaves, C. E. Kefalidis, M. G. Gardiner, F. Tuna, E. J. L. McInnes, W. Lewis, L. Maron, S. T. Liddle, *Chem. Eur. J.* **2017**, *23*, 2950 – 2959.

[7] a) D. M. King, S. T. Liddle, *Coord. Chem. Rev.* **2014**, *266*, 2-15; b) L. Chatelain, R. Scopelliti, M. Mazzanti, *J. Am. Chem. Soc.* **2016**, *138*, 1784-1787; c) N. Tsoureas, A. F. R. Kilpatrick, C. J. Inman, F. G. N. Cloke, *Chem. Sci.* **2016**, *7*, 4624-4632; d) L. Maria, I. C. Santos, V. R. Sousa, J. Marcalo, *Inorg. Chem.* **2015**, *54*, 9115-9126; e) A. R. Fox, P. L. Arnold, C. C. Cummins, *J. Am. Chem. Soc.* **2010**, *132*, 3250-3251; f) P. A. Cleaves, D. M. King, C. E. Kefalidis, L. Maron, F. Tuna, E. J. L. McInnes, J. McMaster, W. Lewis, A. J. Blake, S. T. Liddle, *Angew. Chem. Int. Ed. Engl.* **2014**, *53*, 10412-10415; g) R. K. Thomson, T. Cantat, B. L. Scott, D. E. Morris, E. R. Batista, J. L. Kiplinger, *Nat. Chem.* **2010**, *2*, 723-729; h) D. M. King, F. Tuna, E. J. L. McInnes, J. McMaster, W. Lewis, A. J. Blake, S. T. Liddle, *Science* **2012**, *337*, 717-720; i) W. J. Evans, S. A. Kozimor, J. W. Ziller, *Science* **2005**, *309*, 1835-1838; j) S. Fortier, G. Wu, T. W. Hayton, *J. Am. Chem. Soc.* **2010**, *132*, 6888-6889.

[8] a) H. W. Turner, S. J. Simpson, R. A. Andersen, *J. Am. Chem. Soc.* **1979**, *101*, 2782-2782; b) J. M. Manriquez, P. J. Fagan, T. J. Marks, *J. Am. Chem. Soc.* **1978**, *100*, 3939-3941; c) P. J. Fagan, J. M. Manriquez, E. A. Maatta, A. M. Seyam, T. J. Marks, *J. Am. Chem. Soc.* **1981**, *103*, 6650-6667.

[9] a) J. A. Higgins, F. G. N. Cloke, S. M. Roe, *Organometallics* **2013**, *32*, 5244-5252; b) W. J. Evans, E. Montalvo, S. A. Kozimor, K. A. Miller, *J. Am. Chem. Soc.* **2008**, *130*, 12258-12259; c) J. C. Berthet, J. F. Lemarechal, M. Lance, M. Nierlich, J. Vigner, M. Ephritikhine, *J. Chem. Soc., Dalton Trans.* **1992**, 1573-1577; d) W. J. Evans, K. A. Miller, A. G. DiPasquale, A. L. Rheingold, T. J. Stewart, R. Bau, *Angew. Chem. Int. Ed. Engl.* **2008**, *47*, 5075-5078; e) H. S. La Pierre, H. Kameo, D. P. Halter, F. W. Heinemann, K. Meyer, *Angew. Chem. Int. Ed. Engl.* **2014**, *53*, 7154-7157; f) J. K. Pagano, J. M. Dorhout, K. R. Czerwinski, D. E. Morris, B. L. Scott, R. Waterman, J. L. Kiplinger, *Organometallics* **2016**, *35*, 617-620; g) M. Ephritikhine, *Chem. Rev.* **1997**, *97*, 2193-2242.

[10] C. Camp, J. Pecaut, M. Mazzanti, *J. Am. Chem. Soc.* **2013**, *135*, 12101-12111.

[11] C. J. Windorff, M. R. MacDonald, K. R. Meihaus, J. W. Ziller, J. R. Long, W. J. Evans, *Chem. Eur. J.* **2016**, *22*, 772-782.

[12] J. G. Brennan, R. A. Andersen, A. Zalkin, *J. Am. Chem. Soc.* **1988**, *110*, 4554-4558.

[13] D. M. King, J. McMaster, F. Tuna, E. J. L. McInnes, W. Lewis, A. J. Blake, S. T. Liddle, *J. Am. Chem. Soc.* **2014**, *136*, 5619-5622.

[14] D. Grant, T. J. Stewart, R. Bau, K. A. Miller, S. A. Mason, M. Gutmann, G. J. McIntyre, L. Gagliardi, W. J. Evans, *Inorg. Chem.* **2012**, *51*, 3613-3624.

[15] a) T. Kimura, N. Koiso, K. Ishiwata, S. Kuwata, T. Ikariya, *J. Am. Chem. Soc.* **2011**, *133*, 8880-8883; b) M. P. Shaver, M. D. Fryzuk, *J. Am. Chem. Soc.* **2005**, *127*, 500-501; c) T. Shima, S. W. Hu, G. Luo, X. H. Kang, Y. Luo, Z. M. Hou, *Science* **2013**, *340*, 1549-1552.

[16] M. D. Fryzuk, J. B. Love, S. J. Rettig, V. G. Young, *Science* **1997**, *275*, 1445-1447.

[17] a) K. C. Jantunen, C. J. Burns, I. Castro-Rodriguez, R. E. Da Re, J. T. Golden, D. E. Morris, B. L. Scott, F. L. Taw, J. L. Kiplinger, *Organometallics* **2004**, *23*, 4682-4692; b) E. J. Schelter, J. M. Veauthier, C. R. Graves, K. D. John, B. L. Scott, J. D. Thompson, J. A. Pool-Davis-Tournear, D. E. Morris, J. L. Kiplinger, *Chem. Eur. J.* **2008**, *14*, 7782-7790.

[18] A. E. Guiducci, C. L. Boyd, E. Clot, P. Mountford, *J. Chem. Soc.-Dalton Trans.* **2009**, 5960-5979.
[19] S. C. Bart, C. Anthon, F. W. Heinemann, E. Bill, N. M. Edelstein, K. Meyer, *J. Am. Chem. Soc.* **2008**, *130*, 12536-12546.
[20] a) J. A. H. Frey, G. N. Cloke, S. M. Roe, *Organometallics* **2015**, *34*, 2102–2105; b) E. M. Matson, P. E. Fanwick, S. C. Bart, *Organometallics* **2011**, *30*, 5753-5762; c) F. Calderazzo, G. Dellamico, M. Pasquali, G. Perego, *Inorg. Chem.* **1978**, *17*, 474-479.

CHAPTER 5

Metathesis of a U(V) imido complex: a route to a terminal U(V) sulfide

Introduction[1]

The interest in multiply-bonded uranium pnictogen and chalcogen compounds has grown considerably in recent years.[1] The study of actinide-chalcogen bonds is in part motivated by the efficiency of chalcogen donors in the selective separation of actinides from lanthanides in spent nuclear fuel, a property that has been related to covalent contributions in actinide-chalcogen bonds.[2] Early attempts to prepare terminal sulfido, selenido and tellurido complexes of uranium involved oxidation of a U(III) precursor with a chalcogen-atom donor, and led exclusively to chalcogenide-bridged compounds.[3a, 3b, 3c , 3d , 3e , 3f, 3g] In recent years, a handful of terminal and alkali-capped mononuclear uranium chalcogenides have been prepared and characterised.[4] All characterised terminal sulfido, selenido and tellurido complexes contain a tetravalent uranium ion.[4a, 4c-e, 5] Only one U(IV) complex containing a linear O=U=S^{2+} core has been characterized by Hayton and co-workers.[6] Several terminal mono-oxo complexes of pentavalent uranium[7],[8] and two examples of terminal U(V) nitrides[8d, 9] have been prepared in recent years, but terminal sulfido, selenido and tellurido complexes of U(V) remain undiscovered. Since the degree of covalency in the uranium-chalcogenide bond is expected to be higher in higher oxidation states,[1a] the isolation of a U(V) terminal sulfide is of great interest for elucidating the involvement of 5*f* orbitals in U–S bonding. In general, pentavalent uranium compounds are attractive candidates for the investigation of bonding and magnetic properties due to their simple $5f^1$ configuration,[10] but the number of molecular uranium compounds containing a U(V)–S bond remain rare.[3g, 10b, 11] The presence of stable U(V) cations in chalcogenide materials has also been reported.[12]

[1] Portions of this chapter have been published: R. P. Kelly, M. Falcone, C. A. Lamsfus, R. Scopelliti, L. Maron, K. Meyer, M. Mazzanti, *Chem. Sci.,* **2017**, *8*, 5319
Author contributions: R.P.K. carried out the synthetic experiments and analysed the experimental data; M.F. carried out preliminary synthetic experiments, including the isolation of compound **6** and the synthesis and characterization of compound **7**. M.M. and R.P.K. wrote the manuscript. L.M. carried out the DFT studies and K.M. provided comments. M.M. originated the central idea, coordinated the work, and analyzed the experimental data.

Different approaches have been used in order to prevent the formation of bridging species when preparing U(IV) mono-chalcogenide complexes by oxidation of U(III) compounds.[4b, 4c] Tris(tert-butoxy)siloxide ligands can prevent the formation of a bridging chalcogenide complex. The reaction of the heterobimetallic complex, $[KU(OSi(O^tBu)_3)_4]$, with the two-electron oxidising agent, Ph_3PS, in the presence of 2.2.2-cryptand, led to the isolation of the terminal uranium(IV) monosulfide complex, $[K(2.2.2\text{-cryptand})][US(OSi(O^tBu)_3)_4K]$.[4e] We note that all of the examples mentioned above resulted in the formation of a U(IV) mono-chalcogenide complex in spite of the fact that a two-electron oxidising agent was used in the sulfur-transfer reactions to U(III). A monosulfido complex of U(IV) was also prepared by deprotonation of a hydrosulfido analogue, $[((Ad,MeArO)_3tacn)USH]$ supported by a tripodal hexadentate aminophenolate ligand.[4d] The reported electrochemical studies indicated that this complex could be electrochemically oxidised, most likely to the U(V)≡S species, but preliminary attempts to chemically oxidise and isolate a U(V) sulfido complex were not successful.

In this chapter a new route to isolate a U(V) terminal sulfide using tris(tert-butoxy)siloxide as supporting ligands is presented. This ligand previously allowed for the isolation and characterisation of the U(V) terminal oxo complex, $[UO(OSi(O^tBu)_3)_4K]$,[8b] and of the U(V) terminal imido complex, [K(18c6)]-$[U(NAd)(OSi(O^tBu)_3)_4]$, **1** [13] (Ad = adamantyl). Herein, we show that metathesis reactions of U(V) tetrasiloxide imido complexes with CS_2 and H_2S afford the first U(V) terminal sulfide and trithiocarbonate complexes.

Results and discussion

Attempts to isolate a U(V) terminal sulfide from the chemical oxidation of the uranium(IV) siloxide complex, $[K(2.2.2\text{-cryptand})][US(OSi(O^tBu)_3)_4K]$, only led to decomposition products.

Thus, in our search for a U(V) terminal sulfide, we anticipated that U(V) terminal imido complexes would be the ideal starting materials. Notably, several examples of reactions of transition metal imido compounds with CS_2 have been reported and they usually lead to the formation of sulfide and isothiocyanate products via a cycloaddition pathway.[14] The formation of a U(V) terminal oxo complex from the reaction of a U(V) imido complex with CO_2 has been reported,[8a] but a similar strategy using CS_2 has never been used to prepare terminal uranium sulfides.

Hydrosulfidolysis of imido compounds also represent a successful route to terminal or bridging sulfide complexes of d-block transition metals,[15] but was never applied for *f*-elements.

In our group it was shown that [K(18c6)][U{OSi(O^{t}Bu)$_3$}$_4$] can be used to effect a two-electron reduction of adamantyl azide, affording the U(V) monoimido complex [K(18c6)][U(NAd){OSi(O^{t}Bu)$_3$}$_4$], **1**.[13] With regard to the important effect of alkali cations and crown-ether-bound alkali cations on the reactivity of uranium compounds supported by tris(tert-butoxy)siloxide ligands,[8b, 16] we have prepared the analogous complexes, [U(NAd){OSi(O^{t}Bu)$_3$}$_4$K], **4**, and [K(2.2.2-cryptand)]-[U(NAd){OSi(O^{t}Bu)$_3$}$_4$] **5**, by reduction of adamantyl azide with [KU{OSi(O^{t}Bu)$_3$}$_4$], **2** and [K(2.2.2-cryptand)][U{OSi(O^{t}Bu)$_3$}$_4$], **3**, respectively (Scheme 1).

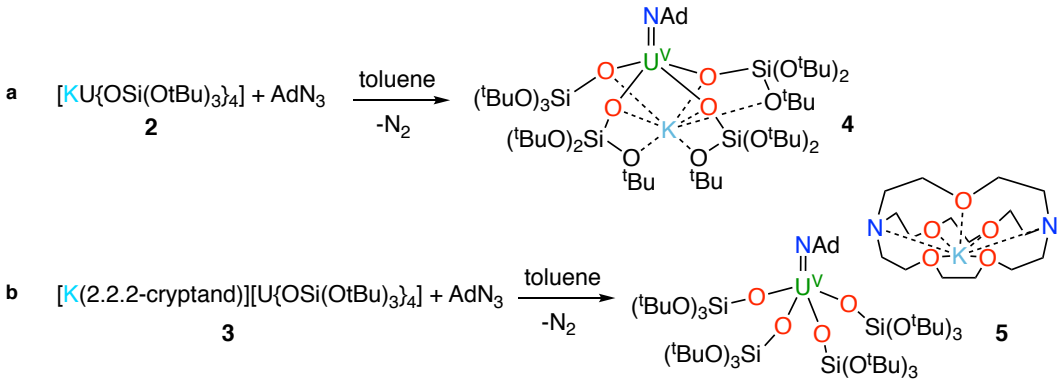

Scheme 1. Synthesis of [U(NAd){OSi(OtBu)$_3$}$_4$K], **4** (**a**) and [U(NAd){OSi(OtBu)$_3$}$_4$], **5** (**b**).

The charge-separated U(III) tetrasiloxide precursor, [K(2.2.2-cryptand)]-[U{OSi(O^{t}Bu)$_3$}$_4$] **3**, is conveniently prepared in high yield by stirring the reported complex, [K U{OSi(O^{t}Bu)$_3$}$_4$] **2**,[8b] with 2.2.2-cryptand in toluene. Complex **3** crystallised from a mixture of THF and hexane as two crystallographically unique pairs of [K(2.2.2-cryptand)]$^+$ and [U{OSi(O^{t}Bu)$_3$}$_4$]$^-$ ions (Figure 1). The four-coordinate uranium ions feature a tetrahedral coordination geometry formed by four monodentate tris(tert-butoxy)siloxide ligands. The structure is very similar to that of [K(18c6)][U(NAd){OSi(O^{t}Bu)$_3$}$_4$] and the U–O bond lengths of the two complexes are comparable (U–O$_{ave}$ = 2.228 Å in [K(18c6)][U(NAd){OSi(O^{t}Bu)$_3$}$_4$]; U–O$_{ave}$ = 2.21 Å in **3**).

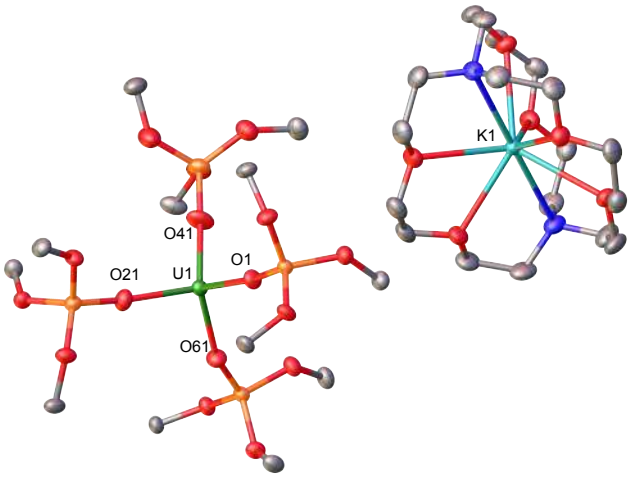

Figure 1. Solid-state molecular structure of one of the crystallographically unique pairs of [K(2.2.2-cryptand)]-[U{OSi(OtBu)$_3$}$_4$], **3**. Thermal ellipsoids set at 50% probability. Hydrogen atoms and methyl groups were omitted for clarity. Selected bond lengths [Å]: U1–O1 = 2.223(4), U1–O21 = 2.193(4), U1–O41 = 2.211(4), U1–O61 = 2.220(4).

Complex **4** is highly soluble in hexane, toluene and THF, whereas **5** is sparingly soluble in toluene but highly soluble in THF. The ^{1}H NMR spectra of **4** and **5** in toluene-d$_8$ are similar to that of the reported complex **1**,[13] and show four paramagnetically shifted resonances attributable to the adamantyl protons, and one peak corresponding to the tert-butyl protons of the siloxide ligands. However, in the case of **5** the siloxide peak is sharp, while in the case of **4** a broad peak is observed, suggesting fluxional binding of the potassium ion in toluene solution for complex **4**. Complex **5** shows three additional cryptand resonances in the ^{1}H NMR spectrum. Dark brown crystals of the heterobimetallic complex **4** crystallised from toluene (Figure 2a). The central uranium ion is five coordinate and it is ligated by four negatively charged oxygen atoms of the tris(tert-butoxy)siloxide ligands, and one nitrogen atom of the imido group. The U–N bond length (1.954(3) Å) is slightly longer than the corresponding bond length in [K(18c6)][U(NAd){OSi(O^{t}Bu)$_3$}$_4$] (1.937(7) Å), while the average U–O bond lengths (2.20(2) Å for [K(18c6)]-[U(NAd){OSi(O^{t}Bu)$_3$}$_4$] and 2.20(3) Å for **4**) of the two complexes are about the same.[13] The incorporation of the potassium ion into the structure of **4** results in significant distortion of the coordination geometry around the uranium ion relative to that found in **1** (Figure 2b).

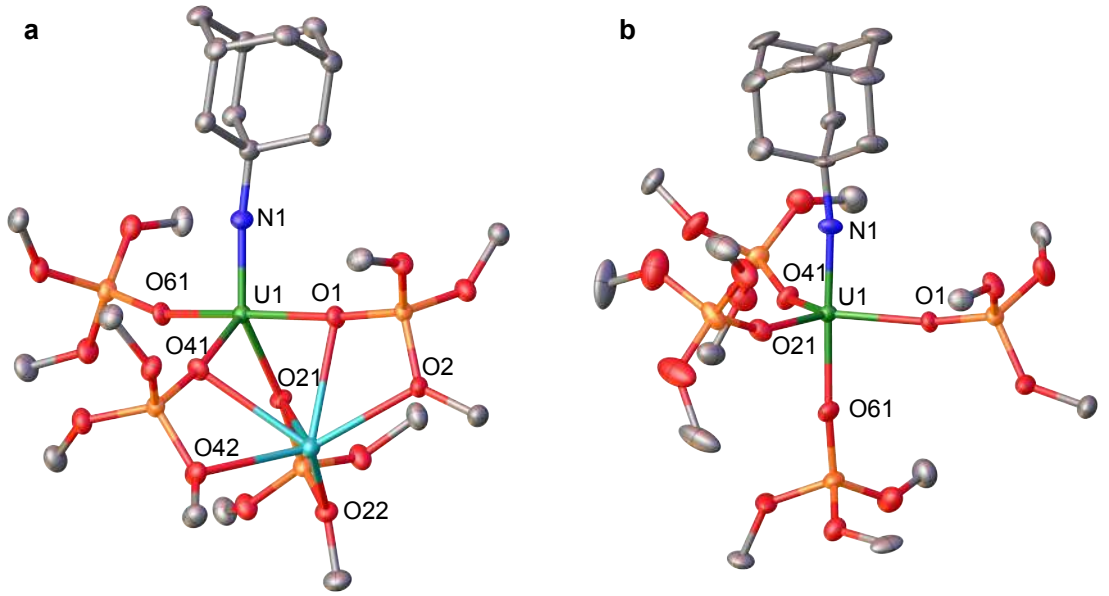

Figure 2. Solid-state molecular structure of [U(NAd){OSi(OtBu)$_3$}$_4$K], **4** (**a**) and of the anion of [K(18c6)]-[U(NAd){OSi(OtBu)$_3$}$_4$], **1** (**b**). Thermal ellipsoids set at 50% probability. Hydrogen atoms and methyl groups were omitted for clarity. Selected bond lengths for **4** [Å]: U1–N1 = 1.954(3), U1–O1 = 2.243(3), U1–O21 = 2.175(3), U1–O41 = 2.190(3), U1–O61 = 2.185(3), K1–O1 = 2.827(3), K1–O2 = 2.631(3), K1–O21 = 3.058(3), K1–O22 = 2.626(3), K1–O41 = 2.822(4), K1–O42 = 2.725(4).

In **1**, the coordination geometry of the uranium centre is roughly trigonal bipyramidal, with three siloxide ligands occupying the equatorial sites, and the axial sites being taken up by a siloxide ligand and an imido group, respectively. However, in **4**, the coordination geometry around the uranium ion is highly distorted due to the coordination of three siloxide ligands to the six-coordinate potassium ion, which fits into a pocket formed by three κ^2O-siloxide ligands.

At first, we investigated the reaction of [U(NAd){OSi(O^{t}Bu)$_3$}$_4$K], **4** with $^{13}CS_2$. An analogous approach has been used to prepare a uranium terminal oxo complex by reaction of a U(V) imido complex with CO_2.[8a] The proposed mechanism for the formation of the terminal oxo involves a [2+2] cycloaddition reaction followed by extrusion of isocyanate to afford the terminal oxo complex.[8a] In the present case, reactions between **4** and one or two equivalents of $^{13}CS_2$ were slow. Monitoring the reactions by ^{1}H NMR spectroscopy showed that in both cases consumption of the starting material took place over two to three days, and it proceeded with the concomitant formation of [U{OSi(O^{t}Bu)$_3$}$_4$] (in 35% yield) and additional unidentified uranium product(s). None of these products could be identified as a terminal sulfide, even when the **4**:CS_2 ratio was 1:1. The ^{13}C NMR spectrum of the crude reaction mixtures in toluene show the presence of the metathesis by-product,

the isothiocyanate S=C=NAd, in both cases, as well as an additional signal at 132 ppm assigned to the perthiodicarbonate $C_2S_6^{2-}$. The formation of an insoluble compound is also observed. The ^{13}C NMR spectrum in DMSO-d_6 of the residue obtained after removal of toluene form the reaction mixture shows the presence of peaks at 267 ppm and 129 ppm assigned to the CS_3^{2-} and to the $C_2S_6^{2-}$ species in a ratio of 1:1.2. Adding 18c6 to a 1:2 toluene reaction mixture of **4** and CS_2 allowed for the crystallisation of the unusual CS_3-coupling product, $[K(18c6)]_2[C_2S_6]$, **6** (Scheme 2).

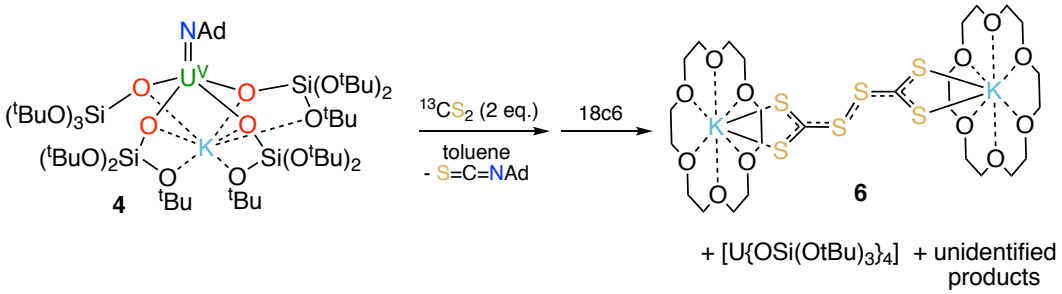

Scheme 2. Reaction of **4** with CS_2: isolation of **6** after addition of 1 equivalent of 18c6.

Perthiodicarbonate species are rare but some examples are known, e.g. $[PPh_4]_2[C_2S_6]$, which formed from aerial oxidation of a reaction mixture of PPh_4Cl and $K_2(CS_3)$.[17] Yellow crystals of **6** crystallised from toluene (Figure 3).

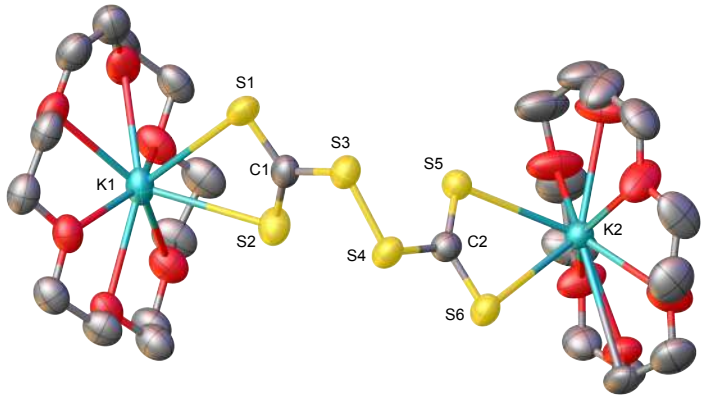

Figure 3. Solid-state molecular structure of $[K(18c6)]_2[C_2S_6]$, **6**. Thermal ellipsoids set at 50% probability. Hydrogen atoms were omitted for clarity. Only one conformation of a disordered 18c6 molecule is shown. Selected bond lengths [Å]: K1–S1 = 3.248(3), K1–S2 = 3.439(3), K2–S5 = 3.222(3), K2–S6 = 3.504(3), C1–S1 = 1.664(8), C1–S2 = 1.670(9), C1–S3 = 1.793(9), C2–S4 = 1.784(9), C2–S5 = 1.660(10), C2–S6 = 1.671(9), S3–S4 = 2.046(3).

The complex features two potassium ions encapsulated by two 18c6 molecules. Each potassium ion is bound to two terminal sulfur atoms of the $[C_2S_6]^{2-}$ dianion. Analysis of the bond lengths shows that the binding of the two sulfur atoms to each eight-

coordinate potassium ion is uneven (K1–S1 = 3.248(3) Å, K1–S2 = 3.439(3) Å; K2–S5 = 3.222(3) Å, K2–S6 = 3.504(3) Å), while the C–S bond lengths indicate delocalisation of the negative charge over the two sulfur atoms bound to each potassium ion (C1–S1 = 1.664(8) Å, C1–S2 = 1.670(9) Å, C1–S3 = 1.793(9) Å). The S–S bond length is 2.046(3) Å, and this, along with the C–S bond lengths, is consistent with the structural parameters reported for $[PPh_4]_2[C_2S_6]$.[17]

Complex **6** plausibly arises from uranium(V)-mediated oxidation of the trithiocarbonate in a putative $[U^V(CS_3)\{OSi(O^tBu)_3\}_4K]$ intermediate. Such an intermediate is likely to be formed from the reaction of a U(V) terminal sulfide, formed from the metathesis of the imido group with a first CS_2 molecule, with a second CS_2 molecule.

The presence of bound potassium ions incorporated into the structure of uranium siloxide complexes has been shown to have an important effect on the reactivity of U(III) complexes with CS_2, and on the stability of the resulting products with respect to trithiocarbonate or tetrathiooxalate ligand loss.[16a] Thus, we anticipated that the analogous reactions carried out with the U(V) imido complex **5**, where the presence of 2.2.2-cryptand prevents cation binding to the siloxides, might enable us to stabilise the U(V) terminal sulfide and terminal trithiocarbonate intermediates.

Indeed, the reaction of **5** with two to five equivalents of CS_2 in toluene afforded the trithiocarbonate complex $[K(2.2.2\text{-cryptand})][U(CS_3)\{OSi(O^tBu)_3\}_4]$, **7** in 57% yield (Scheme 3). The ^{1}H NMR spectrum of **7** in toluene-d_8 exhibits two signals with equal integration ratios at 1.77 ppm and 1.51 ppm, respectively, corresponding to the tert-butoxy protons of the siloxide ligands, indicating a C_2-symmetric species in solution. The ^{13}C NMR spectrum of **7** in toluene shows a broad signal at 180 ppm assigned to the bound thiocarbonate ligand. In addition to this signal, the ^{13}C NMR spectrum of the crude reaction mixture in toluene-d_8 showed the presence of the isothiocyanate product, S=C=NAd, a resonance at 132 ppm assigned to $C_2S_6^{2-}$, and a signal at 247 ppm (free CS_3^{2-}). The ^{1}H NMR spectrum of the reaction mixture also shows the presence of a signal assigned to $[U\{OSi(O^tBu)_3\}_4]$, but in a much smaller amount (8%) compared to what was found in the reaction of **4** with CS_2.

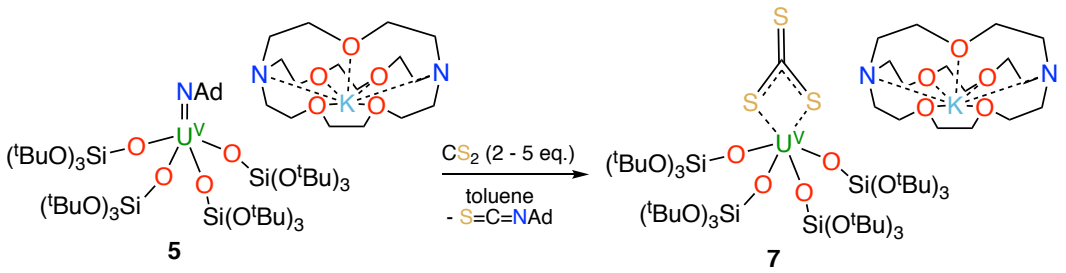

Scheme 3. Synthesis of the terminal U(V) trithiocarbonate complex [K(2.2.2-cryptand)]-[U(CS_3){OSi(OtBu)$_3$}$_4$], **7**.

Dark brown crystals of complex **7** crystallised from toluene (Figure 4). The six-coordinate uranium atom is coordinated by four siloxide oxygen atoms and two sulfur atoms of a terminally-bound κ^2S-trithiocarbonate moiety, affording a distorted octahedral coordination geometry.

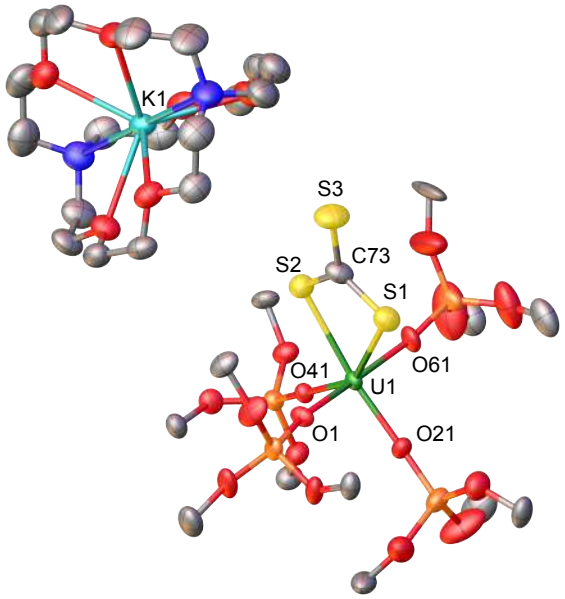

Figure 4. Solid-state molecular structure of [K(2.2.2-cryptand)][U(CS_3){OSi(OtBu)$_3$}$_4$], **7**. Thermal ellipsoids set at 50% probability. Hydrogen atoms were omitted for clarity. Only one conformation of a disordered 18c6 molecule is shown. Selected bond lengths [Å]: U1–S1 2.772(3), U1–S2 2.747(3), U1–O_{ave} 2.14(3), C73–S_{range} 1.68(1) - 1.75(1).

The structure bears similarities to the recently reported terminal U(IV) thiocarbonate [U(TrenTIPS)(κ^2-CS_3)][K(B15C5)$_2$] [18] and to the related U(IV) trithiocarbonate complex, [{K(18c6)}$_2${μ^3-κ^2:κ^2:κ^2-CS_3}{U(OSi(O^{t}Bu)$_3$)$_4$}].[16a] However, in the latter U(IV) complex, the 18c6-bound potassium cation is still able to bind two sulfur atoms of the thiocarbonate group. The average U–O bond length (2.10(3) Å) is noticeably shorter than the corresponding average bond lengths in the U(V) imido complexes, [K(18c6)][U(NSiMe$_3$){OSi(O^{t}Bu)$_3$}$_4$] and [K(18c6)][U(NAd){OSi(O^{t}Bu)$_3$}$_4$] (2.16(2) Å and 2.20(2) Å, respectively), and this is presumably a result of greater steric

congestion in the two imido complexes, although electronic effects cannot be ruled out. The U–S bond lengths (2.747(3) Å and 2.772(3) Å) are shorter than those in the aforementioned terminal (2.8415(8) and 2.8520(10) Å) [18] and $K(18c6)^+$-capped U(IV) trithiocarbonate complex (2.9488(19) Å and 2.951(2) Å).[16a] In the case of the capped complex the difference is greater than would be expected given the difference in ionic radii between U(IV) and U(V) (0.13 Å for six-coordinate ions),[19] probably due to electron-withdrawing effect of the two coordinated $\{K(18c6)\}^+$ units in the U(IV) complex. The C–S bond lengths (1.679(13) Å, 1.696(12) Å and 1.749(14) Å) show similar values (within error) as previously observed for the related U(IV) trithiocarbonate complex, $[\{K(18c6)]\}_2\{\kappa^2\text{-}CS_3\}\{U(OSi(O^tBu)_3)_4\}]$ (1.723(8), 1.711(10) and 1.704(8) Å) [16a] in agreement with charge delocalisation over the CS_3^{2-} unit.

Complex **7** is the first example of a U(V) uranium trithiocarbonate complex and is only the second example of a terminal trithiocarbonate complex in *f*-element chemistry.[18] Complex **7** shows higher stability than a putative trithiocarbonate intermediate formed in the reaction of the K^+ U(V) imido complex, **4** with CS_2. This is probably explained by the fact that in the absence of K^+ cations binding the trithiocarbonate group, oxidation of the trithiocarbonate by U(V) is not a favoured pathway. Complex **7** is likely formed by the nucleophilic addition of a U(V) terminal sulfide intermediate to a CS_2 molecule (Scheme 4). Fast addition of terminal and bridging U(IV) sulfide to CS_2 to afford terminal or bridging U(IV) thiocarbonate complexes has been previously reported.[4e, 20]

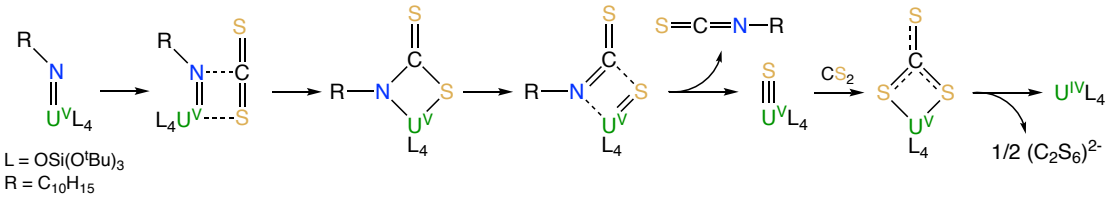

Scheme 4. Proposed pathway for the formation of complex **7** from the reaction of complex **5** with CS_2.

Monitoring the reaction between equimolar amounts of complex **5** and $^{13}CS_2$ by ^1H NMR spectroscopy showed a very slow reaction, due in part to the very low solubility of **5** in toluene, and after ten days, complex **7** and unreacted complex **4** were present in equimolar quantities. There is no evidence of the formation of the U(V) terminal sulfide intermediate under these conditions, probably due to its fast reaction with an

additional CS_2 molecule. We reasoned that using a less bulky imido complex might increase the rate of the first step of the reaction, thereby allowing for the isolation of a terminal sulfide complex, but NMR-scale reactions between [K(2.2.2-cryptand)]-[U(NSiMe$_3$){OSi(O^{t}Bu)$_3$}$_4$] and two equivalents of $^{13}CS_2$ showed that this strategy was unsuitable. The reaction was slow, and although multiple products were formed, it was possible to identify complex **7** in the reaction mixture by ^{1}H NMR spectroscopy. The presence of a terminal sulfide was not detected.

These results show that although the metathesis reaction of the U(V) imido complex with CS_2 leads to a terminal U(V) sulfido complex, the reaction is rather slow and the plausible U(V) terminal sulfide intermediate cannot be isolated due to its rapid reaction with another molecule of CS_2 to afford the trithiocarbonate complex. In an analogous approach, we anticipated that the high basicity of the imido group could be exploited in an acid/base metathesis reaction with H_2S to afford a terminal sulfide product. Indeed, treating a pre-chilled (−40 °C) suspension of [K(2.2.2-cryptand)][U(NAd){OSi(O^{t}Bu)$_3$}$_4$], **4** in toluene with a fresh, commercially available 0.8 M solution of H_2S in THF (1.3 equiv.) afforded the first isolable U(V) terminal sulfide complex, [K(2.2.2-cryptand)][US{OSi(O^{t}Bu)$_3$}$_4$], **8** (Scheme 5) in 41 % yield.

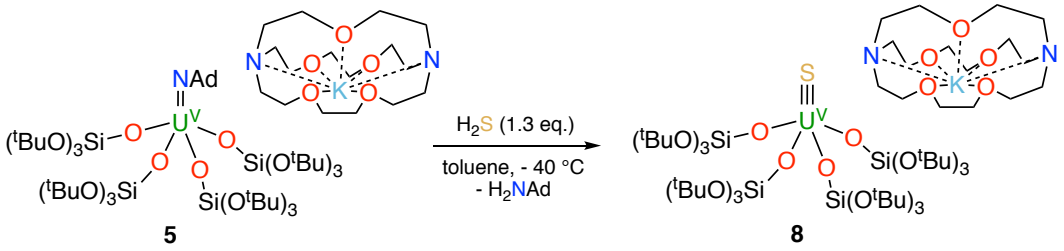

Scheme 5. Synthesis of the terminal U(V) sulfide complex , [K(2.2.2-cryptand)][US{OSi(OtBu)$_3$}$_4$], **8**.

Some unidentified side products also formed in the reaction, but a ^{1}H NMR spectroscopy experiment using naphthalene as an internal standard showed that the conversion rate to the terminal sulfide product was 76%. The ^{1}H NMR spectrum of **8** in toluene-d$_8$ only shows one broad resonance at 1.20 ppm that corresponds to the tert-butoxy protons of the siloxde ligands, along with three signals for the cryptand protons. The fact that only one signal is observed for the siloxide protons suggests that the structure of **8** is fluxional in solution. Complex **8** is reasonably thermally stable and it only showed minor decomposition in solution over the course of a week at room temperature. The formation of the terminal sulfide is likely to involve a

double H-atom transfer from the H_2S to the imido nitrogen. No intermediate reaction product was observed by NMR spectroscopy, suggesting that if the plausible uranium amide/hydrosulfide intermediate is formed (as previously proposed in the hydrosulfidolysis of titanium imido complexes) the H-transfer from the bound SH to the resulting amido group is fast.[15b, 15c]

Dark brown crystals of complex **8** crystallised from toluene as two crystallographically independent units. The molecular structure is shown in Figure 5 and selected bond lengths are listed in Table 1. The uranium atoms in each molecule are ligated by one terminally bound sulfide atom and the negatively charged oxygen atoms of four siloxide ligands, resulting in a distorted trigonal bipyramidal coordination geometry.

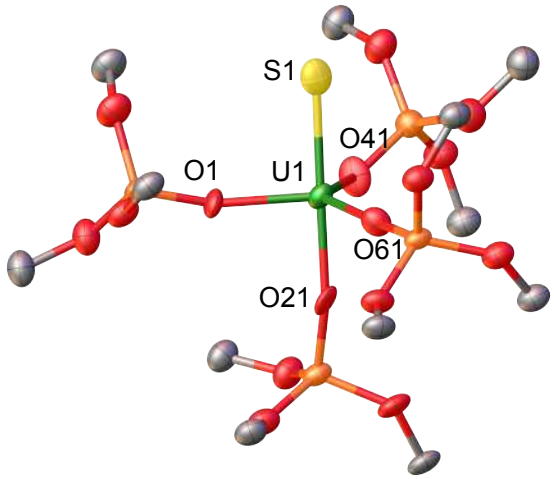

Figure 5. Solid-state molecular structure of the anion of [K(2.2.2-cryptand)][US{OSi(OtBu)$_3$}$_4$], **8**. Thermal ellipsoids set at 50% probability. [K(2.2.2-cryptand)]$^+$, hydrogen atoms were omitted for clarity. Only one conformation of a disordered 18c6 molecule is shown. Selected bond lengths [Å]: U1–S1 2.376(5), U1–O_{ave} 2.10(3).

The U–S bond lengths of the two independent molecules are 2.376(5) Å and 2.396(5) Å, respectively, which are considerably shorter than the corresponding bond length in the U(IV) analogue, [K(2.2.2-cryptand)][US(OSi(O^{t}Bu)$_3$)$_4$K] (2.5220(14) Å).[4e] However, this difference is about what would be expected after accounting for the difference in ionic radii between U(IV) and U(V). The average U–O bond lengths (2.14(3) Å for molecule 1 and 2.13(4) Å for molecule 2, respectively) are longer than the corresponding average bond length in complex **7**. Given that a sulfide ligand is

considerably less bulky than a trithiocarbonate moiety, this difference can probably be ascribed primarily to electronic effects.

Table 1. Selected bond lengths (Å) for complexes **7**·tol and **8**·1.5tol

Structural parameters	**7**·tol	**8**·1.5tol
U1–S1	2.772(3)	2.376(5)
U1–S2	2.747(3)	–
U1–O_{ave}	2.14(3)	2.10(3)
C73–S_{range}	1.68(1)–1.75(1)	–

A ^{1}H NMR experiment showed that complex **7** reacted immediately with 1 equiv. of $^{13}CS_2$ in toluene-d_8 to yield **8** as the only product. This result supports the possibility of **7** as an intermediate in the formation of **8** from **5**.

The X-band EPR spectra of **7** and **8** were measured in a toluene/acetonitrile glass (see Appendix 4). While no signal was detected at room temperature, an EPR signal, featuring broad linewidths (600 to 800 mT), that unambiguously originates from a metal-centred unpaired electron was observed at 10 K for both complexes. In both cases, the EPR signal was fitted with a rhombic set of g-values (g_1 = 1.246; g_2 = 1.03; g_3 = 0.725 for **7** and g_1 = 1.378; g_2 = 1.24; g_3 = 0.25 for **8**) that are comparable to those reported for the octahedral uranium(V) complex, [UO(OSi(O^{t}Bu)$_3$)$_4$K] (g_1 = 1.248; g_2 = 0.856; g_3 = 0.485).[8b]

Computational bonding analysis

In order to investigate the nature of the U–S bond in complexes **7** and **8**, we performed calculations at the B3PW91 level, as this method was successfully applied to describe the U–chalcogen bonds in previous studies.[4d,4e] Firstly, the bonding situation was analysed in the U(V) trithiocarbonate complex **7**. No clear U–S multiple bond character was found. Rather, two σ U–S bonds (HOMO-4 and HOMO-5 in Figure 6) and a C=S double bond (HOMO and HOMO-1 in Figure 6) are found in the MO spectrum. The NBO analysis indicates the same bonding situation, with two σ

bonds that are strongly polarised towards S (77-78% S and 22-22% U), and involve a hybrid 6d/5f orbital at the uranium centre.

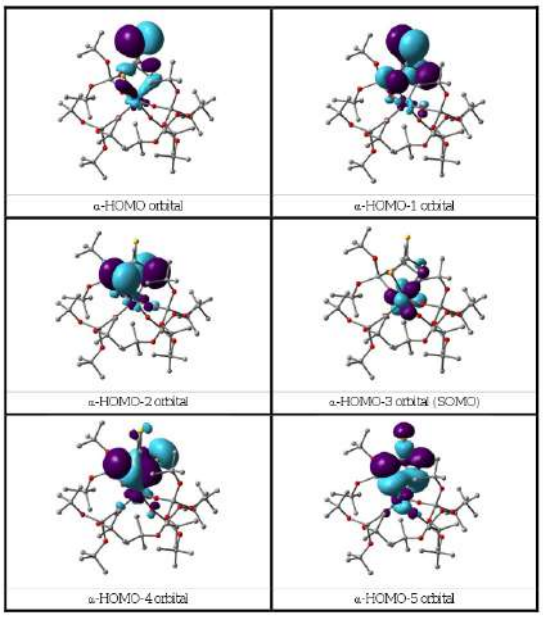

Figure 6. Frontier molecular orbitals of complex **7**.

Finally, the WBI of the U–S bonds are 0.94 and 1.02, in line with a σ bond with highly covalent character. The bonding in the U(IV) dipotassium trithiocarbonate is quite similar to the one found in **7**. Indeed, two σ U–S bonds are found but these bonds are even more polarised than in **7**, with a contribution of 90% from sulfur. This is reflected in the WBI (only 0.47/0.50), indicating a less covalent bond.

However, since the U(IV) trithiocarbonate complex involves the coordination of two potassium atoms, its putative U(V) equivalent was computed to check the influence of the two potassium ions on the bonding. In the latter U(V) complex, the bonding is also consistent with two U–S σ bonds. These bonds appear to be as polarised as in **7**, with a 77/80% contribution from sulfur to the bonding.

On the other hand, the WBI are 0.72/0.75, intermediate between the values found for **7** and the U(IV) compound, in line with an influence of the potassium on the covalency. Indeed, the presence of the interaction between the potassium and the trithiocarbonate decreases the covalency in the U–S bond, mainly because the atomic orbitals of sulfur need to overlap with both U and K. Using similar methods, we analysed the bonding in complex **8** and compared it with the bonding found in its

U(IV) analogue.[4e] Molecular orbital analysis (Figure 7) clearly indicates a triple bond that is similar to that observed for the U(IV) analogue.

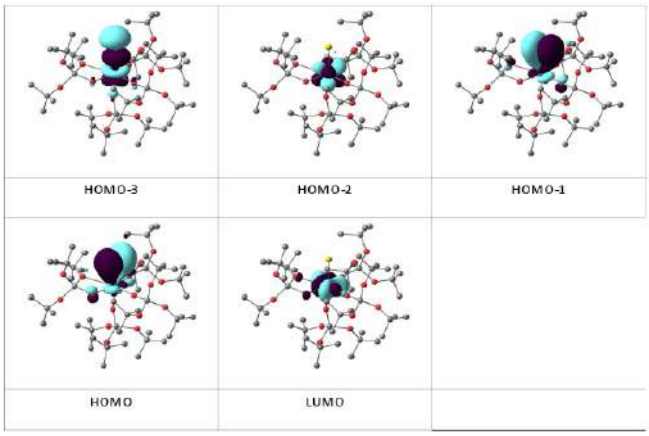

Figure 7. Frontier molecular orbitals of complex **8**.

The HOMO-3 is the σ bond, whereas HOMO-1 and HOMO are the two π orbitals. Natural bonding orbital (NBO) analysis is in line with this bonding description. Indeed, at the first order, three bonding orbitals (1σ and 1π) are found and they are strongly polarised towards S (77%, 80% and 81% for the σ orbital and the two π orbitals, respectively). Finally, the Wiberg Bond Index (WBI) is 2.2, in line with a triple bond with very strong covalent character. This is very close to the value of 2.25 that was found for the U(I)V analogue, indicating that oxidation of the U(IV) complex does not affect the bonding but only removes an electron from one of the 5f orbitals that becomes the LUMO of the U(V) system.

Conclusions

To summarise, we have prepared and fully characterised the first examples of stable terminal U(V) sulfide and thiocarbonate complexes using bulky siloxides as supporting ligands.

DFT calculations were performed to investigate the nature of the U–S bond in complexes **7** and **8**, and the results were compared with the analyses of the analogous U(IV) complexes. Based on this analysis, triple-bond character with strong covalent character is suggested for the U–S bond in the terminal uranium(V) sulfide **8**, in line with previous studies on terminal U(IV) sulfides. Single-bond character was found for the U–S bond in complex **7**, which turned out to be more covalent than in the U(IV) analogue.

In conclusion, we have shown that the metathesis of U(V) imido complexes with CS_2 or H_2S provides a convenient route to terminal sulfides. However, the metathesis reaction with CS_2 was very slow and resulted in nucleophilic addition of the putative sulfide intermediate to CS_2. Moreover, the presence of siloxide-bound cations in the U(V) imido precursor resulted in the isolation of a side-reaction product, the perthiodicarbonate, salt $[K(18c6)]_2[C_2S_6]$, resulting from the oxidation of CS_3^{2-} by U(V).

In contrast, the metathesis of U(V) with H_2S readily forms a stable terminal U(V) sulfide. The hydrosulfidolysis of uranium imides reported here provide a versatile route to uranium terminal chalcogenides that should be easily extended to other uranium oxidation states and to other chalcogenides. Work in this direction is in progress.

Experimental

General procedures. Unless otherwise noted, all manipulations were carried out at ambient temperature under an inert atmosphere using Schlenk techniques and an MBraun glovebox equipped with a purifier unit. The water and oxygen level were always kept at less than 1 ppm. Glassware was dried overnight at 150 °C prior to use. **Starting materials.** The solvents were purchased, in their anhydrous form, from Aldrich or Cortecnec (deuterated solvents), conditioned under argon and vacuum distilled from K/benzophenone (toluene, THF) or sodium dispersion (hexane) or dried over 4 Å molecular sieves for one week (DMSO). All reagents were dried under high-vacuum for 5 days prior to use. $HOSi(OtBu)_3$ was purified by sublimation prior to use. Depleted uranium turnings were purchased from the "Société Industrielle du Combustible Nucléaire" of Annecy (France). $[U(OSi(OtBu)_3)_4K]$, **2** [8b], $[K(18c6)][U\{OSi(OtBu)_3\}_4]$,[13] and $[K(18c6)][U(NAd\{OSi(OtBu)_3\}_4]$, **1** [13] were prepared according to the published procedures. The complex [K(2.2.2-cryptand)]$[U(NSiMe_3)\{OSi(OtBu)_3\}_4]$ was prepared from **3** following a procedure analogous to that reported for $[K(18c6)][U(NSiMe_3)(OSi(O^tBu)_3)_4]$.[13] Synthetic details for the preparation of [K(2.2.2-cryptand)]$[U\{OSi(OtBu)_3\}_4]$, **3**, $[U(NAd)\{OSi(OtBu)_3\}_4K]$, **4**, and [K(2.2.2-cryptand)]$[U(NAd)\{OSi(OtBu)_3\}_4]$, **5** are given in the supporting

information. **NMR and EPR spectroscopy.** NMR spectra were performed in J. Young NMR tubes. ^{1}H and ^{13}C NMR spectra were recorded on a Bruker 400MHz spectrometer. NMR chemical shifts are reported in ppm and were referenced to the residual ^{1}H and ^{13}C signals of the deuterated solvents. EPR spectra of **7** and **8** were measured with a Bruker Elexsys E500 spectrometer working at 9.4 GHz frequency with an oxford ESR900 cryostat for 4–300 K operation. Baseline correction of the raw EPR spectrum was performed with cubic spline (Xepr 2.4b.12, Bruker). Simulations were performed with the Easyspin 5.1.3 program.[21] **Elemental analyses**. Samples were analysed under nitrogen by the elemental analyses department of the EPFL using a Thermo Scientific Flash 2000 Organic Elemental Analyzer.

Synthesis of [K(2.2.2-cryptand)][U(CS$_3$){OSi(OtBu)$_3$}$_4$], 7

[K(2.2.2-cryptand)][U{OSi(OtBu)$_3$}$_4$] (46 mg, 0.025 mmol) was suspended in toluene (0.5 mL) and then $^{13}CS_2$ (7.4 µL, 0.12 mmol) was added by syringe. The mixture was monitored periodically by ^{1}H NMR spectroscopy until there was no more starting material (ca. 10 days). The product crystallised from solution in two batches and the dark brown crystals of **7** were dried under vacuum (26 mg, 57 %). Single crystals suitable for X-ray crystallography were grown from toluene. Anal. calcd for **7** $C_{67}H_{144}KN_2O_{22}S_3Si_4U$ (1815.55): C, 44.32; H, 7.99; N, 1.54. Found C, 44.37; H, 8.22; N, 1.45. ^{1}H NMR (400 MHz, d_8-toluene, 298 K): δ [ppm] 3.24 (brs, 12H, 2.2.2-cryptand), 3.13 (brs, 12H, 2.2.2-cryptand), 2.14 (brs, 12H, 2.2.2-cryptand), 1.77 (brs, 54H, OSiOtBu), 1.51 (brs, 54H, OSi(OtBu)$_3$). ^{13}C NMR (100.6 MHz, d_8-toluene, 298 K): δ [ppm] 180.88 (CS_3), 77.78 (OSiO*C*(CH_3)), 71.80 (OSiO*C*(CH_3)), 70.82 (2.2.2-cryptand) 67.81 (2.2.2-cryptand), 54.08 (2.2.2-cryptand), 32.62 (OSiOC(*CH_3*)), 27.97 (OSiOC(*CH_3*)).

Synthesis of [K(2.2.2-cryptand)][US{OSi(OtBu)$_3$}$_4$], 8

[K(2.2.2-cryptand)][U{OSi(OtBu)$_3$}$_4$] (89 mg, 0.048 mmol) was suspended in toluene (1.5 mL) and the mixture was chilled to −40 °C. A 0.8 M solution of H_2S in thf (75 µL, 0.060 mmol) was added by syringe, immediately giving a dark brown solution. A slight excess (1.3 eq.) of H_2S is needed to ensure consumption of the starting material and the reaction is sensitive to the quality

of the H_2S solution that is used. The resulting dark brown solution was stirred overnight at −40 °C and then for two hours at room temperature the following morning. The solvent was then removed under vacuum, leaving a dark brown oil. Hexane (0.5 mL) was added to the oil and then the mixture was dried under vacuum giving a brown solid. The solid was washed with hexane (3 x 1 mL), and then the resulting solid was recrystallised from toluene several times at −40 °C, affording analytically pure dark brown crystals of **8** (36 mg, 41 %). Single crystals suitable for X-ray crystallography were grown from toluene at −40 °C. Anal. calcd for **8**·0.8toluene $C_{67.75}H_{150.4}KN_2O_{22}SSi_4U$ (1813.12): C, 47.43; H, 8.36; N, 1.55. Found C, 47.46; H, 8.83; N, 1.58. ^{1}H NMR (400 MHz, d_8-toluene, 298 K): δ [ppm] 4.08 (s, 12H, 2.2.2-cryptand), 4.01 (t, 12H, 2.2.2-cryptand), 3.05 (t, 12H, 2.2.2-cryptand), 1.20 (brs, 108H, $OSi(OtBu)_3$). ^{13}C NMR (100.6 MHz, d_8-toluene, 298 K): δ [ppm] 180.88 (CS_3), 73.76 ($OSiOC(CH_3)$), 71.05 ($OSiOC(CH_3)$), 56.38 (2.2.2-cryptand), 32.44 ($OSiOC(CH_3)$).

A conversion experiment using naphthalene as an internal standard determined the conversion of **4** to **8** to be 76 % by ^{1}H NMR spectroscopy.

Reaction of 4 with CS_2: isolation of $[K(18c6)]_2[C_2S_6]$, 6

$^{13}CS_2$ (1.6 μL, 0.027 mmol) was added to a dark brown solution of **4** (20 mg, 0.014 mmol) in d_8-toluene (0.5 mL), and the resulting dark brown solution was kept at room temperature for several days until complete consumption of **4** was observed. Then, 18c6 (3.7 mg, 0.014 mmol) was added. After several days, a few yellow single crystals of $[K(18c6)]_2[C_2S_6]$, **6** deposited. The crystals were reproducibly obtained but attempts to isolate larger amounts only gave mixtures of products.

A conversion experiment using naphthalene as an internal standard determined the conversion of **4** into $[U\{OSi(OtBu)_3\}_4]$ to be 35 % by ^{1}H NMR spectroscopy.

Reaction of 8 with CS_2 to afford 7

A 0.59 M solution of $^{13}CS_2$ in d_8-toluene (5.0 μL, 0.0030 mmol) was added to a brown solution of $[K(2.2.2\text{-cryptand})][US\{OSi(OtBu)_3\}_4]$, **8** (4 mg, 0.0023 mmol) in d_8-toluene (0.5 mL). ^{1}H NMR spectroscopy showed immediate and complete

consumption of **8**, and the appearance of signals corresponding to [K(2.2.2-cryptand)][U(CS_3){OSi($OtBu)_3$}$_4$], **7**.

Bibliography

[1] a) S. T. Liddle, *Angew. Chem. Int. Ed. Engl.* **2015**, *54*, 8604-8641; b) T. W. Hayton, *Dalton Trans* **2010**, *39*, 1145-1158; c) T. W. Hayton, *Chem. Commun.* **2013**, *49*, 2956-2973; d) M. Ephritikhine, *Coord. Chem. Rev.* **2016**, *319*, 35-62; e) M. B. Jones, A. J. Gaunt, *Chem. Rev.* **2013**, *113*, 1137-1198.

[2] a) K. I. M. Ingram, N. Kaltsoyannis, A. J. Gaunt, M. P. Neu, *J. Alloys Compd.* **2007**, *444*, 369-375; b) C. Madic, M. Lecomte, P. Baron, B. Boullis, *Comptes Rendus Physique* **2002**, *3*, 797-811; c) S. R. Daly, J. M. Keith, E. R. Batista, K. S. Boland, D. L. Clark, S. A. Kozimor, R. L. Martin, *J. Am. Chem. Soc.* **2012**, *134*, 14408-14422; d) D. E. Smiles, G. Wu, P. Hrobarik, T. W. Hayton, *J. Am. Chem. Soc.* **2016**, *138*, 814-825; e) M. B. Jones, A. J. Gaunt, J. C. Gordon, N. Kaltsoyannis, M. P. Neu, B. L. Scott, *Chem. Sci.* **2013**, *4*, 1189-1203; f) L. Karmazin, M. Mazzanti, J. Pecaut, *Chem. Commun.* **2002**, 654-655.

[3] a) J. L. Brown, G. Wu, T. W. Hayton, *Organometallics* **2013**, *32*, 1193-1198; b) O. P. Lam, F. W. Heinemann, K. Meyer, *Chem. Sci.* **2011**, *2*, 1538-1547; c) J. G. Brennan, R. A. Andersen, A. Zalkin, *Inorg. Chem.* **1986**, *25*, 1761-1765; d) L. R. Avens, D. M. Barnhart, C. J. Burns, S. D. McKee, W. H. Smith, *Inorg. Chem.* **1994**, *33*, 4245-4254; e) A. J. Gaunt, B. L. Scott, M. P. Neu, *Inorg. Chem.* **2006**, *45*, 7401-7407; f) L. P. Spencer, P. Yang, B. L. Scott, E. R. Batista, J. M. Boncella, *Inorg. Chem.* **2009**, *48*, 11615-11623; g) W. J. Evans, E. Montalvo, J. W. Ziller, A. G. DiPasquale, A. L. Rheingold, *Inorg. Chem.* **2010**, *49*, 222-228.

[4] a) L. Ventelon, C. Lescop, T. Airligue, P. C. Leverd, M. Lance, M. Nierlich, M. Ephritikhine, *Chem. Commun.* **1999**, 659-660; b) J. L. Brown, S. Fortier, R. A. Lewis, G. Wu, T. W. Hayton, *J. Am. Chem. Soc.* **2012**, *134*, 15468-15475; c) D. E. Smiles, G. Wu, T. W. Hayton, *J. Am. Chem. Soc.* **2014**, *136*, 96-99; d) M. W. Rosenzweig, A. Scheurer, C. A. Lamsfus, F. W. Heinemann, L. Maron, J. Andrez, M. Mazzanti, K. Meyer, *Chem. Sci.* **2016**, *7*, 5857-5866; e) J. Andrez, J. Pecaut, R. Scopelliti, C. E. Kefalidis, L. Maron, M. W. Rosenzweig, K. Meyer, M. Mazzanti, *Chem. Sci.* **2016**, *7*, 5846-5856.

[5] a) D. E. Smiles, G. Wu, T. W. Hayton, *Inorg. Chem.* **2014**, *53*, 10240-10247; b) D. E. Smiles, G. Wu, P. Hrobarik, T. W. Hayton, *J. Am. Chem. Soc.* **2016**, *138*, 814-825.

[6] J. L. Brown, S. Fortier, G. Wu, N. Kaltsoyannis, T. W. Hayton, *J. Am. Chem. Soc.* **2013**, *135*, 5352-5355.

[7] a) D. S. J. Arney, C. J. Burns, *J. Am. Chem. Soc.* **1993**, *115*, 9840-9841; b) P. Roussel, R. Boaretto, A. J. Kingsley, N. W. Alcock, P. Scott, *J. Chem. Soc. Dalton Trans.* **2002**, 1423-1428; c) S. Fortier, N. Kaltsoyannis, G. Wu, T. W. Hayton, *J. Am. Chem. Soc.* **2011**, *133*, 14224-14227.

[8] a) S. C. Bart, C. Anthon, F. W. Heinemann, E. Bill, N. M. Edelstein, K. Meyer, *J. Am. Chem. Soc.* **2008**, *130*, 12536-12546; b) O. Cooper, C. Camp, J.

Pecaut, C. E. Kefalidis, L. Maron, S. Gambarelli, M. Mazzanti, *J. Am. Chem. Soc.* **2014**, *136*, 6716-6723; c) D. M. King, F. Tuna, J. McMaster, W. Lewis, A. J. Blake, E. J. L. McInnes, S. T. Liddle, *Angew. Chem. Int. Ed. Engl.* **2013**, *52*, 4921-4924; d) N. Tsoureas, A. F. R. Kilpatrick, C. J. Inman, F. G. N. Cloke, *Chem. Sci.* **2016**, *7*, 4624-4632.

[9] D. M. King, F. Tuna, E. J. L. McInnes, J. McMaster, W. Lewis, A. J. Blake, S. T. Liddle, *Science* **2012**, *337*, 717-720.

[10] a) G. Nocton, P. Horeglad, V. Vetere, J. Pecaut, L. Dubois, P. Maldivi, N. M. Edelstein, M. Mazzanti, *J. Am. Chem. Soc.* **2010**, *132*, 495-508; b) C. R. Graves, J. L. Kiplinger, *Chem. Commun.* **2009**, 3831-3853; c) L. A. Seaman, G. Wu, N. Edelstein, W. W. Lukens, N. Magnani, T. W. Hayton, *J. Am. Chem. Soc.* **2012**, *134*, 4931-4940; d) C. R. Graves, P. Yang, S. A. Kozimor, A. E. Vaughn, D. L. Clark, S. D. Conradson, E. J. Schelter, B. L. Scott, J. D. Thompson, P. J. Hay, D. E. Morris, J. L. Kiplinger, *J. Am. Chem. Soc.* **2008**, *130*, 5272-5285; e) P. L. Arnold, J. B. Love, D. Patel, *Coord. Chem. Rev.* **2009**, *253*, 1973-1978; f) G. Nocton, P. Horeglad, J. Pécaut, M. Mazzanti, *J. Am. Chem. Soc.* **2008**, *130*, 16633–16645.

[11] a) C. R. Graves, B. L. Scott, D. E. Morris, J. L. Kiplinger, *Chem. Commun.* **2009**, 776-778; b) T. Arliguie, M. Fourmigue, M. Ephritikhine, *Organometallics* **2000**, *19*, 109-111; c) C. Camp, M. A. Antunes, G. Garcia, I. Ciofini, I. C. Santos, J. Pecaut, M. Almeida, J. Marcalo, M. Mazzanti, *Chem. Sci.* **2014**, *5*, 841-846.

[12] a) K. Chondroudis, M. G. Kanatzidis, *J. Am. Chem. Soc.* **1997**, *119*, 2574-2575; b) D. L. Gray, L. A. Backus, H. A. K. von Nidda, S. Skanthakumar, A. Loidl, L. Soderholm, J. A. Ibers, *Inorg. Chem.* **2007**, *46*, 6992-6996; c) D. E. Bugaris, J. A. Ibers, *Inorg. Chem.* **2012**, *51*, 661-666.

[13] C. Camp, J. Pecaut, M. Mazzanti, *J. Am. Chem. Soc.* **2013**, *135*, 12101-12111.

[14] a) A. E. Guiducci, C. L. Boyd, P. Mountford, *Organometallics* **2006**, *25*, 1167-1187; b) P. J. Tiong, A. Nova, L. R. Groom, A. D. Schwarz, J. D. Selby, A. D. Schofield, E. Clot, P. Mountford, *Organometallics* **2011**, *30*, 1182-1201; c) S. R. Dubberley, A. Friedrich, D. A. Willman, P. Mountford, U. Radius, *Chem. Eur. J.* **2003**, *9*, 3634-3654.

[15] a) G. Parkin, in *Progress in Inorganic Chemistry, Vol 47, Vol. 47* (Ed.: K. D. Karlin), **1998**, pp. 1-165; b) W. D. Wang, I. A. Guzei, J. H. Espenson, *Inorg. Chem.* **2000**, *39*, 4107-4112; c) D. Swallow, J. M. McInnes, P. Mountford, *J. Chem. Soc., Dalton Trans.* **1998**, 2253-2259.

[16] a) C. Camp, O. Cooper, J. Andrez, J. Pecaut, M. Mazzanti, *J. Chem. Soc.-Dalton Trans.* **2015**, *44*, 2650-2656; b) L. Chatelain, R. Scopelliti, M. Mazzanti, *J. Am. Chem. Soc.* **2016**, *138*, 1784-1787; c) M. Falcone, C. E. Kefalidis, R. Scopelliti, L. Maron, M. Mazzanti, *Angew. Chem. Int. Ed. Engl.* **2016**, *55*, 12290-12294.

[17] A. Muller, E. Krickemeyer, F. Elkatri, D. Rehder, A. Stammler, H. Bogge, F. Hellweg, *Z. Anorg. Allg. Chem.* **1995**, *621*, 1160-1170.

[18] P. A. Cleaves, C. E. Kefalidis, M. G. Gardiner, F. Tuna, E. J. L. McInnes, W. Lewis, L. Maron, S. T. Liddle, *Chem. Eur. J.* **2017**, *23*, 2950 – 2959.

[19] R. D. Shannon, *Acta Crystallogr A* **1976**, *32*, 751-767.

[20] O. P. Lam, L. Castro, B. Kosog, F. W. Heinemann, L. Maron, K. Meyer, *Inorg. Chem.* **2012**, *51*, 781-783.

[21] S. Stoll, A. Schweiger, *J. Magn. Reson.* **2006**, *178*, 42-45.

CHAPTER 6

Nitrogen reduction and functionalization by a multimetallic uranium nitride complex

Introduction[1]

Molecular nitrogen (N_2) is cheap and widely available, but its unreactive nature is a challenge when attempting to functionalize it under mild conditions with other widely available substrates such as carbon monoxide, to produce value-added compounds. Biological N_2 fixation can do this, but the industrial Haber-Bosch process for ammonia production operates under harsh conditions (450 °C and 300 bar), even though both processes are thought to involve multimetallic catalytic sites.[1] And although molecular complexes capable of binding and even reducing N_2 under mild conditions are known, with co-operativity between metal centres considered crucial for the N_2 reduction step[1-2], the multimetallic species involved are usually not well defined, and further transformation of N_2-binding complexes to achieve N–H or N–C bond formation is rare.[1b, 2d, 2f, 2h, 3] Haber noted,[4] before an iron-based catalyst was adopted for the industrial Haber–Bosch process, that uranium and uranium nitride materials are very effective heterogeneous catalysts for ammonia production from N_2. However, few examples of uranium complexes binding N_2 are known,[5] and soluble uranium complexes capable of transforming N_2 into ammonia or organonitrogen compounds have not yet been identified. In this chapter the four-electron reduction of N_2 under ambient conditions is presented. The dinitrogen reduction is effected by a complex with two U(III) ions and three K^+ centers held together by a nitride group and a flexible metalloligand framework. The addition of hydrogen and/or protons, or CO to the resulting N_2^{4-} complex results in the complete cleavage of N_2 with concomitant N–H or N–C bond-forming reactions. These observations establish that a molecular uranium complex can promote the stoichiometric transformation of N_2 into value-added compounds, and that a flexible, electron-rich, multimetallic, nitride-

[1] Portions of this chapter have been published: M. Falcone, L. Chatelain, R. Scopelliti, I. Zivkovic, M. Mazzanti, *Nature,* **2017**, 547, 332
Author contributions: M.F. carried out the synthetic experiments and analysed the experimental data; L.C. carried out preliminary synthetic experiments, including the isolation of the dinitrogen complex. R.S. performed the X-ray single crystal structure analyses; I.Z. carried out and analysed the magnetic measurements; M.M. and M.F. wrote the manuscript.

bridged core unit is a promising starting point for the design of molecular complexes capable of cleaving and functionalizing N_2 under mild conditions.

Results and discussion

We prepared the diuranium(III) nitride complex $[K_3\{[U(OSi(O^tBu)_3)_3]_2(\mu\text{-}N)\}]$, **1**, by reduction of the previously reported [6] diuranium(IV) nitride-bridged complex $[Cs\{[U(O\,Si(O^tBu)_3)_3]_2(\mu\text{-}N)\}]$ with excess KC_8 (10 equiv.) in THF (tetrahydrofuran) at −70 °C. The presence of potassium results in greater solid-state and solution stability of complex **1** compared to the previously reported [7] Cs analogue $[Cs_3\{[U(OSi(O^tBu)_3)_3]_2(\mu\text{-}N)\}]$ ($Cs_3U{-}N{-}U$), allowing for more controlled reactivity. The solid-state molecular structure of complex **1** (Figure 1) features a heterometallic $K_3U{-}N{-}U$ core in which the two uranium(III) are bridged by a nitride group. Three siloxide-ligated K^+ bind the nitride moiety, forming a distorted triangular array that is perpendicular to the U(III)−N−U(III) core with a U–N–U angle of 173.7(8)° and a U–U distance of 4.234(2) Å. Overall, the potassium-siloxide framework results in the presence of three flexible bidentate metalloligands bridging the two uranium ions.

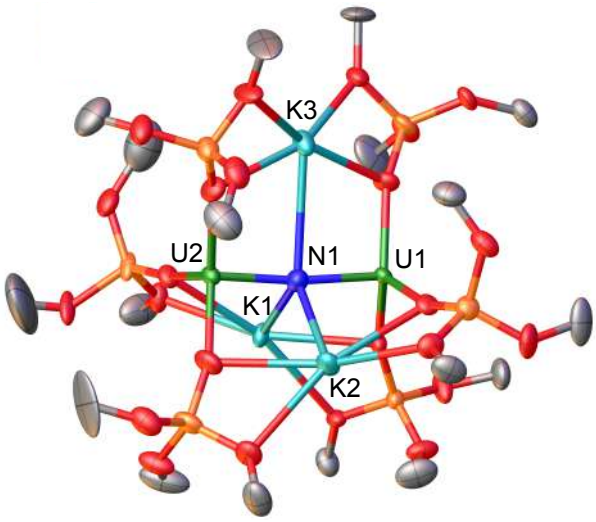

Figure 1. Solid-state molecular structure of $[K_3\{[U(OSi(O^tBu)_3)_3]_2(\mu\text{-}N)\}]$, **1**. Thermal ellipsoids set at 50% probability. Hydrogen atoms and methyl groups were omitted for clarity. Selected bond lengths [Å]: U1–N1 2.129(14), U2–N1 2.111(14), K1–N1 3.115(17), K2–N1 3.017(16), K3–N1 3.243(15), average $U{-}O_{siloxide}$ 2.288(28).

Exposing the multimetallic uranium(III) complex **1** to N_2 (0.5 - 1 atm) at room temperature in the solid state or in a toluene solution affords $[K_3\{[U(OSi(O^tBu)_3)_3]_2(\mu\text{-}N)(\mu\text{-}\eta^2\text{:}\eta^2\text{-}N_2)\}]$, **2**, in 68% isolated yield (Scheme 1).

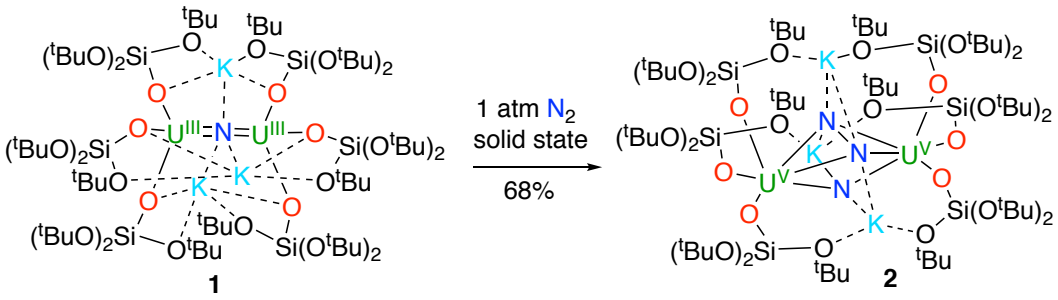

Scheme 1. Four-electron reduction of N_2 by **1** to afford the diuranium(V) complex **2**.

The X-ray crystal structure of **2** (Figure 2) shows one nitrido atom and a side-on-bound hydrazido moiety (N_2^{4-}) bridging two uranium centres in a diamond-shaped geometry with a U–U distance of 3.305(1) Å. The assignment of the three nitrogen atoms in **2** as a hydrazido(4–) ligand and a nitrido(3–) ligand requires a formal oxidation state of +5 for the uranium ions. Each of the three N atoms in **2** is also bound to a siloxide-ligated potassium cation. The U–N3 distance (2.069(2) Å) is in the range of U–N distances reported for nitride-bridged uranium compounds.[6-7] The $U_2(\mu\text{-}\eta^2\text{:}\eta^2\text{-}N_2)$ moiety features U–N bond distances ranging from 2.163(13) Å to 2.311(13) Å, consistent with the presence of U–N single bonds.[8] The value of the N–N bond length (1.521(18) Å) corresponds to the presence of a highly activated bound N_2 that has been reduced to a hydrazido(4–) (N_2^{4-}) moiety. This value is comparable to the observed bond length in hydrazine, H_2NNH_2 (1.47 Å) and falls in the range of values (1.377(3) - 1.635(5) Å) reported for hydrazido complexes.[2a, 2d, 2e, 2g, 9]

The flexible potassium-siloxide framework plays a crucial role in holding together the U–N–U core while it bends upon N_2 binding (the U–N–U angle changes from 173.7(8)° in **1** to 106.0(5)° in **2**).

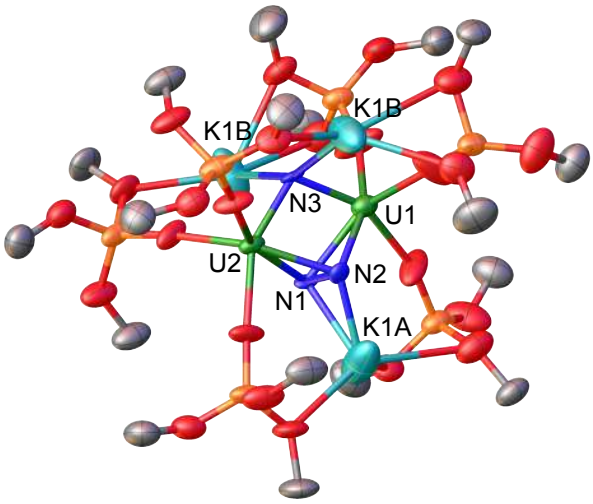

Figure 2. Solid-state molecular structure of $[K_3\{[U(OSi(O^tBu)_3)_3]_2(\mu\text{-}N)(\mu\text{-}\eta^2\text{:}\eta^2\text{-}N_2)\}]$, **2**. Thermal ellipsoids set at 50% probability. Hydrogen atoms and methyl groups were omitted for clarity. Selected bond lengths [Å] and angles: U2–N3 2.071(13), U1–N3 2.068(13), U1–N2 2.163(13), U2–N2 2.247(13), U2–N1 2.234(13), U1–N1 2.311(13), N1–N2 1.521(18), K1A–N1 1.926(14), K1A–N2 2.440(18), K1B–N3#1 3.067(17), K1B–N3 3.182(17), average $U\text{–}O_{siloxide}$ 2.229(15); U1–N1–U2 = 93.3(5)° and U1–N2–U2 = 97.1(5)°. Only one of the three disordered positions (occupancy 0.33) of the N atoms in complex **2** is shown.

The +5 oxidation state of the two uranium centers is supported by electron paramagnetic resonance (EPR) data and variable temperature magnetic data measured with a superconducting quantum interference devide (SQUID). The X-Band EPR spectrum of **2** (Figure 3a) shows an intense signal at 10 K that was fitted with a rhombic set of g-values (g_1 = 1.73; g_2 = 0.78; g_3 = 0.46), confirming the presence of uranium in the +5 oxidation state. The g values of **2** can be compared to those reported for an octahedral uranium(V) monoxo-complex (g_1 = 1.248; g_2 = 0.856; g_3 = 0.485). [10] The solid-state magnetic moment of **2** at 298 K was found to be of 2.06 μ_B per uranium. This value is significantly lower than the theoretical U(V) free ion value (μ_{eff} = 2.54 μ_B) but is in the range of magnetic moments previously reported for U(V) complexes (1.35 - 3.40 μ_B).[11] The value of the magnetic moment decreases gradually with the temperature from a value of 2.92 μ_B per dimer at 300 K to a value of 1.6 μ_B at 50 K and then more rapidly reaching a value of 0.4 μ_B at 2.5 K. This temperature response of the magnetic moment is also characteristic of U(V) complexes. Magnetic susceptibility of **2** (Figure 3b) shows a paramagnetic behaviour from 300 K down to approximately 50 K where a deviation occurs, which can probably be attributed to antiferromagnetic coupling between two uranium spins.

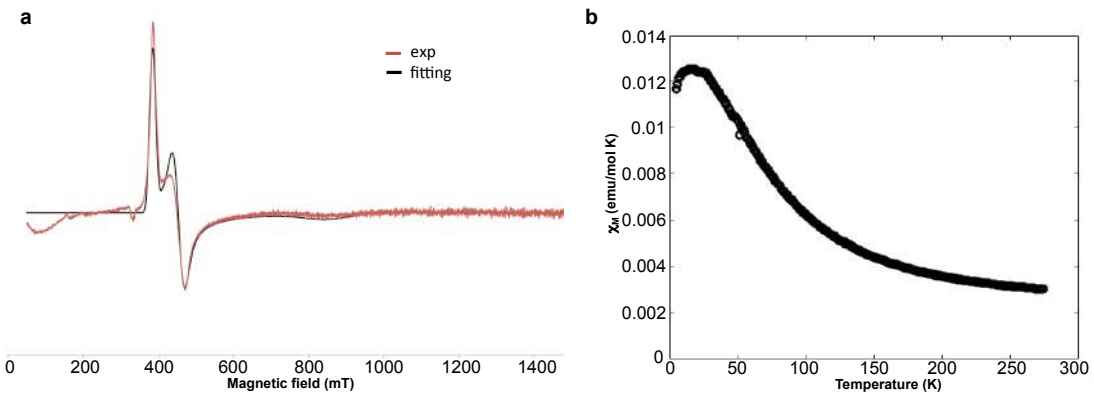

Figure 3. X-band (9.40 GHz) EPR spectrum of crystal of **2** in toluene/hexane glass at 10 K (red line exp., black line fitted) (**a**); plot of measured χ versus temperature (**b**).

Notably, the different metallo-ligand framework provided by the caesium cation in Cs_3U–N–U does not lead to well defined reactivity. Cs_3U–N–U also reacts with N_2 under ambient conditions but the isolation of the reaction products was not successful owing to the concomitant formation of decomposition products. The identity of the specific alkali ion is ordinarily not critical, but a crucial effect of the nature of the cation has been recently shown in models of the iron-based Haber-Bosch process [12] and in models of the oxygen-evolving complex (OEC).[13]

The few N_2-binding uranium complexes reported to date are, with one exception,[5d] all dinuclear complexes with a side-on bridging N_2 (where the N–N distance remains essentially the same as found in free N_2)[5e] or with a side-on bridging N^{2-} moiety resulting from the two-electron reduction of N_2 by mononuclear complexes of uranium(III).[5a-c] We also note that uranium complexes containing the highly activated hydrazido moiety have not been reported so far. Moreover, no information on the reactivity of the dinitrogen in N_2-bound uranium complexes has been reported to date, probably owing to the lability of the bound N_2 in the previously characterized complexes.

Treating **2** with 1 equiv. of 2,4,6-tri-*tert*-butylphenol (Scheme 2a) gives the mono-protonated compound $[K_2\{[U(OSi(O^tBu)_3)_3]_2(\mu\text{-}NH)(\mu\text{-}\eta^2\text{:}\eta^2\text{-}N_2)\}]$, **3**, in 70% yield.

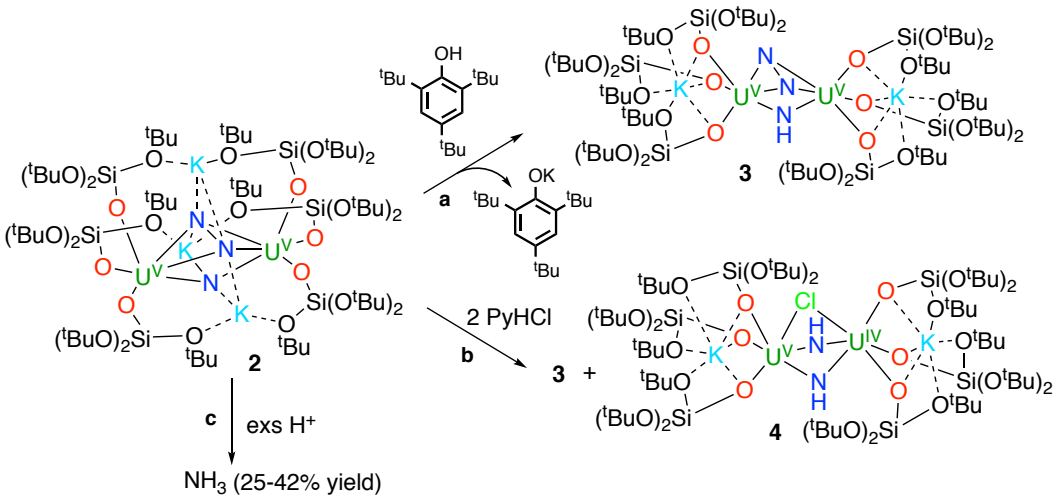

Scheme 2. Protonation reactions of the nitrido (**a**) and hydrazido (**b**) ligands in **2**, affording **3** and **4**, respectively; protonation of **2** with an excess of acid leads to ammonia formation (**c**).

The molecular structure of **3** (Figure 4a) shows two [K{U(OSi(O^{t}Bu)$_3$)$_3$}] fragments bridged by an NH^{2-} ligand and an N_2^{4-} ligand. The geometry of the diamond-shaped U_2N_3 core remains similar to that found in complex **2**, with essentially unchanged U–N distances in the U–N_2^{4-} fragment. The mean value of the U–N3 distances (2.11(5) Å) is longer than that found in the nitride-bridged complex **2** (2.069(2) Å), and is consistent with the presence of a U(V) imido-bridged species.[8]

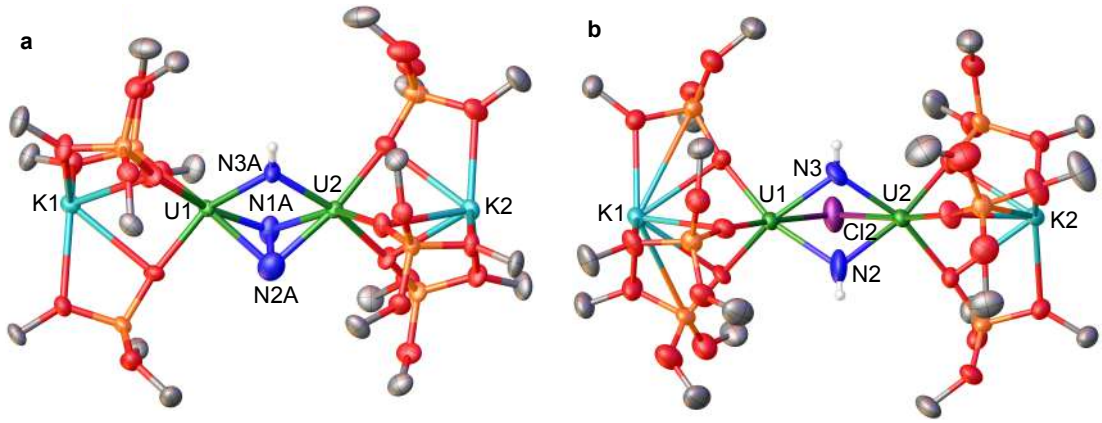

Figure 4. Solid-state molecular structure of [K$_2${[U(OSi(O^{t}Bu)$_3$)$_3$]$_2$(μ-NH)(μ-η^2:η^2-N$_2$)}], **3** (**a**) and of [K$_2${[U(OSi(O^{t}Bu)$_3$)$_3$]$_2$(μ-NH)$_2$(μ-Cl)}], **4** (**b**). Thermal ellipsoids set at 50% probability. Hydrogen atoms and methyl groups were omitted for clarity. Selected bond lengths for **3** [Å]: U1–N1A 2.147(9), U1–N2A 2.295(12), U1–N3A 2.151(8), U2–N1A 2.204(9), U2–N2A 2.244(13), U2–N3A 2.089(8), N1A–N2A 1.492(10), U1–U2 3.3717(2), average U–O$_{siloxide}$ 2.215(5). Selected bond lengths for **4** [Å]: U1–N2 2.23(2), U1–Cl1 2.833(7), U1–N3 2.285(16), U2–N2 2.25(2), U2–Cl1 2.809(7), U2–N3 2.261(17), average U–O$_{siloxide}$ 2.216(11).

Addition of the stronger acids PyHCl, HCl or HBAr^F (BAr^F = [{3,5-(CF$_3$)$_2$C$_6$H$_3$}$_4$B]$^-$ to **2** results also in the protonation of the hydrazido ligand (Scheme 2b), with addition of two equivalents of PyHCl enabling isolation of a few single crystals of a doubly

protonated species with structural parameters consistent with the presence of the bis(imido)-bridged diuranium(IV/V) complex, $[K_2\{[U(OSi(O^tBu)_3)_3]_2(\mu\text{-}NH)_2(\mu\text{-}Cl)\}]$, **4**.

Adding excess PyHCl (20 equiv.) to complex **2** led to the formation of a precipitate, the ^1H NMR spectrum of which (in deuterated DMSO, dimethyl sulfoxide-d_6) shows ammonium chloride ($^{14}NH_4Cl$) as the only product (Figure 5a). This result and the isolation of complex **4** suggest that the protonation of complex **2** leads to the cleavage of dinitrogen. The same experiment with the ^{15}N-labelled complex ^{15}N-**2** gave a ^1H NMR spectrum with signals assigned to $^{15}NH_4Cl$ (doublet) and $^{14}NH_4Cl$ (triplet) in a ratio of 1:0.85 (Figure 5b).

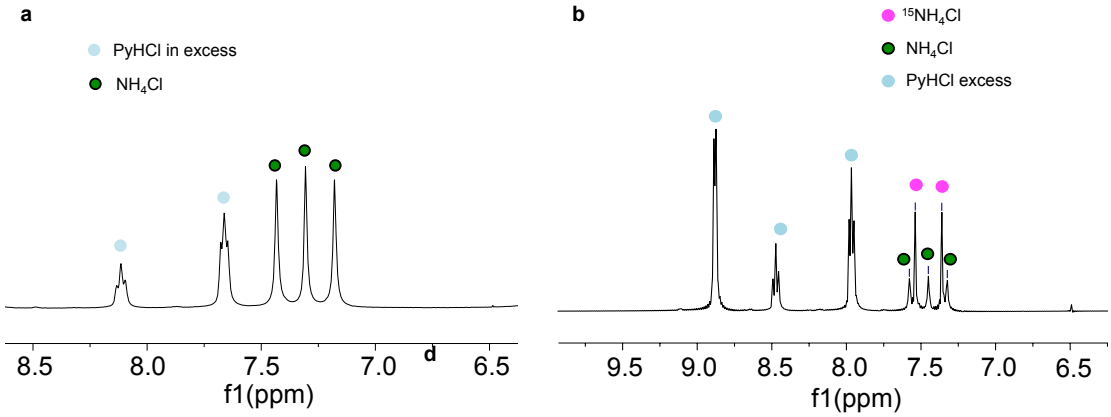

Figure 5. ^1H NMR (400 MHz, DMSO-d_6, 298 K) of the white precipitate formed after addition of excess PyHCl to 2 (**a**); ^1H NMR (400 MHz, DMSO-d_6, 298 K) of the white precipitate formed after addition of excess PyHCl to ^{15}N-**2** (**b**).

The addition of excess $HBAr^F$, PyHCl or HCl to complex **2** resulted in overall yields of ammonia of 25%, 35% and 42% (Scheme 2c), respectively (determined by quantitative NMR spectroscopy and indophenol titration, considering a yield of 100% to be when 1 equiv. of complex **2** gives 3 equiv. of NH_3). The low ammonia yield could reflect hydrazine disproportionation to form N_2.

Because direct hydrogenation of N_2 with hydrogen (H_2) under mild conditions is desirable, yet has been observed only for a few N_2 complexes,[2e, 2g] we also explored functionalizing the bound N_2 in complex **2** with H_2. Letting **2** stand under H_2 (1 atm) at room temperature slowly consumes the complex over two to three weeks. The ^1H NMR spectrum of the final reaction mixture shows only the presence of the free

ligand (10% yield), and no NH_3 is observed among the volatiles. However, adding a solution of HCl in ether to the product of the reaction of **2** with H_2 leads to formation of ammonia in 77% yield (Figure 6a). Adding a solution of HCl in ether to the product of the reaction of ^{15}N-**2** with H_2 leads to the formation of $^{15}NH_4Cl$ and $^{14}NH_4Cl$ (giving a doublet and a triplet signal, respectively, in the ^{1}H NMR spectrum) in a 2:1 ratio, indicating that the three nitrogen atoms are all incorporated in the ammonia generated (Figure 6b).

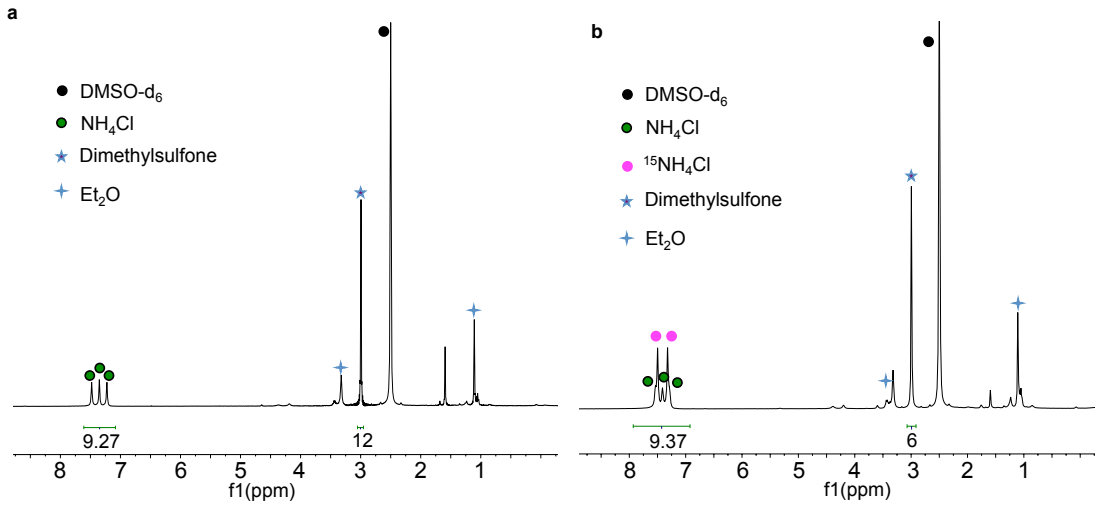

Figure 6. Quantitative ^{1}H NMR (400 MHz, DMSO-d_6, 298 K) of NH_4Cl formed after addition of HCl(Et_2O) to the residual solid of reaction between **2** and H_2 (2 equivalents of dimethylsulfone added) (a); ^{1}H NMR (400 MHz, DMSO-d_6, 298 K) of $^{15}NH_4Cl$ and NH_4Cl formed in ratio 2:1 after addition of HCl(Et_2O) to the residual solid from the reaction between complex ^{15}N-**2** and H_2 (1 equivalent of dimethylsulfone).

The addition of hydrogen to complex **2** might involve protonation of the nitride (as seen for the reactivity of the diuranium(IV) bridging nitride with H_2 in Chapter 4) and the resulting hydride might reduce the N–N single bond, allowing the formation of ammonia upon acid addition, without disproportionation reactions to form N_2. However, H_2 might play a role independently from the protonation of the nitride and formation of a hydride species, as when added to a solution of complex **3**, a slow reaction occurs, even though the species formed could not be characterized. A preliminary structure obtained shows three electron density in the core, but it is not conclusive, as the occupancy of these densities could not be assigned.

Complex **2** also reacts with CO (10 equiv.) in THF or benzene at room temperature to afford the U(IV)/U(IV) oxo/cyanate complex $[K_2\{[U(OSi(O^tBu)_3)_3]_2(\mu\text{-}O)(\mu\text{-}NCO)_2\}]$, **5**, which was isolated by recrystallization from THF in 68% yield (Scheme

3). Elemental analysis supports the assignment of **5** as an oxo/cyanate complex, an assignment further corroborated by the formation of CN^- as a by-product detected by ^{13}C NMR.

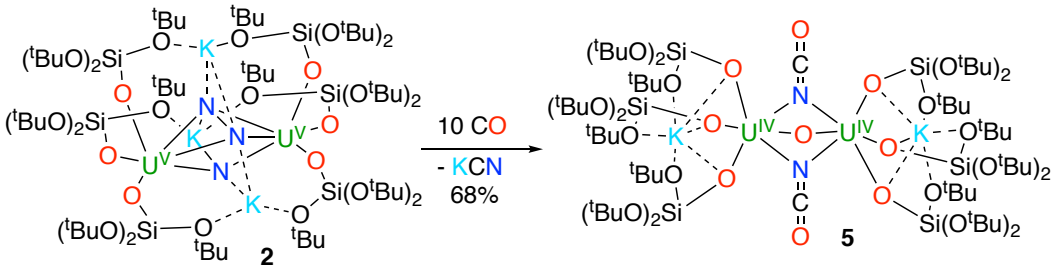

Scheme 3. Reactivity of the nitrido and hydrazido ligands to give a bridging oxo ligand (and cyanide extrusion) and two cyanate ligands, respectively.

The X-ray crystal structure of complex **5** (Figure 7) shows two $[K\{U(OSi(O^tBu)_3)_3\}]$ fragments bridged by an oxo group (O^{2-}) and two cyanate (OCN^-) moieties in a bent geometry, with a U1–O–U2 angle of 108.7(3)° and U–$N_{cyanate}$–U angles of 88.0(3)° and 89.0(3)°. The nitride and the hydrazido ligands thus both react with CO, so that successive reaction of the nitride-bridged diuranium(III) complex **1** with N_2 and CO leads to N_2 cleavage and functionalization by a well-defined uranium complex. The nucleophilic addition of the nitride to CO results in the complete cleavage of the CO triple bond, leading to the formation of a bridging oxo complex and cyanide (CN^-) that is extruded as KCN.

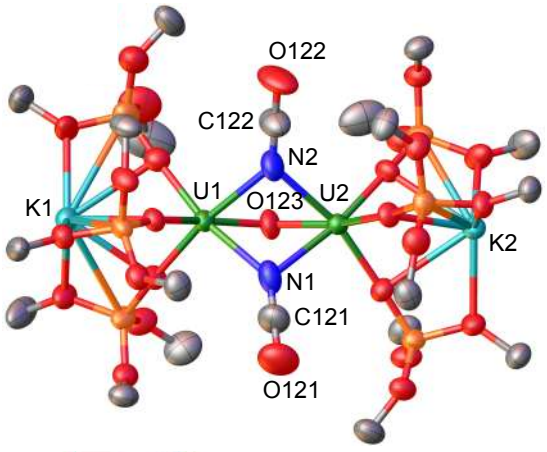

Figure 7. Solid-state molecular structure of $[K_2\{[U(OSi(O^tBu)_3)_3]_2(\mu\text{-}O)(\mu\text{-}NCO)_2\}]$, **5**. Thermal ellipsoids set at 50% probability. Hydrogen atoms and methyl groups were omitted for clarity. Selected bond lengths [Å]: U1–O123 2.161(6), U2–O123 2.161(6), U1–N2 2.493(7), U2–N2 2.517(8), U1–N1 2.521(9), U2–N1 2.534(8), N1–C121 1.244(14), C121–O121 1.207(13), N2–C122 1.217(13), C122–O122 1.215(12), U1–U2 3.5127(3)), average U–$O_{siloxide}$ 2.210(11).

We have recently reported similar reactivity for the nitride-bridged diuranium(IV) complex, $[Cs\{[U(OSi(O^tBu)_3)_3]_2(\mu\text{-}N)\}]$, which completely cleaves the CO triple bond under ambient conditions to yield the oxo/ cyanide diuranium(IV) complex, $[Cs\{[U(OSi(O^tBu)_3)_3]_2(\mu\text{-}CN)(\mu\text{-}O)\}]$.[14] The reductive carbonylation of uranium(V) and uranium(VI) terminal nitrides to afford cyanate has also been reported,[15] but reductive carbonylation of metal dinitrogen complexes is unprecedented. Ligand-induced cleavage of dinitrogen has been achieved with Zr(IV) and Hf(IV) metallocene complexes, but differs from the reactivity of **2** in that addition of excess CO (1 - 4 atm) to the reduced N_2^{4-} in Zr(IV) and Hf(IV) metallocene complexes affords the $[N_2C_2O_2]^{4-}$ (oxamidide) fragment and does not involve metal-centred electron transfer. [2h, 16] The addition of 4 equivalents of 2.2.2cryptand to the nitrogen adduct, **2** leads to immediate precipitation of an unknown product, possibly a species that can be assigned to $[K_{3-x}\{K(cryptand)\}_x\{[U(OSi(O^tBu)_3)_3]_2(\mu\text{-}N)(\mu\text{-}\eta^2\text{:}\eta^2\text{-}N_2)\}]$ and the ^1H NMR spectrum shows only the presence of free cryptand (Figure 8a). When 1 equivalent of cryptand is added in a THF solution, no precipitate is observed and the ^1H NMR spectrum shows a considerable shift of the peak assigned to the siloxide ligands (Figure 8b), which shifts upon addition of other 2 equivalents of cryptand. This preliminary results show that it is possible to remove one or more potassium cations from the core of the molecule. The addition of CO to the reaction mixture in toluene after addition of 4 equivalents of cryptand, in presence of the precipitate, leads to a different proton NMR spectrum but no species could be identified. Further studies should focus on the isolation of the species $[K_{3-x}\{K(cryptand)\}_x\{[U(OSi(O^tBu)_3)_3]_2(\mu\text{-}N)(\mu\text{-}\eta^2\text{:}\eta^2\text{-}N_2)\}]$ and reactivity products to understand the role of the $K\text{-}N_{nitrido}$ and $K\text{-}N_{hydrazido}$ bonds in guiding towards different products.

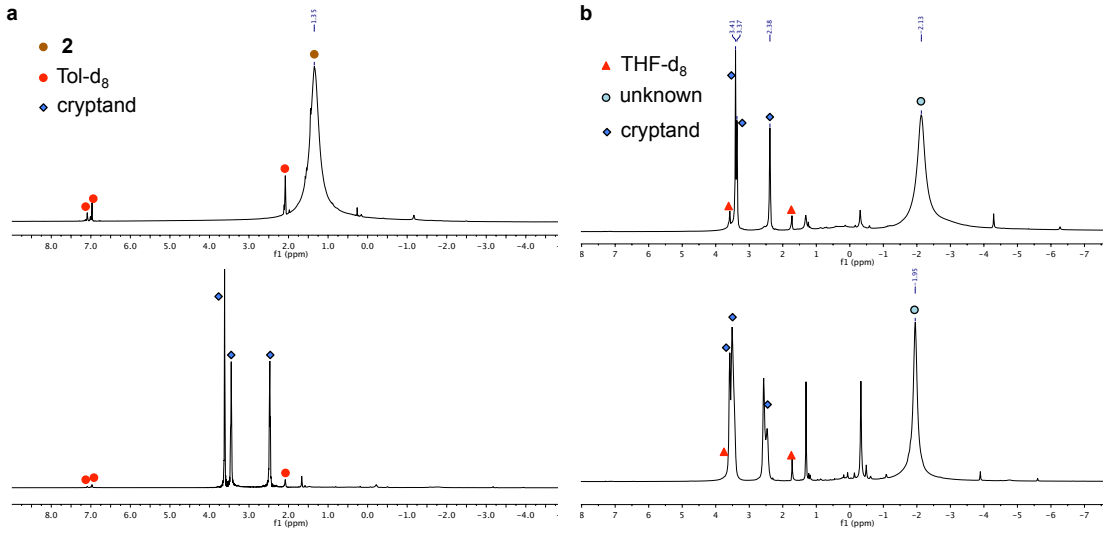

Figure 8. ^{1}H NMR (400 MHz, tol-d_8, 298K) before (top) and after (bottom) addition of 4 equivalents of 2.2.2cryptand to complex **2** in toluene (**a**); ^{1}H NMR (400 MHz, THF-d_8, 298K) after addition of 1 equivalent of 2.2.2cryptand to complex **2** in THF (top) and ^{1}H NMR (400 MHz, THF-d_8, 298K) after addition of 2 other equivalents of 2.2.2cryptand (bottom) (**b**).

The high reactivity of both the nitride and the hydrazido ligands in complex **2** with CO renders it difficult to envisage a possible synthetic cycle that would allow for the transformation of N_2 and CO into cyanate and then restore the U(III)–N–U(III) precursor.

Anticipating reduced reactivity of the protonated nitride group with CO, we explored the reactivity of complex **3**, and found that addition of CO (10 equiv.) to a toluene solution of **3** and standing for 24 h at room temperature gave brown crystals of the cyanate complex, $[K_2\{[U(OSi(O^tBu)_3)_3]_2(\mu\text{-}NH)(\mu\text{-}NCO)\}]$, **6**, in 70% yield (Scheme 4). The high yield suggests that the U(III)/U(IV) complex **6** is the major uranium species formed in this reaction. The ^{13}C NMR spectrum of the reaction mixture of **3** with ^{13}CO in deuterated water does not show free HN^{13}CO or ^{13}CN^{-}.

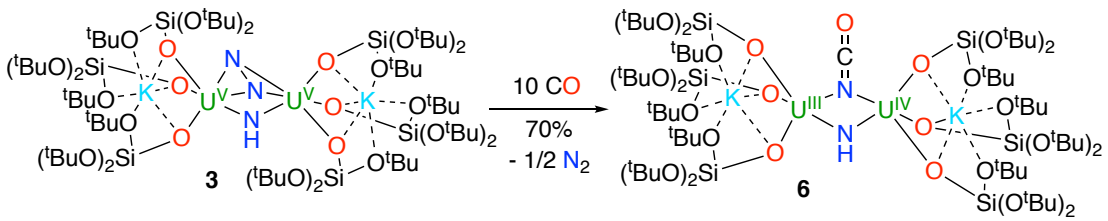

Scheme 4. Reaction of the imido complex **3** with CO to afford **6**, with concomitant release of ½ N_2.

The stoichiometry and the electron balance of the reductive carbonylation of **3** require the concomitant elimination of dinitrogen. Analysis of the headspace from the

reaction of ^{15}N-**3** with CO by GC-MS analysis confirmed the presence of $^{15}N_2$ and $^{14}N^{15}N$ at mass to charge ratios *m/z* = 30 and *m/z* = 29 respectively (see Appendix 5). The X-ray crystal structure of **6** (Figure 9) is consistent with a mixed-valent U(III)/U(IV) complex, with one imido (NH^{2-}) group and one cyanate (NCO^{-}) group (disordered over two crystallo- graphic positions) bridging the two uranium centres in a non-planar diamond-shaped geometry. The mean value of the U–NH distance (2.18(3) Å) is longer than in complex **3** (2.10(5) Å), in agreement with the presence of a uranium(III) centre.

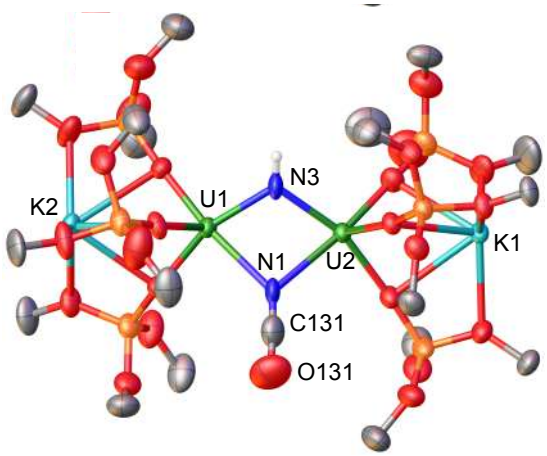

Figure 9. Solid-state molecular structure of $[K_2\{[U(OSi(O^tBu)_3)_3]_2(\mu\text{-}NH)(\mu\text{-}NCO)\}]$, **6**. Thermal ellipsoids set at 50% probability. Hydrogen atoms and methyl groups were omitted for clarity. Selected bond lengths [Å]: U1–N3 2.200(8), U1–N1 2.569(10), U2–N3 2.161(9), U2–N1 2.576(10), N1–C131 1.224(6), C131–O131 1.214(6), average $U–O_{siloxide}$ 2.197(6).

The bridging nitride present in complex **4** is lost upon addition of CO, and a briging oxo is formed. Instead, in complex **6** the imido ligand does not react further with CO, and it is a good candidate for reduction studies, with the aim of performing cycles of nitrogen reduction. Attempt to reduce complex **6** to the starting bridging U(III) nitride, with extrusion of KNCO, resulted inconclusive. After addition of excess KC_8 at –70 °C to a solution of complex **6**, the ^{1}H NMR spectrum shows the presence of free ligand and an unknown species that could not be identified. Further studies should be performed to identify conditions that allow the implementation of a cycle.

Conclusions

The observed difference in reactivity between complex **2** and **3** is probably due to replacement of N^{3-} with a less electron donating NH^{2-} group, which enables U(V) reduction to U(III). Preliminary attempts to reduce complex **6** to regenerate the diuranium(III) precursor have not been successful, and future studies will focus on the

identification of possible synthetic cycles allowing the production of cyanate from N_2 and CO. Bimetallic complexes containing highly activated side-on-bound dinitrogen (N_2^{4-}) that can be further reduced and completely cleaved by the addition of reducing ligands such as H_2 or CO have so far only been reported for group 4 metals.[2d, 2e, 2g, 2h, 2k] In these systems, the intermediate species (probably dinuclear Zr(II) and Hf(II) complexes) involved in N_2 activation were prepared by *in situ* reduction of mononuclear M(IV) complexes under a N_2 atmosphere and not characterized. Ligand-induced N_2 cleavage in these systems also differs from the reactivity of **2** and **3** in that no metal-centred electron transfer is involved,[2g, 2h] while the reaction of the ($U–(N_2)^{4-}$) complex with CO that we report confirms uranium-centred electron transfer that yields different reaction products from those obtained with the group 4 metals. We also note that the higher redox flexibility of uranium makes it well positioned for the implementation of catalytic N–C bond-forming cycles that exploit the assembly of low-valent metals and alkali ions through bridging nitrides as an optimized arrangement for the cooperative binding and activation of dinitrogen; the stable yet flexible U–N–U core can bend to accommodate the N_2 moiety. We envisage that these design principles could also be extended to other metals, provided that the corresponding low-valent nitride complex can be stabilized, and thereby aid the development of new molecular systems for the catalytic transformation of N_2. However, the bridging nitride does not act as a spectator linker atom and it is involved in the reactivity with protons, CO and probably with H_2. In the next chapter the synthesis and reactivity of an analogous diuranium(III) complex with an oxo as linker atom will be described. We anticipated that the oxo linker is less likely to be involved in the reactivity compared to the nitride.

Experimental

Materials. Unless otherwise noted, reagents were purchased from commercial suppliers and used without further purification. Tris(*tert*-butoxy)silanol and 2,4,6-Tri-*tert*-butylphenol were purified by sublimation. The solvents were purchased from Aldrich or Cortecnet (deuterated solvents) in their anhydrous form, conditioned under argon and vacuum distilled from K/benzophenone (toluene, THF, benzene-d_6 and n-hexane). DMSO-d_6 was freeze-degassed and stored over activated 3 Å molecular sieves. The complexes $[Cs\{[U(OSi(O^tBu)_3)_3]_2(\mu\text{-}N)\}$ [6] and $[Cs_3\{[U(OSi(O^tBu)_3)_3]_2(\mu\text{-}N)\}]$ [7] were prepared according to published procedure.

Carbon monoxide (N47 Bt-S 10/200) was purchased from Carbagas and stored over activated 3 Å molecular sieves. N_2 (99.9999% purity) was purchased from Carbagas. ^{13}CO (93.13% ^{13}C) and $^{15}N_2$ (98% ^{15}N) were purchased from Cortecnet and stored over activated 3 Å molecular sieves. All manipulations were carried out under a dry and oxygen free argon atmosphere using Schlenk techniques and an MBraun glovebox equipped with a purifier unit. The water and oxygen levels were always kept at less than 0.1 ppm. Glassware was dried overnight at 140°C before use. **Caution:** Depleted uranium (primary isotope ^{238}U) is a weak α-emitter (4.197 MeV) with a half-life of 4.47×10^9 years. Manipulations and reactions should be carried out in monitored fume hoods or in an inert atmosphere glovebox in a radiation laboratory equipped with α- and β-counting equipment. **^{1}H NMR experiments** were carried out using NMR tubes adapted with J. Young valves. ^{1}H NMR spectra were recorded on Bruker 400 MHz. NMR chemical shifts are reported in ppm with solvent as internal reference. **Elemental analyses** CHN elemental microanalysis were obtained using a Thermo Scientific Flash 2000 Organic Elemental Analyzer at the Institut of Chemistry and Chemical Engineering at EPFL. **IR analyses** were performed with a FT-IR Spectrometer Spectrum one Perkin-Elmer; the measurement for complex **6** was performed with a Perkin Elmer Frontier FT-IR equipped with a liquid nitrogen cooled MCT detector. The sample was placed into the Harrick High Temperature Chamber DRIFT cell under argon atmosphere. Scans were performed in a range between 400 and 4000 cm^{-1} at a resolution of 4 cm^{-1}. **Raman** analysis was performed with a LabRam spectrometer Jobin Yvon Horiba. Excitation line was provided by an Ar laser (532.19 nm).

Synthesis of $[K_3\{[U(OSi(O^tBu)_3)_3]_2(\mu\text{-}N)\}]$, 1

A cold (–70 °C) red-brown solution of $[Cs\{[U(OSi(O^tBu)_3)_3]_2(\mu\text{-}N)\}]$, (223.2 mg, 0.101 mmol, 1 equiv) in THF (2.0 mL) was added onto cold (-70°C) KC_8 (136.8 mg, 1.01 mmol, 10 equiv) under argon. After 5 minutes stirring at −70 °C, the resulting dark purple suspension was evaporated maintaining the reaction flask at cold temperature and the resulting residue was extracted with 1mL of cold n-hexane. The resulting suspension was filtered at –70°C to remove the excess of KC_8 and graphite, which were then washed with cold n-hexane (30 mL). The filtrate was evaporated (1mL). After 4 hours at –70°C, a dark purple solid formed that was collected on a cold filter, yielding 156.8mg of **1** (70%). Elemental analysis performed (under argon)

Anal. Calcd for **1**.0.2(n-hexane) $C_{73.2}H_{2.8}K_3NO_{24}Si_6U_2$: C, 39.87; H, 7.53; N, 0.64. Found: C, 39.92; H, 7.77; N, 0.52. ^{1}H NMR of **1** (400 MHz, THF-d_8, 298 K): δ(ppm) = 1.56 (s, 162H, CH_3 terminal siloxide), (400 MHz, Toluene-d_8, 298 K): δ(ppm) = 1.74 (s, 162H, CH_3 terminal siloxide). ^{13}C NMR (400 MHz, Toluene-d_8, 298 K): δ(ppm) = 32.2 (**C**H_3), 74.7 (**C**Me_3).

Synthesis of [K_3{[U(OSi(O^{t}Bu)$_3$)$_3$]$_2$(μ-N)(μ-η^2-N_2)}], 2

Complex **1**, (128.5 mg, 0.03 mmol), was introduced into a glass tube equipped with a Young valve under argon in the glove box. The tube was then connected to a Schlenk line and evacuated maintaining the tube in liquid nitrogen. The solid was exposed to N_2 (0.5 atm.) for 2 h at room temperature. The colour of the solid changed within few minutes from dark purple to brown. The solid was stirred every 10 minutes. After 2 hours the solid was transferred to the glove box and dissolved in cold toluene. The resulting toluene solution was filtered and left standing at –40 °C. After 2 days, **2** precipitated out of the solution as a microcrystalline brown solid that was vacuum-dried (60 mg, 68% yield). The labelled analogue of complex **2**, [K_3{[U(OSi(O^{t}Bu)$_3$)$_3$]$_2$(μ-N)(μ-η^2-$^{15}N_2$)}], ^{15}N-**2**, is easily prepared using the same procedure by exposing **2** to $^{15}N_2$. ^{1}H NMR (400 MHz, toluene-d_8, 298 K): δ(ppm) = 1.34 (s, 162H, CH_3 terminal siloxide). ^{13}C NMR (400 MHz, toluene-d_8, 298 K): δ(ppm) = 31.4 (**C**H_3), 71.6 (**C**Me_3). Anal. Calcd for [K_3{[U(OSi(O^{t}Bu)$_3$)$_3$]$_2$(μ-N)(μ-η^2-N_2)}] (**$C_{72}H_{162}K_3N_3O_{24}Si_6U_2$**): C, 39.03; H, 7.37; N, 1.90. Found: C, 39.05; H, 7.36; N, 1.63. μ_{eff} (298 K): 2.06μ_B. Raman of powder, υ(cm^{-1}): **2:** 797 (817); ^{15}N-**2**: 785 (1100). No loss of N_2 from **2** is observed under dynamic vacuum in the solid state or after three cycles of freeze-pump-thaw degassing under argon of a toluene or THF solution of **2**. The synthesis can also be performed by exposure of a solution of **1** in THF or toluene solution to N_2 at room temperature but the yield for these reactions is lower due to the low solution stability of **1** at room temperature. When the previously reported cesium analogue [Cs_3{[U(OSi(O^{t}Bu)$_3$)$_3$]$_2$(μ-N)}] is reacted with N_2, the reaction proceeds with similar colour change. The proton NMR spectrum in THF-d_8 of the crude mixture shows the presence of a new peak at –0.2 ppm, the presence of the previously reported U(III)/U(IV), U(IV)/U(IV) nitride complexes [7] and free ligand. The U(III)/U(IV), U(IV)/U(IV) nitride complexes [M_2{[U(OSi(O^{t}Bu)$_3$)$_3$]$_2$(μ-N)}] and [M{[U(OSi(O^{t}Bu)$_3$)$_3$]$_2$(μ-N)}] (M =K , Cs) do not react with N_2.

Synthesis of $[K_2\{[U(OSi(O^tBu)_3)_3]_2(\mu\text{-}NH)(\mu\text{-}\eta^2\text{-}N_2)\}]$, 3

A solution of 2,4,6-tri-tert-butylphenol (2.4 mg, 0.009 mmol, 1 eq) in THF was added to a brown solution of **2** (20 mg, 0.009 mmol, 1 eq) in THF (0.5 mL). The mixture was stirred for 1 h. The colour changed from dark brown to light brown. THF was evaporated and the residue was suspended in toluene. The resulting solution was filtered and let standing at –40 °C. After 24 h, XRD suitable brown crystals of **3** formed (14.7 mg, 70% yield). The ^{15}N labelled complex ^{15}N-**2** was prepared from ^{15}N-**2** following the same procedure**.** Crystals of **3** could also be isolated from the reaction of complex **2** with 2 equivalents of PyHCl in THF, in 24 h from a toluene solution at –40 °C. Proton NMR studies show that addition of one equivalent of PyHCl affords complex **3**, unreacted starting material and other protonation products. From the reaction with two equivalents we have also isolated pale brown crystals of a minor product that cannot be isolated clean in sufficient amount for further analysis. X ray crystallography studies indicate the presence of the diprotonated complex $[K_2\{[U(OSi(O^tBu)_3)_3]_2(\mu\text{-}NH)_2(\mu\text{-}Cl)$, **4.**

^1H NMR of crystals of **3** (400 MHz, THF-d_8, 298 K): δ(ppm) = –1.26 (s, 162H, CH_3 terminal siloxide), 78 (s, 1H, NH). ^1H NMR of crystals of **3** (400 MHz, toluene-d_8, 298 K): δ(ppm) = –1.10 (s, 162H, CH_3 terminal siloxide), ^{13}C NMR (400 MHz, toluene-d_8, 298 K): δ(ppm) = 29.5 (**C**H_3), 71.9 (**C**Me_3). Anal. Calcd for $[K_2\{[U(OSi(O^tBu)_3)_3]_2(\mu\text{-}NH)(\mu\text{-}\eta^2\text{-}N_2)\}]$ **(**$C_{72}H_{163}K_2N_3O_{24}Si_6U_2$) ($C_7H_8$)$_{1.5}$: C, 42.78; H, 7.62; N, 1.81. Found: C, 42.95; H, 7.73; N, 1.54. ^1H NMR of crystals of 4 (400 MHz, THF-d_8, 298 K): δ(ppm) = 0.1 (s, 162H, CH_3 terminal siloxide).

Ammonia formation after addition of excess PyHCl to 2

To a brown solution of **2** (20 mg, 0.009 mmol, 1 eq) in THF (1 mL), an excess of PyHCl was added (20 mg, 0.17 mmol, 20 eq). The mixture was stirred overnight, affording a colourless solution and a white precipitate. The supernatant was removed and the solid was washed twice with 0.5 mL THF. The solid was dried under vacuum and then dissolved in DMSO-d_6. ^1H NMR analysis allowed the detection of ammonium chloride as the only product. The reaction was repeated also with the labelled ^{15}N compound $[K_3\{[U(OSi(O^tBu)_3)_3]_2(\mu\text{-}N)(\mu\text{-}\eta^2\text{-}^{15}N_2)\}]$. The experiment suggests that both the nitride and the hydrazido ligands are transformed into NH_3 by addition of acid. The ratio of $^{15}NH_4Cl$:$^{14}NH_4Cl$ was found to be 1:0.85. The global yield in NH_3 was determined in a separate experiment by integration (with an internal

standard) of the NMR signals to be 35%. ^{1}H NMR of NH_4Cl (400 MHz, DMSO-d_6, 298 K): δ(ppm) = 7.3 (triplet, J = 52 Hz) ^{1}H NMR of $^{15}NH_4Cl$ (400 MHz, DMSO-d_6, 298 K): δ(ppm) = 7.4 (doublet, J = 72 Hz)

Ammonia formation after addition of excess HCl(Et_2O) to 2

To a brown solution of complex **2** (5.2 mg, 0.0023 mmol, 1 eq) in THF (1 mL), an excess of a 2M solution of HCl in Et_2O (34.5 μL, 0.069 mmol, 30 eq) was added. The reaction mixture turned immediately colourless. After 24 h the solvent was removed under vacuum, DMSO-d_6 was added and the amount of ammonia was evaluated by quantitative ^{1}H NMR (dimethylsulfone as internal standard) (42% yield of ammonia).

Ammonia formation after addition of excess $HBAr^F_4 \cdot 2Et_2O$ to 2

A Schlenk flask was charged with a solution of complex $[K_3\{[U(OSi(O^tBu)_3)_3]_2(\mu\text{-}N)(\mu\text{-}\eta^2\text{-}N_2)\}]$ (10 mg, 0.0045 mmol, 1 eq) in 2 mL of Et_2O and it was cooled down at –70 °C. $HBAr^F_4 \cdot 2Et_2O$ (114 mg, 0.11 mmol, 25 eq) was dissolved in Et_2O and cooled down at –70 °C. The $HBAr^F_4 \cdot 2Et_2O$ solution was added and the mixture was stirred for 10 minutes at – 70 °C. The reaction mixture was left stirring at room temperature for 15 minutes. All the volatiles were then vacuum transferred into a Schlenk flask containing a 2 M HCl solution in Et_2O (4 mL). NaO^tBu (40 mg in 3 mL of Et_2O) was added to the residual solid. It was left stirring for 10 minutes at room temperature and then the volatiles were vacuum transferred into the HCl(Et_2O) Schlenk. The HCl(Et_2O) was removed under vacuum and the white solid was dissolved in DMSO-d_6 to evaluate by quantitative ^{1}H NMR (dimethylsulfone as internal standard) the amount of ammonia (25% yield). The same result was obtained in a separate experiment by dissolving the white solid in 20 mL of distilled water for the indophenol test for ammonia quantification (25% yield of ammonia).

Ammonia formation after reaction of 2 with H_2 and HCl(Et_2O)

In an NMR tube, a brown toluene solution of **2** (5.2 mg, 0.0023 mmol) was prepared by dissolving **2** in 0.5 mL of toluene in the glove-box under argon. The solution was freeze-degassed three times and exposed to 1 atmosphere of hydrogen gas. The tube was closed and left for three weeks at room temperature, until disappearance of all the starting material. The ^{1}H NMR spectrum shows only the presence of free ligand in 10% yield. After three weeks, all the volatiles were vacuum transferred into a Schlenk

flask containing a 2 M HCl solution in Et_2O (4 mL). After removal of the HCl(Et_2O) solution under vacuum, no white precipitate was visible. The absence of any amount of ammonium chloride was confirmed by proton NMR. To the residual solid left in the NMR tube, 1 mL of a solution of 2 M HCl in Et_2O was added. Immediately, white solid precipitated out of the solution. HCl(Et_2O) was removed under vacuum and the white solid was titrated in DMSO-d_6 using dimethyl sulfone as internal standard (77% yield in ammonia). Preliminary studies show that hydrogenation of complex **3** does not lead to decomposition, but to the clean formation of a new uranium species.

Reaction of 2 with CO, synthesis of [K_2{[U(OSi(O^{t}Bu)$_3$)$_3$]$_2$(μ-O)(μ-NCO)$_2$}], 5

A brown benzene solution of **2**, (19 mg, 0.0086 mmol, 1 eq) prepared by dissolving **2** in benzene-d_6 (0.5 mL) in the glove-box under argon, was freeze-degassed three times. 10 equivalents of CO were then added at room temperature. The solution turned light yellow. The proton NMR of the reaction mixture shows the presence of only one signal. Benzene was removed and THF (0.1 mL) was added, the suspension was filtered and the resulting solution was left standing at –40 °C. After 48 h X-ray suitable brown crystals **5** formed (13 mg, 68% yield). The ^{15}N labelled complex ^{15}N-**5** was prepared from ^{15}N-**2** following the same procedure**.** IR, ν^{13}**NCO** (cm^{-1}): 2195. ^{13}C NMR of the evaporated reaction mixture (400 MHz, D_2O, 298 K): δ(ppm) = 129 (NCO), 164 (CN). ^{1}H NMR of crystals of complex **5** (400 MHz, C_6D_6, 298 K): δ(ppm)= 1.07 (s, 162H, CH_3 terminal siloxide). ^{13}C NMR of reaction mixture (400 MHz, C_6D_6, 298 K): δ(ppm)= –164 (N**C**O), 30.8 (**C**H$_3$), 73.3 (**C**Me$_3$). Anal. Calcd for [K_2{[U(OSi(O^{t}Bu)$_3$)$_3$]$_2$(μ-O)(μ-NCO)$_2$}] (C$_{74}$H$_{162}$K$_2$N$_2$O$_{27}$Si$_6$U$_2$): C, 39.77; H, 7.31; N, 1.25. Found: C, 39.74; H, 7.21; N, 1.27. ^{13}C NMR of ^{15}N-**5** shows the presence of a broad peak at –163.9 (NCO$^-$). The ^{13}C NMR (^{13}Cigp30; d1=120) in water shows a doublet at 129 ppm (J= 64, ^{15}N^{13}**C**O) and a singlet at 165 ppm (^{13}**C**^{14}N), in ratio 2:1 respectively.

Reaction of 3 with CO, synthesis of [K_2{[U(OSi(O^{t}Bu)$_3$)$_3$]$_2$(μ-NH)(μ-NCO)}], 6

A brown solution of **3** (11.5 mg, 0.0053 mmol, 1 eq) in toluene (0.5 mL) prepared under argon in a tube equipped with a Young valve was freeze-degassed three times. 10 equivalents of CO were added. The solution turned yellow and proton NMR indicate completion within 24 h. X-ray suitable orange crystals of **6** were isolated after letting stand the toluene solution at room temperature for 24h (8 mg, 70% yield).

The ^{15}N labelled complex ^{15}N-**6** was prepared from ^{15}N-**2** following the same procedure**.** Titration of the residual compound present in the mother liquor show the presence of an additional amount of **6** to afford a 80 % overall yield. The proton NMR spectrum showed that when 100 equivalents of CO are added to **3**, a different species identified as a bis-cyanate $[K_2\{[U(OSi(O^tBu)_3)_3]_2(\mu\text{-}NH)(\mu\text{-}NCO)_2\}]$ complex is formed. In contrast the complex **6** does not react with carbon monoxide or with 2,4,6-tri-tert-butylphenol. ^{13}C NMR spectroscopy in D_2O of the residue after solvent evaporation from the reaction mixture obtained from the reaction of **3** with CO (10 equiv.) only shows the presence of the signal at 130.0 ppm assigned to cyanate, no formation of cyanide is observed. The addition of excess PyHCl (20 eq.) to complex ^{15}N-**6** leads to the formation of a precipitate. The proton NMR spectrum in dmso-d_6 of this solid shows the presence of signals assigned to $^{15}NH_4Cl$ (doublet) and $^{14}NH_4Cl$ (triplet) suggesting that hydrazide/nitride exchange occurs during protonation of **2** to yield **3**. IR, $\nu N^{13}CO$ (cm^{-1}): 2135, νNH (cm^{-1}): 3428 ^1H NMR of crystals of **6** (400 MHz, toluene-d_8, 298 K): δ(ppm) = 0.36 (s, 162H, CH_3 terminal siloxide).^{13}C NMR of crystals of **6** (400 MHz, toluene-d_8, 298 K): δ(ppm) = 145 (NCO). Anal. Calcd for $[K_2\{[U(OSi(O^tBu)_3)_3]_2(\mu\text{-}NH)(\mu\text{-}NCO)\}]$ **(**$C_{73}H_{163}K_2N_2O_{25}Si_6U_2$): C, 40.02; H, 7.45; N, 1.28. Found: C, 40.25; H, 7.22; N, 1.67. Preliminary trials of reduction of complex **6** were performed at –70 °C in THF-d_8 by addition of 10 equivalents of KC_8. The ^1H NMR spectrum (400 MHz, toluene-d_8, 233 K) shows the presence of free ligand and of a new species at –1.3 ppm in a ratio 1:0.5 respectively. Attempts to isolate the new species were not successful.

Bibliography

[1] a) B. A. MacKay, M. D. Fryzuk, *Chem. Rev.* **2004**, *104*, 385-401; b) K. C. MacLeod, P. L. Holland, *Nat. Chem.* **2013**, *5*, 559-565.

[2] a) S. Gambarotta, J. Scott, *Angew. Chem. Int. Ed. Engl.* **2004**, *43*, 5298-5308; b) S. F. McWilliams, P. L. Holland, *Acc. Chem. Res.* **2015**, *48*, 2059-2065; c) C. E. Laplaza, C. C. Cummins, *Science* **1995**, *268*, 861-863; d) Y. Ohki, M. D. Fryzuk, *Angew. Chem. Int. Ed. Engl.* **2007**, *46*, 3180-3183; e) J. A. Pool, E. Lobkovsky, P. J. Chirik, *Nature* **2004**, *427*, 527-530; f) M. M. Rodriguez, E. Bill, W. W. Brennessel, P. L. Holland, *Science* **2011**, *334*, 780-783; g) M. D. Fryzuk, J. B. Love, S. J. Rettig, V. G. Young, *Science* **1997**, *275*, 1445-1447; h) D. J. Knobloch, E. Lobkovsky, P. J. Chirik, *Nat. Chem.* **2010**, *2*, 30-35; i) K. Arashiba, Y. Miyake, Y. Nishibayashi, *Nat. Chem.* **2011**, *3*, 120-125; j) Y. Lee, F. T. Sloane, G. Blondin, K. A. Abboud, R. Garcia-Serres, L. J. Murray,

Angew. Chem. Int. Ed. Engl. **2015**, *54*, 1499-1503; k) M. Hirotsu, P. P. Fontaine, P. Y. Zavalij, L. R. Sita, *J. Am. Chem. Soc.* **2007**, *129*, 12690-12691.

[3] a) L. P. Spencer, B. A. MacKay, B. O. Patrick, M. D. Fryzuk, *Proc Natl Acad Sci USA* **2006**, *103*, 17094-17098; b) Y. Nishibayashi, *Inorg. Chem.* **2015**, *54*, 9234-9247.

[4] F. Haber*, Vol. DE 229126*, Haber, F Ammonia German patent DE 229126, **1909**.

[5] a) G. Cloke, F. N., P. B. Hitchcock, *J. Am. Chem. Soc.* **2002**, *124*, 9352-9353; b) A. L. Odom, P. L. Arnold, C. C. Cummins, *Journal of American Chemical Society* **1998**, *120*, 5836-5837; c) S. M. Mansell, N. Kaltsoyannis, P. L. Arnold, *J. Am. Chem. Soc.* **2011**, *133*, 9036-9051; d) W. J. Evans, S. A. Kozimor, J. W. Ziller, *J. Am. Chem. Soc.* **2003**, *125*, 14264-14265; e) P. Roussel, P. Scott, *J. Am. Chem. Soc.* **1998**, *120*, 1070-1071.

[6] C. Camp, J. Pecaut, M. Mazzanti, *J Am Chem Soc* **2013**, *135*, 12101-12111.

[7] L. Chatelain, R. Scopelliti, M. Mazzanti, *J. Am. Chem. Soc.* **2016**, *138*, 1784-1787.

[8] L. P. Spencer, E. J. Schelter, P. Yang, R. L. Gdula, B. L. Scott, J. D. Thompson, J. L. Kiplinger, E. R. Batista, J. M. Boncella, *Angew. Chem. Int. Ed. Engl.* **2009**, *48*, 3795-3798.

[9] M. Hirotsu, P. P. Fontaine, A. Epshteyn, P. Y. Zavalij, L. R. Sita, *J. Am. Chem. Soc.* **2007**, *129*, 9284-+.

[10] O. Cooper, C. Camp, J. Pecaut, C. E. Kefalidis, L. Maron, S. Gambarelli, M. Mazzanti, *J. Am. Chem. Soc.* **2014**, *136*, 6716-6723.

[11] D. R. Kindra, W. J. Evans, *Chem. Rev.* **2014**, *114*, 8865-8882.

[12] K. Grubel, W. W. Brennessel, B. Q. Mercado, P. L. Holland, *J. Am. Chem. Soc.* **2014**, *136*, 16807-16816.

[13] E. Y. Tsui, R. Tran, J. Yano, T. Agapie, *Nat. Chem.* **2013**, *5*, 293-299.

[14] M. Falcone, C. E. Kefalidis, R. Scopelliti, L. Maron, M. Mazzanti, *Angew. Chem. Int. Ed. Engl.* **2016**, *55*, 12290-12294.

[15] P. A. Cleaves, D. M. King, C. E. Kefalidis, L. Maron, F. Tuna, E. J. L. McInnes, J. McMaster, W. Lewis, A. J. Blake, S. T. Liddle, *Angew. Chem. Int. Ed. Engl.* **2014**, *53*, 10412-10415.

[16] D. J. Knobloch, E. Lobkovsky, P. J. Chirik, *J. Am. Chem. Soc.* **2010**, *132*, 10553-10564.

CHAPTER 7

The role of bridging ligands in dinitrogen reduction and functionalization by uranium multimetallic complexes

Introduction[1]

Multimetallic complexes that reduce and functionalize dinitrogen in the absence of strong alkali reducing agents are crucial to establish a structure-activity relationship, but remain extremely rare. In chapter 6, a multimetallic nitride-bridged diuranium(III) complex capable of reducing and functionalizing dinitrogen is described. Here an analogous complex assembled with an oxide instead of a nitride linker is presented. The resulting complex is able to effect the four electrons reduction of dinitrogen, but the reactivity of the resulting oxo/(N_2) complex differs remarkably from that of the nitride/(N_2). Computational studies, performed by prof. C. Corminboeuf et al., show a different bonding scheme for the dinitrogen where the bridging nitride does participate to the binding and to the consequent activation of N_2, while the oxide does not.

A wide range of studies has been directed to the development of metal complexes able to effect the conversion of N_2 into high N-containing organic products in mild conditions[1],[2]. Particularly desirable would be the use of cheap and/or largely available molecules such as CO or CO_2 in combination with dinitrogen for the synthesis of new organic products. Versatile chemical cycles for the production of isocyanates by the molecular fixation of N_2, CO_2 and R_3ECl (E=C, Si, and Ge) have been reported by Sita and coworkers[3]. However, direct dinitrogen cleavage and N–C

[1] Portions of this chapter have been published: M. Falcone, L. Barluzzi, J. Andrez, F. F. Tirani, I. Zivkovic, A. Fabrizio, C. Corminboeuf, K. Severin, M. Mazzanti, *Nature Chemistry,* **2018**, *11*, 154
Author contributions: compounds **2** and **3** were first isolated and characterized by J.A., while their synthesis was optimized by L.B. Compound **4** was isolated, synthetized and characterized by M.F. Compound **5** was isolated by M.F. and further characterized by L.B. Compound **6** was first isolated and characterized by L.B. Reactivity studies with acids and hydrogen were performed by M.F. M.F. and L.B. collaborated all along for the synthesis of compounds and analysis of data. X-ray analyses were performed by F.F.T. Magnetic measurements were performed and analyzed by I.Z. A.F and C.C. performed the DFT calculations. K.S. suggested the use and provided the oxo transfer agent. M.M., M.F. and L.B. wrote the manuscript. M.M. originated the central idea, coordinated the work and analyzed the experimental data.

bond formation from the addition to dinitrogen complexes of cheap carbonated molecules such as CO and CO_2 remains extremely rare[4],[5]. The observed reactivity of complex $[K_3\{[U(OSi(OtBu)_3)_3]_2(\mu\text{-}N)\}]$ (Chapter 6) giving the first example of dinitrogen functionalization at a uranium centre, is ascribed to the multimetallic binding of the bridging dinitrogen to two uranium centres and two potassium cations, that is enabled by the bridging nitride and the flexible potassium-siloxide framework. However, it remains unclear how crucial is the nature of the group (nitride) bridging the two uranium(III) atoms. We therefore set out to explore the possibility of using an oxo group as linker to build multimetallic uranium complexes. Oxo-bridged molecular complexes are attractive models for metal oxide catalysts but usually contain metal centres in high oxidation state. Notably, only one example of a crystallographically characterized U(III)–O–U(III) complex has been reported[6]. This complex and most of the reported structurally characterized diuranium(IV) oxo-bridged complexes have been obtained from the reaction of U(III) complexes with the solvent [7] or the supporting ligand [8] or with adventitious traces of O_2 or water in the solvent. In contrast, the number of rationally synthesised diuranium(IV) oxo-bridged complexes remains limited, probably due to the tendency of these species to undergo further oxidation.[9],[10],[11] In this chapter a novel route for the preparation of a siloxide oxo-bridged diuranium(IV) complex is described. Moreover, the reduction to afford a rare multimetallic oxo-bridged diuranium(III) is presented, together with reactivity studies to prove the effect of the core structure on the reduction and functionalization of dinitrogen, showing that the linker has a crucial role in determining the reactivity of analogous multimetallic N_2 complexes.

Results and discussion

Initial attempts to prepare a diuranium(IV) oxo-bridged complex from the reaction of the previously reported complex $[U(OSi(O^tBu)_3)_3]_2$, **1** [12] with common oxygen atom transfer reagents lead to intractable reaction mixtures (Me_3NO, N_2O) or to the isolation of complex **2** in very low yield (PyNO). However, we were able to reproducibly prepare complex $[\{U(OSi(O^tBu)_3)_3\}_2(\mu\text{-}O)]$, **2**, in 79% yield by treating **1** with the N_2O adduct of the N-heterocyclic carbene 1,3-dimesitylimidazol-2-ylidene (IMes) $IMesN_2O$ [13] in THF at –80 °C (Scheme 1a). The ability of the $IMesN_2O$ to selectively produce the oxodiuranium(IV) complex could be due to the higher reaction rates of this reagent [14] compared to the other used oxygen transfer agents.

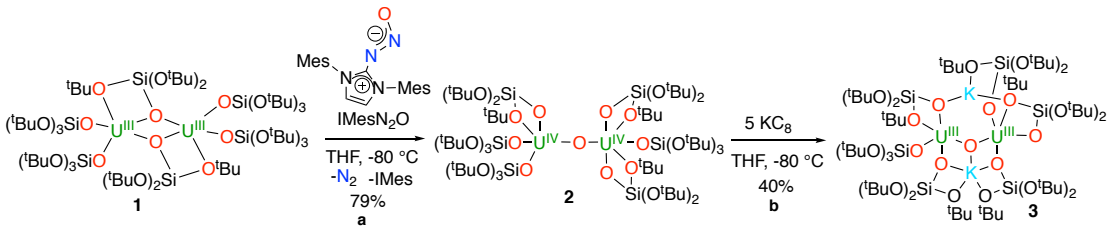

Scheme 1. Reaction of **1** with $IMesN_2O$ affords the diuranium(V) oxo-bridged complex **2** (**a**); reduction of **2** with excess of KC_8 affords the diuranium(III) oxo-bridged complex **3** (**b**).

In the solid-state structure of **2** (Figure 1a), an oxo ligand (O^{2-}) bridges, with an angle that deviates slightly from linearity (172.19(7) Å; U---U 4.2129(9) Å), two inequivalent U(IV) centres. The values of the U(IV)–oxo distances (2.0852(13) and 2.1376(13) Å) fall in the range of those found in analogous oxo-bridged diuranium(IV) complexes (2.0881(4) - 2.147(6) Å) [8, 10a, 10c, 11, 15].

The reduction of complex **2** with 5 equivalents of KC_8 in THF at –80 °C affords the formation of the multimetallic oxo-bridged diuranium(III) complex $[K_2\{[U(OSi(O^tBu)_3)_3]_2(\mu\text{-}O)\}]$, K_2UOU, **3** (Scheme 1b) that can be isolated from a cold (–80 °C) THF solution with a yield of 40 %. The conversion rate is significantly higher (>70%) but isolation results in lower yields due to the low thermal stability of **3**. The structure of **3** (Figure 1b) shows the presence of a neutral complex with two U(III) ions bridged by an oxo ligand that is also bound to a potassium cation located in the pocket formed by four oxygen atoms of the siloxide ligands (K2–O121 =2.913(4) Å). A second potassium cation is coordinated by the oxygen atoms of the siloxide ligands at a non-bonding distance from the oxo group (K1–O121 3.392(4) Å). The values of the U(III)-oxo bond distances (2.178(4) and 2.109(4) Å), are significantly longer than those found for **2** (2.0852(13) and 2.1376(13) Å) and compare well with those found in the only other crystallographically characterized oxo-bridged diuranium(III) complexes. (2.125(13) and 2.094(14) Å).[6] In complex **3**, the two uranium atoms are maintained in close proximity at a U---U distance of 4.2619(5) Å by the oxo group and by the metallo-ligand framework formed by the potassium-bound siloxides. This distance is slightly longer than that found in the nitride bridged diuranium(III) complex $[K_3\{[U(OSi(O^tBu)_3)_3]_2(\mu\text{-}N)\}]$, K_3UNU, (4.234(2) Å)[5]. The U–O–U core (167.4(2)°) in **3** is significantly more bent compared to that of the U–N–U core in the K_3UNU complex (173.7(8)°).

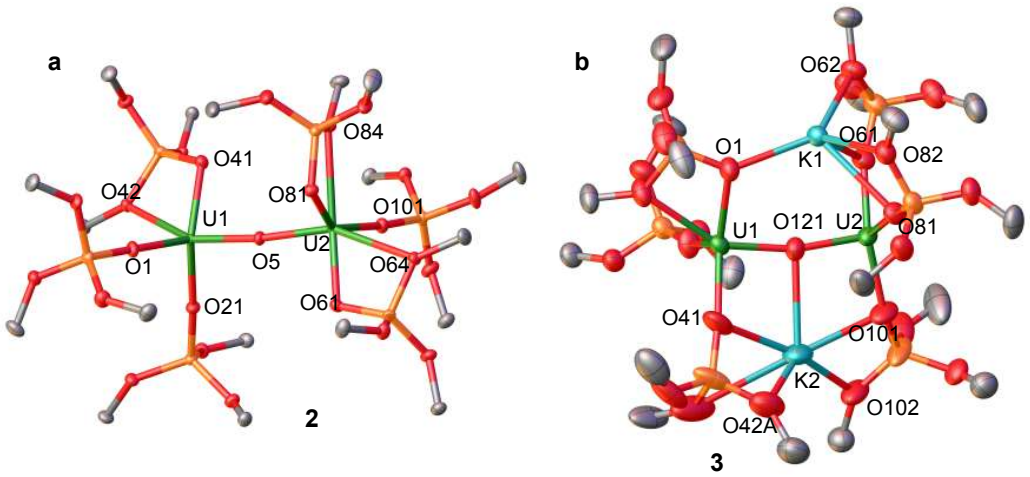

Figure 1. Solid-state molecular structure of [{U(OSi(O^{t}Bu)$_3$)$_3$}$_2$(μ-O)], **2** (**a**) and of [K$_2${[U(OSi(O^{t}Bu)$_3$)$_3$]$_2$(μ-O)}], **3** (**b**). Thermal ellipsoids set at 50% probability. Hydrogen atoms and methyl groups were omitted for clarity. Selected bond lengths for **2** [Å]: U1–O5 2.0852(13), U2–O5 2.1376(13). Selected bond lengths for **3** [Å]: U1–O121 2.178(4), U2–O121 2.109(4), K1–O121 3.392(4), K2–O121 2.913(4).

In order to investigate how the linker affects the reactivity of multimetallic complexes of uranium(III) towards dinitrogen we have investigated the reaction of **3** with N_2. When a toluene solution of **3** is exposed to N_2 (1 atm) at room temperature (Scheme 2), we observe an immediate change in colour from deep red to brown along with disappearance of the ^{1}H NMR signal assigned to **3** and appearance of a new peak.

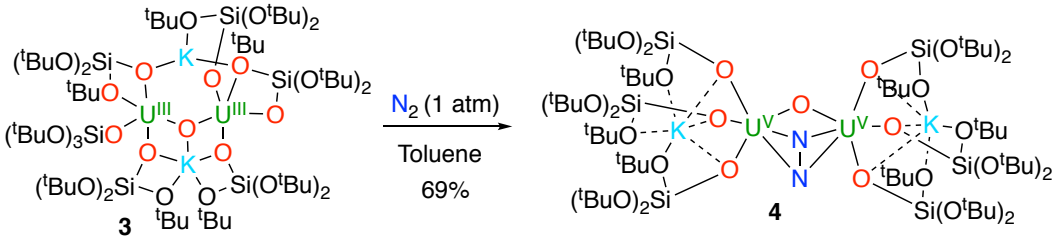

Scheme 2. Reaction of **3** with 1 atm N_2 to afford the hydrazido complex **4**.

Dark brown crystals of the complex [K$_2${[U(OSi(O^{t}Bu)$_3$)$_3$]$_2$(μ-O)(μ-η^2:η^2-N$_2$)}], **4**, were isolated in 70% yield from a toluene solution of **4** at –40 °C. Proton NMR studies showed that complex **4** is stable in toluene at room temperature for several hours. No loss of N_2 from **4** is observed under dynamic vacuum in the solid state or after three cycles of freeze-pump thaw degassing under argon of a toluene solution of **4**. The structure of **4** (Figure 2) reveals the presence of one oxo group (U–O–U = 105.0(3) Å and a side-on (U1–N1A–U2= 99.0(2)° and U1–N2A–U2 = 98.56(18)°), bound hydrazido moiety (N_2^{4-}) bridging two uranium(V) centres in a diamond-shaped

geometry with a short U---U distance of (3.3801(5) Å). Differently from the previously reported U(V) nitrido hydrazido complex [K_3{[$U(OSi(O^tBu)_3)_3]_2$(μ-N)(μ-N_2)}], $K_3UN(N_2)U$, in which three potassium cations were bound to the nitrido and hydrazido groups in the core of the molecule (U---U distance: 3.3052(5) Å), in **4** the two potassium cations are located in the pockets formed by the siloxide ligands and do not bind the core N,N,O atoms. The $U_2(\mu\text{-}\eta^2\text{-}N_2)$ moiety in **4** features U–N bond distances ranging from 2.279(8) to 2.157(17) Å that are comparable to those found in $K_3UN(N_2)U$ (2.311(13) Å to 2.163 (13) Å). The N-N bond length in complex **4** (1.40(1) Å) is comparable to the observed bond length in hydrazine, H_2NNH_2 (1.47 Å) and falls in the range of values (1.377 - 1.548 Å) reported for hydrazido complexes of Zr(IV) and U(V)[2a, 2b, 16].

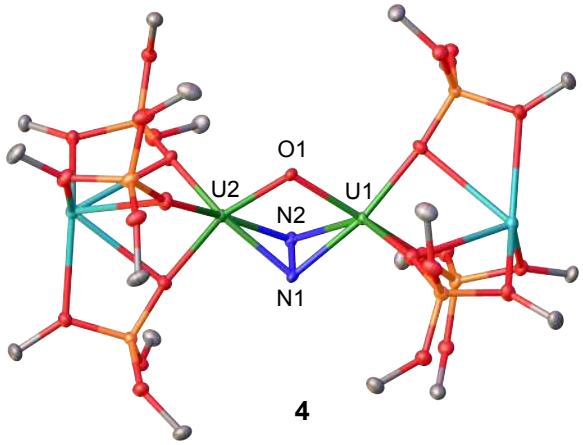

Figure 2. Solid-state molecular structure of [K_2{[$U(OSi(O^tBu)_3)_3]_2$(μ-O)(μ-η^2:η^2-N_2)}], **4**. Thermal ellipsoids set at 50% probability. Hydrogen atoms and methyl groups were omitted for clarity. Selected bond lengths [Å]: U1–O1 2.135(11), U2–O1 2.127(10), U1–N1 2.182(20), U2–N1 2.230(61), U1–N2 2.221(57), U2–N2 2.194(2), N2–N2 1.401(41).

The cation plays a crucial role in N_2 activation by the K_2UOU complex. Notably, preliminary results indicate that when the potassium is replaced by Cs, N_2 binding or reduction is not observed.

The variable-temperature magnetic data measured with a superconducting quantum interference device (SQUID) for complex **4** showed the presence of two uranium ions in the formal oxidation +V confirming the presence of a highly activated bound dinitrogen, reduced to a hydrazido group (N_2^{4-}).

These results show that the two uranium(III) ions, held together by a potassium bound oxo ligand in a multimetallic K_2UOU core, are able to bind dinitrogen and to effect its four electron reduction as previously reported for the nitride-bridged $K_3UN(N_2)U$ [5]

in spite of the lower electron-rich character of the uranium cations in the oxo complex (as a result of the replacement of N^{3-} by O^{2-}). Such a remarkable reactivity is only the second example [5] of four electron reduction of dinitrogen by a uranium complex and indicates that the oxo group also provides a versatile linker for the assembly of highly reactive multimetallic uranium complexes.

Attempts to reduce the N–N single bond by addition of KC_8 at room temperature and at –70 °C did not lead to any conclusive result, as no product could be isolated. When 2 equivalents of KC_8 were added to a toluene solution of **4** at room temperature or at –70 °C, the same proton NMR spectrum was obtained, showing still starting material and two peaks at –4 and 11 ppm in a ratio 1:0.5, possibly belonging to the siloxide ligands of a complex (Figure 3). The presence of the starting material suggests that the reduction at the metal center compete with the N–N reduction.

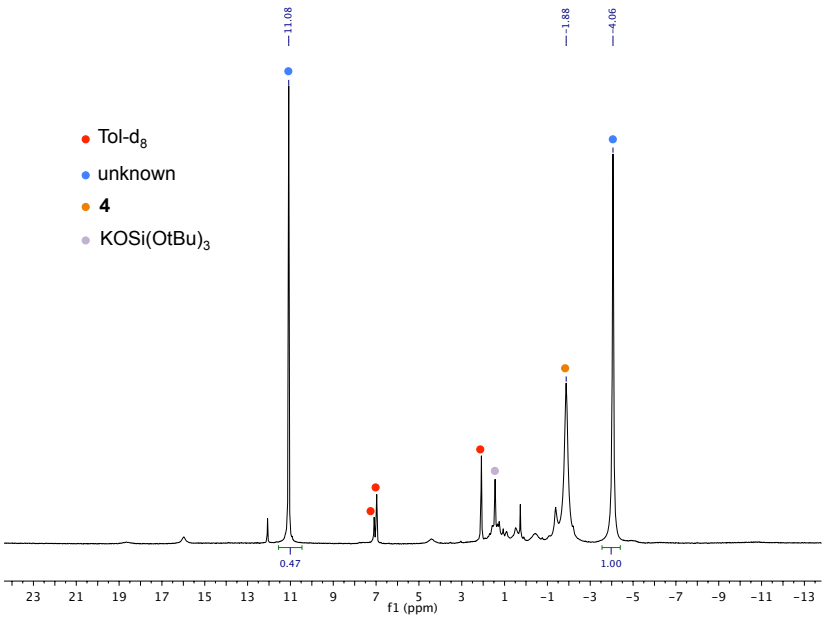

Figure 3. ^{1}H NMR (400 MHz, tol-d_8, 298K) right after addition of 2 equiv. of KC_8 to a solution of complex **4**.

In order to understand how the replacement of the nitride group in $K_3UN(N_2)U$ by an oxo group in **4**, ($K_2UO(N_2)U$) affects the reactivity of the bound dinitrogen we investigated the reaction of **4** with CO, H_2 and H^+.

When a toluene solution of complex **4** is exposed to 3 equivalents of CO (Scheme 3a), the reaction mixture changes immediately colour from dark brown to dark purple. Black crystals of the cyanamido-bridged complex $[K_2\{[U(OSi(O^tBu)_3)_3]_2(\mu\text{-}O)_2(\mu\text{-}NCN)\}]$, **5**, were isolated from a toluene solution at –40 °C with 68% yield.

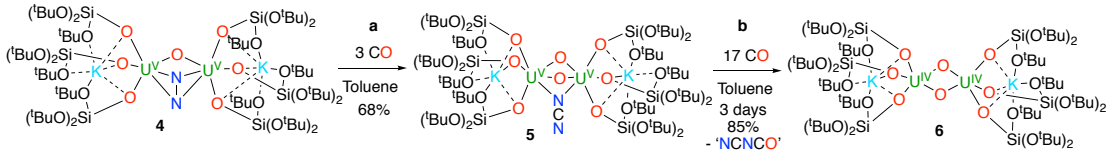

Scheme 3. Reaction in ambient conditions of complex **4** with CO to afford the cyanamido-bridged complex **5** (**a**); complex **5** can react with excess CO to afford the bis-oxo complex **6** (**b**).

The structure of complex **5** (Figure 4a) shows a dinuclear complex in which each uranium atom is coordinated by three siloxide ligands, two bridging oxo groups and a cyanamido ($N{\equiv}C{-}N^{2-}$) ligand adopting a μ-κN,κN bridging mode. The observed C–N bond distances in **5** are in agreement with the presence of a cyanamido ($N{\equiv}C{-}N^{2-}$) ligand (N1–C201=1.302(17) Å and C201–N2=1.23(2) Å) and are in good agreement with those found in previously reported metal complexes containing the bridging cyanamido ligand.[17]

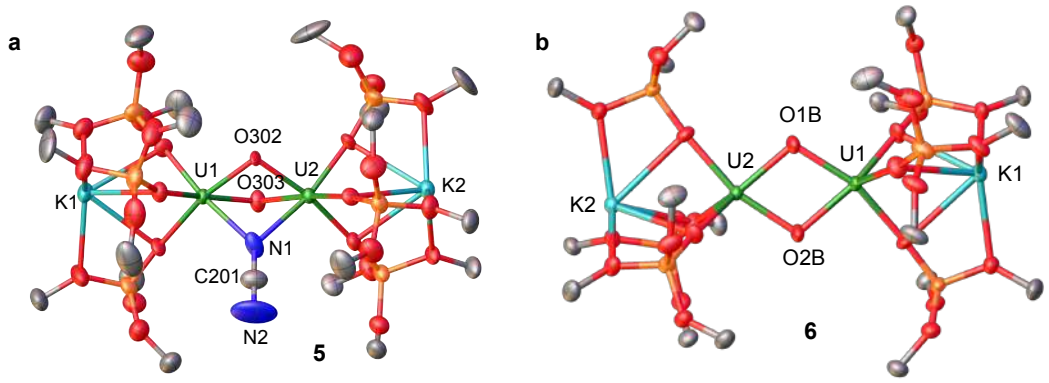

Figure 4. Solid-state molecular structure of $[K_2\{[U(OSi(O^tBu)_3)_3]_2(\mu\text{-}O)_2(\mu\text{-}NCN)\}]$, **5** (**a**) and of $[K_2\{[U(OSi(O^tBu)_3)_3]_2(\mu\text{-}O)_2\}]$, **6** (**b**). Thermal ellipsoids set at 50% probability. Hydrogen atoms and methyl groups were omitted for clarity. Selected bond lengths for **5** [Å]: U1–N1 2.367(10), U1–O302 2.099(6), U2–O302 2.099(6), U2–N1 2.346(9), U1–O301 2.152(7), U2–O301 2.137(7), N1–C201 1.302(17), C201–N2 1.23(2). Selected bond lengths for **6** [Å]: U1–O1B 2.092(5), U1–O2B 2.182(5), U2–O1B 2.155(5), U2–O2B 2.091(5).

The IR spectrum of the isolated compound **5** shows a strong vibration at 2008 cm^{-1}, assigned to the NCN^{2-} ligand, that is shifted at 1942 cm^{-1} for the ^{13}C labelled complex **^{13}C-5** (Figure 5). These values are in the range of those reported (1975 cm^{-1} - 2061 cm^{-1}) [17a, 18] in metal complexes of the cyanamide ligand, and compare well to the value reported for a cyanamide-bridged diuranium(IV) complex (2034 cm^{-1}) where the ligand adopts a linear μ-η^1-κ^1N-κ^1N' binding mode.[17c]

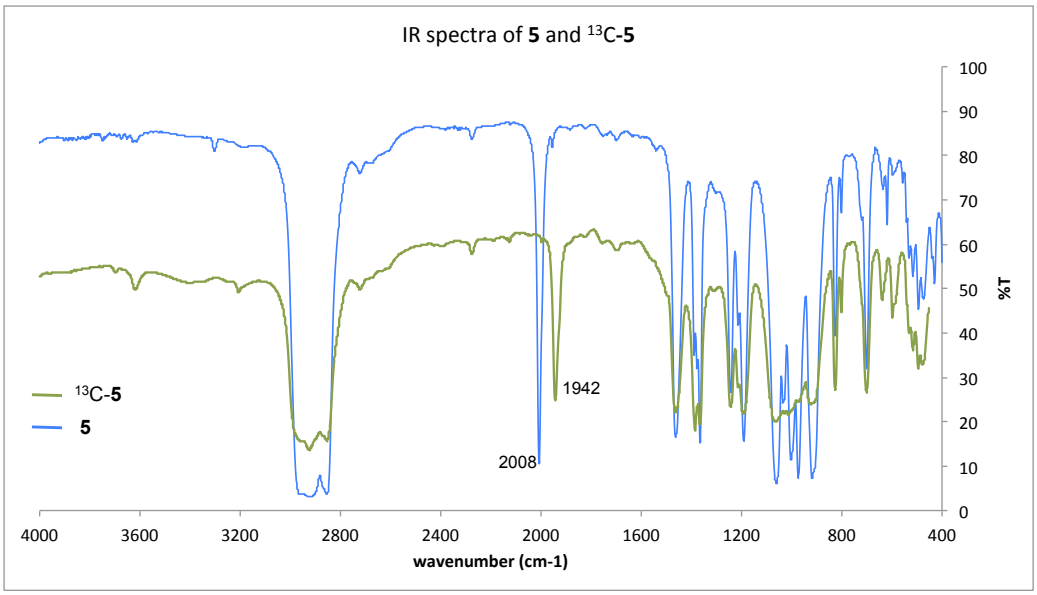

Figure 5. Overlay of the IR spectra of complex **5** (in blue) and ^{13}C-**5** (in green).

In this unique reaction, both the dinitrogen single bond and the CO triple bond are cleaved at room temperature to afford a bridging oxo group and a bridging cyanamide ligand (NCN^{2-}), leaving the oxidation state of the uranium atoms unchanged. The reactivity displayed by the oxo-hydrazido complex **4** differs completely from that observed for other reported hydrazido complexes[4] and in particular from that of the nitrido-hydrazido and imido-hydrazido uranium(V) complexes $K_3UN(N_2)U$ and $K_2U_2(NH)(N_2)]$ respectively.[5] Notably the reaction of the U(V) complexes $[K_3U_2N(N_2)]$ and $[K_2U_2(NH)(N_2)]$ with CO resulted in the reductive carbonylation of the hydrazido ligand leading to formation of U(IV)U(IV) bis-cyanate and U(III)U(IV) mono-cyanate complexes, respectively.[5] The reactivity of **4** with CO also differs from that observed for group 4 dinitrogen complexes. Notably the addition of CO to hydrazido complexes of Hf(IV), results in the addition of 2 CO molecules to the Hf(IV)-bound N_2^{4-} group and the formation of a oxamidide ($[N_2C_2O_2]^{4-}$) bridged Hf(IV) complex.[4]

The novel reactivity suggests that reduction of the uranium centers is less accessible in complex **4** compared to the nitride analogue, but that the strong nucleophilic character of the bound N_2^{4-} group still allow the concomitant cleavage of the CO and N_2 bonds.

However, the addition of excess CO (10 - 100 equivalents) to the isolated cyanamide complex **5** results in the slow transformation of **5** (3 days when 18 equivalents are

used) into the bis-oxo diuranium (IV) complex $[K_2\{[U(OSi(O^tBu)_3)_3]_2(\mu\text{-}O)_2\}]$ **6** (Scheme 3b) with a conversion rate of 85%. The reduction of the uranium cations is accompanied by the elimination of the product of CO addition to the cyanamide that could not be identified. The structure of **6** shows (Figure 4b) the presence of two uranium(IV) cations bridged by two oxo groups. The U–O distances of 2.092(5) - 2.182(5) Å are comparable to those reported in analogous U(IV) bis-oxo diuranium complexes.[19]

The reaction of a toluene solution of complex **4** with excess acid ($HCl(Et_2O)$ or $HBAr^F_4$) alone or in the presence of a reducing agent (KC_8) did not result in the formation of ammonia as previously observed upon addition of excess acid to $K_3UN(N_2)U$, but in the elimination of N_2 (Scheme 4a). A dramatic difference in reactivity between **4** and $K_3UN(N_2)U$ was also observed upon addition of H_2. The reaction of a toluene solution of complex **4** with 1 atmosphere of H_2 for three days at room temperature or one hour at 60 °C leads to the quantitative conversion of **4** into a new species as indicated by ^1H NMR studies (Scheme 4b), showing a signal at 11.96 ppm integrating for two protons. The latter is assigned to the protons deriving from H_2, since the peak disappears when the reaction is carried out with D_2.

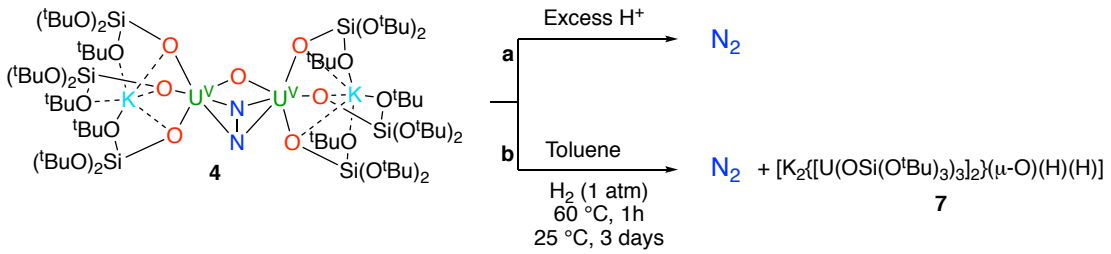

Scheme 4. Reaction of complex **4** with excess acid lead to N_2 release (**a**); reaction with H_2 lead to release of N_2 and formation of the hydride complex **7** (**b**).

GC-MS of the headspace of the reaction mixture showed that evolution of N_2 had occurred during the reaction (see Appendix 6). A yellow solid could be isolated from this reaction and elemental analysis did not show the presence of nitrogen. Furthermore, even in the presence of a reducing agent, the addition of excess acid ($HCl(Et_2O)$) to the product of the reaction of **4** with H_2, did not result in the formation of nitrogen containing products. The recorded data indicate that addition of H_2 to **4** leads to the elimination of N_2 and suggest the formation of a diuranium(IV) oxo bis-hydride complex ($[K_2\{[U(OSi(O^tBu)_3)_3]_2(\mu\text{-}O)(H)(H)]\}$, **7**). The magnetic data measured for complex **7** are in agreement with the presence of U(IV).[20] The same

compound was also obtained from the reaction of the U(III) oxo complex **3** with 1 atm H_2 (for further characterization and reactivity of **7** see Chapter 8). Examples of N_2 elimination following dihydrogen addition have been reported [1b, 21] and are usually indicative of a low degree of activation of the bound dinitrogen.

Thus, the reactivity of the oxo-bridged $K_2UO(N_2)U$ dinitrogen complex differs dramatically from that of the nitride-bridged $K_2UO(N_2)U$ complex, which reacts with H_2 and acid to produce ammonia almost quantitatively (77% conversion of the nitrido and hydrazido groups into ammonia). The difference is probably due both to structural effects arising from differences in the alkali ion-binding mode and to differences in the electronic structure of the two complexes. Dramatic differences in the reactivity of analogous N_2 bound complexes with H_2 have been reported by Chirik and coworkers upon subtle changes of the supporting ligand (from η^5-C_5Me_5 to η^5-C_5Me_4-H),[21] but in that case the change in supporting ligand leads to a different binding mode of the dinitrogen (end-on versus side-on) as result of steric protection by the ligand. In contrast the subtle change from nitride to oxide does not lead to significant steric changes and results in the same binding mode (side-on) and the same degree of reduction of the bound dinitrogen.

Magnetic Data.

In order to further investigate differences in the electronic structure of the oxo and nitride complexes, that may be responsible for difference in reactivity, we carried out magnetic studies, in collaboration with Dr. Ivica Zivkovic. The two dinuclear complexes (**3** and K_3UNU) have a similar magnetic moment (μ = 2.10 μ_B for **3** and μ = 2.04 μB for K_3UNU) at room temperature in agreement with the presence of uranium(III) ions,[20] but show remarkably different magnetic behavior, as is clearly observable in the plots of the magnetic susceptibility (χ) versus T and χT versus T (Figure 6).

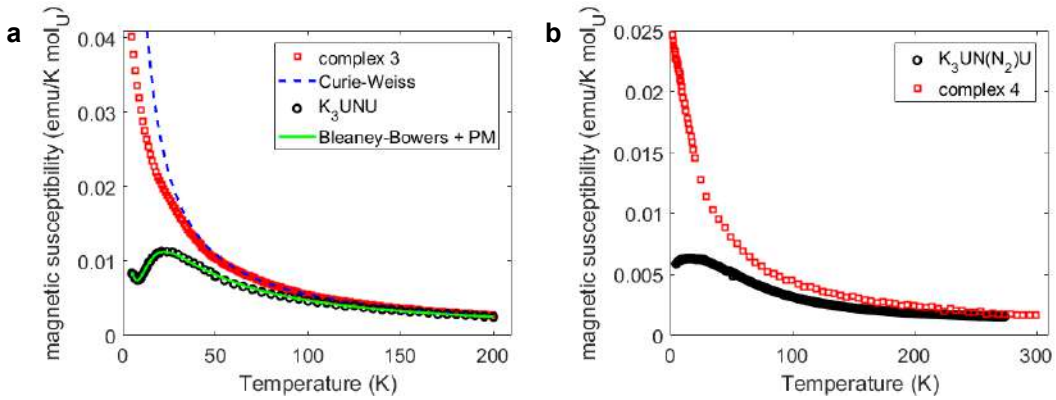

Figure 6. Comparison of the variable-temperature magnetic susceptibility of **3** versus K_3UNU (the green line represents the fitting with the Bleaney-Bowers equation including contribution from paramagnetic impurities (PM) while the dotted blue line represents the fitting with the Curie-Weiss equation) (**a**) and of **4** versus $K_3UN(N_2)U$ (**b**).

The χ versus T plot for the nitride complex K_3UNU exhibits the magnetic behavior of an antiferromagnetically coupled dinuclear complex with a maximum at 23K. In contrast the χ versus T plot for **3** shows the magnetic behavior of two magnetically independent U(III) ions. Similarly, the dinuclear dinitrogen complexes **4** and $K_3UN(N_2)U$ have a similar magnetic moment (μ = 1.75 μ_B for **4** and μ = 1.80 μ_B for $K_3UN(N_2)U$) indicative of the presence of U(V) cations, but show different χ versus T plots suggestive of the presence of two magnetically independent ions in **4** and of an antiferromagnetically coupled system for the nitride complex. These results suggest that the nitride ligand allows for a better communication between the metal centers compared to the oxide.

Computational analysis.

In agreement with the magnetic data, DFT level computations indicate that the singlet, antiferromagnetic state is the most stable at 0 K for the nitride complex, while the triplet, paramagnetic state is the most stable for **3** (Appendix 6 Table 3). As shown in Figure 7 the frontier orbitals (HOMO-5 to LUMO+2) of the $K_3U^{III}NU^{III}$ complex suggests a markedly covalent character of the U–N–U bond. On the other hand, no orbital overlap exists in **3** between the bridging oxide (O^{2-}) and the two uranium centers, which would suggest a strictly ionic type of bonding. Topological analysis of the electron density about the bonds with the bridging atom further supports the difference in bonding character (Appendix 6, Figure 58).

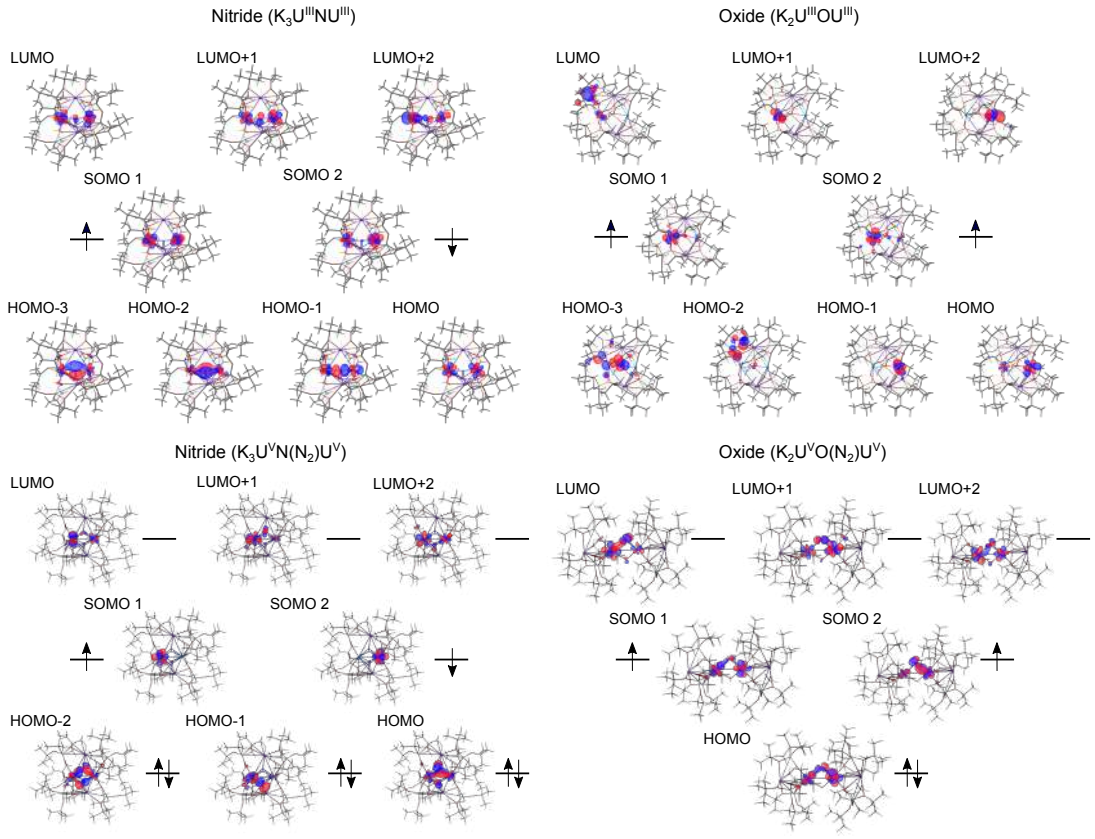

Figure 7. Molecular orbitals of the K_3UNU (top left), K_2UOU (top right), $K_3UN(N_2)U$ (bottom left) and $K_2UO(N_2)U$ (bottom right) complexes. Orbital overlap is present in K_3UNU and $K_3UN(N_2)U$ (covalent character), but not in K_2UOU and $K_2UO(N_2)U$ (ionic character). SOMO, singly occupied molecular orbital; HOMO, highest occupied molecular orbital; LUMO, lowest unoccupied molecular orbital.

The bond character and the spin state of each complex do not change upon complexation of the N_2 substrate. In particular, orbital overlap persists in the nitride case (covalent), while it does not appear in the oxide complex (ionic). As shown in Figure 7, this affects the binding of the N_2 substrate resulting in significant differences between the two complexes. In the case of $K_3UN(N_2)U$, both uranium atoms and both nitrogen atoms from dinitrogen are involved in bonding, while in $K_2UO(N_2)U$ the overlap is asymmetric involving only one uranium atom. Moreover, all N_2 bonding orbitals present a strong component centred on the bridging nitride ligand atom, but none centred on oxygen. Natural Bond Order (NBO) analysis and Wiberg bond index indicate that this results in a decreased N-N bond order (1.4 in **4** and 1.0 in $K_3UN(N_2)U$) and an increased U-N(N_2) bond order in the nitride complex compared to the oxide one. This observation suggests that the bridging nitride does participate to the binding and to the consequent activation of N_2, while the oxide does not. Combined together, the asymmetric orbital overlap and the spectator role of the

bridging oxygen provide a theoretical basis to rationalise the striking difference in reactivity of N_2 substrate in the nitride and oxo complexes.

Conclusions

In summary, bridging oxo groups can be used to support uranium in a low oxidation state, affording multimetallic complexes that effect the reduction and functionalization of dinitrogen. The uranium bound dinitrogen is easily cleaved in ambient condition by carbon monoxide (CO) affording an original compound via N-C bond formation. This provides a route for building organo-nitrogen compounds from cheap resources (notably cyanamide is formed from CO and N_2). We demonstrate that the substitution of a nitride linker with a oxo linker has dramatic effects on the reactivity of the resulting multimetallic uranium(III) complex towards dinitrogen. Specifically, the presence of the oxo linker results in the release of dinitrogen upon addition of dihydrogen while the subsequent addition of hydrogen and acid to the nitride complex leads to ammonia formation. Moreover, the oxo linker leads to unusual reactivity of the uranium bound dinitrogen as a result of structural and electronic differences compared to the nitride-linked diuranium complex. Thus, the results show that both oxo groups and nitride groups can be used as linkers to build low-valent multimetallic complexes for dinitrogen reduction, and on the other hand they show that the nature of the linker affects dramatically the reactivity of the bound dinitrogen. DFT computations and magnetic data indicate a different bonding scheme for the nitride and oxide complexes with amarkedly covalent character of the U–N–U bond and a strictly ionic U–O–U bond. This difference is maintained in the respective dinitrogen complexes where in addition the bridging nitride participates to the binding and to the consequent activation of N_2, while the oxide does not. These results show that, in spite of the presence of the same dinitrogen binding mode, the same supporting ligands and the same oxidation level of the metal centers, the nature of the linker has a significant impact on the degree of N_2 activation.

Experimental

General. All manipulations were carried out under a dry and oxygen free argon atmosphere using Schlenk techniques and an MBraun glovebox equipped with a purifier unit. The water and oxygen levels were always kept at less than 0.1 ppm. Glassware was dried overnight at 140°C before use. Compounds were characterized by elemental analysis, ^{1}H and ^{13}C NMR, IR and single-crystal X-ray diffraction.

^{1}H NMR experiments were carried out using NMR tubes adapted with J. Young valves. ^{1}H NMR spectra were recorded on Bruker 400 MHz. NMR chemical shifts are reported in ppm with solvent as internal reference. **Elemental analyses** were performed with a Thermo Scientific Flash 2000 Organic Elemental Analyzer. Elemental analysis of complex **5** was performed under argon by Analytische Laboratorien GMBH at Lindlar, Germany. **IR analyses** were performed with a FT-IR Spectrometer Perkin-Elmer. The measurements were performed by using nujol mulls between KBr plates. **Starting materials.** Unless otherwise noted, reagents were purchased from commercial suppliers and used without further purification. Tris(*tert*-butoxy)silanol and 2,4,6-tri-*tert*-butylphenol were purified by sublimation. Depleted uranium was purchased from IBILABS (USA). The solvents were purchased from Aldrich or Cortecnet (deuterated solvents) in their anhydrous form, conditioned under argon and vacuum distilled from K/benzophenone (toluene, toluene-d_8 (tol-d_8), tetrahydrofuran (THF), THF-d_8, benzene-d_6 and hexane). DMSO-d_6 was freeze-degassed and stored over activated 3 Å molecular sieves. The complex $[U(OSi(O^tBu)_3)_3]_2$, **1** [12] and $IMesN_2O$ (IMes = N-heterocyclic carbene 1,3-dimesitylimidazol-2-ylidene) [13b, 22] were prepared according to the published procedure. Carbon monoxide (N47 Bt-S 10/200) was purchased from Carbagas and stored over activated 3 Å molecular sieves. N_2 (99.9999% purity) was purchased from Carbagas. ^{13}CO (93.13% 13C) and $^{15}N_2$ (98% 15N) were purchased from Cortecnet and stored over activated 3 Å molecular sieves. **Magnetic data.** Magnetic measurements were performed using a Quantum Design MPMS-5T superconducting quantum interference device (SQUID) magnetometer in a temperature range 2-300 K. The powder sample was enclosed in an evacuated quartz capsule and placed inside a plastic straw. The measurements were performed with applied magnetic field of 0.1 T in the zero-field cooled (ZFC) regime. **Caution:** Depleted uranium (primary isotope ^{238}U) is a weak α-emitter (4.197 MeV) with a half-life of 4.47×10^{9} years. Manipulations and reactions should be carried out in monitored fume hoods or in an

inert atmosphere glovebox in a radiation laboratory equipped with α- and β-counting equipment.

Synthesis of [{U(OSi(O^{t}Bu)$_3$)$_3$}$_2$(μ-O)], 2

A cold yellow suspension of IMesN$_2$O (184.7 mg, 0.53 mmol, 1 eq) in THF (6 mL) was added to a cold solution (–80 °C) of complex [U(OSi(O^{t}Bu)$_3$)$_3$]$_2$, **1** (1.09 g, 0.53 mmol, 1 eq) in THF (6 mL). N_2 evolution was observed. The solution was allowed to react at –80 °C for 4 h. Monitoring the reaction mixture by ^{1}H NMR in THF-d$_8$ shows that the reaction is complete after 4 hours at –80 °C and some solid has formed. The resulting suspension was taken to dryness and the solid residue was washed several times with cold (–40 °C) toluene (2mL), until complete removal of the IMes carbene formed during the reaction, to afford [{U(OSi(O^{t}Bu)$_3$)$_3$}$_2$(μ-O)], **2**, as a pink solid (0.87 g, 79 % yield). X-ray suitable crystals were obtained by leaving standing a 0.005 M solution of **2** in toluene at –40 °C overnight. ^{1}H NMR of the solid (400 MHz, tol-d$_8$, 298 K): δ (ppm) = 0.49 (s, CH_3 terminal siloxide). ^{13}C NMR of the solid (400 MHz, tol-d$_8$, 298 K): δ (ppm) = 70.16 (s, (**C**(CH$_3$)$_3$),), δ (ppm) = 25.97 (s, (C(**C**H$_3$)$_3$)). Anal. Calcd for **2** $C_{72}H_{162}O_{25}Si_6U_2$: C, 41.72; H, 7.88; N, 0.00. Found: C, 41.46; H, 7.77; N, 0.00. When the reaction is carried out at higher temperatures, a larger number of by-products are formed and the yield in complex **2** is significantly reduced. Complex **2** is stable in THF and toluene solution at room temperature for, respectively, 24 and 6 hours, but decomposes slowly over time to afford unidentified species and [U(OSi(O^{t}Bu)$_3$)$_4$]. The decomposition is complete after 20-30 days.

Reactivity of complex [{U(OSi(O^{t}Bu)$_3$)$_3$}$_2$], 1 with N$_2$O, Me$_3$NO, and PyNO

The reaction of complex **1** with N_2O, PyNO, or Me$_3$NO resulted in mixtures of several products independently of the stoichiometry used, the temperature (25 °C, –40 °C or –80 °C) and of the solvent used (THF and hexane were used, toluene could not be used because **1** reacts with toluene). In some cases, the formation of complex **2** was observed, but only as a minor product. The highest reaction yield that could be obtained using a 1:1 stoichiometric ratio at –80 °C in hexane was 9%. In the case of the reaction of **1** with Me$_3$NO at –80°C in hexane, only one product is formed that could not be identified.

Synthesis of $[K_2\{[U(OSi(O^tBu)_3)_3]_2(\mu\text{-}O)\}]$, 3

Excess KC_8 (48.3 mg, 0.355 mmol, 5 eq) was added to a cold solution (–80 °C) of $[\{U(OSi(OtBu)_3)_3\}_2(\mu\text{-}O)]$, **2** (148.1 mg, 0.071 mmol, 1 eq) in THF (3 mL). The suspension was stirred at –80 °C for 15 minutes. The reaction mixture was then filtered on cooled (–80 °C) glassware in order to remove graphite and unreacted KC_8. The resulting dark red solution was concentrated to 1 mL and the solution was kept at –80 °C for 1h leading to the formation of a red precipitate. The suspension was filtered on cold glassware affording 61.9 mg of $[K_2\{[U(OSi(O^tBu)_3)_3]_2(\mu\text{-}O)\}]$, **3** (40 % yield). X-ray suitable crystals were obtained by leaving standing a THF solution (0.07 M) of **3** at –40 °C overnight. ^{1}H NMR of the solid (400 MHz, THF-d_8, 298 K): δ (ppm) = –0.04 (s, CH_3 terminal siloxide). ^{1}H NMR of the solid (400 MHz, tol-d_8, 298 K): δ (ppm) = 0.10 (s, CH_3 terminal siloxide). ^{13}C NMR of the solid (400 MHz, THF-d_8, 298 K): δ (ppm) = 69.67 (s, $\mathbf{C}(CH_3)_3$), 27.77 (s, $C(\mathbf{C}H_3)_3$). Anal Calcd for **3** $C_{72}H_{162}O_{25}Si_6K_2U_2$: C, 40.21; H, 7.59; N, 0.00. Found: C, 40.09; H, 7.63; N, 0.00. The isolated yield is quite low (40 %) due to the good solubility of the complex in THF, but the effective yield is higher. Notably, when N_2 is directly added to the reaction mixture obtained by reacting **2** with KC_8, the resulting dinitrogen complex $[K_2\{[U(OSi(O^tBu)_3)_3]_2(\mu\text{-}O)(\mu\text{-}N_2)\}]$, **4,** is isolated in 70% yield, indicating that the yield in complex **3** is at least of 70%. The use of lower amounts of KC_8 or of higher reaction temperatures (–40 °C) in the synthesis of **3** results in the presence of larger amounts of unidentified by-products and to significantly lower yields. Complex **3** is not stable at room temperature in THF solution. Decomposition starts immediately after dissolution and is complete after 12 hours.

Reactivity of $[Cs_2\{[U(OSi(O^tBu)_3)_3]_2(\mu\text{-}O)\}]$, 3.Cs with N_2

A cold solution (–40 °C) of $[\{U(OSi(OtBu)_3)_3\}_2(\mu\text{-}O)]$, **2** (36.5 mg, 0.0176 mmol, 1 eq) in THF (1.5 mL) was added to cold (–40 °C) Cs (11.7 mg, 0.088 mmol, 5 eq). The reaction mixture was left stirring at –40 °C for 1h. After this time, the reaction mixture turned dark red and ^{1}H NMR monitoring of the reaction showed that the reaction was complete. The reaction mixture was filtered and the flask was transferred to a Schlenk line and was degassed by freeze-pump-thawing three times. N_2 (1 atm) was added to the solution at room temperature. The reaction mixture was monitored by ^{1}H NMR spectroscopy. No reaction with N_2 was observed.

Synthesis of complex $[K_2\{[U(OSi(O^tBu)_3)_3]_2(\mu\text{-}O)(\mu\text{-}N_2)\}]$, 4

A dark red solution of complex $[K_2\{[U(OSi(O^tBu)_3)_3]_2(\mu\text{-}O)\}]$, **3** (31.7 mg, 0.015 mmol) in toluene (0.5 mL) was prepared in a Schlenk tube in the glove box under argon. The tube was transferred to the Schlenk line and was degassed by freeze-pump-thawing three times. N_2 (1 atm) was added to the solution at room temperature. The solution turned immediately dark brown. ^{1}H NMR shows immediate complete conversion to complex **4**. The toluene solution was left standing at –40 °C for 24 h yielding to X-ray suitable crystals of complex $[K_2\{[U(OSi(O^tBu)_3)_3]_2(\mu\text{-}O)(\mu\text{-}N_2)\}]$, **4** (22 mg, 69% yield). The ^{15}N labeled complex **^{15}N-4** was prepared with the same procedure from $^{15}N_2$. ^{1}H NMR of **4** (400 MHz, tol-d_8, 298 K): δ(ppm) = –1.88 (s, CH_3 terminal siloxide). Anal. Calcd for **4**(toluene)$_2$ $C_{72}H_{162}N_2O_{25}K_2Si_6U_2(C_7H_8)_2$: C, 43.71; H, 7.59; N, 1.19. Found: C, 43.62; H, 7.45; N, 1.10. Magnetic moment at room temperature 1.752 μ_B.

Reaction of $[K_2\{[U(OSi(O^tBu)_3)_3]_2(\mu\text{-}O)(\mu\text{-}N_2)\}]$, 4 with acids

Addition of one equivalent of 2,4,6-tri-*tert*-butylphenol to 4. When one equivalent of 2,4,6-tri-*tert*-butylphenol was added to a solution of **4** in THF-d_8 the ^{1}H NMR spectrum showed formation of $KOSi(O^tBu)_3$ and other unidentified species.

Addition of excess HCl(Et_2O) to 4. Excess HCl(Et_2O) (34 mL of a 2M solution, 30 equivalents) was added to a toluene solution of complex **4** (5 mg). The mixture turned immediately colorless, along with the formation of a pale green precipitate. All volatiles were removed under vacuum and DMSO-d_6 was added for ammonia detection (dimethylsulfone added as internal standard). No ammonia formation was detected.

Addition of KC_8 and $HBAr^F$ to 4. When 10 equivalents of KC_8 were added at –80 °C to a solution of complex **4** in Et_2O and subsequently 30 equivalents of $HBAr^F$ in Et_2O were added, neither ammonium chloride or hydrazine were detected by ^{1}H NMR or UV spectroscopy, respectively.

Nitrogen detection after addition of excess HCl to complex 4.

A reaction tube was charged with a toluene (1mL) solution of $[K_2\{[U(OSi(O^tBu)_3)_3]_2(\mu\text{-}O)(\mu\text{-}N_2)\}]$ (10.6 mg) and it was closed with a silicon septum and secured with a metallic clip. 30 equivalents of 2M HCl in Et_2O were added via syringe through the septum. The headspace was injected into a GC-MS.

The measurement confirmed the formation of N_2. The same experiment was performed with **^{15}N-4** to confirm the formation of $^{15}N_2$.

Reaction of complex [K_2{[U(OSi(O^{t}Bu)$_3$)$_3$]$_2$(μ-O)(μ-N_2)}], 4 with CO: synthesis of [K_2{[U(OSi(O^{t}Bu)$_3$)$_3$]$_2$(μ-O)$_2$(μ-NCN)}], 5

A dark brown solution of complex **4** (81.0 mg, 0.037 mmol) in toluene (1 mL) prepared in a glove box under argon was transferred to a Schlenk line, was degassed by freeze-pump-thawing and 3 equivalents of CO were added. The color of the solution turned immediately purple. The solution was concentrated to 0.2 mL and left standing at –40 °C for 24 h, affording XRD suitable crystals of complex [K_2{[U(OSi(O^{t}Bu)$_3$)$_3$]$_2$(μ-O)$_2$(μ-NCN)}]**, 5** (55.4 mg, 67.8 % yield). ^{1}H NMR of **5** (400 MHz, tol-d_8, 298 K): δ(ppm) = 1.15 (s, CH_3 terminal siloxide), 1.32 (s, CH_3 terminal siloxide). The ^{13}C labelled analogue ^{13}C-**5** was prepared with the same procedure using ^{13}CO. ^{13}C NMR of ^{13}C-**5** (400 MHz, tol-d_8, 298 K): δ(ppm) = 261.63 (N^{13}CN), 73.16 (**C**(CH$_3$)$_3$), 32.06 (C(**C**H$_3$)$_3$). IR of **5**: 2008 cm^{-1}; IR of ^{13}C-**5**: 1942 cm^{-1}. Anal. Calcd for **5** $C_{73}H_{162}N_2O_{26}K_2Si_6U_2$: C, 39.73; H, 7.40; N, 1.27; Found: C, 40.12; H, 7.49; N, 1.02. The reaction of **4** with CO to afford **5** is immediate. The addition of larger amounts of CO (10-100 equivalents) to complex **5** slowly (the reaction time depends on the CO amount) affords new products as shown by ^{1}H NMR.

Reactivity of complex [K_2{[U(OSi(O^{t}Bu)$_3$)$_3$]$_2$(μ-O)$_2$(μ-NCN)}], 5 with excess of CO

A dark violet solution of complex [K_2{[U(OSi(O^{t}Bu)$_3$)$_3$]$_2$(μ-O)$_2$(μ-NCN)}], **5** (3.6 mg, 1 eq) in tol-d_8 (0.5 mL) was degassed by freeze-pump-thawing three times. ^{13}CO (18 eq) was added. After 3 days, the color of the reaction mixture turned yellow. The solution was concentrated to 0.1 mL and left standing overnight at –40 °C to obtain XRD suitable crystals. In an equivalent experiment, the conversion rate was calculated by quantitative ^{1}H NMR spectroscopy after adding 11.8 mg (57.5 eq) of naphtalene as a standard. The complex [K_2{[U(OSi(O^{t}Bu)$_3$)$_3$]$_2$(μ-O)$_2$}], **6** was formed with a conversion of 85%. The ^{13}C spectrum shows an additional product that could not be identified.

Independent synthesis of $[K_2\{[U(OSi(O^tBu)_3)_3]_2(\mu\text{-}O)_2\}]$, 6

Excess KC_8 (27.5 mg, 0.203 mmol, 5 eq) was added to a cold solution (–80 °C) of $[\{U(OSi(OtBu)_3)_3\}_2(\mu\text{-}O)]$, **2** (84.2 mg, 0.041 mmol, 1 eq) in THF (3 mL). The suspension was stirred at –80 °C for 15 minutes. The reaction mixture was then filtered on cooled glassware in order to remove graphite and unreacted KC_8. The solid was washed with cold THF. The resulting dark red solution was concentrated to 3 mL and connected to a Schlenk line. The solution was degassed by freeze-pump-thawing and 1 equivalent of N_2O was added. The color turned immediately green. The solution was then brought to dryness and the resulting solid was dissolved in 1.5 mL of toluene. The solution was left standing at –40 °C overnight affording the formation of $[K_2\{[U(OSi(O^tBu)_3)_3]_2(\mu\text{-}O)_2\}]$ as a green crystalline solid (51.1 mg, 58% yield). ^{1}H NMR of **6** (400 MHz, tol-d_8, 298 K): δ(ppm) = –1.38 (s, CH_3 terminal siloxide)**.** Anal. Calcd for **6**(toluene)$_{1.7}$ $C_{72}H_{162}O_{26}K_2Si_6U_2(C_7H_8)_{1.7}$: C, 43.37; H, 7.62; N, 0.00. Found: C, 43.13; H, 8.04; N, 0.00.

Reaction of complex $[K_2\{[U(OSi(O^tBu)_3)_3]_2(\mu\text{-}O)(\mu\text{-}N_2)\}]$, 4 with H_2 (1 atm)

A brown solution of complex **4** in toluene (42.0 mg, 0.006 mmol) was degassed by freeze-pump-thawing and 1 atm of H_2 was added. The reaction was followed by ^{1}H NMR, which showed consumption of the starting material and concomitant appearance of a new species showing a signal assigned to the siloxide protons at –1.42 ppm and a signal corresponding to two protons at 11.96 ppm, within 24 h. When the mixture was heated at 60 °C, the reaction was complete after 1 h affording the same signals in the ^{1}H NMR spectrum. When the solution resulting from the reaction at high temperature was concentrated to half the volume and left standing at –40 °C for 24 h a yellow solid was recovered (28.9 mg, 69% yield). The conversion rate of the reaction, calculated by ^{1}H NMR with naphthalene as internal standard, is quantitative on the base of the siloxide protons. The peak integrating for two protons at 11.96 ppm is absent from the spectrum of the complex **4** reacted with D_2. The addition of H_2 to **^{15}N-4** results in the same proton NMR spectrum as that obtained from the reaction of **4** with H_2. No signal was observed in the ^{15}N NMR spectrum.

^{1}H NMR (400 MHz, tol-d_8, 298 K): δ(ppm) = –1.42 (s, 162H, CH_3 of terminal siloxide ligands), 12.0 (broad s, 1.99H). ^{13}C NMR of crude reaction mixture (400 MHz, tol-d_8, 298 K): δ(ppm) = 25.75 (q, C(**C**H_3)$_3$), 71.1 (s, **C**(CH_3)$_3$). The same ^{1}H

NMR spectrum is observed when complex **3** is reacted with H_2. The elemental analysis of the complex isolated from the reaction of **4** in the presence of 1 atm H_2 does not show the presence of nitrogen (reproduced twice). The elemental analysis and the presence of a signal assigned to two hydride protons in the ^{1}H NMR spectrum are in agreement with the presence of the U(IV) bis-hydride complex $[K_2\{[U(OSi(O^tBu)_3)_3]_2(\mu\text{-}O)\ (H)_2\}]$, **7**. GC-MS analysis of the headspace after reaction of **4** and **^{15}N-4** with H_2 show the presence of N_2 or $^{15}N_2$ respectively. Anal. Calcd for **7**(toluene)$_2$ $C_{72}H_{164}O_{25}K_2Si_6U_2(C_7H_8)_2$: C, 44.20; H, 7.76; N, 0.00. Found: C, 44.43; H, 7.71; N, 0.00. Anal. Calcd for **7** $C_{72}H_{164}O_{25}K_2Si_6U_2$: C, 40.17; H, 7.68; N, 0.00. Found: C, 40.09; H, 7.83; N, 0.00. The same compound can also be isolated in 68% yield upon addition of 1 atm H_2 to a solution of **3** in toluene, by letting stand the reaction mixture at –40 °C for 24 hours. Anal. Calcd for 7(toluene)$_{1.5}$ (as isolated from the reaction of **3** with H_2) $C_{72}H_{164}O_{25}K_2Si_6U_2(C_7H_8)_{1.5}$: C, 43.25; H, 7.74; N, 0.00. Found: C, 43.08; H, 7.86; N, 0.00. The magnetic data measured for **7** (Appendix 6, Figure 55-56) are in agreement with the presence of a U(IV) complex. Upon addition of one equivalent of 2,4,6-tri-*tert*-butylphenol to this compound no reaction was observed. When the reaction of **4** with H_2 is carried out at room temperature and in the presence of less that 1 atm of H_2 the ^{1}H NMR spectrum of the resulting final reaction product appears the same as for the reaction performed at 1 atm at room temperature or at 60 °C but the elemental analysis shows the presence of variable amounts of dinitrogen content. These data suggest that in these conditions hydrogenation of the coordinated dinitrogen may occur, but in a non-reproducible fashion.

Addition of excess HCl(Et_2O) after reaction of 4 with H_2.

After reaction of **4** with H_2, the NMR tube was connected with an adaptor to a Schlenk tube containing 2 mL of HCl(Et_2O) (2M). The acid solution was degassed by freeze-pump-thawing. All the volatiles were collected into the HCl(Et_2O) solution. HCl(Et_2O) was removed under vacuum, but no formation of solid was observed. A large excess (>100 eq) of HCl(Et_2O) was added at room temperature to the solid residue left in the NMR tube. The solution turned immediately light green and a light green/white precipitate was formed. After 10 minutes, the acid solution was removed under vacuum and the residual solid was dissolved in DMSO-d_6 (1 equivalent of dimethylsulfone was added as internal standard) for the quantitative ammonium

chloride detection. The ^{1}H NMR showed no signal for ammonium chloride or hydrazinium chloride and showed a peak at 3.3 ppm, assigned to water (probably arising from the protonation of the oxo group), and free ligand.

Reaction of 4 with 5 atm H_2

The reaction of **4** with 5 atm H_2 leads to complete disappearance of the ^{1}H signals of complex **4** in the ^{1}H NMR spectrum. Only one peak of $HOSi(O^tBu)_3$ could be assigned in the ^{1}H NMR spectrum after reaction. The volatiles were collected into $HCl(Et_2O)$ (2M) while addition of an excess HCl (Et_2O) (2M) was added to the solid residue of the resulting reaction mixtures. Both reactions did not lead to the detection of ammonium chloride or hydrazinium salts.

Bibliography

[1] a) R. J. Burford, M. D. Fryzuk, *Nature Reviews Chemistry* **2017**, *1*; b) M. P. Shaver, M. D. Fryzuk, *Adv. Synth. Catal.* **2003**, *345*, 1061-1076.

[2] a) J. A. Pool, E. Lobkovsky, P. J. Chirik, *Nature* **2004**, *427*, 527-530; b) M. D. Fryzuk, J. B. Love, S. J. Rettig, V. G. Young, *Science* **1997**, *275*, 1445-1447; c) B. L. Wang, G. Luo, M. Nishiura, S. W. Hu, T. Shima, Y. Luo, Z. M. Hou, *J. Am. Chem. Soc.* **2017**, *139*, 1818-1821.

[3] A. J. Keane, W. S. Farrell, B. L. Yonke, P. Y. Zavalij, L. R. Sita, *Angew. Chem. Int. Ed. Engl.* **2015**, *54*, 10220-10224.

[4] D. J. Knobloch, E. Lobkovsky, P. J. Chirik, *Nat. Chem.* **2010**, *2*, 30-35.

[5] M. Falcone, L. Chatelain, R. Scopelliti, I. Zivkovic, M. Mazzanti, *Nature* **2017**, *547*, 332-+.

[6] W. J. Evans, S. A. Kozimor, J. W. Ziller, *Polyhedron* **2004**, *23*, 2689-2694.

[7] C. P. Larch, F. G. N. Cloke, P. B. Hitchcock, *Chem. Commun.* **2008**, 82-84.

[8] I. Castro-Rodriguez, K. Olsen, P. Gantzel, K. Meyer, *Chem. Commun.* **2002**, 2764-2765.

[9] J. X. Wang, Y. Gurevich, M. Botoshansky, M. S. Eisen, *J. Am. Chem. Soc.* **2006**, *128*, 9350-9351.

[10] a) O. P. Lam, S. C. Bart, H. Kameo, F. W. Heinemann, K. Meyer, *Chem. Commun.* **2010**, *46*, 3137-3139; b) L. Castro, O. P. Lam, S. C. Bart, K. Meyer, L. Maron, *Organometallics* **2010**, *29*, 5504-5510; c) S. Fortier, J. L. Brown, N. Kaltsoyannis, G. Wu, T. W. Hayton, *Inorg. Chem.* **2012**, *51*, 1625-1633; d) J. C. Berthet, J. F. Lemarechal, M. Nierlich, M. Lance, J. Vigner, M. Ephritikhine, *J. Organomet. Chem.* **1991**, *408*, 335-341; e) A. C. Schmidt, A. V. Nizovtsev, A. Scheurer, F. W. Heinemann, K. Meyer, *Chem. Commun.* **2012**, *48*, 8634-8636; f) A. S. P. Frey, F. G. N. Cloke, M. P. Coles, P. B. Hitchcock, *Chem. Eur. J.* **2010**, *16*, 9446-9448; g) L. R. Avens, D. M.

Barnhart, C. J. Burns, S. D. McKee, W. H. Smith, *Inorg. Chem.* **1994**, *33*, 4245-4254.

[11] a) M. Falcone, C. E. Kefalidis, R. Scopelliti, L. Maron, M. Mazzanti, *Angew Chem Int Edit* **2016**, *55*, 12290-12294; b) M. Falcone, L. Chatelain, M. Mazzanti, *Angew. Chem. Int. Ed. Engl.* **2016**, *55*, 4074-4078.

[12] V. Mougel, C. Camp, J. Pecaut, C. Coperet, L. Maron, C. E. Kefalidis, M. Mazzanti, *Angew. Chem. Int. Ed. Engl.* **2012**, *51*, 12280-12284.

[13] a) A. G. Tskhovrebov, B. Vuichoud, E. Solari, R. Scopelliti, K. Severin, *J. Am. Chem. Soc.* **2013**, *135*, 9486-9492; b) A. G. Tskhovrebov, E. Solari, M. D. Wodrich, R. Scopelliti, K. Severin, *Angew. Chem. Int. Ed. Engl.* **2012**, *51*, 232-234.

[14] T. D. Palluccio, E. V. Rybak-Akimova, S. Majumdar, X. C. Cai, M. G. Chui, M. Temprado, J. S. Silvia, A. F. Cozzolino, D. Tofan, A. Velian, C. C. Cummins, B. Captain, C. D. Hoff, *J. Am. Chem. Soc.* **2013**, *135*, 11357-11372.

[15] H. S. La Pierre, K. Meyer, in *Prog. Inorg. Chem., Vol. 58* (Ed.: K. D. Karlin), **2014**, pp. 303-415.

[16] a) M. D. Fryzuk, T. S. Haddad, S. J. Rettig, *J. Am. Chem. Soc.* **1990**, *112*, 8185-8186; b) Y. Ohki, M. D. Fryzuk, *Angew. Chem. Int. Ed. Engl.* **2007**, *46*, 3180-3183.

[17] a) M. H. V. Huynh, P. S. White, C. A. Carter, T. J. Meyer, *Angew. Chem. Int. Ed. Engl.* **2001**, *40*, 3037-3039; b) Y. Tanabe, S. Kuwata, Y. Ishii, *J. Am. Chem. Soc.* **2002**, *124*, 6528-6529; c) D. J. Mindiola, Y. C. Tsai, R. Hara, Q. H. Chen, K. Meyer, C. C. Cummins, *Chem. Commun.* **2001**, 125-126.

[18] H. Kajitani, Y. Tanabe, S. Kuwata, M. Iwasaki, Y. Ishii, *Organometallics* **2005**, *24*, 2251-2254.

[19] a) A.-C. Schmidt, F. W. Heinemann, W. W. Lukens, Jr., K. Meyer, *J. Am. Chem. Soc.* **2014**, *136*, 11980-11993; b) J. G. Reynolds, A. Zalkin, D. H. Templeton, N. M. Edelstein, *Inorg. Chem.* **1977**, *16*, 1090-1096.

[20] D. R. Kindra, W. J. Evans, *Chem. Rev.* **2014**, *114*, 8865-8882.

[21] J. A. Pool, W. H. Bernskoetter, P. J. Chirik, *J. Am. Chem. Soc.* **2004**, *126*, 14326-14327.

[22] A. G. Tskhovrebov, E. Solari, M. D. Wodrich, R. Scopelliti, K. Severin, *J. Am. Chem. Soc.* **2012**, *134*, 1471-1473.

CHAPTER 8

CO_2 and CO/H_2 conversion to methoxide by a uranium(IV) hydride

Introduction[1]

The search for more sustainable and selective catalysts for the production of oxygenates from CO or CO_2 hydrogenation continues to drive interest in the homogeneous reduction of CO and CO_2 by molecular hydride complexes.[1] Most studies have focused on d block transition metals, but f block hydrides, because of their different reactivity, may open up new routes for the transformation and reduction of CO and CO_2 to valuable products.[1f, 1j] The reduction of CO_2 to methanol by molecular hydride complexes was previously reported for early transition metals[1f] in high oxidation state but never for f elements. In particular, the two examples of CO_2 functionalization by uranium hydrides reported so far have both resulted in formate formation.[2] The reaction of early d block[1c] and 4f block[1j, 3] metal hydrides with CO has also received less attention than for mid- late-transition metals. However, early d block and f metal hydrides provide pertinent mechanistic and functional models of the surface mediated hydride transfer to CO in the heterogeneously catalysed Fischer-Tropsch process used on the industrial scale for the conversion of a CO/H_2 mixture to higher hydrocarbons and oxygenate products.[1c, 4] CO addition to mononuclear (Sm,[3a] Ce[3b]) and polynuclear hydrides (Yb[3c], Lu[3e]) of the 4f block led to the isolation of ethenediolate, etheneolate, propeneolate or oxomethylene ($[OCH_2]^{2-}$) complexes. Further reactivity of such complexes with H_2 was only reported for the dinuclear cerium product $[\{(1,2,4\text{-}(Me_3C)_3C_5H_2)_2Ce\}_2(\eta^2\text{-}OCH_2)]$ that reacts with H_2 to yield cerium methoxide and cerium hydride complexes.[3b] Conversion of CO to methoxide was also reported for a mononuclear thorium(IV) hydride complex in the presence of H_2 (6 atm) but the products were not crystallographically characterized.[5]

[1] Portions of this chapter are published: M. Falcone, R. Scopelliti, M. Mazzanti, *Journal of the American Chemical Society,* **2019**, DOI:10.1021/jacs.9b02235
Author contributions: M.F. carried out the synthetic experiments and analysed the experimental data. R.S. performed the X-ray measurements. M.F. and M.M originated the idea and wrote the manuscript.

Spectroscopic evidence of the formation of Th-formyl and Th-oxomethylene intermediates was reported but these intermediates were not isolated.[6] [5] In contrast, the only reported example of CO/H_2 conversion to methoxide mediated by a uranium(III) complex reported by Cloke and coworkers was not found to involve an hydride or formyl intermediate, and a mechanism involving hydrogenation of a C_2O_2 intermediate was suggested.[7] Notably, several U(III) complexes were found to promote the reductive coupling of CO to yield enediolate, deltate, or squarate products.[8] Surprisingly, the functionalization of CO or CO_2 by uranium hydrides remains poorly studied probably due to the scarce number of uranium hydrides reported so far. In spite of the tremendous advances made in the field of organo-actinide chemistry in the past three decades,[9] since the seminal work from the early 1980s [10] only a few additional examples of uranium hydrides have been reported.[2, 9g, 10c, 11] In this chapter the synthesis of a stable dinuclear diuranium(IV) bis-hydride is presented. The addition of H_2 to the U(III)–O–U(III) core of the previously reported [12] complex $[K_2\{[U(OSi(O^tBu)_3)_3]_2(\mu\text{-}O)\}]$, **1** affords, $[K_2\{[U(OSi(O^tBu)_3)_3]_2(\mu\text{-}O)(\mu\text{-}H)_2\}]$, **2**, that is stable with respect to H_2 loss. The bis-hydride complex **2** effects the reduction of CO in ambient conditions to the oxomethylene dianion that reacts further with hydrogen to afford a methoxide hydride complex. Moreover, we show that complex **2** acts as a powerful hydride donor that can reduce CO_2 beyond formate to afford methanol.

Results and discussion

When a cold solution (–80 °C) of $[K_2\{[U(OSi(O^tBu)_3)_3]_2(\mu\text{-}O)\}]$, **1** in toluene is exposed to 1 atm of H_2 the reaction mixture changes colour from dark red to yellow within 15 minutes. The proton NMR spectrum shows the disappearance of the signals of **1** and the appearance of a new species assigned as the bis-hydride-bridging diuranium(IV) complex $[K_2\{[U(OSi(O^tBu)_3)_3]_2(\mu\text{-}O)(\mu\text{-}H)_2\}]$, **2** (Scheme 1). The solid-state structure of compound **2**, determined by X-ray crystallography (Figure 1) shows two six-coordinate U(IV) ions, bridged by an oxo ligand (O^{2-}) which is disordered over three positions, with an overall occupancy of one oxygen, with angles U1–O121–U2, U1–O122–U2 and U1–O123–U2 of 105.7(3)°, 104.2(6)° and 103.4(8)°, respectively, and average U–O distance of 2.154(24) Å. The rest of the

electron density found in the core, is attributed to the presence of two bridging hydrides, disordered over the same three positions.

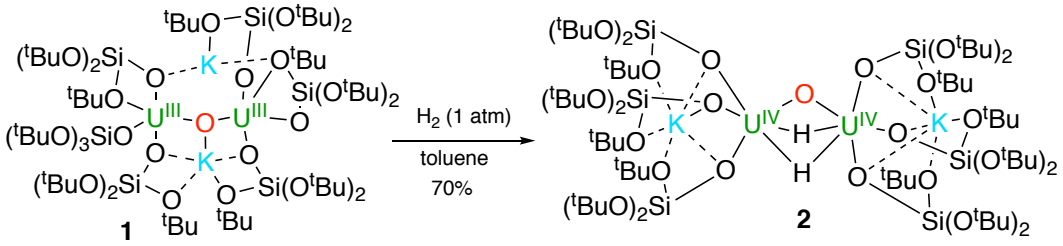

Scheme 1. Synthesis of the bis-hydride diuranium(IV) complex **2**. Only the -O^{t}Bu groups bound to the metals are shown.

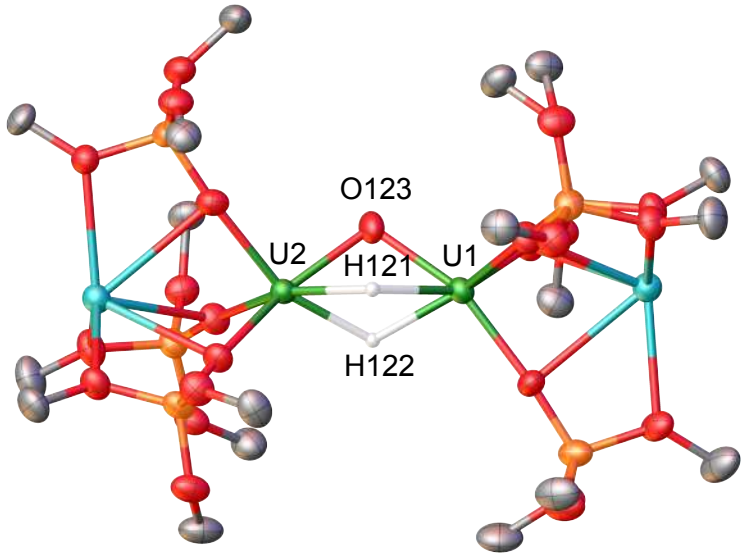

Figure 1. Solid-state molecular structure of $[K_2\{[U(OSi(O^tBu)_3)_3]_2(\mu\text{-}O)(\mu\text{-}H)_2\}]$, **2.** Thermal ellipsoids set at 50% probability. Hydrogen atoms and methyl groups were omitted for clarity. Selected bond lengths [Å]: O123–U1 2.141(19), U1–H122 2.012(15), U1–H121 2.010(15), U2–O123 2.198(19), U2–H122 2.011(15), U2–H121 2.009(15).

The ^{1}H NMR spectrum of **2** shows a signal at 12 ppm integrating for two protons that is absent in the spectrum of the deuterated analogue of **2** (**D-2**), and was assigned to the two bridging hydride ligands. Thus, the highly reactive U(III)–O–U(III) complex **1**, cleaves molecular hydrogen in ambient conditions acting as a two-electron reducing agent to yield two U(IV) ions and two bridging hydrides. The uranium(IV) bis-hydride **2** shows a remarkable stability with respect to H_2 elimination both in solution and solid state. This contrasts with the tendency of the $[(C_5Me_5)_2U(H)(\mu\text{-}H)]_2$ complex [10c] to readily lose H_2 at room temperature in solution and incited us to investigate the reactivity of **2** towards electrophilic small molecules. We found that **2**

reacts readily with two equivalents of MeCN in toluene solution, to yield $[K_2\{[U(OSi(O^tBu)_3)_3]_2(\mu\text{-}O)(\mu\text{-}\kappa^2\text{-}NC(CH_3)NCH_2CH_3)\}]$, **3** (Scheme 2), where two U(IV) centers are bridged by a dianionic ligand produced from the reductive coupling of two acetonitrile molecules. The reaction is likely to proceed at first with the attack of the acetonitrile triple bond by the two hydride ligands to afford a metal imido species (M-NCH_2CH_3) that rapidly reacts with a second acetonitrile molecule to afford the dianionic bidentate fragment -$NC(CH_3)NCH_2CH_3$.

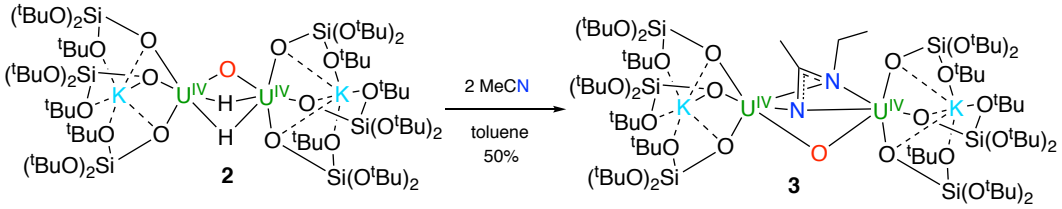

Scheme 2. Reactivity of complex **2** with acetonitrile, to give complex **3**. Only the -O^{t}Bu groups bound to the metals are shown.

The solid-state structure of compound **3**, determined by X-ray crystallography (Figure 2) shows two six-coordinate U(IV) ions, bridged by an oxo ligand (U1–O121 2.124(11) Å, U2–O121 2.106(11) Å) and by the two nitrogen atoms of the dianionic ligand. The –$NC(CH_3)N$ fragment lies in a plane perpendicular to the U1–U2 axis. The two equal N–C distances (N121–C121 1.34(2) Å, N122–C121 1.33(2) Å) and the geometry of C121 imply an sp^2 hybridization of the carbon and the delocalization of the double bound between the three atoms N121–C121–N122.

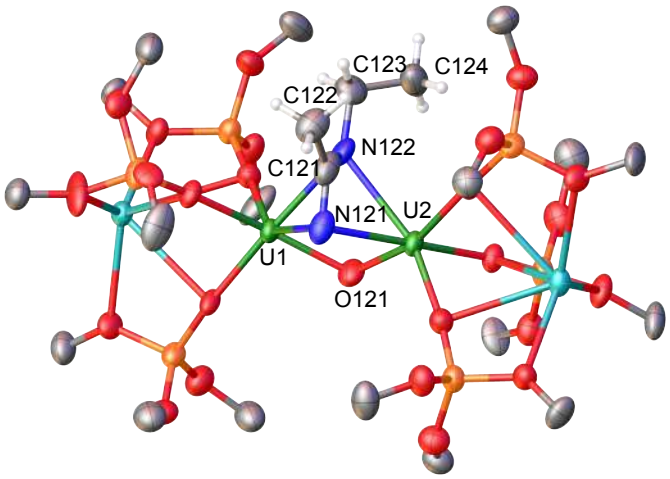

Figure 2. Solid-state molecular structure of $[K_2\{[U(OSi(O^tBu)_3)_3]_2(\mu\text{-}O)(\mu\text{-}\kappa^2\text{-}NC(CH_3)NCH_2CH_3)\}]$, **3.** Thermal ellipsoids set at 50% probability. Hydrogen atoms and methyl groups were omitted for clarity. Selected bond

lengths [Å]: U1-O121 2.124(11), U1-N121 2.360(12), U1-N122 2.650(13), U2-O121 2.106(11), U2-N121 2.458(13), U2-N122 2.555(13).

Further confirmations of the nature of the bridging dianionic ligand were given by ^{1}H NMR spectroscopy. The ^{1}H NMR spectrum confirmed the presence of a CH_2CH_3 fragment and when acetonitrile was reacted with the deuterated analogue **D-2**, the ^{1}H NMR resonances assigned to the CH_2 group were not observed, demostrating that the two hydrides are transferred to the nitrile carbon. Moreover, the HMQC experiment (Figure 3a) showed three correlation peaks (peak 1 attributed to an impurity which is formed with time): peak 2 shows correlation between the peak at 73.25 ppm (carbon) and the peak at –72.8 ppm (proton) which integrates for 3 protons (CH_3); peak 3 shows correlation between the peak at 22.7 ppm (carbon) and –51.5 ppm (proton) which integrates for 3 protons (CH_3); peak 4 shows correlation between the peak at 32.5 ppm (carbon) and –85.3 ppm (proton) which integrates for 2 protons (CH_2). Correlation is found between the peaks at 72.8 and –85.3 ppm (Figure 3b) showing that these two signals belong to vicinal protons, in agreement with a CH_2CH_3 group.

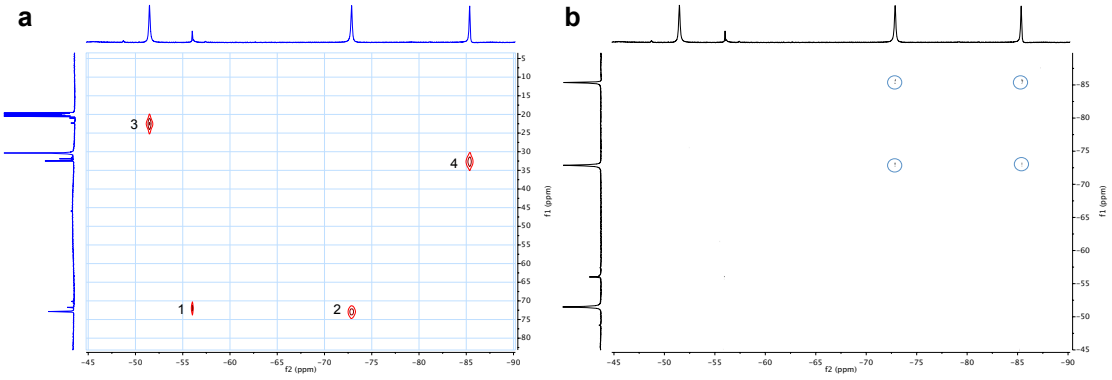

Figure 3. HMQC (600 MHz, tol-d_8, 298K) of crytals of **3** (**a**); COSY (600 MHz, tol-d_8, 298K) of crystals of **3** (**b**).

Previously, reductive coupling of acetonitrile by the U(III) hydride $[\{(C_5Me_5)_2UH\}_2]$ was reported to yield a diaminocyanopentadienyl dianion and H_2 but none of the hydrogen atoms in the $(C_6N_3H_7)^{2-}$ dianion were found to arise from the U-bound hydrides.[13] The facile reduction of acetonitrile by complex **2** incited us to explore its reactivity with CO and CO_2 and the possibility of converting them into methoxide.

Upon addition of 1 equivalent of CO to a toluene solution of complex **2**, an immediate reaction occurs and the ^{1}H spectrum indicates full conversion of the diuranium(IV)

bis-hydride complex into a new species, identified as complex $[K_2\{[U(OSi(O^tBu)_3)_3]_2(\mu\text{-}CH_2O)(\mu\text{-}O)\}]$, **4** (Scheme 3 a)). The ^1H NMR spectrum of **4** shows a signal at −130 ppm, which integrates for 2 protons and splits into a doublet in the ^1H NMR spectrum of the ^{13}C labeled analogue **^{13}C-4** (see Appendix 7), in agreement with the formation of the CH_2O fragment from ^{13}CO addition to **2**. The molecular structure of complex **4** (Figure 4a) shows two six-coordinate U(IV) atoms bridged by an oxo ligand and an oxomethylene dianion, in a side-on $\mu\text{-}\kappa^2(O):\kappa^2(C)$ coordination mode, perpendicular to the U1–U2 axis. The two ligands are disordered over two positions in the core of the molecule with an overall occupancy of 1 for each atom. The C53–O45 bond distance of 1.31(3) Å, is comparable to those found in the complexes $[(1,2,4\text{-}(Me_3C)_3C_5H_2)_2Ce](\mu\text{-}OCH_2)$ (1.39(1) Å) [3b] and $[Zr(\eta^8\text{-}C_8H_8(OAr)]_2(\mu\text{-}CH_2O)$, (1.313(14) Å),[14] consistent with the presence of a C–O single bond and a sp^3 carbon atom. The presence of an hypervalent carbon is probably an artefact due to the superposition of two symmetry related enantiomers with a $\mu\text{-}\kappa^1:\kappa^1$ bound CH_2O. A similar artifact was found in the $[(1,2,4\text{-}(Me_3C)_3C_5H_2)_2Ce](\mu\text{-}OCH_2)$ complex.[3b]

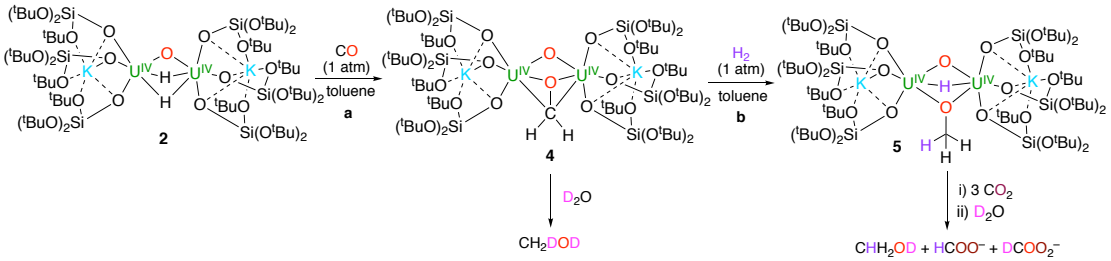

Scheme 3. Reduction of carbon monoxide to oxomethylene(2–) (**a**) and subsequent reaction with hydrogen to give the methoxide complex, **5** (**b**).

The CO triple bond undergoes a four-electron reduction by the two hydrides in **2** to yield two new C-H bonds. The oxomethylene ligand is likely to form via the insertion of CO into the U-H bond to afford a formyl intermediate that then adds a second hydride ligand. Overall, the diuranium(III) complex **1** mediates the stepwise conversion of H_2 and CO to yield a CH_2O^{2-} dianion which is readily transformed into methanol by addition of D_2O. The detection of a triplet at 50 ppm (^{13}C-deuterium coupling) in the ^{13}C NMR spectrum of **4** in D_2O reveals the presence of CH_2DOD. The formation of methanol was also confirmed by GC-MS. Addition of excess CO to

4 results in the slow complete conversion into a new species that was not further characterized.

Because of the anticipated nucleophilic character of the CH_2O^{2-} carbon, we also investigated the possibility of direct heterolytic cleavage of H_2 to afford methoxide. The addition of 1 atm H_2 to complex **4**, resulted in the clean formation of a new species, identified as the methoxide complex $[K_2\{[U(OSi(O^tBu)_3)_3]_2(\mu\text{-}OCH_3)(\mu\text{-}O)(\mu\text{-}H)\}]$, **5** (Scheme 3 b)). The proton NMR spectrum of **5** shows the presence of a peak at −104 ppm, which integrates for 3H and splits into a well-resolved doublet in the ^{1}H NMR spectrum when **^{13}C-4** is used. The proton-coupled ^{13}C NMR spectrum of **5** shows a quadruplet at −348 ppm, in agreement with the presence of the methoxide group (see Appendix 7). The singlet found in the spectrum at 41 ppm, which integrates for one proton, was assigned to a bridging hydride. When D_2 is added to **^{13}C-4** the hydride signal disappear and the doublet at −104 ppm integrates for two protons, in agreement with the formation of $[K_2\{[U(OSi(O^tBu)_3)_3]_2(\mu\text{-}OCH_2D)(\mu\text{-}O)(\mu\text{-}D)\}]$, **D-5**.

The molecular structure of **5** (Figure 4b) shows two six-coordinate U(IV) atoms bridged by an oxo ligand, an hydride (the oxo and the hydride are disordered over two positions with an occupancy of 1 for each atom) and a methoxide ligand that bridges the metal centers through the oxygen atom. The U–O_{oxo} distances of 2.204(18), 2.182(19) Å and the U–O–U angle 102.1(9)° are similar to those found in **4.**

The solution magnetic moment determined by the Evan's method for complexes **2**, **4** and **5,** is in agreement with the presence of U(IV) for all complexes, indicating that the oxidation state of the uranium remains unchanged during reactivity.

Finally, upon addition of 3 equivalents of CO_2 to complex **5**, the carbon NMR spectrum in D_2O showed the presence of formate, bicarbonate and methanol. The formation of formate confirms unambiguously the presence of the hydride ligand in **5**.

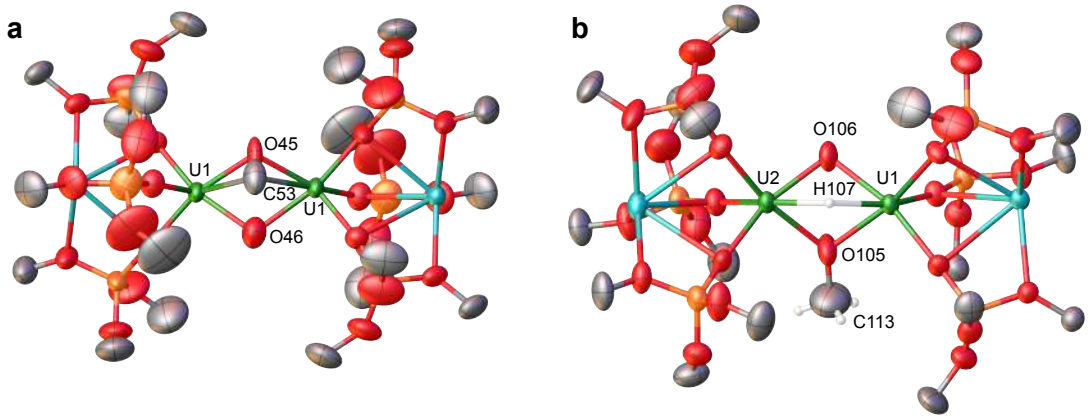

Figure 4. Solid-state molecular structure of **4** (**a**) and **5** (**b**). Thermal ellipsoids set at 50% probability. Hydrogen atoms and methyl groups were omitted for clarity. Selected bond lengths [Å] for **4**: U1–O46 2.115(13), U1–O45 2.198(10), U1–C53 2.617(18), C53–O45 1.31(3); for **5**: U1–O106 2.204(18), U1–O105 2.295(12), U2–O106 2.182(19), U2–O105 2.309(12), U1–H107 1.999(15), U2–H107 2.000(15), O105–C113 1.44(3).

The facile non-reversible heterolytic cleavage of dihydrogen by **4** is the result of cooperative H_2 activation by the two Lewis acid uranium centers and the nucleophilic oxomethylene ligand. Metal-ligand cooperative reactivity towards small molecules is rare in actinide chemistry[15] but we recently reported the cooperative H_2 cleavage by a bifunctional metal nitride.[2b]

These results prompted us to explore the reduction of CO_2 by complex **2**. Upon addition of 3 equivalents of CO_2 to **2** at room temperature, a mixture of products formed immediately. Crystals of complex $[K_2\{[U(OSi(O^tBu)_3)_3]_2(\mu\text{-}CO_3)(\mu\text{-}HCOO)_2\}]$, **6** were isolated and characterized by X-ray analysis. The solid-state structure of compound **6** (Figure 5) shows two seven-coordinate U(IV) ions, bridged by two formate ligands and a carbonate ligand, indicating that both the U–H and the U–O bonds undergo CO_2 insertion. The U–O bond distances for the formate ligands range between 2.338(11) and 2.403(12) Å and are similar to those found in the only other example of a formate- bridged diuranium(IV) complex (2.409(3) and 2.356(3) Å).[2b] Both hydrogens of the formate moieties were located in the Fourier difference map. The carbonate ligand bridges the two metal centers in a $\mu\text{–}\eta^2(O,O'):\eta^2(O'',O')$ mode with an average U–O bond distance for the carbonate ligand of 2.448(30) Å.

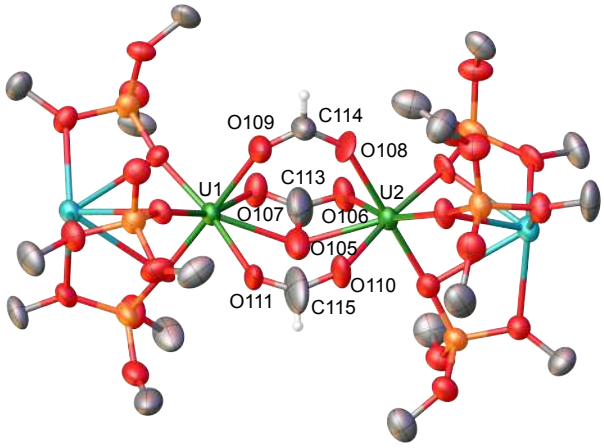

Figure 5. Solid-state molecular structure of **6.** Thermal ellipsoids set at 50% probability. Hydrogen atoms and methyl groups were omitted for clarity. Selected bond lengths [Å]: U1–O109 2.361(13), U1–O111 2.403(12), U1–O105 2.409(14), U1–O107 2.448(13), U1–C113 2.835(19), U2–O108 2.338(11), U2–O110 2.400(11), U2–O106 2.455(13), U2–O105 2.482(14).

Interestingly, the ^{13}C NMR spectrum in D_2O of the reaction mixture of **2** with CO_2 (3 equiv.) shows, in addition to formate and carbonate, the presence of CH_3OD which was confirmed by GC-MS analysis (see Appendix 7). This suggests that a methoxide complex is also formed in the reaction of **2** with CO_2. Indeed, when 0.5-1 equivalents of CO_2 were added to a solution of **2** (Scheme 4), the proton NMR spectrum shows the presence of unreacted **2** but also the presence of signals corresponding to complex $[K_2\{[U(OSi(O^tBu)_3)_3]_2(\mu\text{-}OCH_3)(\mu\text{-}O)(\mu\text{-}H)\}]$, **5** and to the previously reported diuranium(IV) bis-oxo complex $[K_2\{[U(OSi(O^tBu)_3)_3]_2(\mu\text{-}O)_2\}]$.[12]

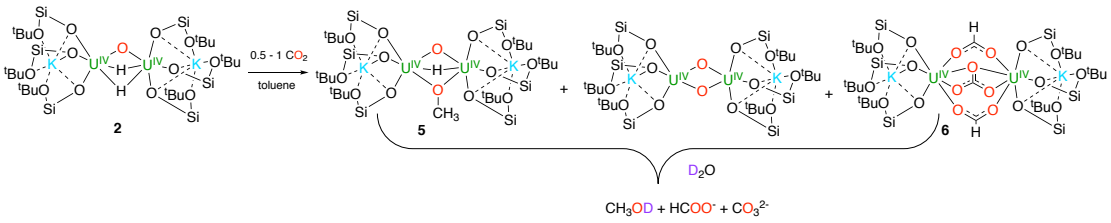

Scheme 4. Reduction of carbon dioxide by complex **2**, to give a mixture of compounds, **5**, **6** and bis-oxo. Only the –O^{t}Bu groups bound to a metal are shown.

The absence of ^{13}C–deuterium coupling for the ^{13}C NMR signal assigned to CH_3OD confirms that all the protons leading to methanol formation originate from the hydrides ligands in **2**. Stepwise formation of formate, methylene diolate and methoxide complexes has been proposed for the heterogeneously catalyzed hydrogenation of CO_2 in industrial processes. An analogous mechanism was proposed for the conversion of CO_2 to methoxide by the zirconocene hydrido complex

$Cp_2Zr(H)Cl$ (Schwartz's reagent) [16] with carbon dioxide on the basis of spectroscopic studies.[17]

A plausible mechanism for methoxide formation from the reaction of **2** with CO_2 involves the transfer of three hydrides from two molecules of **2** to a CO_2 molecule followed by oxide abstraction to afford **5** and the previously reported diuranium(IV) bis-oxo complex (Scheme 5).

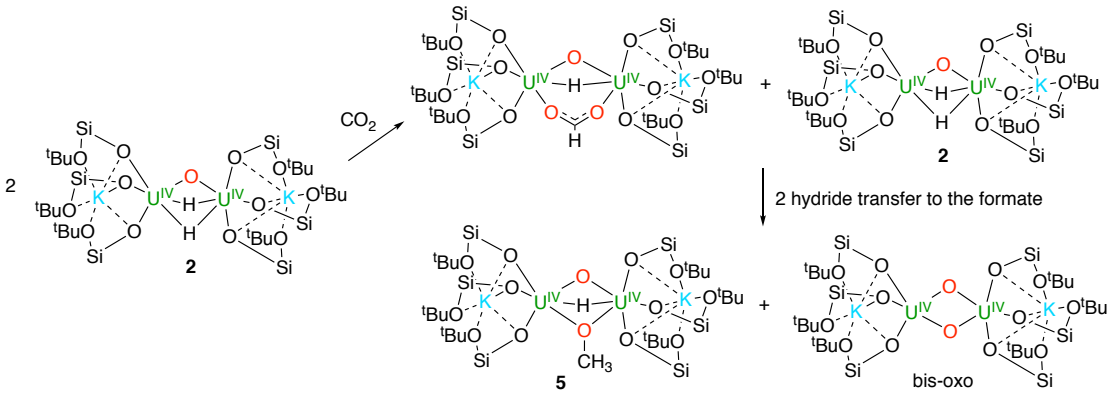

Scheme 5. Proposed mechanism for the formation of the CH_3O^- ligand from the reaction of **2** with CO_2. Only the -O^{t}Bu bound to a metal are shown.

After the insertion of a molecule of CO_2 into a U–H bond has occurred, the resulting formate undergoes the intermolecular reduction of the formate ligand by a second dihydride complex **2** to afford the methoxide complex **5.** No evidence of methylene diolate intermediates could be found. The formate reduction to methoxide is a competitive pathway compared to the insertion of CO_2 in the second U–H bond to yield **6**, even in the presence of excess CO_2. However, the amount of methoxide formed increases at lower CO_2 to **2** ratios and, only in these conditions, the identification of **5** and bis-oxo was possible. Notably, the quantitative evaluation by ^{13}C NMR spectroscopy of the reaction products after hydrolysis of the reaction mixture showed formate:methanol ratios of 1:1.75 for the 1:1 (**2**:CO_2) and of 1:0.25 for the 1:3 (**2**:CO_2) reaction.

The insertion of CO_2 into the uranium(IV)-hydride bond has some rare precedents[2, 18] and in two cases the resulting U(IV) formate was crystallographically characterized.[2] The insertion of CO_2 into the U(IV)–O bond to afford carbonate was also reported.[19] However, the reduction of CO_2 to methoxide by a uranium hydride complex has not yet been reported.

Conclusions

In conclusion we have shown that the scaffold provided by siloxide ligands and a bridging oxo enables the non-reversible addition of H_2 to the diuranium(III) complex **1** to afford a stable diuranium(IV) bis-hydride complex. The reactivity shown by this oxo- and hydride- bridged complex differs significantly from that of previously reported U(IV) bis-hydride complexes supported by cyclopentadienyl ligands, that are unstable with respect to hydrogen loss.[2a, 10c]i Notably the complex **2** does not undergo elimination of H_2 either spontaneously or promoted by substrates. In contrast the hydrides in the reported oxo- hydride- bridged complex show high reductive activity towards different substrates. The oxide bridge holds the uranium cations together during reactivity and facilitates the isolation of uranium-bound reduction products. Carbon monoxide reduction results in the isolation of a unique diuranium(IV) oxomethylene bridged complex that cleaves H_2 at room temperature, affording a methoxide as the unique product. The oxide-supported diuranium(IV) hydride also effects the reduction of carbon dioxide to afford methoxide which is unprecedented in f element chemistry. These results show that polynuclear oxide-supported hydrides are excellent candidates for the conversion of CO and CO_2 to methoxide, furthering the understanding of analogous transformation at metal oxide surfaces.

Experimental

General Methods. All manipulations were carried out under a dry and oxygen free argon atmosphere using Schlenk techniques and an MBraun glovebox equipped with a purifier unit. The water and oxygen levels were always kept at less than 0.1 ppm. Glassware was dried overnight at 140 °C before use. Compounds were characterized by elemental analysis, ^{1}H and ^{13}C NMR spectroscopies, IR spectroscopy and single-crystal X-ray diffraction. **^{1}H NMR experiments** were carried out using NMR tubes adapted with J. Young valves. ^{1}H and ^{13}C NMR spectra were recorded on Bruker 400 MHz and 600 MHz spectrometers. NMR chemical shifts are reported in ppm with solvent as internal reference. **Elemental analyses** were performed with a Thermo Scientific Flash 2000 Organic Elemental Analyzer. **IR analyses** were performed with a FT-IR Spectrometer Perkin-Elmer. The measurements were performed using nujol mulls between KBr plates. **Starting materials.** Unless otherwise noted, reagents were

purchased from commercial suppliers and used without further purification. Tris(*tert*-butoxy)silanol was purified by sublimation. Depleted uranium was purchased from IBILABS (USA). The solvents were purchased from Aldrich or Cortecnet (deuterated solvents) in their anhydrous form, conditioned under argon and vacuum distilled from K/benzophenone (toluene, toluene-d_8 (tol-d_8), tetrahydrofuran (THF), THF-d_8 and acetonitrile (MeCN)). DMSO-d_6 was degassed by three freeze-pump-thaw cycles and stored over activated 3 Å molecular sieves. The complexes $[\{U(OSi(O^tBu)_3)_3\}_2(\mu\text{-}O)]$, and $[K_2\{[U(OSi(O^tBu)_3)_3]_2(\mu\text{-}O)\}]$, **1** were prepared according to their published procedures.[12] Carbon monoxide (N47 Bt-S 10/200) was purchased from Carbagas. ^{13}CO (93.13% ^{13}C), $^{13}CO_2$ (93.13% ^{13}C) and D_2 (99.8% D) were purchased from Cortecnet and stored over activated 3 Å molecular sieves. **Caution:** Depleted uranium (primary isotope ^{238}U) is a weak α-emitter (4.197 MeV) with a half-life of 4.47×10^9 years. Manipulations and reactions should be carried out in monitored fume hoods or in an inert atmosphere glovebox in a radiation laboratory equipped with α- and β-counting equipment.

Synthesis of complex $[\{U(OSi(O^tBu)_3)_3\}_2(\mu\text{-}O)(\mu\text{-}H)_2]$, 2.

Excess KC_8 (32.0 mg, 0.240 mmol, 5 equiv.) was added to a cold solution (−80 °C) of $[\{U(OSi(OtBu)_3)_3\}_2(\mu\text{-}O)]$ (97.2 mg, 0.05 mmol, 1 equiv.) in THF (3 mL). The suspension was stirred at −80 °C for 15 minutes. The reaction mixture was then filtered on cooled glassware. All the volatiles were removed under vacuum at −80 °C and cold toluene (2 mL) added to afford a solution of $[K_2\{[U(OSi(O^tBu)_3)_3]_2(\mu\text{-}O)\}]$, **1**. The ^1H NMR spectrum of the solution in toluene-d_8 confirmed the presence of **1** as a pure species and the complex was reacted without further purification to increase the overall yield and purity of the final product (complex **1** decomposes readily at room temperature and is highly soluble). The reaction tube was transferred to a Schlenk line and degassed by freeze-pump-thaw cycles. Hydrogen gas (1 atm) was added into the tube and the reaction mixture was left stirring at room temperature. The reaction mixture turned from dark red to yellow within 15 min. The toluene solution was left standing at −40 °C for 24 h, yielding X-ray suitable crystals of complex $[K_2\{[U(OSi(O^tBu)_3)_3]_2(\mu\text{-}O)(\mu\text{-}H)_2\}]$, **2** (72.0 mg, 70% yield). ^1H NMR of crystals of **2** (400 MHz, tol-d_8, 298 K): δ (ppm) = 12.0 (s, 2H), −1.42 (s, CH_3 terminal siloxide). ^{13}C NMR of crystals of **2** (400 MHz, tol-d_8, 298 K): δ (ppm) = 71.11 (s, $\mathbf{C}(CH_3)_3$), 25.81 (s, $C(\mathbf{C}H_3)_3$). Anal. Calcd for $C_{72}H_{164}O_{25}K_2Si_6U_2(C_7H_8)_{1.5}$: C, 43.25; H, 7.74;

N, 0.00. Found: C, 43.25; H, 7.64; N, 0.00. Magnetic moment calculated by Evans method: 2.78 μ_B. When D_2 was added to a solution of **1**, the complex $[K_2\{[U(OSi(O^tBu)_3)_3]_2(\mu\text{-}O)(\mu\text{-}D)_2\}]$, **D-2** was isolated with similar yield and the proton NMR spectrum showed disappearance of the peak at 12 ppm.

Synthesis of $[K_2\{[U(OSi(O^tBu)_3)_3]_2(\mu\text{-}O)(\mu\text{-}k^2\text{-}NC(CH_3)NCH_2CH_3)\}]$, 3.

MeCN (9 mL of a 3M solution in tol-d_8, 0.027 mmol, 2.25 equiv.) was added to a yellow solution of $[K_2\{[U(OSi(O^tBu)_3)_3]_2(\mu\text{-}O)(\mu\text{-}H)_2\}]$, **2** (25.6 mg, 0.012 mmol) in toluene-d_8 (0.6 mL). The colour of the solution did not change upon addition, but the ^{1}H NMR spectrum of the reaction mixture after addition showed the complete disappearance of **2** and the appearance of new signals assigned to $[K_2\{[U(OSi(O^tBu)_3)_3]_2(\mu\text{-}O)(\mu\text{-}k^2\text{-}NC(CH_3)NCH_2CH_3)\}]$, **3**. The solution was left standing at −40 °C and X-ray suitable yellow crystals of $[K_2\{[U(OSi(O^tBu)_3)_3]_2(\mu\text{-}O)(\mu\text{-}k^2\text{-}NC(CH_3)NCH_2CH_3)\}]$, **3** were collected (16.2 mg, 60% yield). ^{1}H NMR of crystals of **3** (400 MHz, tol-d_8, 298 K): δ (ppm) = 1.55 (s, CH_3 terminal siloxide), −51 (s, 3H, C(C**H**$_3$)), −73 (s, 3H, CH_2C**H**$_3$), −85 (s, 2H, C**H**$_2$$CH_3$). ^{13}C NMR of crystals of **3** (400 MHz, tol-d_8, 298 K): δ (ppm) = 73.3 (s, **C**$(CH_3)_3$), 30.8 (s, C(**C**$H_3)_3$), 22.7 (s, C(**C**H_3)). Anal. Calcd for $C_{76}H_{170}N_2O_{25}K_2Si_6U_2(C_7H_8)$: C, 42.84; H, 7.71; N, 1.20. Found: C, 42.86; H, 7.22; N, 1.52. The ^{1}H NMR spectrum of the reaction mixture after addition of 1 equivalent of MeCN to **2** showed the presence of complex **3** and unreacted complex **2**. Single crystals isolated from this reaction confirmed the presence of **3**. When 2 equivalents of MeCN were added to a solution of **D-2**, the species $[K_2\{[U(OSi(O^tBu)_3)_3]_2(\mu\text{-}O)(\mu\text{-}k^2\text{-}NC(CH_3)NCD_2CH_3)\}]$, **D-3** was formed as confirmed by ^{1}H NMR spectroscopy.

Synthesis of $[K_2\{[U(OSi(O^tBu)_3)_3]_2(\mu\text{-}CH_2O)(\mu\text{-}O)\}]$, 4.

^{13}CO (0.012 mmol, 1 equiv.) was added to a solution of **2** (26.5 mg, 0.012 mmol), which had been degassed by freeze-pump-thaw cycles. The colour of the solution changed from yellow-greenish to pale yellow immediately and the ^{1}H NMR spectrum showed the disappearance of the resonances of the starting material and the appearance of those of a new species. The solution was left standing at −40 °C for 24 h. X-ray suitable crystals of complex $[K_2\{[U(OSi(O^tBu)_3)_3]_2(\mu\text{-}^{13}CH_2O)(\mu\text{-}O)\}]$, **^{13}C-4**, were recovered (18.6 mg, 70% yield). The quantitative ^{13}C NMR spectrum of **^{13}C-4** in D_2O showed the presence of one equivalent of methanol which was referenced to

^{13}C labelled potassium acetate, $CH_3{}^{13}COOK$ used as internal standard, confirming the presence of the bound oxomethylene dianion in **^{13}C-4**. Methanol formation was also identified by GC-MS analysis on the non-labelled analogue **4** in H_2O: M^+: 31 m/z. ^1H NMR (400 MHz, tol-d_8, 298 K): δ (ppm) = −1.13 (s, CH_3 terminal siloxide), −130 (d, 2H, $^{13}CH_2O^{2-}$). ^{13}C NMR (400 MHz, tol-d_8, 298 K): δ (ppm) = 71.06 (s, $\mathbf{C}(CH_3)_3$), 26.06 (s, $C(\mathbf{C}H_3)_3$), 22.72 (s, CH_2O^{2-}). ^{13}C NMR (400 MHz, D_2O, 298 K): δ (ppm) = 49 (triplet, $^{13}CH_2DOD$). Anal Calcd for $C_{73}H_{164}O_{26}K_2Si_6U_2(C_7H_8)_{0.2}$ **4**: C, 40.63; H, 7.59; N, 0.00. Found: C, 40.55; H, 7.25; N, 0.00. Magnetic moment calculated by Evans method: 2.75 m_B. When excess ^{13}CO is used, complex **^{13}C-4** is formed and was found to slowly react with additional ^{13}CO. The ^1H NMR spectrum shows disappearance of the resonances for **^{13}C-4** and the appearance of those of a new species that remains unidentified. The reaction of **^{13}C-4** with ^{13}CO is complete after 1 week. The ^{13}C NMR in D_2O of the final reaction mixture does not show the presence of methanol, suggesting that an attack of the nucleophilic carbon of the oxomethylene dianion of **^{13}C-4** on ^{13}CO has occurred. When ^{13}CO was added to a solution of **D-2**, the species $[K_2\{[U(OSi(O^tBu)_3)_3]_2(\mu\text{-}^{13}CD_2O)(\mu\text{-}O)\}]$, **D-4** was formed as confirmed by ^1H NMR spectroscopy, which showed the disappearance of the CH_2 signal.

Synthesis of $[K_2\{[U(OSi(O^tBu)_3)_3]_2(\mu\text{-}OCH_3)(\mu\text{-}O)(\mu\text{-}H)\}]$, 5.

A yellow solution of complex **2** (27.1 mg, 0.013 mmol) in toluene-d_8 (0.6 mL), was degassed by freeze-pump-thawing and ^{13}CO (0.013 mmol, 1 equiv.) was added. When the reaction with ^{13}CO was complete and all **2** had been converted into **4**, H_2 (1 atm) was added to the resulting solution. The mixture turned from yellow to light brown. The ^1H NMR spectrum shows that a new species is formed and does not evolve with time. The excess H_2 was removed under vacuum and the solution was left standing for 24 h, yielding X-ray suitable crystals of complex $[K_2\{[U(OSi(O^tBu)_3)_3]_2(\mu\text{-}OCH_3)(\mu\text{-}O)(\mu\text{-}H)\}]$, **5** (20.8 mg, 75 %). ^1H NMR (400 MHz, tol-d_8, 298 K): δ (ppm) = −0.05 (s, CH_3 terminal siloxide), −104 (d, 3H, CH_3O), 41 (s, 1H, H^-). ^{13}C NMR (^1H coupled) (400 MHz, tol-d_8, 298 K): δ (ppm) = 71.54 (s, $\mathbf{C}(CH_3)_3$), 28.5 (q, $C(\mathbf{C}H_3)_3$), −348 (q, CH_3O). Anal Calcd for mixture of $C_{73}H_{166}O_{26}K_2Si_6U_2$, **5**: C, 40.17; H, 7.67; N, 0.00. Found: C, 40.30; H, 7.34; N, 0.00. ESI-MS: M^+ 2184 m/z, MK^+ 2222 m/z. Magnetic moment calculated by Evans method: 2.37 m_B. The protonation of the hydroxo group was ruled out because of the absence of bands that could be assigned to a hydroxo ligand in the IR spectrum of **5** (see Supporting info). When D_2 is added to a toluene

solution of complex **4**, the species $[K_2\{[U(OSi(O^tBu)_3)_3]_2(\mu\text{-}CH_2DO)(\mu\text{-}O)(\mu\text{-}D)\}]$, **D-5** is formed. In the ^1H NMR spectrum of this reaction, the signal at 41 ppm disappears and the doublet at −104 ppm integrates for 2H. When CO (1 atm) and H_2 (1 atm) were added to **1** simultaneously in a pressurized vessel, complex **5** was formed as the only product. When 3 equivalents of $^{13}CO_2$ were added to a toluene solution of **5**, immediate reaction was observed to afford a new species. The ^{13}C NMR spectrum of this species in D_2O showed the presence of formate, confirming the presence of the hydride ligand in complex **5** that undergoes facile insertion of CO_2 in the U–H bond. ^{13}C NMR of the crude mixture after addition of 3 equivalents of $^{13}CO_2$ to **5** (400 MHz, D_2O, 298 K): δ (ppm) = 172.4 ($HCOO^-$), 161.6 (DCO_3^-), 50.4 (CH_3OD).

Reaction of 2 with CO_2: isolation of $[K_2\{[U(OSi(O^tBu)_3)_3]_2(\mu\text{-}CO_3)(\mu\text{-}HCOO)_2\}]$, 6.

CO_2 (0.03 mmol, 3 equiv.) was introduced into a yellow solution of $[K_2\{[U(OSi(O^tBu)_3)_3]_2(\mu\text{-}O)(\mu\text{-}H)_2\}]$, **2** (23.3 mg, 0.01 mmol), which was previously degassed by freeze-pump-thaw cycles . The colour of the solution turned light blue immediately. After 24 h at −40 °C light blue crystals were formed (20.6 mg). The ^1H NMR spectrum of the light blue crystals showed a mixture of products. Complex $[K_2\{[U(OSi(O^tBu)_3)_3]_2(\mu\text{-}CO_3)(\mu\text{-}HCOO)_2\}]$, **6** could be identified among the products by X-ray diffraction. The ^{13}C NMR spectra both in toluene-d_8 and in deuterated water indicated the formation of two different products that co-precipitate. The ^{13}C NMR spectra of the light blue crystals in D_2O showed the presence of $HCOO^-$, CO_3^{2-} and CH_3OD in a ratio 1:0.5:0.25 respectively. The presence of methanol was confirmed by GC-MS analysis. ^1H NMR of the light blue crystals (400 MHz, tol-d_8, 298 K): δ (ppm) = 12 (s, broad), 1.37 (s), 1.22 (s), -4.30 (s, broad). ^{13}C NMR of the light blue crystals (400 MHz, tol-d_8, 298 K): δ (ppm) = 73.25 (s, $\mathbf{C}(CH_3)_3$), 30.75 (s, $C(\mathbf{C}H_3)_3$), 130, 105, −216 (three ^{13}C for CH_3O^-, $HCOO^-$ and CO_3^{2-}). ^{13}C NMR of the light blue crystals (600 MHz, D_2O, pD 12, 298 K): δ (ppm) = 172 ($HCOO^-$), 168 (CO_3^{2-}), 50 (CH_3OD). GC-MS anal. for $^{13}CH_3OH$ M^+: 32 m/z. When 0.5 or 1 equivalents of $^{13}CO_2$ were added to a solution of **2**, the ^1H NMR spectrum showed the presence of complex **5**, the bis(oxo) complex $[K_2\{[U(OSi(O^tBu)_3)_3]_2(\mu\text{-}O)_2\}]$,[12] and starting material **2**. The ^{13}C NMR spectrum in D_2O after addition of 1 equiv. $^{13}CO_2$ showed the presence of $HCOO^-$, CO_3^{2-} and

CH_3OD in a ratio 1:0.8:1.75 respectively. ^{13}C NMR after addition of 1 equiv. of $^{13}CO_2$ (600 MHz, D_2O, pD 12, 298 K): δ (ppm) = 172 ($HCOO^-$), 169 (CO_3^{2-}), 49.7 (CH_3OD).

Bibliography

[1] a) M. D. Anker, C. E. Kefalidis, Y. Yang, J. Fang, M. S. Hill, M. F. Mahon, L. Maron, *J. Am. Chem. Soc.* **2017**, *139*, 10036-10054; b) R. Lalrempuia, C. E. Kefalidis, S. J. Bonyhady, B. Schwarze, L. Maron, A. Stasch, C. Jones, *J. Am. Chem. Soc.* **2015**, *137*, 8944-8947; c) N. M. West, A. J. M. Miller, J. A. Labinger, J. E. Bercaw, *Coord. Chem. Rev.* **2011**, *255*, 881-898; d) M. A. Rankin, C. C. Cummins, *J. Am. Chem. Soc.* **2010**, *132*, 10021-10023; e) T. J. Hadlington, C. E. Kefalidis, L. Maron, C. Jones, *Acs Catalysis* **2017**, *7*, 1853-1859; f) K. A. Grice, *Coord. Chem. Rev.* **2017**, *336*, 78-95; g) J. Y. Ye, R. C. Cammarota, J. Xie, M. V. Vollmer, D. G. Truhlar, C. J. Cramer, C. C. Lu, L. Gagliardi, *Acs Catalysis* **2018**, *8*, 4955-4968; h) E. A. Romero, T. X. Zhao, R. Nakano, X. B. Hu, Y. T. Wu, R. Jazzar, G. Bertrand, *Nature Catalysis* **2018**, *1*, 743-747; i) X. H. Shi, C. P. Hou, C. L. Zhou, Y. Y. Song, J. H. Cheng, *Angew. Chem. Int. Ed. Engl.* **2017**, *56*, 16650-16653; j) T. Shima, Z. M. Hou, in *Recent Development in Clusters of Rare Earths and Actinides: Chemistry and Materials, Vol. 173* (Ed.: Z. Zheng), **2017**, pp. 315-335.

[2] a) J. A. Higgins, F. G. N. Cloke, S. M. Roe, *Organometallics* **2013**, *32*, 5244-5252; b) M. Falcone, L. N. Poon, F. F. Tirani, M. Mazzanti, *Angew Chem Int Edit* **2018**, *57*, 3697-3700.

[3] a) W. J. Evans, J. W. Grate, R. J. Doedens, *J. Am. Chem. Soc.* **1985**, *107*, 1671-1679; b) E. L. Werkema, L. Maron, O. Eisenstein, R. A. Andersen, *J. Am. Chem. Soc.* **2007**, *129*, 2529-2541; c) G. M. Ferrence, R. McDonald, J. Takats, *Angew. Chem. Int. Ed. Engl.* **1999**, *38*, 2233-2237; d) J. H. Cheng, M. J. Ferguson, J. Takats, *J. Am. Chem. Soc.* **2010**, *132*, 2; e) T. Shima, Z. Hou, *J. Am. Chem. Soc.* **2006**, *128*, 8124-8125.

[4] B. H. Davis, M. L. Occelli, *Advances in Fischer−Tropsch Synthesis Catalysts and Catalysis*, CRC, Boca Raton, FL, , **2009**.

[5] D. A. Katahira, K. G. Moloy, T. J. Marks, *Organometallics* **1982**, *1*, 1723-1726.

[6] P. J. Fagan, K. G. Moloy, T. J. Marks, *J. Am. Chem. Soc.* **1981**, *103*, 6959-6962.

[7] A. S. P. Frey, F. G. N. Cloke, M. P. Coles, L. Maron, T. Davin, *Angew. Chem. Int. Ed. Engl.* **2011**, *50*, 6881-6883.

[8] a) B. Wayland, X. F. Fu, *Science* **2006**, *311*, 790-791; b) O. T. Summerscales, F. G. N. Cloke, P. B. Hitchcock, J. C. Green, N. Hazari, *Science* **2006**, *311*, 829-831; c) O. T. Summerscales, F. G. N. Cloke, P. B. Hitchcock, J. C. Green, N. Hazari, *J. Am. Chem. Soc.* **2006**, *128*, 9602-9603; d) A. S. Frey, F. G. N. Cloke, P. B. Hitchcock, I. J. Day, J. C. Green, G. Aitken, *J. Am. Chem. Soc.* **2008**, *130*, 13816-13817; e) B. M. Gardner, J. C. Stewart, A. L. Davis, J. McMaster, W. Lewis, A. J. Blake, S. T. Liddle, *Proc Natl Acad Sci USA* **2012**,

109, 9265-9270; f) P. L. Arnold, Z. R. Turner, R. M. Bellabarba, R. P. Tooze, *Chem. Sci.* **2011**, *2*, 77-79; g) N. Tsoureas, O. T. Summerscales, F. G. N. Cloke, S. M. Roe, *Organometallics* **2013**, *32*, 1353-1362.

[9] a) H. Liu, T. Ghatak, M. S. Eisen, *Chem. Commun.* **2017**, *53*, 11278-11297; b) B. S. Billow, B. N. Livesay, C. C. Mokhtarzadeh, J. McCracken, M. P. Shores, J. M. Boncella, A. L. Odom, *J Am Chem Soc* **2018**, *140*, 17369-17373; c) N. H. Anderson, S. O. Odoh, Y. Y. Yao, U. J. Williams, B. A. Schaefer, J. J. Kiernicki, A. J. Lewis, M. D. Goshert, P. E. Fanwick, E. J. Schelter, J. R. Walensky, L. Gagliardi, S. C. Bart, *Nat. Chem.* **2014**, *6*, 919-926; d) M. B. Jones, A. J. Gaunt, *Chem. Rev.* **2013**, *113*, 1137-1198; e) P. L. Arnold, Z. R. Turner, *Nat. Rev. Chem.* **2017**, *1*; f) S. T. Liddle, *Angew. Chem. Int. Ed. Engl.* **2015**, *54*, 8604-8641; g) M. R. MacDonald, M. E. Fieser, J. E. Bates, J. W. Ziller, F. Furche, W. J. Evans, *J. Am. Chem. Soc.* **2013**, *135*, 13310-13313; h) W. L. Huang, P. L. Diaconescu, in *Advances in Organometallic Chemistry, Vol 64, Vol. 64* (Ed.: P. J. Perez), **2015**, pp. 41-75; i) D. E. Smiles, G. Wu, P. Hrobarik, T. W. Hayton, *J. Am. Chem. Soc.* **2016**, *138*, 814-825.

[10] a) H. W. Turner, S. J. Simpson, R. A. Andersen, *J. Am. Chem. Soc.* **1979**, *101*, 2782-2782; b) J. M. Manriquez, P. J. Fagan, T. J. Marks, *J. Am. Chem. Soc.* **1978**, *100*, 3939-3941; c) P. J. Fagan, J. M. Manriquez, E. A. Maatta, A. M. Seyam, T. J. Marks, *J. Am. Chem. Soc.* **1981**, *103*, 6650-6667.

[11] a) W. J. Evans, E. Montalvo, S. A. Kozimor, K. A. Miller, *J. Am. Chem. Soc.* **2008**, *130*, 12258-12259; b) J. C. Berthet, J. F. Lemarechal, M. Lance, M. Nierlich, J. Vigner, M. Ephritikhine, *J. Chem. Soc., Dalton Trans.* **1992**, 1573-1577; c) W. J. Evans, K. A. Miller, A. G. DiPasquale, A. L. Rheingold, T. J. Stewart, R. Bau, *Angew. Chem. Int. Ed. Engl.* **2008**, *47*, 5075-5078; d) H. S. La Pierre, H. Kameo, D. P. Halter, F. W. Heinemann, K. Meyer, *Angew. Chem. Int. Ed. Engl.* **2014**, *53*, 7154-7157; e) M. Ephritikhine, *Chem. Rev.* **1997**, *97*, 2193-2242; f) J. K. Pagano, J. M. Dorhout, R. Waterman, K. R. Czerwinski, J. L. Kiplinger, *Chem. Commun.* **2015**, *51*, 17379-17381.

[12] M. Falcone, L. Barluzzi, J. Andrez, F. F. Tirani, I. Zivkovic, A. Fabrizio, C. Corminboeuf, K. Severin, M. Mazzanti, *Nat. Chem.* **2019**, *11*, 154–160.

[13] W. J. Evans, K. A. Miller, J. W. Ziller, *Angew. Chem. Int. Ed. Engl.* **2008**, *47*, 589-592.

[14] P. Berno, C. Floriani, A. Chiesivilla, C. Guastini, *J. Chem. Soc. Chem. Commun.* **1991**, 109-110.

[15] J. J. Kiernicki, S. L. Staun, M. Zeller, S. C. Bart, *Organometallics* **2017**, *36*, 665-672.

[16] G. Fachinetti, C. Floriani, A. Roselli, S. Pucci, *J. Chem. Soc. Chem. Commun.* **1978**, 269-270.

[17] N. E. Schlorer, S. Berger, *Organometallics* **2001**, *20*, 1703-1704.

[18] a) J. C. Berthet, M. Ephritikhine, *New J. Chem.* **1992**, *16*, 767-768; b) K. G. Moloy, T. J. Marks, *Inorganica Chimica Acta-F-Block Elements Articles and Letters* **1985**, *110*, 127-131.

[19] a) H. S. La Pierre, K. Meyer, in *Prog. Inorg. Chem., Vol. 58* (Ed.: K. D. Karlin), **2014**, pp. 303-415; b) L. Castro, O. P. Lam, S. C. Bart, K. Meyer, L. Maron, *Organometallics* **2010**, *29*, 5504-5510.

CONCLUSIONS AND PERSPECTIVES

The objective of this work was related to the development and study of multimetallic uranium systems for the transformation of small molecules. To the best of our knowledge, before this work, the ability of uranium multimetallic complexes in activating small molecules was essentially unexplored. Moreover, the evaluation of the nature of the bonding in uranium complexes it is of great fundamental interest, together with the understanding of the ligands role in reactivity.

Firstly, we demonstrated that bridging nitride ligands in uranium chemistry could be highly reactive, contrary to what is found for d-block metal bridging nitrides. The ligand based reactivity of the diuranium(IV) bridging nitride complex allowed us to isolate the first example of CO_2 addition to a $U–N_{nitride}$ bond, to give a dicarbamate ligand, and to the isolation of the product of complete CO cleavage. The dicarbamate-bridging group could be released only in water, causing the concomitant decomposition of the complex. In contrast, the cyanide ligand formed upon CO cleavage could be transferred to substrates such as methyl triflate or trimethylsilyl iodide. Such reactions are stoichiometric, as the oxophilicity of the uranium metal does not facilitate the product release, and the nitride is consumed as a source of nitrogen for the N–C bond formation. However, the importance of these reactions is found in the single activation and coordination steps. These steps gie insight into species that might be involved in the mechanism of existing industrial processes and lead, in the long term, to the development of improved catalysts. Additionally, the high nucleophilicity of the bridging nitride was shown to effect the reversible cleavage of dihydrogen, yielding an hydrido/imido complex, which readily transfer the hydride to carbon dioxide. The interest in H_2 activation originates from the need of efficient and selective catalysts for both CO_2 hydrogenation and ammonia formation from N_2 and H_2. Further studies should focus on stabilizing diuranium(III) hydride species in order to exploit the hydride reducing power combined with the reducing power of the metal center.

Secondly, we have shown that well designed multimetallic complexes of U(III), in which the metal centers are linked by nitride or oxide ligands, can perform multielectron transfer and activate inert molecule, such as dinitrogen. Despite the general thought that uranium(III) complexes could only reversibly activate dinitrogen

or reducing it by two electrons, we have shown that the diuranium(III) bridging nitride complex can react with N_2 to give the first example in uranium chemistry of a highly activated side-on-bound dinitrogen (N_2^{4-}) product, resulting from a four electron reduction. The N–N single bond could be further reduced and completely cleaved by the addition of reducing agent such as H_2 or CO. This difference compared to the previous examples present in literature, is due to the combination of three factors: the reducing power of uranium in the +III oxydation state, the multimetallic nature of the complex and the flexibility given by the metallo-ligand framework. If such hydrazido complexes were isolated for group 4 metals, the intermediate species have not been characterized and the N_2 cleavage does not involve metal-centered electron transfer, while the reaction of the uranium nitride/hydrazido complex with CO involves a uranium-centred electron transfer.

However, for a potential N_2 catalytic transformation into value added products, the bridging atom should act as a spectator atom. A bridging oxide could provide a good alternative to the bridging nitride, which was shown to react with protons, CO and with H_2. The analogous diuranium(III) oxo complex could be synthetized and the reactivity towards N_2 appeared to be similar as for the nitride. However, the substitution of the linker atom from a nitride to an oxide ligand had a dramatic effect on the reactivity with further reactants. Specifically, the presence of the oxo linker resulted in the release of dinitrogen upon addition of H_2 while with the subsequent addition of hydrogen and acid to the nitride complex, ammonia was formed. Further studies should explore the possibility of synthetizing bridging sulphide or bridging phosphide complexes to find the spectator linker atom that allows the complete cleavage of N_2 upon addition of CO or H_2.

In parallel to the reactivity studies, DFT calculations on selected compounds revealed the nature of the uranium-ligand bonding to uranium. We identified a route using the methatesis of a mononuclear uranium imido complex for the synthesis of the first example of a stable terminal U(V) sulphide complex. This complex showed both ligand based and metal based reactivity. DFT calculations revealed a triple-bond character with strong covalent character for the terminal sulphide. Moreover, the frontier molecular orbitals of the diuranium(III) bridging nitride and bridging oxide engaged in nitrogen activation, have been compared. DFT studies and magnetic data revealed a different bonding scheme for the nitride and oxide complexes with markedly covalent character of the U–N–U bond and a strictly ionic U–O–U bond. In

contrary to the oxide ligand, the bridging nitride appears to be involved in the binding and activation of N_2, showing that the choice of the linker has a significant impact on the degree of N_2 activation.

The results reported in this work highlight the potential of uranium nitrides in promoting N–C bond-formation reactions, from cheap resources such as N_2 and CO. However, for the selective catalytic synthesis of organic molecules from metal nitrides and abundant feestock such as CO_2 or CO, a nitride species must form from N_2 and be cyclically transferred to a substrate. Six-electron transfer to N_2 to give a bis-nitride species would be desirable. As the examples of uranium complexes in the +II oxidation state are increasing, multimetallic U(II) complexes might be a possible target for such reactivity. Alternatively, the multimetallic approach could be used to build a flexible ligand framework able to host three uranium cations.

"...Now is the time to understand more, so that we may fear less" – M. Curie

APPENDIX

APPENDIX 1

Supporting information for Chapter 2

1. NMR Spectroscopic data

tert-Bu transfer from ligand to nitrogen in complex 1.

Figure S1. ^{1}H NMR spectra (298 K, 400 MHz, toluene-d_8) of decomposition of complex **1**, at room temperature and 65 °C for 30h.

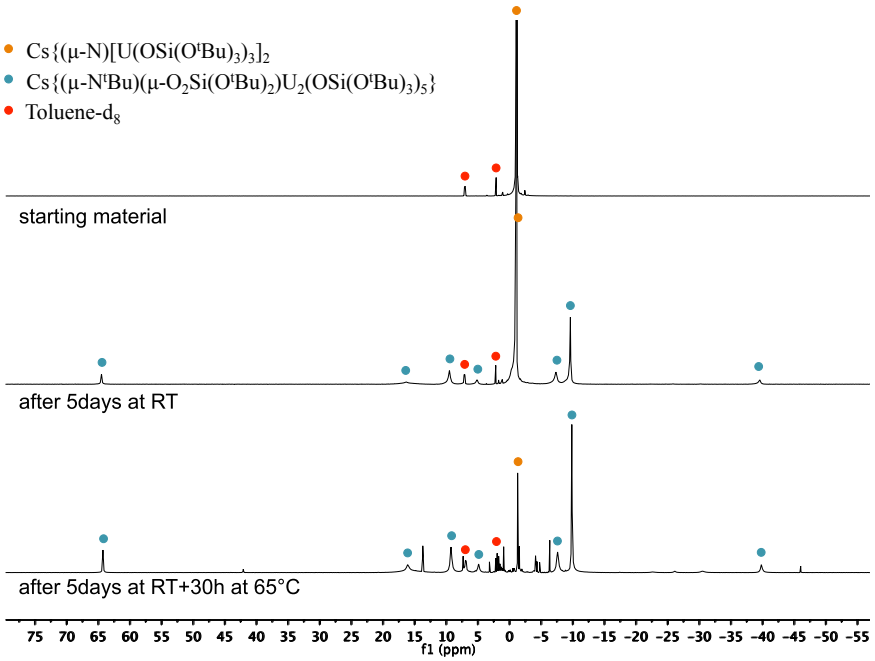

Figure S2. ^{1}H NMR spectra (298 K, 400 MHz, toluene-d_8) of decomposition of complex **1**, at 80 °C.

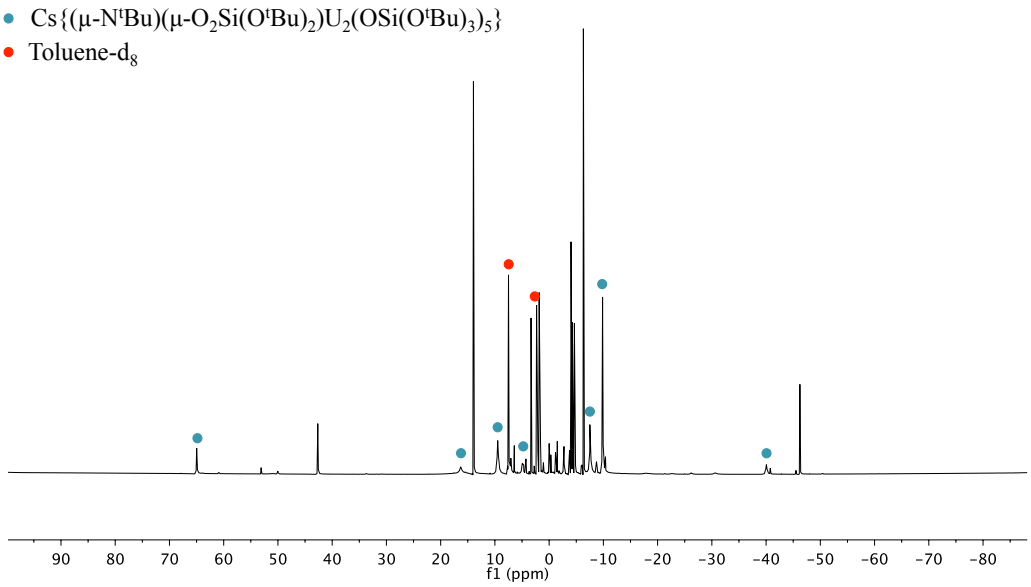

Figure S3. ^{1}H NMR spectrum (298 K, toluene-d_8, 400 MHz) of isolated crystals of complex **2**.

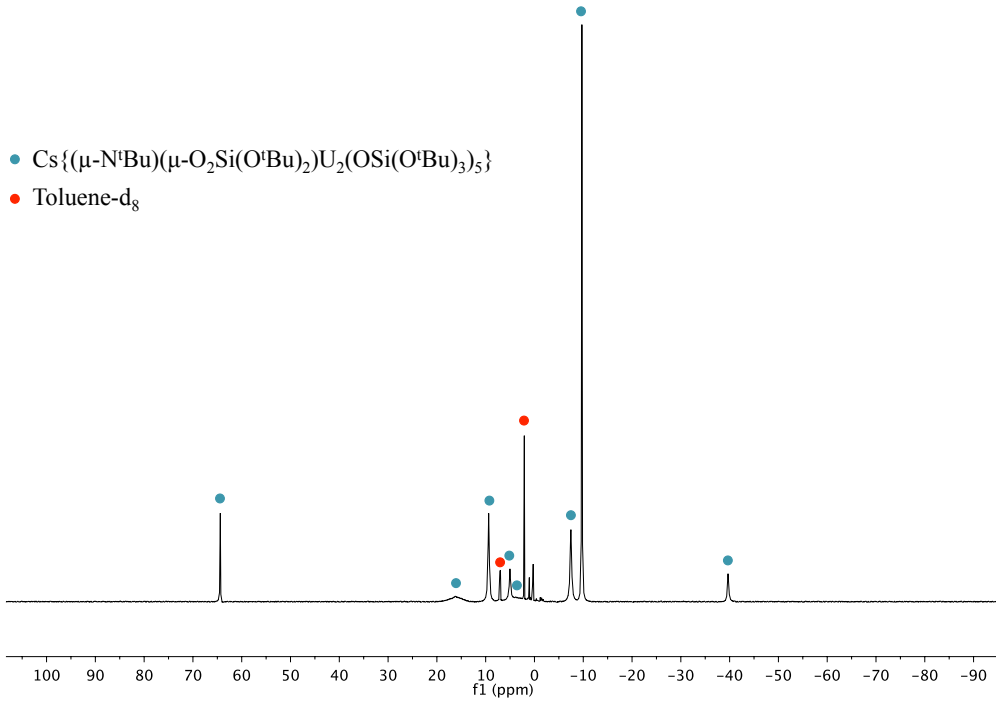

Figure S4. ^{1}H NMR spectrum (298K, 400 MHz, THF-d_8) of complex **2** after addition of 18crown6.

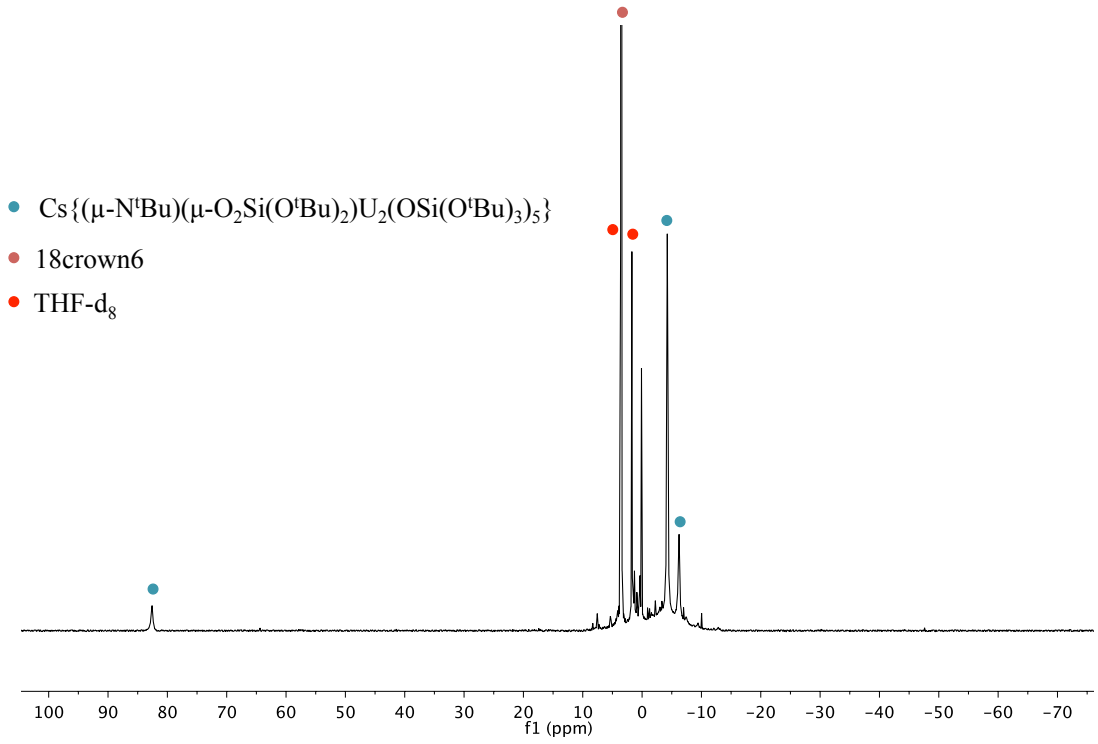

Reaction of complex 1 with CS_2.

Figure S5. ^{1}H NMR spectrum (298 K, 400 MHz, toluene-d_8) after addition of 1 equivalent of CS_2 to complex **1**.

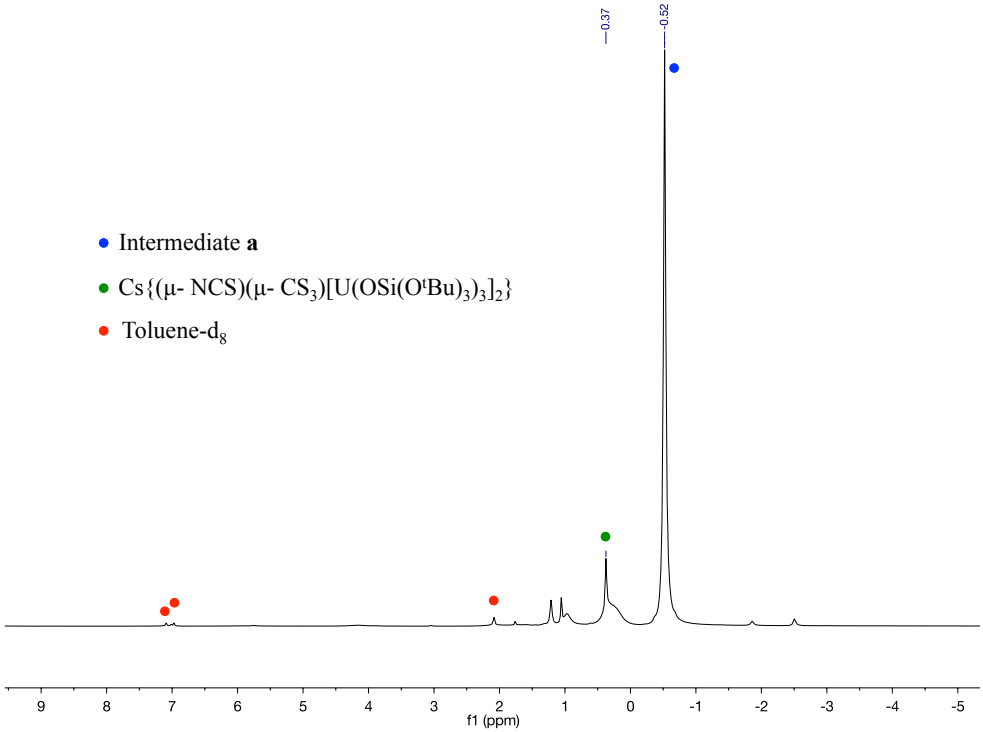

Figure S6. ^{13}C NMR spectrum (298 K, 400 MHz, toluene-d_8) after addition of 1 equivalent of CS_2 to complex **1**.

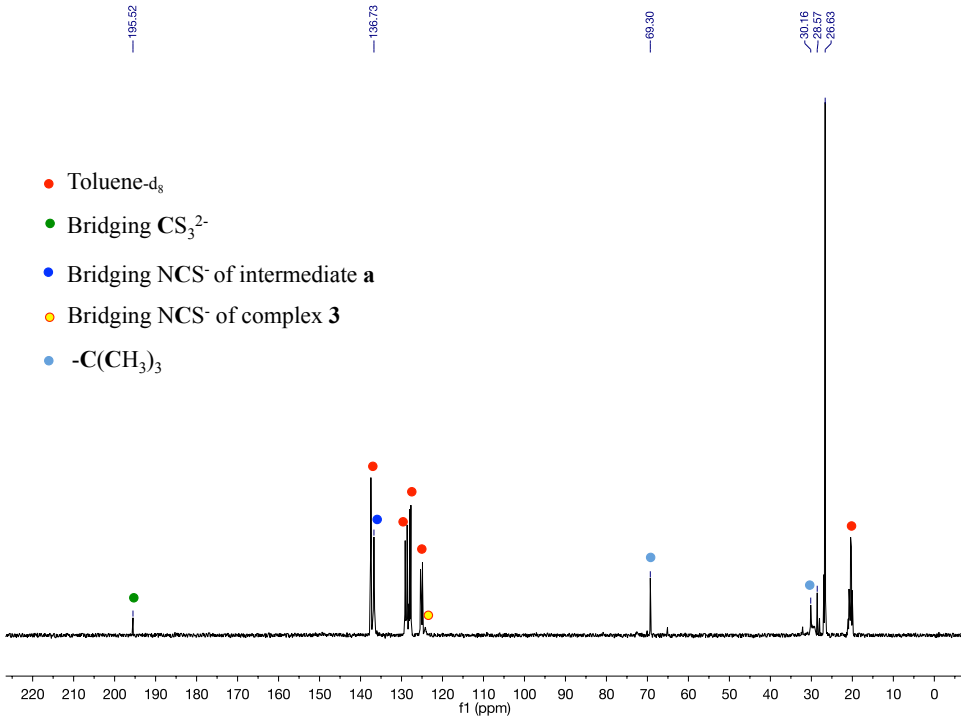

Figure S7. ^{13}C NMR spectra (298 K, 400 MHz, DMSO-d_6) of the reaction mixture after addition of 1 equivalent of CS_2 to complex **1**.

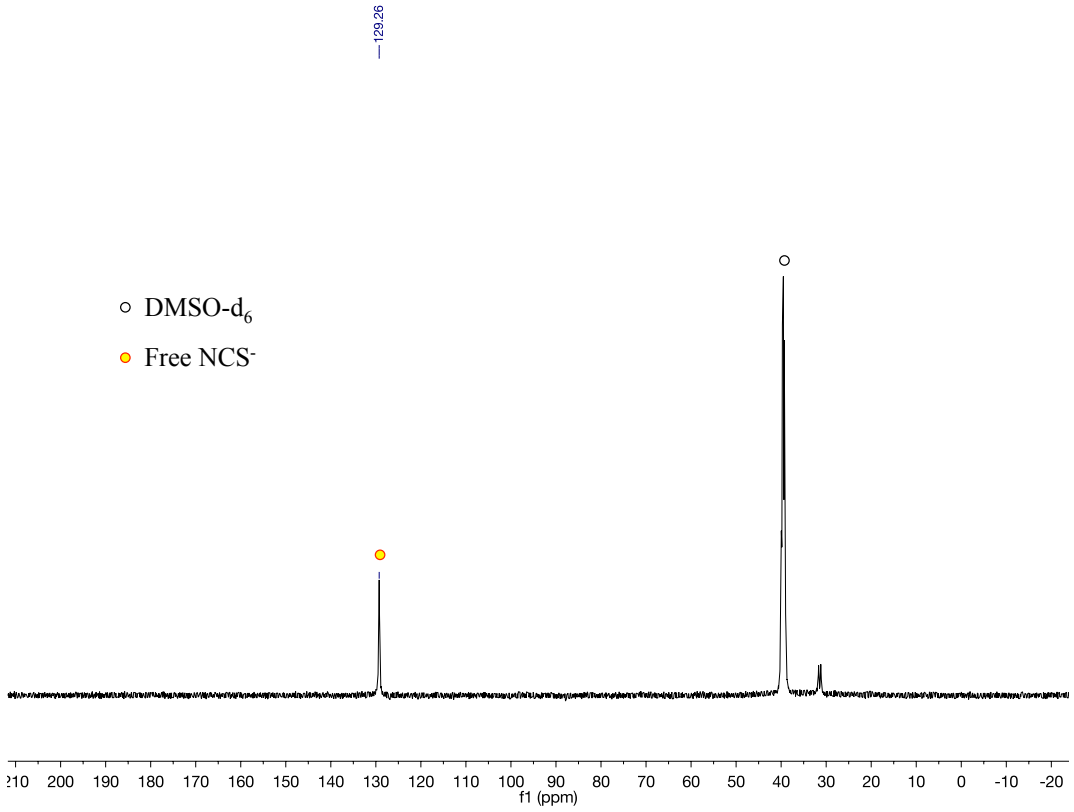

Figure S8. ^{1}H NMR spectra (298 K, 400 MHz, toluene-d_8) of the crude mixture, before and after addition of 2 equivalents of CS_2 to complex **1**.

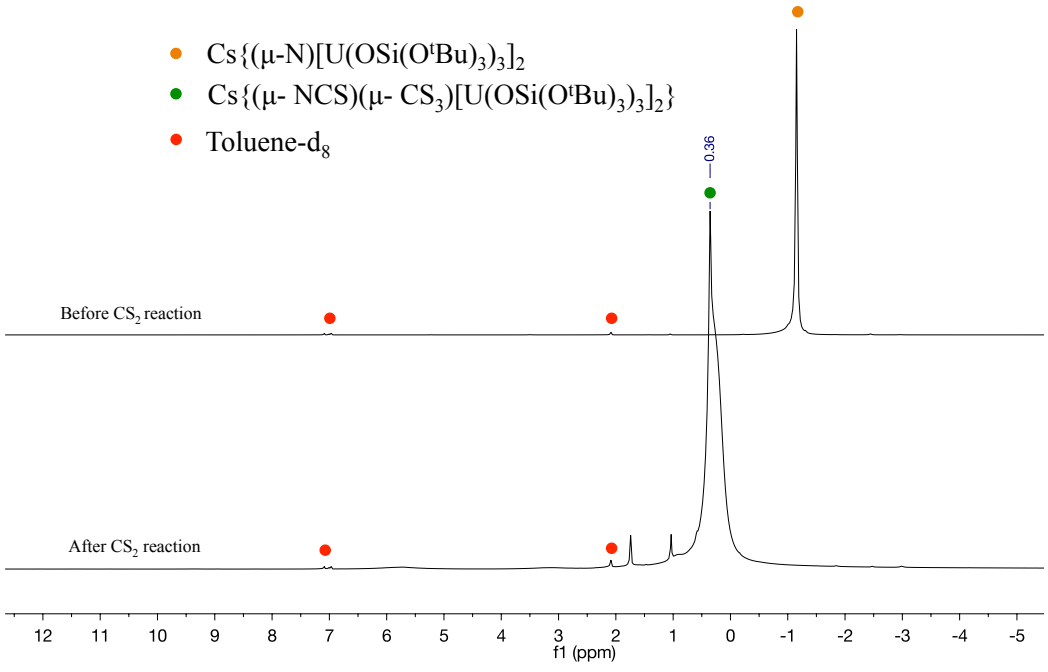

Figure S9. Low temperature ^{1}H NMR spectrum (233 K, 400 MHz, toluene-d_8) of the crude mixture after addition of 2 equivalents of CS_2 to complex **1**.

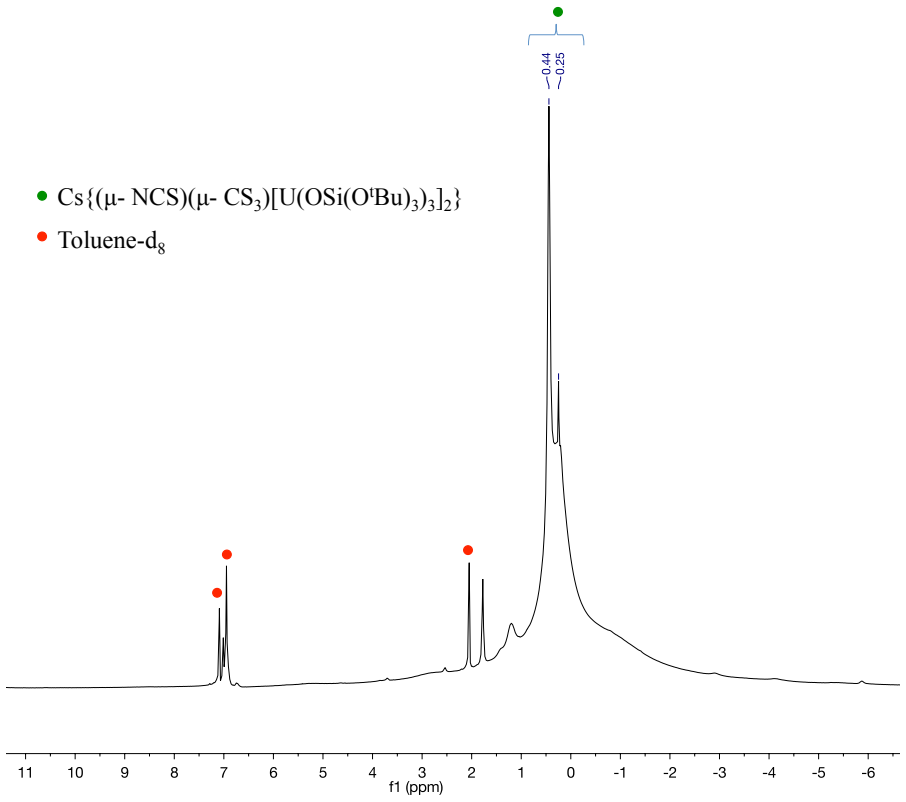

Figure S10. ^{1}H NMR spectrum (298 K, 400 MHz, toluene-d_8) of crystals of **3**.

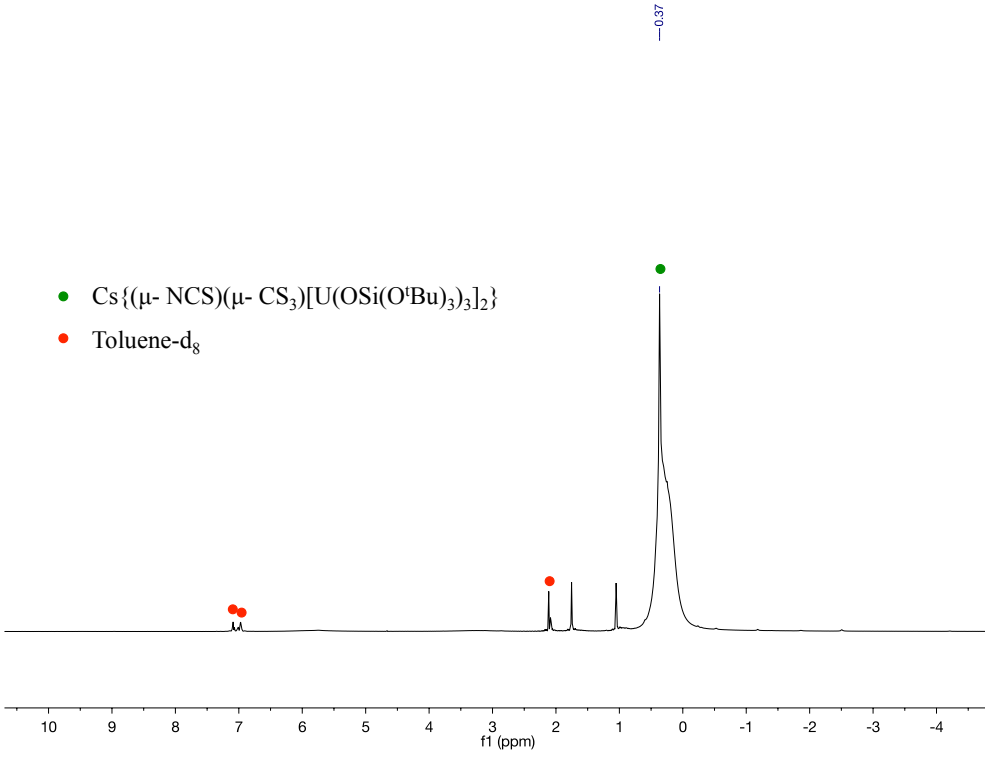

Figure S11. ^{13}C NMR spectrum (298 K, 400 MHz, toluene-d_8) of crystals of **3**.

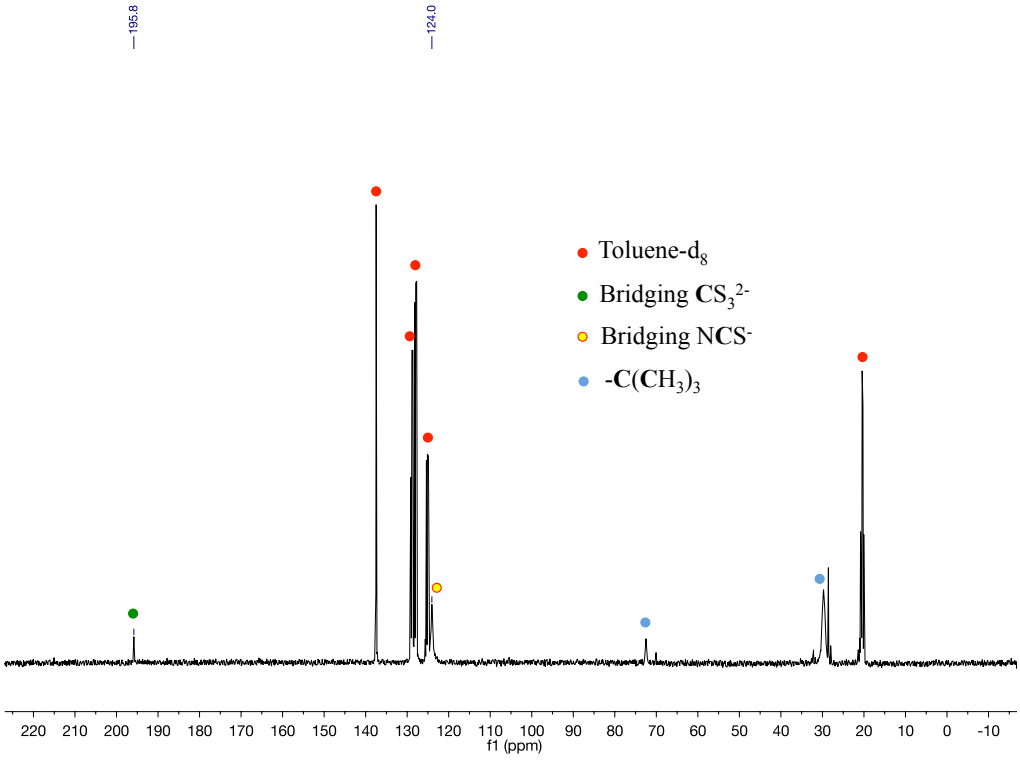

Figure S12. ^{13}C NMR spectrum (298 K, 400 MHz, DMSO-d_6) of crystals of **3**.

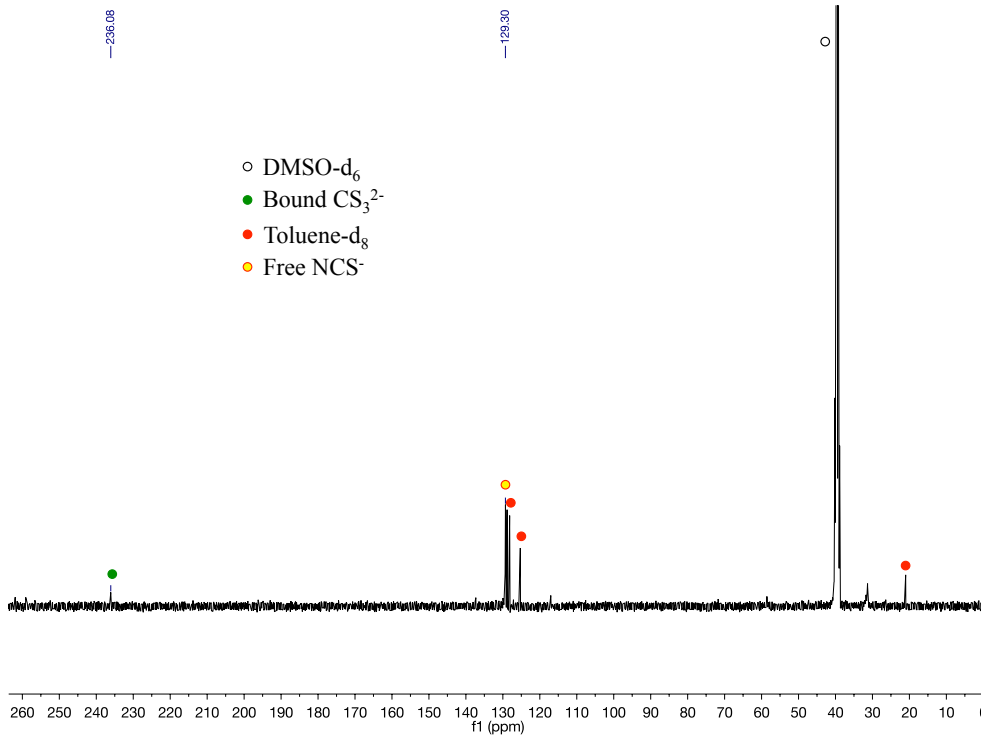

Figure S13. ^{1}H NMR spectrum (298 K, 400 MHz) of a solution of crystals of **3** in toluene-d_8 after 24 h at room temperature.

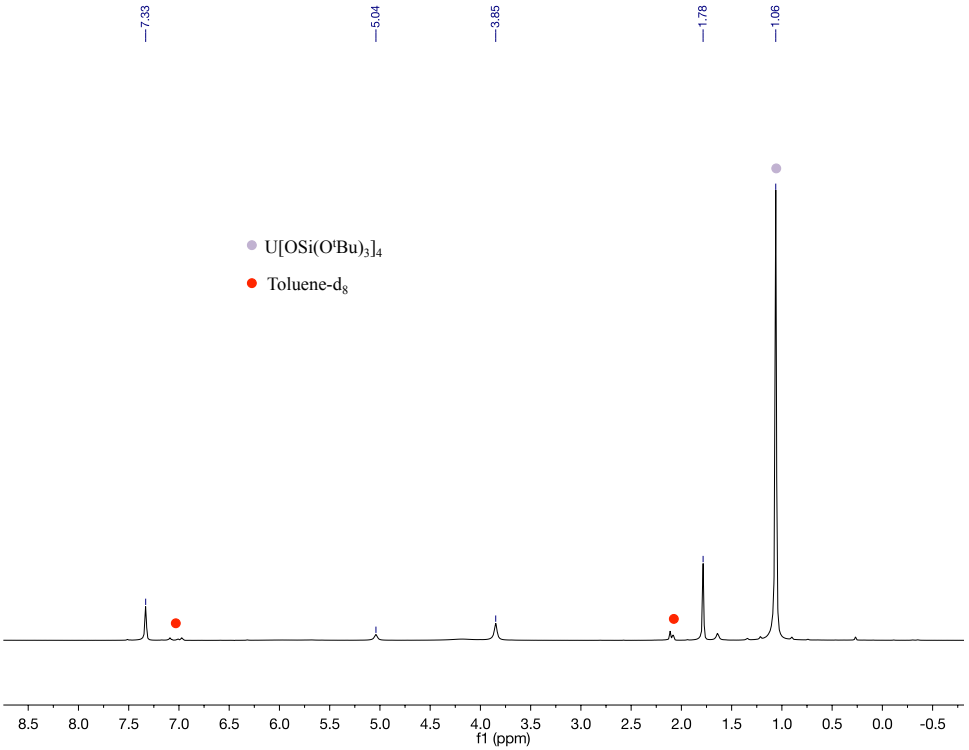

Figure S14. ^{13}C NMR spectrum (298 K, 400 MHz) in DMSO-d_6 of the crude mixture after addition of 2 equivalents of CS_2 to complex **1** to afford **3**, recorded after 24 h at room temperature.

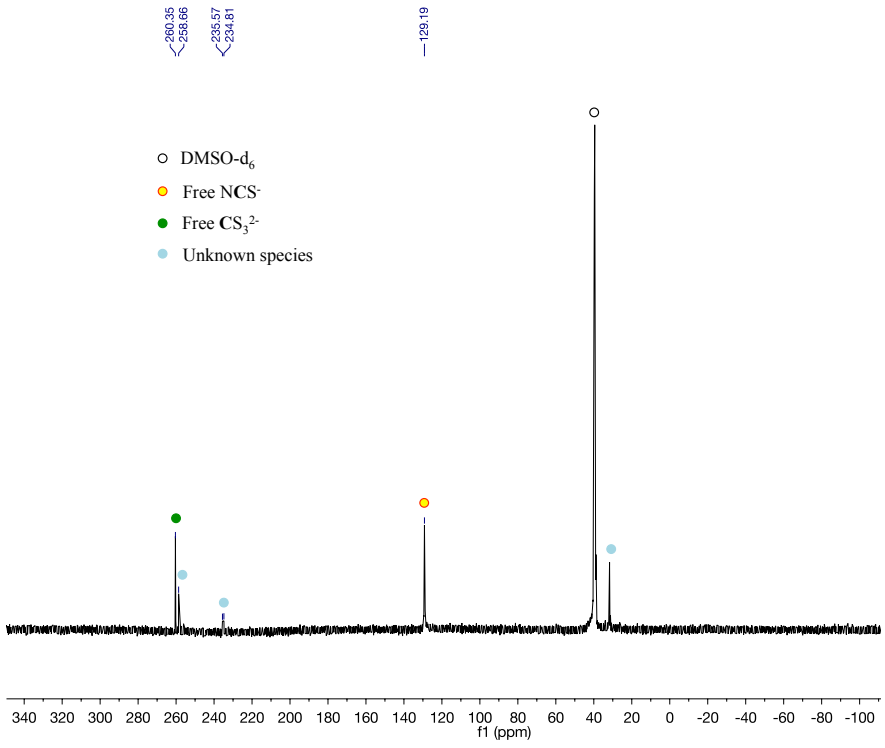

Figure S15. ^{13}C NMR spectrum (298 K, 400 MHz) in D_2O of crystals of **3**.

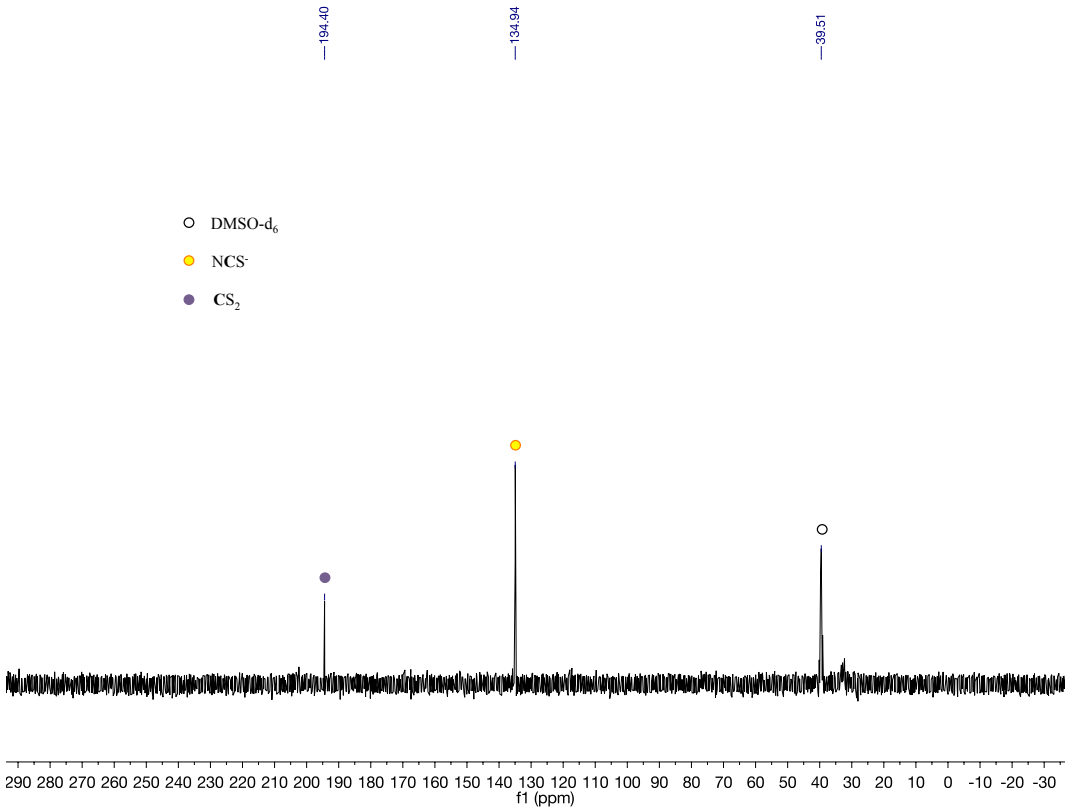

Reaction of complex 1 with CO_2.

Figure S16. ^{1}H NMR spectra (298K, 400MHz, toluene-d_8) after addition of 1 equivalent of CO_2 (a) and a second equivalent of CO_2 (b) to complex **1**.

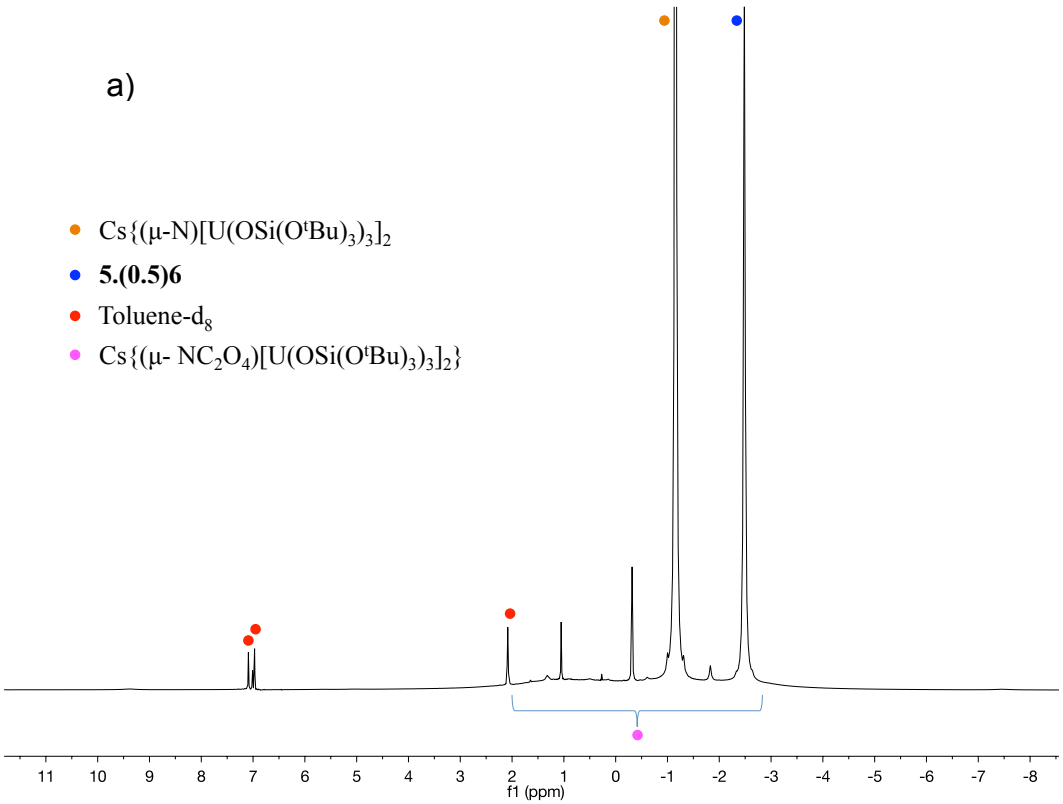

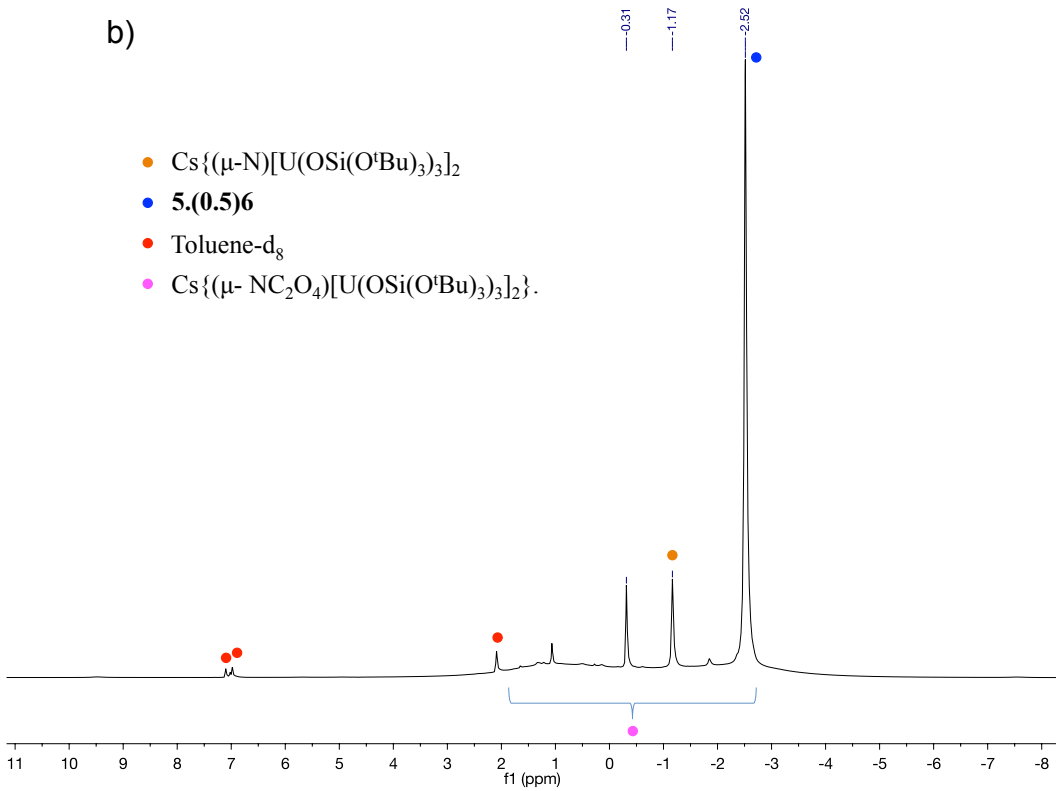

Figure S17. ^{1}H NMR spectrum (298 K, 400 MHz, toluene-d_8) after addition of 2.5 equivalents of CO_2 to complex **1**.

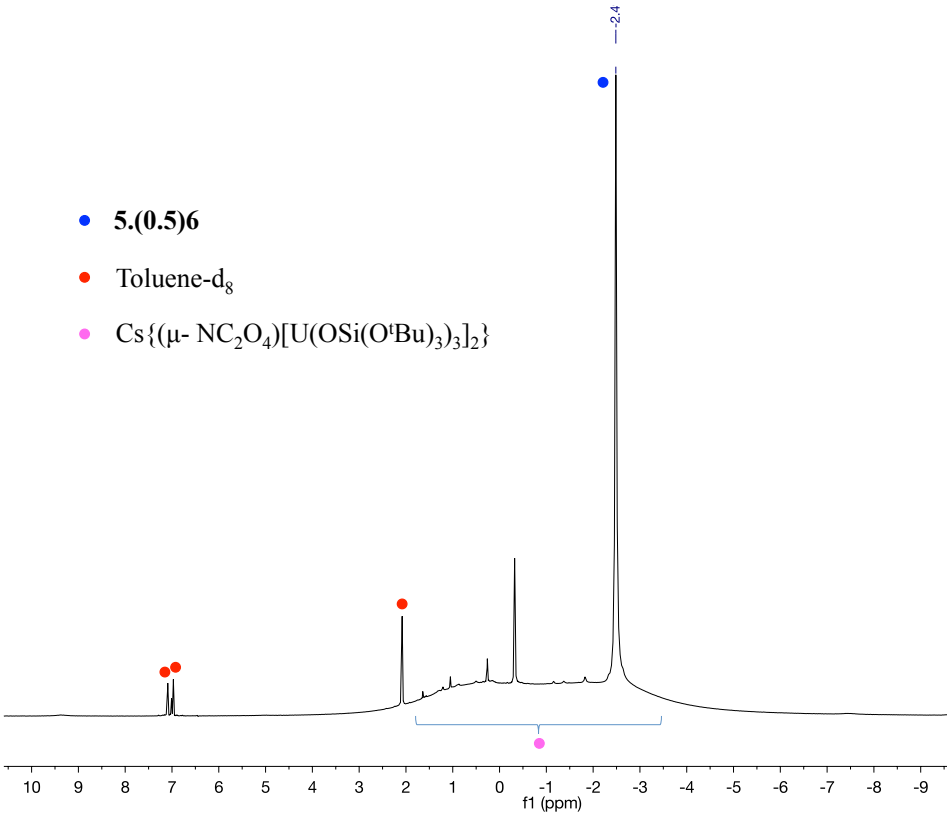

Figure S18. ^{1}H NMR spectrum (298 K, 400 MHz, toluene-d_8) after addition of 3 equivalents of CO_2 to complex **1**.

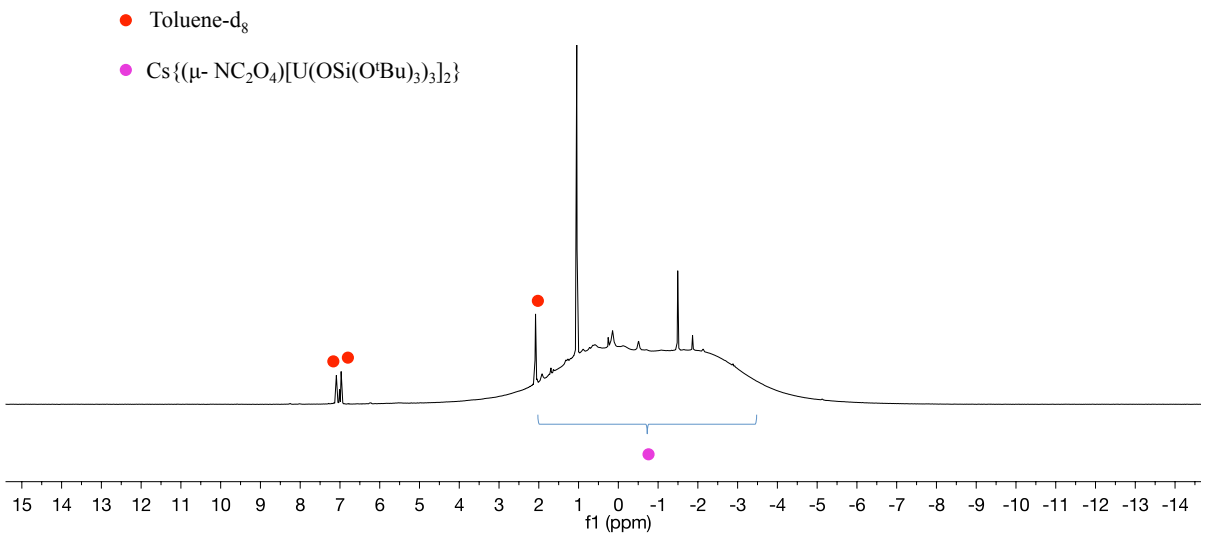

Figure S19. ^{13}C NMR spectrum (298 K, 400 MHz, toluene-d_8) of the crude mixture from reaction of **1** with 3 equivalents of CO_2.

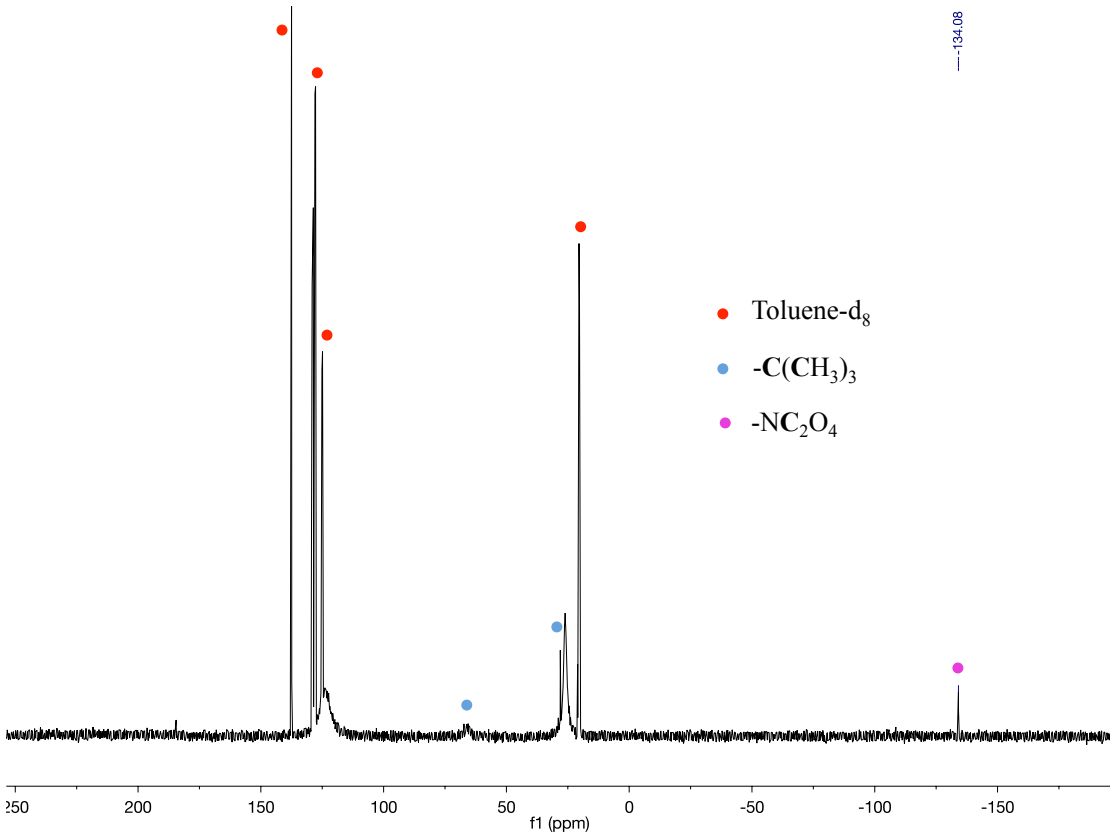

Figure S20. ^{1}H NMR spectrum (298 K, 400 MHz) in toluene-d_8 of crystals of **4**.

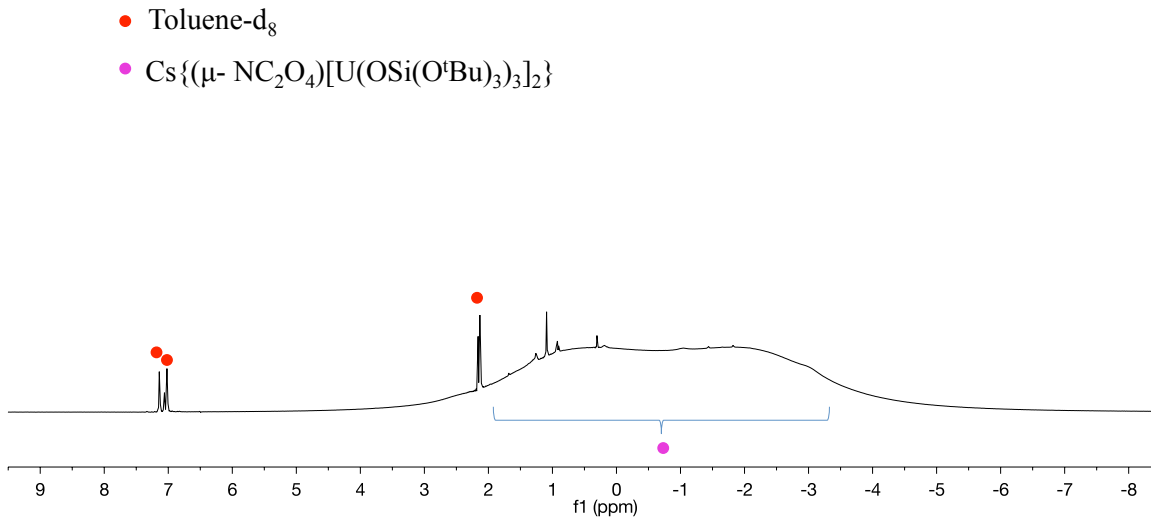

Figure S21. ^{13}C NMR spectrum (298 K, 400 MHz) in toluene-d_8 of crystals of **4**.

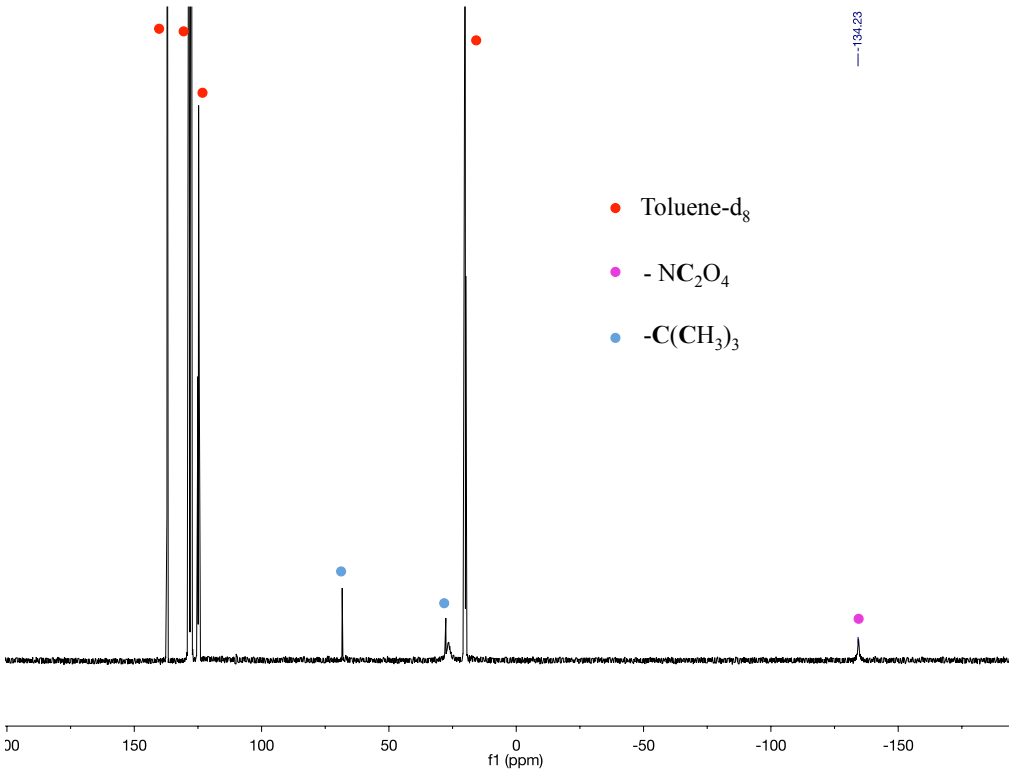

Figure S22. ^{1}H NMR spectrum (298 K, 400 MHz) in THF-d_8 of crystals of **4**.

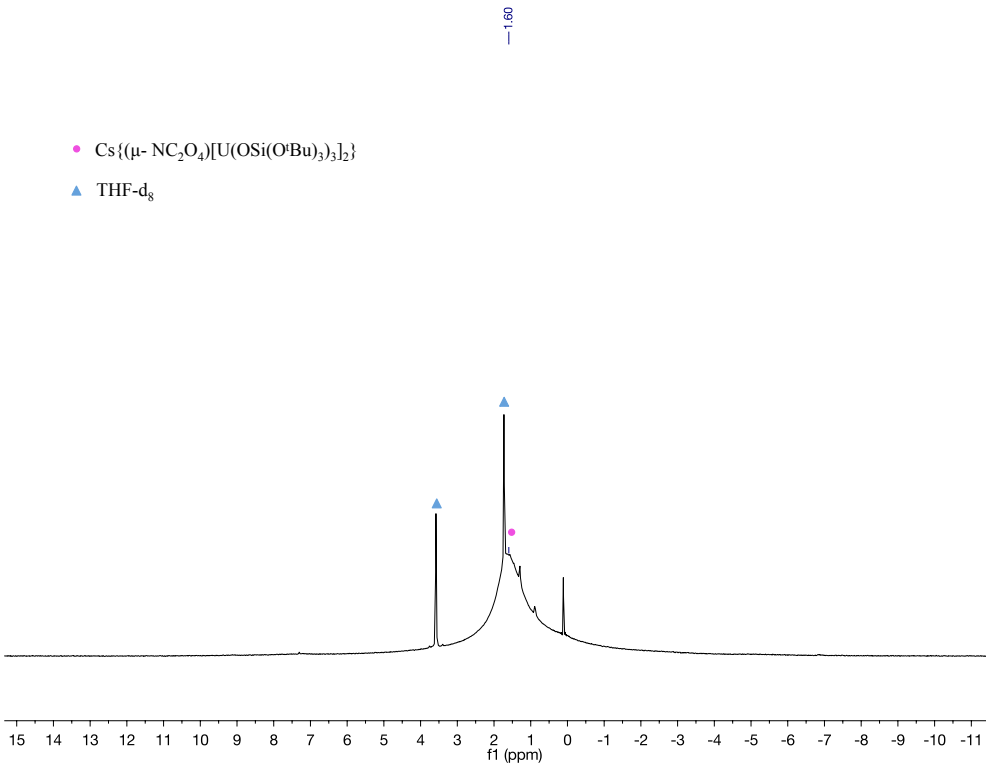

Figure S23. ^{1}H NMR spectrum (298 K, 400 MHz, Toluene-d_8) of crystals of **5.(0.5)6** grown from reaction of complex **1** with 1 eq of CO_2.

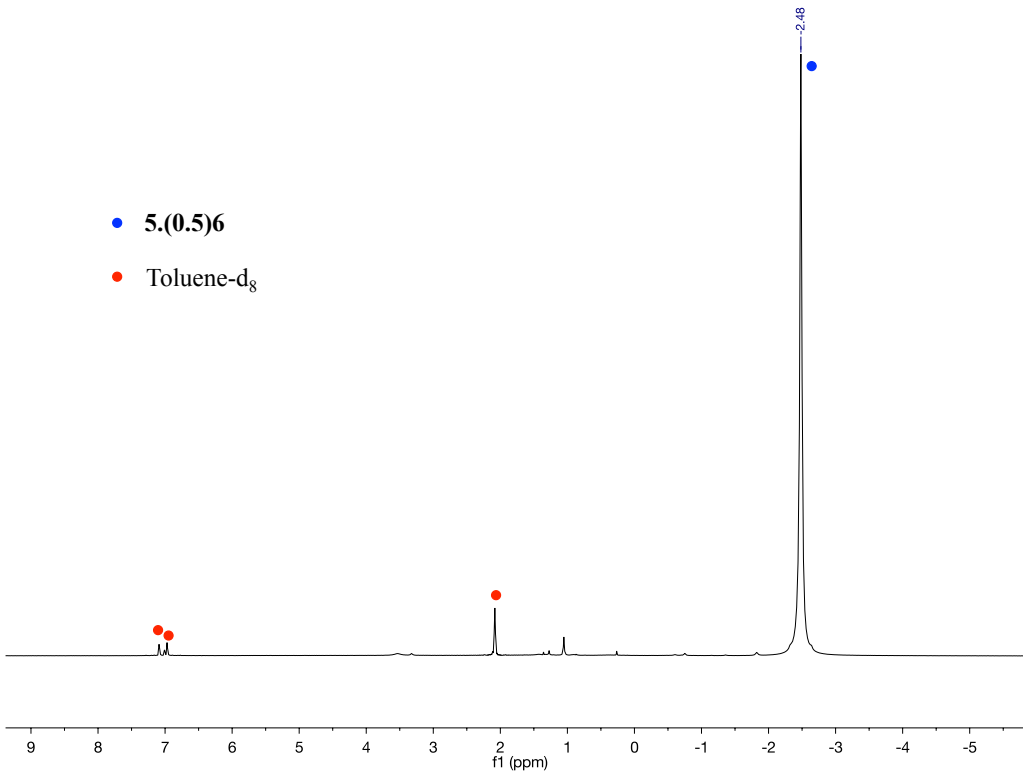

Figure S24. ^{13}C NMR spectrum (298 K, 400 MHz, DMSO-d_6) of crystals of **5.(0.5)6** (a) and ^{13}C NMR spectrum (298 K, 400 MHz, DMSO-d_6) of KNCO (b).

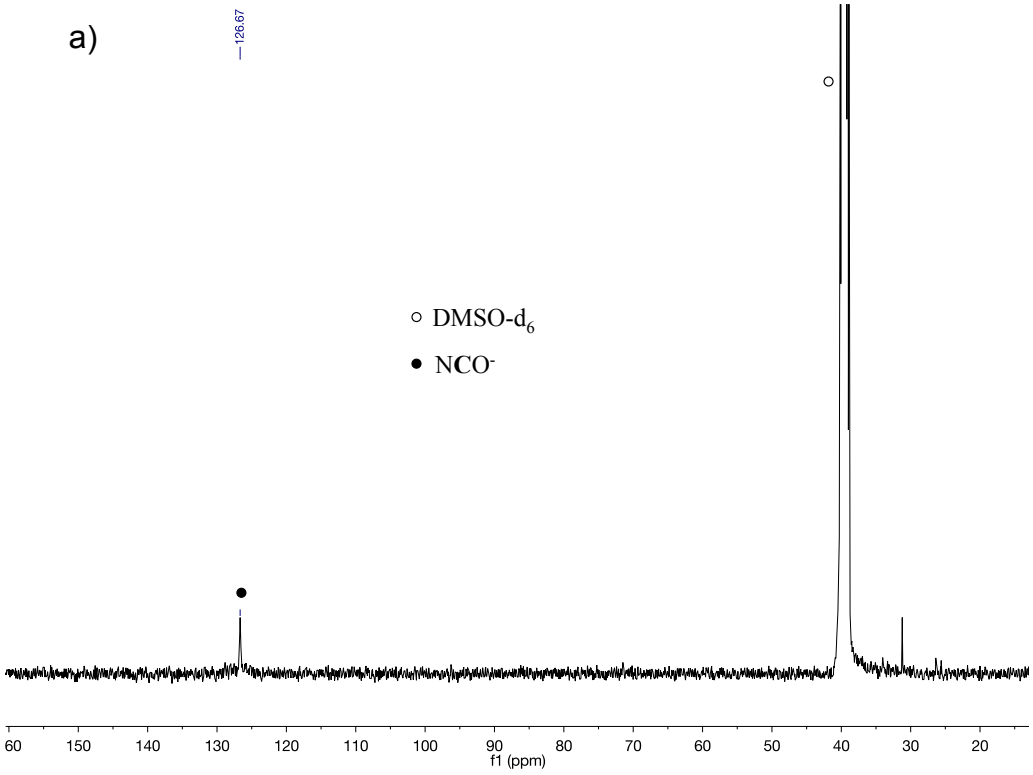

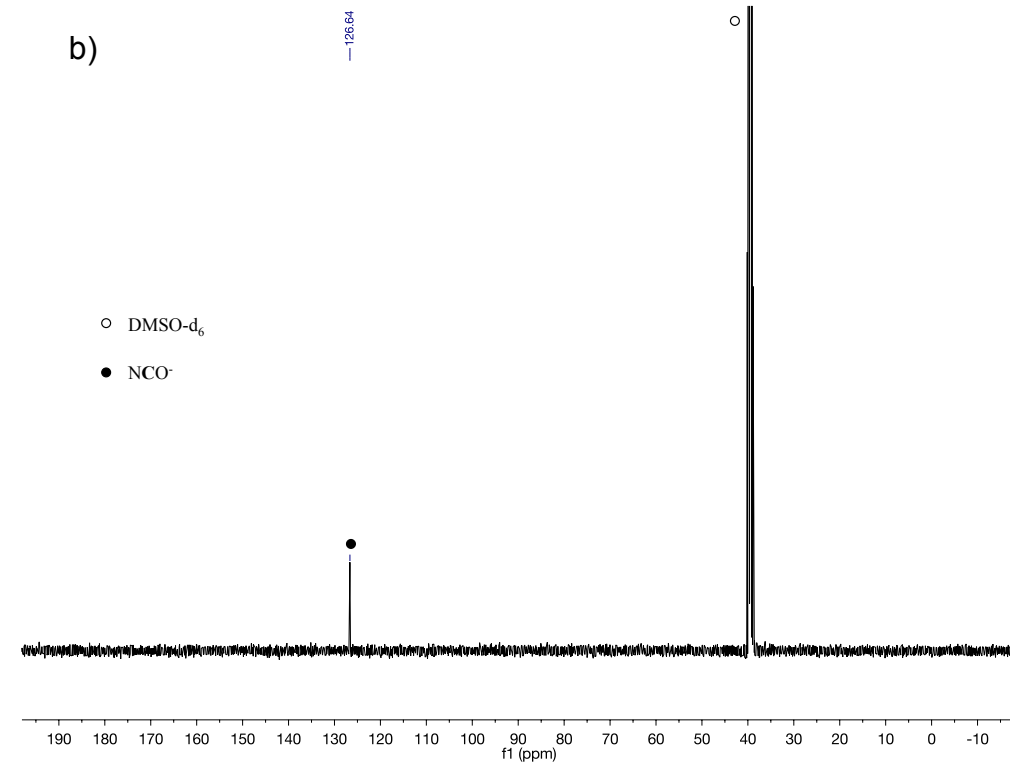

2. Crystallographic data

X-ray Experimental Part:

The diffraction data of **2** and **4** were measured at low temperature [120(2) K] using Mo Ka radiation on a Bruker APEX II CCD diffractometer equipped with a kappa geometry goniometer. The data collection of compounds **3** and **5.(0.5)6** were measured at low temperature [140(2) K] using Cu Ka radiation on an Agilent Technologies SuperNova dual system in combination with an Atlas CCD detector. The data sets of **2** and **4** were reduced by EvalCCD[1] and then corrected for absorption using SADABS Bruker software.[2] The data sets of **3** and **5.(0.5)6** were reduced by Crysalis PRO then corrected for absorption using ABSPACK Oxford-diffraction program.[3] Empirical absorption correction for **2**, **3** and **4** and analytical absorption correction for **5.(0.5)6** were applied. Space groups were determined from systematic absences, and they were confirmed by the successful solution of the structure. The **2** structure was solved by direct methods using the SHELXTL 6.14 package[4] whereas the **3**, **4** and **5.(0.5)6** structures were solved using Superflip software.[5] All non-hydrogen atoms were found by difference Fourier syntheses and refined on F^2. Hydrogen atoms were fixed in ideal position. Experimental details for X-ray data collections of **2**, **3**, **4** and **5.(0.5)6** are given in Table S1. CCDC numbers 1445287-1445290 contain the supplementary crystallographic data for this paper. These data can be obtained free of charge from The Crystallographic Data Centre via www.ccdc.cam.ac.uk/data_request/cif. Figure Graphics are generated using MERCURY 2.3 Supplied with Cambridge Structural Database; CCDC: Cambridge, U.K., 2004-2009.

[1] A. J. M. Duisenberg, L. M. J. Kroon-Batenburg, A. M. M. Schreurs, *J. Appl. Crystallogr*. **2003**, *36*, 220-229

[2] R. H. Blessing, *Acta Crystallogr., Sect. A* **1995**, *51*, 33-38

[3] CrysAlisPro CCD. CrysAlisPro RED, ABSPACK, CrysAlis PRO. Agilent Technologies, Yarnton, England, Agilent (**2010**)

[4] G. M. Sheldrick, *Acta Crystallogr.,Sect A* **2008**, *64*, 112-122

[5] L. Palatinus, G. Chapuis, *J. Appl. Crystallogr.*, **2007**, *40*, 786-790

Table S1: X-Ray crystallographic data.

	2.(toluene)	**3.(toluene)$_{1.5}$**	**4.(toluene)**	**5.(0.5) 6. (toluene)$_{0.5}$**
Formula	$C_{79}H_{170}CsNO_{24}Si_6U_2$	$C_{84.5}H_{174}CsNO_{24}S_4Si_6U_2$	$C_{81}H_{170}CsNO_{28}Si_6U_2$	$C_{225}H_{494}Cs_3N_2O_{78}Si_{18}U_6$
Crystal size (mm)	0.501 x 0.276 x 0.225	0.830 x 0.438 x 0.433	0.451 x 0.294 x 0.273	0.2799 x 0.1975 x 0.0656
cryst syst	Monoclinic	Triclinic	Triclinic	Triclinic
space group	Cc	P-1	P-1	P-1
volume (Å^3)	10778.7(17)	5828.2(3)	5546.5(11)	7911.2(2)
a (Å)	17.750(2)	13.1814(3)	13.5234(11)	13.9806(2)
b (Å)	23.0544(15)	18.0071(5)	17.323(3)	14.1774(3)
c (Å)	26.6029(14)	27.0562(7)	25.6987(18)	45.0404(5)
α (deg)	90.00	71.915(2)	74.324(8)	87.9767(12)
β (deg)	98.056(11)	81.875(2)	84.119(6)	88.3244(11)
γ (deg)	90.00	72.973(2)	73.180(11)	62.4770(18)
Z	4	2	2	1
formula weight (g/mol)	2295.67	2494.00	2383.69	6808.75
density (g cm^{-3})	1.415	1.421	1.427	1.429
absorption coefficient (mm^{-1})	3.461	3.275	3.368	3.537
F(000)	4664.0	2534	2420	3451
temp (K)	120.15	140.00(10)	120(2)	139.99(13)
total no. reflections	84087	75612	125376	84909
unique reflections [R(int)]	29267 [0.0234]	27974 [0.0627]	46120 [0.0535]	32237 [0.0403]
Final R indices [I > 2σ(I)]	R1 = 0.0250, wR2 = 0.0691	R_1 = 0.0801, wR_2 = 0.1792	R1 = 0.0527, wR2 = 0.1034	R_1 = 0.0681, wR_2 = 0.1342
Largest diff. peak and hole (e.A^{-3})	0.91 and -1.62	7.05/-2.01	1.279 and -1.527	4.51 and -2.58
GOOF	1.198	1.056	1.183	1.117

APPENDIX 2

Supporting information for Chapter 3

1. NMR Spectroscopic data

NMR for complex [Cs{[U(OSi(O^{t}Bu)$_3$)$_3$]$_2$(μ-CN)(μ-O)}], 2

Figure S1. ^{1}H NMR (400 MHz, toluene-d$_8$, 298 K) before and after reaction of complex [Cs{[U(OSi(O^{t}Bu)$_3$)$_3$]$_2$(μ-N)}], with CO, at room temperature.

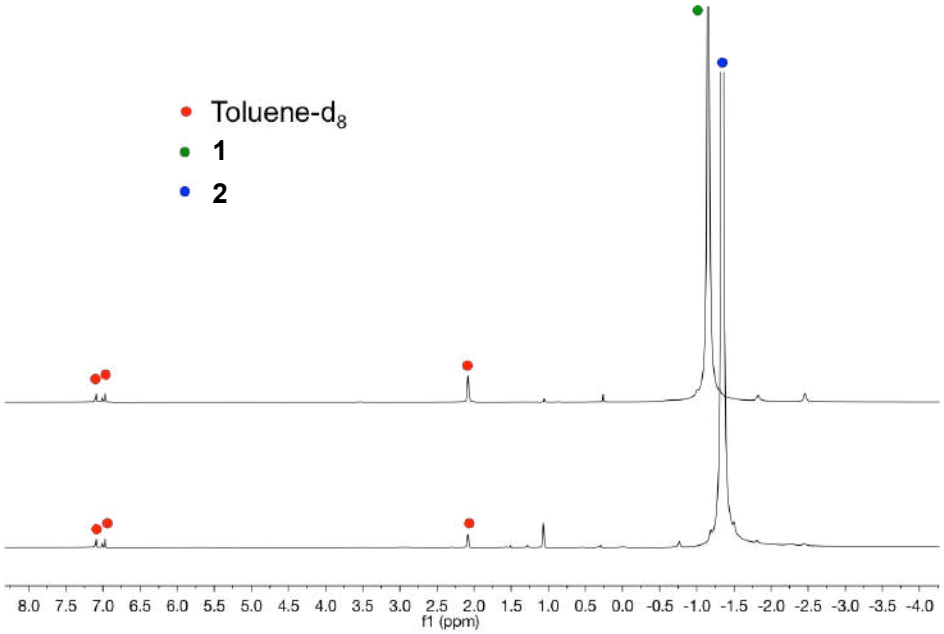

Figure S2. ^{1}H NMR (400 MHz, toluene-d$_8$, 298 K) of isolated crystals of **2**.

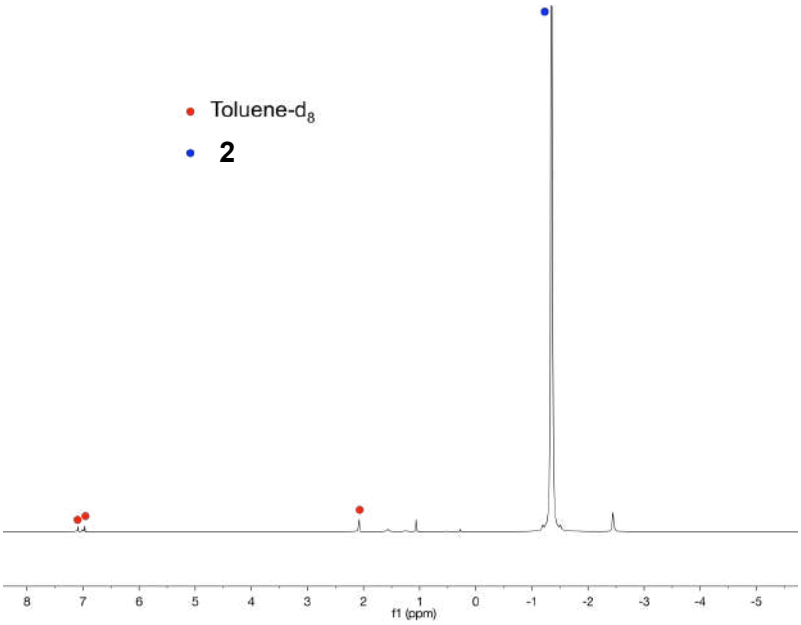

Figure S3. ^{13}C NMR (400 MHz, benzene-d_6, 298 K) of crystals of **2**.

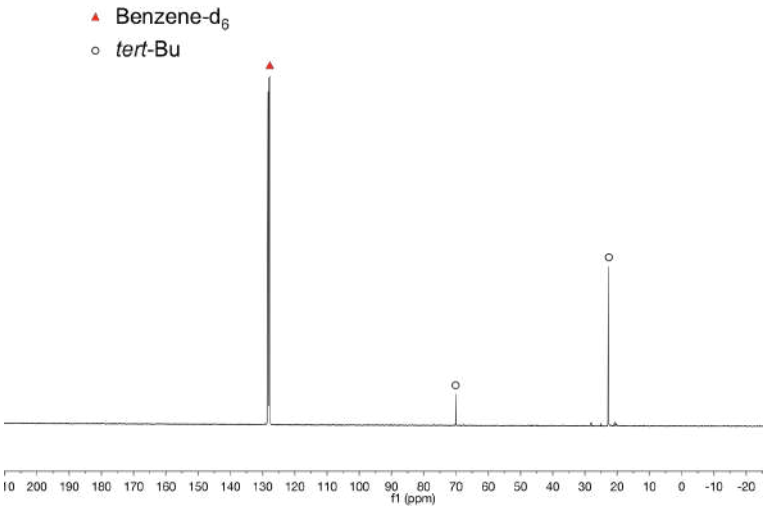

Figure S4. ^{13}C NMR (400 MHz, benzene-d_8, 298 K, O1P = 700) of crystals of **2**.

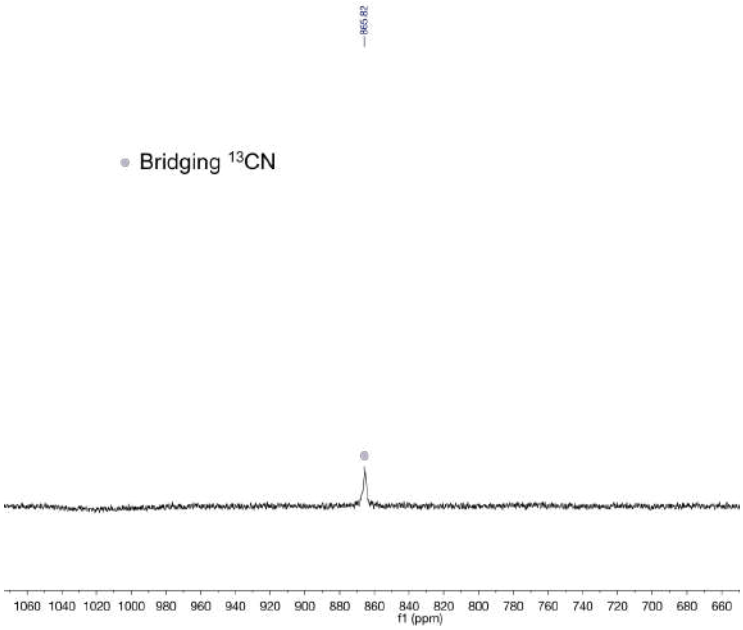

Figure S5. ^{1}H NMR (400 MHz, toluene-d_8, 298 K) of crystals of **2** after 3 days at room temperature showing only small traces of the scrambling product $[U(OSi(OtBu)_3)_4]$.

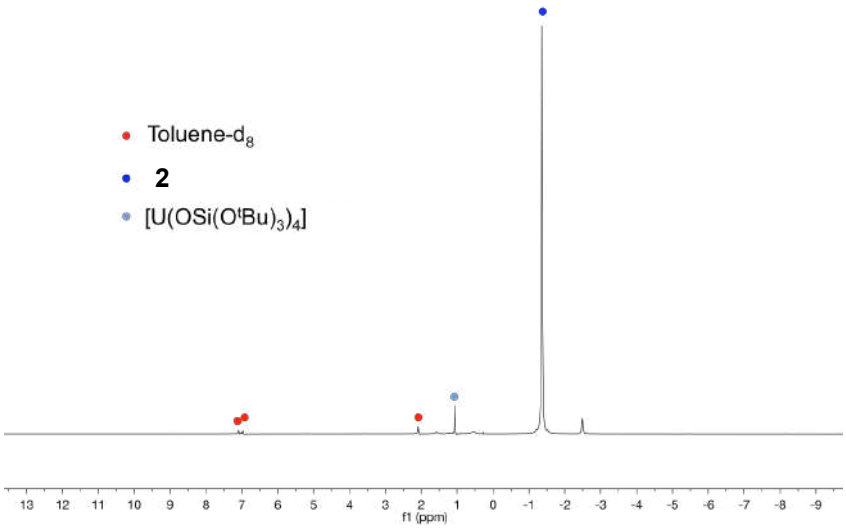

Figure S6. ^{1}H NMR (400 MHz, benzene-d_6, 298 K) of crystals of **2** at different temperatures showing that ligand scrambling occurs at 60°C.

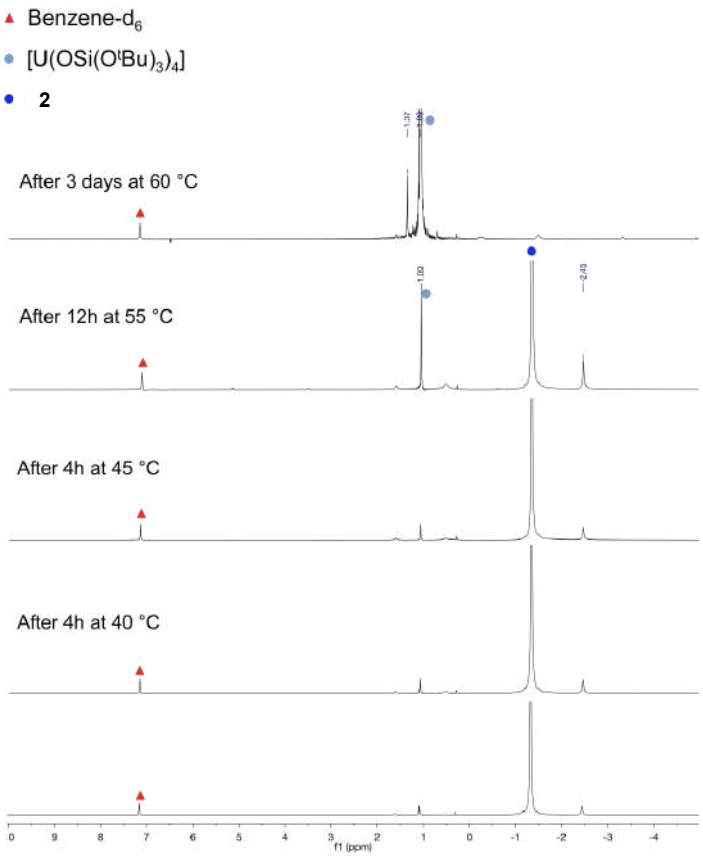

Reaction of [Cs{[U(OSi(O^{t}Bu)$_3$)$_3$]$_2$(μ-^{13}CN)(μ-O)}], 2 with MeOTf

Figure S7. ^{1}H NMR (400 MHz, benzene-d$_6$, 298 K) of the reaction mixture 1 hour after the addition of MeOTf to **2** at room temperature.

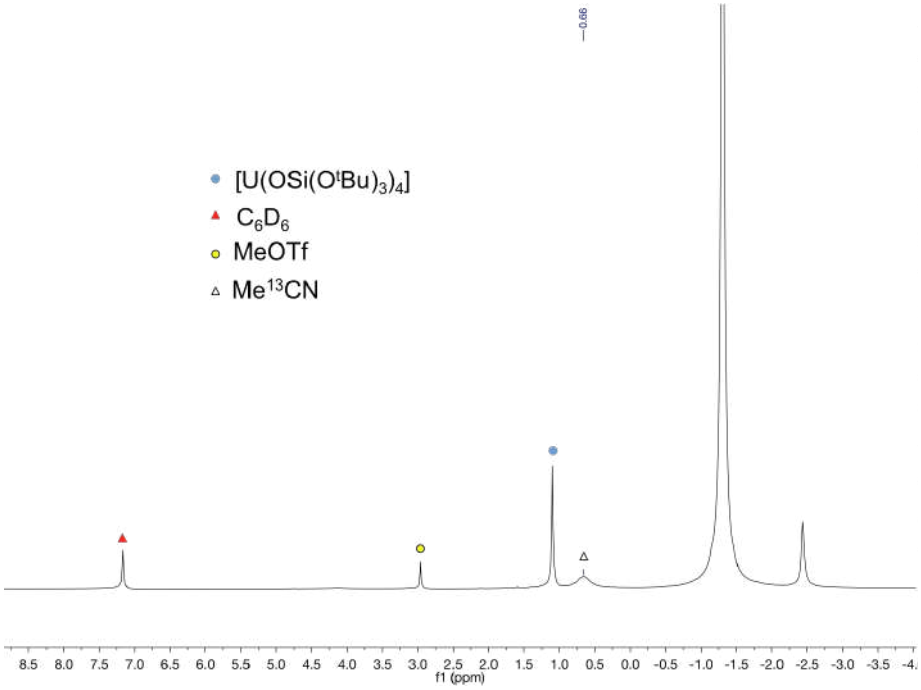

Figure S8. ^{13}C NMR (400 MHz, benzene-d$_6$, 298 K) of reaction mixture between ^{13}C-**2** and MeOTf, after 1h at room temperature.

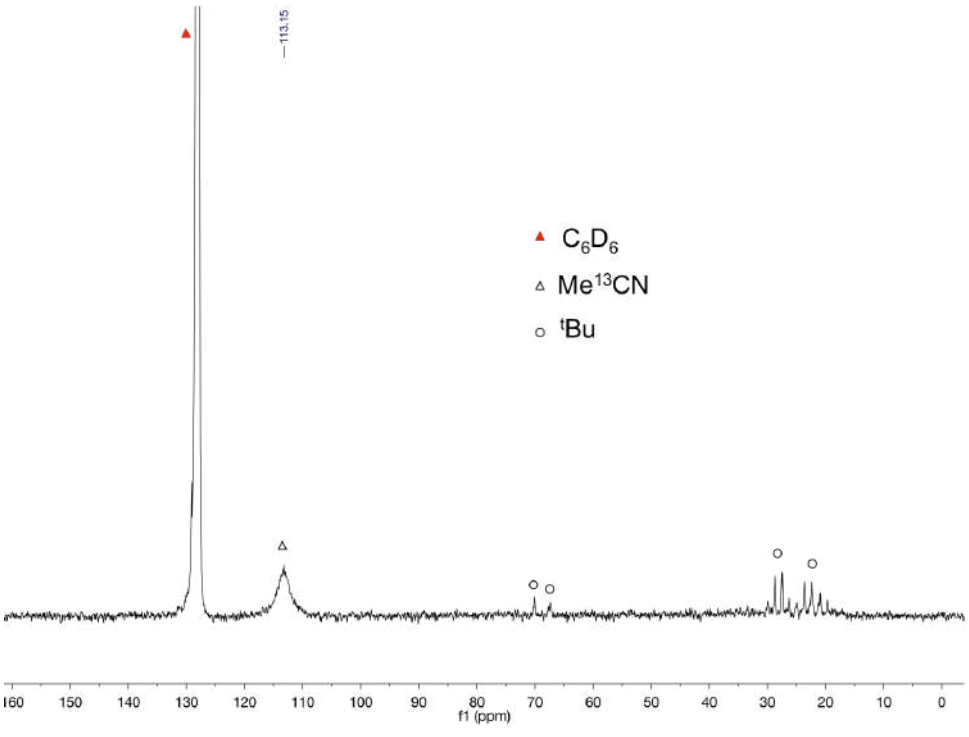

Figure S9. ^{1}H NMR (400 MHz, benzene-d_6, 298 K) of reaction mixture between **2** and MeOTf, after heating at 50 °C for 3 days.

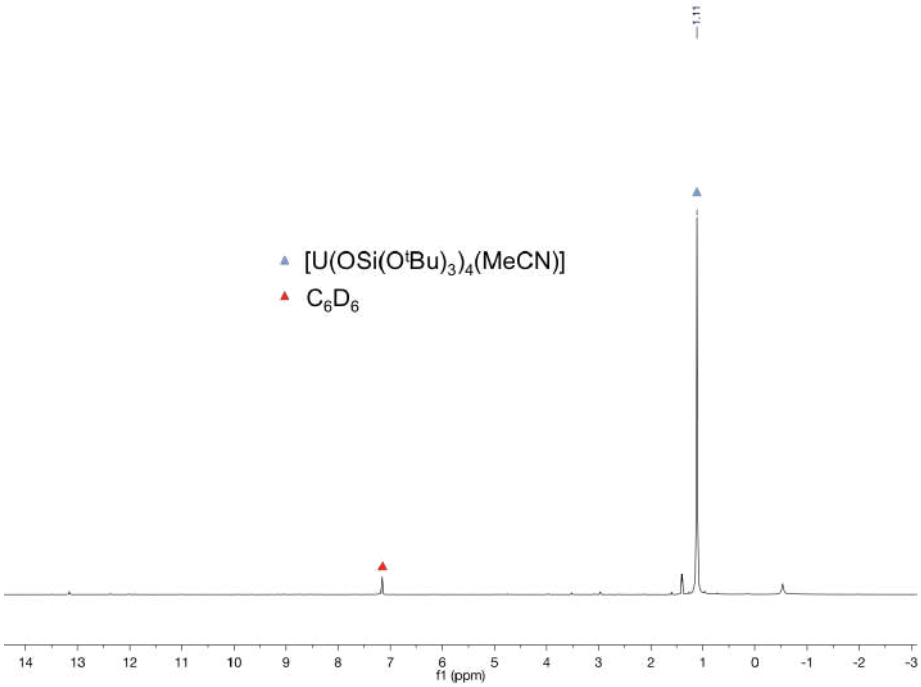

Figure S10. ^{13}C NMR (400 MHz, benzene-d_6, 298 K) of reaction mixture between ^{13}C-**2** and MeOTf, after heating at 50 °C for 3 days.

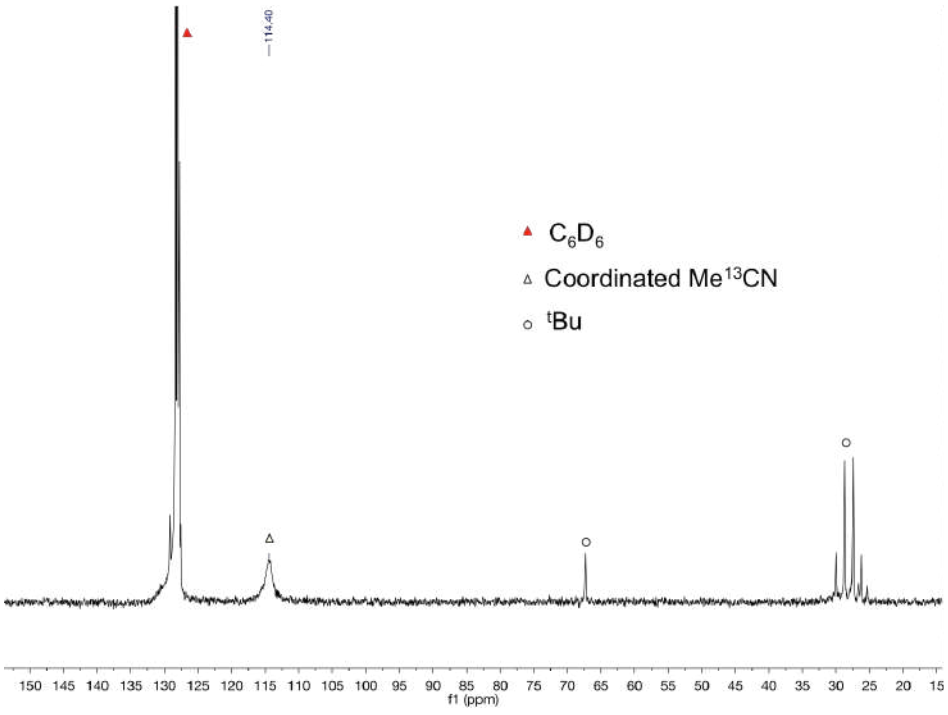

Reaction of [Cs{[U(OSi(O^{t}Bu)$_3$)$_3$]$_2$(μ-^{13}CN)(μ-O)}], 2 with Me$_3$SiI

Figure S11. ^{1}H NMR (400 MHz, benzene-d$_6$, 298 K) immediately after addition of Me$_3$SiI to **2** at room temperature showing the complete disappearance of the signals of **2** and the appearance of a new species (probably a oxo iodide intermediate).

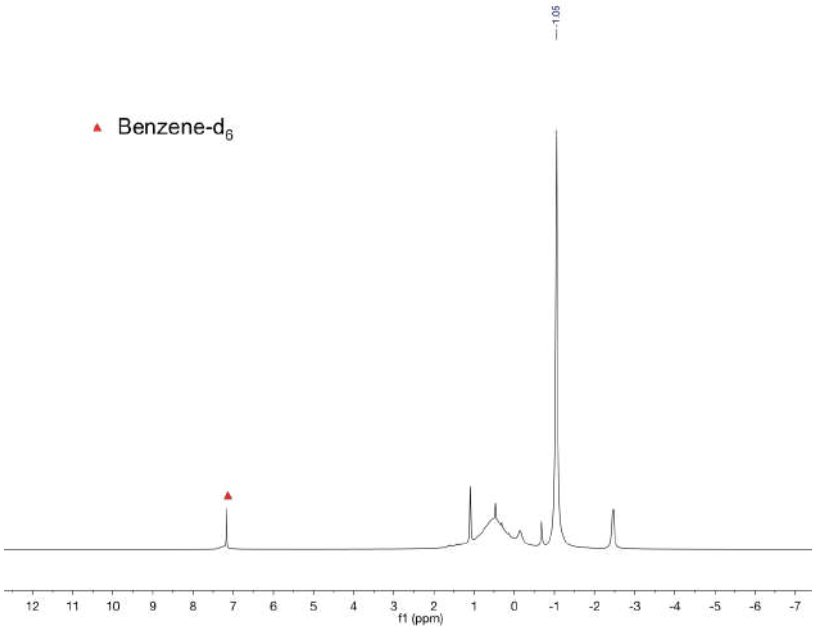

Figure S12. ^{13}C NMR (400 MHz, benzene-d$_6$, 298 K) immediately after addition of Me$_3$SiI to **2** at room temperature.

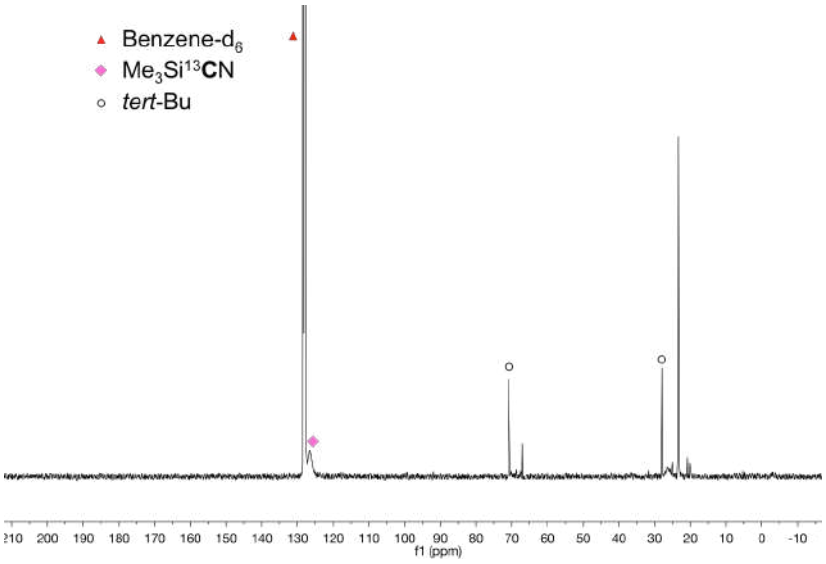

Figure S13. ^{1}H NMR (400 MHz, benzene-d_6, 298 K) 48 h after the addition of Me_3SiI to **2**, at room temperature showing that ligand scrambling has occurred.

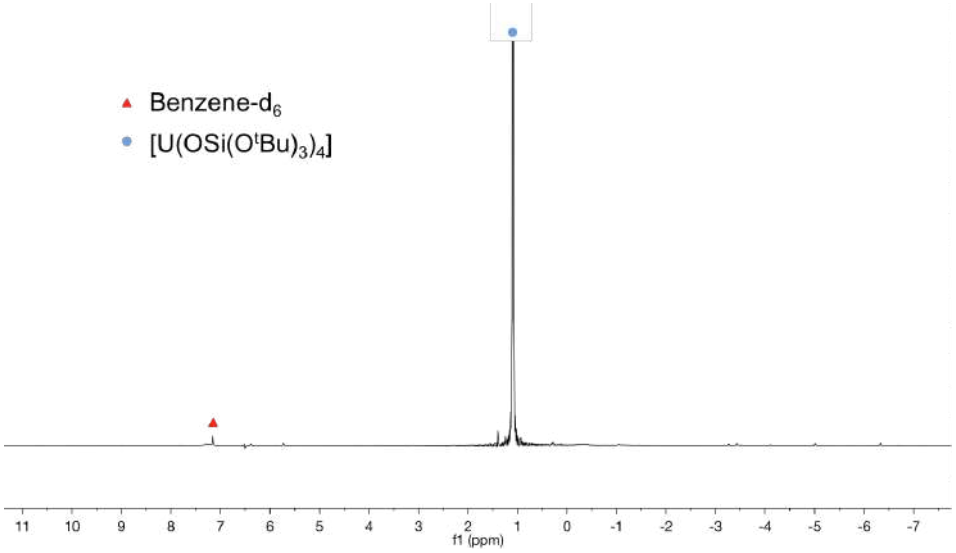

Figure S14. ^{13}C NMR (400 MHz, benzene-d_6, 298 K) 48 h after the addition of Me_3SiI to **2**, at room temperature.

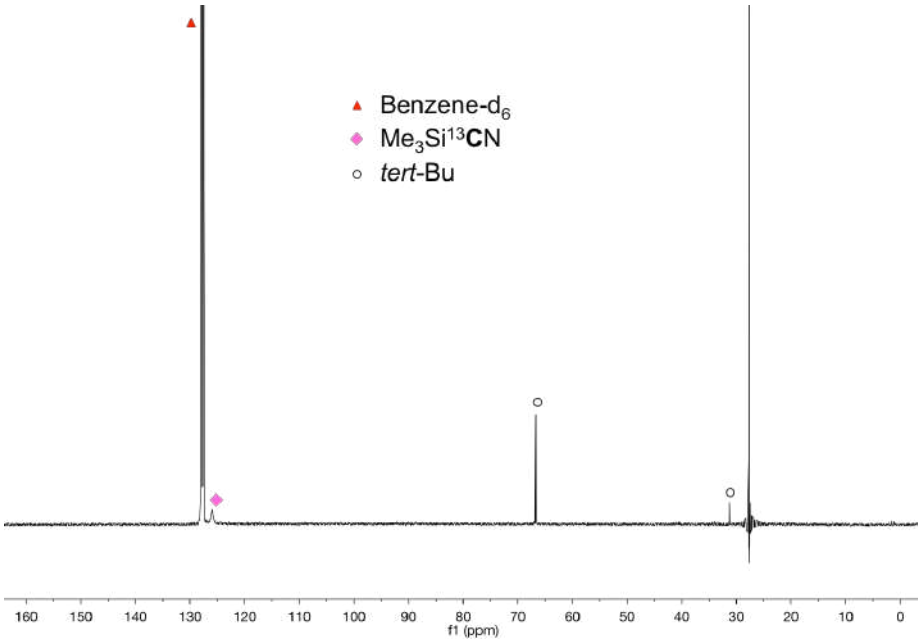

Figure S15. ^{13}C NMR (400 MHz, benzene-d_6, 298 K, O1P = 700) 48 h after the addition of Me_3SiI to **2**, at room temperature showing the disappearance of the signal assigned to ^{13}CN.

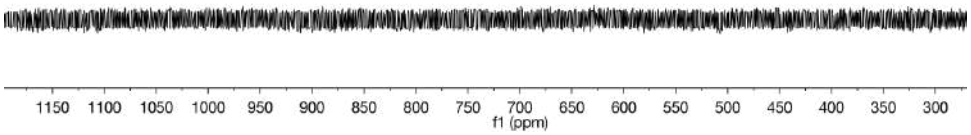

Reaction of $[Cs\{[U(OSi(O^tBu)_3)_3]_2(\mu\text{-}N)\}]$, 1 with 1 eq of MeOTf

Figure S16. ^1H NMR (400 MHz, toluene-d_8, 298 K) right after addition of 1 equivalent of MeOTf to the **1** at room temperature.

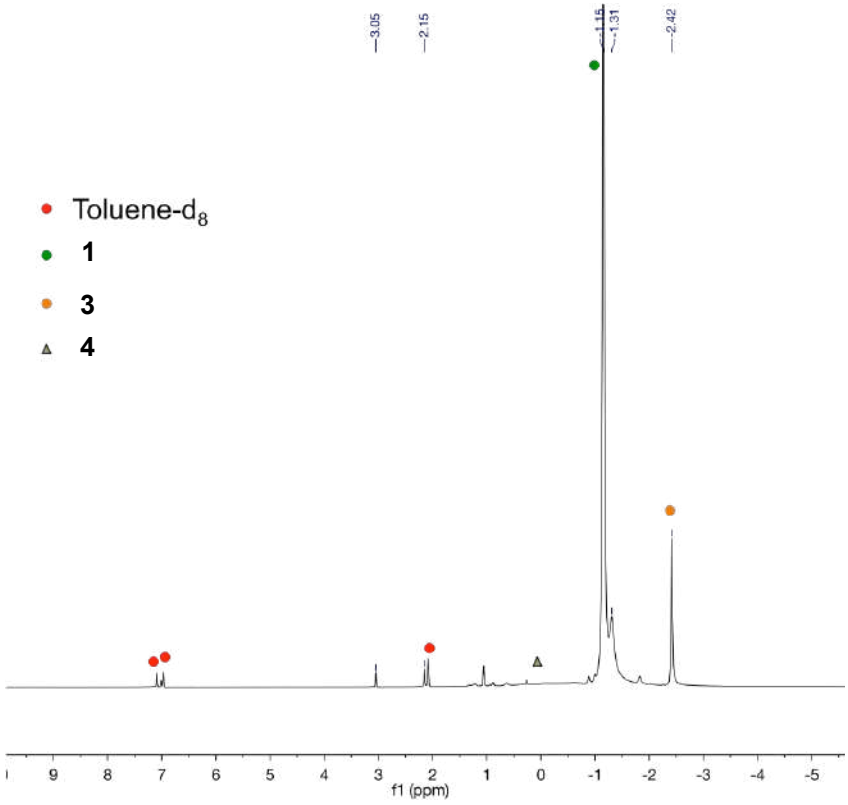

Figure S17. ^{1}H NMR (400 MHz, toluene-d_8, 298 K) 24 h after the addition of 1 equivalent of MeOTf to **1** at room temperature.

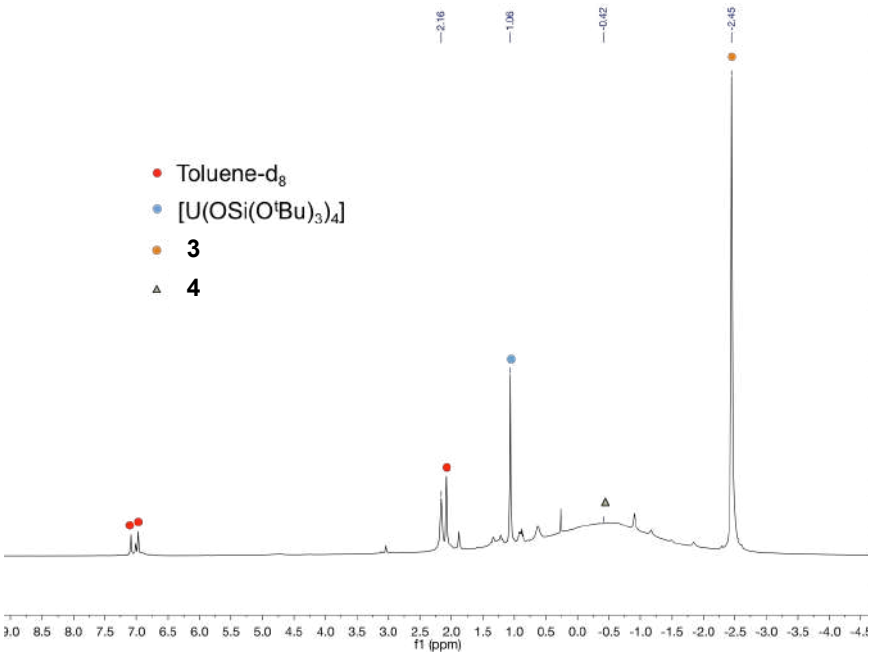

Reaction of complex 1 with 2 eq of MeOTf

Figure S18. ^{1}H NMR (400 MHz, toluene-d_8, 298 K) immediately after addition of 2 equivalents of MeOTf to the complex **1** at room temperature.

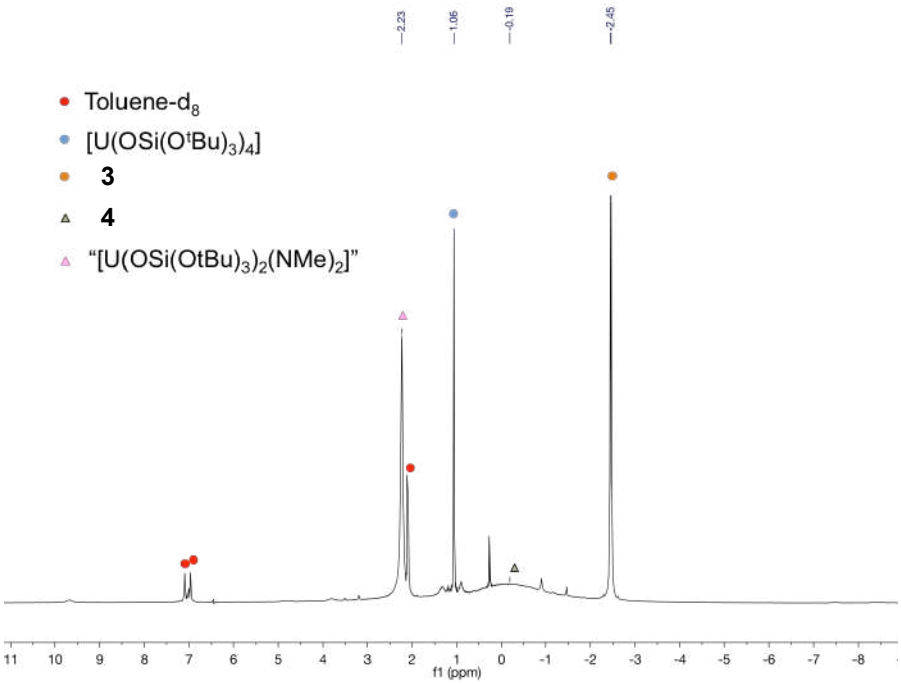

Figure S19. ^{1}H NMR (400 MHz, toluene-d_8, 298 K) of **3**.

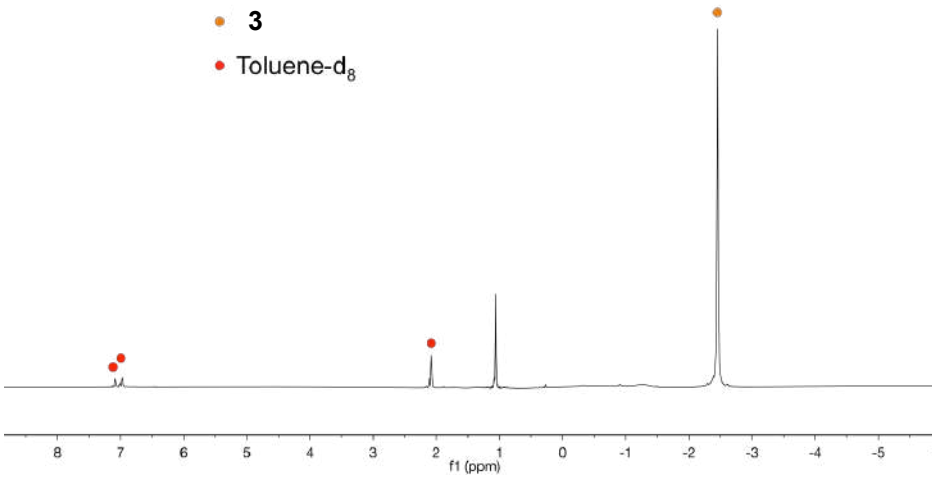

Figure S20. a) ^{1}H NMR (400 MHz, toluene-d_8, 298 K) of the supernatant from the reaction of **1** with two equiv. of MeOTf after removal of crystals of complex **3**; b) of the same solution after 12h. The broad peak assigned to complex **4** decreases with time while the signals at 2.19 and 1.06 ppm, increase with time.

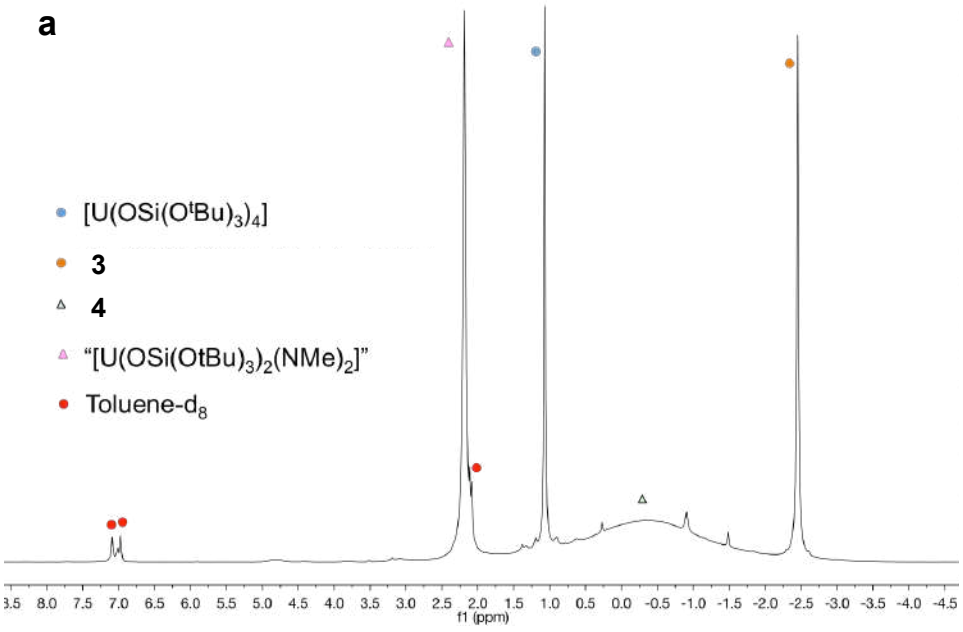

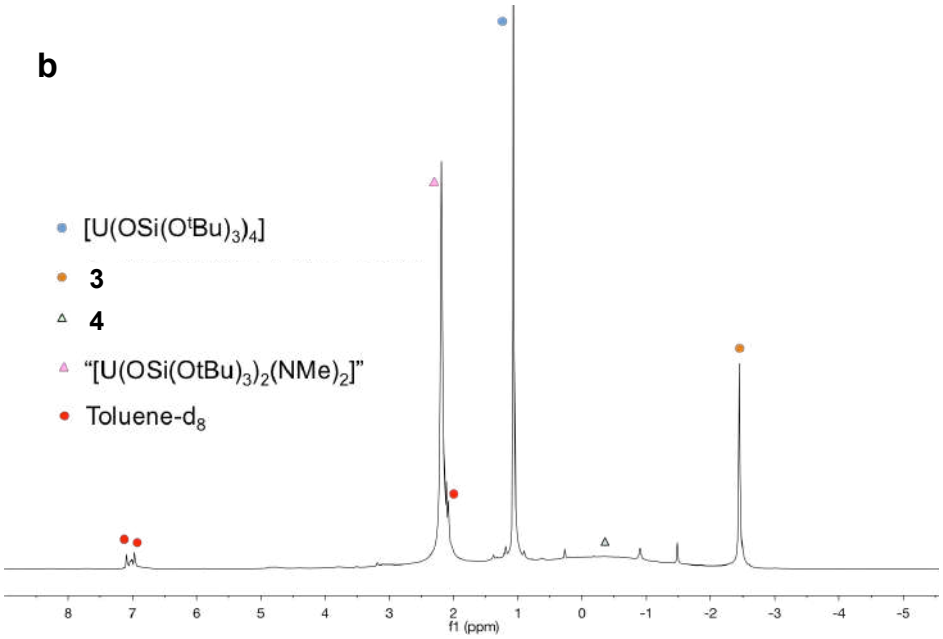

2. Crystallographic data

X-ray experimental part:

The diffraction data of **3** were measured at low temperature [120(2) K] using Mo K_a radiation on a Bruker APEX II CCD diffractometer equipped with a kappa geometry goniometer. The datasets were reduced by EvalCCD[1] and then corrected for absorption.[2] The data collection of compounds **2** and **4** were measured at low temperature [140(2) K] using Cu K_a radiation on an Agilent Technologies SuperNova dual system in combination with an Atlas CCD detector. The data reduction was carried out by Crysalis PRO.[3] The solutions and refinements were performed by SHELX.[4] The crystal structures were refined using full-matrix least-squares based on F^2 with all non hydrogen atoms anisotropically defined. Hydrogen atoms were placed in calculated positions by means of the "riding" model.

In order to obtain reasonable geometric and displacement parameters several restraints (EADP instruction) and constraints (ISOR, SIMU, SADI instructions) were applied to the light atoms of the crystal structures. The split model combined with some restrains (SADI, SIMU cards) was used to treat the severe disorder found in some *tert*-Butyl moieties (compound **3**).

The X-ray crystallographic data for the structures of compounds **2**–**4** reported in this article have been deposited in the Cambridge Crystallographic Data Centre under (CCDC), under deposition nos. CCDC 1487352 (**2**), 1487350 (**3**) and 1487351 (**4**).

These data can be obtained free of charge from The Cambridge Crystallographic Data Centre (www.ccdc.cam.ac.uk/data_request/cif).

Table S1: X-Ray crystallographic data.

	2	**3.$(C_7H_8)_2$**	**4**
Formula	$C_{73}H_{162}CsNO_{25}Si_6U_2$	$C_{88}H_{178}Cs_2F_6O_{30}S_2Si_6U_2$	$C_{74}H_{168}N_2O_{24}Si_6U_2$
Crystal size (mm)	0.51 x 0.39 x 0.34	0.71 x 0.34 x 0.28	0.19 x 0.17 x 0.11
cryst syst	Triclinic	Triclinic	Triclinic
space group	*P*-1	*P*-1	*P*-1
volume ($Å^3$)	5215.07	3112.8(7)	5227.07(18)
a (Å)	13.9709(3)	13.7314(14)	13.9896(3)
b (Å)	16.4278(3)	14.5926(13)	14.2811(3)
c (Å)	25.4347(5)	17.991(3)	30.3880(6)
α (deg)	72.1166(18)	107.671(12)	90.5624(16)
β (deg)	86.4115(16)	104.975(9)	102.3095(17)
γ (deg)	70.0134(18)	103.913(8)	117.363(2)
Z	2	1	2
formula weight (g/mol)	2231.55	2804.84	2114.70
density (g cm^{-3})	1.421	1.496	1.344
absorption coefficient (mm^{-1})	12.512	3.338	9.804
F(000)	2260	1410	2172
temp (K)	140(2)	120(2)	140(2)
total no. reflections	38700	67583	39643
unique reflections [R(int)]	21112 [0.0257]	23049 [0.0565]	21084 [0.0353]
Final R indices	R1 = 0.0531,	R1 = 0.0467,	R1 = 0.0688,

[I > 2σ(I)]	wR2 = 0.1421	wR2 = 0.0976	wR2 = 0.1668
Largest diff. peak and hole ($e.A^{-3}$)	4.488 and -3.956	3.389 and -3.968	9.429 and -4.678
GOOF	1.023	1.111	1.068

Computational Details

Geometry optimizations were performed with the Gaussian09[5] suite of programs (revision D.02) using the Becke's 3-parameter hybrid functional,[6] combined with the non-local correlation functional provided by Perdew/Wang.[7] Since in this study we have considered the full system (including the counter-cation), a more sophisticated combination of basis sets was applied in order to obtain reasonable computational times without losing accuracy. This "cabbage-like" computational protocol was previously described in details and found to give consistent and reliable results in previous studies by our group on a related type of reactivity.[8] In particular, for the uranium atoms the quasi-relativistic energy-consistent 5f-in-core pseudopotentials for the fixed oxidation states III, IV, and V were used, retrieved from Stuttgart-Cologne group's database, in combination with their corresponding adapted energy-optimized valence basis sets (of double-zeta quality) and augmented by a *f* polarization function.[9]For cesium and silicon atoms the corresponding effective core potentials were chosen in combination with their adapted basis sets, and augmented by an extra set of polarisation function for the latter.[10] For the rest atoms that belong to the first coordination sphere the 6-31G(d,p) basis set is used, as well as for the substrates CO and MeOTf.[11] For all the remaining atoms, meaning the carbon and the hydrogen atoms of the ligands, the minimal 3-21G basis set was applied.[12] All stationary points have been identified as either minimum (Nimag=0) or transition states (Nimag=1) by performing analytical vibrational frequencies. Intrinsic Reaction Paths (IRPs) were traced from the various transition structures to obtain the connected intermediates.[13]

[1] A. J. M. Duisenberg, L. M. J. Kroon-Batenburg, A. M. M. Schreurs, *J. Appl. Crystallogr.* **2003**, *36*, 220-229.
[2] R. H. Blessing, *Acta Crystallogr., Sect. A* **1995**, *51*, 33-38.
[3] CrysAlisPro CCD, CrysAlisPro RED , ABSPACK, CrysAlis PRO. Agilent Technologies, release 1.171.3843, Yarnton, England., **2015**.
[4] G. M. Sheldrick, *Acta Crystallogr., Sect. A* **2008**, *64*, 112-122.
[5] R. Gaussian 09.
[6] A. D. Becke, *J. Chem. Phys.* **1993**, *98*, 5648-5652.
[7] J. P. Perdew, Y. Wang, *Phys.Rev. B* **1992**, *45*, 13244-13249.
[8] a) V. Mougel, C. Camp, J. Pecaut, C. Coperet, L. Maron, C. E. Kefalidis, M. Mazzanti, *Angew. Chem. Int. Ed. Engl.* **2012**, *51*, 12280-12284; b) O. Cooper, C. Camp, J. Pecaut, C. E. Kefalidis, L. Maron, S. Gambarelli, M. Mazzanti, *J. Am. Chem. Soc.* **2014**, *136*, 6716-6723; c) A.-C. Schmidt, F. W. Heinemann, C. E. Kefalidis, L. Maron, P. W. Roesky, K. Meyer, *Chem. Eur. J.* **2014**, *20*, 13501-13506; d) C. Camp, L. Chatelain, C. E. Kefalidis, J. Pecaut, L. Maron, M. Mazzanti, *Chem. Commun.* **2015**, *51*, 15454-15457.
[9] a) A. Moritz, X. Cao, M. Dolg, *Theor. Chem. Acc.* **2007**, *118*, 845-854; b) A. Moritz, M. Dolg, *Theor. Chem. Acc.* **2008**, *121*, 297-306.
[10] a) A. Bergner, M. Dolg, W. Kuchle, H. Stoll, H. Preuss, *Mol. Phys.* **1993**, *80*, 1431-1441; b) A. Hollwarth, M. Bohme, S. Dapprich, A. W. Ehlers, A. Gobbi, V. Jonas, K. F. Kohler, R. Stegmann, A. Veldkamp, G. Frenking, *Chem. Phys. Lett.* **1993**, *208*, 237-240.
[11] a) Ditchfie.R, W. J. Hehre, J. A. Pople, *J. Chem. Phys.* **1971**, *54*, 724-728; b) P. C. Hariharan, J. A. Pople, *Theoretica Chimica Acta* **1973**, *28*, 213-222; c) W. J. Hehre, Ditchfie.R, J. A. Pople, *J. Chem. Phys.* **1972**, *56*, 2257-2261.
[12] J. S. Binkley, J. A. Pople, W. J. Hehre, *J. Am. Chem. Soc.* **1980**, *102*, 939-947.
[13] a) C. Gonzalez, H. B. Schlegel, *J. Chem. Phys.* **1989**, *90*, 2154-2161; b) C. Gonzalez, H. B. Schlegel, *J. Phys. Chem.* **1990**, *94*, 5523-5527.

APPENDIX 3

Supporting information for Chapter 4

1. NMR Spectroscopic data

NMR data for complex 2

Figure S1. ^{1}H NMR (400 MHz, tol-d_8, 298 K) of the crude reaction mixture before (bottom) and after (top) addition of 1 atm H_2 to a toluene solution of **1**.

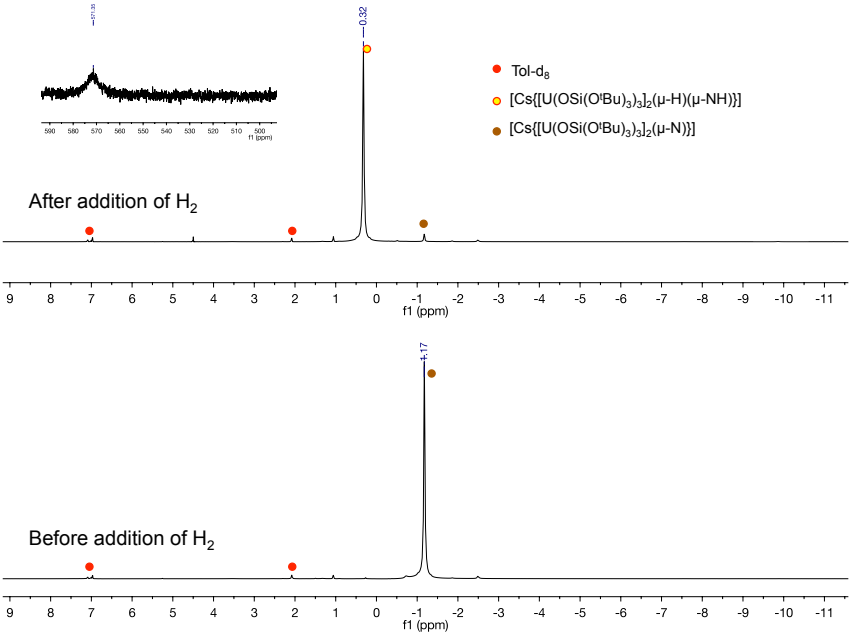

Figure S2. ^{1}H NMR (400 MHz, tol-d_8, 298 K) of the crude reaction mixture before (bottom) and after (top) addition of 1 atm D_2 to a toluene solution of **1**.

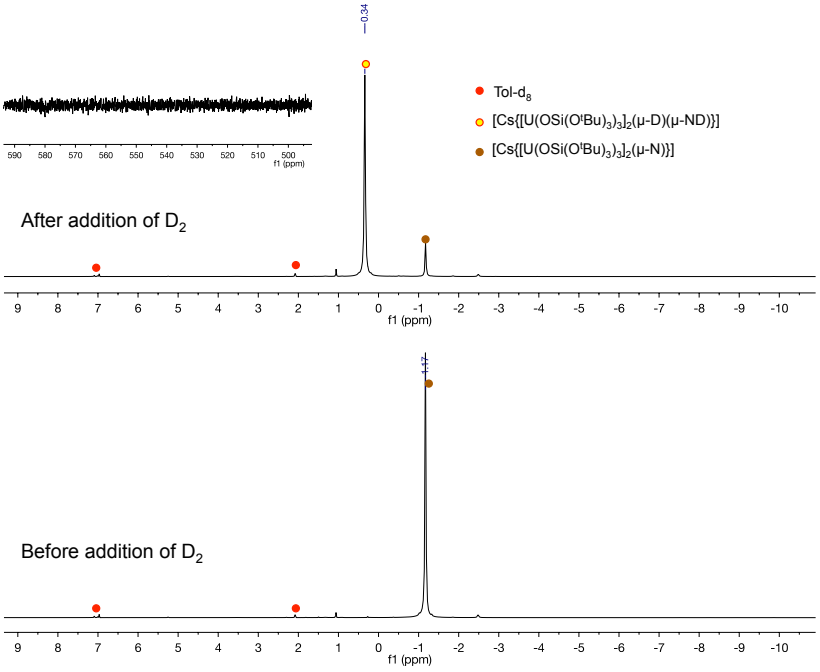

Figure S3. ^{1}H NMR (400 MHz, tol-d_8, 298 K) of the crude reaction mixture of **1** reacted with 1 atm H_2, at different times after removal of the H_2 headspace.

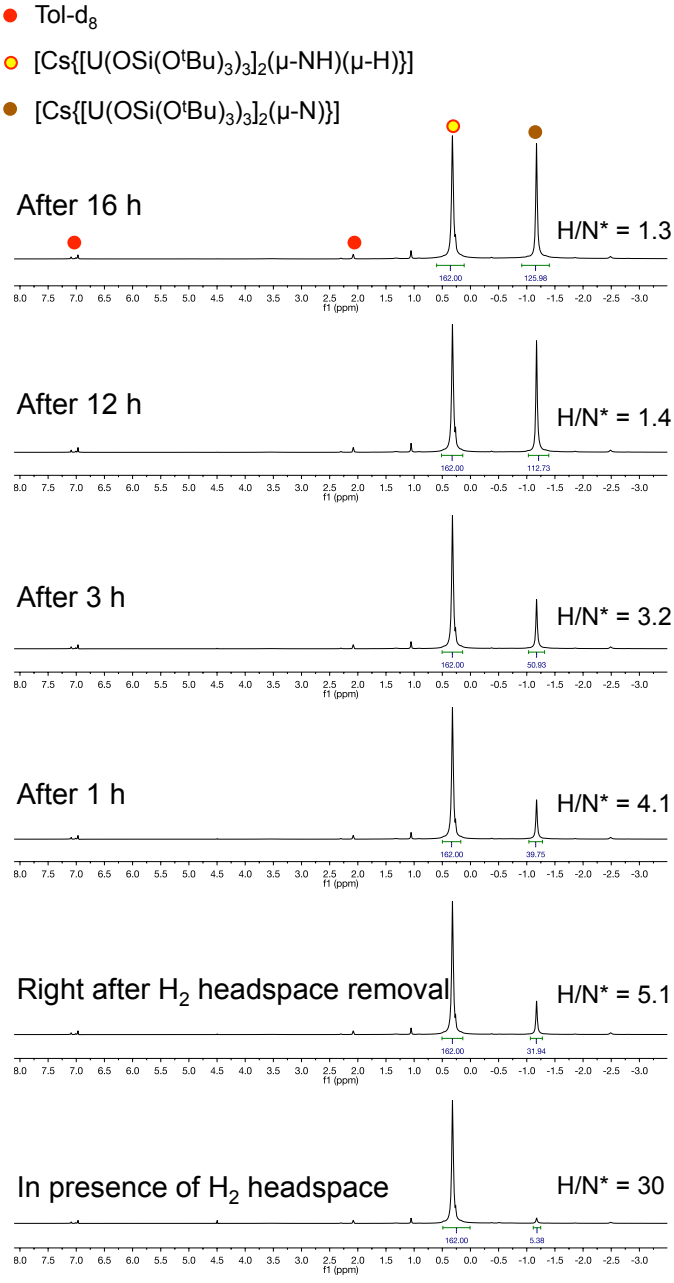

* Ratio area Hydride/Nitride

Figure S4. ^{1}H NMR (400 MHz, tol-d_8, 298 K) of the crude reaction mixture of **1** reacted with 1 atm H_2 (without removing the headspace).

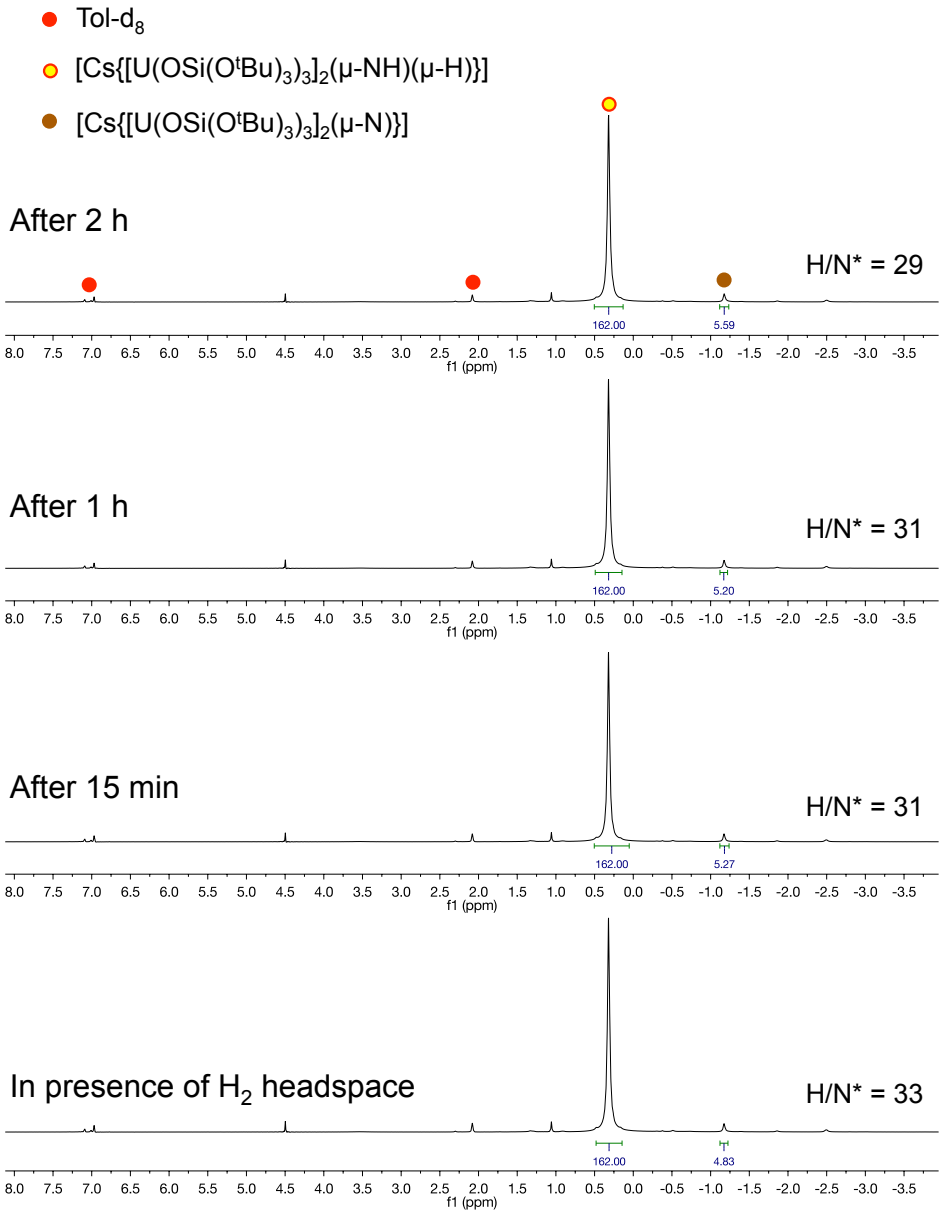

* Ratio area Hydride/Nitride

Figure S5. ^{1}H NMR (400 MHz, tol-d_8, 298 K) of the isolated crystals of **2** after filtration under vacuum for a few minutes (sample used for IR spectroscopy).

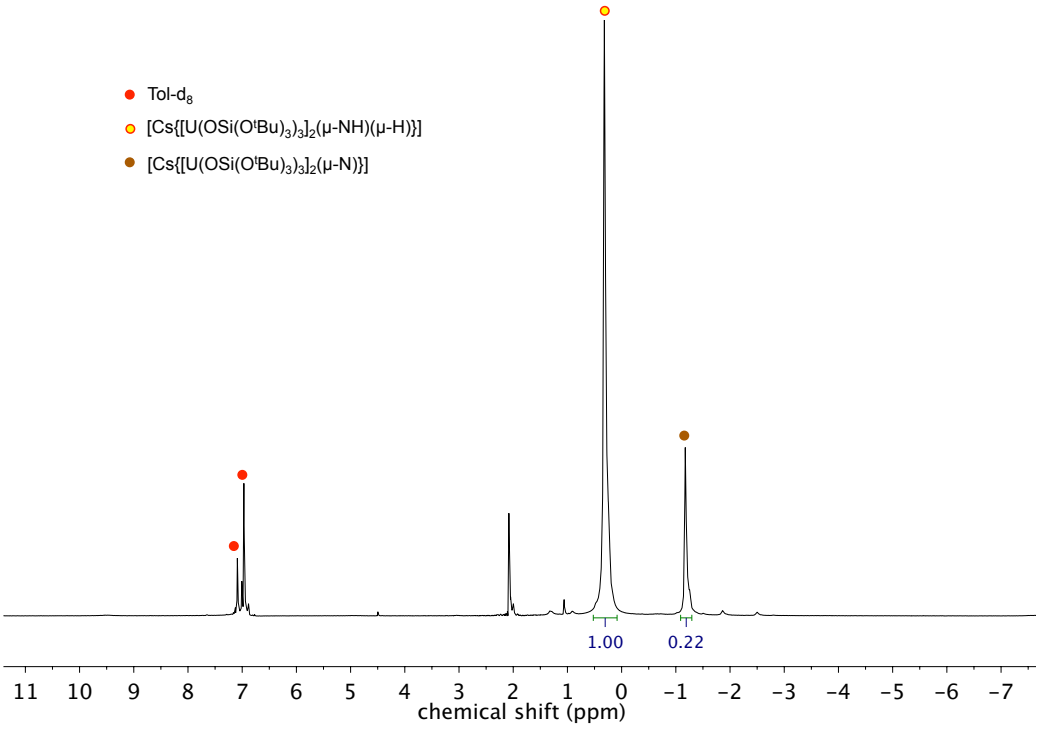

Figure S6. ^{1}H NMR (400 MHz, tol-d_8, 298 K) of the crude reaction mixture of **1** with 1 atm H_2, after leaving the solid residue under vacuum for 1 h.

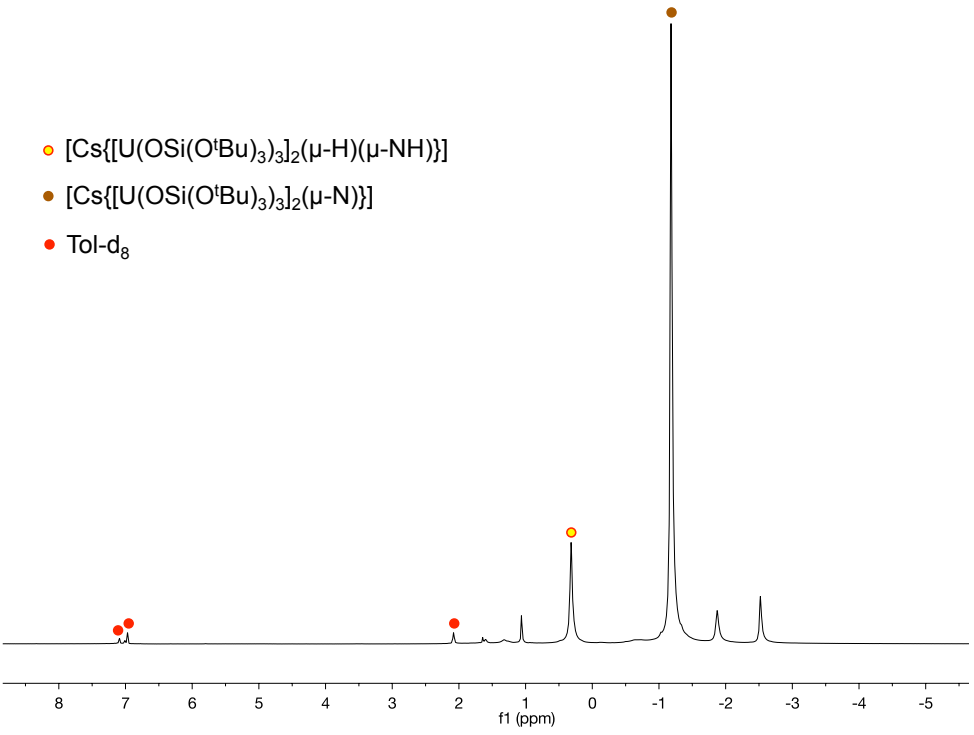

NMR data for complex 3

Figure S7. ^{1}H NMR (400 MHz, tol-d_8, 298 K) of the crude reaction mixture before (bottom) and after (top) addition of 1 equivalent of MeCN to complex **2**.

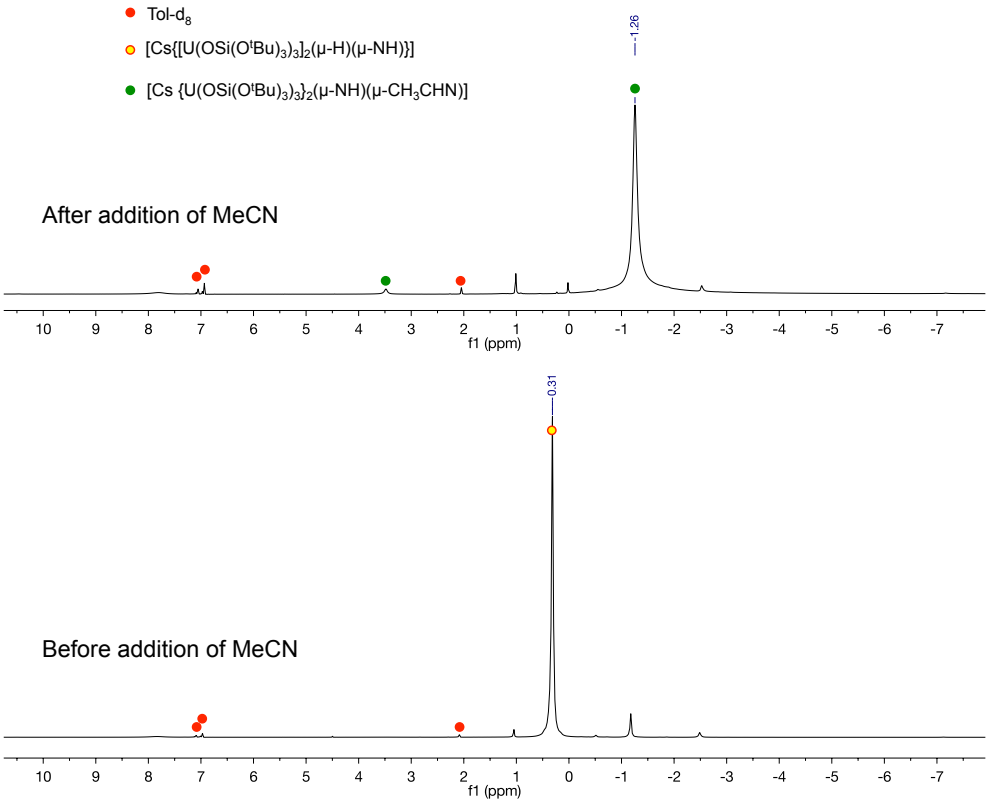

Figure S8. ^{13}C NMR (400 MHz, tol-d_8, 298 K) of the crude reaction mixture of complex **2** with 1 equivalent of MeCN.

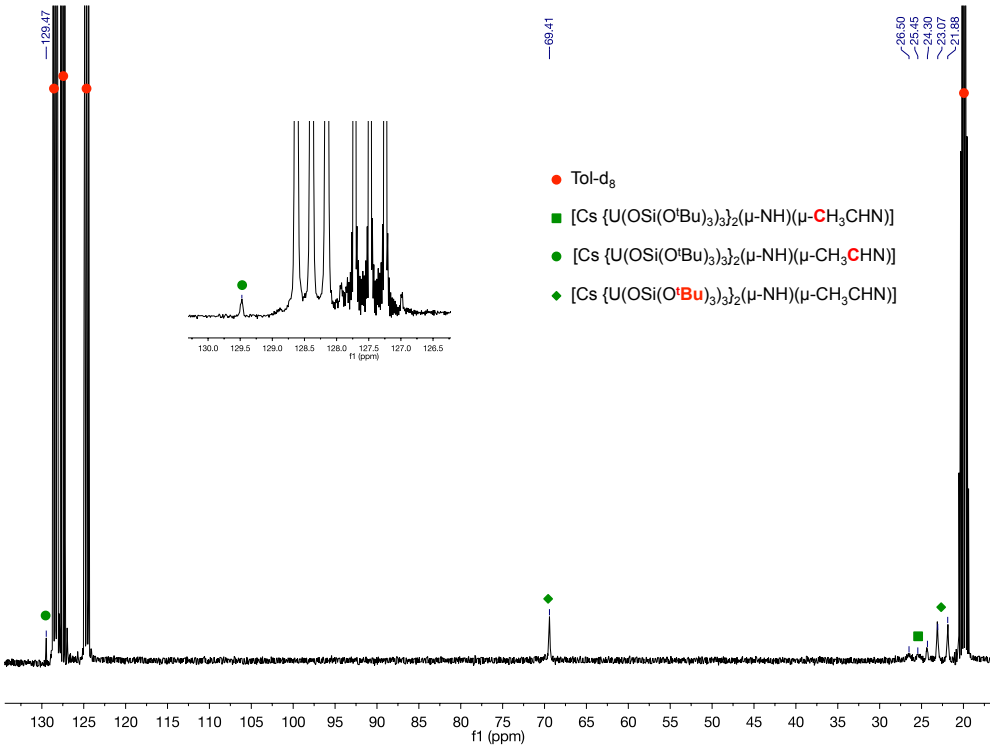

Figure S9. ^{1}H NMR (400 MHz, tol-d_8, 298 K) of crystals of complex **3**.

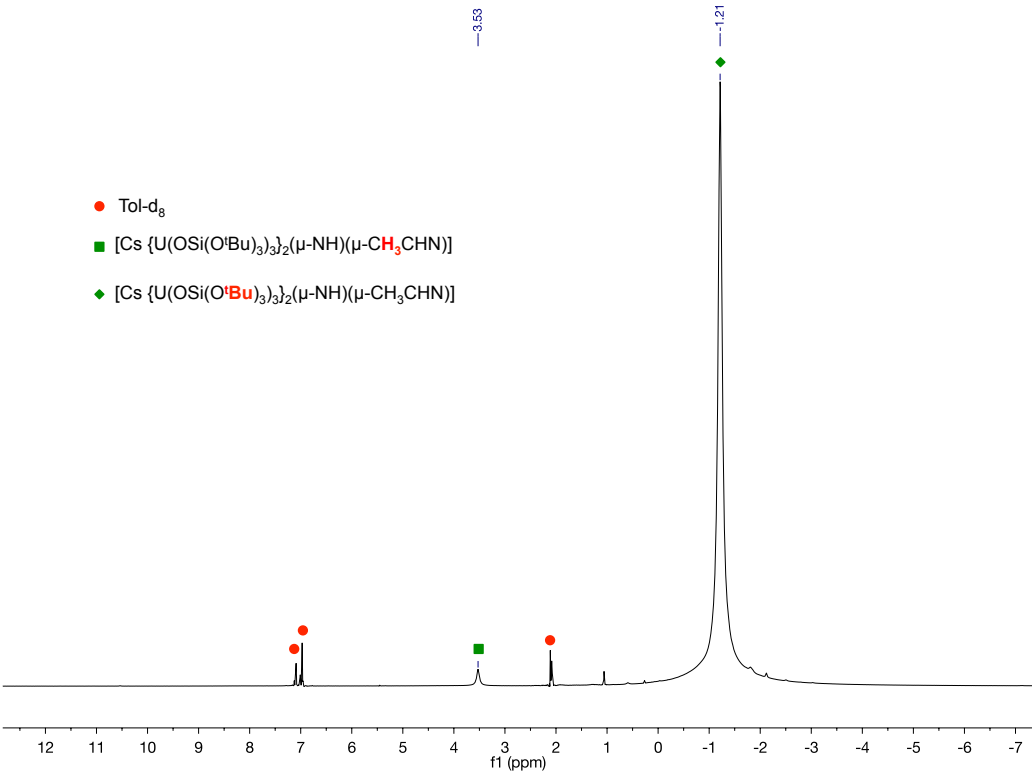

Figure S10. ^{13}C NMR (400 MHz, tol-d_8, 298 K) of crystals of complex **3**.

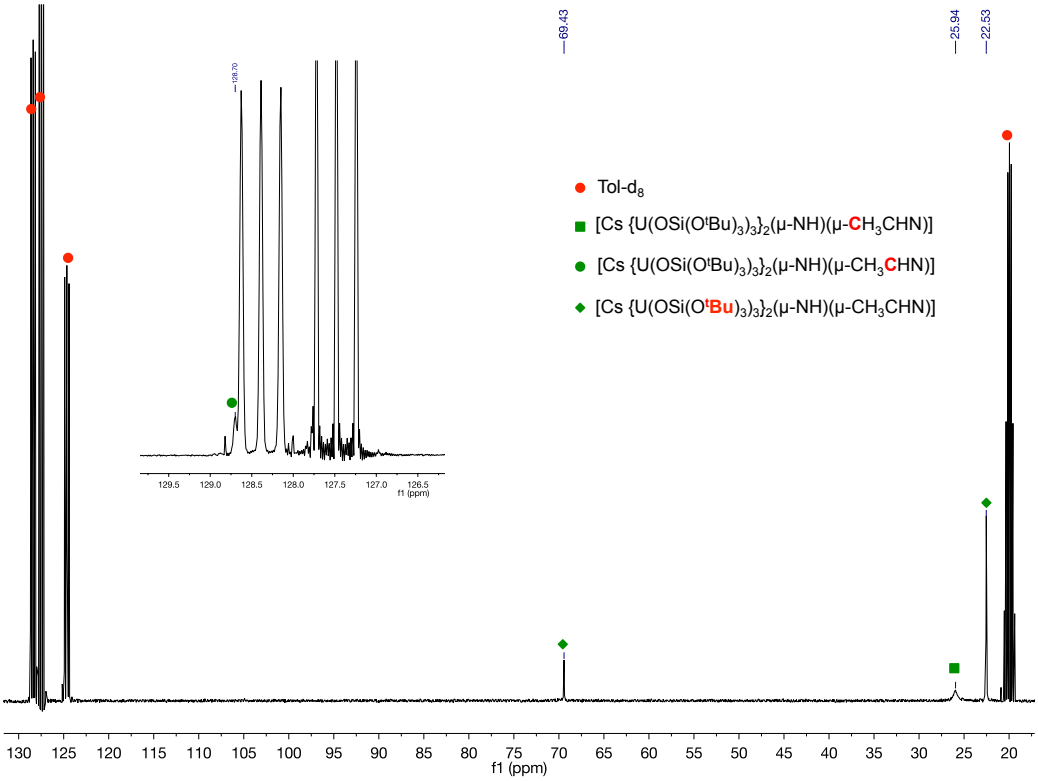

NMR data for complex 4

Figure S11. ^{1}H NMR (400 MHz, tol-d_8, 298 K) of the crude reaction mixture of complex **2** with 2 CO_2.

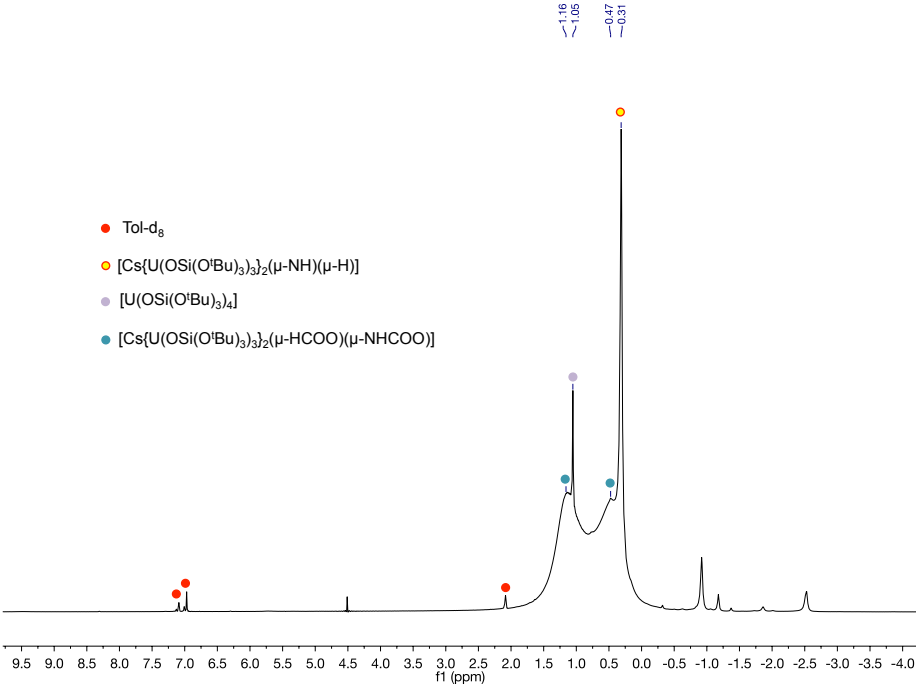

Figure S12. ^{1}H NMR (400 MHz, tol-d_8, 298 K) of the crude reaction of [Cs(μ-NH)(μ-H){U(OSi(O^{t}Bu)$_3$)$_3$}$_2$], **2** (bottom) and of [Cs(μ-ND)(μ-D){U(OSi(O^{t}Bu)$_3$)$_3$}$_2$], **D_2-2** (top) with 2 CO_2.

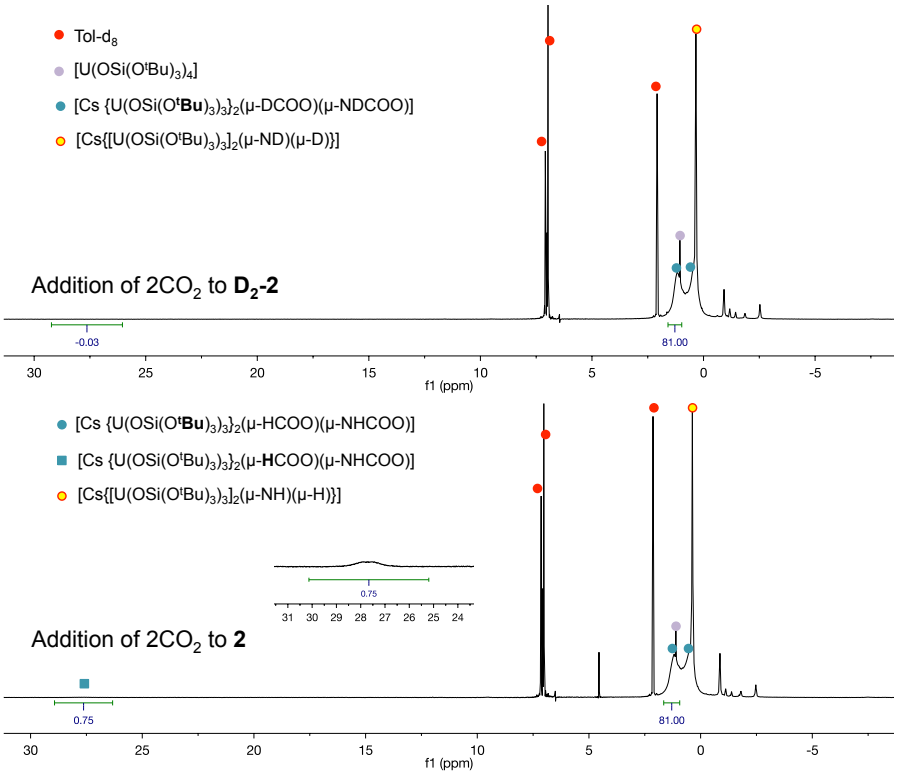

Figure S13. ^{13}C NMR (400 MHz, tol-d_8, 298 K) of crystals of complex **4**.

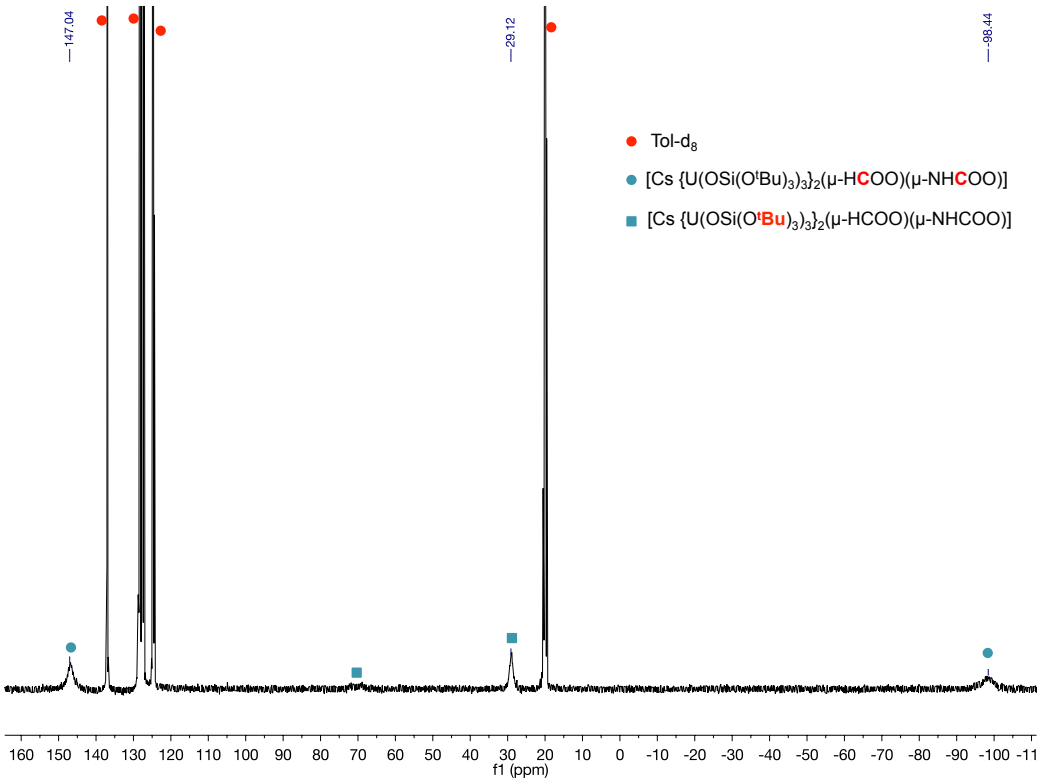

Figure S14. ^{1}H NMR (400 MHz, tol-d_8, 298 K) of the crude reaction mixture after the successive addition of CO_2 to complex **2**.

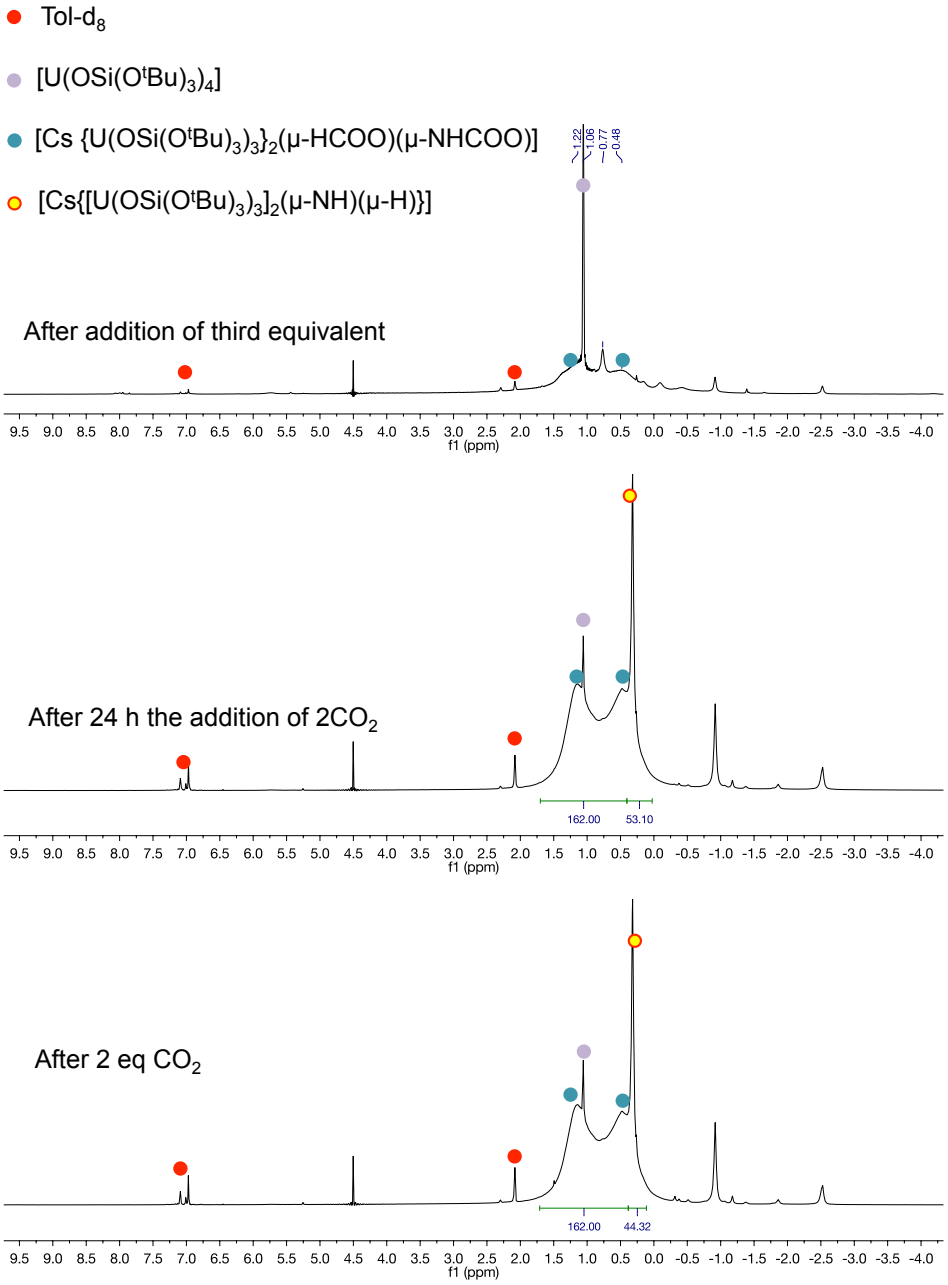

2. IR spectra

Figure S15. Infrared spectra of **1** and of a mixture of **1** and **2**.

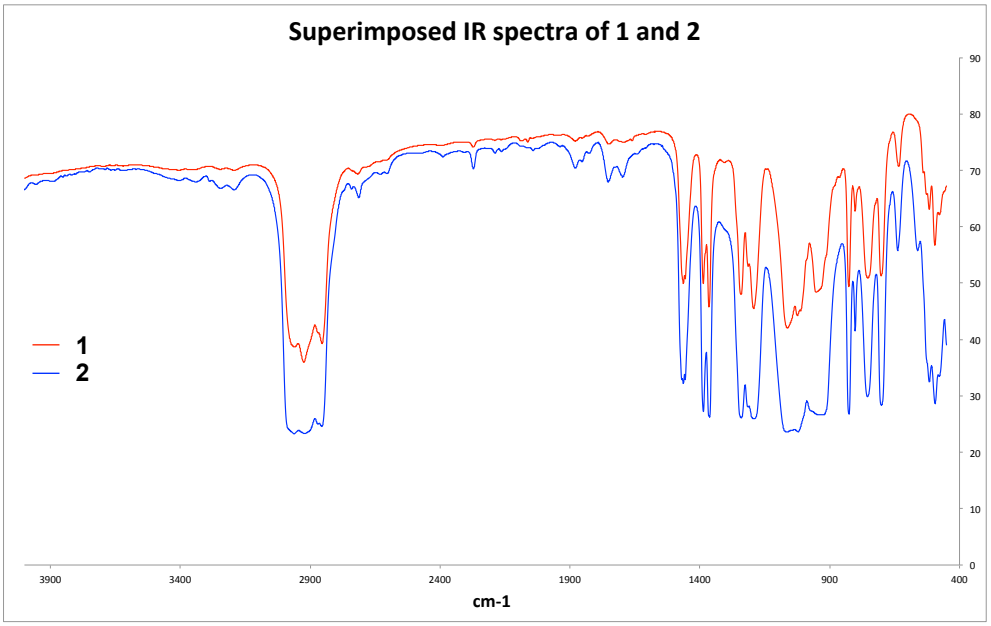

Figure S16. Infrared spectrum of **3**.

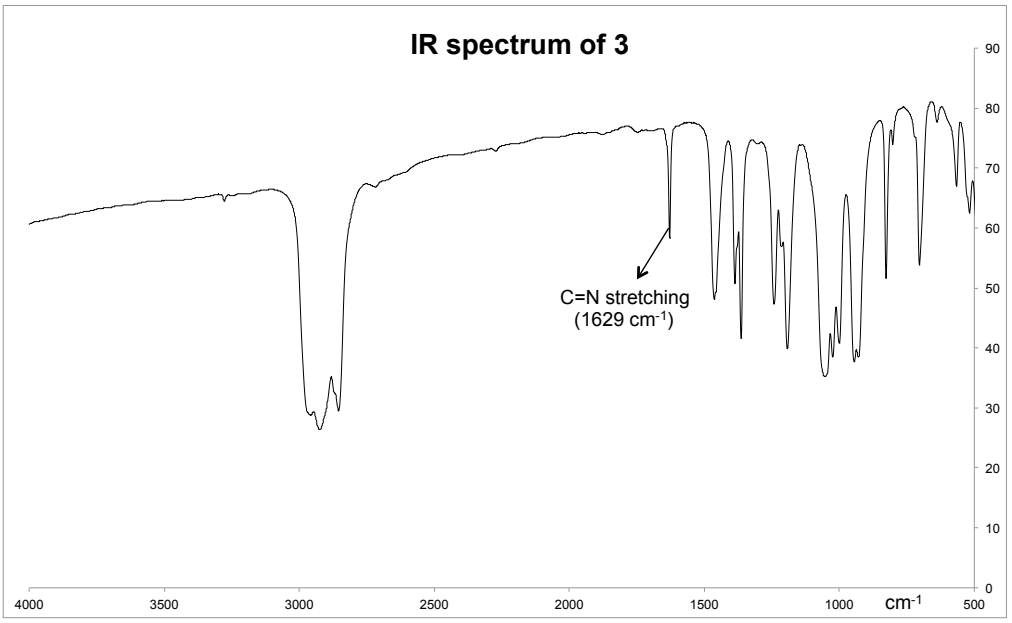

Figure S17. Infrared spectra of **4** and **^{13}C-4**.

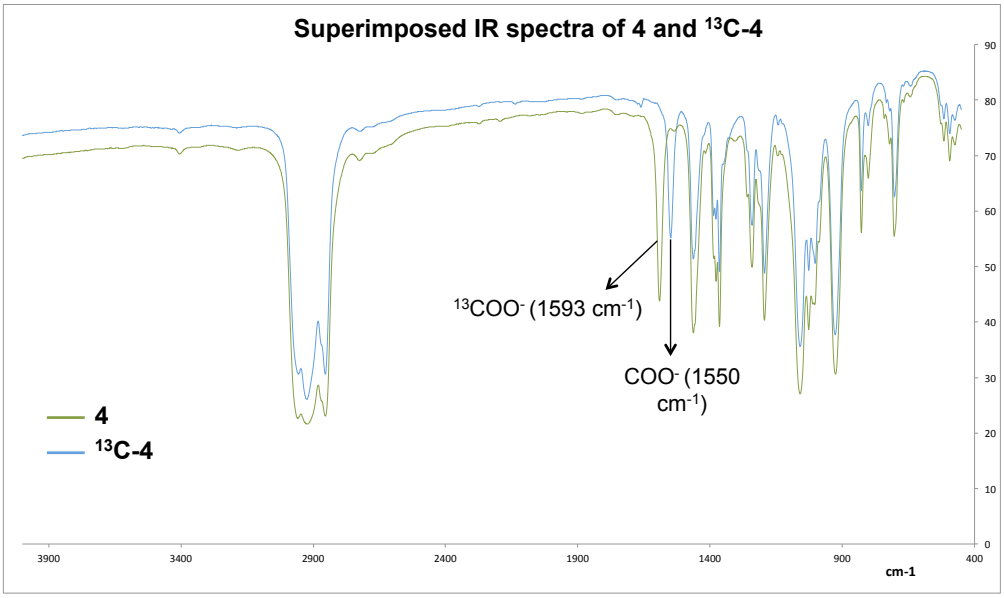

3. X-ray Crystallography

CCDC 1814913, 1587291, 1587292 and 1587293 contain the supplementary crystallographic data for the structures of complexes **2**, **3**, **4** and **1.2** respectively.

Bragg-intensities were collected at 140(1) K, using Mo*K*α radiation for **2** and Cu*K*α radiation for **4**, on a Rigaku SuperNova dual system diffractometer equipped with an Atlas CCD detector. The datasets were reduced and corrected for absorption, with the help of a set of faces enclosing the crystals as snugly as possible, with CrysAlis^{Pro}.[1]

The X-ray diffraction data of **3** were measured at 120(2) K using Mo*K*α radiation on a Bruker APEX II CCD kappa diffractometer. The dataset was reduced by EvalCCD[2] and then corrected, by modelling an empirical transmission surface as sampled by multiple symmetry-equivalent and/or azimuth rotation-equivalent intensity measurements by real spherical harmonic functions of even order, for absorption.[3]

2, 3 and **4** were solved by means of SHELXT.[6] **2** was refined with SHELXL-2018 (release 1),[7] **3** and **4** with SHELXL-2017 (release 1).[4] All non-hydrogen atoms were refined, using full-matrix least-squares based on $|F|^2$, anisotropically, but the hydrogen atoms (except for the hydride in **2**) were placed at calculated positions by means of the "riding" model.

In the structure of **2**, one of the uranium atom is disordered over two positions found in a difference map and refined anisotropically with half occupancies without applying any kind of restraint. The hydride bridge was found in a difference map and refined isotropically. Some t-butoxyl and t-butyl groups of the ligand were disordered over two positions found in a difference map and refined anisotropically imposing distance and similarity restraints (SADI, RIGU and SIMU) for the least-squares refinement. An accessible void of 186 $Å^3$ found in difference map and believed to be due to evaporated toluene molecules was removed by using the SQUEEZE algorithm of PLATON.[8]

The completeness of the measurement is 99.7 % up to 25.3°, but our measurement originally extended to a higher theta, namely 32.6° resulting in lower completeness.

In the structure of **3**, the hydrogen atom of the imide bridge was placed at a calculated position. Most of the ligand is disordered over two orientations, located in difference maps, which were refined anisotropically, but under distance and similarity restraints (SADI, DFIX, RIGU and SIMU). Additional electron density found in difference maps (due to highly disordered solvent molecules) was removed with the help of the solvent-masking program in OLEX2.[5]

In the structure of **4**, the hydrogen atoms of the formate and the carbamate bridges were placed at calculated position. Some t-butyl and t-butoxyl groups of the ligand are disordered over two positions, found in difference maps, and refined anisotropically imposing distance and similarity restraints (SADI and SIMU). Additional electron density found in difference maps (due to highly disordered solvent molecules) was removed with the help of the solvent-masking program in OLEX2.[5]

Table S1. X-ray crystallographic data.

	2	**3**	**4**
Formula	$C_{72}H_{164}CsNO_{24}Si_6U_2$	$C_{74}H_{167}CsN_2O_{24}Si_6U_2$	$C_{74}H_{164}CsNO_{28}Si_6U_2$
Crystal size (mm^3)	0.616 x 0.361 x 0.257	0.388 x 0.240 x 0.227	0.325 x 0.191 x 0.186
cryst syst	Triclinic	Triclinic	Monoclinic
space group	$P\bar{1}$	$P\bar{1}$	$P2_1/n$
volume ($Å^3$)	5160.5(2)	5504.0(11)	11326.72(19)
a (Å)	13.9801(3)	13.691(2)	18.61084(18)
b (Å)	16.2906(4)	14.3033(5)	24.05413(19)
c (Å)	25.1860(5)	31.806(4)	26.4001(3)
α (deg)	72.4692(19)	80.272(7)	90
β (deg)	81.9636(17)	87.262(11)	106.5858(10)
γ (deg)	70.816(2)	63.766(5)	90
Z	2	2	4
formula weight (g/mol)	2205.54	2246.60	2293.56
density ($g\ cm^{-3}$)	1.419	1.356	1.345
absorption coefficient (mm^{-1})	3.611	3.387	11.557
F(000)	2236	2280	4648
temp (K)	140.00(10)	120(2)	140.01(10)
total no. reflections	65732	75204	125780
unique reflections [R_{int}]	34159 [0.0328]	24991 [0.0411]	23733 [0.0517]
Final R indices [$I > 2\sigma(I)$]	$R_1 = 0.0410$, $wR_2 = 0.0952$	$R_1 = 0.0483$, $wR_2 = 0.0853$	$R_1 = 0.0314$, $wR_2 = 0.0803$
Largest diff. peak and hole ($e.A^{-3}$)	2.922 and -2.433	1.539 and -1.252	3.103 and -0.969
GOOF	1.027	1.128	1.028

[1] CrysAlisPRO, Rigaku Oxford Diffraction, **2015**.
[2] A. J. M. Duisenberg, L. M. J. Kroon-Batenburg, A. M. M. Schreurs, *J. Appl. Crystallogr.* **2003**, *36*, 220-229.
[3] R. H. Blessing, *Acta Crystallogr., Sect. A* **1995**, *51*, 33-38.
[4] G. M. Sheldrick, *Acta Crystallogr. C* **2015**, *71*, 3-8.
[5] O. V. Dolomanov, L. J. Bourhis, R. J. Gildea, J. A. K. Howard, H. Puschmann, *J. Appl. Crystallogr.* **2009**, *42*, 339-341.

APPENDIX 4

Supporting information for Chapter 5

1. NMR Spectroscopic data

Figure S1. ^{1}H NMR (400 MHz, THF-d_8, 298 K) spectrum of [K(2.2.2-cryptand)][U{OSi(OtBu)$_3$}$_4$], **3**. **Note**: L = OSi(OtBu)$_3$

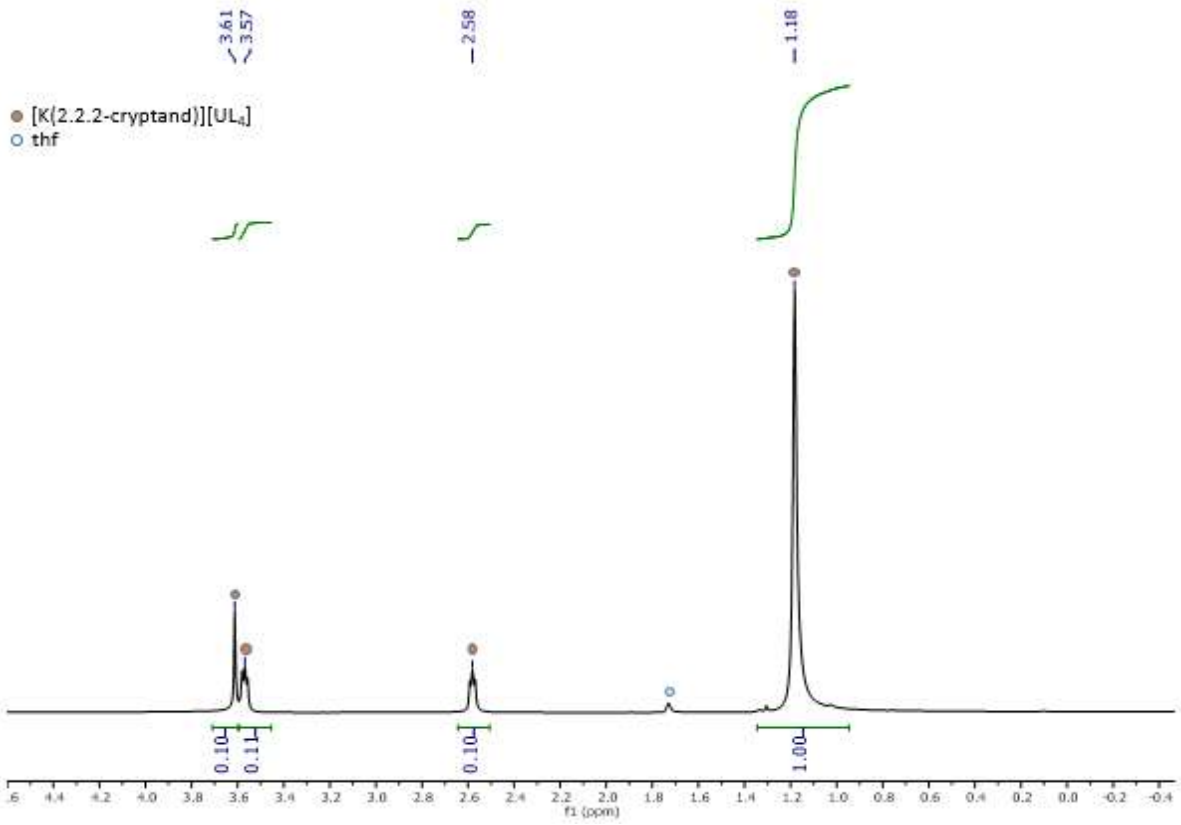

Figure S2. ^{1}H NMR (400 MHz, toluene-d_8, 298 K) spectrum of [U(NAd){OSi(OtBu)$_3$}$_4$K], **4**.

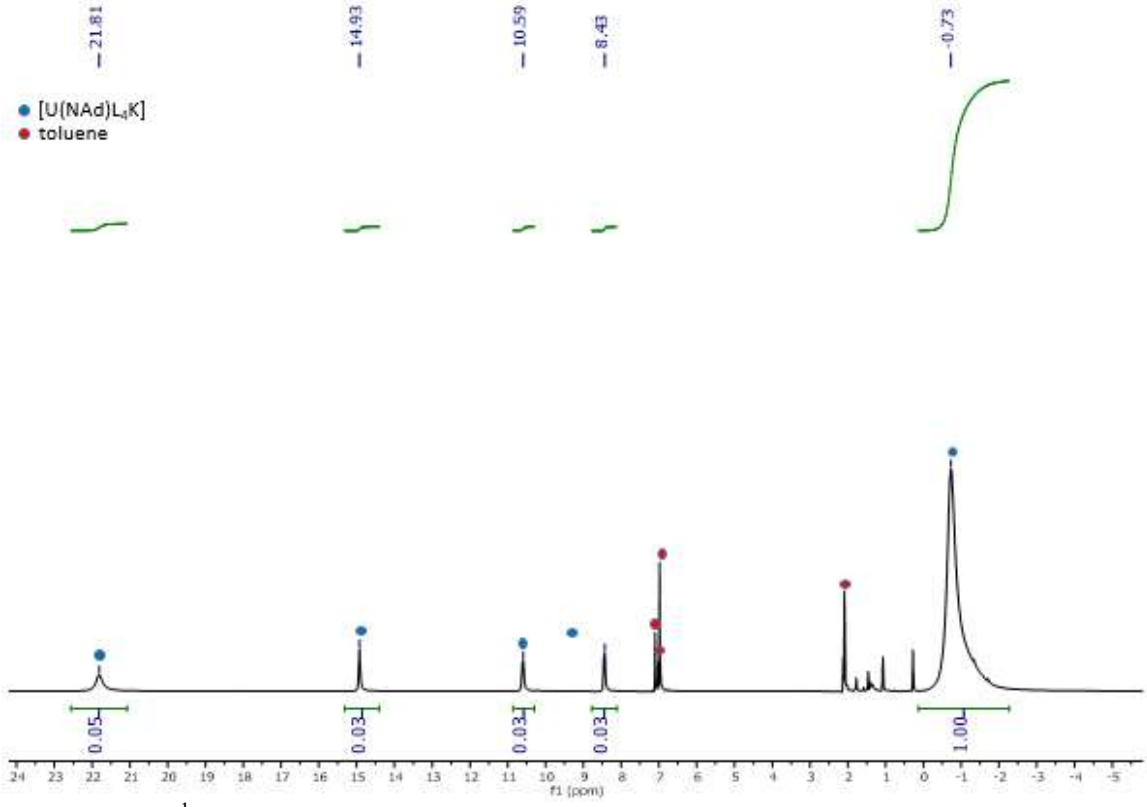

Figure S3. ^{1}H NMR (400 MHz, toluene-d_8, 298 K) spectrum of [K(2.2.2-cryptand)][U(NAd){OSi(OtBu)$_3$}$_4$], **5**.

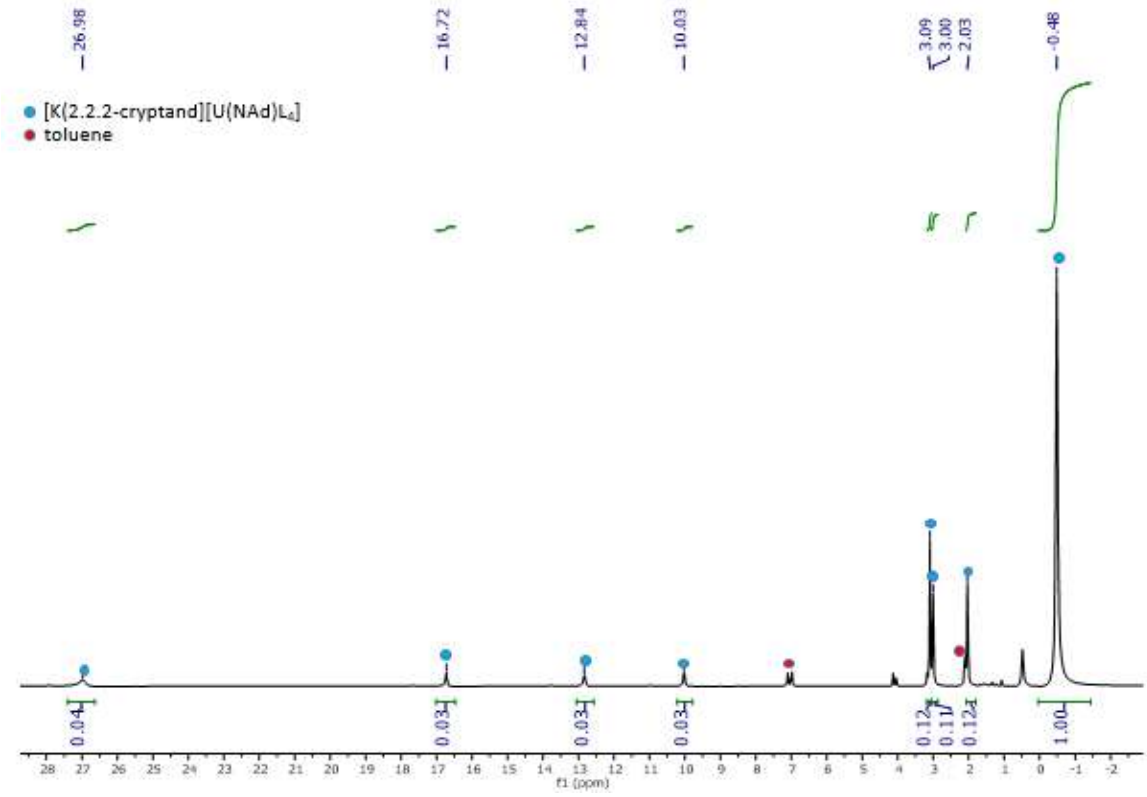

Figure S4. ^{1}H NMR (400 MHz, THF-d_8, 298 K) spectrum of [K(2.2.2-cryptand)][U(NAd){OSi(OtBu)$_3$}$_4$], **5**.

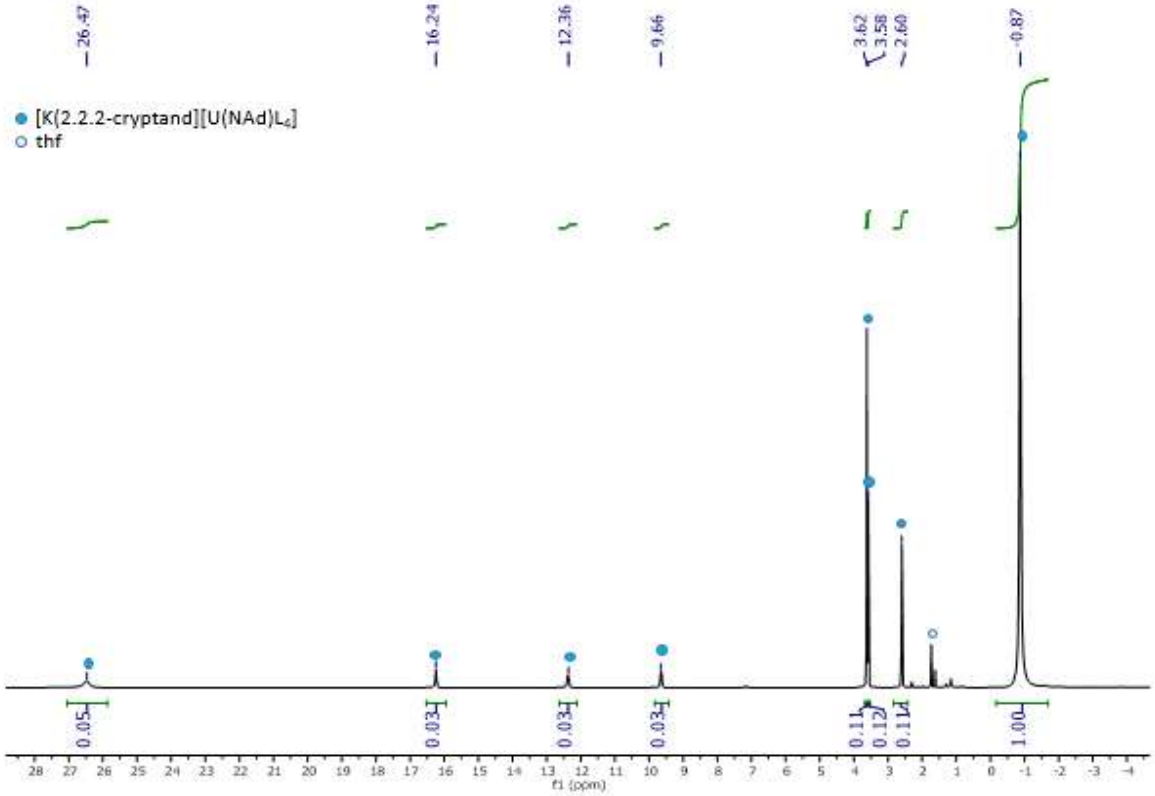

Figure S5. ^{1}H NMR (400 MHz, toluene-d_8, 298 K) spectrum of [K(2.2.2-cryptand)][U(CS_3){OSi(OtBu)$_3$}$_4$], **7**.

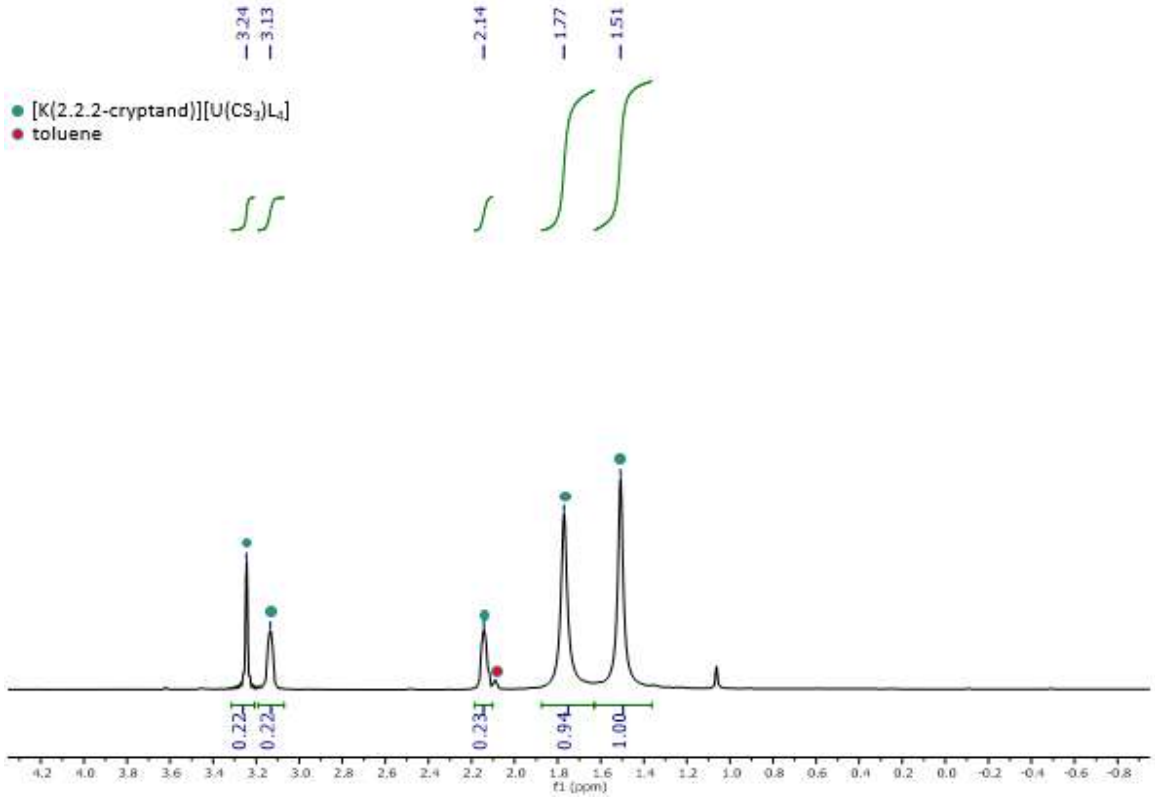

Figure S6. ^{13}C NMR (400 MHz, toluene-d_8, 298 K) spectrum of [K(2.2.2-cryptand)][U(CS_3){OSi(OtBu)$_3$}$_4$], **7**.

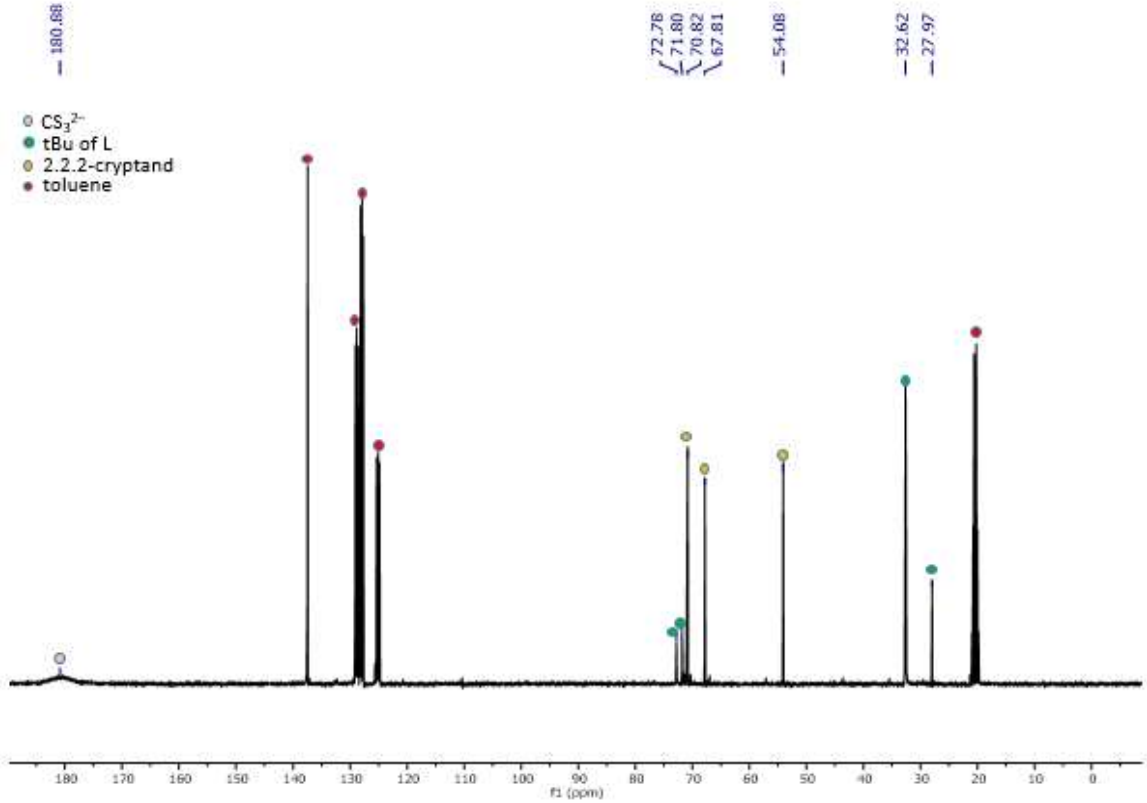

Figure S7. ^{1}H NMR (400 MHz, toluene-d_8, 298 K) spectrum of [K(2.2.2-cryptand)][US{OSi(OtBu)$_3$}$_4$], **8**.

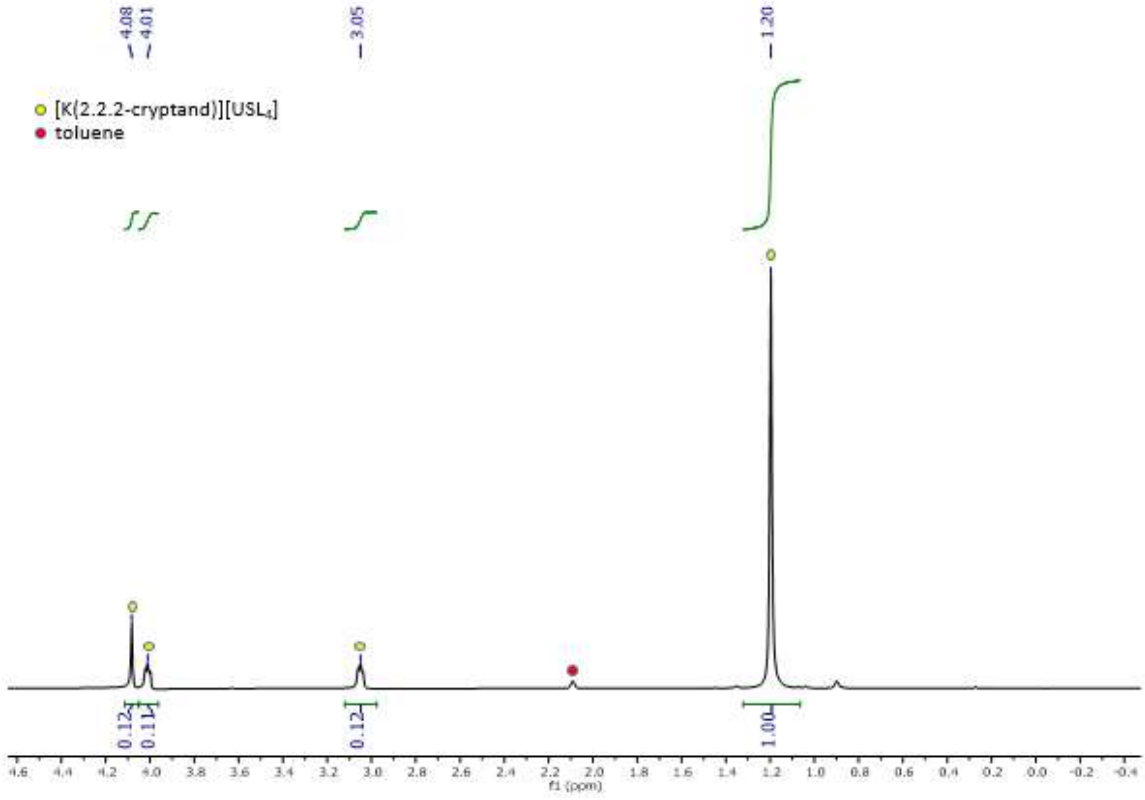

Figure S8. ^{13}C NMR (400 MHz, toluene-d_8, 298 K) spectrum of [K(2.2.2-cryptand)][US{OSi(OtBu)$_3$}$_4$], **8**.

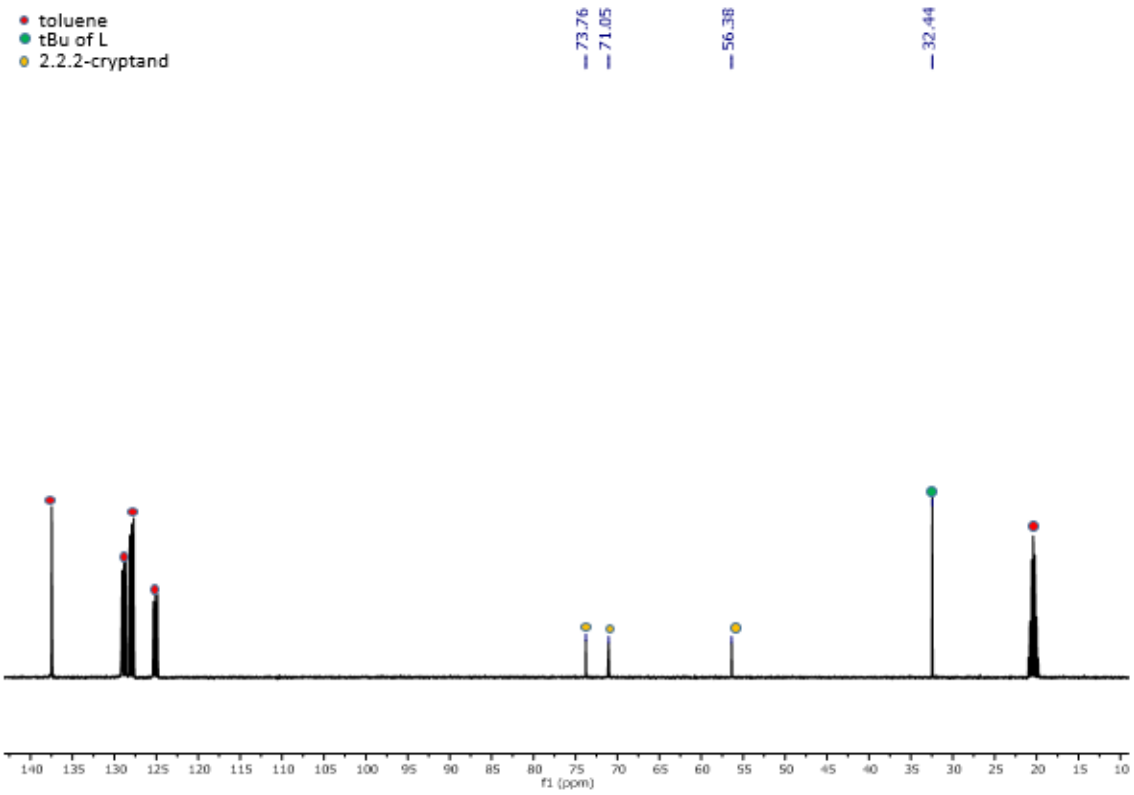

Figure S9. ^{1}H NMR spectrum (400 MHz, toluene-d_8, 298 K) of the crude reaction mixture 2–3 days after the addition of $^{13}CS_2$ (1 eq.) to a solution of **4** (1 eq.).

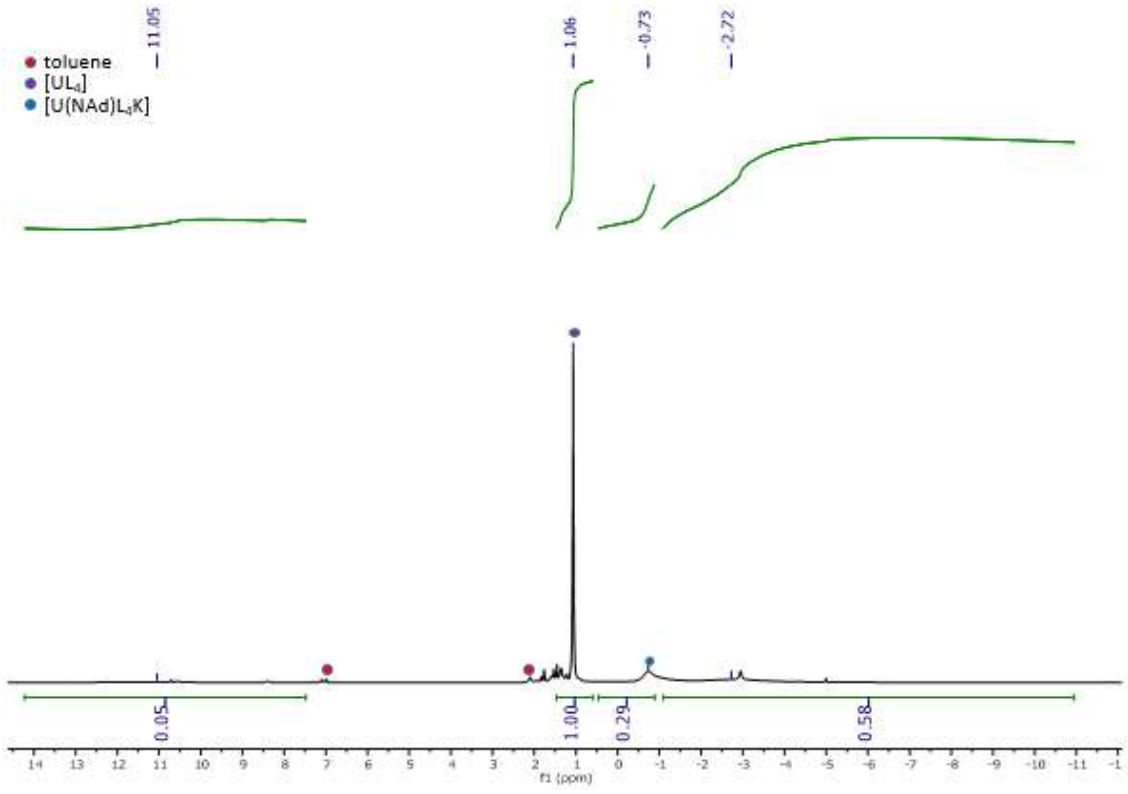

Figure S10. ^{13}C NMR spectrum (100.6 MHz, d_8-toluene, 298 K) of the crude reaction mixture several days after the addition of $^{13}CS_2$ (1 eq.) to a solution of **4** (1 eq.).

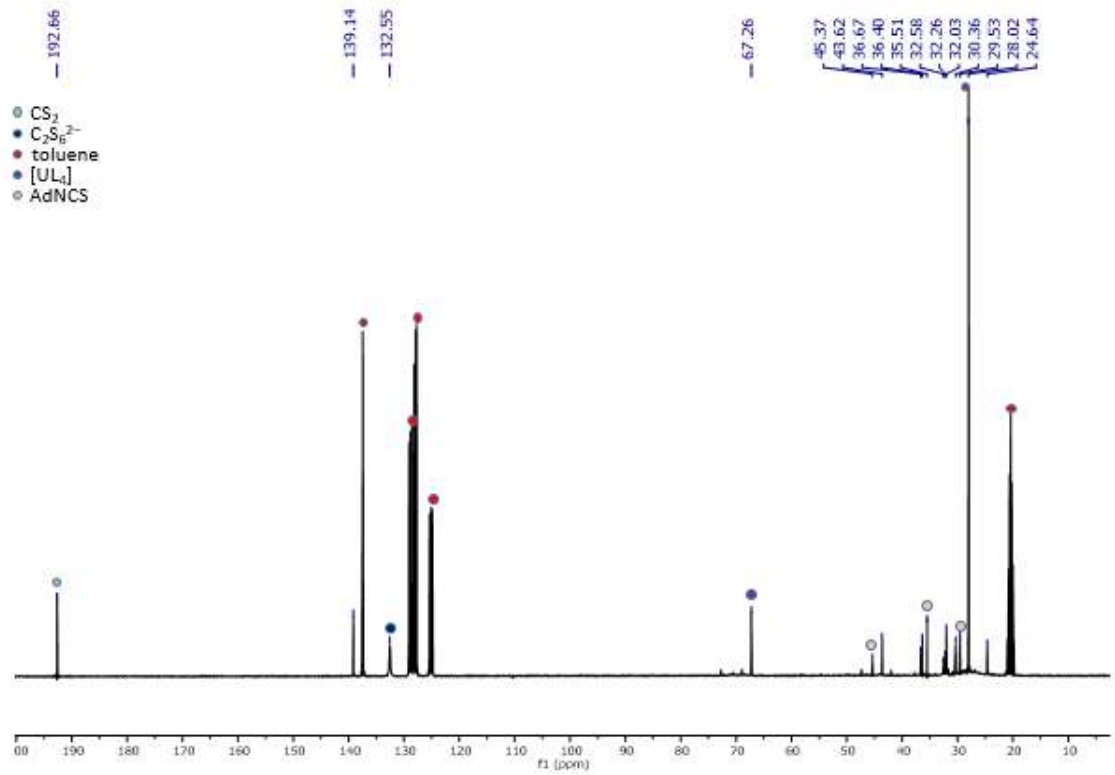

Figure S11. ^{1}H NMR spectrum (400 MHz, toluene-d_8, 298 K) of the crude reaction mixture 2–3 days after the addition of $^{13}CS_2$ (2 eq.) to a solution of **4** (1 eq.). The conversion of **4** into [U{OSi(OtBu)$_3$}$_4$] was determined to be 35 % by quantitative ^{1}H NMR spectroscopy with naphthalene as an internal standard.

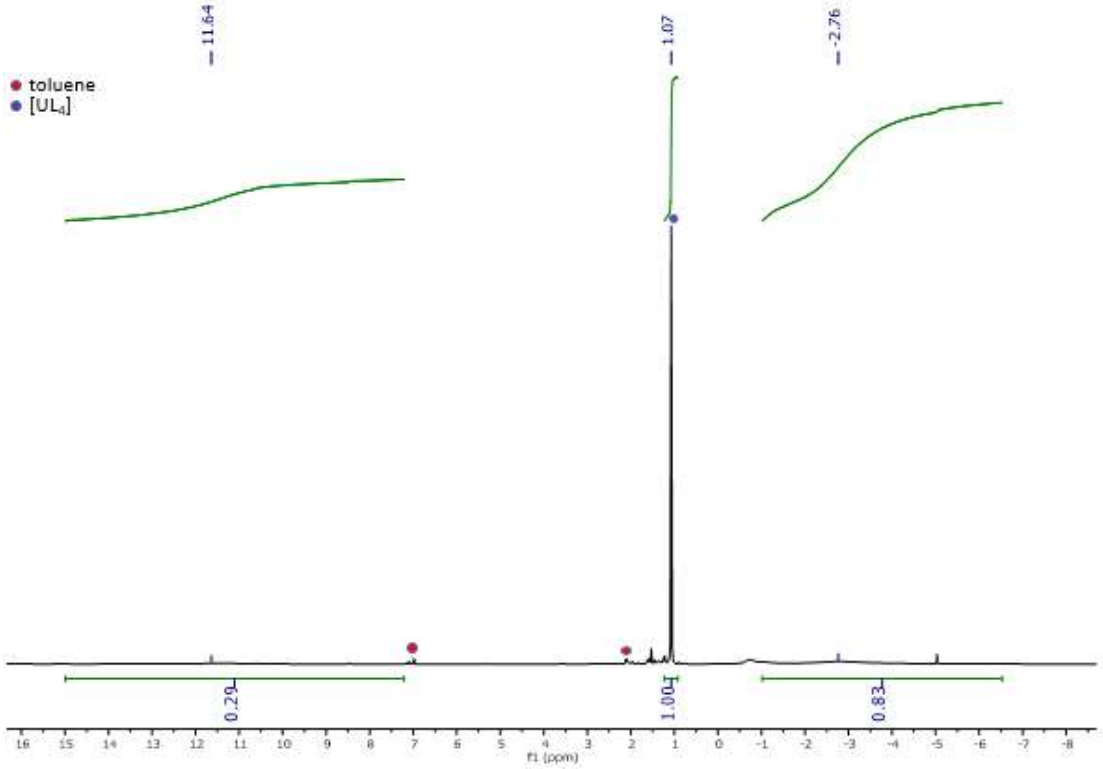

Figure S12. ^{13}C NMR spectrum (100.6 MHz, toluene-d_8, 298 K) of the crude reaction mixture 2–3 days after the addition of $^{13}CS_2$ (2 eq.) to a solution of **4** (1 eq.) (a solid is also present in the reaction mixture).

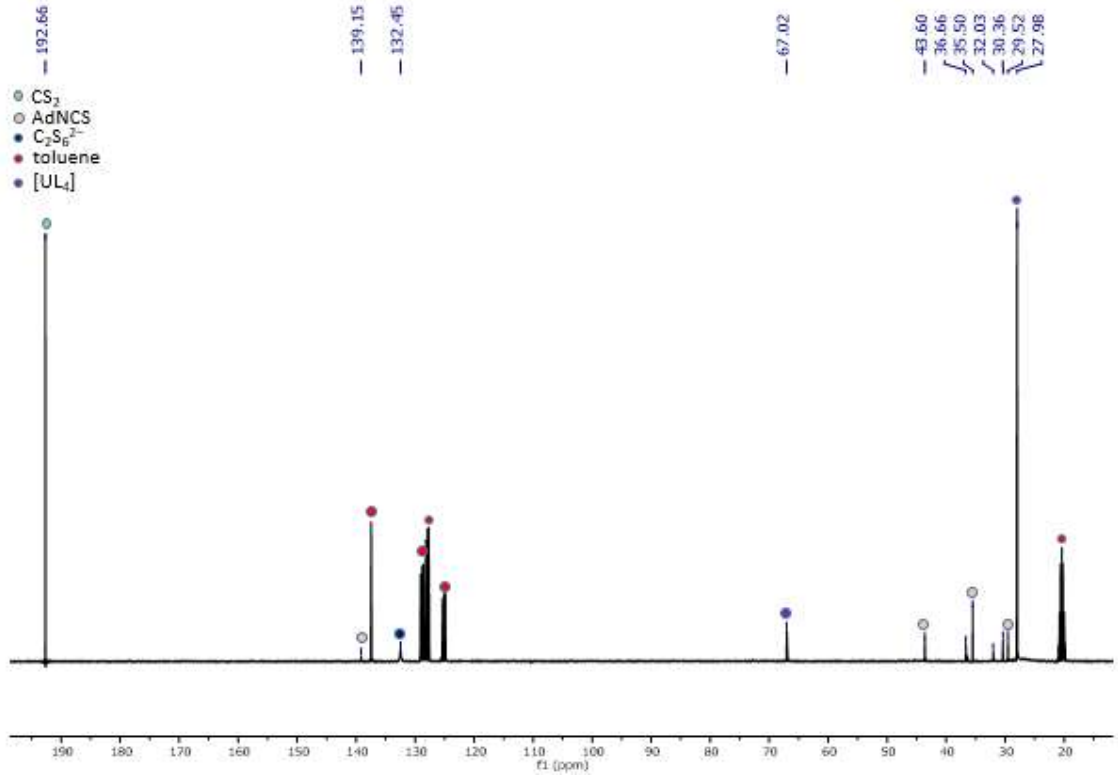

Figure S13. ^{13}C NMR spectrum (100.6 MHz, DMSO-d_6, 298 K) of the residue obtained after toluene was removed from the crude reaction mixture resulting from the addition of $^{13}CS_2$ (2 eq.) to a solution of **4** (1 eq.).

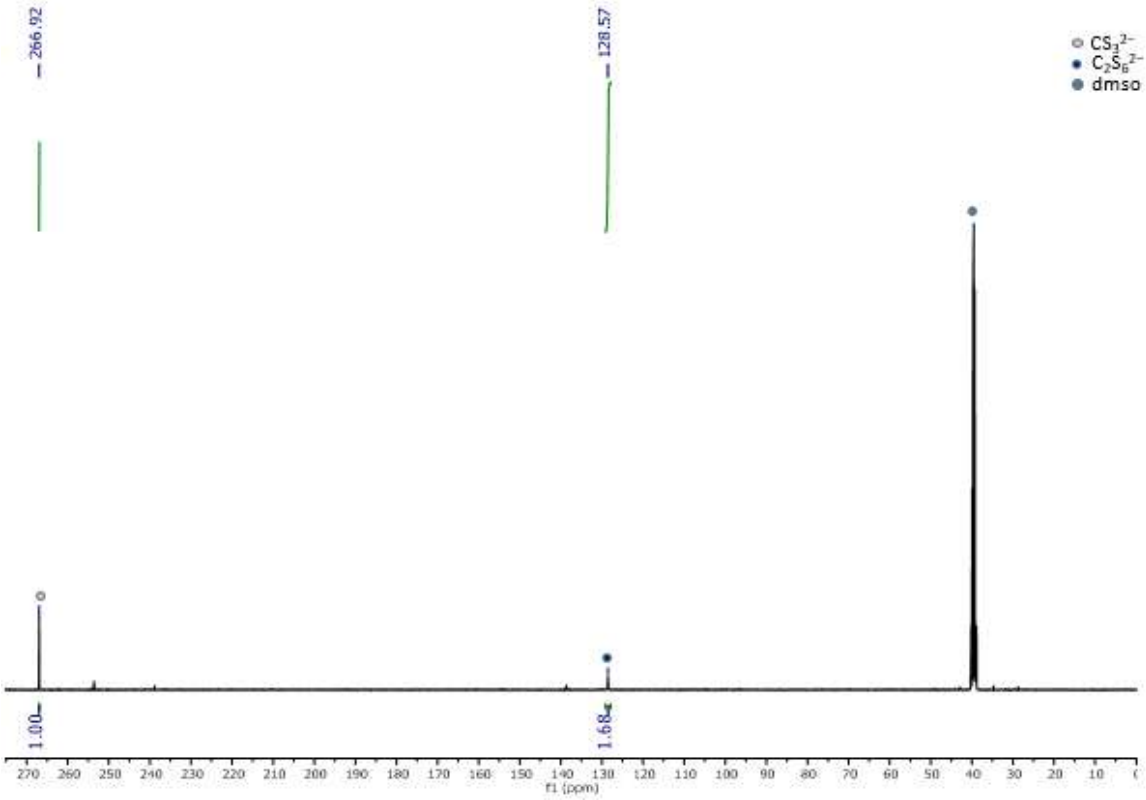

Figure S14. ^{1}H NMR spectrum (400 MHz, toluene-d_8, 298 K) of the crude reaction mixture 2–3 days after the addition of $^{13}CS_2$ (1 eq.) to a solution of **1** (1 eq.).

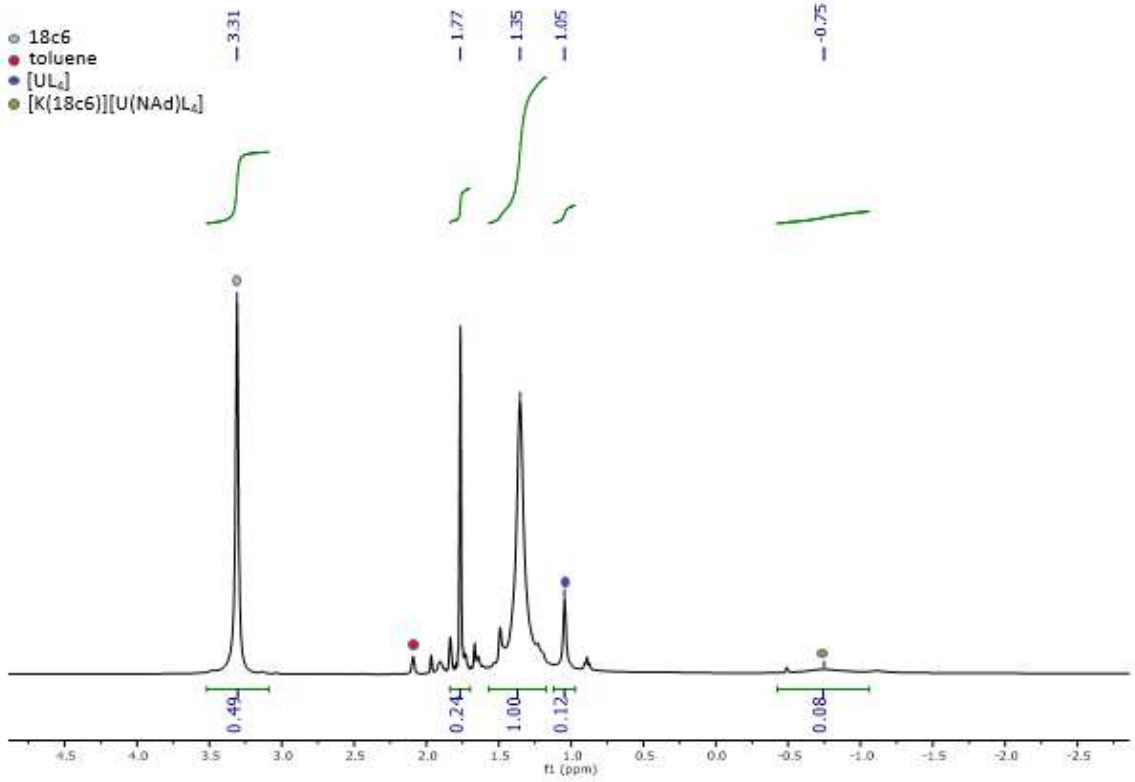

Figure S15. ^{1}H NMR spectrum (400 MHz, toluene-d_8, 298 K) of the crude reaction mixture 2–3 days after the addition of $^{13}CS_2$ (2 eq.) to a solution of **1** (1 eq.).

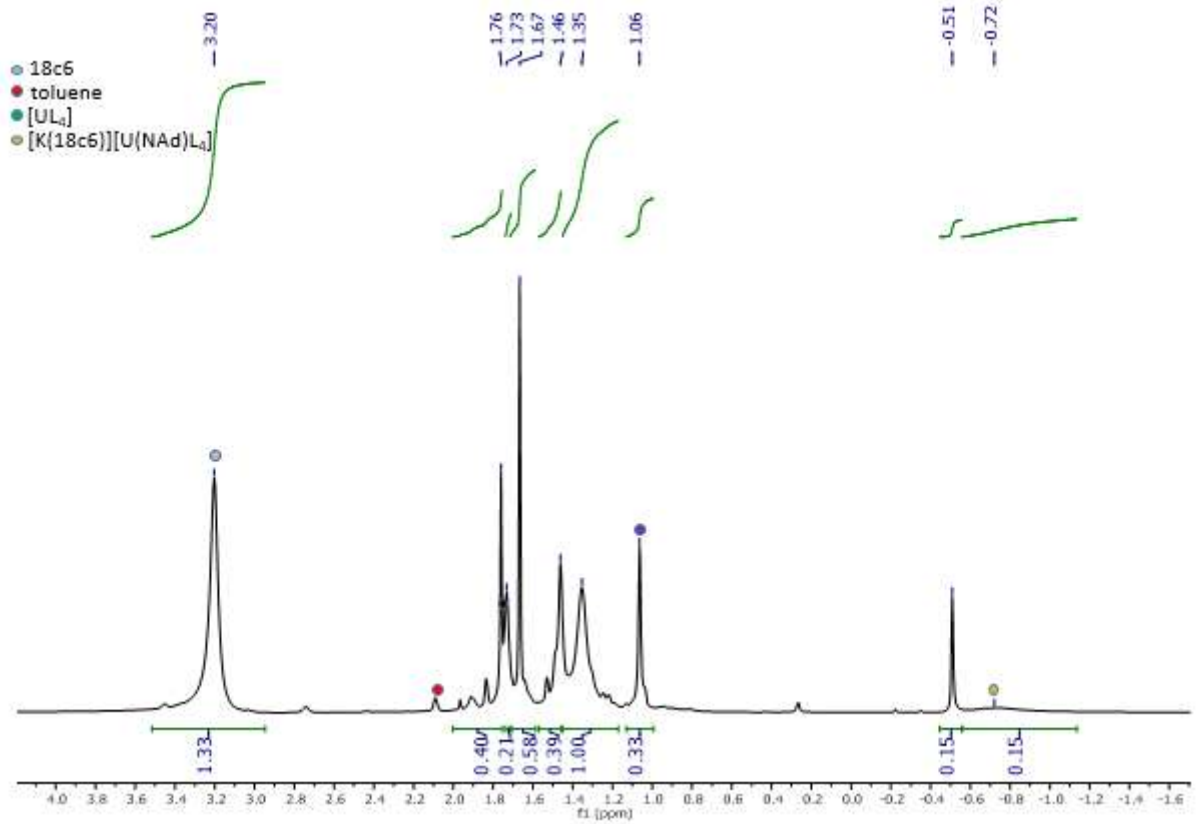

Figure S16. ^{1}H NMR spectrum (400 MHz, toluene-d_8, 298 K) after addition of 2.2.2-cryptand (1 eq.) to the crude reaction mixture obtained three days after the addition of $^{13}CS_2$ (2 eq.) to a solution of **1** (1 eq.). The conversion of **1** into [U{OSi(OtBu)$_3$}$_4$] was determined to be 9 % by quantitative ^{1}H NMR spectroscopy with naphthalene as an internal standard.

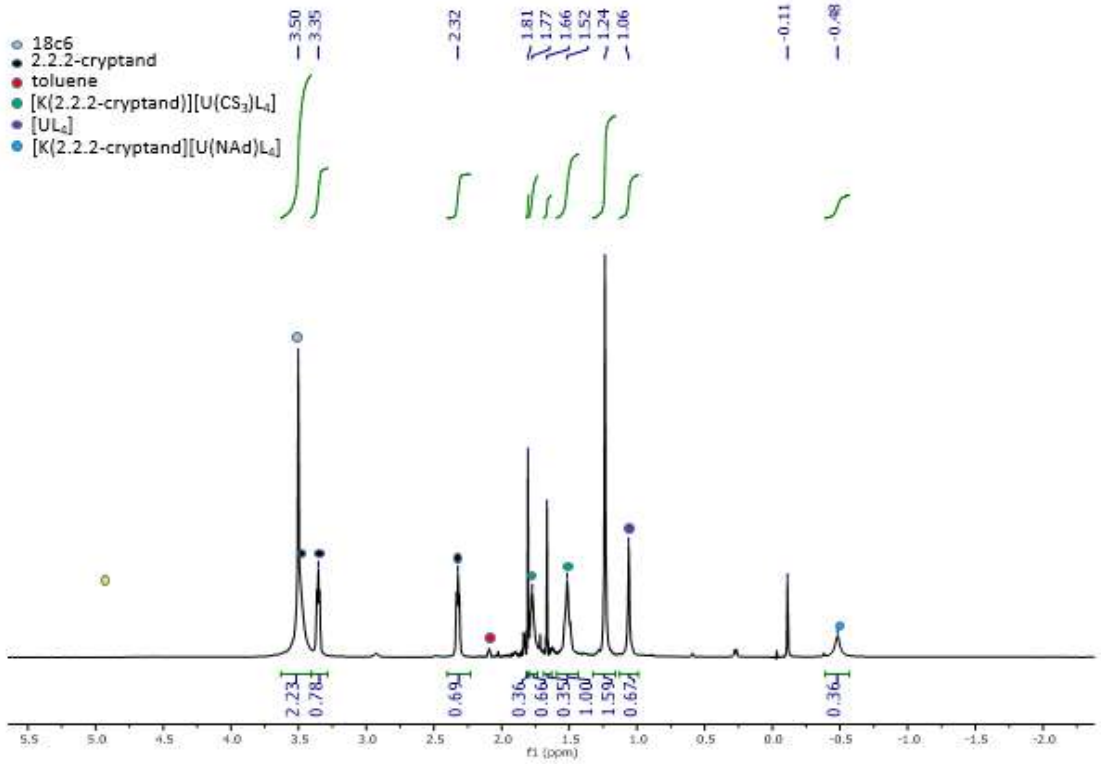

Figure S17. ^{13}C NMR spectrum (100.6 MHz, toluene-d_8, 298 K) of the crude reaction mixture 2–3 days after the addition of $^{13}CS_2$ (2 eq.) to a solution of **1** (1 eq.).

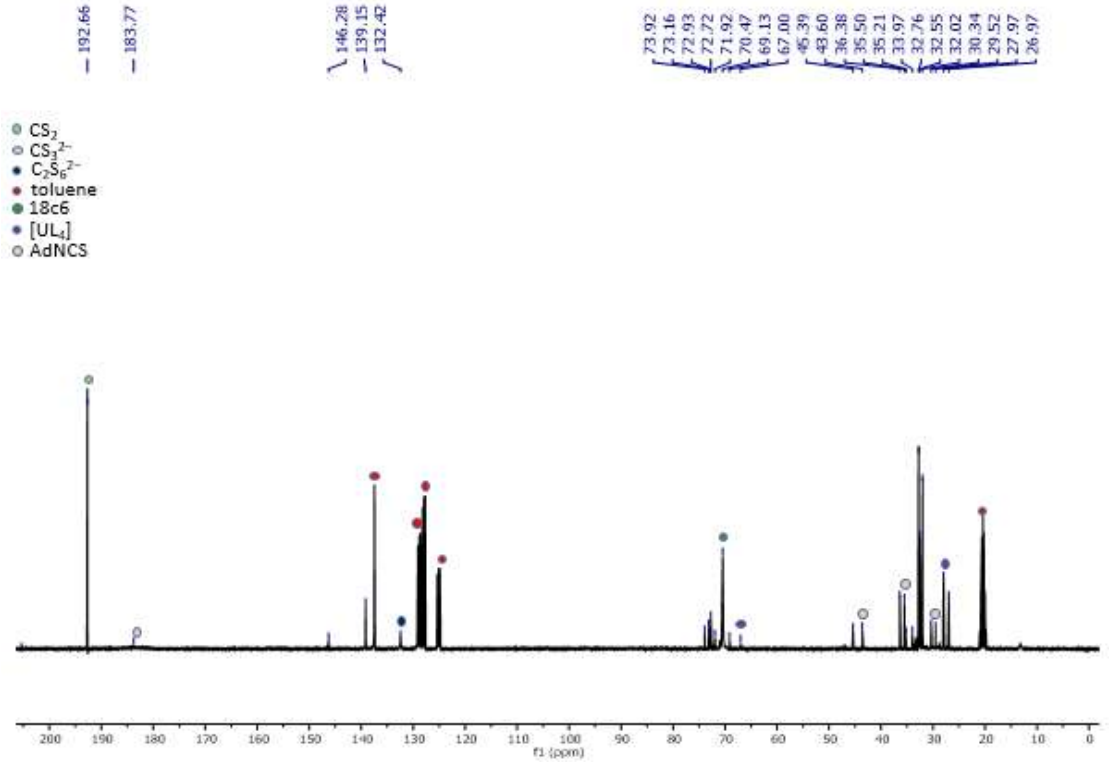

Figure S18. ^{1}H NMR spectra (400 MHz, toluene-d_8, 298 K) over time of the crude reaction mixture after the addition of $^{13}CS_2$ (1 eq.) to a suspension of **5** (1 eq.), affording **7**.

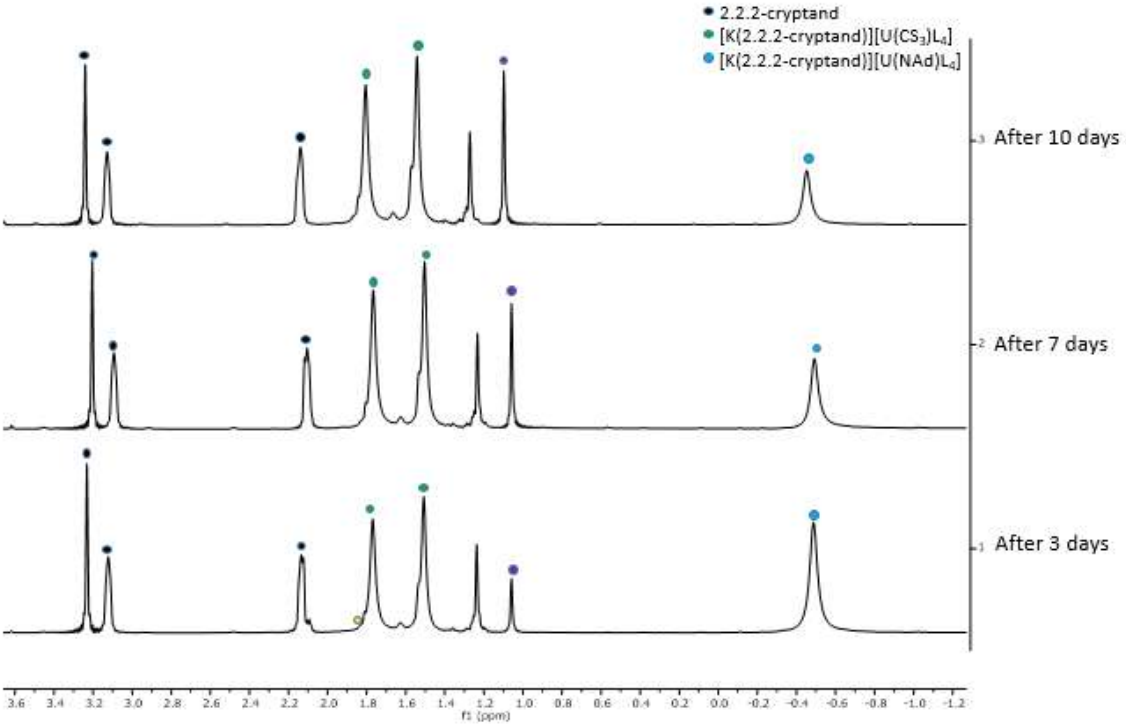

Figure 19. ^{1}H NMR spectra (400 MHz, toluene-d_8, 298 K) over time of the crude reaction mixture after the addition of $^{13}CS_2$ (2 eq.) to a suspension of **5** (1 eq.), affording **7**.

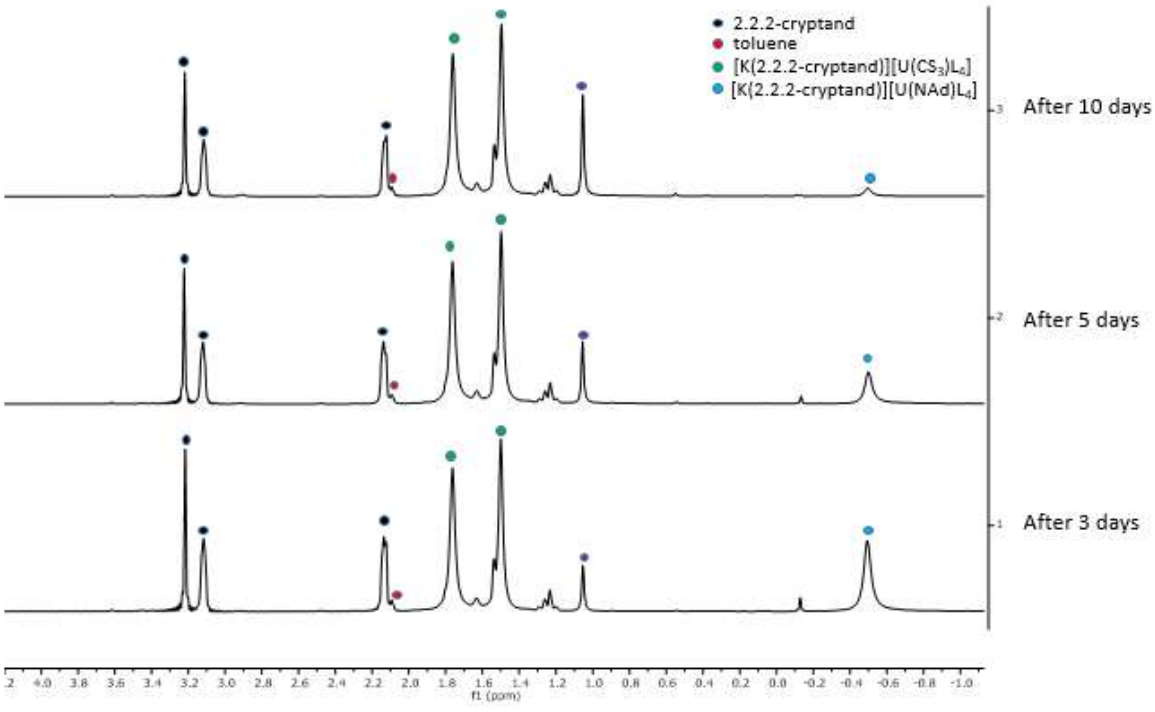

Figure S20. ^{1}H NMR spectrum (400 MHz, toluene-d_8, 298 K) of the crude reaction mixture ca. 10 days after the addition of $^{13}CS_2$ (2 eq.) to a suspension of **5** (1 eq.), affording **7**. The conversion of **1** into [U{OSi(OtBu)$_3$}$_4$] was determined to be 8 % by quantitative ^{1}H NMR spectroscopy with naphthalene as an internal standard.

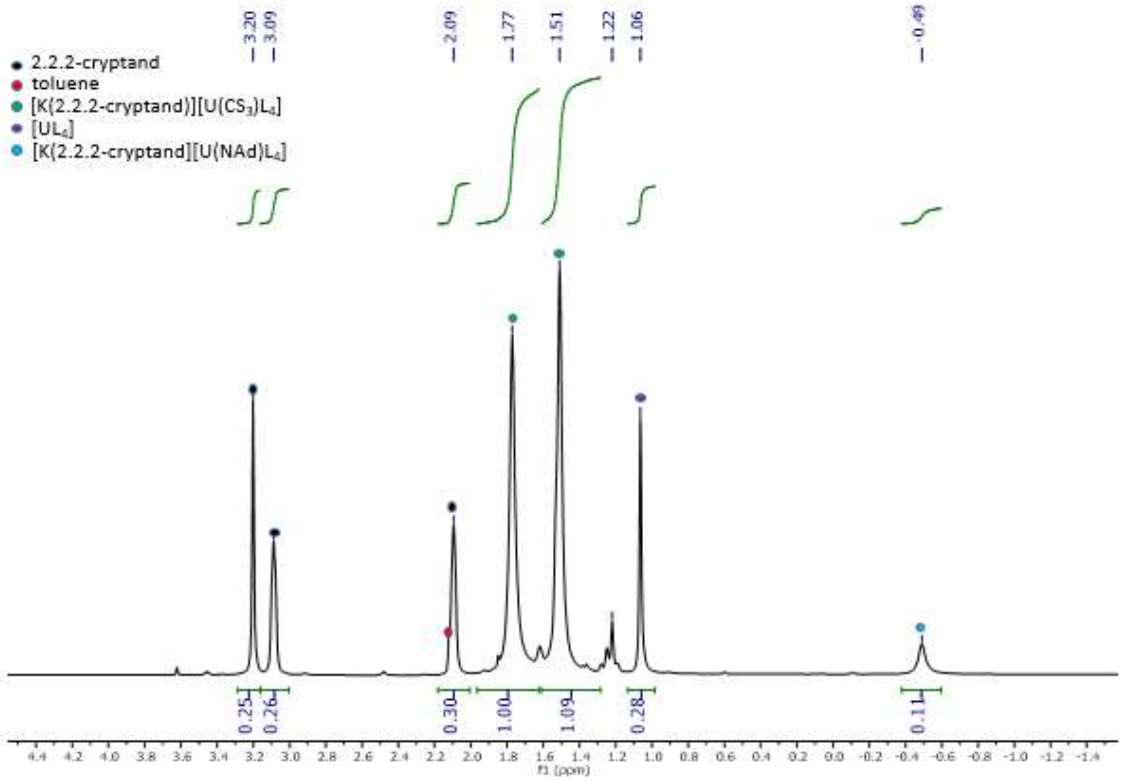

Figure S21. ^{13}C NMR spectrum (100.6 MHz, toluene-d_8, 298 K) of the crude reaction mixture ca. 10 days after the addition of $^{13}CS_2$ (2 eq.) to a suspension of **5** (1 eq.), affording **7**.

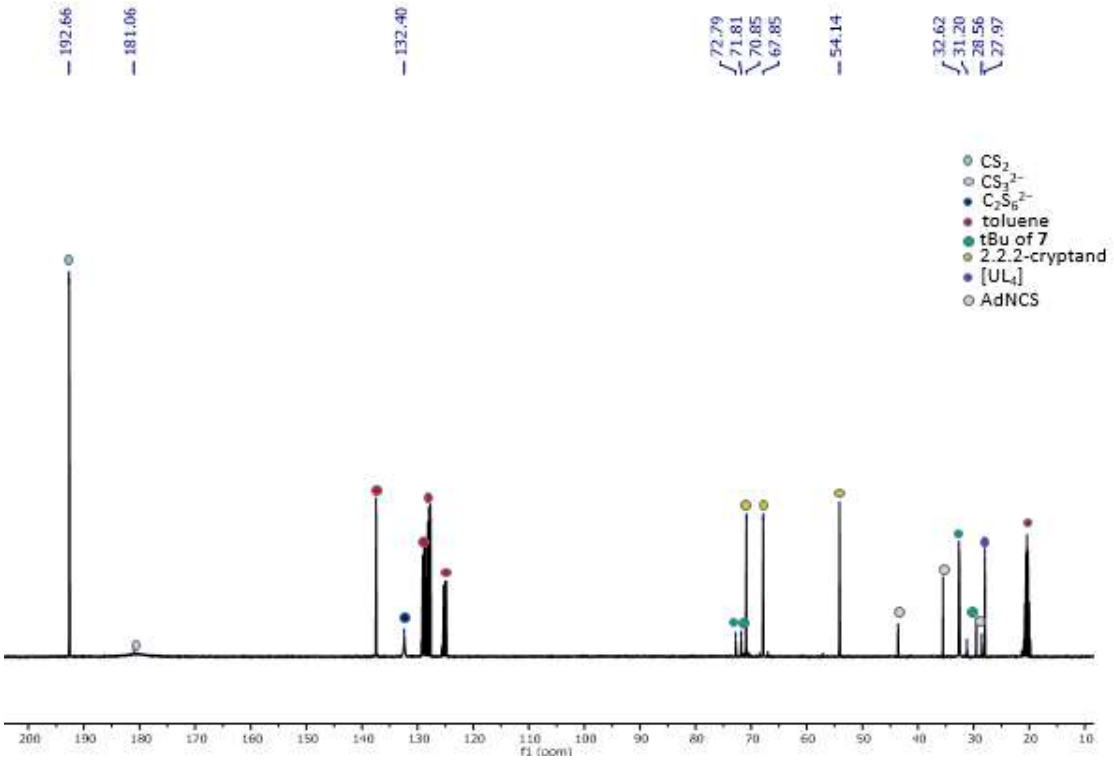

Figure S22. ^{1}H NMR spectra (400 MHz, toluene-d_8, 298 K) over time of the crude reaction mixture after the addition of $^{13}CS_2$ (1 eq.) to a solution of [K(2.2.2-cryptand)][U(NSiMe$_3$){OSi(OtBu)$_3$}$_4$] (1 eq.), affording **7**.

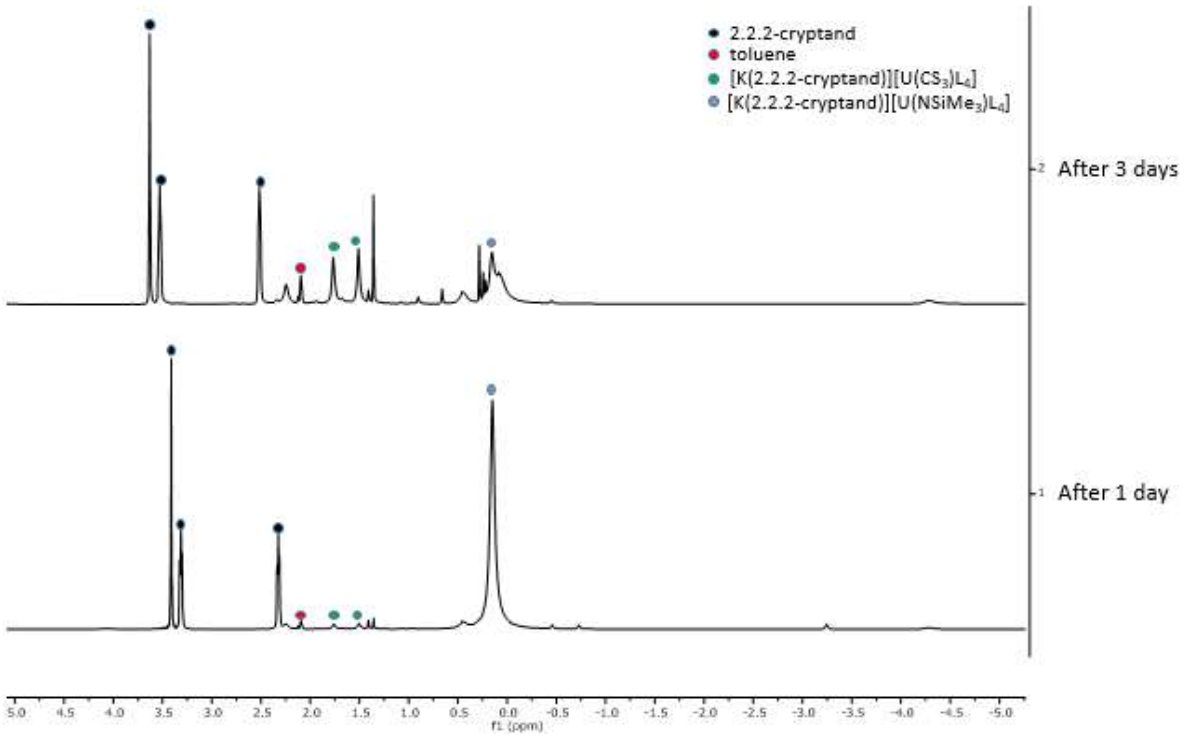

Figure S23. ^{1}H NMR spectra (400 MHz, toluene-d_8, 298 K) over time of the crude reaction mixture after the addition of H_2S (1.3 eq.) to a suspension of **5** (1 eq.), affording **8**. The reaction mixture was stored at −40 °C between measurements.

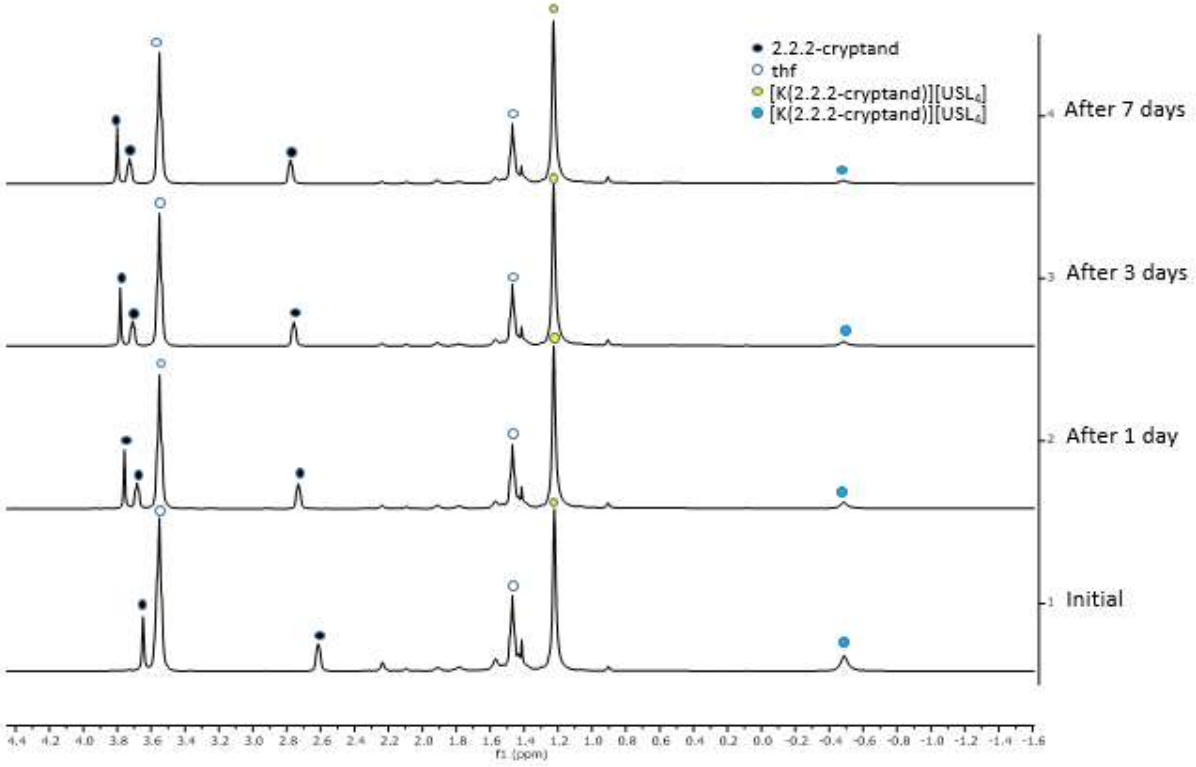

Figure S24. Monitoring the stability of **8** in toluene-d_8 over time by ^{1}H NMR spectroscopy (400 MHz, toluene-d_8, 298 K).

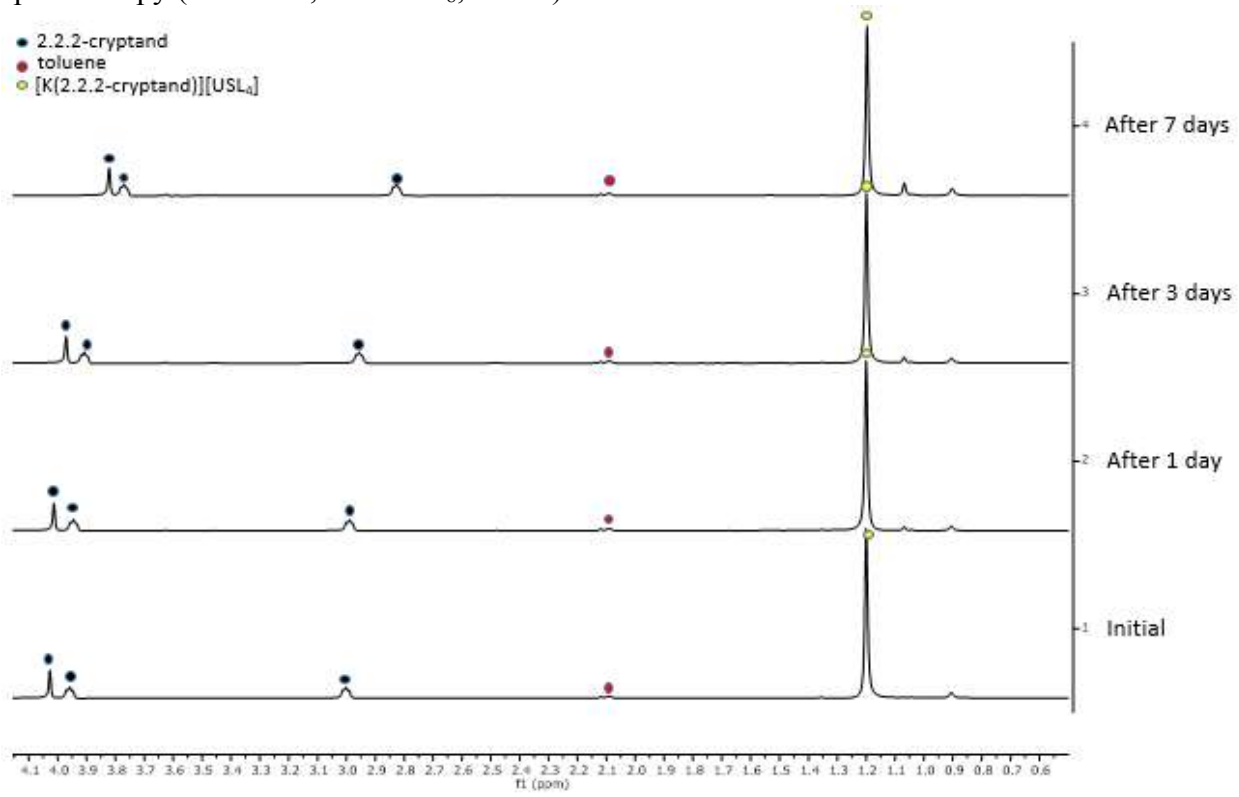

Figure S25. Conversion of **8** into **7** by reaction with $^{13}CS_2$ (1.3 eq.) as shown by ^{1}H NMR spectroscopy (400 MHz, toluene-d_8, 298 K).

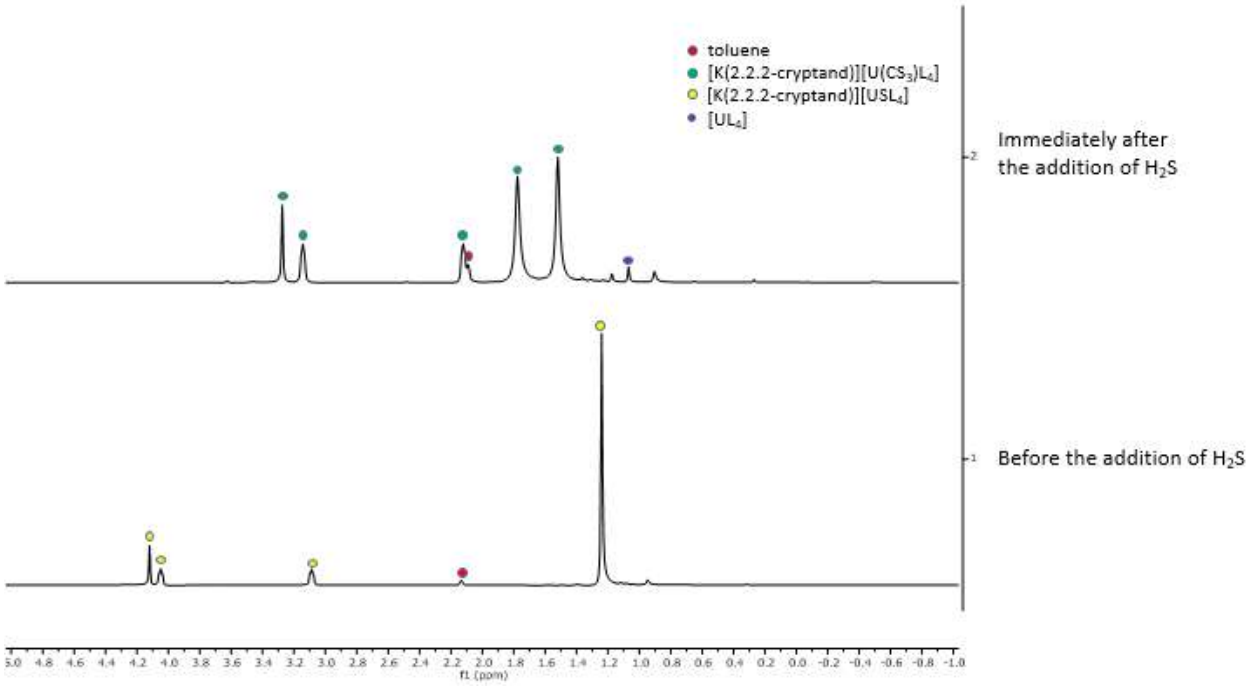

Figure S26. ^{1}H NMR spectrum (400 MHz, toluene-d_8, 298 K) of [K(2.2.2-cryptand)][U(NSiMe$_3$){OSi(OtBu)$_3$}$_4$].

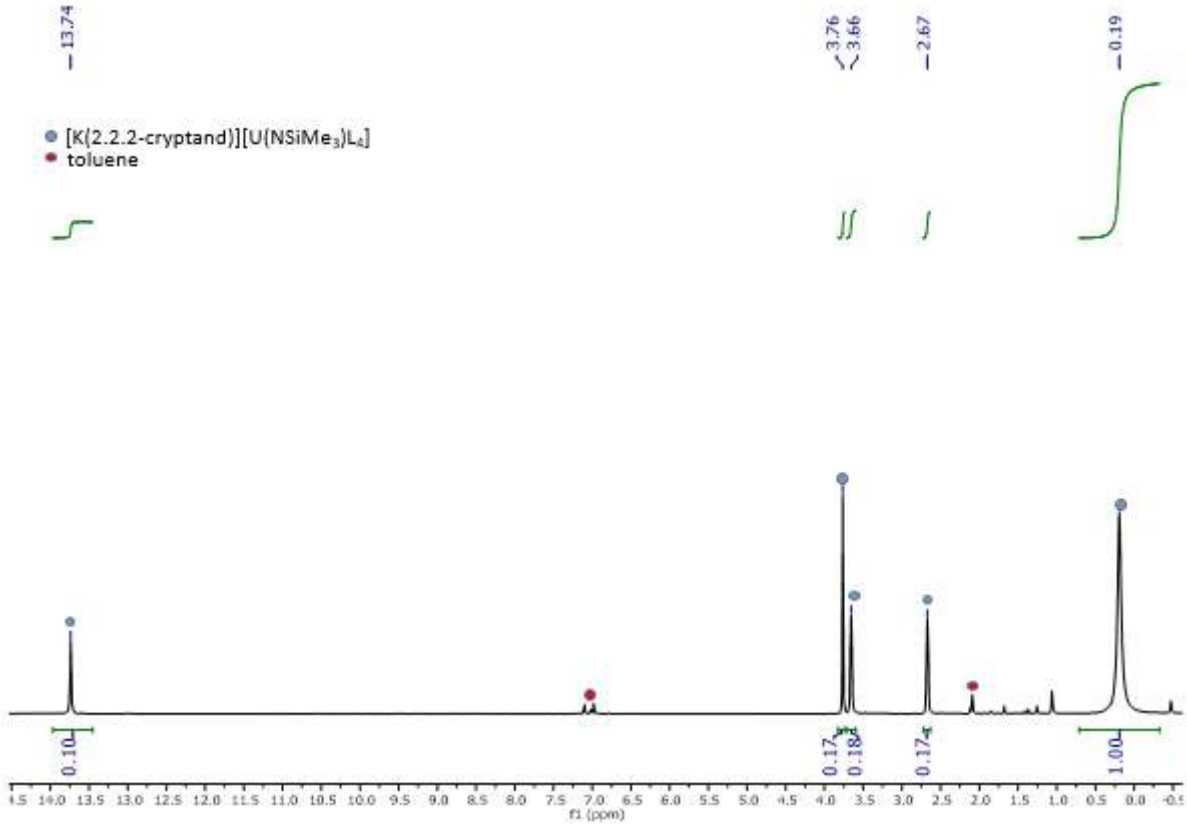

2. EPR spectra

Figure S27. Band (9.40 GHz) EPR spectrum of crystals of **7** (top) and **8** (bottom) in a 1:1 toluene/hexane glass at 10 K (black lines) and simulated EPR spectra of **7** and **8** (red lines).

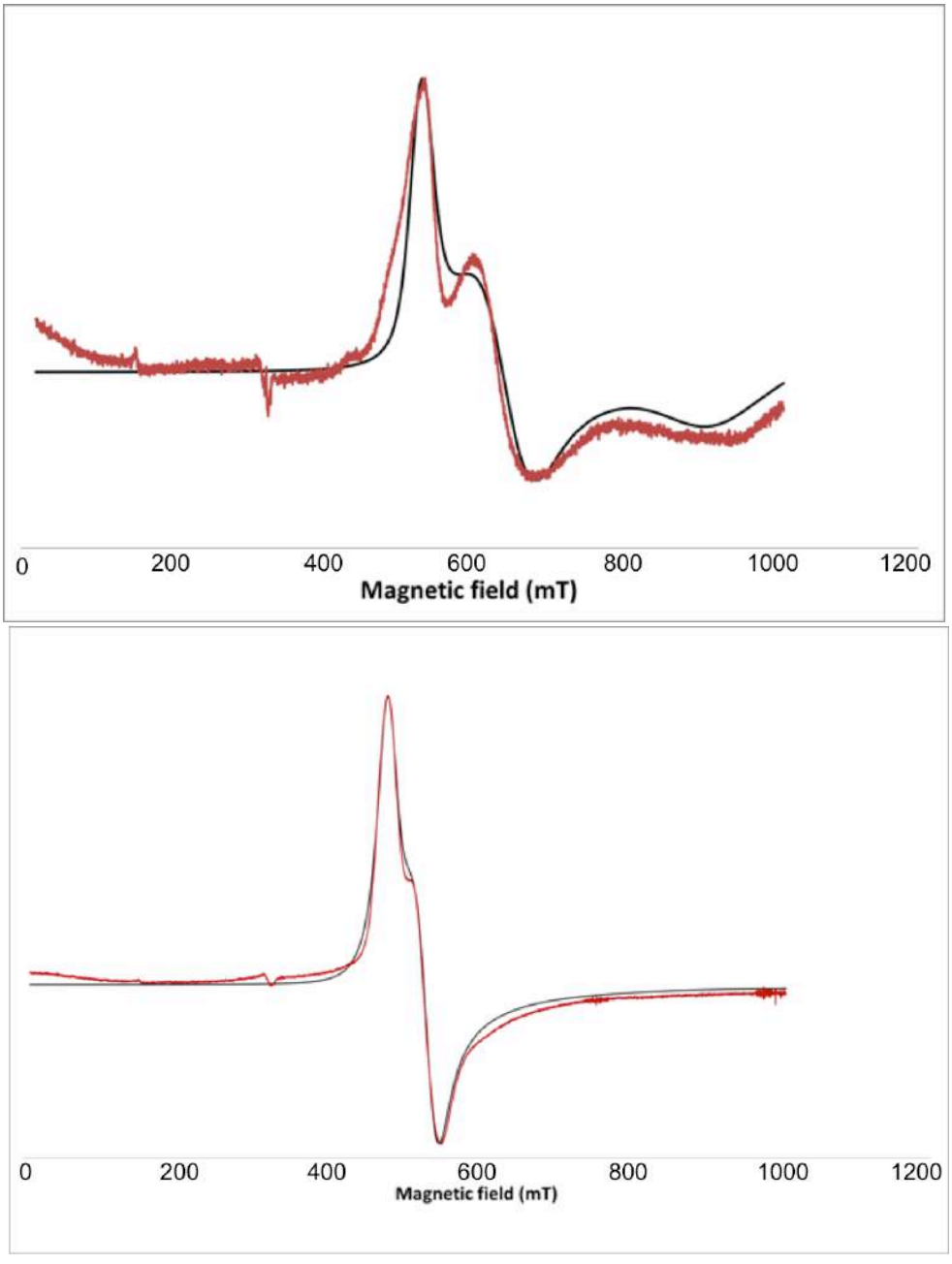

3. Electrochemistry

Figure S28. Cyclic voltammogram trace of [K(2.2.2-cryptand)][US{OSi(OtBu)$_3$}$_4$] (**8**) in an 0.1 M solution of [NBu$_4$][PF$_6$] in thf (Pt electrode, 100 mV/s scan rate).

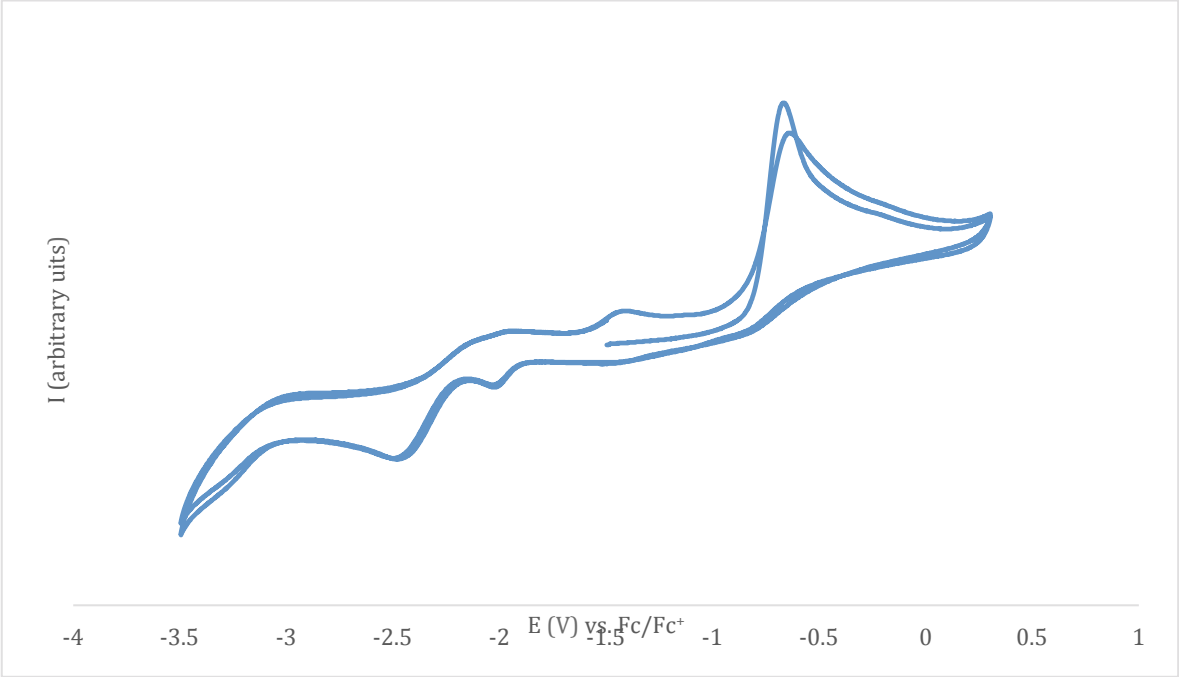

Figure S29. Cyclic voltammogram trace of [K(2.2.2-cryptand)][US{OSi(OtBu)$_3$}$_4$K] in an 0.1 M solution of [NBu$_4$][PF$_6$] in thf (Pt electrode, 100 mV/s scan rate).

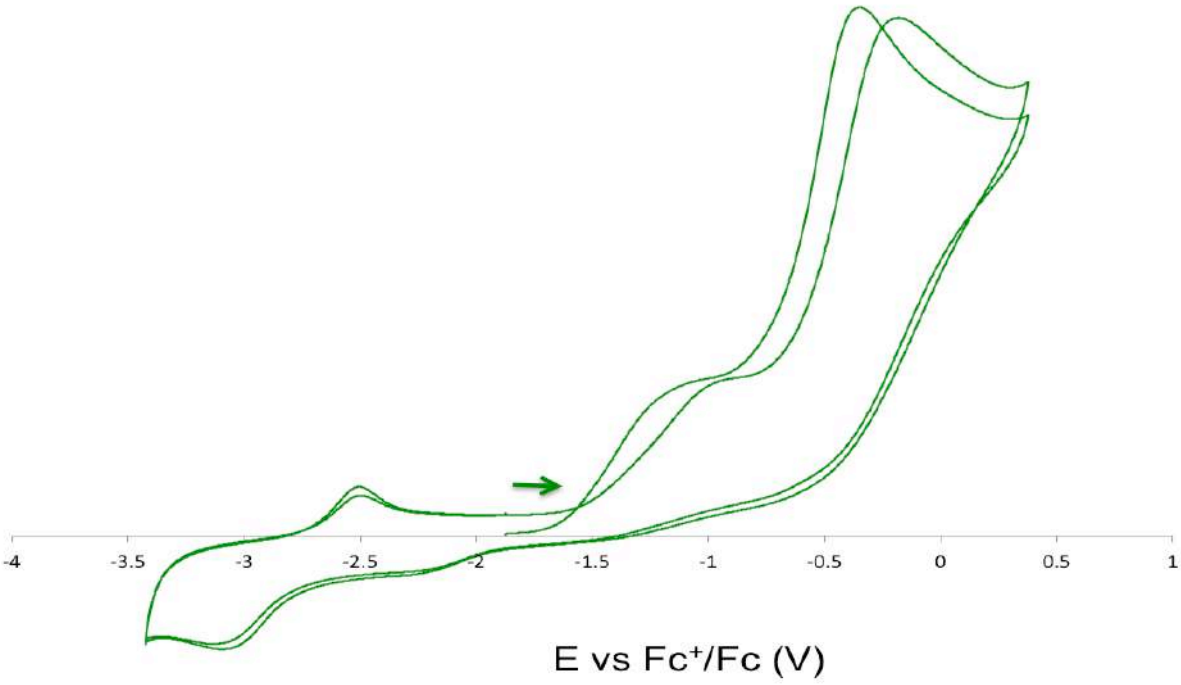

4. Crystallographic data

Crystallographic data for X-ray analyses of all complexes are given in Table S1. Figure graphics were generated using MERCURY 3.9: Cambridge, U.K., 2001-2016. CCDC-1535285 (**7**), CCDC-1535286 (**6**), CCDC-1535287 (**8**) CCDC-1535288 (**4**) and CCDC-1535289 (**3**) contain the supplementary crystallographic data for this paper. The data can be obtained free of charge from Cambridge Crystallographic Data Centre, 12 Union Road, Cambridge, CB2 1EZ, UK (fax: ++44-1223-336-033; e-mail: deposit@ccdc.cam.ac.uk).

Bragg-intensities of **3**, **4**, **6**, **7** and **8** were measured at low temperature [100 K and 140 K (compound **8**)], respectively using Cu *K*α radiation (l = 1.54184 Å) on a Rigaku SuperNova dual system diffractometer equipped with an Atlas CCD detector for compound **3** and **7** and equipped with an Atlas S2 CCD detector for compound **4**, **6** and **8**. The datasets were reduced and then corrected for absorption with CrysAlisPro.[1]

The solutions and refinements for the structures were performed by SHELXT[2] and SHELXL-2016 (release 6),[2] respectively. In the case of **7**, the solution and refinement for the structure were performed by SHELX-97.[3] The crystal structures were refined using full-matrix least-squares based on F^2 with all non-hydrogen atoms anisotropically defined. The hydrogen atoms were placed in calculated positions by means of the "riding" model.

In the case of **4**, the structure contained half toluene molecule in the asymmetric unit and it was disordered along a two-fold axis. The atoms were refined anisotropically and in order to have a convergent least-squares refinement, distance and similarity restraints (SADI, SIMU, ISOR and FLAT) were applied.

In the case of **6**, the structure was refined as a two-component twin with HKLF 5 file obtained by treating the data with CrysAlisPro[1] yielding to the value of 0.432(2) for the BASF parameter. One 18c6 is disordered over two positions. The atoms of each orientation were located in difference Fourier map. The major and minor parts were refined anisotropically, but distance and similarity restraints (DFIX, SADI, ISOR and SIMU) were used for a convergent least-squares refinement, yielding to site occupancy ratios of 0.511(5)/ 0.489(5). The second 18c6 was just partially disordered over two positions but treated in the same way yielding to site occupancy ratios of 0.64(1)/ 0.36(1). In Compound **7**, light atoms (C and O) showed unstable anisotropic

behaviour and restraints (SIMU 0.02 card) were necessary to handle them. In the case of **8**, the structure was refined as a two-component twin crystal and data (in HKLF 5 format) were obtained by treating the data with CrysAlisPro[1] yielding to the value of 0.448(1) for the BASF parameter. The structure included one molecule of toluene in the asymmetric unit, it was disordered over an inversion centre and refined in a 'PART -1' environment. The atoms were refined anisotropically, but distance and similarity restraints (DFIX and SIMU) were employed for a stable least-squares refinement.

Table S1. Crystal data and structure refinement for **3**.

Empirical formula	$C_{66}H_{144}KN_2O_{22}Si_4U$	
Formula weight	1707.31	
Temperature	100.01(10) K	
Wavelength	1.54184 Å	
Crystal system	Orthorhombic	
Space group	$P2_12_12_1$	
Unit cell dimensions	a = 25.92909(16) Å	α = 90°
	b = 26.18261(18) Å	β = 90°
	c = 26.16679(16) Å	γ = 90°
Volume	17764.41(19) Å^3	
Z	8	
Density (calculated)	1.277 Mg/m^3	
Absorption coefficient	6.590 mm^{-1}	
F(000)	7176	
Crystal size	0.398 x 0.261 x 0.144 mm^3	
Theta range for data collection	3.376 to 75.505°.	
Index ranges	$-32 \le h \le 25$, $-31 \le k \le 32$, $-32 \le l \le 25$	
Reflections collected	134443	
Independent reflections	36333 [$R_{(int)}$ = 0.0346]	
Completeness to theta = 67.684°	100.0 %	
Refinement method	Full-matrix least-squares on F^2	
Data / restraints / parameters	36333 / 0 / 1802	
Goodness-of-fit on F^2	1.096	
Final R indices [I>2sigma(I)]	R_1 = 0.0301, wR_2 = 0.0677	
R indices (all data)	R_1 = 0.0312, wR_2 = 0.0683	
Absolute structure parameter	0.108(3)	
Largest diff. peak and hole	1.753 and -1.698 e.Å^{-3}	

Table S2. Crystal data and structure refinement for **4**·tol.

Empirical formula	$C_{123}H_{254}K_2N_2O_{32}Si_8U_2$	
Formula weight	3052.25	
Temperature	100.01(10) K	
Wavelength	1.54184 Å	
Crystal system	Orthorhombic	
Space group	*Fdd*2	
Unit cell dimensions	a = 92.6284(8) Å	α = 90°
	b = 24.32104(17) Å	β = 90°
	c = 13.71515(11) Å	γ = 90°
Volume	30897.7(4) Å^3	
Z	8	
Density (calculated)	1.312 Mg/m^3	
Absorption coefficient	7.453 mm^{-1}	
F(000)	12768	
Crystal size	0.330 x 0.240 x 0.202 mm^3	
Theta range for data collection	3.731 to 76.194°.	
Index ranges	$-116 \leq h \leq 112$, $-30 \leq k \leq 30$, $-17 \leq l \leq 9$	
Reflections collected	48571	
Independent reflections	12702 [$R_{(int)}$ = 0.0395]	
Completeness to theta = 67.684°	100.0 %	
Absorption correction	Gaussian	
Max. and min. transmission	0.323 and 0.162	
Refinement method	Full-matrix least-squares on F^2	
Data / restraints / parameters	12702 / 93 / 818	
Goodness-of-fit on F^2	1.034	
Final R indices [I>2sigma(I)]	R_1 = 0.0252, wR_2 = 0.0639	
R indices (all data)	R_1 = 0.0255, wR_2 = 0.0642	
Absolute structure parameter	-0.028(3)	
Largest diff. peak and hole	1.108 and -1.151 e.Å^{-3}	

Table S3. Crystal data and structure refinement for **6**.

Empirical formula	$C_{26}H_{48}K_2O_{12}S_6$	
Formula weight	823.20	
Temperature	100.02(11) K	
Wavelength	1.54184 Å	
Crystal system	Monoclinic	
Space group	$P2_1/c$	
Unit cell dimensions	a = 19.133(2) Å	α = 90°
	b = 9.4570(7) Å	β = 111.465(12)°
	c = 22.775(2) Å	γ = 90°
Volume	3835.1(7) $Å^3$	
Z	4	
Density (calculated)	1.426 Mg/m^3	
Absorption coefficient	5.699 mm^{-1}	
F(000)	1736	
Crystal size	0.134 x 0.109 x 0.084 mm^3	
Theta range for data collection	2.481 to 75.784°.	
Index ranges	$-23 \le h \le 24$, $-11 \le k \le 11$, $-28 \le l \le 28$	
Reflections collected	9167	
Independent reflections	9167 [$R_{(int)}$ = 0.0946]	
Completeness to theta = 67.684°	100.0 %	
Absorption correction	Gaussian	
Max. and min. transmission	0.801 and 0.635	
Refinement method	Full-matrix least-squares on F^2	
Data / restraints / parameters	9167 / 1778 / 598	
Goodness-of-fit on F^2	0.907	
Final R indices [I>2sigma(I)]	R_1 = 0.0829, wR_2 = 0.2090	
R indices (all data)	R_1 = 0.1504, wR_2 = 0.2432	
Largest diff. peak and hole	0.843 and -0.510 e.$Å^{-3}$	

Table S4. Crystal data and structure refinement for **7**·tol.

Identification code	**7**·tol
Empirical formula	$C_{74}H_{152}KN_2O_{22}S_3Si_4U$
Formula weight	1907.65
Temperature	140(2) K
Wavelength	1.54184 Å
Crystal system	Monoclinic
Space group	$P2_1$

Unit cell dimensions	a = 13.8270(3) Å	α = 90°.
	b = 24.6484(5) Å	β = 99.042(3)°.
	c = 14.3945(4) Å	γ = 90°.
Volume	4844.9(2) Å^3	
Z	2	
Density (calculated)	1.308 Mg/m^3	
Absorption coefficient	6.686 mm^{-1}	
F(000)	2002	
Crystal size	0.24 x 0.17 x 0.12 mm^3	
Theta range for data collection	3.24 to 76.47°.	
Index ranges	$-17 \le h \le 15$, $-31 \le k \le 21$, $-18 \le l \le 17$	
Reflections collected	37530	
Independent reflections	15546 [$R_{(int)}$ = 0.0802]	
Completeness to theta = 76.47°	98.3 %	
Absorption correction	Gaussian	
Max. and min. transmission	0.562 and 0.292	
Refinement method	Full-matrix least-squares on F^2	
Data / restraints / parameters	15546 / 457 / 989	
Goodness-of-fit on F^2	1.052	
Final R indices [I>2sigma(I)]	R_1 = 0.0627, wR_2 = 0.1516	
R indices (all data)	R_1 = 0.0722, wR_2 = 0.1607	
Absolute structure parameter	-0.027(7)	
Largest diff. peak and hole	5.562 and -3.158 e.Å^{-3}	

Table S5. Crystal data and structure refinement for **8**·1.5tol.

Empirical formula	$C_{73}H_{152}KN_2O_{22}SSi_4U$	
Formula weight	1831.51	
Temperature	100.01(10) K	
Wavelength	1.54184 Å	
Crystal system	Triclinic	
Space group	$P\bar{1}$	
Unit cell dimensions	a = 14.4445(4) Å	α = 82.352(3)°
	b = 14.4565(6) Å	β = 84.245(3)°
	c = 47.0418(18) Å	γ = 78.583(3)°
Volume	9515.4(6) Å^3	
Z	4	
Density (calculated)	1.278 Mg/m^3	
Absorption coefficient	6.387 mm^{-1}	

F(000)	3852
Crystal size	0.264 x 0.111 x 0.052 mm^3
Theta range for data collection	2.852 to 76.401°.
Index ranges	$-17 \leq h \leq 18$, $-18 \leq k \leq 17$, $-59 \leq l \leq 59$
Reflections collected	37472
Independent reflections	37472 [$R_{(int)} = 0.0811$]
Completeness to theta = 67.684°	98.2 %
Absorption correction	Gaussian
Max. and min. transmission	1.000 and 0.401
Refinement method	Full-matrix least-squares on F^2
Data / restraints / parameters	37472 / 978 / 1973
Goodness-of-fit on F^2	1.093
Final R indices [I>2sigma(I)]	$R_1 = 0.0906$, $wR_2 = 0.2307$
R indices (all data)	$R_1 = 0.0931$, $wR_2 = 0.2320$
Extinction coefficient	n/a
Largest diff. peak and hole	4.635 and -4.135 e.$Å^{-3}$

5. Computational data

All the structures reported in this study were fully optimised with the Becke's 3-parameter hybrid functional combined with the non-local correlation functional provided by Perdew/Wang (denoted as B3PW91).[4] The Stuttgart-Dresden RECP (relativistic effective core potential) 5*f*-in-valence was used for uranium atom in combination with its adapted basis set.[5]However, in some cases, the 5*f*-in-core ECP augmented by a *f* polarisation function (α = 1.0) was used for the fixed oxidation state IV or V of the uranium atom.[6] In addition, silicon atoms were treated with the corresponding Stuttgart-Dresden RECP in combination with its adapted basis sets,[7] each one augmented by an extra set of polarisation functions.[8] For the rest of the atoms, the 6-31G(d,p) basis set was used.[9] For analysing the bonding situation in the complexes of interest, we mainly used natural bond orbital analysis (NBO) using Weinhold's methodology.[10] Also, the Multiwfn program,[11] was used for obtaining the composition of the molecular orbitals, based on natural atomic orbital method,[12] as well as the Wiberg bond order analysis in a Löwdin orthogonalised basis. The Chemcraft program was used for the visualisation of the molecular orbitals. [13] Finally, the GAUSSIAN09 program suite was used in all calculations.[14]

Figure S30. Molecular orbitals of the putative $U^{V}K_2$ complex

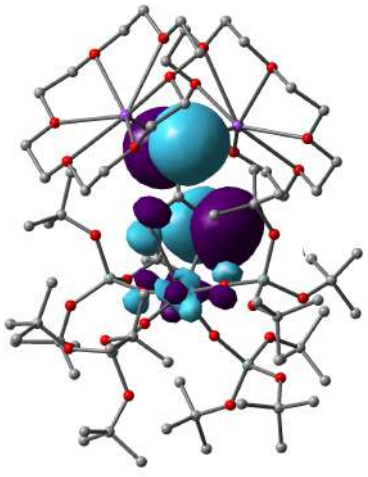	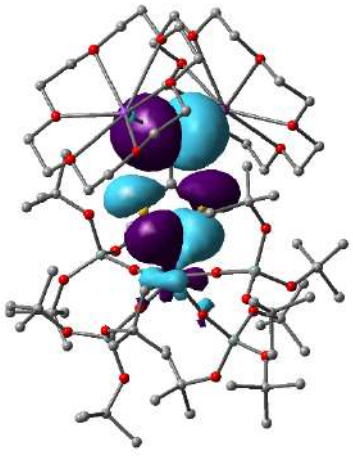
α-HOMO orbital	α-HOMO-1 orbital

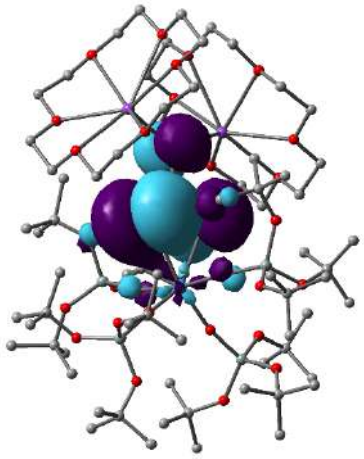	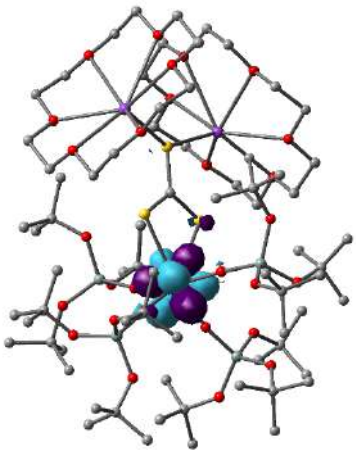
α-HOMO-2 orbital	α-HOMO-3 orbital (orbital f)
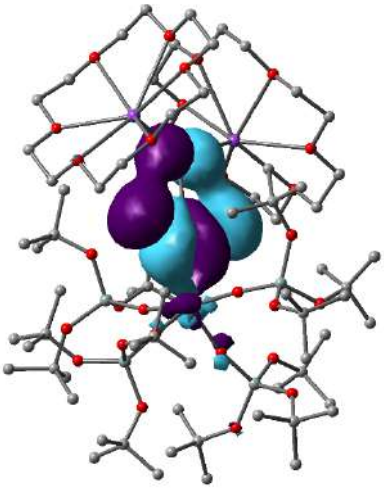	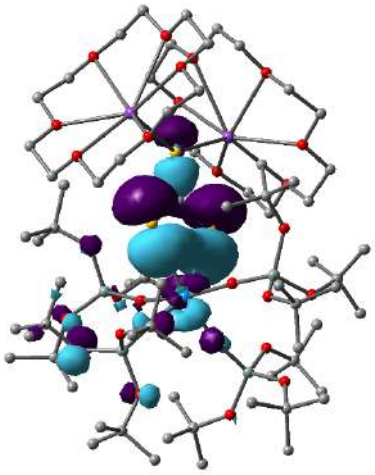
α-HOMO-4 orbital	α-HOMO-10 orbital

[1] CrysAlisPRO, *Rigaku Oxford Diffraction* **2015**.
[2] G. M. Sheldrick, *Acta Crystallogr. C* **2015**, *71*, 3-8.
[3] G. M. Sheldrick, *Acta Crystallogr., Sect. A* **2008**, *64*, 112-122.
[4] a) A. D. Becke, *J. Chem. Phys.* **1993**, *98*, 5648-5652; b) J. P. Perdew, Y. Wang, *Phys.Rev. B* **1992**, *45*, 13244-13249.
[5] a) W. Kuchle, M. Dolg, H. Stoll, H. Preuss, *J. Chem. Phys.* **1994**, *100*, 7535-7542; b) X. Y. Cao, M. Dolg, H. Stoll, *J. Chem. Phys.* **2003**, *118*, 487-496; c) X. Y. Cao, M. Dolg, *Journal of Molecular Structure-Theochem* **2004**, *673*, 203-209.
[6] A. Moritz, X. Cao, M. Dolg, *Theor. Chem. Acc.* **2007**, *118*, 845-854.
[7] A. Bergner, M. Dolg, W. Kuchle, H. Stoll, H. Preuss, *Mol. Phys.* **1993**, *80*, 1431-1441.
[8] A. W. Ehlers, M. Bohme, S. Dapprich, A. Gobbi, A. Hollwarth, V. Jonas, K. F. Kohler, R. Stegmann, A. Veldkamp, G. Frenking, *Chem. Phys. Lett.* **1993**, *208*, 111-114.

[9] a) Ditchfie.R, W. J. Hehre, J. A. Pople, *J. Chem. Phys.* **1971**, *54*, 724-728; b) W. J. Hehre, Ditchfie.R, J. A. Pople, *J. Chem. Phys.* **1972**, *56*, 2257-2261; c) P. C. Hariharan, J. A. Pople, *Theoretica Chimica Acta* **1973**, *28*, 213-222.
[10] a) F. Weinhold, *The Encyclopedia of Computational Chemistry*, Chichester, **1998**; b) A. E. Reed, L. A. Curtiss, F. Weinhold, *Chem. Rev.* **1988**, *88*, 899-926.
[11] T. Lu, F. W. Chen, *J. Comput. Chem.* **2012**, *33*, 580-592.
[12] T. Lu, F. W. Chen, *Acta Chim. Sinica* **2011**, *69*, 2393-2406.
[13] http://www.chemcraftprog.com.
[14] R. Gaussian 09.

APPENDIX 5

Supporting information for Chapter 6

1. NMR Spectroscopic data

Figure S1. ^{1}H NMR (400 MHz, THF-d_8, 298K) of [Cs{[U(OSi(O^{t}Bu)$_3$)$_3$]$_2$(μ-N)}] before (bottom) and after (top) addition of excess KC_8 to yield **1** (**a**); ^{1}H NMR (400 MHz, C_7D_8, 298K) of the crude mixture before (bottom) and after (top) addition of N_2 to complex **1** (**b**).

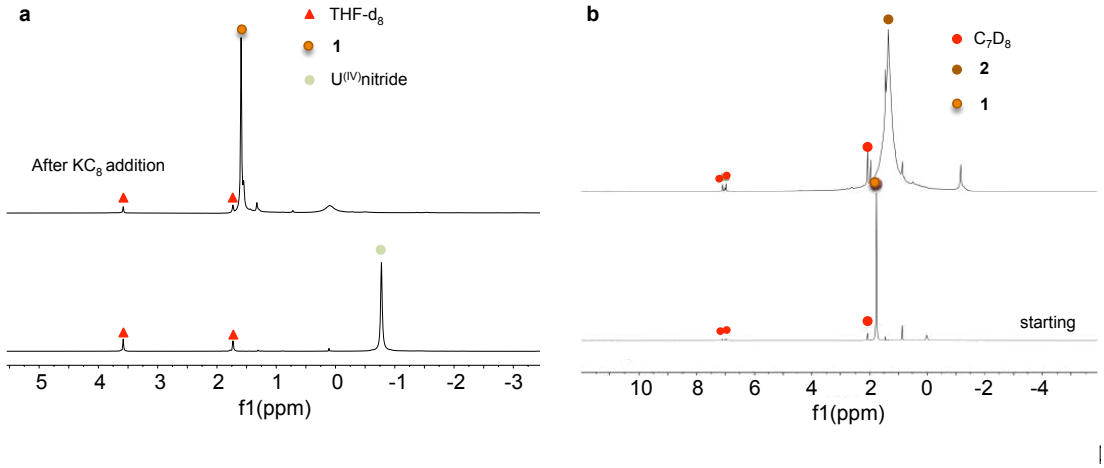

Figure S2. ^{1}H NMR (400 MHz, C_7D_8, 298K) of crystals of complex **3**.

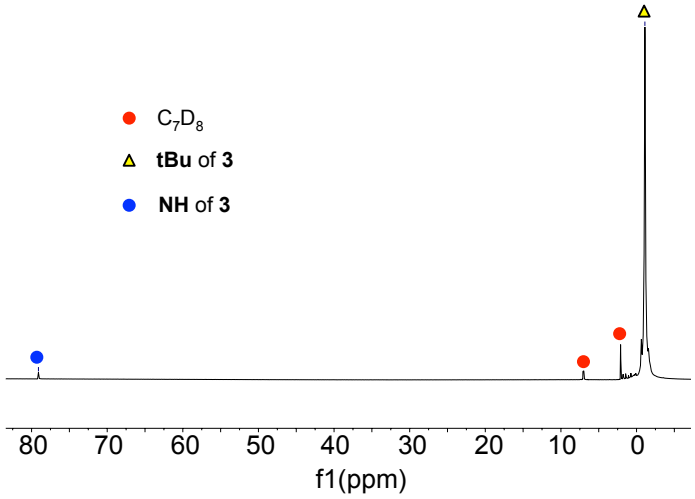

Figure S3. ^{1}H NMR (400 MHz, THF-d_8, 298K) of the successive addition of 1 equiv. PyHCl (up to 7 equiv.) to **2**.

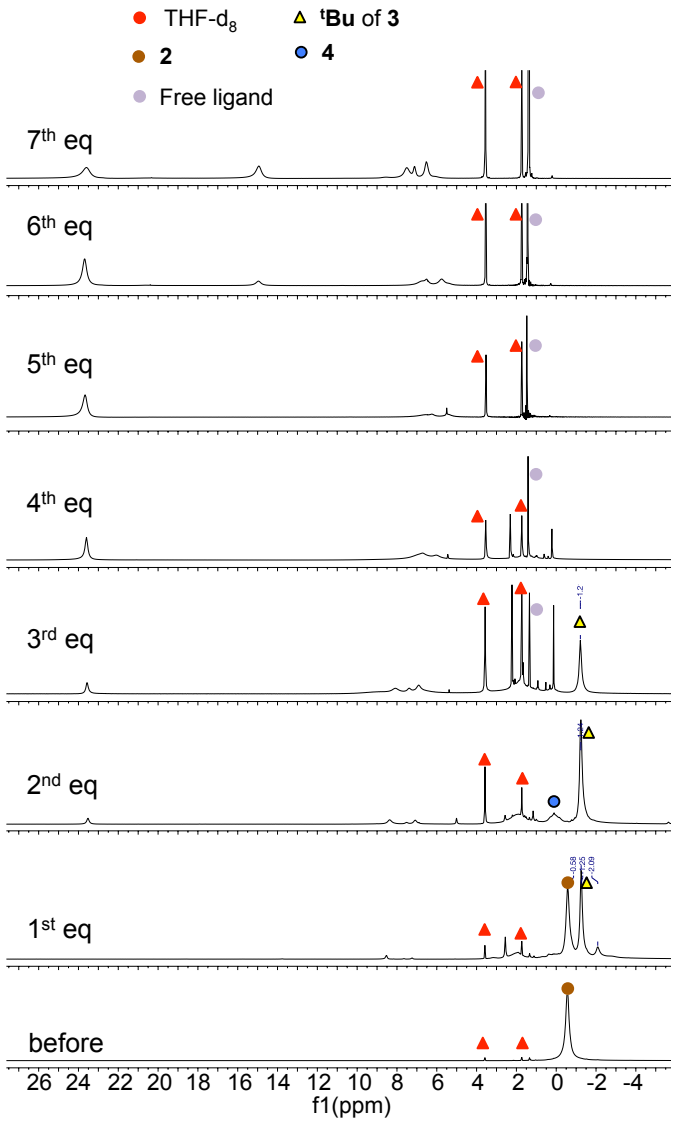

Figure S4. ^{1}H NMR (400 MHz, C_7D_8, 298K) of the crude reaction mixture at different times after reaction of **2** with H_2 (1 atm) at room temperature.

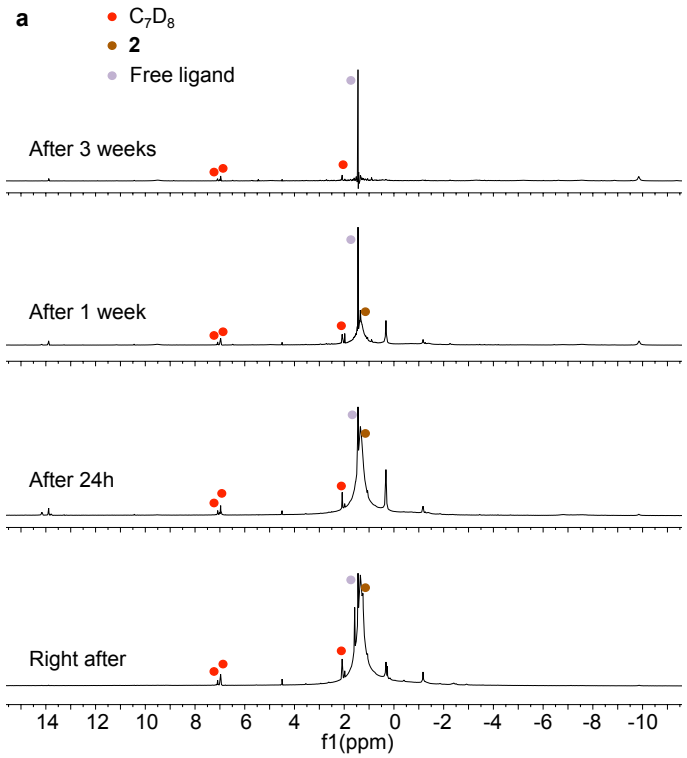

Figure S5. ^{1}H NMR (400 MHz, C_6D_6, 298K) of the crude mixture 1 hour after addition of 10 equiv. of CO to **2** to afford **5** (**a**); ^{1}H NMR (400 MHz, C_6D_6, 298K) of crystals of **5** (**b**).

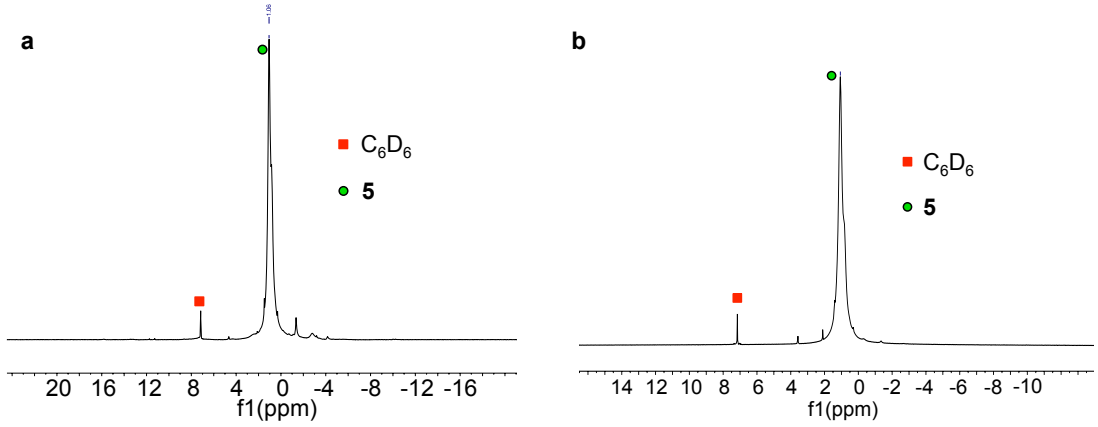

Figure S6. ^{13}C NMR (400 MHz, D_2O, 298K) of the crude mixture after addition of 10 equiv. of CO to complex **2** showing the presence of CN^- and OCN^- in a 1:2 ratio.

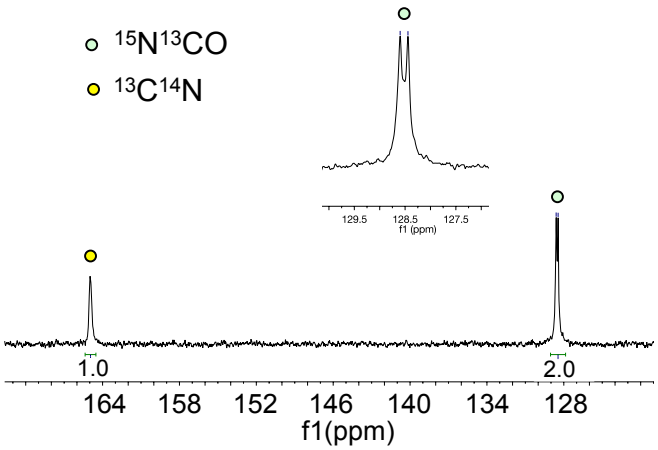

Figure S7. ^1H NMR (400 MHz, C_7D_8, 298K) of crystals of **6** (**a**); ^{13}C NMR (400 MHz, C_7D_8, 298K) of crystals of **6** (**b**).

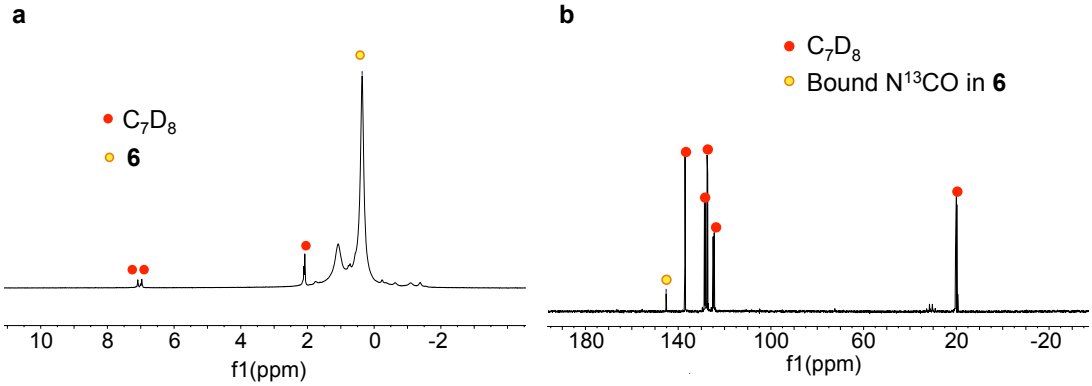

Figure S8. ^{13}C NMR (400 MHz, D_2O, 298K) of the crude mixture after addition of 10 equiv. of CO to complex **3**.

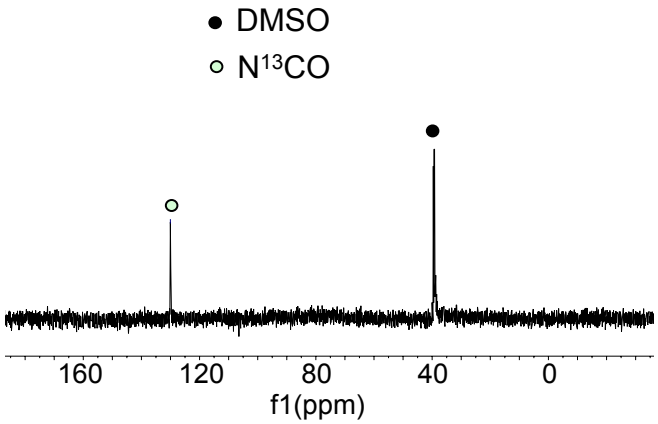

Figure S9. Mass spectrum of the gas evolved during the reaction of ^{15}N-**3** with CO, showing formation of $^{14}N^{15}N$ and $^{15}N_2$ with m/z = 29 and 30, respectively. The peak at m/z = 28 arises from $^{14}N_2$ and CO. $^{14}N^{15}N$ and $^{14}N_2$ arise from nitride/N_2 scrambling during the synthesis of **3**.

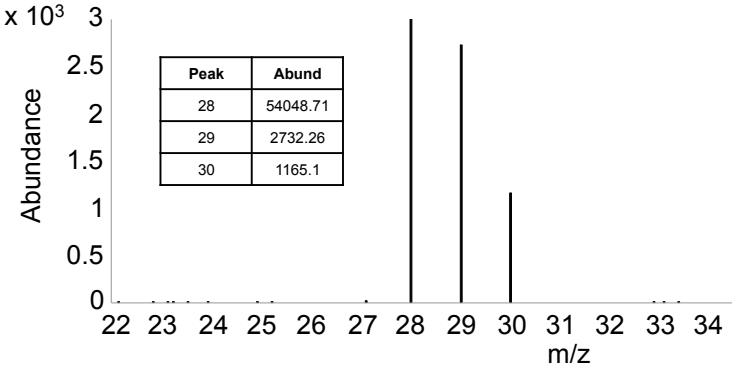

Figure S10. ^{1}H NMR (400 MHz, DMSO-d_6, 298K) of crystals of the white precipitate formed after addition of excess PyHCl (20 equiv.) to ^{15}N-**6**.

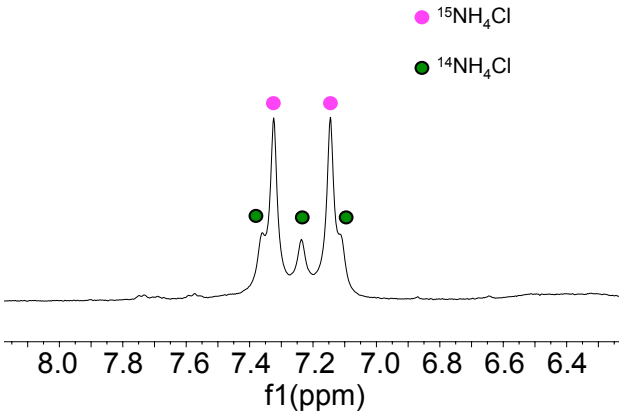

2. Crystallographic data

The diffraction data of **1** were measured at low temperature [100(2) K] using Mo K_a radiation on a Bruker APEX II CCD diffractometer equipped with a kappa geometry goniometer. The dataset was reduced by EvalCCD[1] and then corrected for absorption.[2] The data collection of **2** and **3, 5** and **6** were performed at low temperature [140(2) K for **2**, **3**, **5** and **6**; 100(2) K for **4**] using Cu K_a radiation on a Rigaku SuperNova dual system in combination with an Atlas CCD detector. The data reduction was carried out by Crysalis PRO. [3] The solution and refinement of the structure was performed with SHELXS-97[4] and SHELXL-2016 (released 4),[5]. The crystal structures were refined using full-matrix least-squares based on F^2 with all non hydrogen atoms anisotropically defined. Hydrogen atoms were placed in calculated

positions by means of the "riding" model. In the case of **1**, extensive disorder was encountered during the refinement of one –OSi(O*t*-butyl)$_3$ moiety and the split model combined with reasonable restraints (SADI, SIMU cards) was employed to correctly treat it. Some geometrical restraints (SADI card) were applied to **3** *t*-butyl substituents and all carbon atoms were refined anisotropically but their thermal parameters were submitted to restraints (SIMU). The SQUEEZE [6] algorithm of Platon was employed in the last stages of refinement to take into account spurious electron density peaks, likely due to disordered solvent molecules. In the case of **2**, K and N atoms displayed a disordered arrangement complicated by symmetry (3-fold axes); K was treated by the split model whereas in the case of nitrogen atoms the occupancies were fixed to 1/3 for symmetry reasons. The displacement parameters of N1 and N3 were constrained by means of the EADP command. As for **1**, restraints (ISOR card) were applied to the thermal parameters of all carbons. Additional electron density found in the difference Fourier map (due to highly disordered solvent) of compounds **3, 4, 5** and **6** was treated by the SQUEEZE algorithm of PLATON.[6] The μ_2-N_2 molecule and the μ_2-NH group bridging the metal centres in **3** were split into two orientations. The major and minor parts were refined anisotropically, but distance and similarity restraints (DFIX, SIMU and ISOR) had to be applied for a convergent least-square refinement, yielding to site occupancy ratios of 0.57(2)/ 0.43(2). In **4** the μ_2-Cl and μ_2-NH bridging metal centres were split into two orientations. Two parts were modelled over two half-occupied sites, that were refined anisotropically, but distance and similarity restraints (SADI, SIMU and ISOR) had to be applied for a convergent least-square refinement. In **6** the μ_2-NCO bridging metal centres was split into two orientations. The major and minor parts were refined anisotropically, but distance and similarity restraints and constrains (DFIX, SADI, ISOR and EADP) had to be applied for a convergent least-square refinement, yielding to site occupancy ratios of 0.57(1)/ 0.43(1).

Table S1: X-Ray crystallographic data for complexes 1, 2 and 3.

	1	**2**	**3.Toluene**
Formula	$C_{72}H_{162}K_3NO_{24}Si_6U_2$	$C_{72}H_{162}K_3N_3O_{24}Si_6U_2$	$C_{79}H_{171}K_2N_3O_{24}Si_6U_2$
Crystal size (mm)	0.402 x 0.111 x 0.046	0.20 x 0.15 x 0.10	0.724 x 0.487 x 0.308
cryst syst	Monoclinic	Trigonal	Triclinic
space group	C 2/c	R-3	P-1
volume ($Å^3$)	23766(5)	16076.0(5)	5792.02(17)
a (Å)	56.507(9)	23.8684(3)	14.21015(19)
b (Å)	14.4927(15)	23.8684(3)	17.5116(3)
c (Å)	29.069(3)	32.5838(7)	25.4916(4)
α (deg)	90	90	79.0803(14)
β (deg)	93.331(10)	90	88.6143(12)
γ (deg)	90	120	68.5980(14)
Z	8	6	2
formula weight (g/mol)	2187.92	2215.95	2269.98
density (g cm^{-3})	1.223	1.373	1.302
absorption coeff (mm^{-1})	2.940	10.615	9.518
F(000)	8944	6792	2328
temp (K)	100(2)	140.00(13)	140.00(10)
total refl	124838	40364	43331
unique refl [R(int)]	21850 [R(int) = 0.0946]	7339 [R(int) = 0.0409]	23323 [R(int) = 0.0405]
Final R indices [I > 2σ(I)]	R_1 = 0.1066, wR_2 = 0.2327	R_1 = 0.0450, wR_2 = 0.1091	R_1 = 0.0514, wR_2 = 0.1345
Largest diff. peak and hole (e.$Å^{-3}$)	2.638 and -2.276	2.646 and -3.263	4.056 and -4.974
GOF	1.150	1.026	1.038

Table S2: X-Ray crystallographic data for complexes 4, 5 and 6.

	4	**5.THF**	**6**
Formula	$C_{72}H_{164}ClK_2N_2O_{24}Si_6U_2$	$C_{78}H_{170}K_2N_2O_{28}Si_6U_2$	$C_{73}H_{163}K_2N_2O_{25}Si_6U_2$
Crystal size (mm)	0.205 x 0.191 x 0.109	0.38 x 0.33 x 0.27	0.585 x 0.463 x 0.382
cryst syst	Monoclinic	Monoclinic	Monoclinic
space group	P 2_1	C2/c	P 2_1
volume ($Å^3$)	5550.2(2)	23761.0(10)	5584.7(3)
a (Å)	13.9073(3)	49.0711(15)	13.9643(4)
b (Å)	18.2458(4)	18.0309(6)	18.1361(5)
c (Å)	21.9160(5)	26.9338(6)	22.0812(6)
α (deg)	90	90	90
β (deg)	93.603(2)	94.389(2)	92.980(2)
γ (deg)	90	90	90
Z	2	8	2
formula weight (g/mol)	2200.29	2306.95	2191.84
density (g cm^{-3})	1.317	1.290	1.303
absorption coeff (mm^{-1})	10.129	9.31	3.092
F(000)	2250	9456	2242
temp (K)	100.01(10)	140.0(1)	140.09(13)
total refl	42431	79798	83917
unique refl [R(int)]	20626 [R(int) = 0.0557]	24371 [R(int) = 0.071]	26650 [R(int) = 0.0439]
Final R indices [I > 2σ(I)]	R_1 = 0.0503, wR_2 = 0.1274	R_1 = 0.0616, wR_2 = 0.1531	R_1 = 0.0471, wR_2 = 0.1084
Largest diff. peak and hole ($e.Å^{-3}$)	3.506 and -1.612	3.69 and -1.69	2.191 and -1.246

GOF	1.032	1.071	1.030

3. Magnetic and EPR analyses

Magnetic measurements were performed using a Quantum Design MPMS-5T superconducting quantum interference device (SQUID) magnetometer in a temperature range 2-300 K. The powder sample was enclosed in an evacuated quartz capsule and placed inside a plastic straw. The measurements were performed with applied magnetic field of 0.1 T in the zero-field cooled (ZFC) regime. The solid-state magnetic moment of **2** at 298 K was found to be of 2.06 μ_B (where μ_B is Bohr magneton units) per uranium. This value is significantly lower than the theoretical U^V free ion value (μ_{eff} = 2.54 μ_B) but is in the range of magnetic moments previously reported for U^V complexes (1.35–3.40 μ_B).[7] The value of the magnetic moment decreases gradually with the temperature from a value of 2.92 μ_B per dimer at 300 K to a value of 1.6 μ_B at 50 K and then more rapidly reaching a value of 0.4 μ_B at 2.5 K. This temperature response of the magnetic moment is also characteristic of U^V complexes. Magnetic susceptibility of 2 (Extended data Fig. 7b) shows a paramagnetic behaviour from 300 K down to approximately 50 K where a deviation occurs, which can probably be attributed to antiferromagnetic coupling between two uranium spins. The value of the magnetic moment per uranium is of 2.06μ_B at 298K. The X-Band (9.40 GHz) EPR spectrum of **2** (Extended data Fig.7a) was measured on a solution of **2** (2 mg, 0.0009 mmol) in 170 µL of a mixture of toluene/n-hexane (1:1), with a Bruker Elexsys E500 spectrometer working at 9.4 GHz frequency with an oxford ESR900 cryostat for 4-300 K operation. Baseline correction of the raw EPR spectrum was performed with cubic spline (Xepr 2.4b.12, Bruker). Simulations were performed with the Easyspin 5.1.3 program.[8] The X-Band (9.40 GHz) EPR spectrum of complex **2** shows an intense signal at 10 K that was fitted with a rhombic set of g-values (g_1 = 1.73; g_2 = 0.78; g_3 = 0.46), confirming the presence of uranium in the +5 oxidation state. The g values of **2** can be compared to those reported for an octahedral uranium(V) monoxo-complex (g_1 = 1.248; g_2 = 0.856; g_3 = 0.485).[9]

[1] A. J. M. Duisenberg, L. M. J. Kroon-Batenburg, A. M. M. Schreurs, *J. Appl. Crystallogr.* **2003**, *36*, 220-229.
[2] R. H. Blessing, *Acta Crystallogr., Sect. A* **1995**, *51*, 33-38.
[3] CrysAlisPRO, Rigaku Oxford Diffraction, **2015**.
[4] G. M. Sheldrick, *Acta Crystallogr., Sect. A* **2008**, *64*, 112-122.
[5] G. M. Sheldrick, *Acta Crystallogr., Sect. A* **2015**, *71*, 3-8.
[6] a) PLATON, A. L. Spek, *Acta Crystallogr., Sect. D* **2009**, *65*, 148-155; b) A. L. Spek, *Acta Crystallogr. Sect. C* **2015**, *71*, 9-18.
[7] D. R. Kindra, W. J. Evans, *Chem. Rev.* **2014**, *114*, 8865-8882.
[8] S. Stoll, A. Schweiger, *J. Magn. Reson.* **2006**, *178*, 42-45.
[9] O. Cooper, C. Camp, J. Pecaut, C. E. Kefalidis, L. Maron, S. Gambarelli, M. Mazzanti, *J. Am. Chem. Soc.* **2014**, *136*, 6716-6723.

APPENDIX 6

Supporting information for Chapter 7

1. NMR Spectroscopic data

NMR data for 2

Figure 1. ^{1}H NMR (400 MHz, tol-d_8, 298 K) of the residue after solvent removal from the crude reaction mixture after addition of IMesN_2O to **1** in THF at 233K.

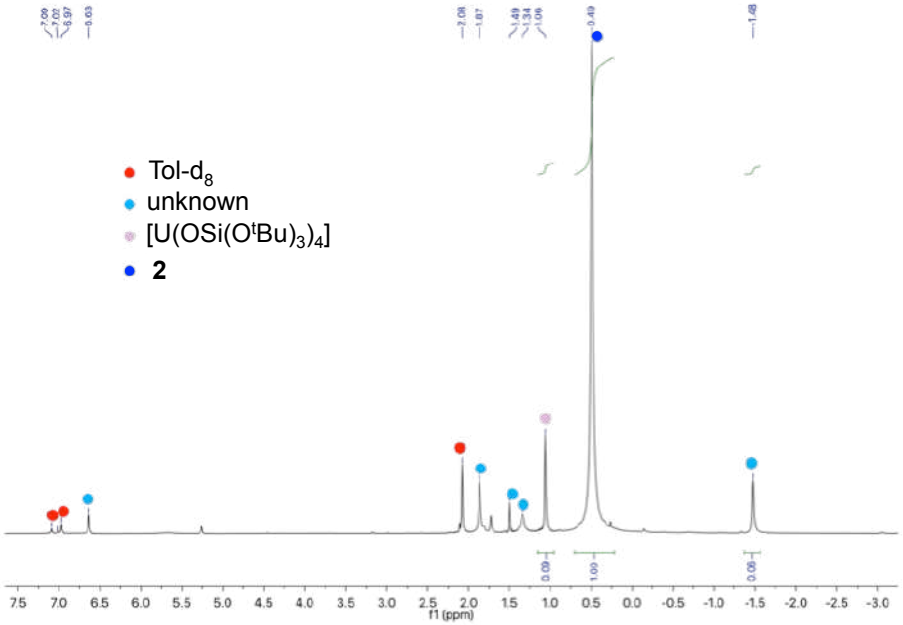

Figure 2. ^{1}H NMR (400 MHz, tol-d_8, 298 K) of crystals of **2**.

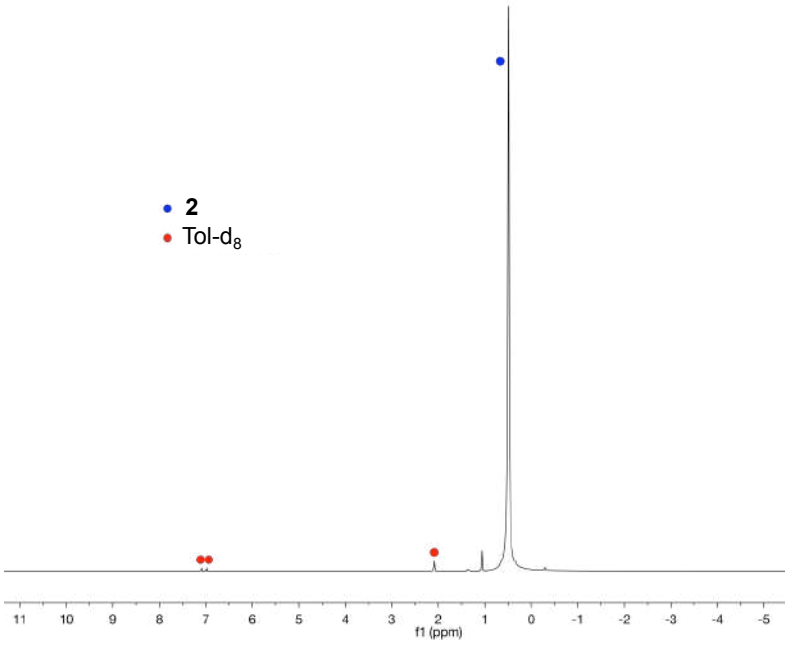

Figure 3. ^{13}C NMR (400 MHz, tol-d_8, 298 K) of crystals of **2**.

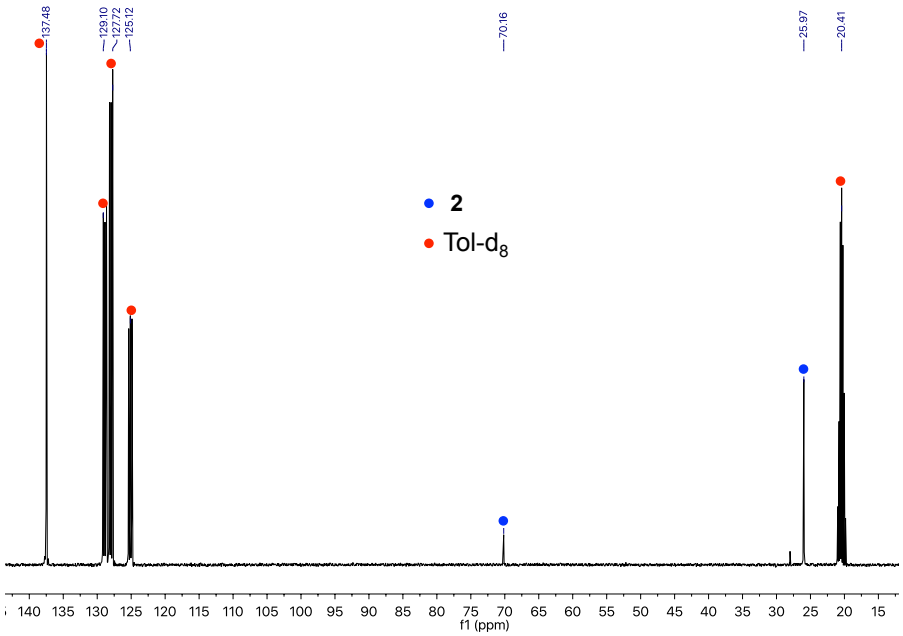

Figure 4. ^{1}H NMR (400 MHz, tol-d_8, 298 K) of a solution of crystals of **2** after 6h at room temperature.

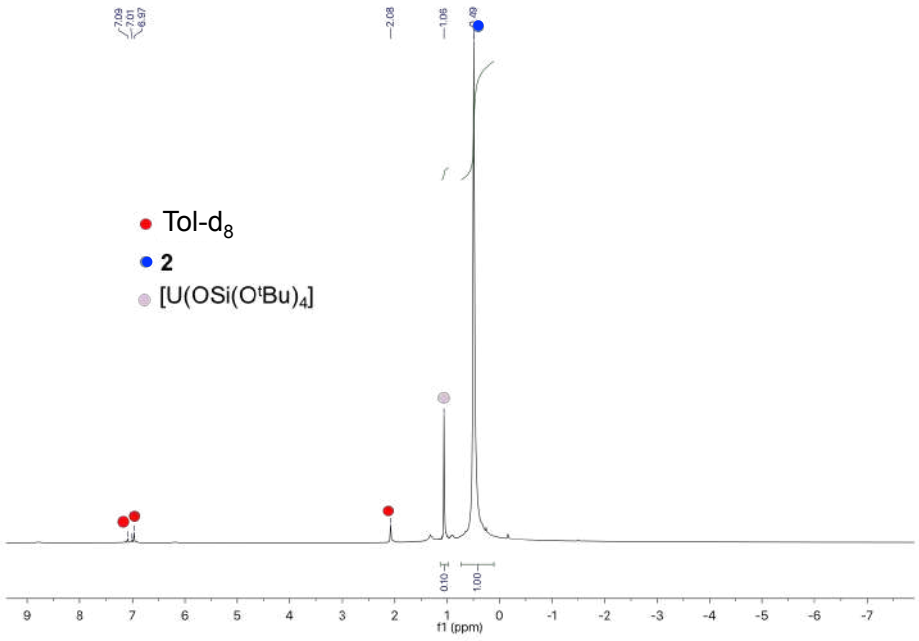

Figure 5. ^{1}H NMR (400 MHz, tol-d_8, 298 K) of a solution of crystals of **2** after 1 week at room temperature.

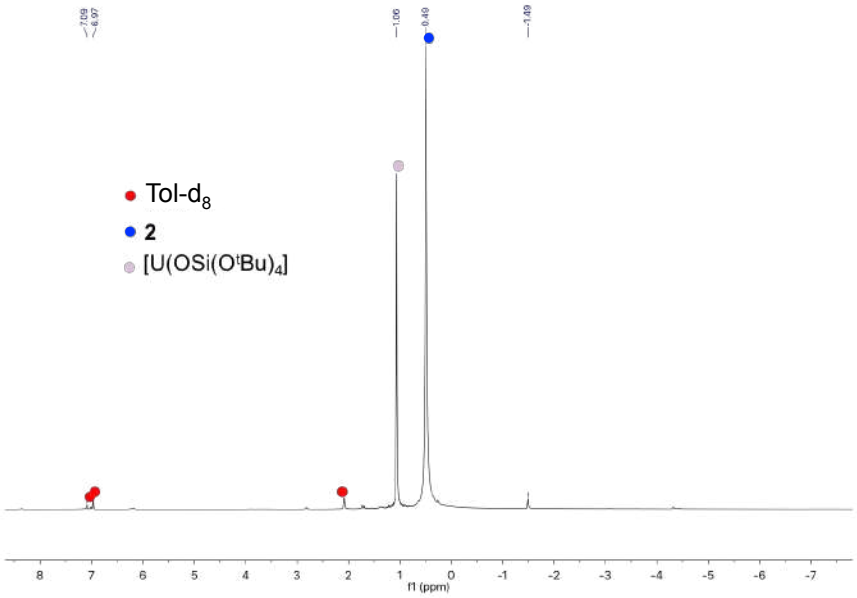

Figure 6. ^{1}H NMR (400 MHz, tol-d_8, 298 K) of a solution of crystals of **2** after 20 days at room temperature.

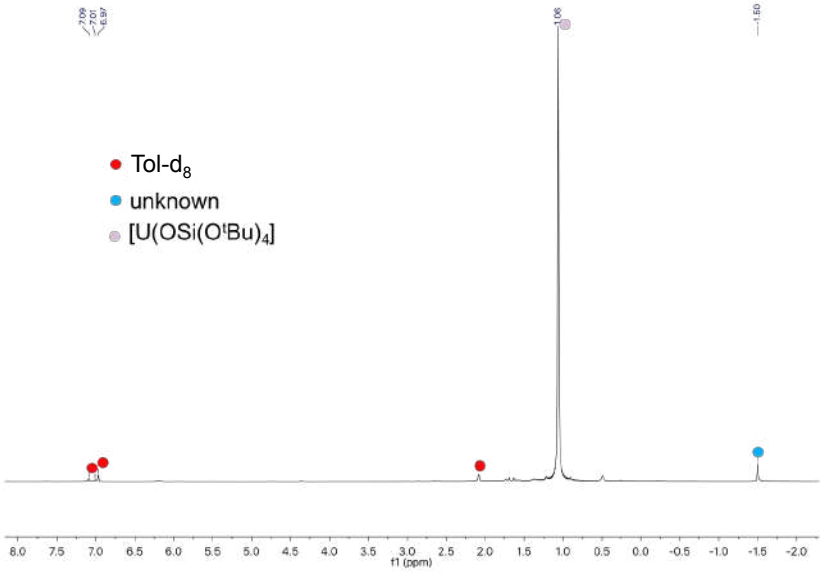

Figure 7. ^{1}H NMR (400 MHz, THF-d_8, 298 K) of a solution of crystals of **2** at room temperature, at different times.

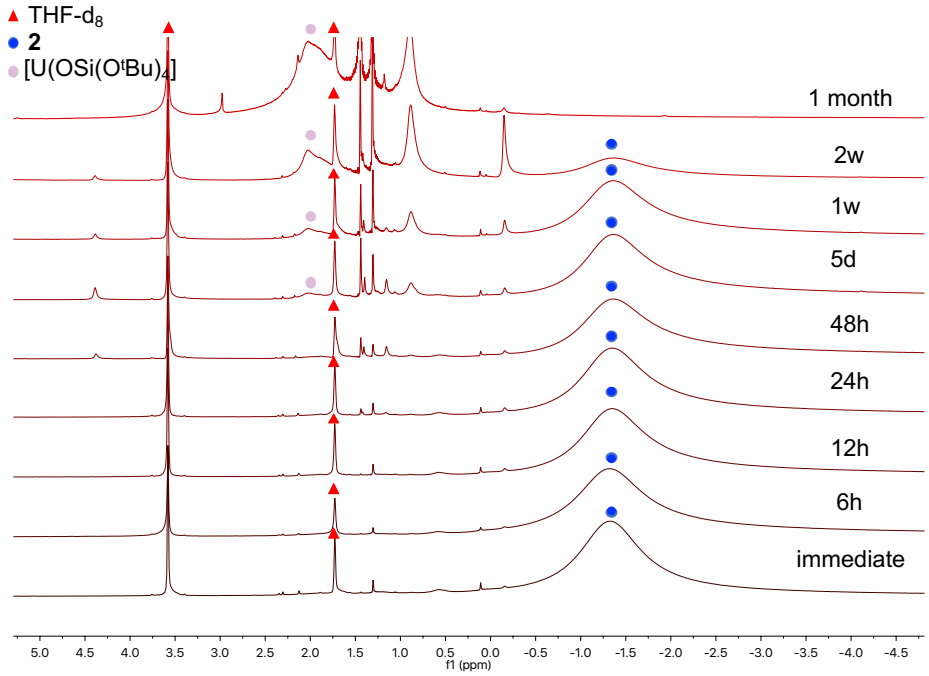

Figure 8. ^{1}H NMR (400 MHz, THF-d_8, 298 K) of the reaction mixture after addition at 193 K, of 1 eq of N_2O in hexane to complex **1**.

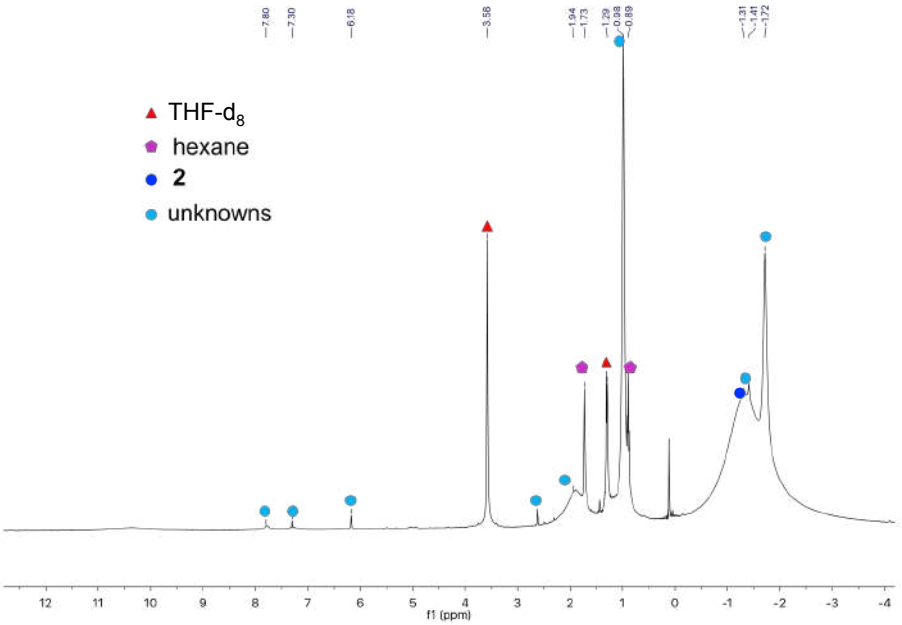

Figure 9. ^{1}H NMR (400 MHz, THF-d_8, 298 K) of the crude reaction mixture after addition of 1 eq N_2O in THF at 298 K to complex **1**.

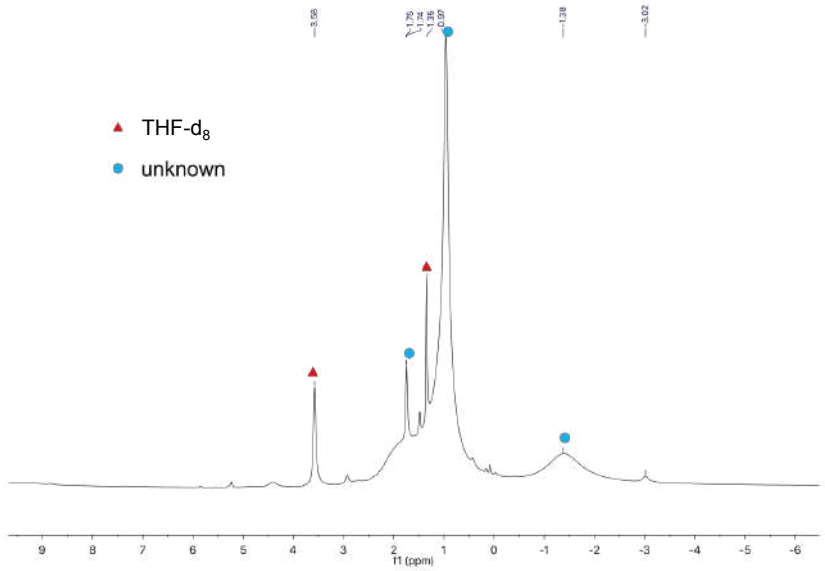

Figure 10. ^{1}H NMR (400 MHz, tol-d_8, 233 K) of the crude reaction mixture after addition of 1 eq PyNO in hexane at 193 K, to complex **1**.

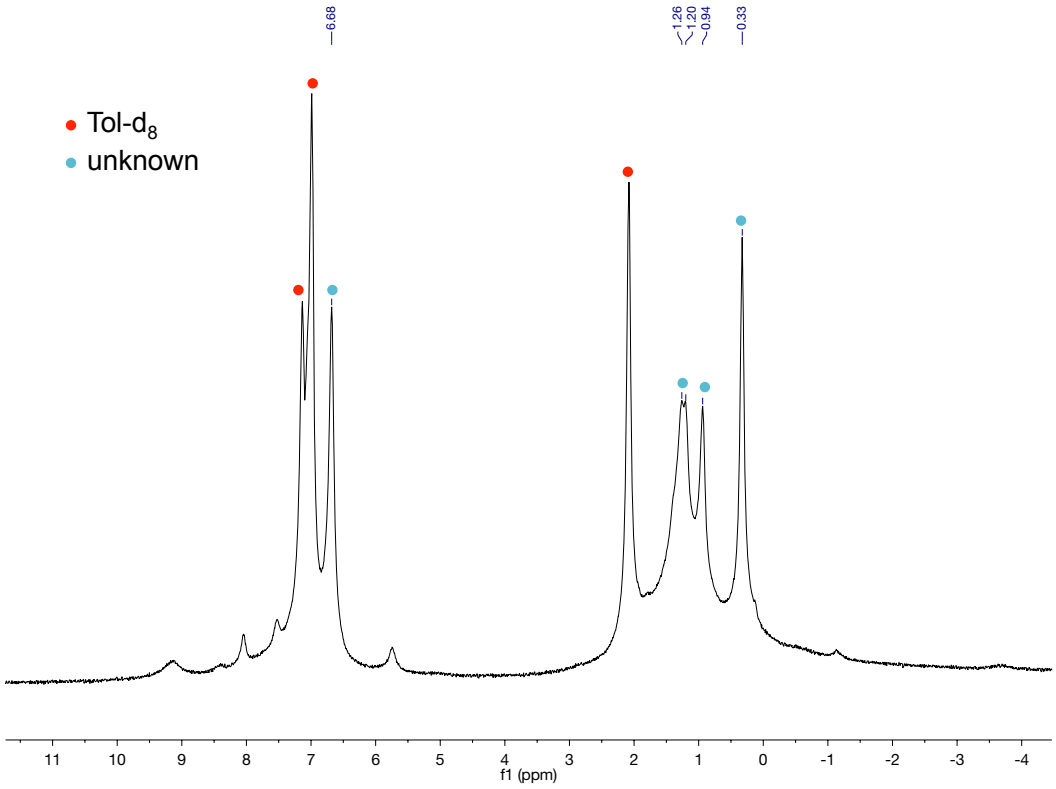

Figure 11. ^{1}H NMR (400 MHz, tol-d_8, 233 K) of the crude reaction mixture after addition of 1 eq Me_3NO as a solution in THF at 193 K, to complex **1**.

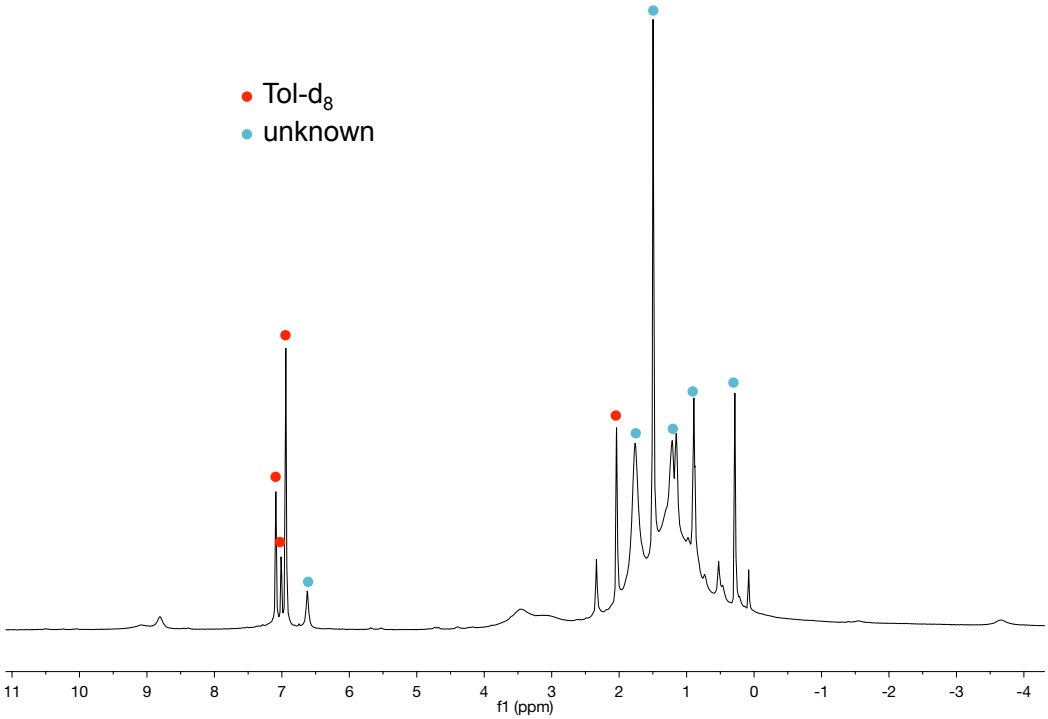

Figure 12. ^{1}H NMR (400 MHz, THF-d_8, 298 K) of the crude reaction mixture after addition of 1 eq Me_3NO in hexane at 193 K, to complex **1**.

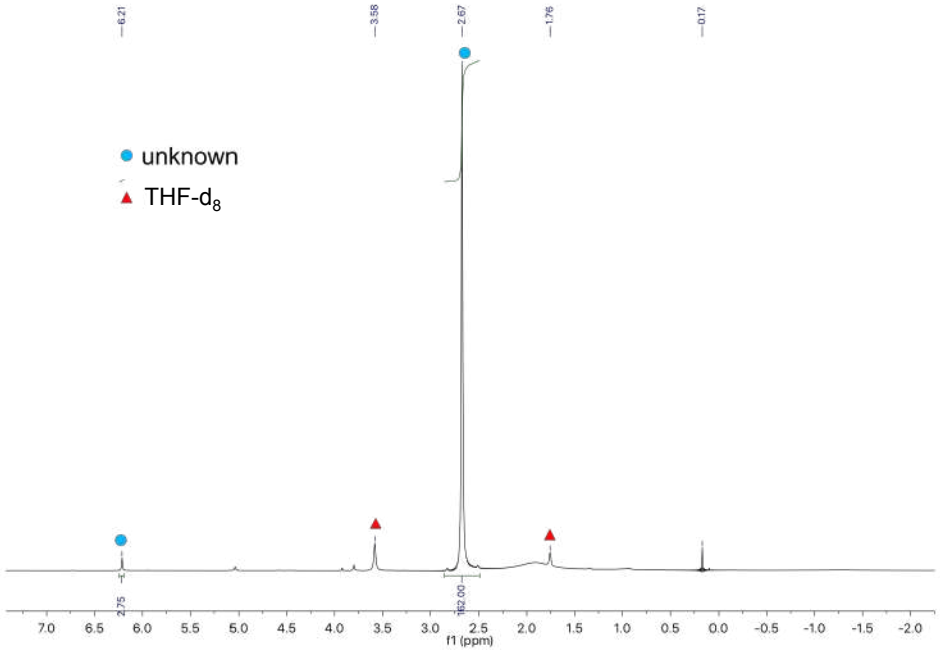

NMR data of 3

Figure 13. ^{1}H NMR (400 MHz, tol-d_8, 298 K) of the crude reaction mixture after addition of 5 eq. KC_8 at 193 K to complex **2** in THF.

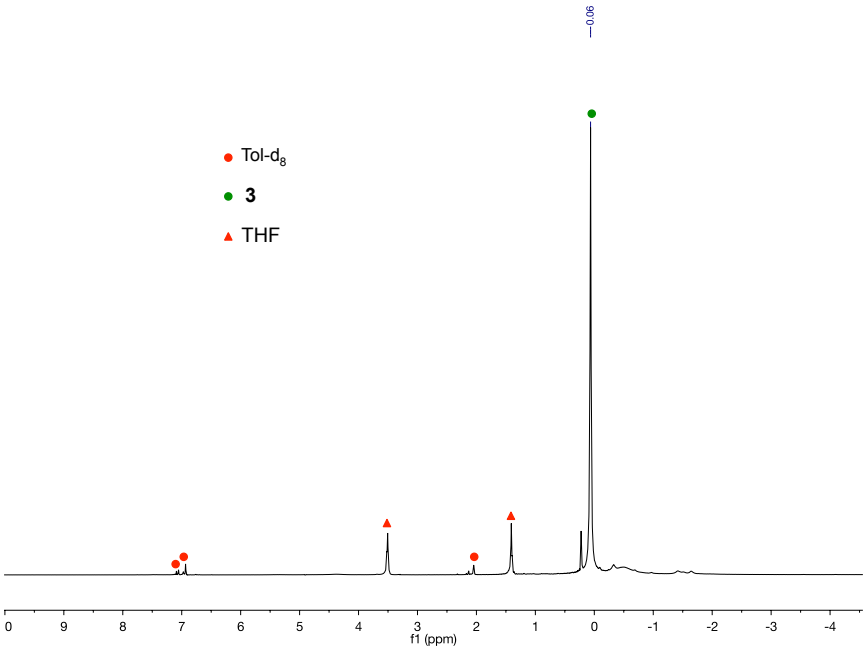

Figure 14. ^{1}H NMR (400 MHz, THF-d_8, 298 K) of crystals of **3**.

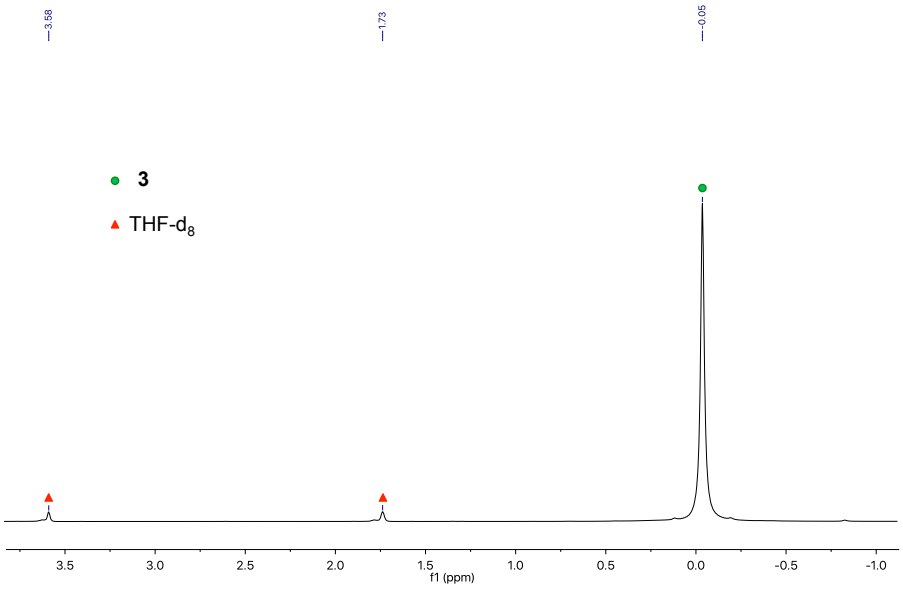

Figure 15. ^{1}H NMR (400 MHz, tol-d_8, 298 K) of crystals of **3**.

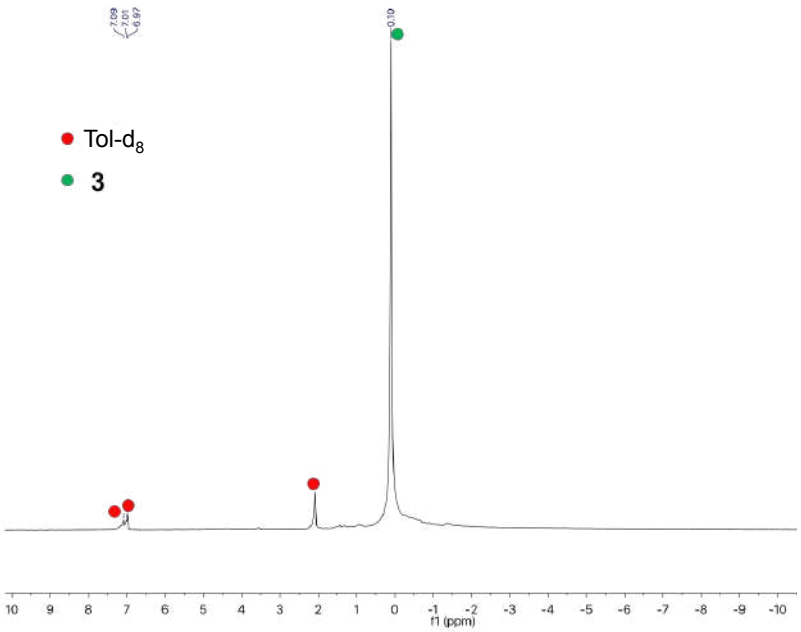

Figure 16. ^{1}H NMR (400 MHz, THF-d_8, 298 K) of a solution of crystals of **3** kept at room temperature measured at different times.

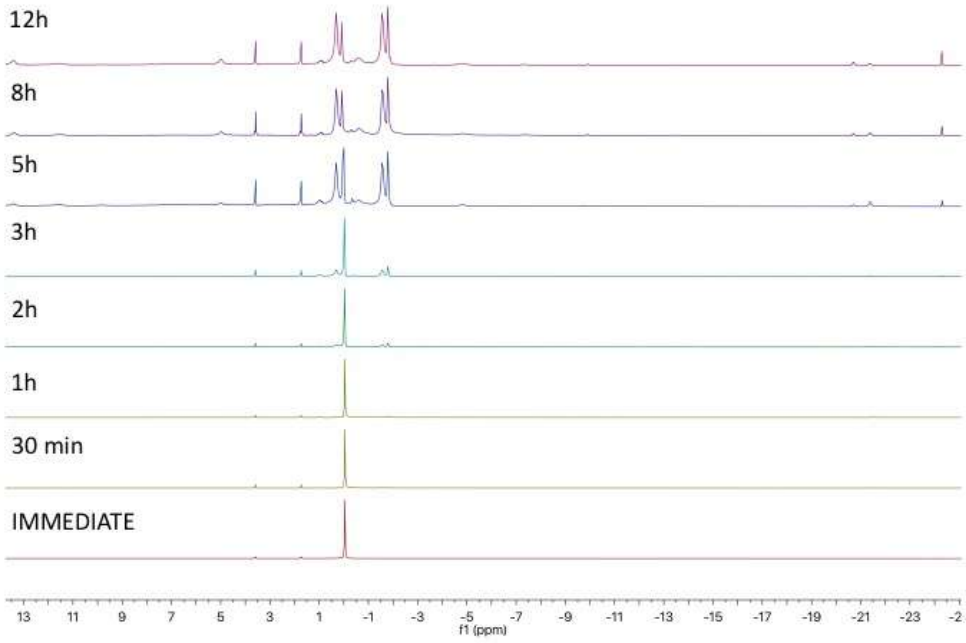

Figure 17. ^{1}H NMR (400 MHz, THF-d_8, 298 K) of a solution of crystals of **3** after 12h at 298K.

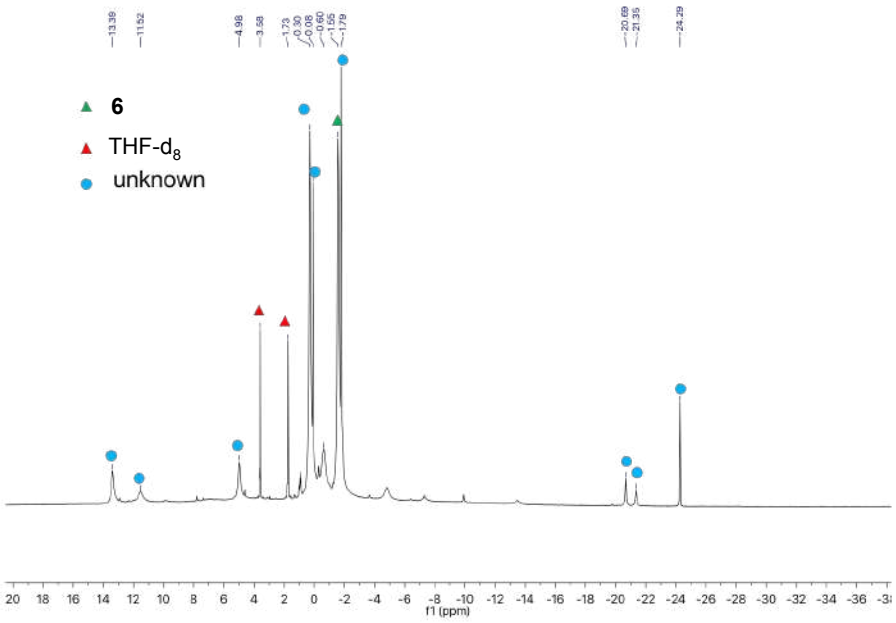

Figure 18. ^{1}H NMR (400 MHz, tol-d_8, 298 K) of **3** in toluene at room temperature measured at different times.

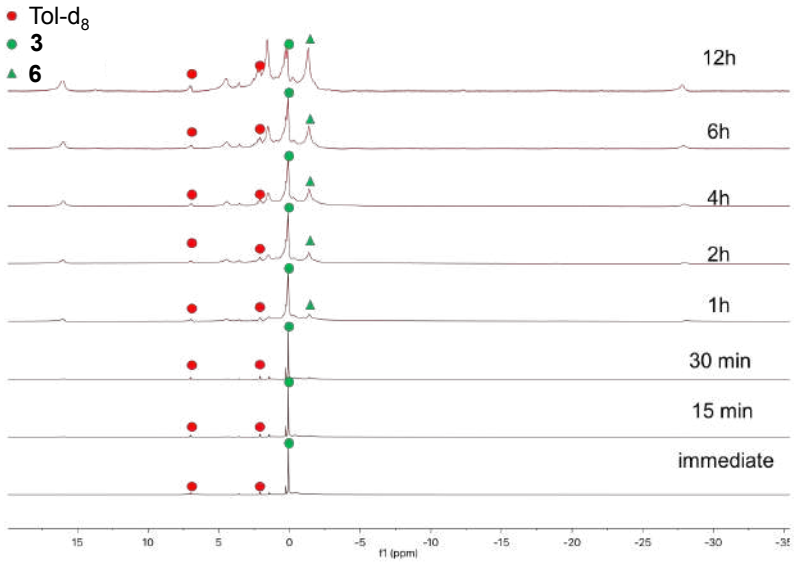

NMR data of 3.Cs

Figure 19. ^{1}H NMR (400 MHz, tol-d_8, 298 K) of complex **3.Cs**.

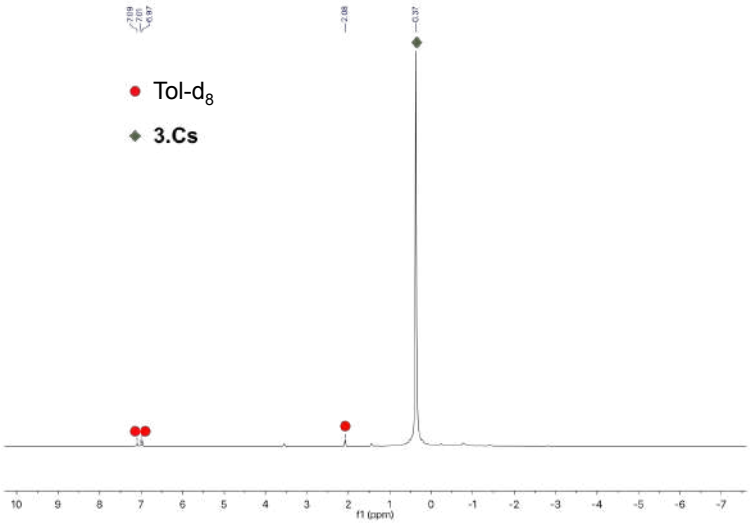

Figure 20. ^{1}H NMR (400 MHz, tol-d_8, 298 K) immediately after addition of N_2 to complex **3.Cs** at 298K in toluene.

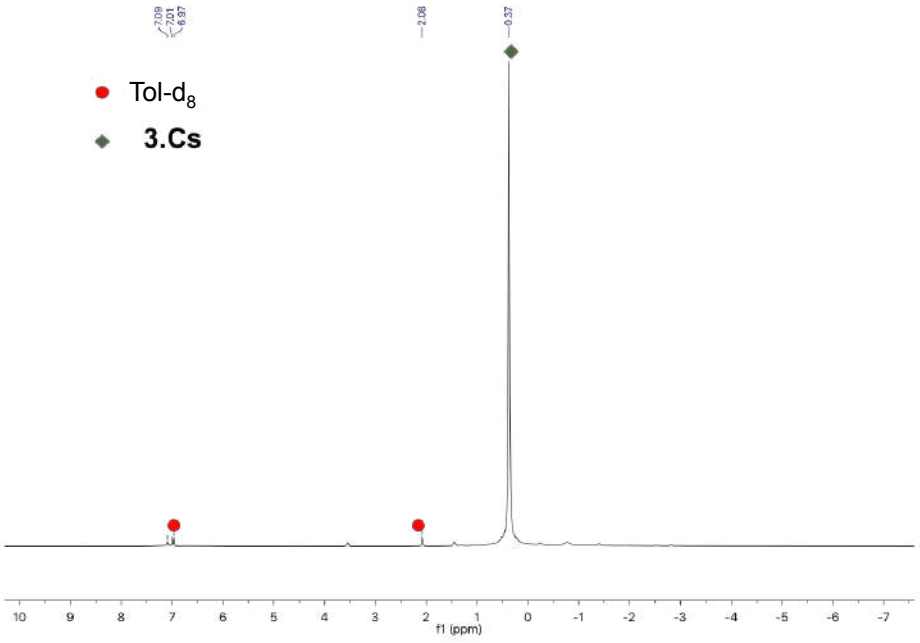

NMR data of 4

Figure 21. ^{1}H NMR (400 MHz, tol-d_8, 298 K) of the reaction mixture immediately after addition of N_2 (1 atm) to complex **3**.

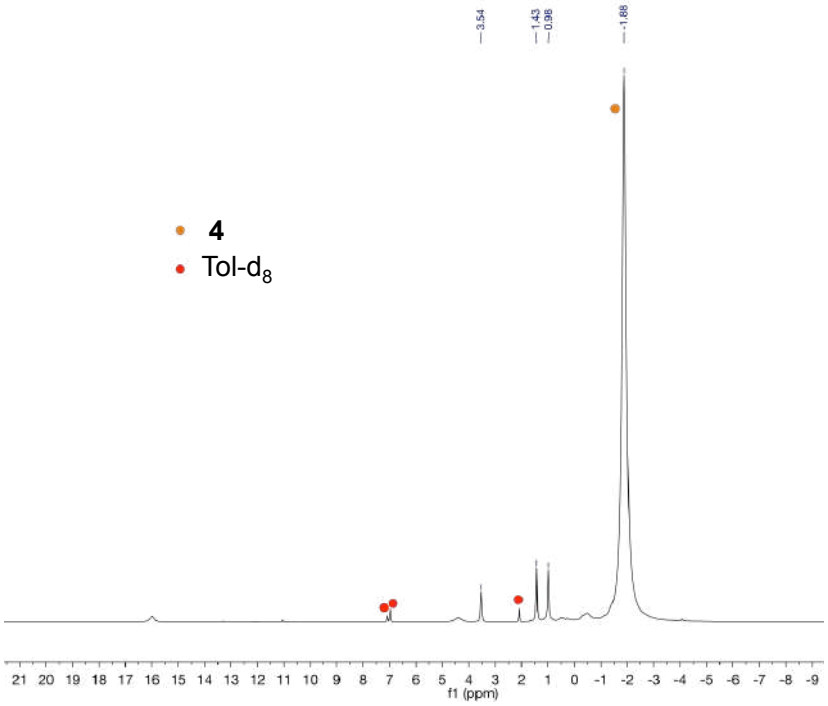

Figure 22. ^{1}H NMR (400 MHz, tol-d_8, 298 K) of crystals of complex **4**.

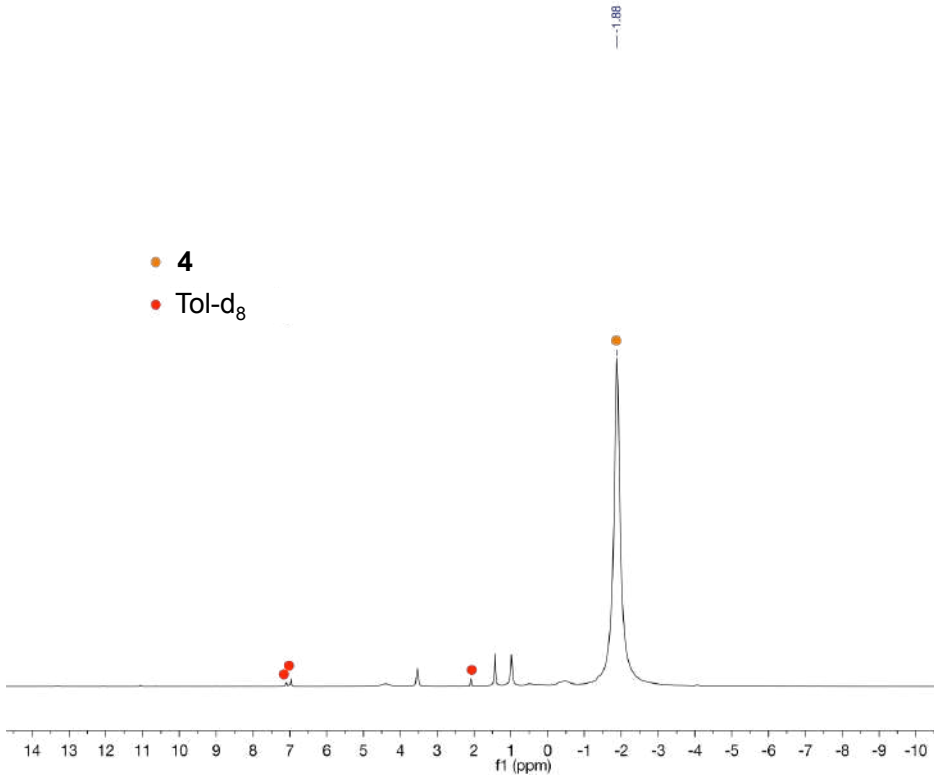

Figure 23. ^{1}H NMR (400 MHz, THF-d_8, 298 K) after addition of one equivalent of 2,4,6-tri-*tert*-butylphenol to **4**.

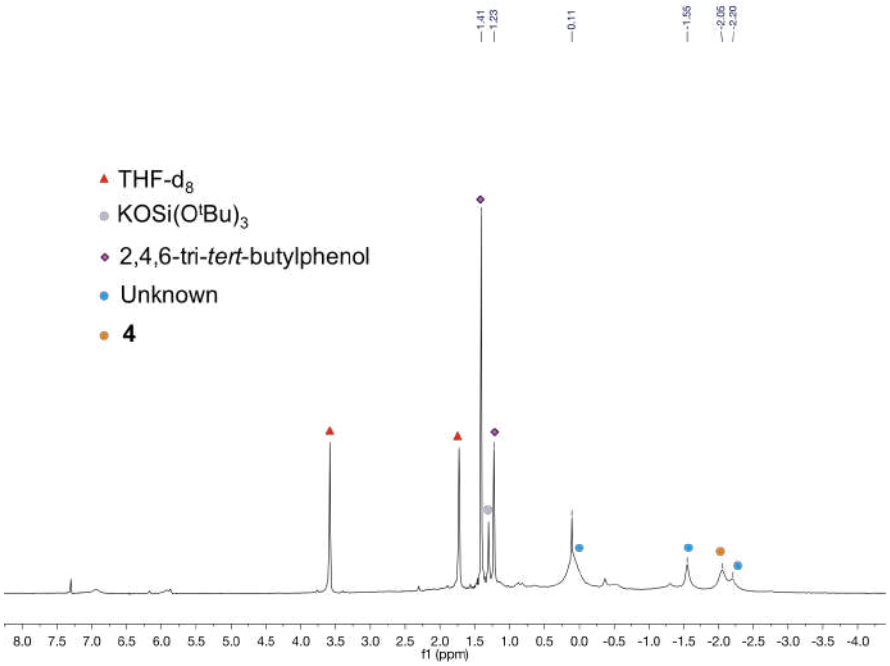

Figure 24. ^{1}H NMR (400 MHz, DMSO-d_6, 298 K) of the crude reaction mixture after addition of excess HCl(Et_2O) to complex **4**.

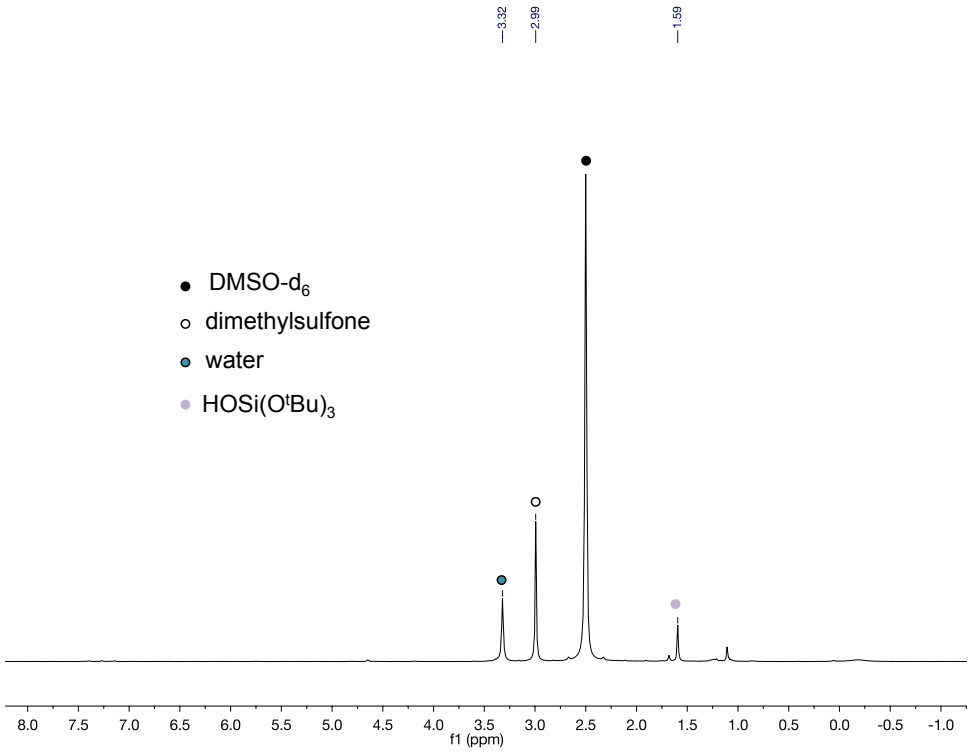

NMR data of 5

Figure 25. ^{1}H NMR (400 MHz, tol-d_8, 298 K) of the reaction mixture immediately after addition of 3 eq of CO to complex **4**.

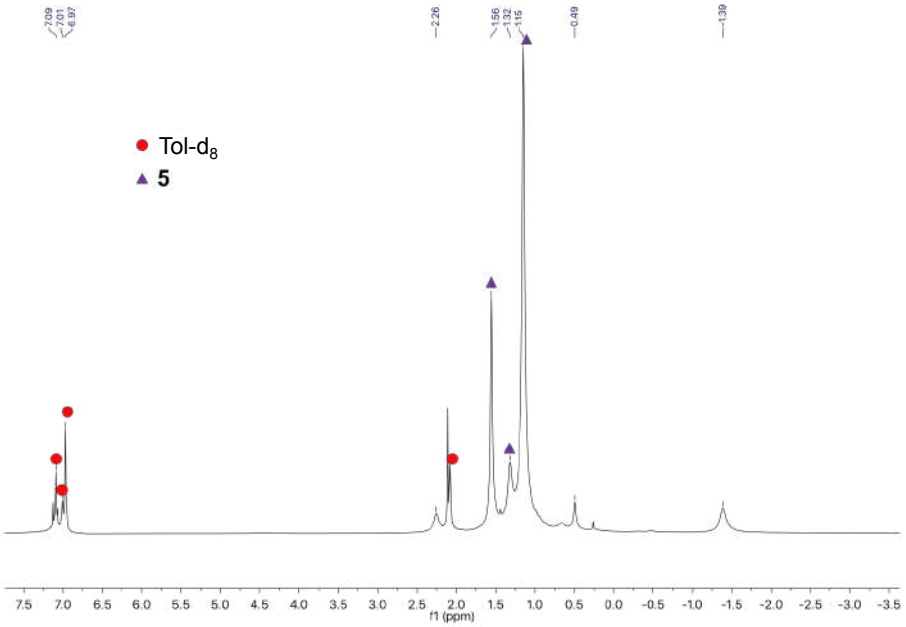

Figure 26. ^{1}H NMR (400 MHz, tol-d_8, 298 K) of crystals of **5**.

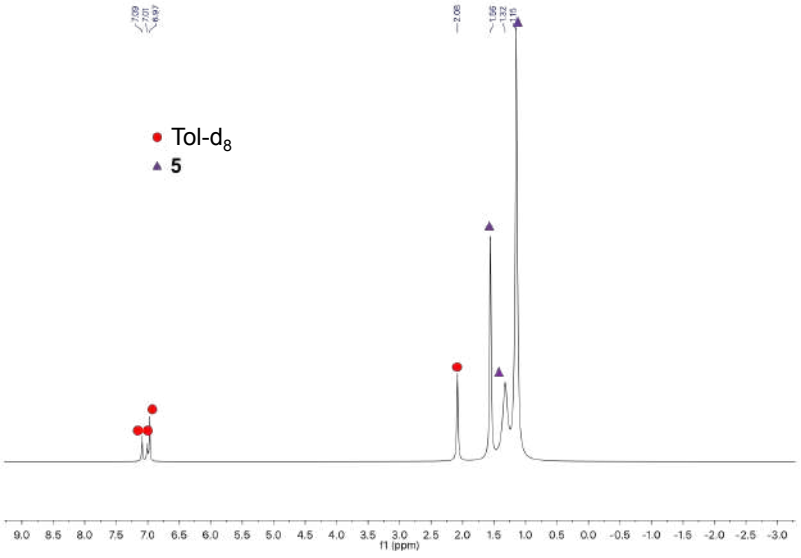

Figure 27. ^{1}H NMR (400 MHz, tol-d_8, 298 K) of the crude reaction mixture immediately after addition of 18 equivalents of CO to a solution of complex **5**.

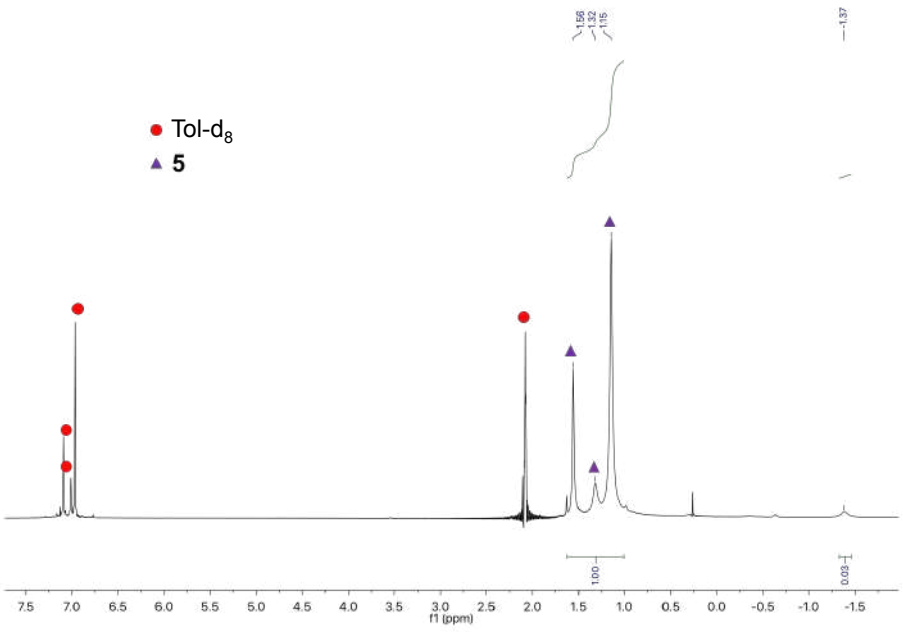

Figure 28. ^{1}H NMR (400 MHz, tol-d_8, 298 K) of the crude reaction mixture 3 days after addition of 18 equivalents of CO to a solution of isolated complex **5**.

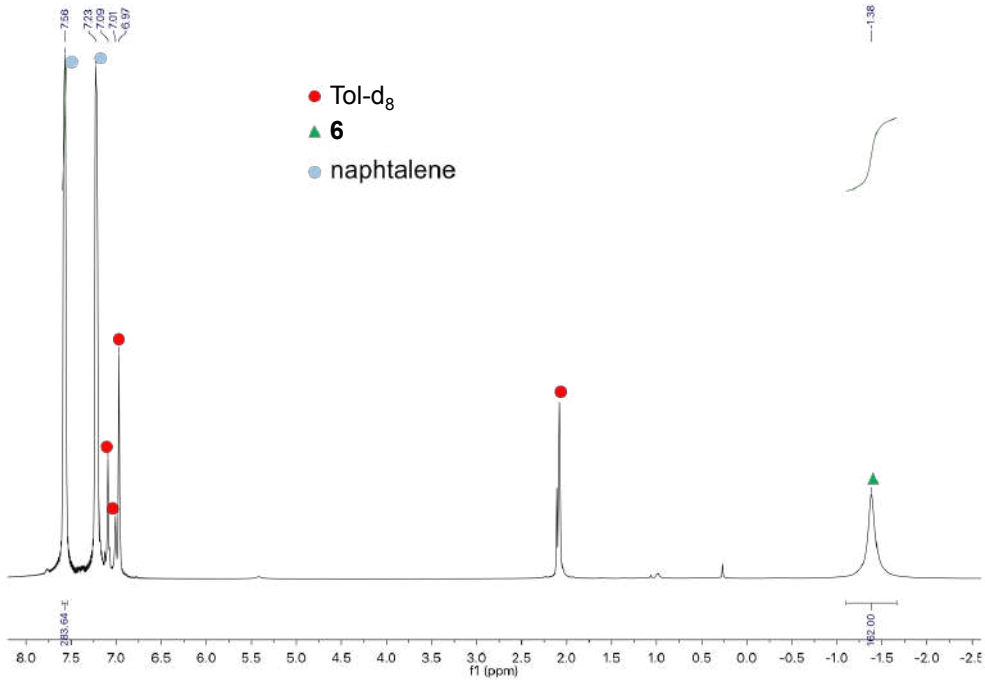

Figure 29. ^{13}C NMR (400 MHz, C_6D_6, 298 K) of the crude reaction mixture 8 days after addition of 10 equivalents of ^{13}CO to a solution of isolated complex **5**.

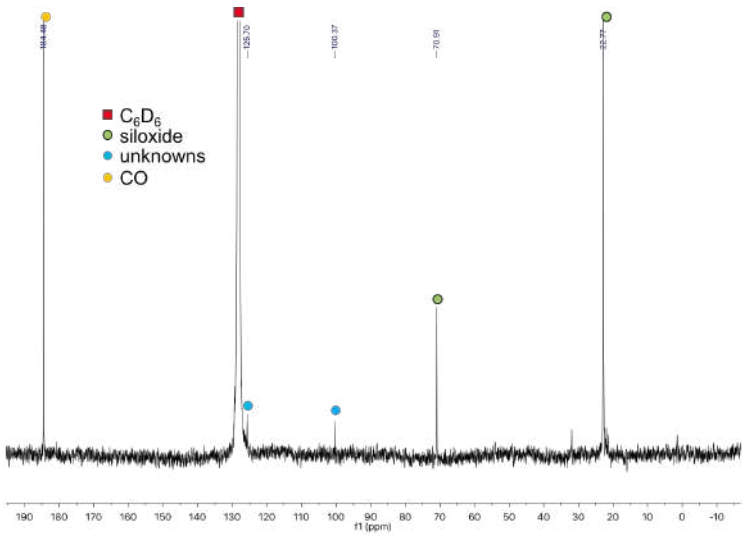

NMR data for 6

Figure 30. ^{1}H NMR (400 MHz, THF-d_8, 298 K) immediately after reaction of **3** with 1 equivalent of N_2O.

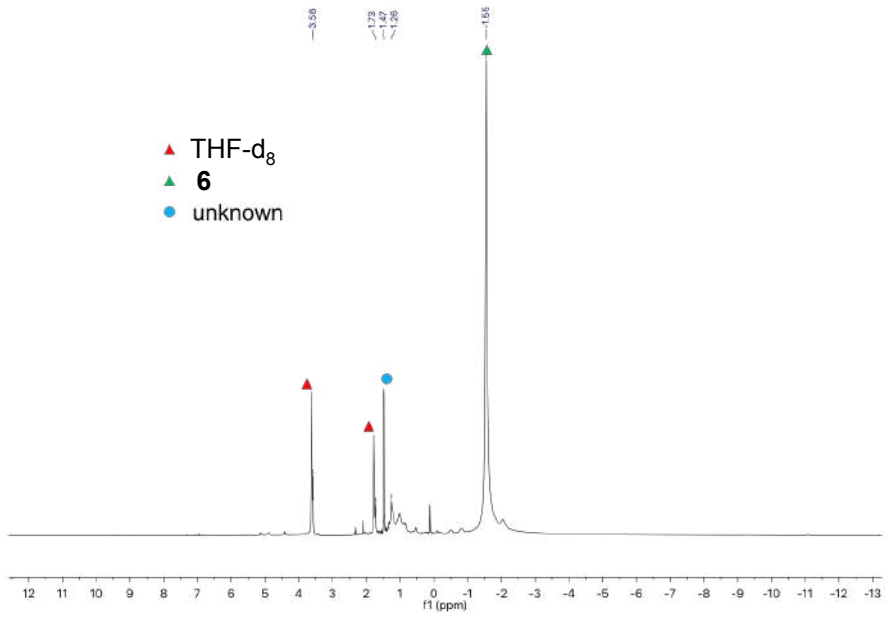

Figure 31. ^{1}H NMR (400 MHz, tol-d_8, 298 K) of isolated crystals of **6**.

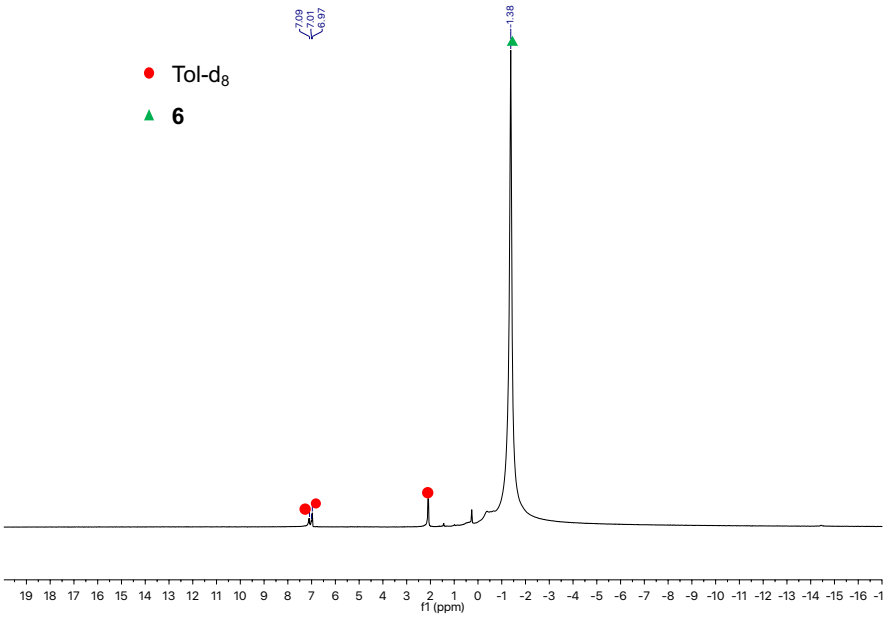

NMR data for the reactivity of 4 and 3 with H_2

Figure 32. ^{1}H NMR (400 MHz, tol-d_8, 298 K) before and after reaction of **4** with 1 atm of H_2.

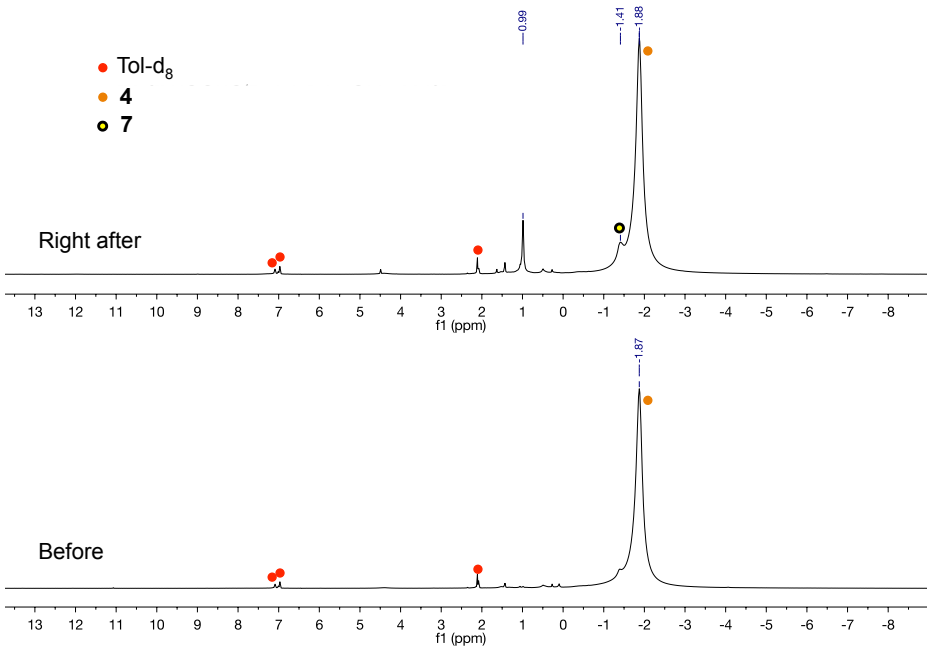

Figure 33. ^{1}H NMR (400 MHz, tol-d_8, 298 K) of the crude reaction mixture 3 days after the addition of 1 atm of H_2 to **4**.

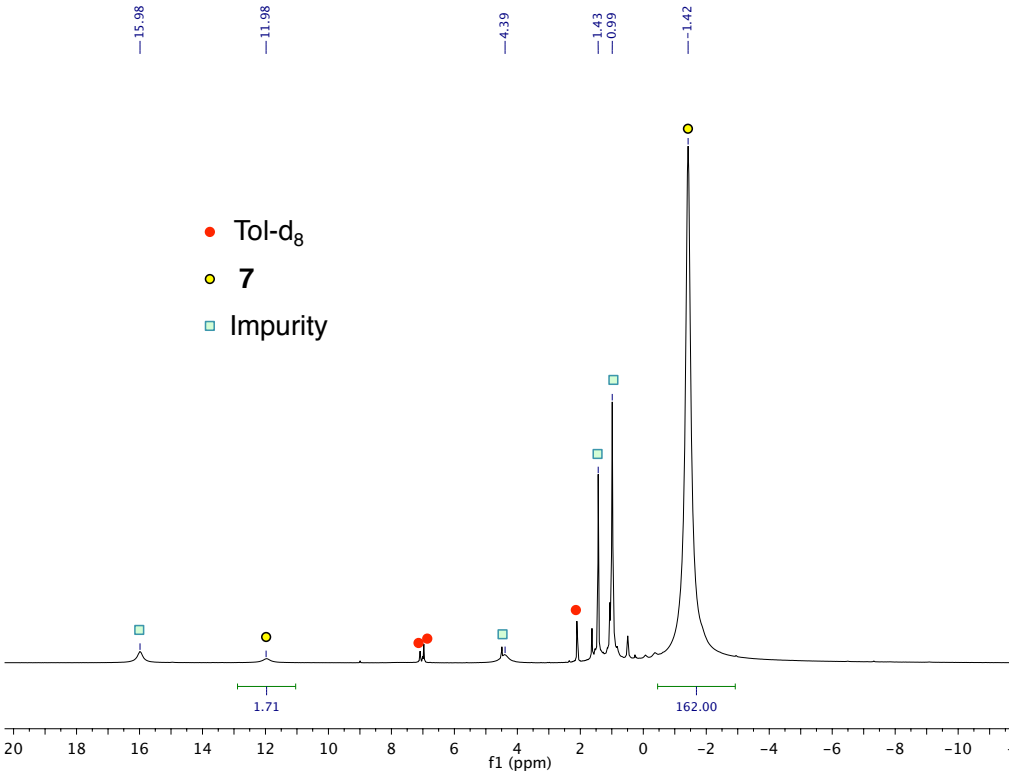

Figure 34. ^{1}H NMR (400 MHz, tol-d_8, 298 K) of crystals of ^{15}**N-7**.

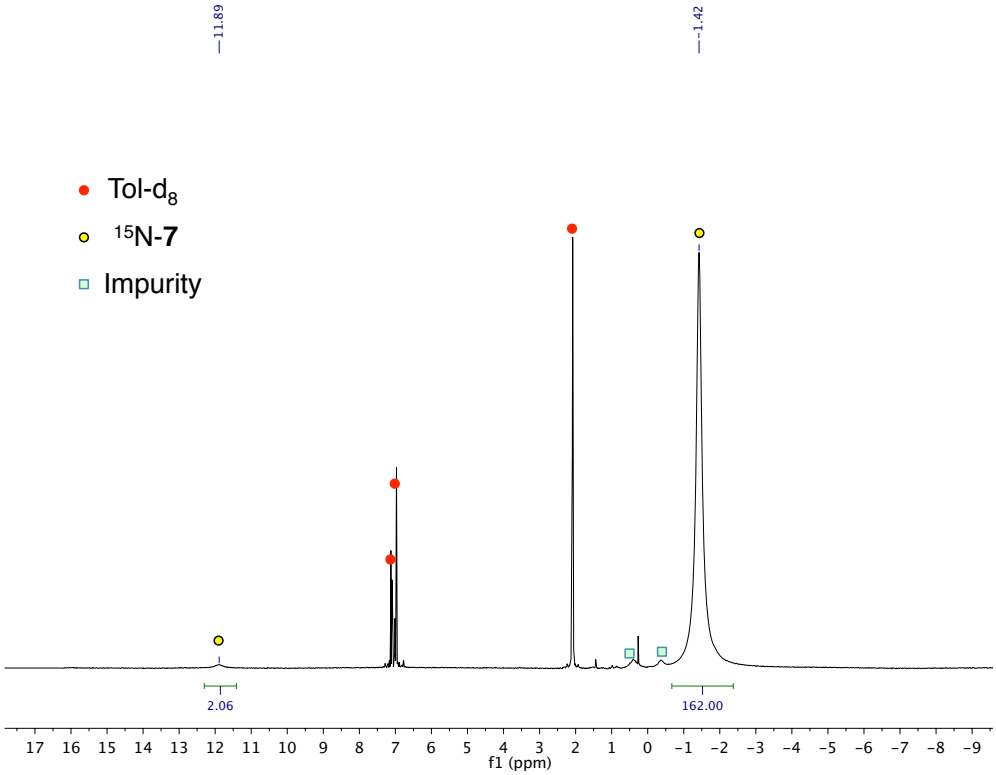

Figure 35. Quantitative ^{1}H NMR (400 MHz, tol-d_8, 298 K) of the crude mixture from reaction of **4** with H_2, after heating for 1 h at 60 °C.

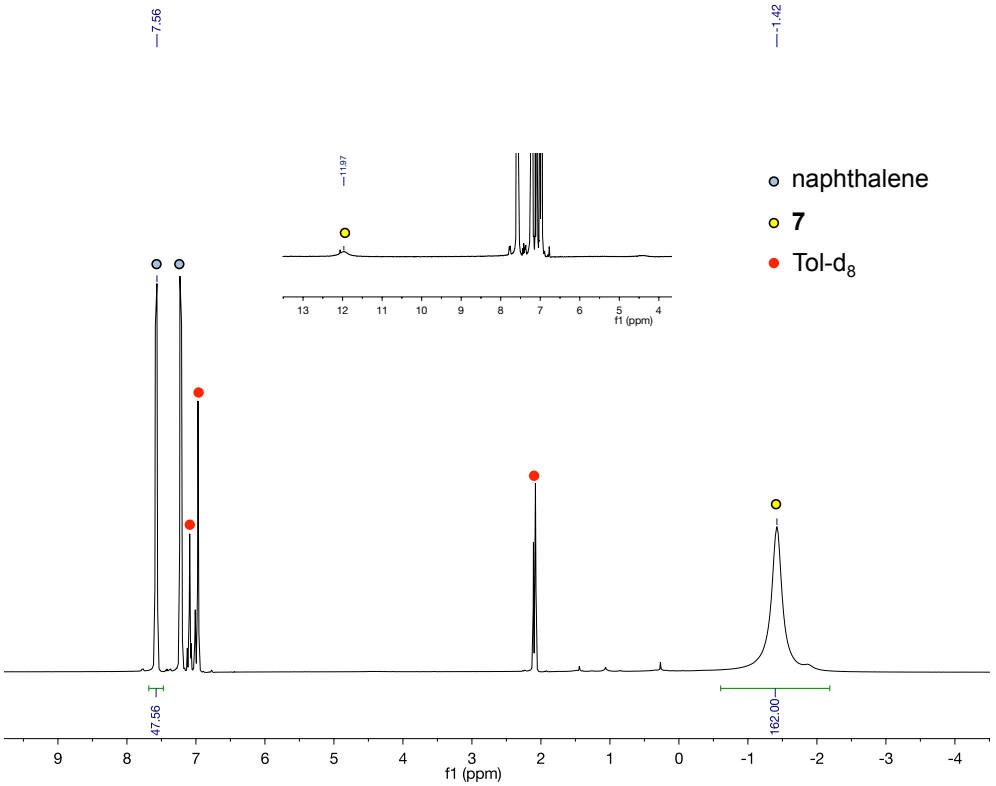

Figure 36. ^{1}H NMR (400 MHz, tol-d_8, 298 K) kept 1 h at 60 °C after the addition of D_2 to **4**.

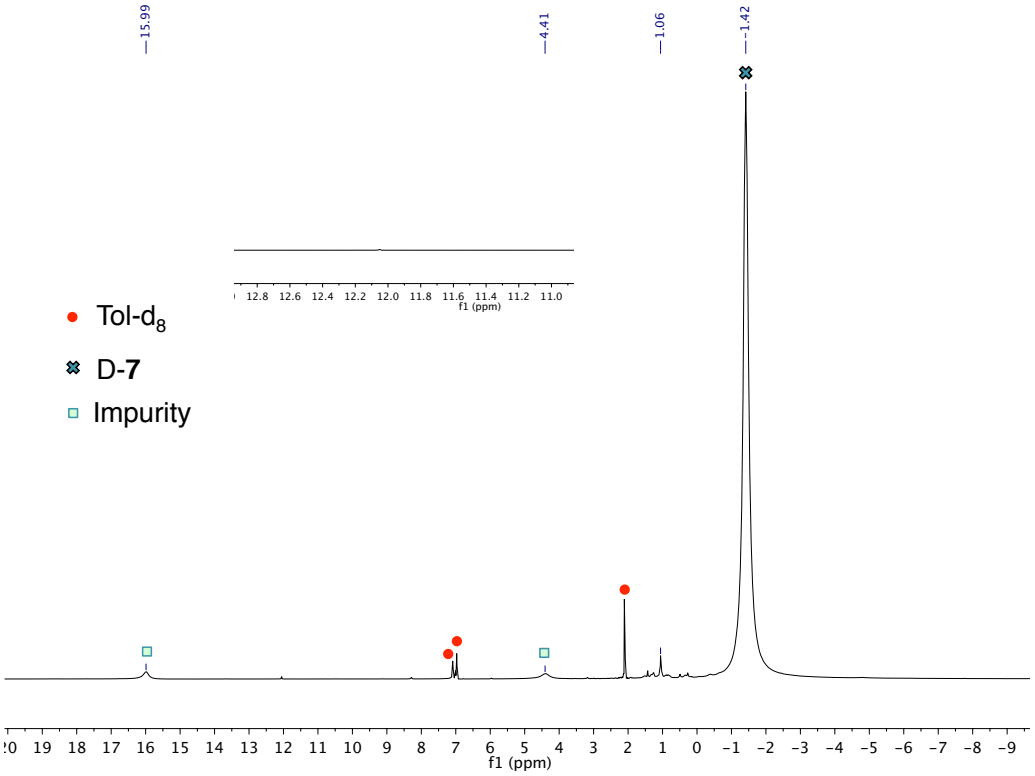

Figure 37. ^{1}H NMR (400 MHz, DMSO-d_6, 298 K) of the crude mixture from the reaction of the compound isolated from the reaction of **4** with H_2 (at room temperature) with excess HCl(Et_2O).

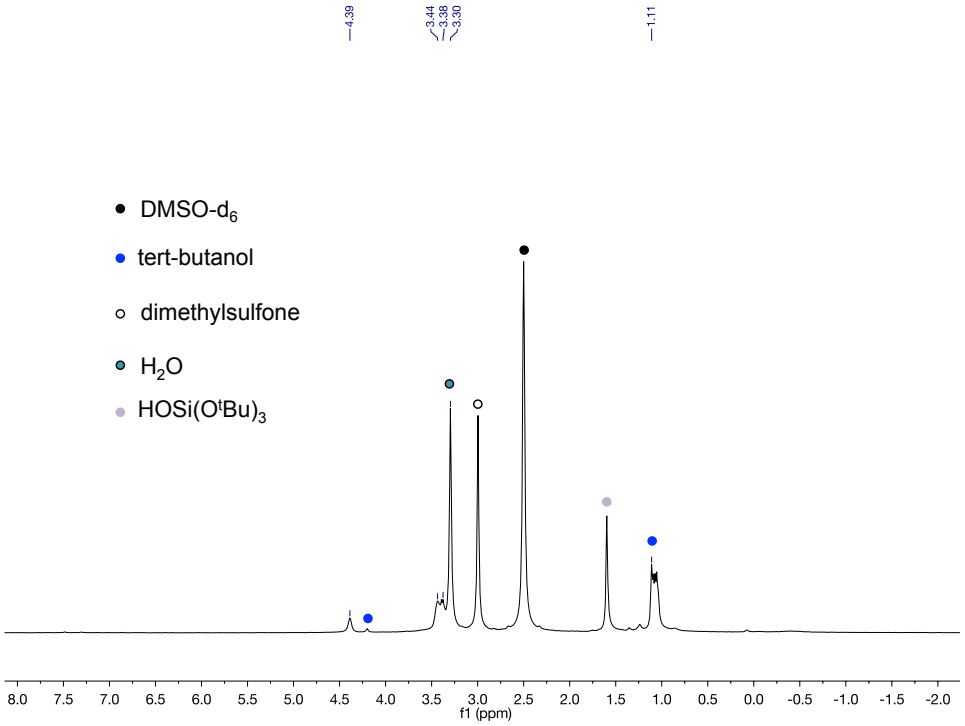

Figure 38. ^{1}H NMR (400 MHz, tol-d_8, 298 K) of the crude reaction mixture before (top) ad after consecutive additions of H_2 (middle) and CO (bottom) to **4**.

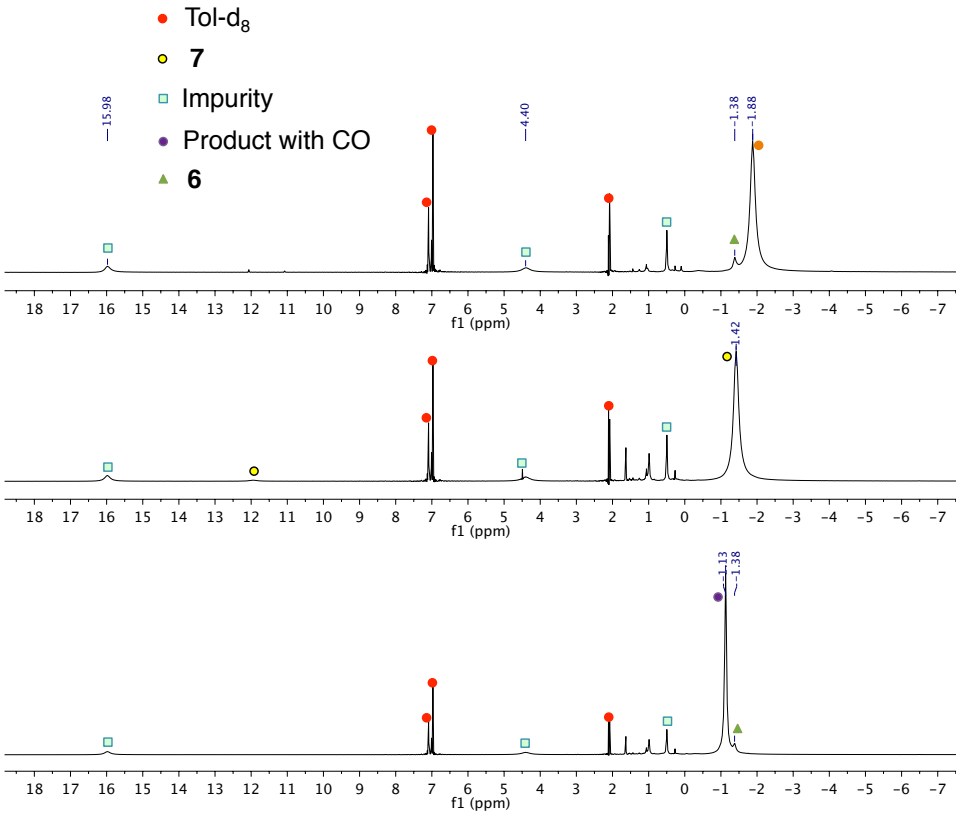

Figure 39. ^{1}H NMR (400 MHz, tol-d_8, 298 K) of the crude mixture after addition of 5 atm H_2 to **4**.

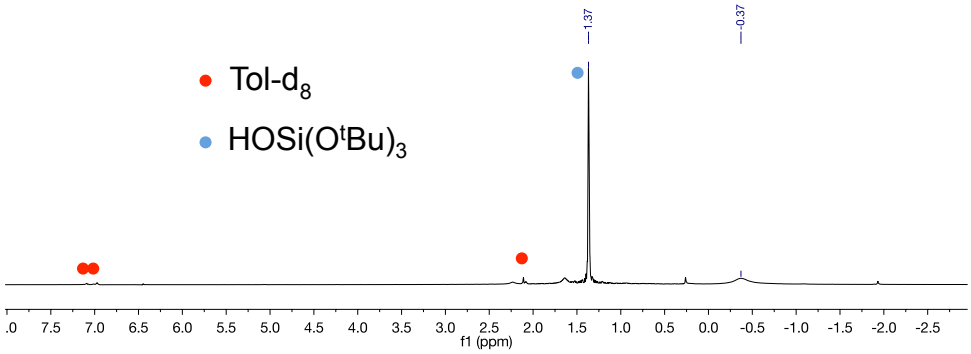

Figure 40. ^{1}H NMR (400 MHz, tol-d_8, 298 K) of the crude mixture after addition of 1 atm H_2 to **3**.

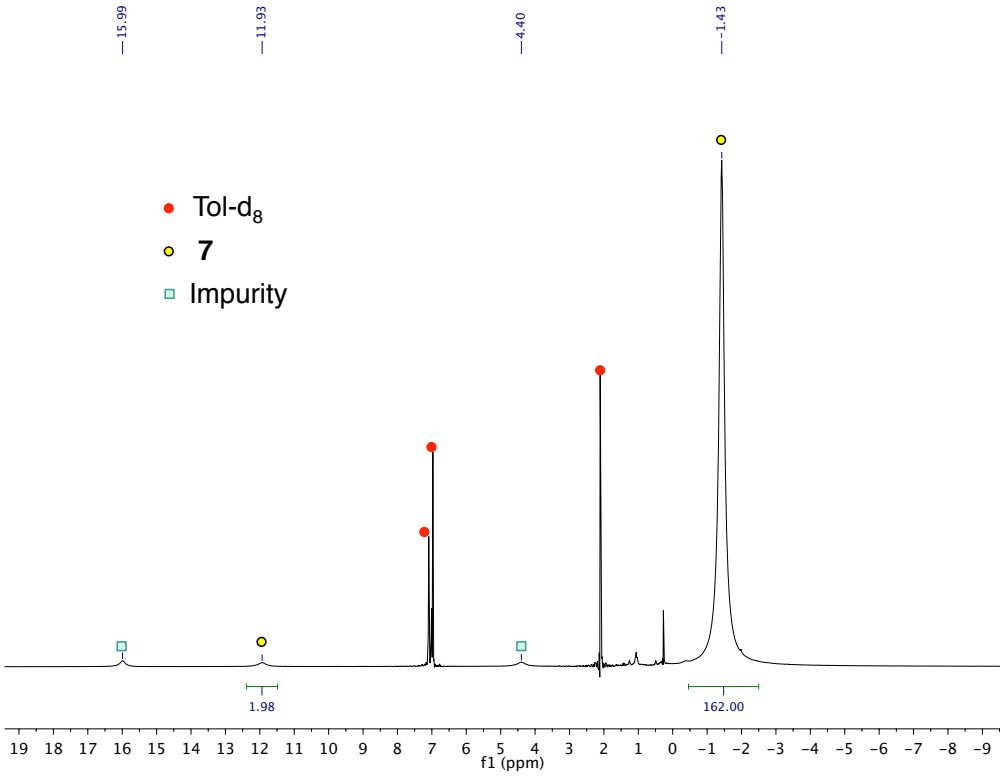

Figure 41. ^{1}H NMR (400 MHz, tol-d_8, 298 K) of complex **7** as isolated after addition of 1 atm H_2 to **3**.

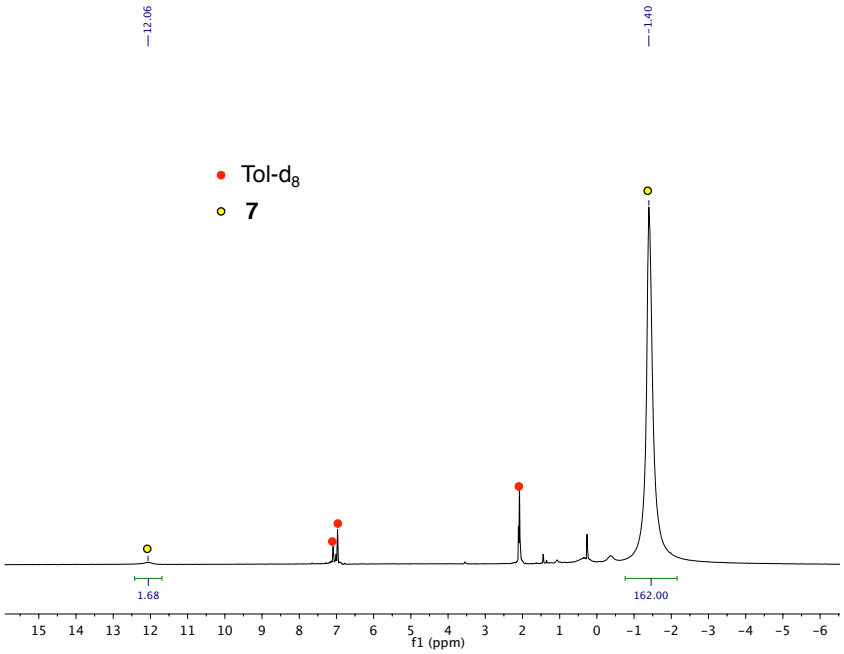

Figure 42. ^{1}H NMR (400 MHz, tol-d_8, 298 K) of the crude mixture before and after addition of 1 atm D_2 to **3** (impurities are due to the decomposition of 3 during reaction at room temperature).

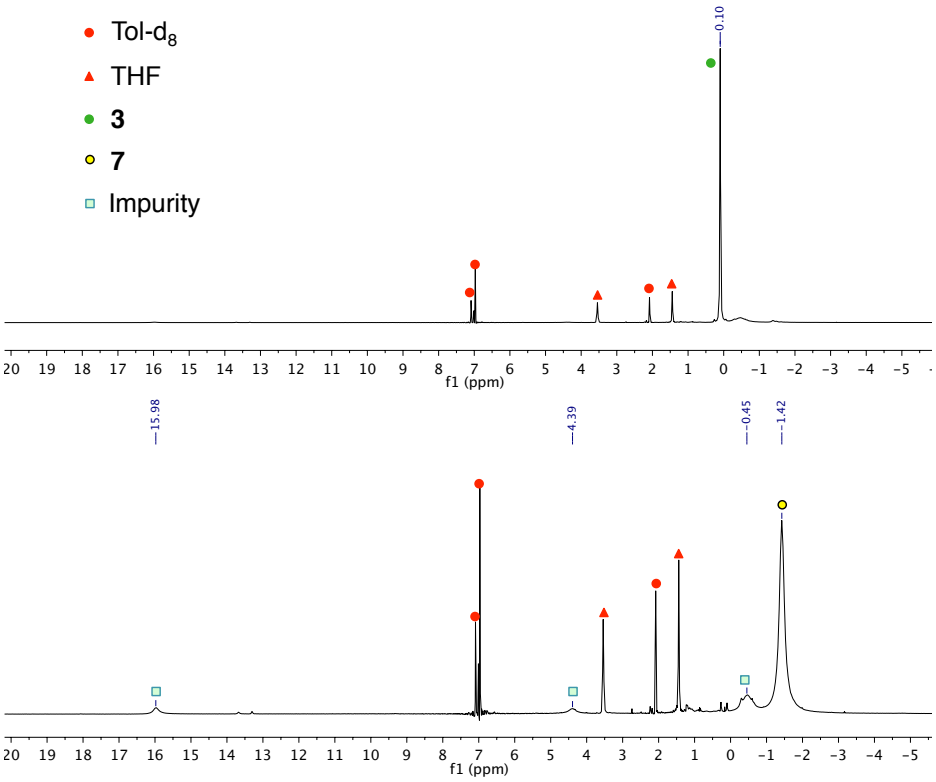

Figure 43. ^{1}H NMR (400 MHz, tol-d_8) at variable temperatures of **7**.

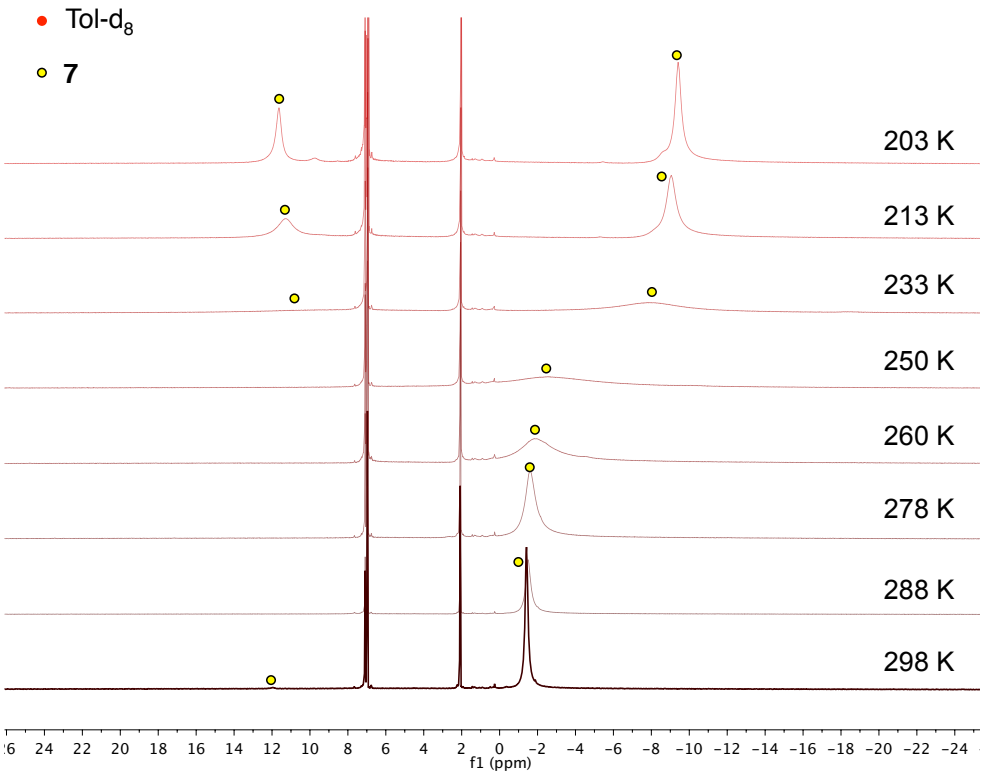

Figure 44. ^{1}H NMR (400 MHz, tol-d_8) at variable temperatures of the product isolated after addition of 1 atm of H_2 to **3**.

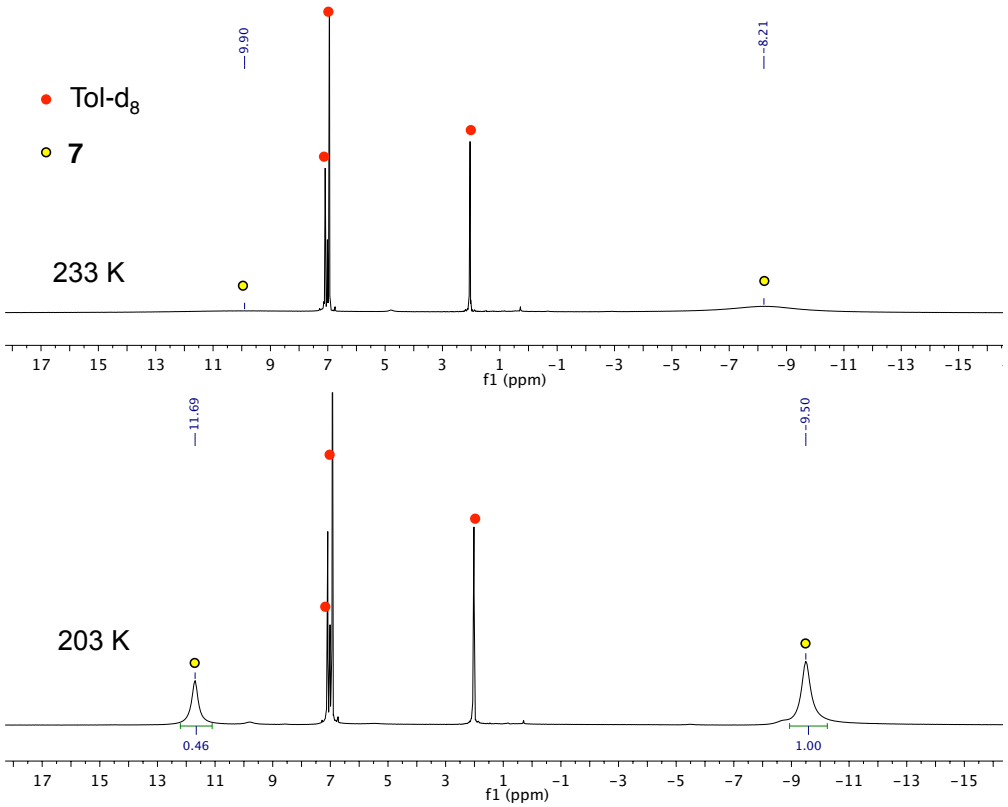

2. MS spectra from GC-MS measurements

Figure 45. Nitrogen detection after reaction of **4** with excess HCl.

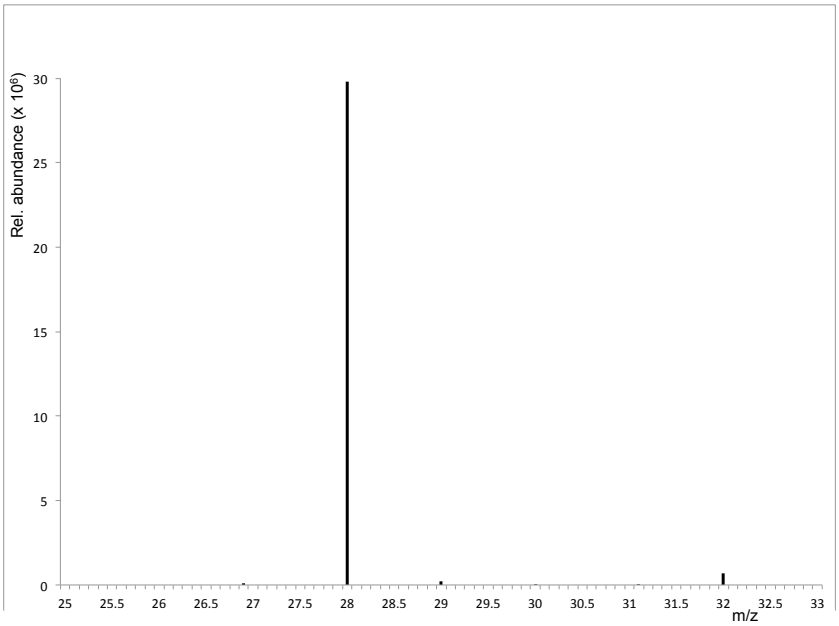

Figure 46. Nitrogen detection after reaction of **^{15}N-4** with excess HCl.

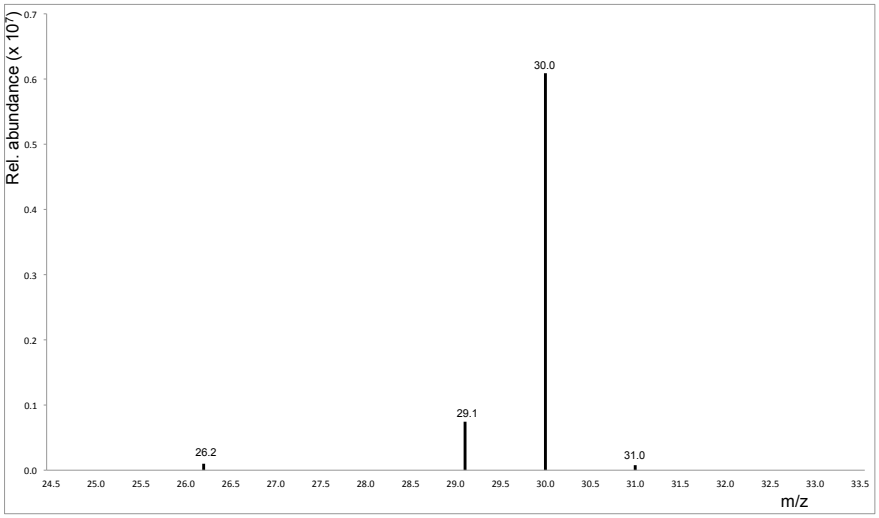

Figure 47. Nitrogen detection after addition of H_2 (1 atm, 1h at 60 °C) to **4**.

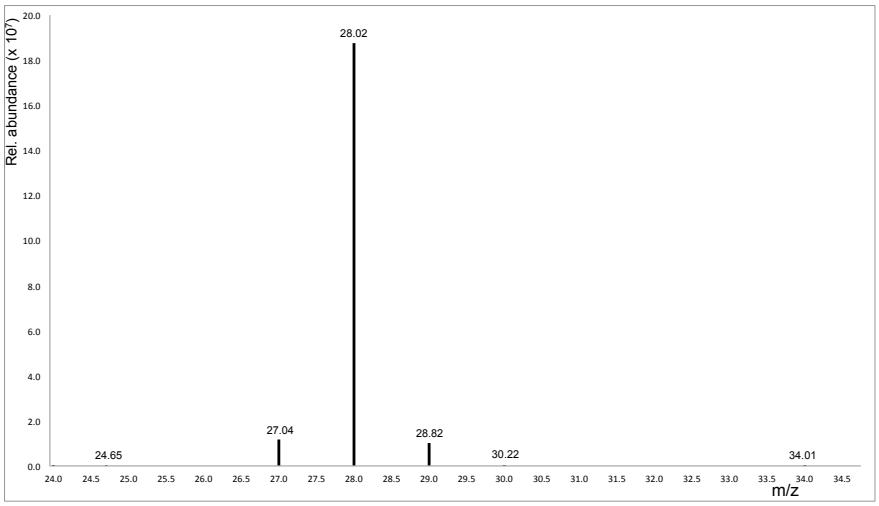

Figure 48. Nitrogen detection after addition of H_2 (1 atm, 1h, 60 °C) to **^{15}N-4**.

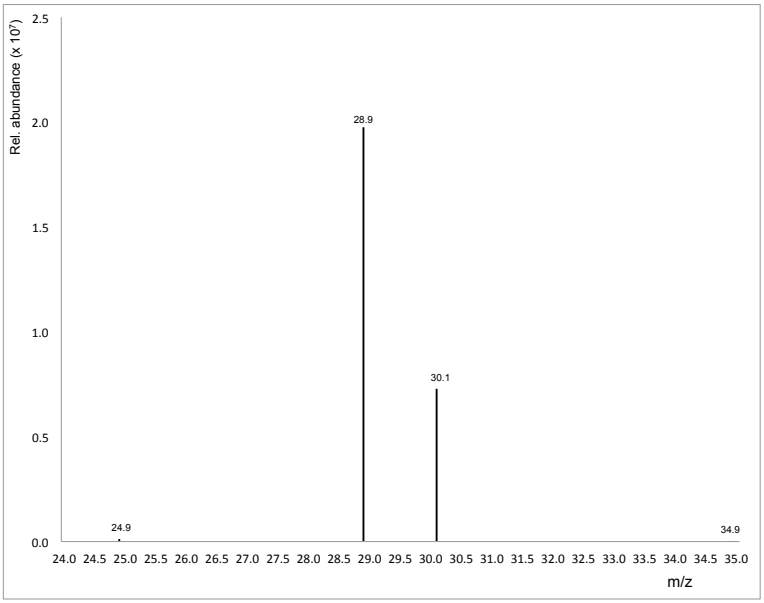

3. IR spectra

Figure 49. IR spectrum of **5**.

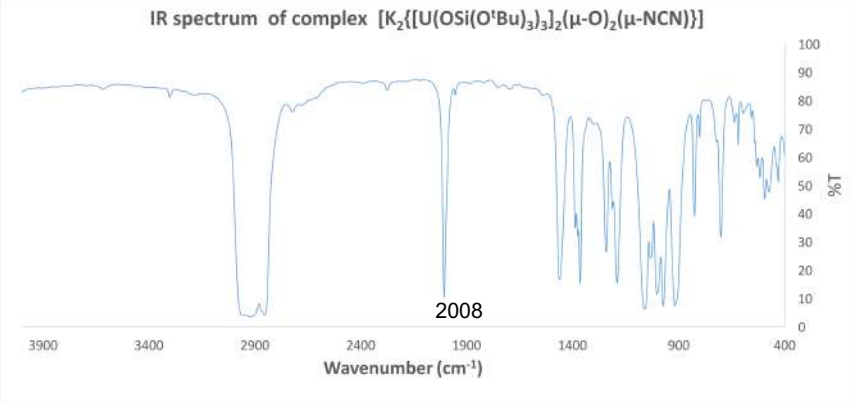

Figure 50. IR spectrum of ^{13}**C-5**.

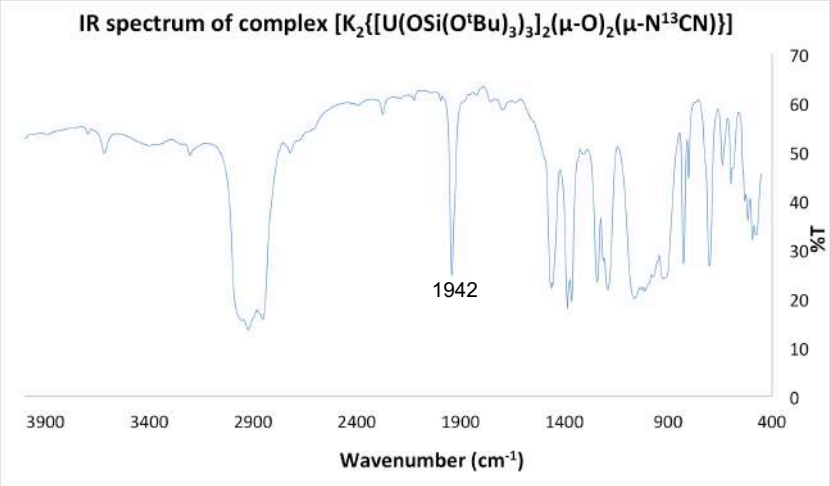

Figure 51. IR spectrum of 7 obtained from addition of H_2 to **4** (orange) and from addition of H_2 to **3** (blue).

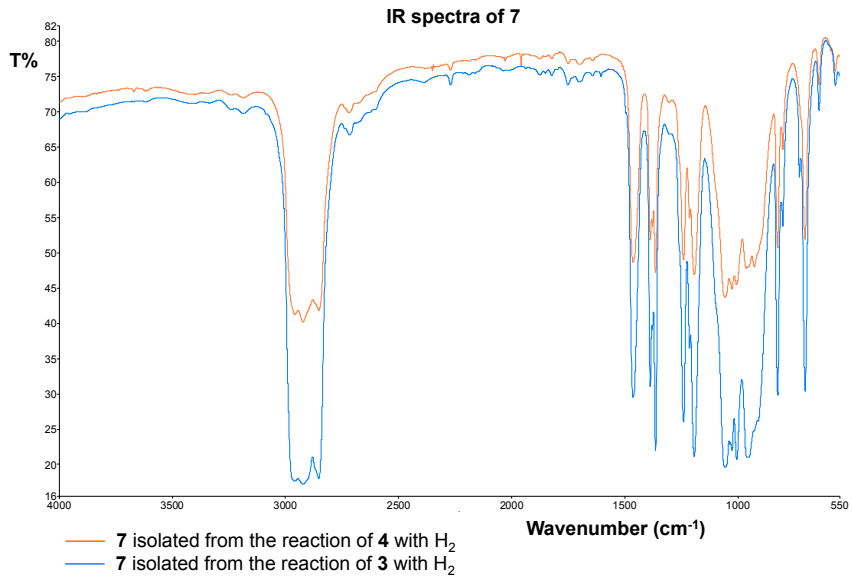

4. Crystallographic data

The X-ray diffraction data of **2** were measured at 100 K using MoK_α radiation on a Bruker APEX II CCD kappa diffractometer. The dataset was reduced by EvalCCD[1] and then corrected, by modelling an empirical transmission surface as sampled by multiple symmetry-equivalent and/or azimuth rotation-equivalent intensity measurements by real spherical harmonic functions of even order, for absorption[2].

Bragg-intensities of **3, 4** and **5** were collected at 140 K and those of **6** at 100 K using Cu K_α radiation. A Rigaku SuperNova dual system diffractometer with an Atlas S2 CCD detector was used for compounds **4**, **5**, and **6**, and one equipped with an Atlas CCD detector for compound **3**. The datasets were reduced and then corrected for absorption, with the help of a set of faces enclosing the crystals as snugly as possible, with CrysAlis^{Pro}[3].

The solutions and refinements for the structures were performed by the latest available version of SHELXT[4] and SHELXL,[5] respectively, except the structure solution of **2** that was obtained by SHELXS-97[6]. All non-hydrogen atoms were refined anisotropically using full-matrix least-squares based on $|F|^2$, but the hydrogen atoms were placed at calculated positions by means of the "riding" model.

In the structure of **3**, The contributions of highly disordered solvent molecules were removed from the model by the SQUEEZE algorithm of PLATON[7].

In the case of **4**, each of the bridging hydrazido and oxo ligands are disordered over three positions found in a difference Fourier map and refined anisotropically. For the least-squares refinement, the distance and similarity restraints (SADI and SIMU) were applied. The structure of **5** was refined as a two-component inversion twin yielding a BASF parameter of 0.467(8). In the structure of **6**, each of the bridging oxo ligands are disordered over two positions found in a difference map and refined anisotropically by applying distance and similarity restraints (SADI and SIMU) for the least-squares refinement. Highly disordered solvent molecules were removed with the help of the solvent-masking program in OLEX2[8].

Table 1. X-ray crystallographic data of **2**, **3** and **4**.

	2	**3**	**4**
Formula	$C_{72}H_{162}O_{25}Si_6U_2$	$C_{72}H_{162}K_2O_{25}Si_6U_2$	$C_{72}H_{162}K_2N_2O_{25}Si_6U_2$
Crystal size (mm^3)	0.491 x 0.462 x 0.453	0.243 x 0.200 x 0.149	0.260 x 0.235 x 0.170

cryst syst	Triclinic	Monoclinic	Triclinic
space group	*P*1	$P2_1/c$	*P*
volume (Å^3)	4988.7(13)	10917.5(4)	5754.67(16)
a (Å)	13.3490(13)	15.4845(4)	14.1735(2)
b (Å)	16.186(3)	26.0288(5)	17.4801(3)
c (Å)	25.445(3)	27.5024(6)	25.4162(4)
α (deg)	71.451(13)	90	79.0497(12)
β (deg)	80.481(9)	99.961(2)	88.5818(12)
γ (deg)	73.743(9)	90	68.7349(14)
Z	2	4	2
formula weight (g/mol)	2072.61	2150.81	2178.83
density (g cm^{-3})	1.380	1.309	1.257
absorption coefficient (mm^{-1})	3.376	10.068	9.562
F(000)	2124	4400	2228
temp (K)	100(2)	139.99(10)	140.00(10)
total no. reflections	133395	46467	42155
unique reflections [R(int)]	39997 [0.0262]	21972 [0.0408]	23173 [0.0198]
Final R indices [I > 2σ(I)]	R1 = 0.0302, wR2 = 0.0439	R1 = 0.0418, wR2 = 0.1045	R1 = 0.0257, wR2 = 0.0639
Largest diff. peak and hole (e.A^{-3})	1.103 and -1.218	2.099 and -1.918	2.262 and -1.259
GOOF	1.157	1.022	1.035

Table 2. X-ray crystallographic data of **5**, and **6**.

	5(C_7H_8)	**6**
Formula	$C_{80}H_{170}K_2N_2O_{26}Si_6U_2$	$C_{72}H_{162}K_2O_{26}Si_6U_2$
Crystal size (mm^3)	0.206 x 0.068 x 0.056	0.158 x 0.129 x 0.102
cryst syst	Monoclinic	Triclinic
space group	$P2_1$	*P*
volume (Å^3)	5520.03(7)	5726.8(3)
a (Å)	13.96090(10)	14.2026(3)
b (Å)	17.98093(13)	17.4810(4)
c (Å)	22.01302(17)	25.3076(6)
α (deg)	90	79.203(2)
β (deg)	92.6473(8)	88.9716(18)
γ (deg)	90	68.330(2)
Z	2	2
formula weight (g/mol)	2298.97	2166.81

density (g cm^{-3})	1.383	1.257
absorption coefficient (mm^{-1})	10.006	9.608
F(000)	2356	2216
temp (K)	140.00(10)	100.00(10)
total no. reflections	40549	43509
unique reflections [R(int)]	20377 [0.0405]	23197 [0.0258]
Final R indices [I > 2σ(I)]	R1 = 0.0376, wR2 = 0.0962	R_1 = 0.0346, wR_2 = 0.0808
Largest diff. peak and hole ($e.A^{-3}$)	1.776 and -2.501	3.407 and -3.060
GOOF	1.042	1.030

5. Magnetic Data

Figure 52. Plot of measured $1/(\chi - \chi_0)$ vs T for complex **4**.

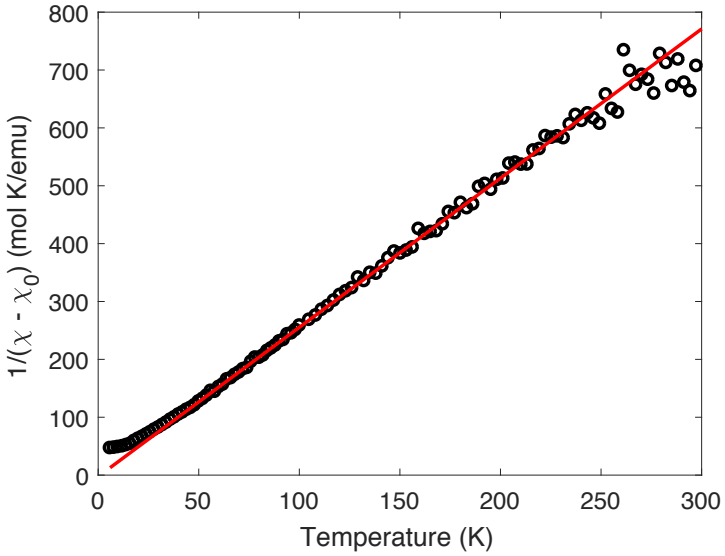

Figure 53. Plot of effective moment vs T for complex **4**.

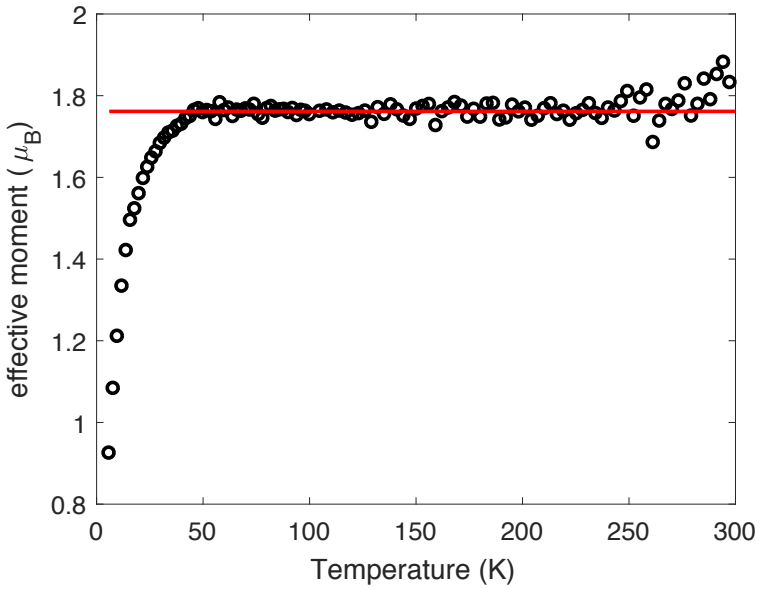

Figure 54. Plot of measured $1/(\chi - \chi_0)$ vs T for complex **7**.

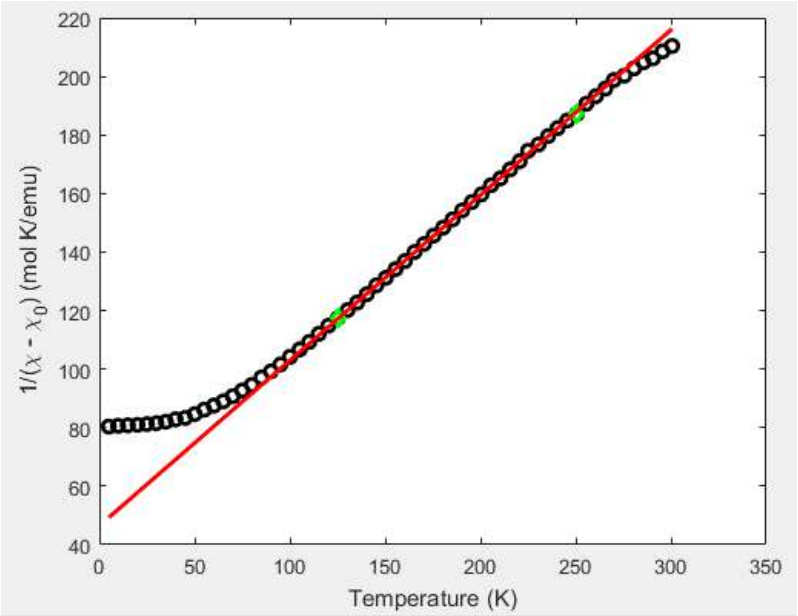

Figure 55. Plot of effective moment vs T for complex **7**.

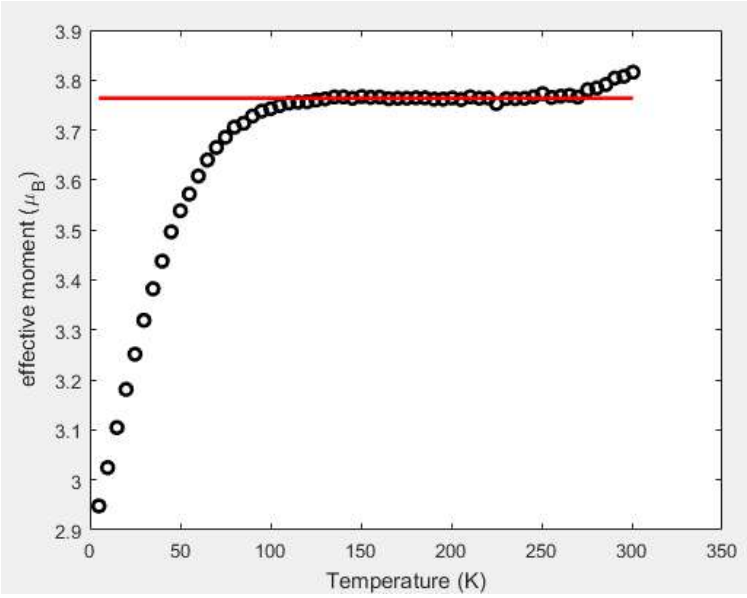

6. Computational Analysis

a. Computational Details

Density functional theory (DFT) computations on the experimentally synthesized $K_3U^{III}NU^{III}$ and $K_2U^{III}OU^{III}$ compounds, as well as their N_2 complexes, have been performed with the M06L[12] functional in combination with the 6-31G** basis set for all first, second and third row atoms, while the LanL2DZ basis set and corresponding effective core potentials were chosen for U and K (78 and 10 core electrons respectively). Scalar relativistic effects for U were included through the LanL2DZ ECPs. The X-Ray resolved structures of all compounds were retained with the exception of the hydrogen and N_2 positions, which were fully relaxed. All DFT computations were performed within the unrestricted open-shell formalism in Gaussian16.[13] The electron density about the bridging U-N-U and U-O-U bonds has been analyzed with the Density Overlap Region Indicator (DORI[14]) in combination with a modified version of the DGRID software.

b. Spin State Stability

Tables 3 and 4 respectively report the relative spin stability for the lowest spin multiplicities of the $K_3U^{III}NU^{III}/K_2U^{III}OU^{III}$ and $K_3U^{V}N(N_2)U^{V}/K_2U^{V}O(N_2)U^{V}$

complexes. The electronic energies are computed at the M06L/LanL2DZ/6-31G** level.

Table 3. Electronic energies in kcal mol^{-1} at M06L/LanL2DZ/6-31G** of the lowest spin multiplicities relative to the most stable state of $K_3U^{III}NU^{III}$ and $K_2U^{III}OU^{III}$.

Spin Multiplicity	Nitride	Oxide
Singlet	0.0	100.68
Triplet	2.10	0.0
Quintet	6.57	14.66
Septet	15.20	23.69

Table 4. Electronic energies in kcal mol^{-1} at M06L/LanL2DZ/6-31G** of the lowest spin multiplicities relative to the most stable state of $K_3U^{V}N(N_2)U^{V}$ and $K_2U^{V}O(N_2)U^{V}$.

Spin Multiplicity	Nitride	Oxide
Singlet	0.0	45.85
Triplet	1007.79	0.0

c. DORI Analysis

The electron density about the bridging bond has been analyzed using the Density Overlap Region Indicator (DORI).[14] Figure 58 shows the DORI basins and their integrated value for both $K_3U^{III}NU^{III}$ and $K_2U^{III}OU^{III}$.

Figure 58. Integral of the electron density within a) U-N-U and b) U-O-U DORI basins [$e/bohr^3$]. DORI isovalue set to 0.8.

The higher value of the integrated electronic density in the basins of the nitride complex indicates a more covalent character of the bridging bond.

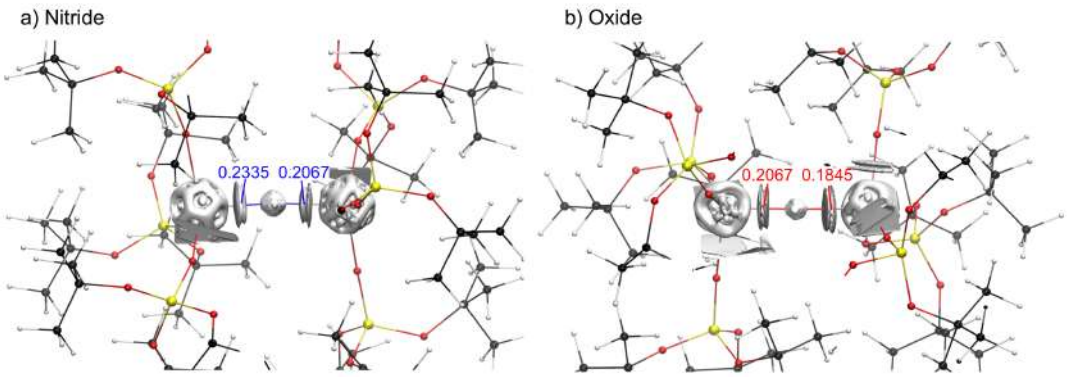

d. Natural Bond Analysis

Tables 5 and 6 report the Wiberg bond index matrix computed respectively on the $K_3U^VN(N_2)U^V$ and $K_2U^VO(N_2)U^V$.

Table 5. $K_2U^VO(N_2)U^V$: Wiberg bond index in the natural atomic orbital basis.

	U(1)	U(2)	N(1)	N(2)	O
U(1)	-	-	0.62	0.45	0.75
U(2)	-	-	0.85	0.68	1.02
N(1)	0.62	0.85	-	1.4	-
N(2)	0.45	0.68	1.4	-	-
O	0.75	1.02	-	-	-

Table 6. $K_3U^VN(N_2)U^V$: Wiberg bond index in the natural atomic orbital basis.

	U(1)	U(2)	N(1)	N(2)	N(bridging)
U(1)	-	-	1.12	1.27	2.14
U(2)	-	-	0.80	0.65	0.78
N(1)	1.12	0.80	-	1.0	-
N(2)	1.27	0.65	1.0	-	-
N(bridging)	2.14	0.78	-	-	-

[1] A. J. M. Duisenberg, L. M. J. Kroon-Batenburg, A. M. M. Schreurs, *J. Appl. Crystallogr.* **2003**, *36*, 220-229.
[2] R. H. Blessing, *Acta Crystallogr., Sect. A* **1995**, *51*, 33-38.
[3] CrysAlisPRO, Rigaku Oxford Diffraction, **2015**.
[4] G. M. Sheldrick, *Acta Crystallogr., Sect. A* **2015**, *71*, 3-8.
[5] G. M. Sheldrick, *Acta Crystallogr. C* **2015**, *71*, 3-8.
[6] G. M. Sheldrick, *Acta Crystallogr., Sect. A* **2008**, *64*, 112-122.
[7] PLATON, A. L. Spek, *Acta Crystallogr., Sect. C* **2015**, *71*, 9-18.
[8] O. V. Dolomanov, L. J. Bourhis, R. J. Gildea, J. A. K. Howard, H. Puschmann, *J. Appl. Crystallogr.* **2009**, *42*, 339-341.

APPENDIX 7

Supporting information for Chapter 8

1. NMR Spectroscopic data

NMR data for complex 2

Figure S1. ^{1}H NMR (400 MHz, tol-d_8, 298K) of the crude mixture after addition of H_2 to **1**.

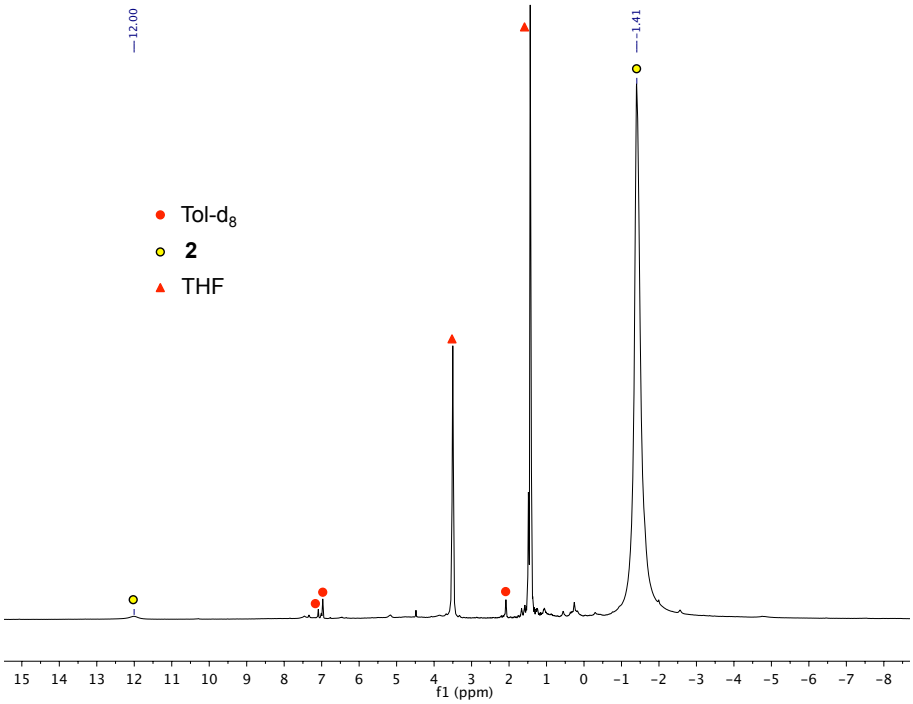

Figure S2. ^{1}H NMR (400 MHz, tol-d_8, 298K) of the crystals of **2**

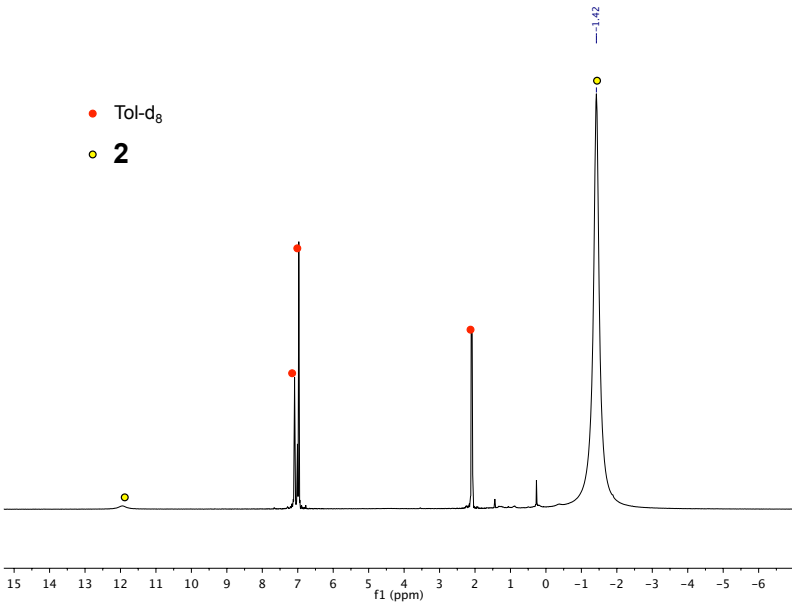

Figure S3. ^{1}H NMR (400 MHz, tol-d_8, 298K) of the crystals of **D-2.**

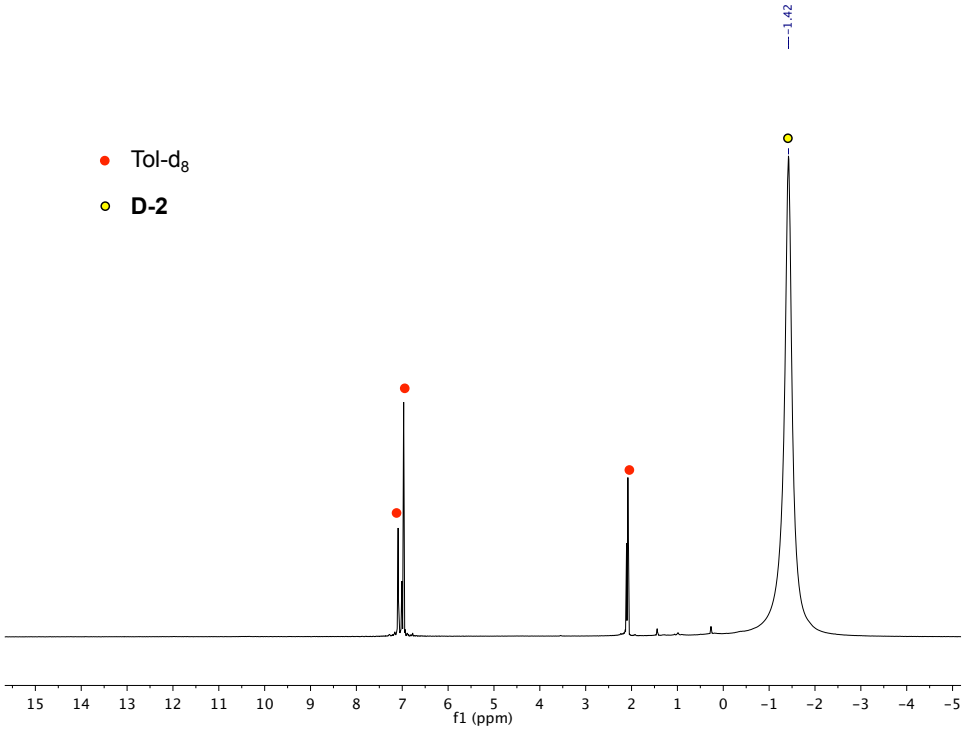

NMR data of complex 3

Figure S4. ^{1}H NMR (400 MHz, tol-d_8, 298K) of the crude reaction mixture after addition of 1 eq of MeCN to **2**

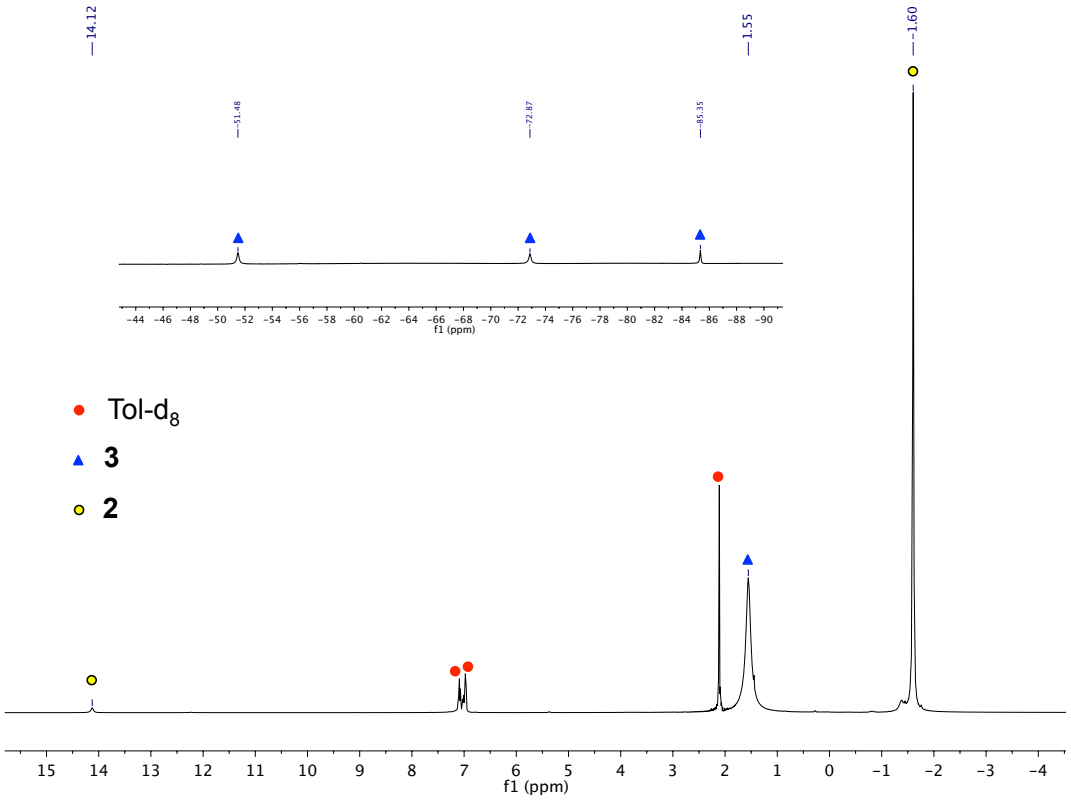

Figure S5. ^{1}H NMR (400 MHz, tol-d_8, 298K) of the crude reaction mixture after addition of 2 equivalents of MeCN to **2**

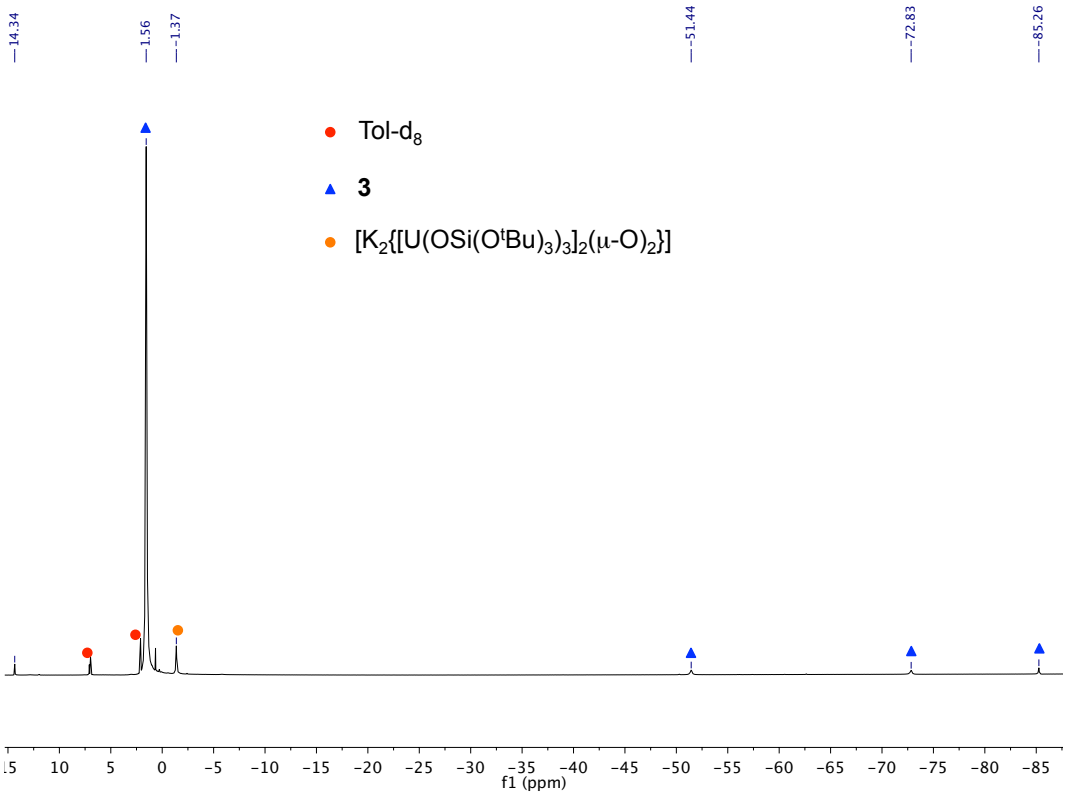

Figure S6. ^{1}H NMR (400 MHz, tol-d_8, 298K) of the crystals of **3**

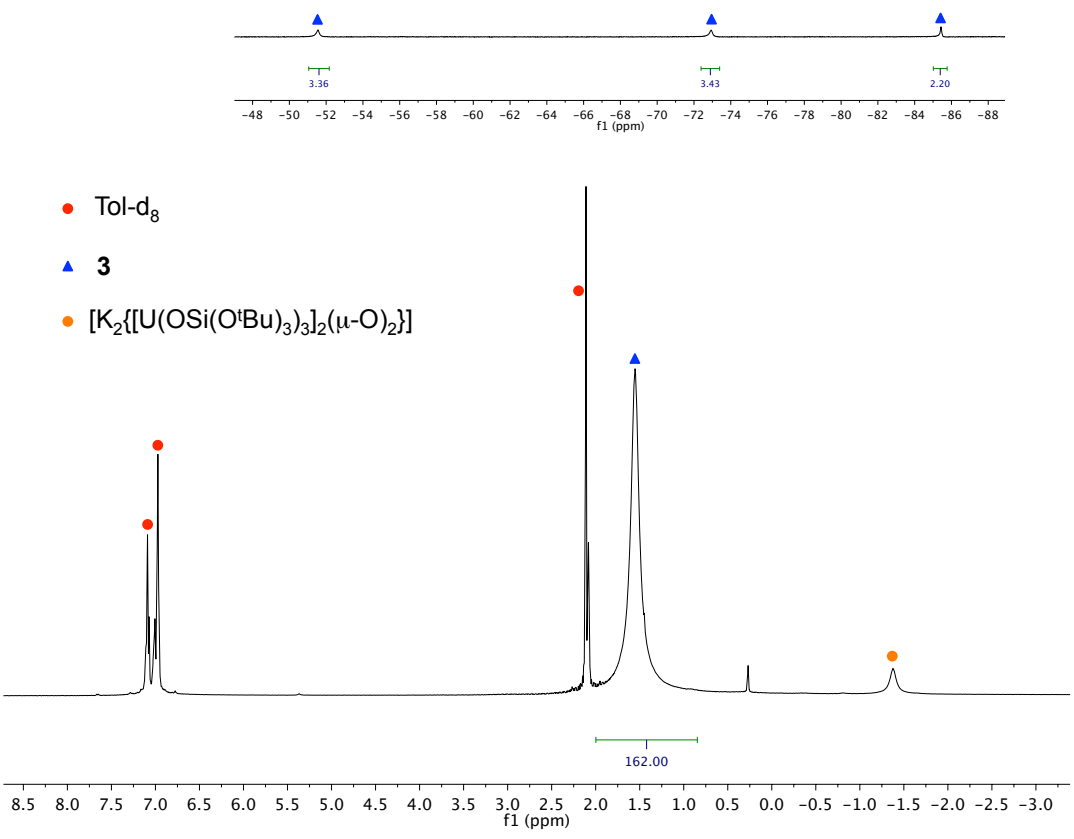

Figure S7. ^{1}H NMR (400 MHz, tol-d_8, 298K) of the crystals of **D-3**.

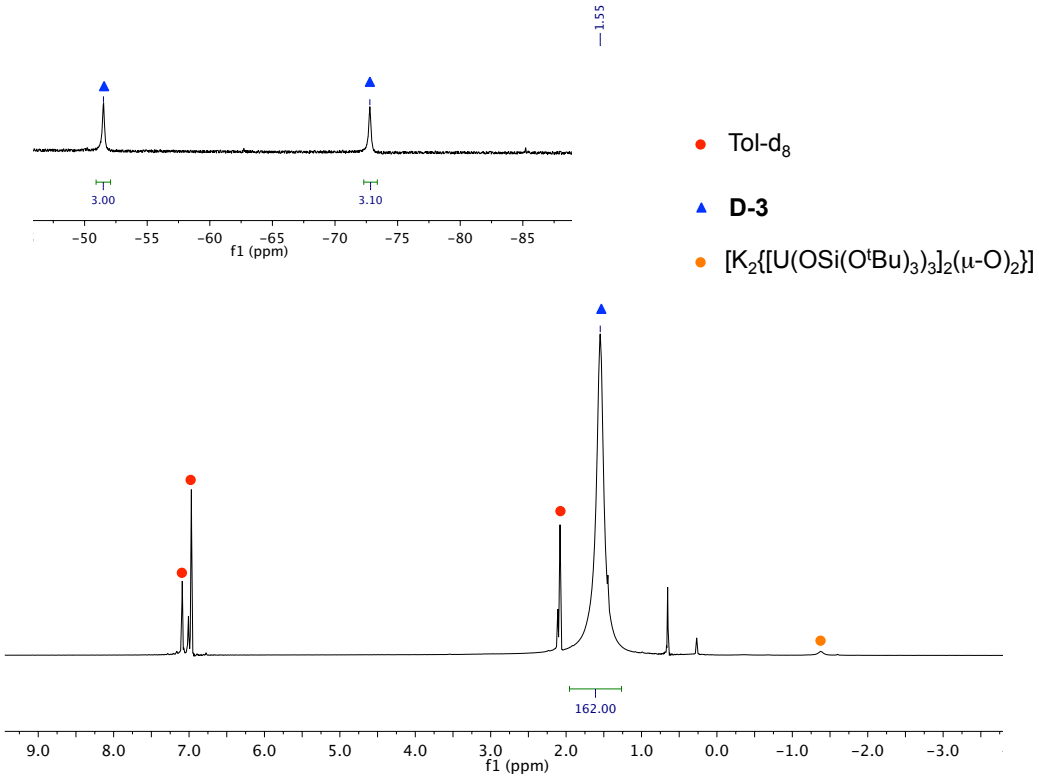

Figure S8. ^{13}C NMR (400 MHz, tol-d_8, 298K) of the crystals of **3**

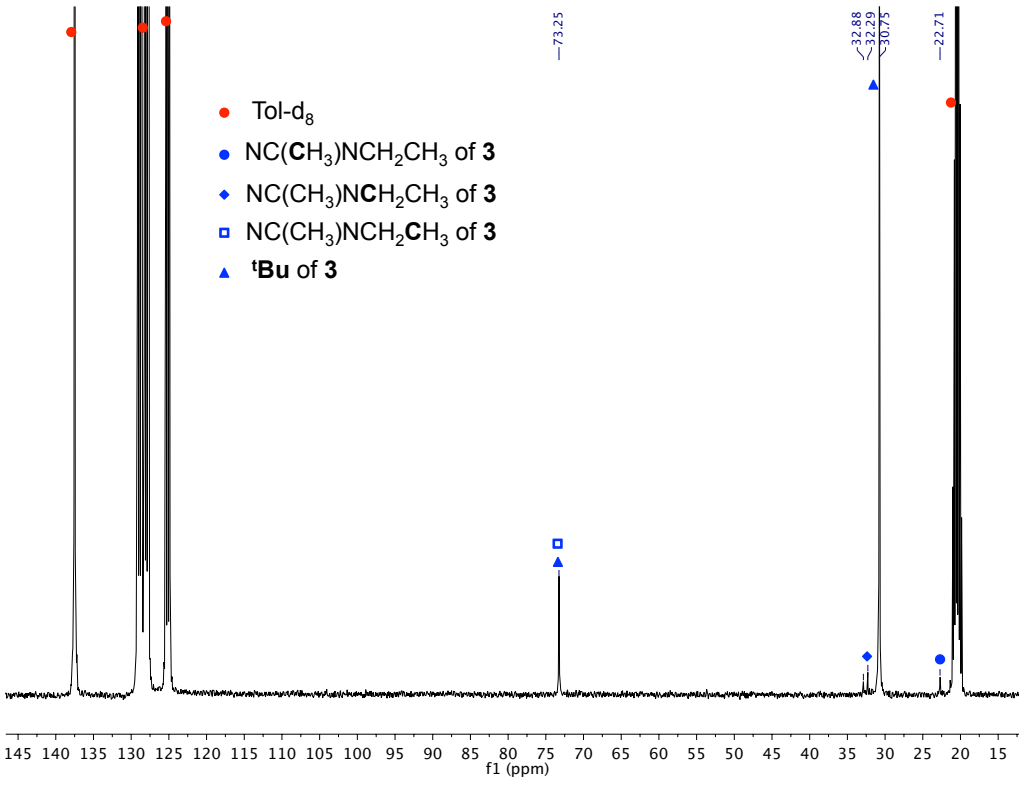

Figure S9. HMQC (600 MHz, tol-d_8, 298K) of the crystals of **3**

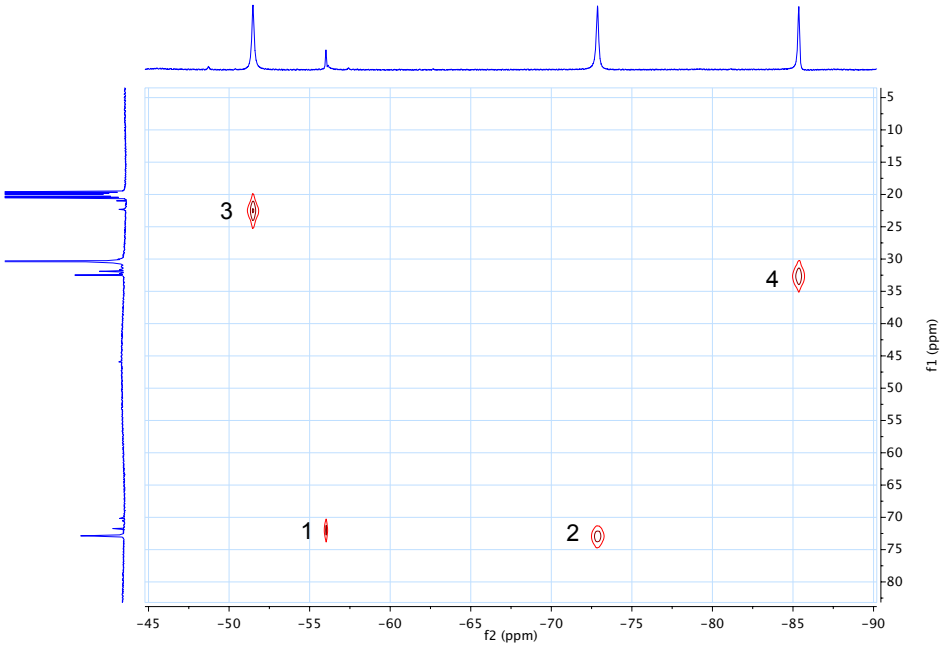

Figure S10. COSY (600 MHz, tol-d_8, 298K) of the crystals of **3**

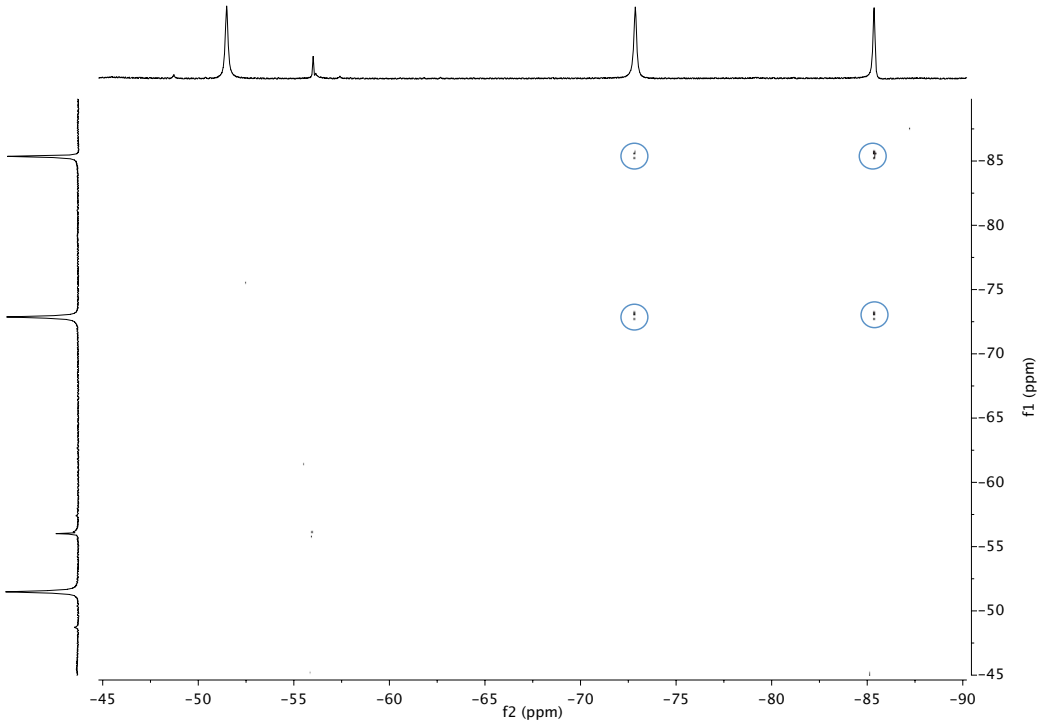

NMR data for the reaction of 2 with CO

Figure S11. ^{1}H NMR (400 MHz, tol-d_8, 298K) after addition of ^{13}CO to **2**.

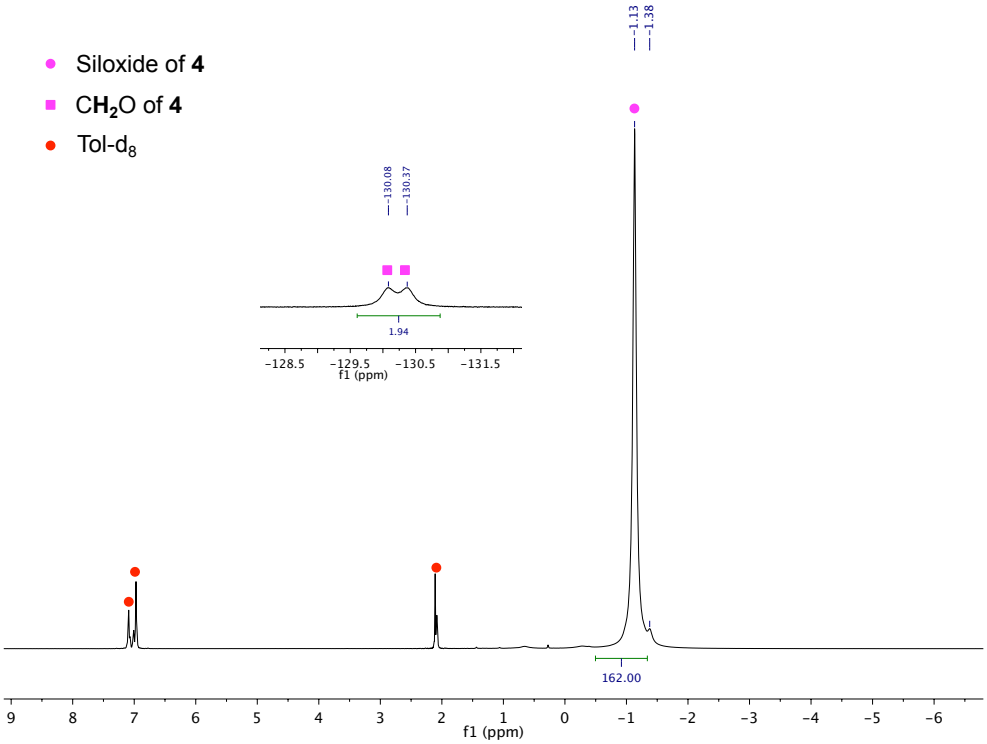

Figure S12. ^{1}H NMR (400 MHz, tol-d_8, 298K) of crystals of **4**.

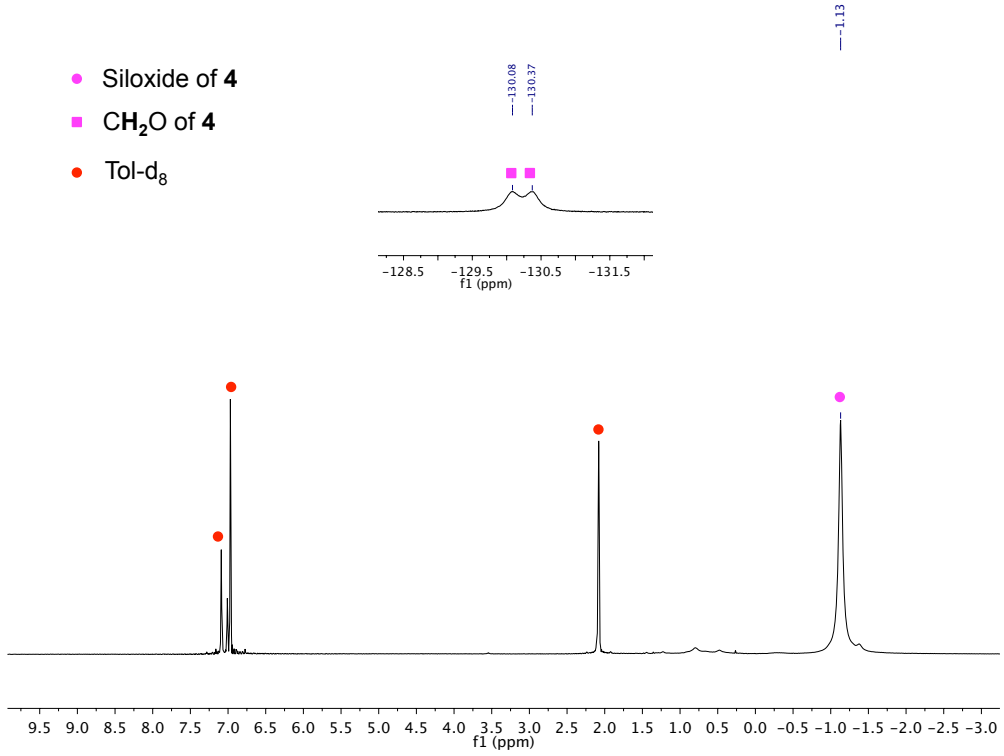

Figure S13. ^{1}H NMR (400 MHz, tol-d_8, 298K) of crystals of **D-4**.

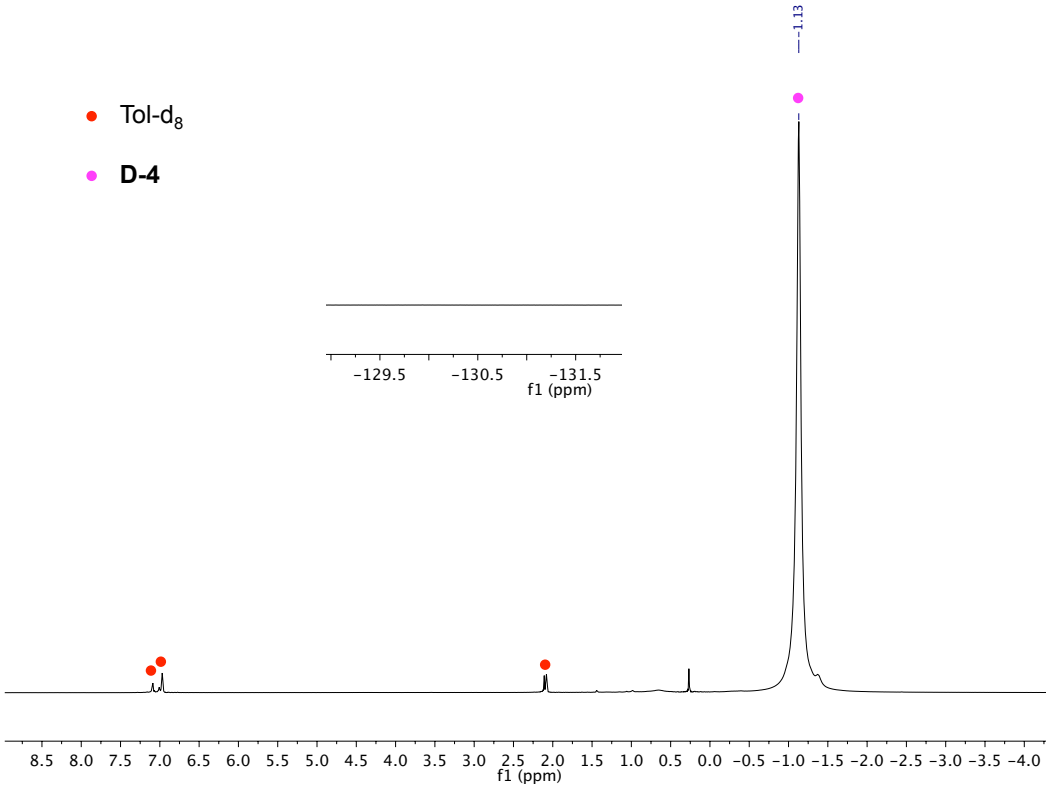

Figure S14. ^{13}C NMR (400 MHz, tol-d_8, 298K) immediately after addition of excess ^{13}CO to **2**.

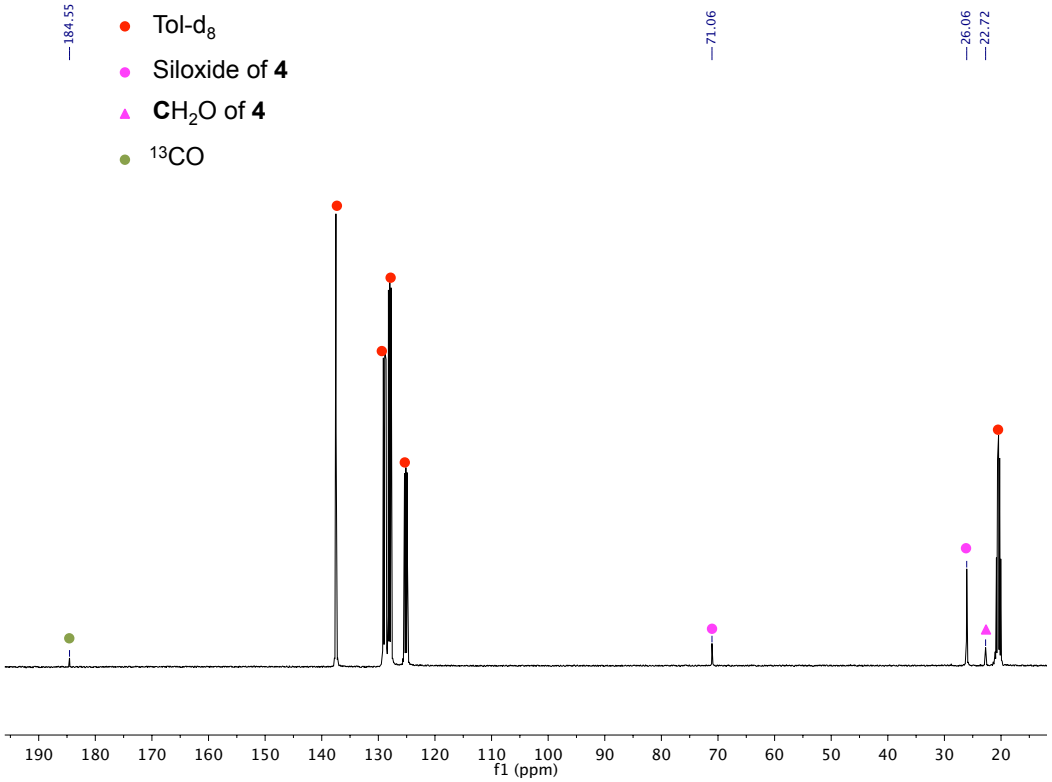

Figure S15. ^{13}C NMR (400 MHz, D_2O, 298K) after addition of ^{13}CO to **2**.

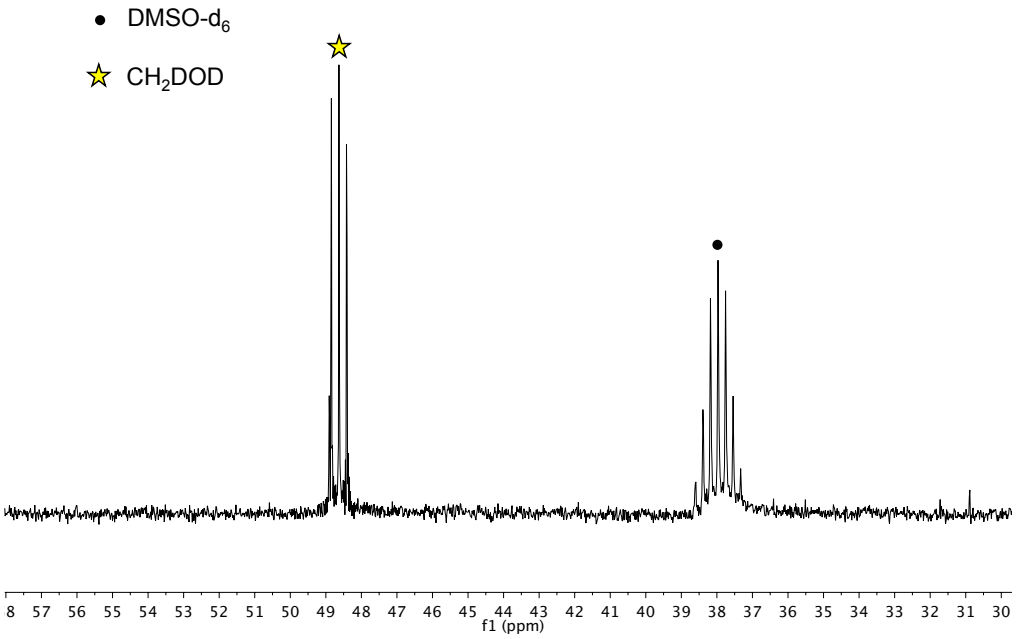

Figure S16. ^{1}H NMR (400 MHz, tol-d_8, 298K) of the evolution with time of the crude mixture of **4** in presence of excess ^{13}CO.

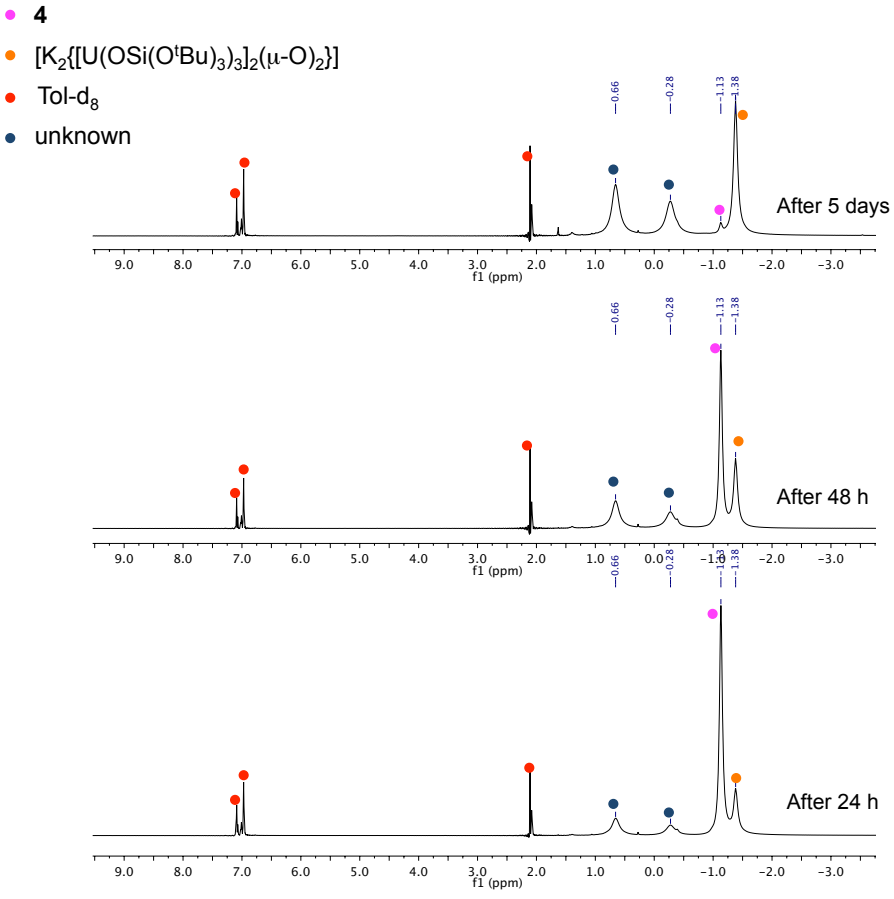

Figure S17. ^{1}H NMR (400 MHz, tol-d_8, 298K) of the crystals obtained from the evolution with time of **4**, in presence of excess ^{13}CO.

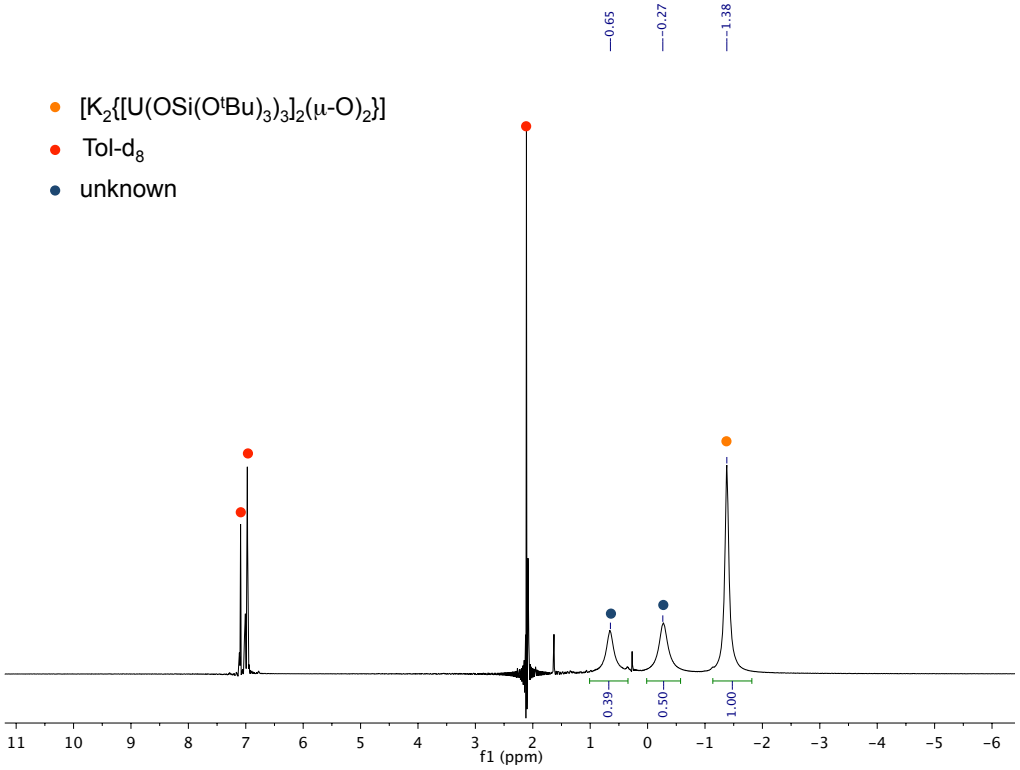

Figure S18. ^{13}C NMR (400 MHz, D_2O, 298K) of the crystals obtained from the evolution with time of **4**, in presence of excess ^{13}CO.

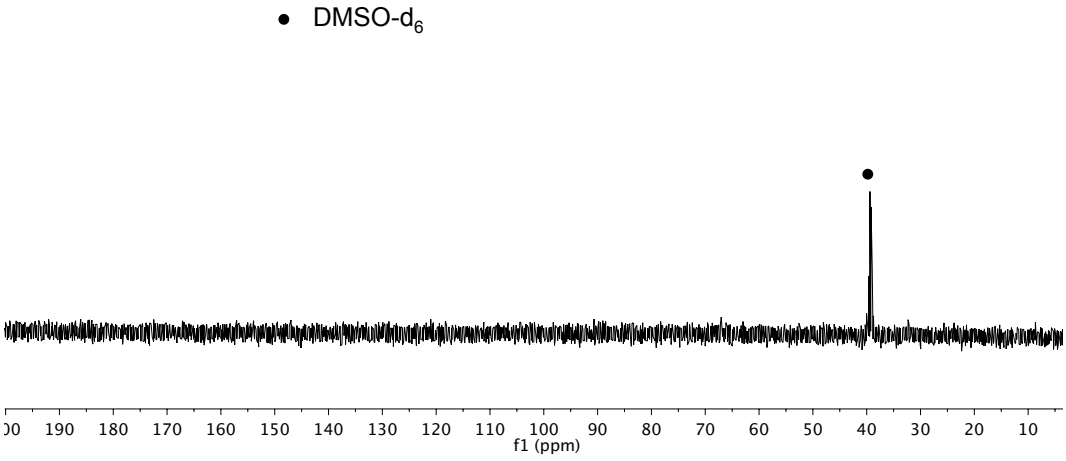

NMR data for the addition of H_2 to 4

Figure S19. ^{1}H NMR (400 MHz, tol-d_8, 298K) of the reaction mixture after subsequent additions of ^{13}CO and H_2 to **2**.

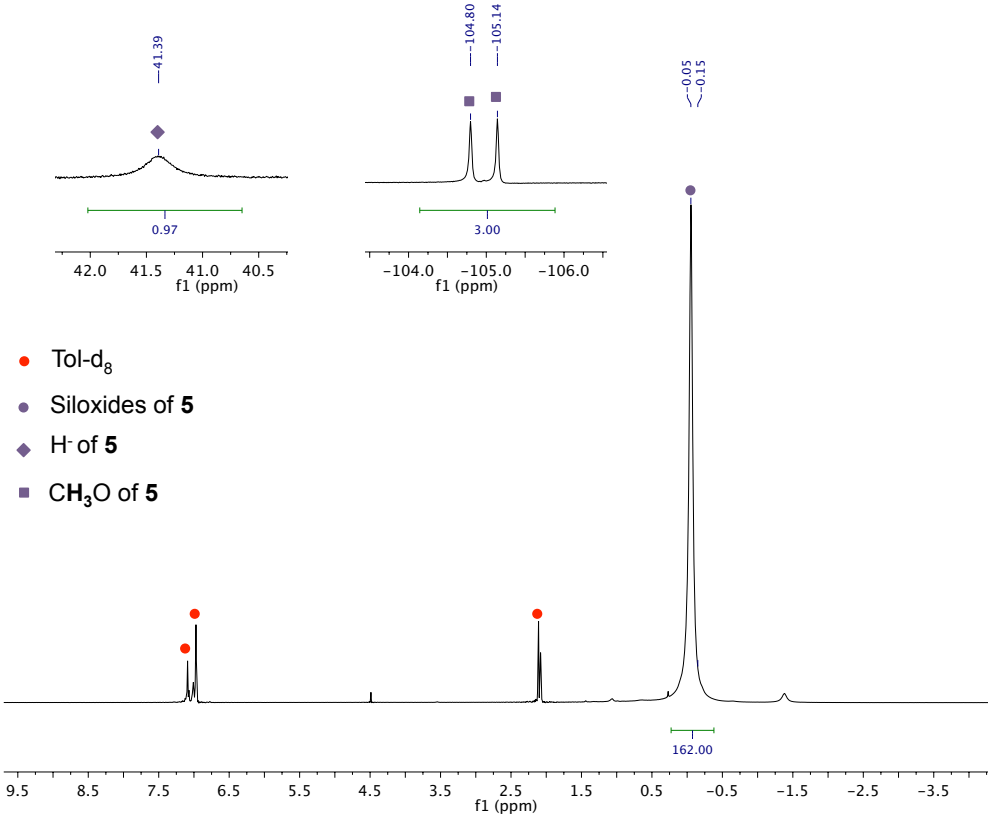

Figure S20. ^{1}H NMR (400 MHz, tol-d_8, 298K) of the reaction mixture after subsequent additions of ^{13}CO and D_2 to **2**.

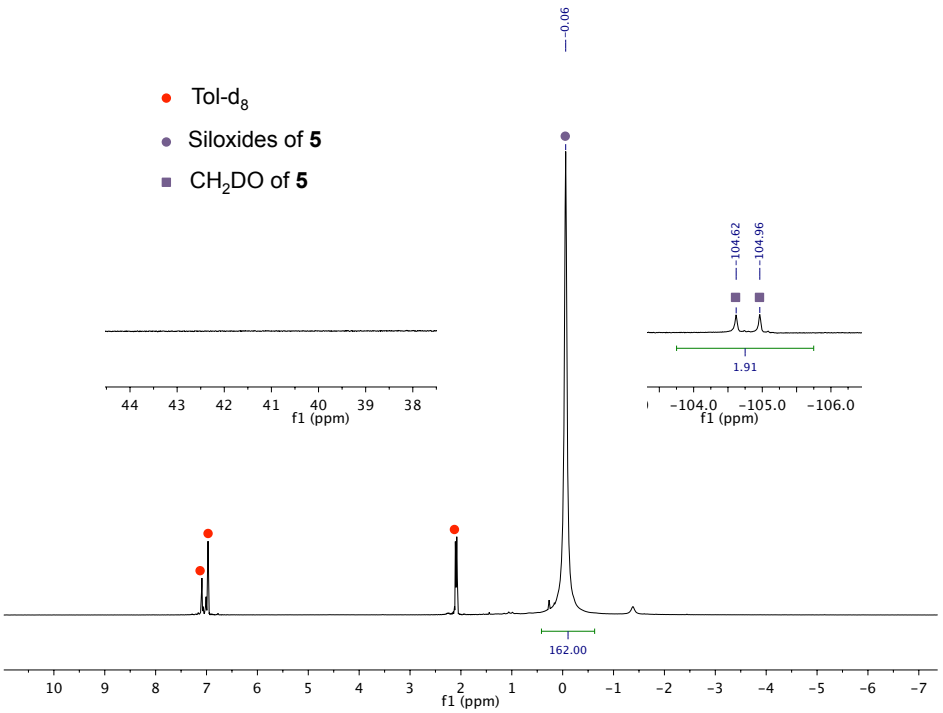

Figure S21. ^{1}H NMR (400 MHz, tol-d_8, 298K) of crystals of **5**.

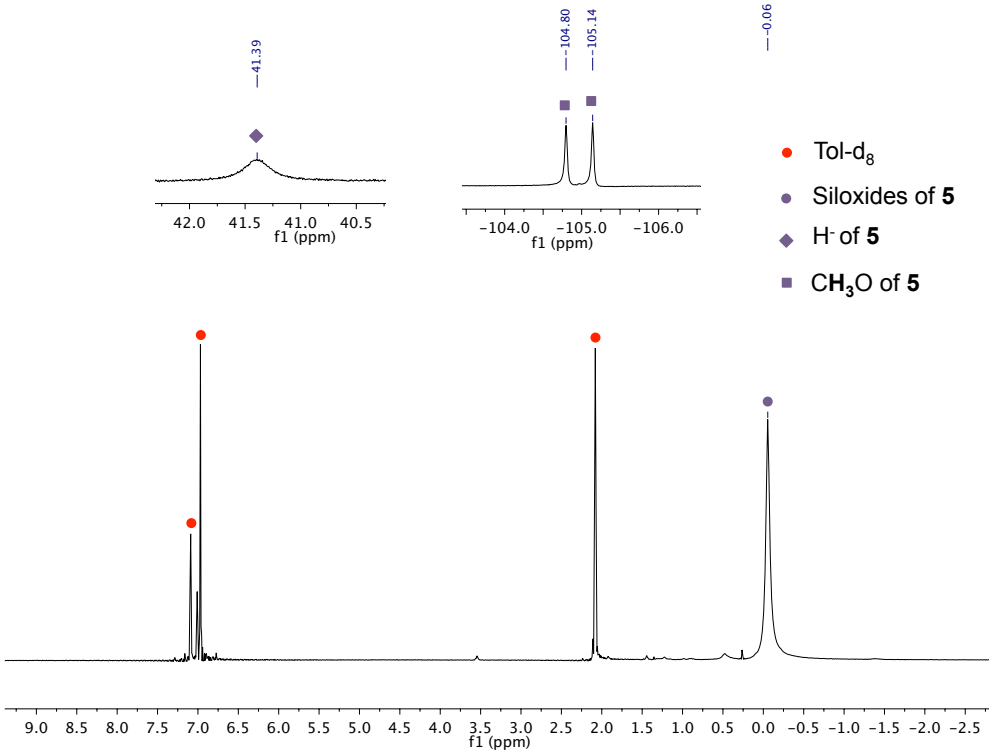

Figure S22. Proton coupled ^{13}C NMR (400 MHz, tol-d_8, 298K) of the reaction mixture after subsequent addition of ^{13}CO and H_2 to **2**.

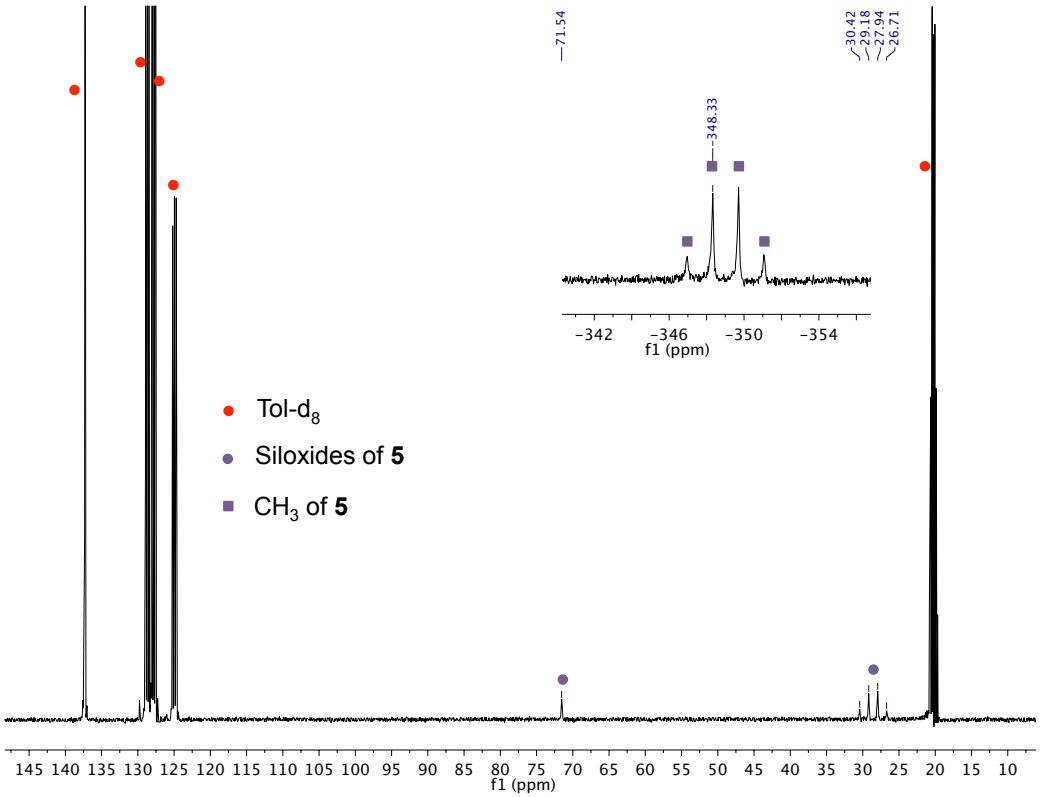

Figure S23. ^{13}C NMR (400 MHz, D_2O, 298K) of the reaction mixture after subsequent addition of ^{13}CO, H_2 and 3 equivalents of $^{13}CO_2$ to **2**.

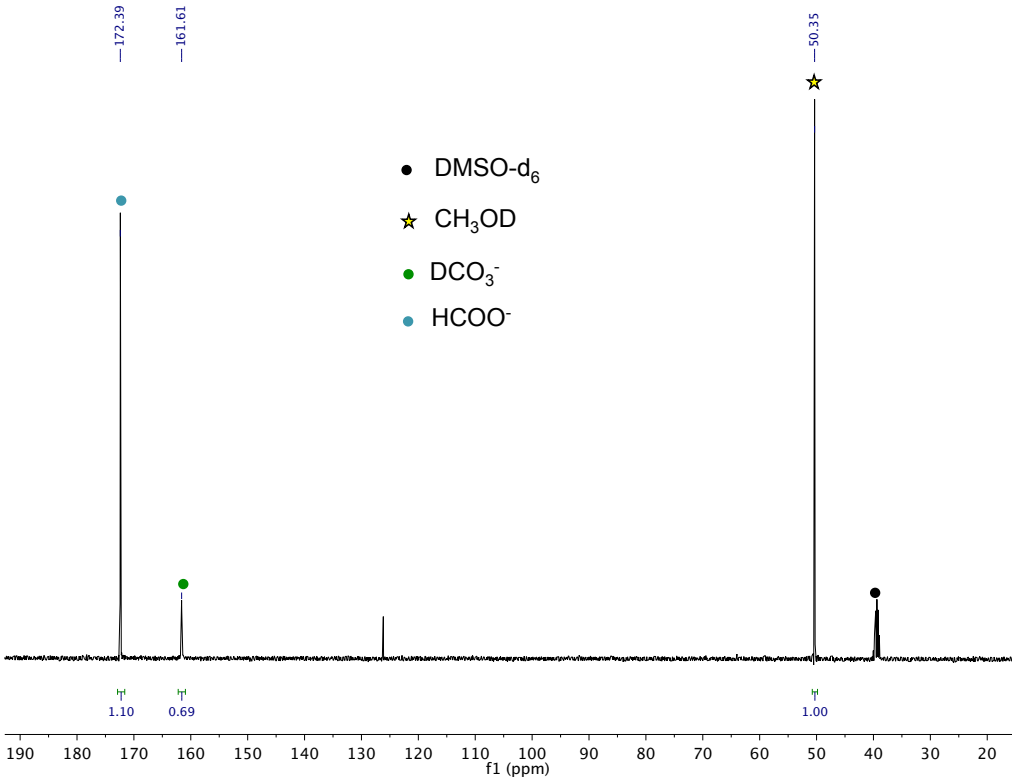

NMR data for the reaction of 2 with 3 equivalents of CO_2

Figure S24. ^{1}H NMR (400 MHz, tol-d_8, 298K) of the crude reaction mixture after addition of 3 equivalents of $^{13}CO_2$ to **2**.

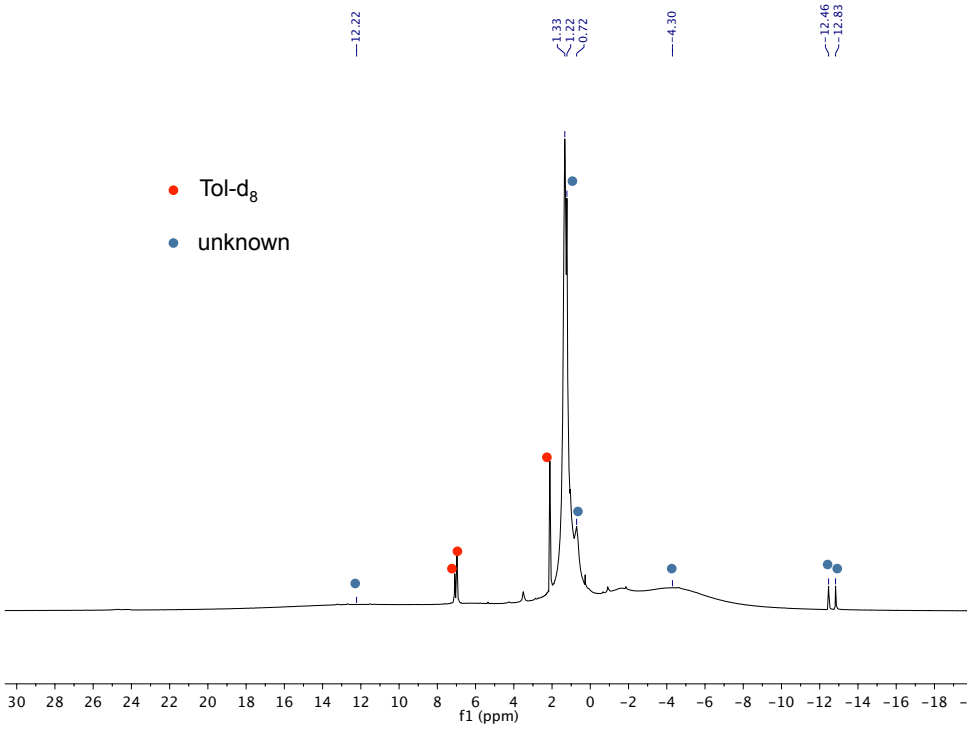

Figure S25. ^{13}C NMR (400 MHz, tol-d_8, 298K) of the crude reaction mixture after addition of 3 equivalents of $^{13}CO_2$ to **2**.

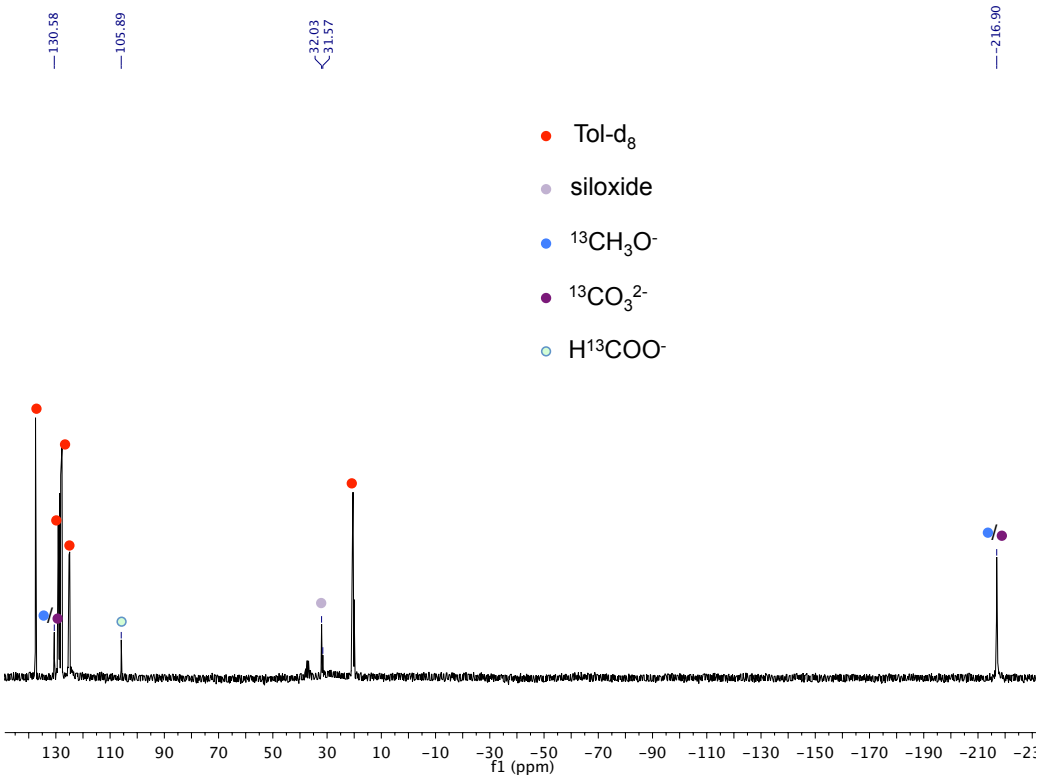

Figure S26. ^{1}H NMR (400 MHz, tol-d_8, 298K) of the light blue crystals obtained after addition of $3CO_2$ to **2**. The ratio at which the different products crystallize is not reproducible. Crystals a) and b) are obtained from two different reactions with 3 CO_2.

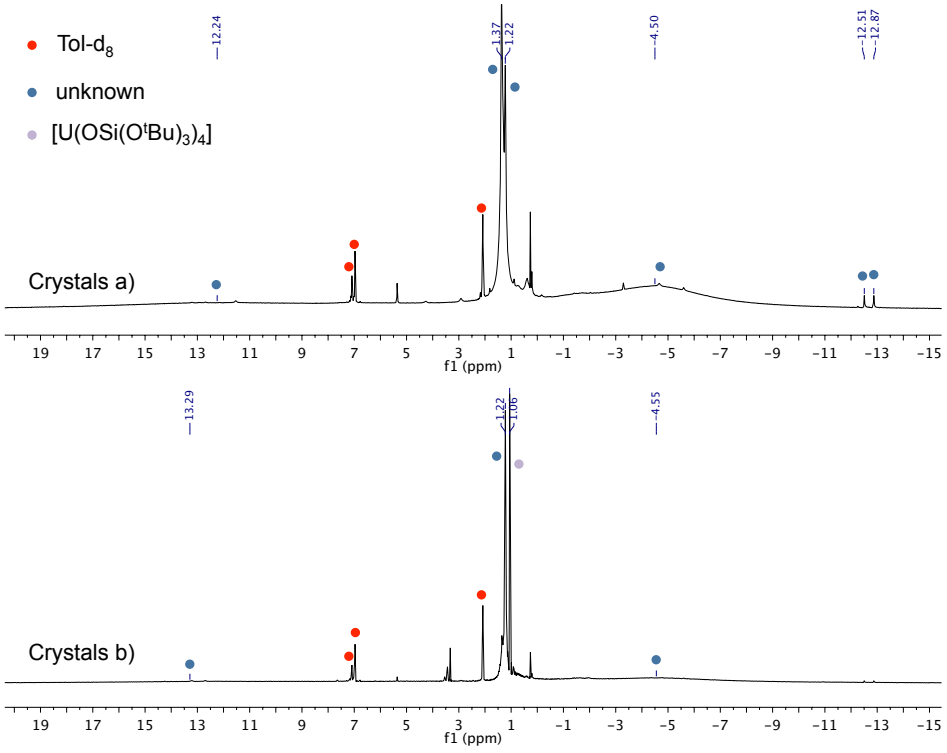

Figure S27. ^{13}C NMR (400 MHz, tol-d_8, 298K) of the light blue crystals obtained after addition of 3 CO_2 to **2**. The ratio at which the different products crystallize is not reproducible. Crystals a) and b) are obtained from two different reactions with 3 CO_2 (the same batches as Figure S26.

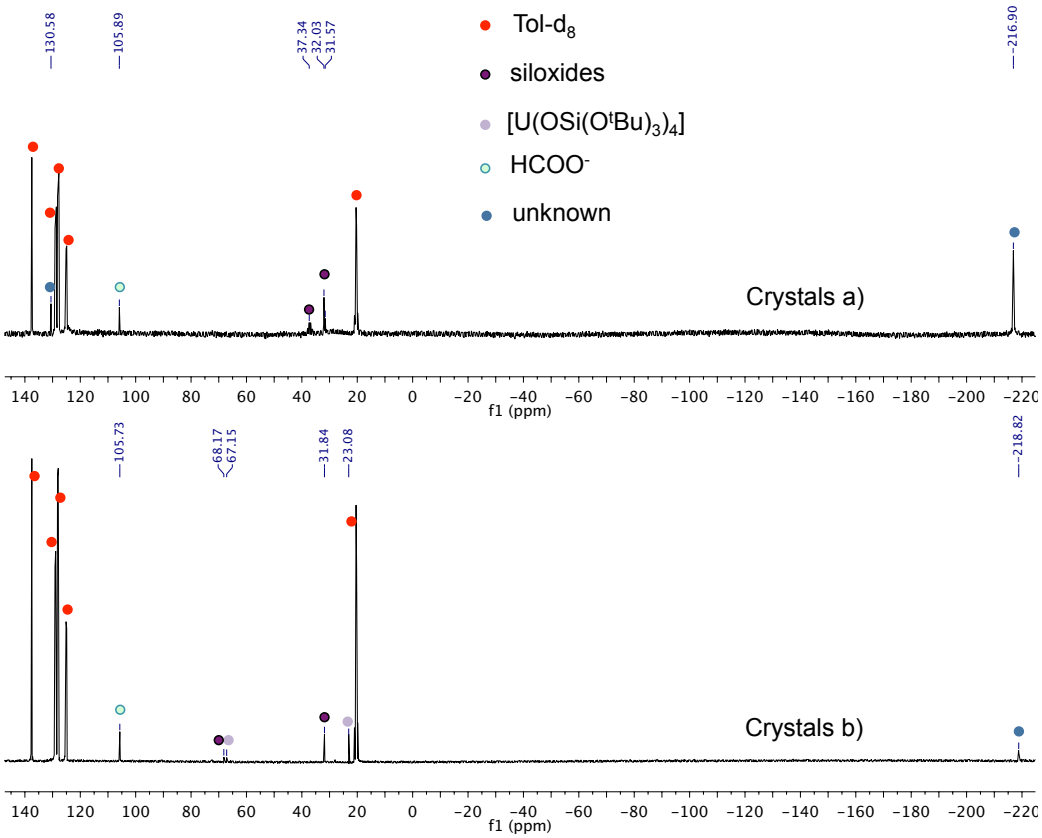

Figure S28. ^{13}C NMR (400 MHz, D_2O, 298K) of the light blue crystals obtained after addition of 3 CO_2 to **2**. The same peaks are found when different crystals or crude mixture are used.

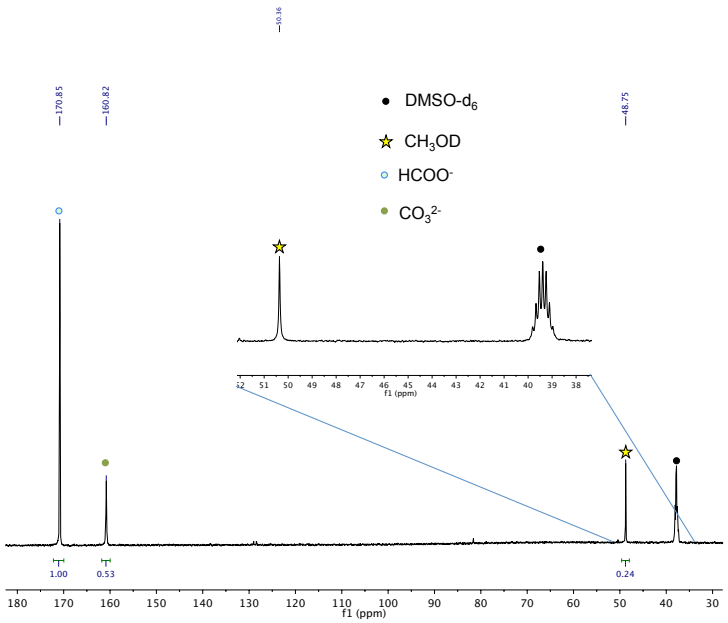

Figure S29. ^{1}H NMR (400 MHz, tol-d_8, 298K) after addition of 1 eq of CO_2

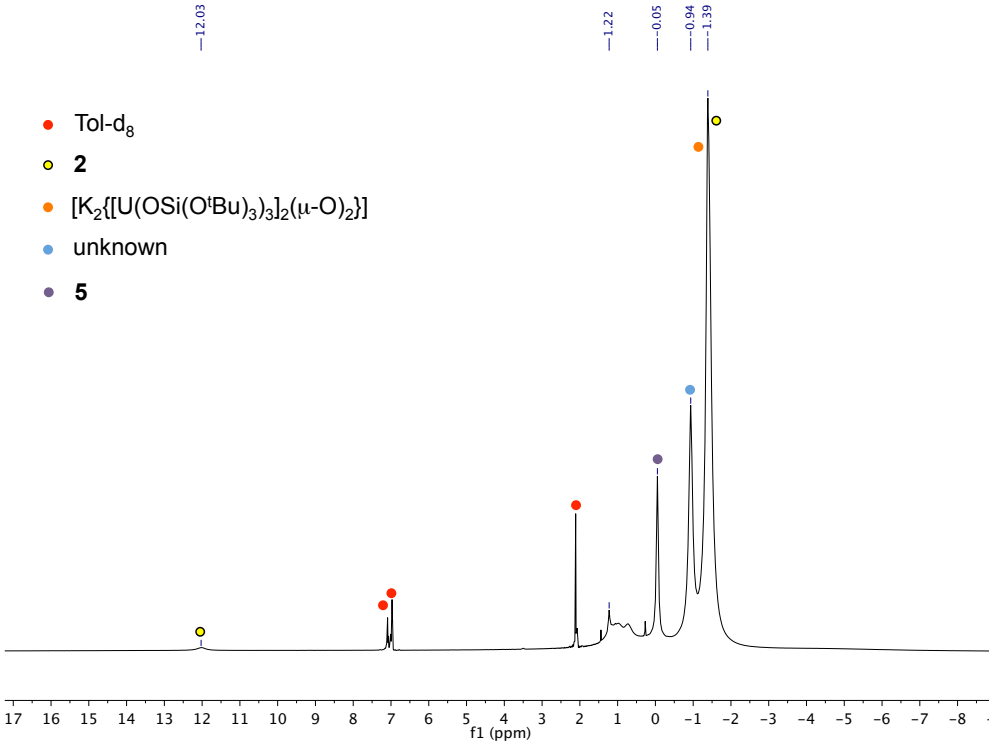

Figure S30. ^{13}C NMR (400 MHz, D_2O, 298K) after addition of 1 eq of CO_2

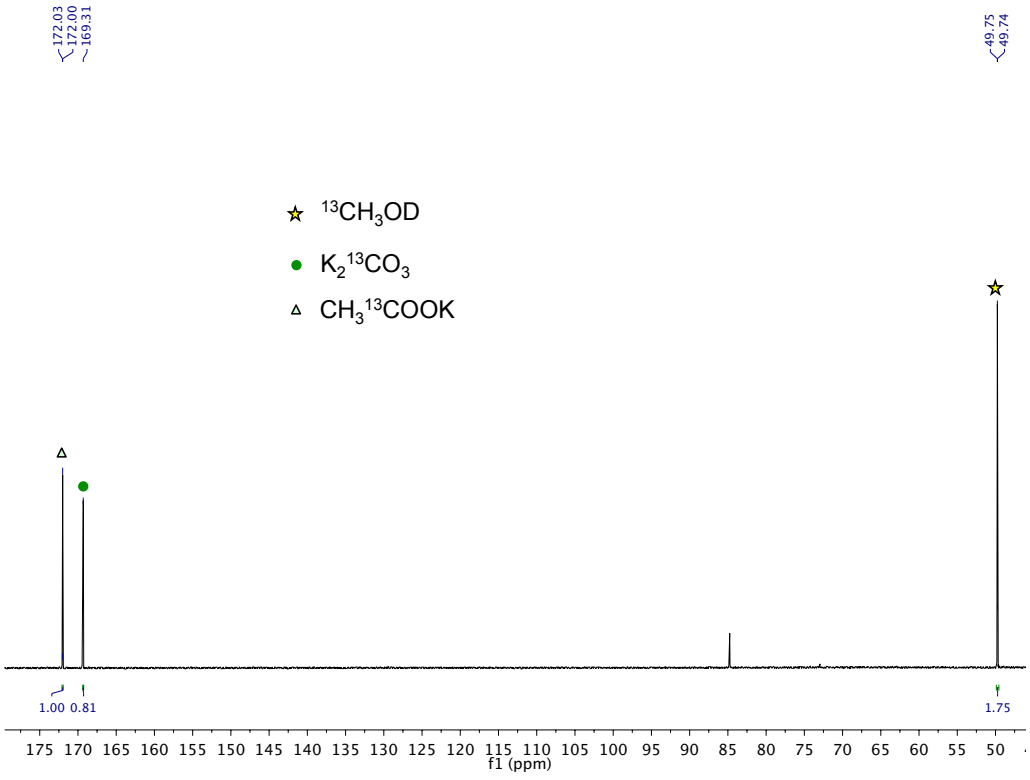

Figure S31. ^{1}H NMR (400 MHz, tol-d_8, 298K) after addition of 2 eq of CO_2

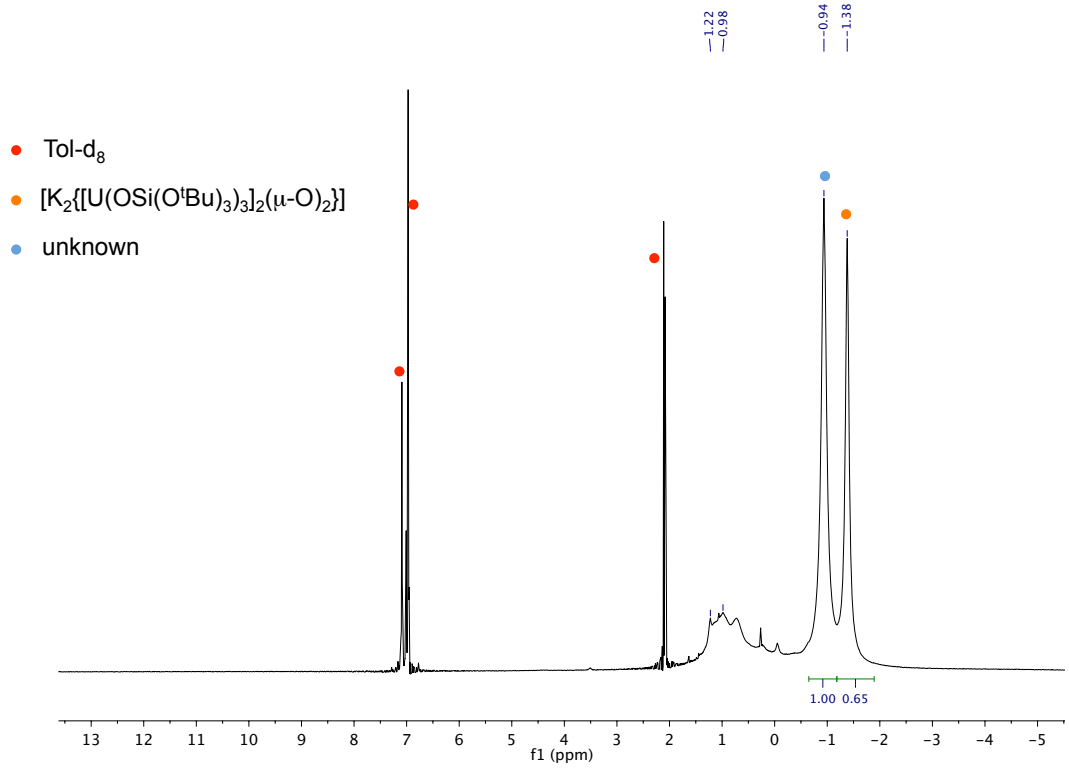

2. Evan's Method

A capillary with pure deuterated solvent was sealed and a sample 0.01 M of **2** in tol-d_8 was prepared. The capillary and the solution of **2** were placed in an NMR tube and the difference in chemical shift between the two solvent peaks is detected and used to calculate the magnetic moment. To the same sample, subsequent additions of CO and H_2 were made and the same measurement performed (the solvent was freezed before removal of the headspace and addition of CO or H_2).

Diamagnetic contribution was calculated from the *Bain, G.A.; Berry, J. F. Diamagnetic Corrections and Pascal's Constants. J.Chem. Educ.* ***2008****, 85 (4), 532.*

Calculated values of magnetic moments: 2.78 m_B (for **2**), 2.75 m_B (for **5**) and 2.37 m_B (for **6**). These values are in agreement with the absence of changes in the oxidation state of the uranium center during the reaction with CO and H_2.

Figure S32. ^{1}H NMR (400 MHz, tol-d_8, 298K) of solutions of complex **2** (top), **4** (middle) and **5** (bottom). Complex **4** and **5** were obtained by subsequent additions of CO and H_2 to isolated complex **2**.

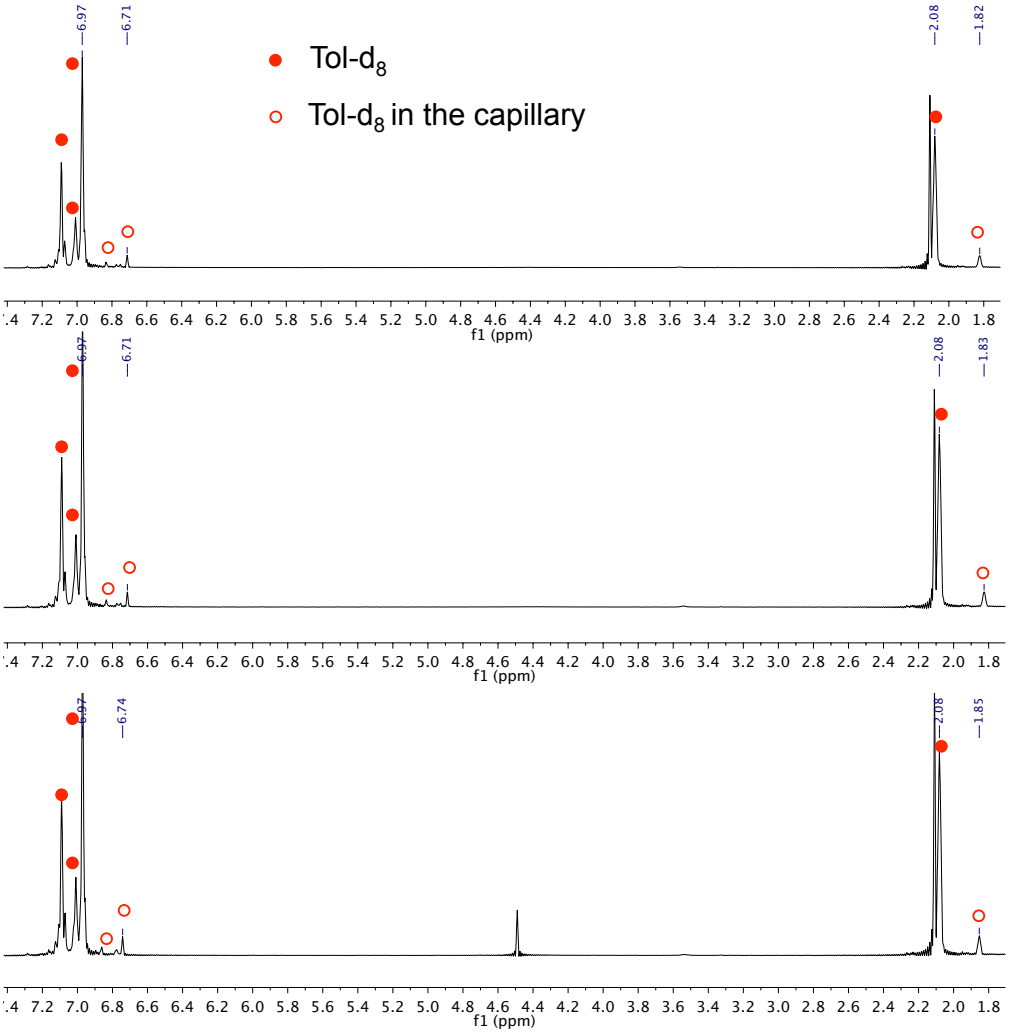

3. GC-MS and ESI-MS data

Figure S33. Detection of $^{13}CH_3OH$ by GC-MS, formed in D_2O from the mixture of products formed after addition of CO_2 to complex **2**.

The deuterium is replaced by proton in the column, as proved by the injection of a standard solution of CH_3OD.

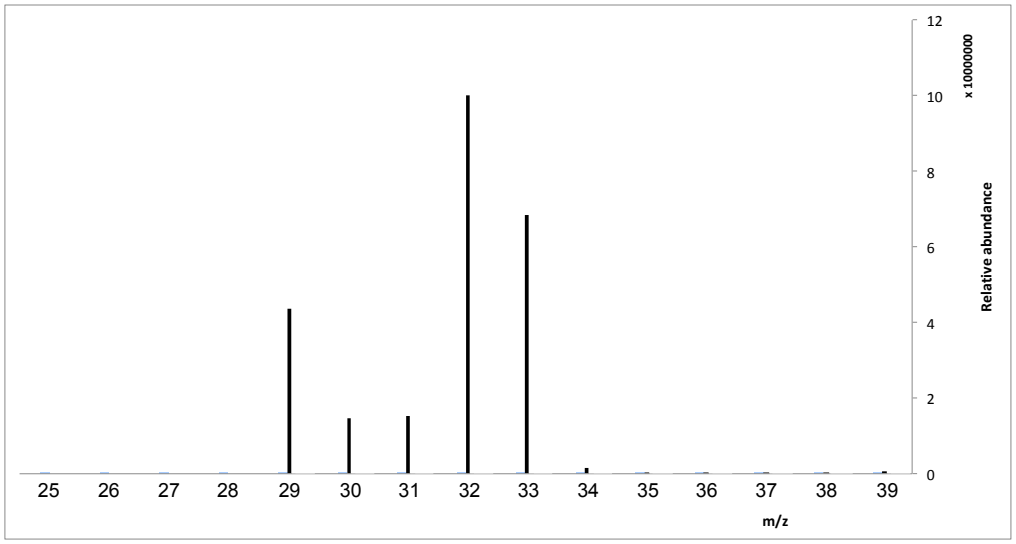

Figure S34. ESI-MS spectrum of a THF solution of complex **5**. MH^+ 2184 m/z, MK^+ 2222 m/z.

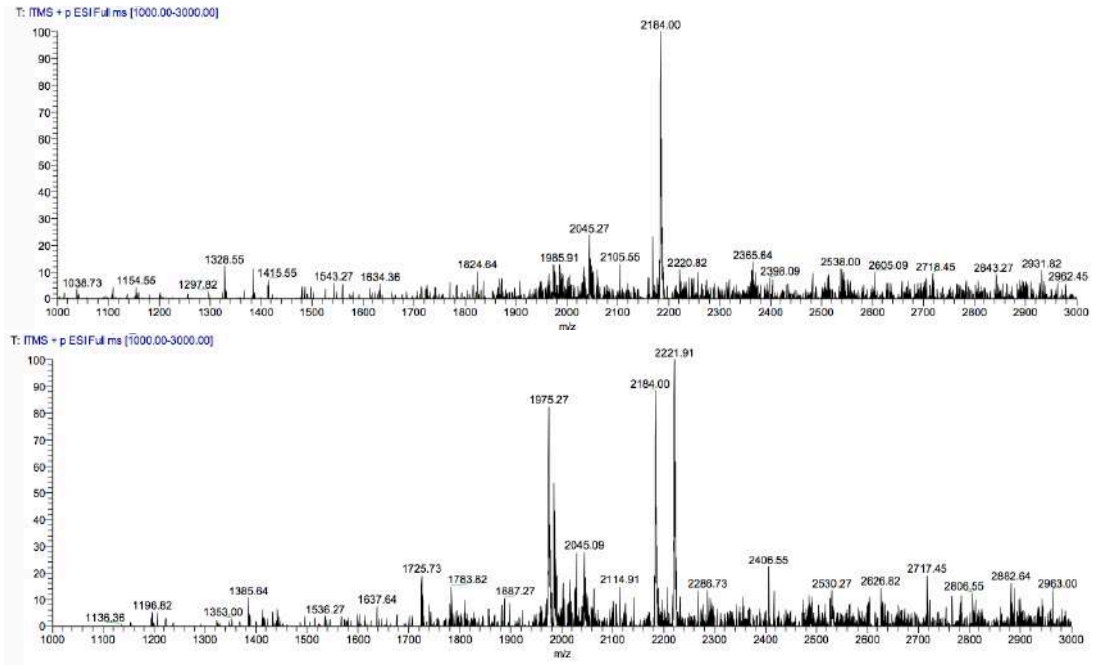

4. IR spectra

Figure S35. IR spectrum of complex **2**.

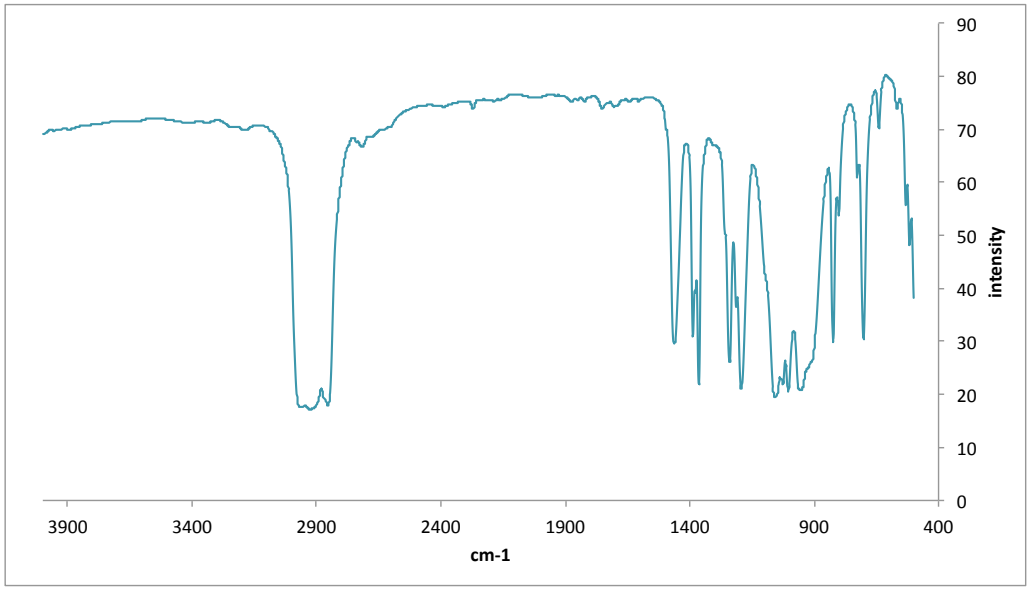

Figure S36. IR spectrum of complex **4**.

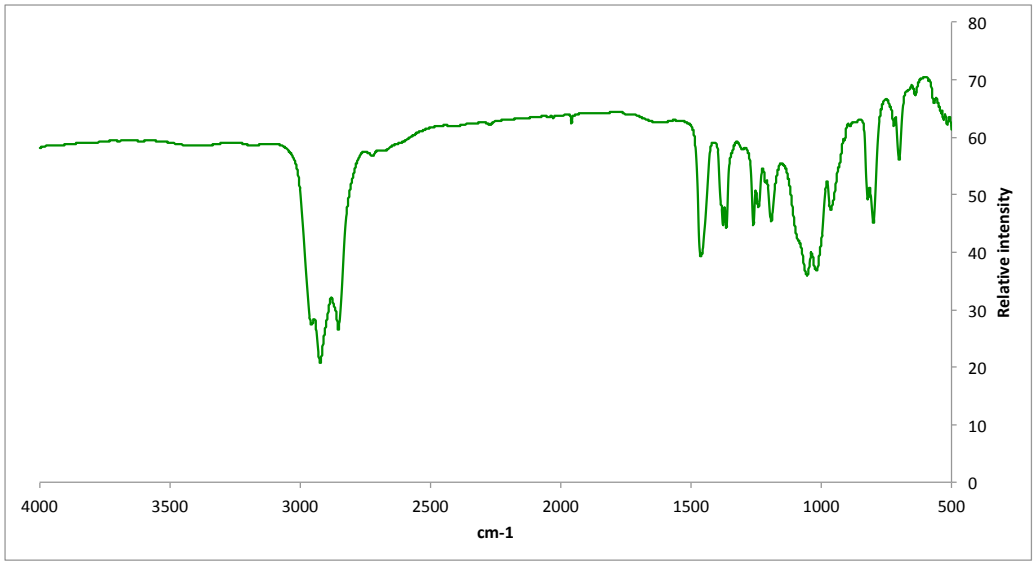

Figure S37. IR spectrum of complex **5**.

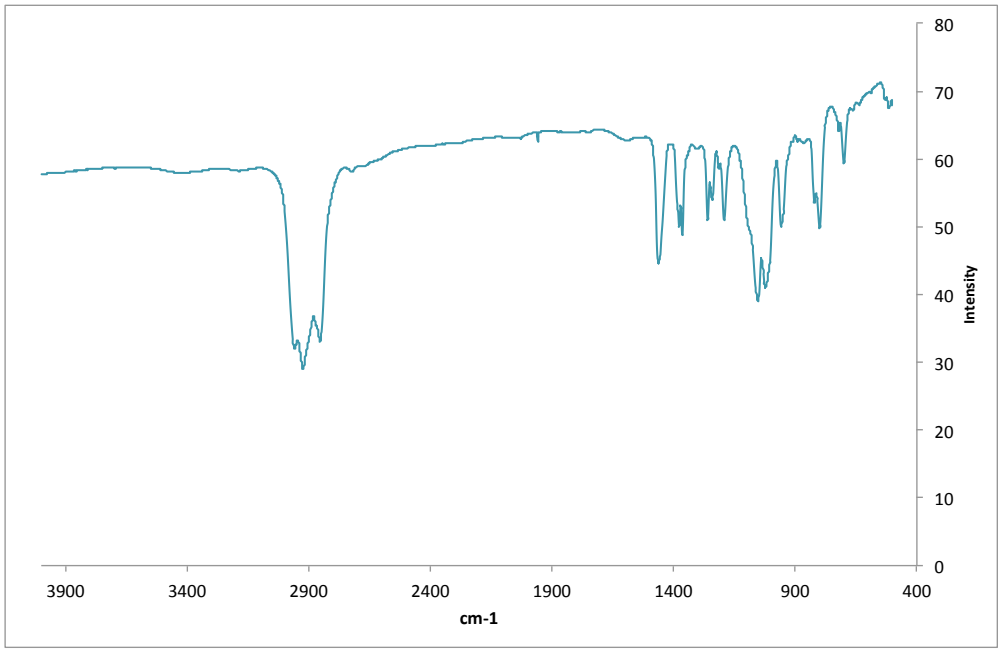

5. X-ray data

Table 1. X-ray data for complex **2 -4**.

	2(C_8H_8)	**3**	**4**
Formula	$C_{79}H_{172}O_{25}Si_6U_2$	$C_{76}H_{170}K_2O_{25}Si_6U_2$	$C_{73}H_{162}K_2O_{26}Si_6U_2$
Crystal size (mm^3)	0.340 x 0.181 x 0.154	0.239 x 0.093 x 0.076	0.268 x 0.195 x 0.171
cryst syst	Triclinic	Monoclinic	Monoclinic
space group	*P*-1	$P2_1/c$	$P2_1/n$
volume ($Å^3$)	5783.3(2)	11108.6(5)	5546.47(9)
a (Å)	14.2030(3)	23.8521(7)	14.26268(13)
b (Å)	17.5377(4)	13.9941(4)	17.70163(18)
c (Å)	25.3851(4)	33.3790(8)	21.97679(18)
α (deg)	78.8955(18)	90	90
β (deg)	88.5451(15)	94.406(2)	91.5652(8)
γ (deg)	68.930(2)	90	90
Z	2	4	2
formula weight (g/mol)	2244.96	2234.93	2178.82
density (g cm^{-3})	1.289	1.336	1.305
absorption coefficient (mm^{-1})	9.525	9.921	9.923
F(000)	2304	4584	2228
temp (K)	140.00(10)	139.99(10)	140.01(10)
total no. reflections	29080	67482	62550
unique reflections [R(int)]	29080	19457 [0.1174]	11623[0.0348]

Final R indices [I > 2σ(I)]	R1 = 0.0435, wR2 = 0.1290	R1 = 0.0976, wR2 = 0.2384	R1 = 0.0532, wR2 = 0.1430
Largest diff. peak and hole (e.A^{-3})	1.833 and -2.169	7.762 and -2.150	2.621 and -2.834
GOOF	1.048	1.080	1.038

Table 2. X-ray data for complex **5** and **6**.

	5	**6**
Formula	$C_{73}H_{166}K_2O_{26}Si_6U_2$	$C_{75}H_{163}K_2O_{31}Si_6U_2$
Crystal size (mm^3)	0.696 x 0.067 x 0.050	0.252 x 0.155 x 0.112
cryst syst	Monoclinic	Orthorhombic
space group	$P2_1$	$P2_12_12_1$
volume (Å^3)	5578.99(18)	11573.4(5)
a (Å)	13.9751(2)	13.5015(3)
b (Å)	18.1064(3)	18.6524(5)
c (Å)	22.0854(5)	45.9564(12)
α (deg)	90	90
β (deg)	93.337(2)	90
γ (deg)	90	90
Z	2	4
formula weight (g/mol)	2182.85	2283.84
density (g cm^{-3})	1.299	1.311
absorption coefficient (mm^{-1})	9.865	9.570
F(000)	2236	4668
temp (K)	140.00(10)	140.00(10)
total no. reflections	23280	85892
unique reflections [R(int)]	23280	23679 [0.1369]
Final R indices [I > 2σ(I)]	R1 = 0.0454, wR2 = 0.1192	R1 = 0.0582, wR2 = 0.1267
Largest diff. peak and hole (e.A^{-3})	1.493 and -2.289	1.585 and -2.105
GOOF	1.042	0.964

X-ray Experimental Part:

The diffraction data for all compounds were measured at low temperature [140 K] using Cu K_a radiation on a Rigaku SuperNova dual system in combination with Atlas type CCD detector. The data reduction was carried out by *CrysAlis*^{Pro}.[1]

The solutions and refinements were performed by *SHELXT*[2] and *SHELXL*[3], respectively. The crystal structures were refined using full-matrix least-squares based on F^2 with all non hydrogen atoms anisotropically defined. Hydrogen atoms were placed in calculated positions by means of the "riding" model.

For compound **2**, the central core contains 1 oxygen atoms and 2 hydrides and they are disordered over three different sites along the metal-metal axes. The overall occupancies for oxygen sump up to 1 while the hydrogens have each an occupancy of 2/3. Some restraints have been applied to disordered moieties (card DFIX, SADI and SIMU) to get acceptable geometries and atomic parameters. Some constraints (EADP card) have been used for the displacement parameters of the central oxygens.

For compound **3**, some similarity restraints have been employed in the case of a disordered ligand (SADI and SIMU cards).

In the case of compound **4**, all light atoms (C, O) have been submitted to similarity restraints (SIMU card); further restraints have been included to model disordered moieties (RIGU, SADI, DFIX, ISOR cards). The central part of the dimer contains one O and one CH_2O and they are disordered by symmetry.

For compound **5**, the core of the dimer contains one CH_3O, one O and 1 H (these latter two are disordered over two positions). Plenty of restraints have been employed for the refinement of carbons and oxygens and to get reasonable ellipsoids and geometries (DFIX, SADI, SIMU, RIGU, ISOR cards).

In the case of compound **6**, the central part of the complex contains 2 $HCOO^-$ and 1 CO_3^{2-}, some restraints were used for the refinement of some disordered moieties and to adjust some geometries in the core of the dimer (SADI, SIMU and RIGU cards).

Additional electron density (due to disordered solvent) found in the difference Fourier map of all compounds except **4** was treated by the *SQUEEZE* algorithm of *PLATON*.[4]

Pseudo merohedral twinning was found for compound **2** and 5 and treated directly by *CrysAlis*^{Pro} [1] obtaining these BASF factors: 0.195(1), 0.0916(8) (**2**), 0.263(1) (**5**).

1) *CrysAlis*^{Pro}, Rigaku Oxford Diffraction, release 1.171.39.46, 2018.
2) *SHELXT* - Integrated space-group and crystal-structure determination¸ G. M. Sheldrick**,** *Acta Crystallogr.*, *Sect. A* **2015**, *71*, 3-8.
3) *SHELXL* - Crystal structure refinement, G. M. Sheldrick**,** *Acta Crystallogr.*, *Sect. C* **2015**, *71*, 3-8.
4) *PLATON*, A.L.Spek, *Acta Crystallogr*., *Sect. D* **2009**, *65*, 148-155.

CURRICULUM VITAE

EDUCATION

- **March 2015** **PhD in Coordination Chemistry**
  at École Polytechnique Fédérale de Lausanne (EPFL)

  "Small molecule activation by molecular uranium complexes"
  Supervisor: Prof. Marinella Mazzanti

- **October 2011** **Master's Degree in Organic Chemistry (110/110 cum laude)**
  at Università di Pisa

  Thesis: "Supramolecular Chiral Aggregates: chirooptical study"
  Supervisor: Prof. Lorenzo Di Bari

- **October 2007** **Bachelor's Degree in Chemistry (105/110)**
  at Università di Parma

LIST OF PUBLICATIONS

- **M. Falcone**, L. Chatelain, M. Mazzanti, "Nucleophilic Reactivity of a Nitride-Bridged Diuranium(IV) Complex: CO_2 and CS_2 Functionalization", *Angewandte Chemie Int. Ed.*, **2016**, *55*, 4074
- **M. Falcone**, C. E. Kefalidis, R. Scopelliti, L. Maron, M. Mazzanti, "Facile CO Cleavage by a Multimetallic CsU_2 Nitride Complex", *Angewandte Chemie Int. Ed.*, **2016**, *55*, 12290
- **M. Falcone**, L. Chatelain, R. Scopelliti, M. Mazzanti, "CO cleavage and CO_2 Functionalization under Mild Conditions by a Multimetallic CsU_2 Nitride Complex", *CHIMIA*, **2017**, *71*, 209
- **M. Falcone**, L. Chatelain, R. Scopelliti, I. Zivkovic, M. Mazzanti, "Nitrogen Reduction and functionalization by a multimetallic uranium nitride complex", *Nature*, **2017**, *547*, 332
- R. P. Kelly, **M. Falcone**, C. A. Lamsfus, R. Scopelliti, L. Maron, K. Meyer, M. Mazzanti, "Metathesis of a U^V imido complex: a route to a terminal U^V sulfide", *Chem. Sci.*, **2017**, *8*, 5319
- **M. Falcone**, L. N. Poon, F. F. Tirani, M. Mazzanti, "Reversible Dihydrogen Activation and Hydride Transfer by a Uranium Nitride Complex", *Angewandte Chemie Int. Ed.*, **2018**, *57*, 3697
- **M. Falcone**, M. Mazzanti, "Four-electron Reduction and Functionalization of N_2 by a Uranium(III) Bridging Nitride", *CHIMIA*, **2018**, *72*, 199

- **M. Falcone**, L. Barluzzi, J. Andrez, F. F. Tirani, I. Zivkovic, A. Fabrizio, C. Corminboeuf, K. Severin, M. Mazzanti, "The role of bridging ligands in dinitrogen reduction and functionalization by uranium multimetallic complexes", *Nature Chemistry*, **2018**, *11*, 154
- M. Falcone, R. Scopelliti, M. Mazzanti, "CO_2 and CO/H_2 Conversion to Methoxide by a Uranium(IV) Hydride", *forthcoming*

CONFERENCES

- Swiss Chemical Society conference (SCS) 2015 at Lausanne, EPFL
- Coordination Chemistry International Conference ICCC 2016 in Brest
- Swiss Chemical Society conference (SCS) 2016 in Zurich, ETH
- Gordon Conference "Inorganic Reaction Mechanism", 2017, Texas
- Swiss Chemical Society conference (SCS) 2017 in Bern, University of Bern
- Gordon Conference "Inorganic Chemistry", 2018, New England
- ICFE10, 2018, EPFL, Lausanne
- Swiss Chemical Society conference (SCS) 2018 in Lausanne, EPFL

AWARDS

- Award for best poster presentation at SCS conference in Zurich, 2016
- Award for best oral presentation at SCS conference in Bern, 2017
- Inorganics (Open access Journal) Travel Awards 2018

**Ce document a été imprimé au Centre d'impression EPFL,
imprimerie climatiquement neutre, certifiée myClimate.**